

Carbon Materials: Chemistry and Physics 10
Series Editors: Franco Cataldo · Paolo Milani

Mircea Vasile Diudea

Multi-shell Polyhedral Clusters

 Springer

Carbon Materials: Chemistry and Physics

Volume 10

Series editors

Franco Cataldo

Soc. Lupi Chemical Research Institute Dipto. Ricerca e Sviluppo

Roma

Italy

Paolo Milani

Università Milano-Bicocca Dipto. Fisica

Milano

Italy

Carbon Materials: Chemistry and Physics aims to be a comprehensive book series with complete coverage of carbon materials and carbon-rich molecules. From elemental carbon dust in the interstellar medium, to the most specialized industrial applications of the elemental carbon and derivatives. With great emphasis on the most advanced and promising applications ranging from electronics to medicinal chemistry.

The aim is to offer the reader a book series which not only should be made of self-sufficient reference works, but should stimulate further research and enthusiasm.

More information about this series at <http://www.springer.com/series/7825>

Mircea Vasile Diudea

Multi-shell Polyhedral Clusters

 Springer

Mircea Vasile Diudea
Department of Chemistry
Faculty of Chemistry and Chemical Engineering
Babes-Bolyai University
Cluj-Napoca, Romania

ISSN 1875-0745 ISSN 1875-0737 (electronic)
Carbon Materials: Chemistry and Physics
ISBN 978-3-319-64121-8 ISBN 978-3-319-64123-2 (eBook)
DOI 10.1007/978-3-319-64123-2

Library of Congress Control Number: 2017951136

© Springer International Publishing AG 2018

This work is subject to copyright. All rights are reserved by the Publisher, whether the whole or part of the material is concerned, specifically the rights of translation, reprinting, reuse of illustrations, recitation, broadcasting, reproduction on microfilms or in any other physical way, and transmission or information storage and retrieval, electronic adaptation, computer software, or by similar or dissimilar methodology now known or hereafter developed.

The use of general descriptive names, registered names, trademarks, service marks, etc. in this publication does not imply, even in the absence of a specific statement, that such names are exempt from the relevant protective laws and regulations and therefore free for general use.

The publisher, the authors and the editors are safe to assume that the advice and information in this book are believed to be true and accurate at the date of publication. Neither the publisher nor the authors or the editors give a warranty, express or implied, with respect to the material contained herein or for any errors or omissions that may have been made. The publisher remains neutral with regard to jurisdictional claims in published maps and institutional affiliations.

Printed on acid-free paper

This Springer imprint is published by Springer Nature
The registered company is Springer International Publishing AG
The registered company address is: Gewerbestrasse 11, 6330 Cham, Switzerland

Preface

Nanoworld is the world seen at the size of 10^{-9} m; searching matter at this depth started since 1970 when Eiji Osawa had enounced the conjecture that the truncated icosahedron could be a molecule, later called C_{60} . Then, in 1985, Kroto, Curl, and Smalley got spectral evidence that C_{60} , which shows a single peak in ^{13}C -NMR, is a real molecule. They were awarded the Nobel Prize in 1995 for this historical discovery. Macroscopic synthesis of C_{60} came later, in 1990, by the work of Kraetschmer and collaborators. Iijima reported in 1991 the synthesis of nanotubes; the period after these pioneering discoveries is commonly called the “Nanoera.” Development of computers and technology enabled researchers and industry to go further in research and applications, promoting an explosive development of electronics, optoelectronics, telecommunications, education, etc. Thereafter, the most important event (for the actual book) was the recognition of quasi-crystals as ordered, nonperiodic matter, the class to which the multi-shell clusters belong. Dan Shehtman was the Noble Prize winner for these results in 2011. . . then the book was started to be written. . .

Topology is the mathematical study of shapes; the multi-shell clusters concerned herein are referred to as sets of shapes, arranged, in an abstract space, in increasing rank (as Egon Schulte proposed in 1980), rather than in the geometrical higher dimensional space. Cluster models representing primary atomic arrangement are needed to understand the actual structure and then the undergoing transformations, both in concept and experimental realization and in the computational treatment. However, there is little reference to crystallographic entities, e.g., real crystal networks and quasi-crystals. Also, this book does not provide all possible structures of a given set of restrictive conditions; it rather gives chosen, representative examples. This book about multi-shell clusters could be more inspiring for architects or visual artists in making monumental, artistic works, by its aesthetic message.

The structure of this book is as follows:

An introduction to the Chemical Graph Theory is made in the first chapter. It is a description through the eye of a chemist of the basic notions of Graph Theory: definitions, topological matrices and indices, counting polynomials, etc.

Chapter 2 describes some of the most important operations on maps that enabled the design of the multi-shell clusters, as is shown in the following chapters.

In Chap. 3, rigorous definitions in polyhedra and polytopes of higher rank are given with a view to helping in the effort of counting structural elements and naming and extracting mathematical and physicochemical properties of multi-shell clusters. Some examples of polytope realization are given at the end of this chapter.

Chapter 4 deals with the complexity and methods of investigation and characterization of multi-shell clusters, such as centrality index counted on layer matrices and the ring signature index, calculated on rings around each vertex/atom of the cluster. Theory about these descriptors is given as well as case studies providing data on topology, defined on connectivity rather than geometry.

From Chaps. 5–9, the topological study is directed to multi-shell clusters classified according to the point group symmetry of the parent Platonic clusters, used as seeds in the design of more complex clusters with the aid of map operations.

Chapter 10 speaks about chiral multi-tori, spongy structures, the complexity of which is given by the high genus surface in which they are embedded.

Chapter 11 opens a gate to the spongy hypercubes, developed on the Platonic solids. The designed structures were characterized by topological (figure) counting and by Omega and Cluj counting polynomials.

Finally, Chap. 12 provides a bound to the real world by energy computation, in an attempt to find multi-shell cluster (or corresponding networks) candidates to the status of real chemical/mineral clusters.

Chapters 2, 5–10, and 12 have Atlas sections that detail the discussed structures; the number of these figures is listed in separate files, in each chapter, while the figure number is associated with the name of clusters within all the text, tables, and figures included, for an easier identification.

The book includes personal research results of the author, in connection with his activity within the Topo Group Cluj, Romania. It is addressed to students and researchers in the interdisciplinary field of Chemistry, Physics, and Mathematics as well as to architects and visual artists. Hin-files of the structures illustrated in this book are deposited online, at www.esmc.ro, available on request.

I was aided in this effort by my younger colleagues, Dr. Csaba L. Nagy and Dr. Atena Pirvan-Moldovan, Faculty of Chemistry and Chemical Engineering, “Babes-Bolyai” University, Cluj, Romania, with quantum chemical and symmetry calculation, figure design, and error checking, while writing the book, which I highly appreciate. Many thanks are addressed to Dr. Attila Bende (Molecular and Biomolecular Physics Department, National Institute for R&D of Isotopic and Molecular Technologies, Cluj, Romania), Dr. Beata Szeffler (Department of Physical Chemistry, Faculty of Pharmacy, Collegium Medicum, Nicolaus Copernicus University, Bydgoszcz, Poland), Dr. Zahra Khalaj (Department of Physics,

Shahr-e-Qods Branch, Islamic Azad University, Tehran, Iran), and Dr. Igor Baburin (Technische Universität Dresden, Theoretische Chemie, Germany) for a fruitful collaboration.

Cluj-Napoca, Romania
January 22, 2017

Mircea Vasile Diudea

Acknowledgements

The author deeply acknowledges Franco Catadlo and Paolo Milani, the Editors of Series “Carbon materials: Chemistry and Physics” who first accredited the idea of a book on multi-shell clusters; many thanks are addressed to Steffen Pauly, Arda Alkan, and Magesh Kaarthick Sundaramoorthy from the Springer Team for their technical assistance.

Contents

1	Basic Chemical Graph Theory	1
1.1	Basic Definitions in Graphs	1
1.2	Topological Matrices and Indices	5
1.2.1	Adjacency Matrix	5
1.2.2	Distance Matrix	6
1.2.3	Detour Matrix	7
1.2.4	Combinatorial Matrices	8
1.2.5	Wiener Matrices	8
1.2.6	Cluj Matrices	9
1.2.7	Distance-Extended Matrices	11
1.2.8	Walk Matrices	12
1.2.9	Reciprocal Matrices	14
1.2.10	Layer and Shell Matrices	14
1.3	Topological Symmetry	18
	References	19
2	Operations on Maps	23
2.1	Dual d	23
2.2	Medial m	25
2.3	Truncation t	26
2.4	Polygonal Mapping p_n	26
2.5	Snub s	27
2.6	Leapfrog l	27
2.7	Quadrupling q	28
2.8	Septupling s_n	29
	References	34
3	Definitions in Polytopes	37
3.1	Polyhedra	37
3.2	n -Dimensional Structures	40
3.3	Abstract Structures	43

3.3.1	Posets	44
3.3.2	Vertex Figure	45
3.3.3	Abstract Polytope	46
3.4	Polytope Realization	47
3.4.1	P-Centered Clusters	47
3.4.2	Cell-in-Cell Clusters	49
3.4.3	24-Cell and Its Derivatives	51
	References	53
4	Symmetry and Complexity	55
4.1	Euler Characteristic	56
4.2	Topological Symmetry	57
4.3	Centrality Index	58
4.4	Ring Signature Index	59
4.4.1	Ring Signature in a Translational Network	61
4.4.2	Ring Signature in Spongy Structures of Higher Rank	63
4.4.3	Ring Signature in Spongy Hypercubes	66
4.4.4	Truncation Operation	66
4.5	Pairs of Map Operation	69
	References	74
5	Small Icosahedral Clusters	77
5.1	Small Cages: Source of Complex Clusters	77
5.2	Truncated MP Icosahedral Clusters	78
5.3	Clusters by Medial Operation	79
5.4	Clusters of Higher Rank	80
	References	124
6	Large Icosahedral Clusters	125
6.1	Small Complex Clusters	125
6.2	Icosahedral Clusters Derived from the C_{45} Seed	127
6.3	Clusters of Dodecahedral Topology	132
6.4	Clusters of Icosahedral Topology	133
6.5	Rhomb Decorated Clusters	135
	References	185
7	Clusters of Octahedral Symmetry	187
7.1	Small Clusters as Seeds for Complex Structures	187
7.2	Clusters Decorated by Octahedra	188
7.3	Clusters Decorated by Dodecahedra	189
7.4	Rhomb Decorated Octahedral Clusters	190
7.5	Cubic Net Transforming	193
	References	245
8	Tetrahedral Clusters	247
8.1	Small Tetrahedral Clusters	247
8.2	Tetrahedral Clusters of Higher Rank	248
8.3	Tetrahedral Clusters Derived From Ada20	248

8.4	Tetrahedral Hyper-structures Decorated with Only Dodecahedra	251
	References	279
9	C₆₀ Related Clusters	281
9.1	Structures Derived from the Cluster P ³² @dC ₆₀ .33	281
9.2	Stellated Clusters	282
9.3	C ₇₅₀ Related Structures	284
9.3.1	Duals of C ₇₅₀ and Related Structures	287
9.3.2	Medials of C ₇₅₀ and Related Clusters	287
9.3.3	Truncated C ₇₅₀ and Related Clusters	290
	References	334
10	Chiral Multi-tori	335
10.1	Design of Chiral Multi-tori	335
10.2	Dodecahedron Related Structures	338
10.3	Cube Related Structures	340
10.4	Tetrahedron Related Structures	341
10.5	C ₆₀ Related Structures	342
	References	361
11	Spongy Hypercubes	363
11.1	Simple Toroidal Hypercubes	363
11.2	Complex Toroidal Hypercubes	365
11.3	Tubular Hypercubes	366
11.4	Spongy Hypercubes	367
11.5	Truncation of Hypercube	370
11.6	Counting Polynomials in Hypercubes	372
11.6.1	Omega Polynomial	372
11.6.2	Cluj Polynomials	377
	References	383
12	Energetics of Multi-shell Clusters	385
12.1	Introduction	385
12.2	C ₂₀ Aggregation	386
12.3	Hyper-graphenes by D ₅ Substructures	389
12.4	Hyper-graphenes by C ₆₀ Units	389
12.5	C ₆₀ Aggregates with Tetrahedral and Icosahedral Symmetry	393
12.6	C ₆₀ Network by [2+2] Cycloaddition	396
12.7	Computational Methods	400
	References	436
	Index	439

List of Abbreviations

<i>d</i>	Dual
<i>l</i>	Leapfrog
<i>m</i>	Medial
<i>t</i>	Truncated
CO	Cuboctahedron
DCO	Dual cuboctahedron
ID	Icosidodecahedron
hP	Half polyhedron
MC	Medial cube
LDCO	Leapfrog (of dual) of cuboctahedron
MDCO	Medial (of dual) of cuboctahedron
MMC	Medial (of medial) of cube
RCO	Rhombicuboctahedron
RID	Rhombicosidodecahedron
SC	Snub cube
SD	Snub dodecahedron
TC	Truncate cube
TCO	Truncate cuboctahedron
TID	Truncate icosidodecahedron
TMC	Truncate (of medial) of cube
TO	Truncate octahedron
TT	Truncate tetrahedron
XAYb	Figure at the bottom of the main figure XAY

Chapter 1

Basic Chemical Graph Theory

Graph Theory applied in Chemistry is called Chemical Graph Theory. This interdisciplinary science takes problems (like isomer enumeration, structure elucidation, etc.) from Chemistry and solve them by Mathematics (using tools from Graph Theory, Set Theory or Combinatorics), thus influencing both Chemistry and Mathematics. Partitioning of a molecular property and reconstructing it from fragmental contributions is one of the main tasks of this theory. For further discussion, some basic definitions in Graph Theory are needed.

1.1 Basic Definitions in Graphs

A *graph* $G(V, E)$ is a pair of two sets, V and E , $V = V(G)$ being a finite nonempty set and $E = E(G)$ a binary relation defined on V (Harary 1969). A graph can be visualized by representing the elements of V by points/vertices and joining pairs of vertices (i, j) by an edge/bond if and only if $(i, j) \in E(G)$. The number of vertices in G equals the cardinality $n = |V(G)|$ of this set. The term *graph* was introduced by Sylvester (1874). There is a variety of graphs, some of them being mentioned below.

A *path graph* is a non-branched chain. A *tree* is a branched structure. A *star* is a set of vertices joined in a common vertex. A *cycle* is a chain which starts and ends in one and the same vertex (Fig. 1.1).

A *complete graph* K_n is the graph of with any two vertices are adjacent. The number of edges in such a graph is $n(n-1)/2$. Fig. 1.2 illustrates the complete graphs with $n = 1-5$.

In a *bipartite graph*, the vertex set V can be partitioned in two disjoint subsets: $V_1 \cup V_2 = V(G)$; $V_1 \cap V_2 = \emptyset$ such that any edge $(i, j) \in E(G)$ joins V_1 with V_2 (Harary 1969; Trinajstić 1983; Diudea 2010). A graph is bipartite if and only if all its cycles are even (Ionescu 1973). If any vertex $i \in V_1$ is adjacent to any vertex $j \in V_2$ then G is a *complete bipartite graph*, $K_{m,n}$, with $m = |V_1|$ and $n = |V_2|$ and the

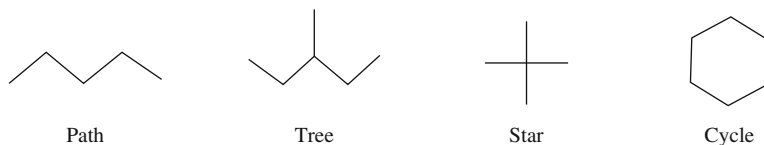


Fig. 1.1 A variety of graphs

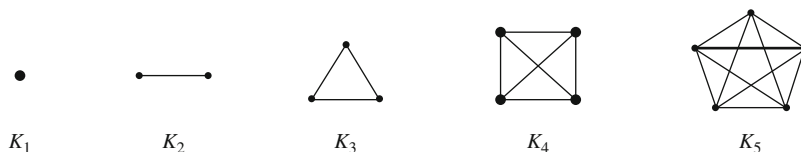


Fig. 1.2 Complete graphs K_n ; $n = 1-5$

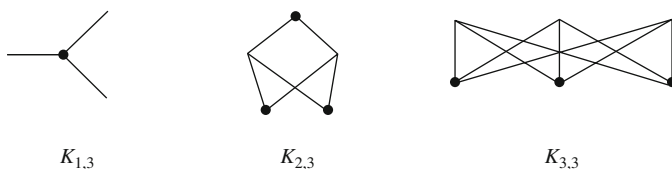


Fig. 1.3 Complete bipartite graphs

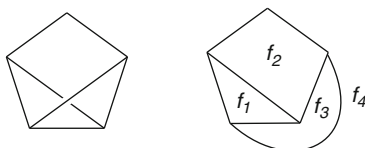


Fig. 1.4 A planar graph and its faces

number of edges being $m \times n$. A *star* is a complete bipartite graph $K_{1,n}$. Fig. 1.3 illustrates some complete bipartite graphs.

A *planar graph* is a graph that can be drawn in the plane with no edge intersections (Harary 1969). The regions defined by a plane graph are called *faces* f , the infinite region being the *exterior face* (see the face f_4 in Fig. 1.4). For any spherical polyhedron with $v = |V|$ vertices, $e = |E|$ edges and $f = |F|$ faces, the Euler (1752–1753) formula is true: $v - e + f = 2$. A graph is planar if and only if it has no subgraphs homeomorphic to K_5 or $K_{3,3}$ (Kuratowski 1930).

A *subgraph* of a graph G is a graph $G_1 = (V_1, E_1)$ having $V_1 \subset V$ and $E_1 \subset E$ (Fig. 1.5).

A *homeomorph* of a graph G is a graph resulted by inserting vertices of degree 2 (Fig. 1.6).

A graph G is *labeled*, $G(Lb)$, when its points are distinguished (e.g. by their numbers) from those of the corresponding abstract graph. There are $n!$ possibilities of numbering a graph of order n .

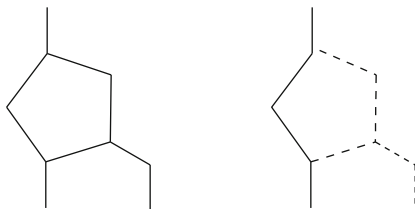


Fig. 1.5 A graph and one of its subgraphs

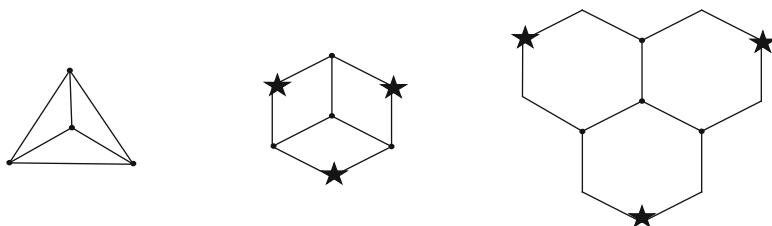


Fig. 1.6 Homeomorphs of the tetrahedron

Two graphs $G = (V, E)$ and $G_1 = (V_1, E_1)$ are *isomorphic* (written $G \cong G_1$) if there exists a function $f: V \rightarrow V_1$ which is a bijection (one-to-one and onto) and for any vertices $i, j \in V(G)$ $(i, j) \in E(G) \leftrightarrow (f(i), f(j)) \in E_1(G_1)$. The function f is called an isomorphism. If f is the permutation operation, then there exists a permutation for which $G(Lb)$ and $G_1(Lb)$ coincide and then f is an *automorphism*.

A *walk* w_n is an alternating sequence of vertices and edges $v_1, e_1, \dots, v_{n-1}, e_{n-1}, v_n$ in which any two subsequent vertices are adjacent: $(v_i, v_{i+1}) \in E(G)$. Revisiting of vertices and edges of G is allowed. Set, in a walk w_n , the vertices $V(w_n)$ and the traversed edges $E(w_n)$; the length of the walk is defined as the cardinality of its edge set: $l(w_n) = |E(w_n)|$. If the walk starts and ends in one and the same vertex (i.e., $v_1 = v_n$) the walk is a closed (or a self-returning) walk, otherwise it is an open walk. If no other conditions are imposed, the walk is called a random walk (Harary 1969; Diudea 2010).

A *path* p_n (or a *self-avoiding walk*) is the walk whose vertices are visited once. Its vertices v_1, v_2, \dots, v_n are all-distinct and no branching is allowed. The length of the path is $l(p_n) = |E(p_n)|$. If the path joining i and j is minimal, it is called a *topological distance* or a *geodesic*; if the path is maximal, it is called a *detour*.

A *circuit/cycle* is a closed path, thus being both self-returning and self-avoiding walk.

A *trail* (i.e., *Eulerian walk*) is a walk with all its edges distinct. Revisiting of vertices is allowed.

A path is *Hamiltonian* if it visits once all the vertices in G . If such a path is a closed one, then it is a *Hamiltonian circuit*. Fig. 1.7 illustrates the above discussed walks.

When $l(p_{ij})$ is expressed in number of edges, the distance is called *topological distance*; when it is measured in *meters* or submultiples (nm, pm) it is a *metric distance*. Vertex *degree* $d(i)$ is the number of edges incident in that vertex. If all the

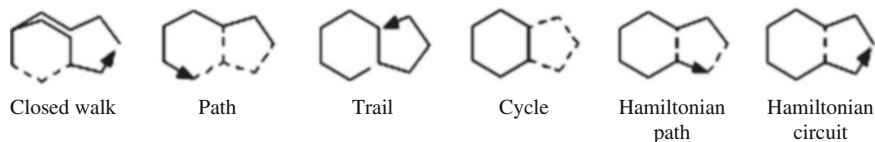


Fig. 1.7 A variety of walks

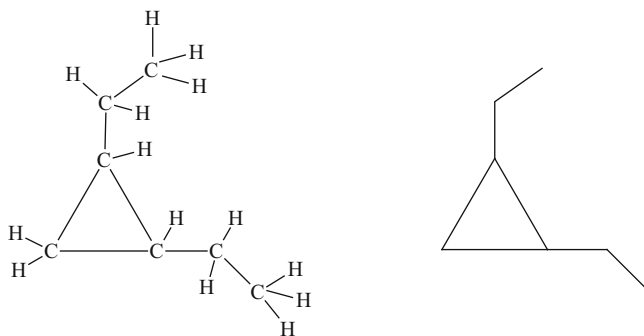


Fig. 1.8 A molecular graph and its hydrogen depleted representation

vertices in G have the same degree, the graph is called a d -regular graph; otherwise it is irregular.

An *invariant* of a graph is a graph theoretical property, which is preserved up to isomorphism; it remains unchanged, irrespective of the numbering or pictorial representation of G .

A *chemical graph* is a model of a chemical system, used to characterize the interactions among its components: atoms, bonds, groups of atoms or molecules. It is also called a *reaction graph* (Diudea et al. 2002, 2006).

A structural formula of a chemical compound can be represented by a *molecular graph*, its vertices being atoms and edges corresponding to covalent bonds. Usually hydrogen atoms are not depicted in which case we speak of *hydrogen depleted molecular graphs* (Fig. 1.8).

A graph is said *connected* if any two vertices i and j are the endpoints of a path; otherwise it is disconnected.

The *distance* d_{ij} between two vertices i and j is the length of a *shortest* path joining them, if any: $d_{ij} = \min l(p_{ij})$; otherwise $d_{ij} = \infty$. A shortest path is often called a *geodesic* (Harary 1969).

The *eccentricity* of a vertex i , ecc_i , is the maximum topological distance between i and any vertex j of G : $ecc_i = \max d_{ij}$. The *radius* of a graph, $r(G)$, is the minimum eccentricity among all vertices i in G : $r(G) = \min ecc_i = \min \max d_{ij}$. Conversely, the *diameter* of a graph, $d(G)$, is the maximum eccentricity in G : $d(G) = \max ecc_i = \max \max d_{ij}$.

The *detour* δ_{ij} between two vertices i and j is the length of a *longest* path joining these vertices, if any: $\delta_{ij} = \max l(p_{ij})$; otherwise $\delta_{ij} = \infty$.

In a connected, non-directed graph, the distance and the detour are *metrics*, that is, for any vertices i, j and k , the following equivalence relations are true

$$\begin{aligned} m(i, j) &\geq 0; \quad m(i, j) = 0 \leftrightarrow i = j \\ m(i, j) &= m(j, i) \\ m(i, j) + m(i, k) &\geq m(j, k) \end{aligned}$$

Within this book, only molecular graphs will be considered.

1.2 Topological Matrices and Indices

A molecular graph can be represented by a sequence of numbers, a polynomial, a single number or a matrix. These representations are aimed to be unique, for a given structure. Topological matrices can be accepted as a rational basis for designing topological indices (Randić 1991).

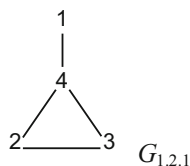
1.2.1 Adjacency Matrix

Since early nineteenth century, a matrix $A(G)$ has been associated to an organic molecule to show its atomic adjacency/connectivity (Sylvester 1874). This is a square table, of dimensions $n \times n$, whose entries are

$$[A(G)]_{ij} = \begin{cases} 1 & \text{if } i \neq j \text{ and } (i, j) \in E(G) \\ 0 & \text{if } i = j \text{ or } (i, j) \notin E(G) \end{cases}$$

$A(G)$ characterizes a graph up to isomorphism. It allows the reconstruction of the graph. $A(G)$ is symmetric vs. its main diagonal, so that the transpose $A^T(G)$ leaves $A(G)$ unchanged: $A^T(G) = A(G)$ (Trinajstić 1983). Figure 1.9 illustrates the adjacency matrix. If instead 1, the bond order is used, the corresponding matrix is called the *connectivity matrix* $C(G)$, with information identical to a connection table. Raising at a power e , of a square matrix, can be eluded by applying the algorithm of Diudea et al. (1994). It evaluates a (topological) property of a vertex I by iterative summation of the first neighbors contributions. The algorithm, called eW_M , is defined as

$$\begin{aligned} M + I &= {}^0W_M \\ [{}^{e+1}W_M]_{ii} &= \sum_j ([M]_{ij} [{}^eW_M]_{ji}) \\ [{}^{e+1}W_M]_{ij} &= [{}^eW_M]_{ij} = [M]_{ij} \end{aligned}$$



	A	1w_i	A ²	2w_i	A ³	3w_i
1	0 0 0 1	1	1 1 1 0	3	0 1 1 3	5
2	0 0 1 1	2	1 2 1 1	5	1 2 3 4	10
3	0 1 0 1	2	1 1 2 1	5	1 3 2 4	10
4	1 1 1 0	3	0 1 1 3	5	3 4 4 2	13

Fig. 1.9 Adjacency matrices A_n ; $n = 1-3$, for the graph $G_{1,2,1}$

where M is any square matrix; the diagonal elements $[{}^eW_M]_{ii}$ equal the row sum RS_i of M^e and are *walk degrees* ${}^e w_{M,i}$ (weighted by the property collected in M —Diudea et al. 2002)

$$[{}^eW_M]_{ii} = \sum_j [M^e]_{ij} = {}^e w_{M,i}$$

The half sum of the local invariants ${}^e w_{M,i}$ in G is a global invariant, called the *walk number* ${}^e W_M$.

$${}^e W_M = {}^e W_M(G) = \frac{1}{2} \sum_i {}^e w_{M,i}$$

When $M = A$, the quantity ${}^e W_M$ (or simply ${}^e W$) represents the so called *molecular walk count*.

The sum of diagonal elements in a square matrix is called the *trace* $Tr(M^e) = \sum_i [M^e]_{ii}$ (Trinajstić 1983). The half sum of diagonal elements provides the global invariant ${}^e SRW_M$ (*Self Returning Walk*) ${}^e SRW_M = (1/2) \sum_i [M^e]_{ii} = MOM(M^e)$ which equals the *moment* of order e of the matrix M , $MOM(M^e)$. When $M = A$, the elements $[A^e]_{ii}$ count both self-returning walks and circuits of length e . (Diudea et al. 2002) $MOM(A^e)$ is related to the spectral properties of molecular graphs (e.g., the energy of molecular orbitals—Graovac and Babić 1990). Figure 1.10 shows the *graphical evaluation* of ${}^e w_i$ and ${}^e W$ numbers.

1.2.2 Distance Matrix

Distance matrix $D(G)$ was introduced by Harary (1969). It is a square symmetric table, of dimensions $n \times n$, whose entries are defined as

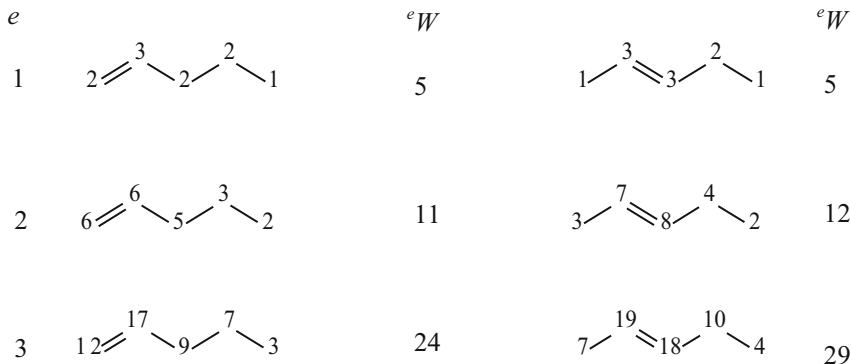


Fig. 1.10 Graphical evaluation of ${}^e w_i$ and ${}^e W$: $e = 1-3$

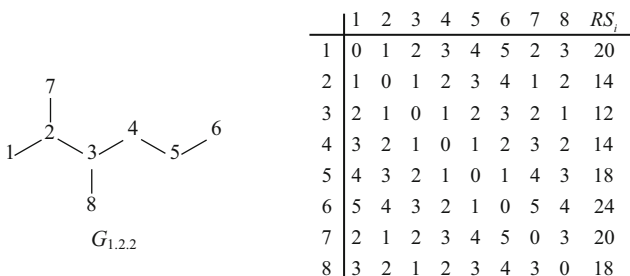


Fig. 1.11 Distance matrix $D(G_{1,2,4})$

$$[D(G)]_{ij} = \begin{cases} \min l(p_{i,j}), & \text{if } i \neq j \\ 0 & \text{if } i = j \end{cases}$$

The non-diagonal entries of this matrix are just the topological distance between i and j . Figure 1.11 illustrates the distance matrix.

The half sum of all entries in $D(G)$ provides the well-known Wiener W topological index

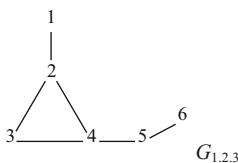
$$W = W(G) = (1/2) \sum_i \sum_j [D]_{ij}$$

When one considers the genuine distances between atoms (i.e., the distances measured through space), the *3D geometric matrix* is obtained (Crippen 1977).

1.2.3 Detour Matrix

In cycle-containing graphs, when the shortest path (i.e., geodesic) is replaced by the longest path between two vertices i and j , the *Detour matrix* $\Delta(G)$ can be

Fig. 1.12 Detour matrix
 $\Delta(G_{1,2,3})$



0	1	2	3	4	5	6	RS_i
1	0	1	3	3	4	5	16
2	1	0	2	2	3	4	12
3	3	2	0	2	3	4	14
4	3	2	2	0	1	2	10
5	4	3	3	1	0	1	12
6	5	4	4	2	1	0	16

constructed (Harary 1969; Diudea et al. 2002; Lukovits 1996; Amić and Trinajstić 1995)

$$[\Delta(G)]_{ij} = \begin{cases} \max l(p_{i,j}), & \text{if } i \neq j \\ 0 & \text{if } i = j \end{cases}$$

Figure 1.12 shows a Detour matrix.

1.2.4 Combinatorial Matrices

Two path-calculated matrices have been proposed (Diudea 1996; Diudea et al. 1998): the *distance-path* D_p (Fig. 1.13) and the *detour-path* Δ_p (Fig. 1.14), whose elements are combinatorially calculated from the classical matrices, distance D (or *distance-edge*) and detour Δ (or *detour-edge*)

$$[D_p]_{ij} = \begin{cases} np(i,j), (i,j) \in D(G), & \text{if } i \neq j \\ 0 & \text{if } i = j \end{cases} \quad (1.1)$$

$$[\Delta_p]_{ij} = \begin{cases} np(i,j), (i,j) \in \Delta(G), & \text{if } i \neq j \\ 0 & \text{if } i = j \end{cases} \quad (1.2)$$

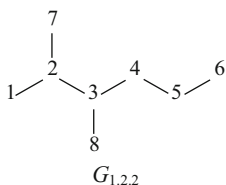
$$np(i,j) = \binom{[M]_{ij} + 1}{2} = (1/2) \left\{ ([M]_{i,j})^2 + [M]_{i,j} \right\}; M = D; \Delta$$

In the above, $np(i,j)$ is the number of *internal paths* (Klein et al. 1995) of length $1 \leq |p| \leq l(i,j)$ included in the path $p(i,j)$.

Half-sum of entries in these matrices provide the Hyper-Wiener and Hyper-Detour indices (Lukovits 1996; Diudea et al. 1998).

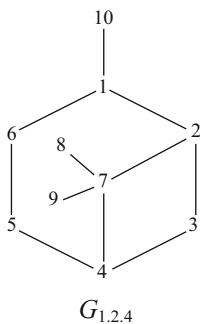
1.2.5 Wiener Matrices

Randić proposed the so-called Wiener matrix, W , and exploited it as a source of structural invariants, useful in *QSPR/QSAR* (Randić et al. 1993, 1994).



	1	2	3	4	5	6	7	8	RS_i
1	0	1	3	6	10	15	3	6	44
2	1	0	1	3	6	10	1	3	25
3	3	1	0	1	3	6	3	1	18
4	6	3	1	0	1	3	6	3	23
5	10	6	3	1	0	1	10	6	37
6	15	10	6	3	1	0	15	10	60
7	3	1	3	6	10	15	0	6	44
8	6	3	1	3	6	10	6	0	35

Fig. 1.13 Distance-path matrix $D_p(G_{1,2,2})$



	1	2	3	4	5	6	7	8	9	10
1	0	15	21	6	10	15	21	28	28	1
2	15	0	15	10	6	10	15	21	21	21
3	21	15	0	15	21	15	21	28	28	28
4	6	10	15	0	15	10	15	21	21	10
5	10	6	21	15	0	15	21	28	28	15
6	15	10	15	10	15	0	15	21	21	21
7	21	15	21	15	21	15	0	1	1	28
8	28	21	28	21	28	21	1	0	3	36
9	28	21	28	21	28	21	1	3	0	36
10	1	21	28	10	15	21	28	36	36	0

Fig. 1.14 Detour-path matrix $\Delta_p(G_{1,2,4})$

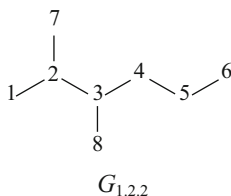
In trees, the non-diagonal entries in such a matrix are defined as:

$$[W_{e/p}]_{i,j} = n_{i,e/p} \times n_{j,e/p}$$

where n_i and n_j denote the number of vertices lying on the two sides of the edge/path, e/p (having i and j as endpoints); when defined on edge, the half-sum of entries give the Wiener index while defined on path, the hyper-Wiener index is calculated. W_e is calculated from W_p by relation $W_e = W_p \bullet A$, where the symbol \bullet indicates the Hadamard (Horn and Johnson 1985) pair-wise matrix product: $[M_a \bullet M_b]_{ij} = [M_a]_{ij} [M_b]_{ij}$. In fact, W_e is an adjacency matrix weighted by the number of external paths which include a given edge e . Fig. 1.15 illustrates this matrix.

1.2.6 Cluj Matrices

Cluj matrices $CJ(G)$ have been proposed by Diudea (Diudea 1997a; Diudea et al. 1997a, b; Janežič et al. 2007); they are defined on Cluj fragments $CJ_{i,j,p}$ which



	1	2	3	4	5	6	7	8	RS _i
1	0	7	5	3	2	1	1	1	20
2	7	0	15	9	6	3	7	3	50
3	5	15	0	15	10	5	5	7	62
4	3	9	15	0	12	6	3	3	51
5	2	6	10	12	0	7	2	2	41
6	1	3	5	6	7	0	1	1	24
7	1	7	5	3	2	1	0	1	20
8	1	3	7	3	2	1	1	0	18

Fig. 1.15 Wiener matrix $W_{el_p}(G_{1,2,2})$: the italicized entries represent W_e matrix

collect vertices v lying closer to i than to j , the endpoints of a path $p(i, j)$. These fragments represent the vertex proximities (see also Gutman 1994) of i vs. any vertex j , joined by the path p , with the distances measured in the subgraph $G \setminus p$:

$$CJ_{i,j,p} = \{v | v \in V(G); D_{(G \setminus p)}(i, v) < D_{(G \setminus p)}(j, v)\}$$

The entries in CJ matrices are taken, by definition, as the maximum cardinality among all such fragments: $[UCJ]_{i,j} = \max_p |CJ_{i,j,p}|$; it is because, in graphs containing rings, more than one path can join the pair (i, j) , thus resulting more than one fragment related to i (with respect to j and path p). Cluj matrices are defined by using either *distance* or *detour* concepts: when path p belongs to the set of distances $DI(G)$, the suffix DI is added to the name of matrix; when path p belongs to the set of detours $DE(G)$, the suffix is DE; when the matrix symbol is not followed by a suffix, it is by default DI.

Cluj matrices are defined in any graph and, except for some symmetric graphs, are unsymmetric: UCJDI, UCJDE. Symmetric Cluj matrix SCJ can be obtained by the Hadamard multiplication of UCJ with its transpose: $SCJ = UCJ \bullet UCJ^T$. The edge-based symmetric matrix is calculable from the path-based one: $SCJ_e = SCJ_p \bullet A$. Fig. 1.16 illustrates the Cluj matrices in a ring-containing graph.

In trees, the path joining any two vertices is unique, then $CJ_{i,j,p}$ represents the set of external paths passing through i to j . Fig. 1.17 illustrates the Cluj matrix in a tree graph. In calculating CJ matrix, the path $p(i, j)$ is characterized by a single endpoint, however, the information is twice: the row-sum is identical to that provided by W_e matrix while the column-sum equals that in the distance D matrix.

Indices derived from topological matrices (see above) are calculated as half sum of matrix entries

$$I(G) = (1/2) \sum_i \sum_j [M]_{ij} = \sum_{i>j} [M]_{ij} = (1/2) uMu^T$$

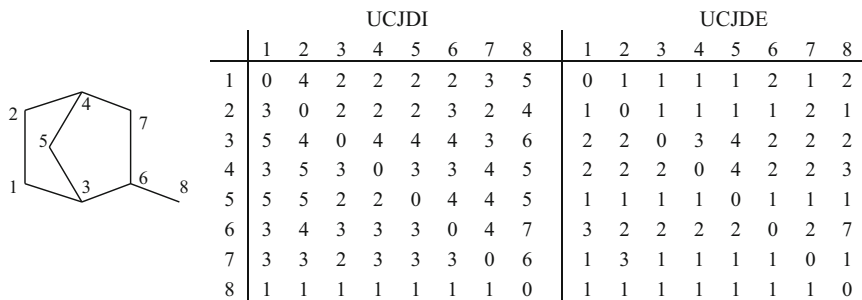


Fig. 1.16 Cluj matrices in a ring-containing graph $G_{1,2,5}$

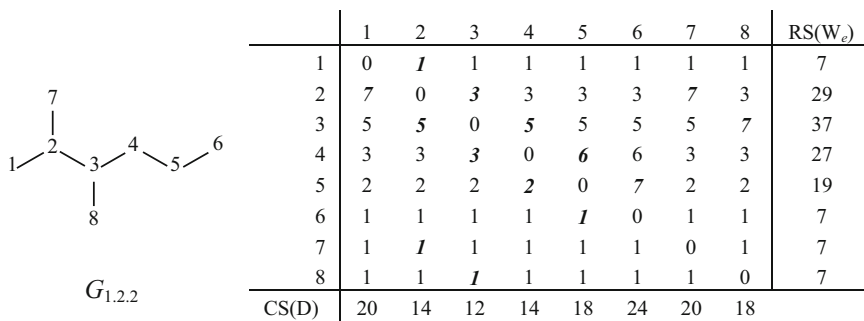
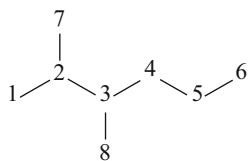


Fig. 1.17 Cluj matrix $UCJ_{e/p}$ ($G_{1,2,4}$); the italicized entries represent UCJ_e matrix

where u and u^T are the unit vector (of order n) and its transpose (Estrada and Rodriguez 1997; Estrada et al. 1997). In trees, the following equalities hold: $SCJ_p = W_p$; $SCJ_e = W_e$. The half-sum in the symmetric Cluj matrices provides the Wiener W and hyper-Wiener WW indices, from SCJ_e and SCJ_p , respectively. Relation with Cluj polynomial $CJS(x)$ (calculated as the first derivative in $x = 1$, see Chap. 11) is as follows: $\sum_i \sum_j [UCJ_e]_{ij} = CJS(1)$

1.2.7 Distance-Extended Matrices

Diudea (1997a, b) has performed the Hadamard product on the unsymmetric Cluj matrix: $[D \bullet UCJ]_{i,j} = [D]_{i,j} \cdot [UCJ]_{i,j}$ to provide a new matrix, that shows in trees, the equalities: $CS(D \bullet UCJ) = CS(D_p)$ and $RS(D \bullet UCJ) = RS(W_p)$. This matrix (illustrated in Fig. 1.18) is a direct proof of the theorem of Klein et al. (1995): in trees, the sum of all internal paths (given by D_p) equals the sum of all external paths (given by W_p) with respect to all pairs (i, j) . Thus, the half-sum of entries in $D \bullet UCJ$ equals the hyper-Wiener WW index (Diudea and Gutman 1998).



	1	2	3	4	5	6	7	8	RS(W_p)
1	0	1	2	3	4	5	2	3	20
2	7	0	3	6	9	12	7	6	50
3	10	5	0	5	10	15	10	7	62
4	9	6	3	0	6	12	9	6	51
5	8	6	4	2	0	7	8	6	41
6	5	4	3	2	1	0	5	4	24
7	2	1	2	3	4	5	0	3	20
8	3	2	1	2	3	4	3	0	18
CS(D_p)	44	25	18	23	37	60	44	35	

Fig. 1.18 Distance-extended Cluj matrix $D \cdot UCJ(G_{1.2.2})$

1.2.8 Walk Matrices

Diudea (1996, 1999) has proposed the *walk matrix*, $W_{(M_1 M_2 M_3)}$, defined by the principle of a *single endpoint characterization of a path*

$$[W_{M_1 M_2 M_3}]_{ij} = [M_2]_{ij} W_{M_1 i} [M_3]_{ij} = \left[RS \left((M_1)^{[M_2]_{ij}} \right) \right]_i [M_3]_{ij}$$

where $W_{M_1 i}$ is the *walk degree* of the vertex i , of extent $[M_2]_{ij}$, weighted by the property collected in M_1 and M_3 (i.e., the i th row-sum of the matrix M_1 , raised to power $[M_2]_{ij}$ and multiplied by the entries of M_3); the diagonal entries are zero. It is a square, (in general) non-symmetric matrix that mixes three square matrices, in fact being a true matrix operator (see below).

Let first $(M_1 M_2 M_3)$ be $(M_1 1 1)$, where 1 is the matrix with “1” off-diagonal elements. The entries of matrix $W_{(M_1 1 1)}$ will be

$$[W_{(M_1 1 1)}]_{ij} = [RS(M_1)]_i = W_{M_1, i}$$

Next, consider the combination $(M_1 1 M_3)$; the corresponding walk matrix can be written as the Hadamard product

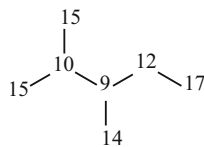
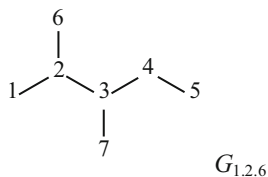
$$W_{(M_1 1 M_3)} = W_{(M_1 1 1)} \cdot M_3$$

Examples in Fig. 1.19 are for the case: $M_1 = A$ and $M_3 = D$.

The sum of all entries in $W_{(M_1 1 M_3)}$ can be calculated by

$$u W_{(M_1 1 M_3)} u^T = \sum_i [RS(W_{(M_1 1 M_3)})]_i = u(M_1 M_3) u^T$$

where u and u^T are the unit vector (of order n) and its transpose. The above equation represents a joint of Cramer and Hadamard matrix algebra, by means of



A(G)									D(G;RS(D _i))								
	1	2	3	4	5	6	7	RS _i		1	2	3	4	5	6	7	RS _i
1	0	1	0	0	0	0	0	1	1	0	1	2	3	4	2	3	15
2	1	0	1	0	0	1	0	3	2	1	0	1	2	3	1	2	10
3	0	1	0	1	0	0	1	3	3	2	1	0	1	2	2	1	9
4	0	0	1	0	1	0	0	2	4	3	2	1	0	1	3	2	12
5	0	0	0	1	0	0	0	1	5	4	3	2	1	0	4	3	17
6	0	1	0	0	0	0	0	1	6	2	1	2	3	4	0	3	15
7	0	0	1	0	0	0	0	1	7	3	2	1	2	3	3	0	14

W _(A11) (G)									W _(D11) (G)								
	1	2	3	4	5	6	7	RS _i		1	2	3	4	5	6	7	RS _i
1	0	1	1	1	1	1	1	6	1	0	15	15	15	15	15	15	90
2	3	0	3	3	3	3	3	18	2	10	0	10	10	10	10	10	60
3	3	3	0	3	3	3	3	18	3	9	9	0	9	9	9	9	54
4	2	2	2	0	2	2	2	12	4	12	12	12	0	12	12	12	72
5	1	1	1	1	0	1	1	6	5	17	17	17	17	0	17	17	102
6	1	1	1	1	1	0	1	6	6	15	15	15	15	15	0	15	90
7	1	1	1	1	1	1	0	6	7	14	14	14	14	14	14	0	84

(A1D) = W _(A11) • D									W _(D1A) = W _(D11) • A								
	1	2	3	4	5	6	7	d _i SD _i		1	2	3	4	5	6	7	d _i SD _i
1	0	1	2	3	4	2	3	15	1	0	15	0	0	0	0	0	15
2	3	0	3	6	9	3	6	30	2	10	0	10	0	0	10	0	30
3	6	3	0	3	6	6	3	27	3	0	9	0	9	0	0	9	27
4	6	4	2	0	2	6	4	24	4	0	0	12	0	12	0	0	24
5	4	3	2	1	0	4	3	17	5	0	0	0	17	0	0	0	17
6	2	1	2	3	4	0	3	15	6	0	15	0	0	0	0	0	15
7	3	2	1	2	3	3	0	14	7	0	0	14	0	0	0	0	14
AD _j	24	14	12	18	28	24	22	142	AD _i	10	39	36	26	12	10	9	142

Fig. 1.19 $W_{(M_1M_2M_3)}$ algebra; d_iSD_i are local contributions to the *degree-distance* index (Dobrynin and Kochetova 1994)

$W_{(M_1M_3)}$. The row-sum vector in $W_{(M_1M_3)}$ can be achieved by the pair-wise product of the row-sums in M_1 and M_3 , respectively

$$[RS(W_{(M_1M_3)})]_i = [RS(M_1)]_i \cdot [RS(M_3)]_i$$

This vector represents a collection of pair-wise products of local (topological) properties (encoded as row-sums in M_1 and M_3). When $M_1 = M_3 = M$, then the sum of entries can be written as

$$uW_{(M_nM)}u^T = u((M)^nM)u^T = u(M^{n+1})u^T$$

thus proving that $W_{(M_1M_2M_3)}$ is a true matrix operator.

A particular case of the walk matrix, $RW_{(AD_1)}$ (i.e., the reciprocal of $W_{(AD_1)}$) is identical to the *restricted random walk* matrix proposed by Randić (1995), (see also Diudea and Randić 1997).

1.2.9 Reciprocal Matrices

In Chemical Graph Theory, the distance matrix accounts for *through bond* interactions of atoms in molecules. However, these interactions decrease as the distance between atoms increases. This reason led to the introduction, by the QSAR Group of Timisoara (Ciubotariu 1987; Ciubotariu et al. 2004) and next by the groups of Balaban (Ivanciuc et al. 1993) and Trinajstić (Plavšić et al. 1993), of the *reciprocal distance* matrix, RD. The entries in this matrix are defined by

$$[RD]_{ij} = 1/[D]_{ij}$$

RD matrix allows the calculation of a Wiener analogue number, called the *Harary index* (Plavšić et al. 1993), in the honor of Frank Harary. Several matrices having entries as *reciprocal* (topological) *property*: $[RM]_{i,j} = 1/[M]_{i,j}$; $M = W_{elp}$, D_p , and UCJ have been proposed by Diudea (1997c).

1.2.10 Layer and Shell Matrices

1.2.10.1 Layer Matrices

Layer matrices (Skorobogatov and Dobrynin 1988) have been proposed in connection with sequences of walks (Halberstam and Quintas 1982; Bonchev et al. 1989; Dobrynin 1993); they are built up on the layer partitions in a graph.

Let $G(v)_k$ be the k th layer of vertices v lying at distance k , in the partition $G(i)$

$$G(v)_k = \{v | d_{i,v} = k\}$$

$$G(i) = \{G(v)_k; k \in [0, 1, \dots, ecc_i]\}$$

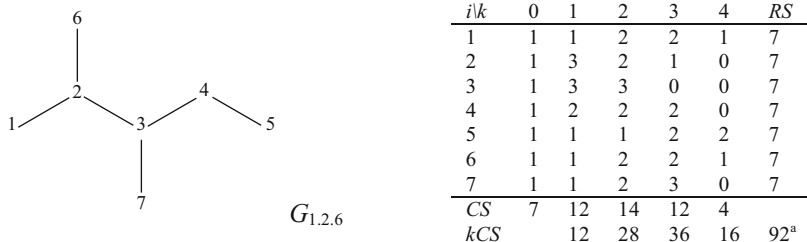


Fig. 1.20 Layer matrix of counting $LC(G_{1,2,6})$; ${}^a 2 \times$ Wiener index

with ecc_i being the *eccentricity* of i . The entries in the layer matrix (of vertex property) LM (Diudea 1994, 2010; Diudea et al. 1994; Diudea and Ursu 2003) are defined as

$$[LM]_{i,k} = \sum_{v|d_{i,v}=k} p_v$$

Layer matrix is a collection of the above defined entries:

$$LM(G) = \left\{ [LM]_{i,k}; i \in V(G); k \in [0, 1, \dots, d(G)] \right\}$$

with $d(G)$ being the diameter of the graph (i.e., the largest distance in G). The zero column is just the column of vertex properties, $[LM]_{i,0} = p_i$. When $p_i = 1$ (i.e., the counting property), LM matrix is named LC (i.e., Layer matrix of Counting—Fig. 1.20). Any atomic/vertex property can be considered as p_i . Moreover, any square matrix M can be taken as *info matrix*, i.e., the matrix supplying local/vertex properties, as row-sum RS , column-sum CS or diagonal entries, as implemented in TopoCluj software (Ursu and Diudea 2005).

1.2.10.2 Shell Matrices

Entries in the shell matrix ShM (of vertex pair property, Diudea and Ursu 2003) are defined as

$$[ShM]_{i,k} = \sum_{v|d_{i,v}=k} [M]_{i,v}$$

The shell matrix is a collection of the above defined entries:

$$ShM(G) = \left\{ [ShM]_{i,k}; i \in V(G); k \in [0, 1, \dots, d(G)] \right\}$$

A shell matrix, $\text{ShM}(G)$, will partition the entries of a square matrix according to the vertex-distance partitions in the graph. The zero column entries $[\text{ShM}]_{i,0}$ can be the diagonal entries of the info matrix. Tables 1.1, 1.2 and 1.3 exemplify the Shell matrix of Cluj matrices for $G_{1.2.6}$

Let now consider the behavior of the edge-calculated matrices: adjacency A , W_e and UCJ_e matrices. These are sparse matrices, with non-zero entries only at $k = 1$, the other columns in the shell matrix being null (see Table 1.4). In case of UCJ_e matrix, the column-sum equals the first derivative (in $x = 1$) of Cluj polynomial $CJ\text{-Sum}(x)$ (see Sect. 11.6.2).

Table 1.1 Shell matrix of UCJ

		ShUCJ($G_{1.2.6}$)								UCJ($G_{1.2.6}$)						
$i \setminus k$	0	1	2	3	4	RS		1	2	3	4	5	6	7	RS	
1	0	1	2	2	1	6		0	1	1	1	1	1	1	6	
2	0	15	6	3	0	24		6	0	3	3	3	6	3	24	
3	0	15	13	0	0	28		4	4	0	5	5	4	6	28	
4	0	8	4	4	0	16		2	2	2	0	6	2	2	16	
5	0	1	1	2	2	6		1	1	1	1	0	1	1	6	
6	0	1	2	2	1	6		1	1	1	1	1	0	1	6	
7	0	1	2	3	0	6		1	1	1	1	1	1	0	6	
CS	0	42	30	16	4	92 ^a	CS	15	10	9	12	17	15	14	92	
CS·k		42	60	48	16	166 ^b										

^a2 × Wiener index W

^b2 × hyper-Wiener index WW (Wiener 1947; Randić 1993)

Shell matrix of UCJ (the bold values indicate entries in UCJ_e matrix)

Table 1.2 Shell matrix of UCJ^T

		ShUCJ ^T ($G_{1.2.6}$)								UCJ ^T ($G_{1.2.6}$)						
$i \setminus k$	0	1	2	3	4	RS		1	2	3	4	5	6	7	RS	
1	0	6	5	3	1	15		0	6	4	2	1	1	1	15	
2	0	6	3	1	0	10		1	0	4	2	1	1	1	10	
3	0	6	3	0	0	9		1	3	0	2	1	1	1	9	
4	0	6	4	2	0	12		1	3	5	0	1	1	1	12	
5	0	6	5	4	2	17		1	3	5	6	0	1	1	17	
6	0	6	5	3	1	15		1	6	4	2	1	0	1	15	
7	0	6	5	3	0	14		1	3	6	2	1	1	0	14	
CS	0	42	30	16	4	92 ^a	CS	6	24	28	16	6	6	6	92 ^a	
CS·k		42	60	48	16	166 ^b										

^a2 × Wiener index W

^b2 × hyper-Wiener index WW

Table 1.3 Shell matrix of the symmetric Cluj matrix SCJ

	ShSCJ($G_{1.2.6}$)							SCJ($G_{1.2.6}$)							
$i \setminus k$	0	1	2	3	4	RS		1	2	3	4	5	6	7	RS
1	0	6	5	3	1	15		0	6	4	2	1	1	1	15
2	0	24	9	3	0	36		6	0	12	6	3	6	3	36
3	0	28	13	0	0	41		4	12	0	10	5	4	6	41
4	0	16	8	4	0	28		2	6	10	0	6	2	2	28
5	0	6	5	4	2	17		1	3	5	6	0	1	1	17
6	0	6	5	3	1	15		1	6	4	2	1	0	1	15
7	0	6	5	3	0	14		1	3	6	2	1	1	0	14
CS	0	92	50	20	4	166 ^a	CS	15	36	41	28	17	15	14	166
CS-k		92	100	60	16	268 ^b									

^a2 × hyper Wiener index

^b2 × Tratch index (Tratch et al. 1990)

Table 1.4 Shell matrices of edge-defined info matrices

	ShA($G_{1.2.6}$)						ShW _e ($G_{1.2.6}$)						ShUCJ _e ($G_{1.2.6}$)						
$i \setminus k$	0	1	2	3	4	RS	0	1	2	3	4	RS	0	1	2	3	4	RS	
1	0	1	0	0	0	1	0	6	0	0	0	6	0	1	0	0	0	0	1
2	0	3	0	0	0	3	0	24	0	0	0	24	0	15	0	0	0	0	15
3	0	3	0	0	0	3	0	28	0	0	0	28	0	15	0	0	0	0	15
4	0	2	0	0	0	2	0	16	0	0	0	16	0	8	0	0	0	0	8
5	0	1	0	0	0	1	0	6	0	0	0	6	0	1	0	0	0	0	1
6	0	1	0	0	0	1	0	6	0	0	0	6	0	1	0	0	0	0	1
7	0	1	0	0	0	1	0	6	0	0	0	6	0	1	0	0	0	0	1
CS	0	12				12 ^a	0	92				92 ^b	0	42					42 ^c

^a2 × e

^b2 × W

^cCJS(x = 1) = v × e

1.2.10.3 Centrality Index

On the above layer/shell matrices, a *centrality index* (Diudea and Ursu 2003; Ursu and Diudea 2005) is calculated as

$$C(\text{LM} \setminus \text{ShM})_i = \left[\sum_{k=1}^{ecc_i} \left([\text{LM} \setminus \text{ShM}]_{ik}^{2k} \right)^{1/(ecc_i)^2} \right]^{-1}$$

$$C(\text{LM} \setminus \text{ShM}) = \sum_i C(\text{LM} \setminus \text{ShM})_i$$

This index allows the finding of the graph center (e.g. the vertex having the largest C_i value) and provides an ordering of graph vertices according to their centrality.

1.3 Topological Symmetry

Molecular geometry and their crystals is completely described by the 230 symmetry groups of the space (Hargittai and Hargittai 2010; Petitjean 2007). Symmetry of molecules is reflected in several properties, such as dipole moments, IR vibrations, ^{13}C -NMR signals etc., that are dependent on the spatial structure of molecules. Molecular topology reveals a different type of symmetry: the *topological symmetry* (i.e., constitutional symmetry). It is defined in terms of *connectivity*, as a constitutive principle of molecules and expresses equivalence relationships among elements of graph: vertices, bonds, faces or larger subgraphs. It makes use of Group Theory formalism while the geometrical aspects are disregarded.

Let $G_1 = (V_1, E_1)$ and $G_2 = (V_2, E_2)$ be two graphs and a function f , mapping the vertices of V_1 onto the vertices belonging to the set V_2 , $f: V_1 \rightarrow V_2$. That is, the function f makes a one-to-one correspondence between the vertices of the two sets. The two graphs are called *isomorphic*, $G_1 \approx G_2$, if there exists a mapping f that preserves adjacency (i.e., if $(i, j) \in E_1$, then $(f(i), f(j)) \in E_2$).

Using notions of the Group action (Hungerford 1974; Mirman 1999), in which every element of the group acts like as a one-to-one mapping, the group G is said to act on a set X if there is a function ϕ such that $\phi: G \times X \rightarrow X$ and for any element $x \in X$, there exists the relation $\phi(g, \phi(h, x)) = \phi(gh, x)$, for all $g, h \in G$, with $\phi(e, x) = x$, e being the identity element of G . The mapping ϕ is called a group action while the set $\{\phi(gx) | g \in G\}$ is called the *orbit* of x . For a permutation σ on n objects, the permutation matrix is an $n \times n$ matrix P_σ , with elements $x_{ij} = 1$ if $i = \sigma(j)$ and 0 otherwise. For any permutation σ and τ on n objects, $P_\sigma P_\tau = P_{\sigma\tau}$, while the set of all permutation matrices is a group isomorphic to the symmetry group S_n on n symbols. A permutation σ of the vertices of a graph $H(V, E)$ (V being the set of vertices and E the set of edges in H) belongs to an automorphism group G if one satisfies the relation $P_\sigma^T A P_\sigma = A$, where A is the adjacency matrix of the graph H . Given $\text{Aut}(H) = \{\sigma_1, \dots, \sigma_m\}$, the matrix $S_G = [s_{ij}]$, where $s_{ij} = \sigma_i(j)$, is called a solution matrix for H and its calculation will provide the automorphism group of H .

Given a graph $H(V, E)$ and the automorphism group $\text{Aut}(H)$, two vertices, $i, j \in V$ are called *equivalent* if $\{\phi(ij) | i, j \in \text{Aut}(H)\}$, in other words, they belong to the same orbit of automorphisms. Suppose v_1, v_2, \dots, v_m are m disjoint *automorphic partitions* of the set of vertices $V(H)$, then: $V = V_{v_1} \cup V_{v_2} \cup \dots \cup V_{v_m}$ and $V_{v_i} \cap V_{v_j} = \emptyset$. All the automorphisms of a graph form a group (Gutman and Polanski 1986; Razinger et al. 1993; Balasubramanian 1994, 1995a, b, c).

Let now consider a vertex invariant (i.e., a topological index), $In = In_1, In_2, \dots, In_m$, which assigns a value In_i to the vertex i . Two vertices i and j of a molecular graph (with vertices meaning the atoms and edges the bonds in the molecule) belong to the same *invariant class* if $In_i = In_j$. The partitioning in *classes* of vertices/atoms leads to m classes, with v_1, v_2, \dots, v_m atoms in each class; such a partitioning may differ from the *orbits of automorphism* i.e. *classes of equivalence*, since no vertex invariant is known so far to always discriminate two non-equivalent vertices in any graph. The classes of vertices are eventually *ordered* according to

some rules. Note that topological symmetry equals the maximum geometrical symmetry a molecular graph can have. Also note that topological symmetry, arising from graph automorphisms, can be defined the same way as the Euclidean symmetry (Petitjean 2007).

In Chemistry, such a study could answer to the question if two molecular graphs represent or not one and the same chemical compound.

Within this book, topological symmetry/equivalence classes will be evaluated by means of Centrality index (see Sect. 1.2.10.3) and checked by adjacency matrix permutations.

References

- Amić D, Trinajstić N (1995) On the detour matrix. *Croat Chem Acta* 68:53–62
- Balasubramanian K (1994) Computer generation of automorphism graphs of weighted graphs. *J Chem Inf Comput Sci* 34:1146–1150
- Balasubramanian K (1995a) Computer generation of nuclear equivalence classes based on the three-dimensional molecular structure. *J Chem Inf Comput Sci* 35:243–250
- Balasubramanian K (1995b) Computational strategies for the generation of equivalence classes of Hadamard matrices. *J Chem Inf Comput Sci* 35:581–589
- Balasubramanian K (1995c) Computer perception of molecular symmetry. *J Chem Inf Comput Sci* 35:761–770
- Bonchev D, Mekenyan O, Balaban AT (1989) Iterative procedure for the generalized graph center in polycyclic graphs. *J Chem Inf Comput Sci* 29:91–97
- Ciubotariu D (1987) Structură-reactivitate în clasa derivaților acidului carbonic. PhD Thesis, Timisoara, Romania
- Ciubotariu D, Medeleanu M, Vlaia V, Olariu T, Ciubotariu C, Dragos D, Seiman C (2004) Molecular van der Waals space and topological indices from the distance matrix. *Molecules* 9:1053–1078
- Crippen GM (1977) A novel approach to calculation of conformation: distance geometry. *J Comput Phys* 24:96–107
- Diudea MV (1994) Layer matrices in molecular graphs. *J Chem Inf Comput Sci* 34:1064–1071
- Diudea MV (1996) Walk numbers $^{\circ}W_M$: Wiener-type numbers of higher rank. *J Chem Inf Comput Sci* 36:535–540
- Diudea MV (1997a) Cluj matrix invariants. *J Chem Inf Comput Sci* 37:300–305
- Diudea MV (1997b) Cluj matrix, CJ_n : source of various graph descriptors. *MATCH Commun Math Comput Chem* 35:169–183
- Diudea MV (1997c) Indices of reciprocal property or Harary indices. *J Chem Inf Comput Sci* 37:292–299
- Diudea MV (1999) Valencies of property. *Croat Chem Acta* 72:835–851
- Diudea MV (2010) Nanomolecules and nanostructures—polynomials and indices, MCM, No. 10. University Kragujevac, Serbia
- Diudea MV, Gutman I (1998) Wiener-type topological indices. *Croat Chem Acta* 71:21–51
- Diudea MV, Randić M (1997) Matrix operator, $W_{(M1, M2, M3)}$ and Schultz-type numbers. *J Chem Inf Comput Sci* 37:1095–1100
- Diudea MV, Ursu O (2003) Layer matrices and distance property descriptors. *Indian J Chem* 42A:1283–1294
- Diudea MV, Topan MI, Graovac A (1994) Layer matrices of walk degrees. *J Chem Inf Comput Sci* 34:1071–1078

- Diudea MV, Parv B, Gutman I (1997a) Detour-Cluj matrix and derived invariants. *J Chem Inf Comput Sci* 37:1101–1108
- Diudea M, Parv B, Topan MI (1997b) Derived Szeged and Cluj indices. *J Serb Chem Soc* 62:267–276
- Diudea MV, Katona G, Lukovits I, Trinajstić N (1998) Detour and Cluj-detour indices. *Croat Chem Acta* 71:459–471
- Diudea MV, Gutman I, Jäntschi L (2002) *Molecular topology*. NOVA, New York
- Diudea MV, Florescu MS, Khadikar PV (2006) *Molecular topology and its applications*. EFICON, Bucharest
- Dobrynin AA (1993) Degeneracy of some matrix invariant and derived topological indices. *J Math Chem* 14:175–184
- Dobrynin AA, Kochetova AA (1994) Degree distance of a graph: a degree analogue of the Wiener index. *J Chem Inf Comput Sci* 34:1082–1086
- Estrada E, Rodriguez L (1997) Matrix algebraic manipulation of molecular graphs, Harary- and MTI-like molecular descriptors. *MATCH Commun Math Comput Chem* 35:157–167
- Estrada E, Rodriguez L, Gutierrez A (1997) Matrix algebraic manipulation of molecular graphs, distance and vertex-adjacency matrices. *MATCH Commun Math Chem* 35:145–156
- Euler L (1752–1753) *Elementa doctrinae solidorum*. *Novi Comm Acad Scient Imp Petrop* 4:109–160
- Graovac A, Babić D (1990) The evaluation of quantum chemical indices by the method of moments. *Int J Quantum Chem Quantum Chem Symp* 24:251–262
- Gutman I (1994) A formula for the Wiener number of trees and its extension to graphs containing cycles. *Graph Theory Notes NY* 27:9–15
- Gutman I, Polansky OE (1986) *Mathematical concepts in organic chemistry*. Springer, Berlin, pp 108–116
- Halberstam FY, Quintas LV (1982) Distance and path degree sequences for cubic graphs. Pace University, New York. A note on table of distance and path degree sequences for cubic graphs, Pace University, New York
- Harary F (1969) *Graph theory*. Addison-Wesley, Reading
- Hargittai M, Hargittai I (2010) *Symmetry through the eyes of a chemist*. Springer, Dordrecht
- Horn RA, Johnson CR (1985) *Matrix analysis*. Cambridge University Press, Cambridge
- Hungerford TW (1974) *Algebra*. Graduate texts in mathematics, vol 73. Springer, New York (Reprint of the original 1980)
- Ionescu T (1973) *Graphs-applications (in Romanian)*, Ed. Ped., Bucharest
- Ivanciuc O, Balaban TS, Balaban AT (1993) Reciprocal distance matrix, related local vertex invariants and topological indices. *J Math Chem* 12:309–318
- Janežič D, Miličević A, Nikolić S, Trinajstić N (2007) *Graph theoretical matrices in chemistry*. Mathematical chemistry monographs. University Kragujevac, Kragujevac
- Klein DJ, Lukovits I, Gutman I (1995) On the definition of the hyper-Wiener index for cycle-containing structures. *J Chem Inf Comput Sci* 35:50–52
- Kuratowski K (1930) Sur le Problème des Courbes Gauches en Topologie. *Fund Math* 15:271–283
- Lukovits I (1996) The detour index. *Croat Chem Acta* 69:873–882
- Mirman R (1999) *Point groups, space groups, crystals, molecules*. World Scientific, River Edge
- Petitjean M (2007) A definition of symmetry. *Symmetry Cult Sci* 18:99–119
- Plavšić D, Nikolić S, Trinajstić N, Mihalić Z (1993) On the Harary index for the characterization of chemical graphs. *J Math Chem* 12:235–250
- Randić M (1991) Generalized molecular descriptors. *J Math Chem* 7:155–168
- Randić M (1993) Novel molecular description for structure-property studies. *Chem Phys Lett* 211:478–483
- Randić M (1995) Restricted random walks on graphs. *Theor Chim Acta* 92:97–106
- Randić M, Guo X, Oxley T, Krishnapriyan H (1993) Wiener matrix: source of novel graph invariants. *J Chem Inf Comput Sci* 33:700–716

- Randić M, Guo X, Oxley T, Krishnapriyan H, Naylor L (1994) Wiener matrix invariants. *J Chem Inf Comput Sci* 34:361–367
- Razinger M, Balasubramanian K, Munk ME (1993) Graph automorphism perception algorithms in computer-enhanced structure elucidation. *J Chem Inf Comput Sci* 33:197–201
- Skorobogatov AV, Dobrynin AA (1988) Metric analysis of graphs. *MATCH Commun Math Comput Chem* 23:105–151
- Sylvester JJ (1874) On an application of the new atomic theory to the graphical representation of the invariants and covariants of binary quantics—with three appendices. *Am J Math* 1:64–90
- Tratch SS, Stankevich MI, Zefirov NS (1990) Combinatorial models and algorithms in chemistry. The expanded Wiener number—a novel topological index. *J Comput Chem* 11:899–908
- Trinajstić N (1983) *Chemical graph theory*. CRC Press, Boca Raton
- Ursu O, Diudea MV (2005) TOPOCLUJ software program. Babes-Bolyai University, Cluj
- Wiener H (1947) Structural determination of paraffin boiling points. *J Am Chem Soc* 69:17–20

Chapter 2

Operations on Maps

Structures discussed in this book are represented by simple, non-directed (molecular) graphs. Their design is based on “operations on maps”, merely applied on the Platonic solids: tetrahedron (T), cube (C), octahedron (O), dodecahedron (D) and icosahedron (I). A map M is a discretized surface domain while the operations on maps are topological modifications of a parent map. All the parameters herein presented refer to regular maps (i.e., having all vertices and faces of the same degree/size). The symmetry of parents is preserved by running these operations. Several operations are known (under various names/symbols) and currently used to decorate/transform a given mathematical object. The reader is invited to consult some publications in this respect (Johnson 1966; Pisanski and Randić 2000; Diudea 2010, Conway et al. 2008; Hart 2015; Grünbaum and Shephard 1987). In the following, only the most important operations will be detailed.

2.1 Dual d

Dual $d(P)$ is obtained by setting a point in the center of each face of a polyhedron P , then joining two such points if their corresponding faces share a common edge. It is the Poincaré dual; vertices of $d(P)$ represent faces in the parent polyhedron and vice-versa. If the starting polyhedron (i.e., the seed) is a three-connected one (e.g., the Platonic solids), of figure sequence $\{v, e, f\}$ (i.e., vertices, edges and faces), one obtains $\{f, e, v\}$ in the dual polyhedron; dual of the dual returns the original polyhedron (or an isomorphic of it): $d(d(P)) = P$. Tetrahedron is self-dual while the other Platonics form pairs: $d(C) = O$; $d(D) = I$ (see Fig. 2.1).

Dualization is an operation in any dimension and can be written, with the Schläfli (1901) symbols, as the reverted polytope figure sequence (see Chap. 3): $\{a, b, c, \dots, y, z\}$ becomes $\{z, y, \dots, c, b, a\}$ in the dual polytope; however, its realization complicates with the increase of polytope dimension. Within this book, only the *cell-dual* cd will be illustrated in some interesting cases.

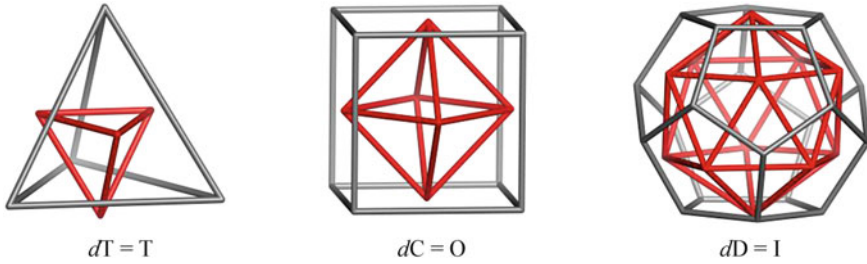


Fig. 2.1 Platonic solids as dual-pairs

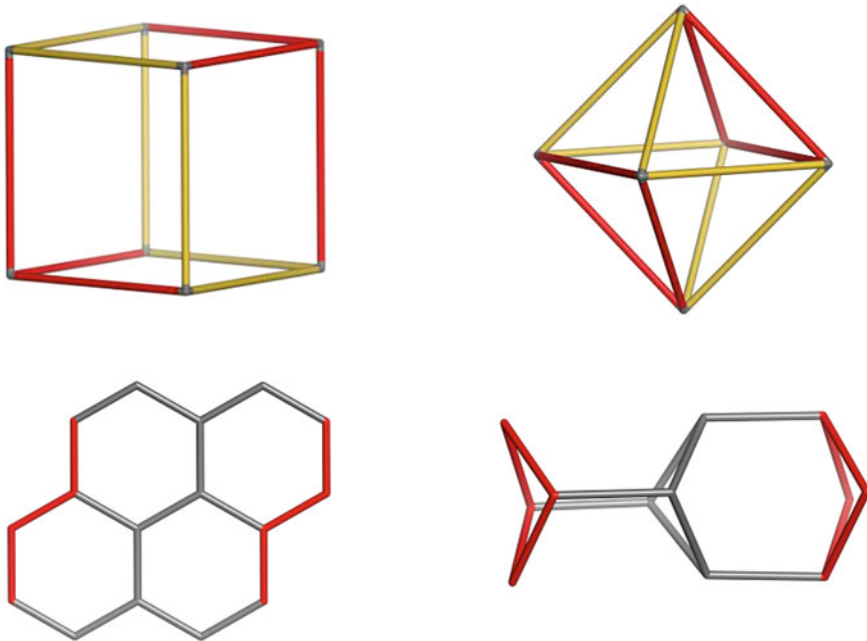


Fig. 2.2 Petrie (skew) hexagons (in yellow) of the cube C and octahedron O (top); embedding of the cube petrial in the torus (resulted by identifying the red edges of four hexagons—left, bottom—to form a tube and then by identifying the squares at the two ends of the tube—right, bottom)

A Petrie dual (or Petrial) is also known (Coxeter 1973, 1974); it is a map having vertices and edges of the original polyhedron and whose faces are the set of Petrie polygons. The Petrie polygon of a polyhedron is a skew polygon of which every two consecutive edges (but not three) belong to one of the faces of the parent polygon. For the Platonic polyhedra (T, C, O, D and I), the Petrie polygons are: three squares, four hexagons, four hexagons, six decagons and six decagons, respectively. Figure 2.2 illustrates the Petrie polygons in case of cube and octahedron, respectively.

Petrie polygon for a regular polytope of n dimensions is a skew polygon such that every $(n - 1)$ consecutive sides (but not n) belong to one of the facets of the

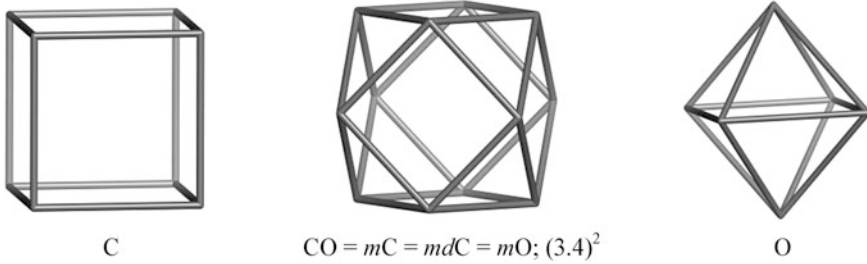


Fig. 2.3 Medial m operation (synonyms: *ambo*; *rectification*) provides a graph symmetric between a polyhedron and its dual

parent polytope. For every regular polytope there exists an orthogonal projection onto a plane (i.e., the Coxeter plane of the symmetry group of the polygon) such that one Petrie polygon becomes a regular polygon while the remainder of the projection appear interior to it.

Petrieals are useful in visualizing the symmetric structure of higher-dimensional regular polytopes.

2.2 Medial m

Medial $m(P)$ is obtained by pairwise joining the midpoints of parent edges if pair edges span an angle. Medial is always a 4-valent graph, symmetric between the parent polyhedron and its dual, that is $m(P) = m(d(P))$. The figure sequence of the truncated polyhedron is: $\{e, 2e, e+2\}$, e being the number of edges in the parent (three-connected) polyhedron. This operation rotates the parent s -gonal faces by π/s . By medial, edges of the parent polyhedron are reduced to a point; this property can be used in topological analysis of edges. This operation (illustrated in Fig. 2.3) is also known as *rectification* or even *ambo* (Conway notation). Applying twice mm (medial of a medial) is the same as *expansion* operation of Conway (Conway et al. 2008) or Johnson's *cantellation* operation (Johnson 1966).

Rectification is a complete vertex-truncation; the resulting polytope is bounded by vertex figure facets and the rectified facets of the parent polytope. If an n -polytope is $(n - 1)$ -rectified, its facets become points and the polytope becomes its dual. However, a rectified 4-polytope $\{p, q, r\}$ is not the same as the rectified $\{r, q, p\}$; a further truncation (namely a *bitruncation*) is needed to make it symmetric between a 4-polytope and its dual.

2.3 Truncation t

Truncation $t(P)$ cuts off the neighborhood of each vertex by a plane, such that it intersects each edge incident in that vertex. The truncated polyhedron has the figure sequence: $\{2e, 3e, e+2\}$; it is always a three-connected graph. Truncation is an operation in any dimension that cuts polytope vertices, creating a new facet instead of each vertex (Pisanski and Randić 2000). This was the main operation used by Archimedes in building its well-known 13 solids while the term originates from Kepler.

A *bitruncation* is a deeper truncation that removes all the original edges but leaves an interior part of the original faces. The bitruncated cube: $2t\{4, 3\}$ is the truncated octahedron, as an example.

In higher dimensions, truncations has various names, as runcination (4-polytopes) or sterication (5-polytopes). *Omnitruncation* is a truncation of a rectification (see Sect. 2.3).

Edge-truncation is a chamfering or a quadrupling (see below) for polyhedra; it retains original vertices while edges are replaced by hexagons. In 4-polytopes, an edge-truncation replaces edges with bipyramids. Fig. 2.4 illustrates the truncation operation in 3-polytopes.

2.4 Polygonal Mapping p_n

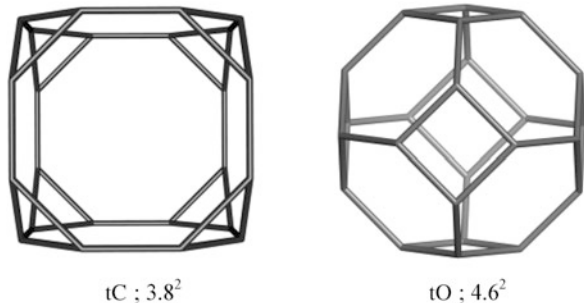
Polygonal $p_n(P)$ operation is achieved by adding a new vertex in the center of each face of a polyhedral graph, next put $n - 3$ points on the boundary edges. Connect the central point with one vertex on each edge (the endpoints included): the parent face will be covered by triangles ($n = 3$), squares ($n = 4$) and pentagons ($n = 5$), respectively. The transformed polyhedron figure sequence is: $\{(n - 2)e + 2, ne, 2e\}$. Fig. 2.5 gives examples of the p_n operations realization (Diudea and Nagy 2007).

Other names are used for these operations:

p_3 —*stellation* st , or *triangulation*, or also *kiss* k (Conway notation);

dual of stellation dp_3 is a *bitruncation* (or *leapfrog*, see Sect. 2.6)

Fig. 2.4 Truncation of cube (left) and octahedron (right)



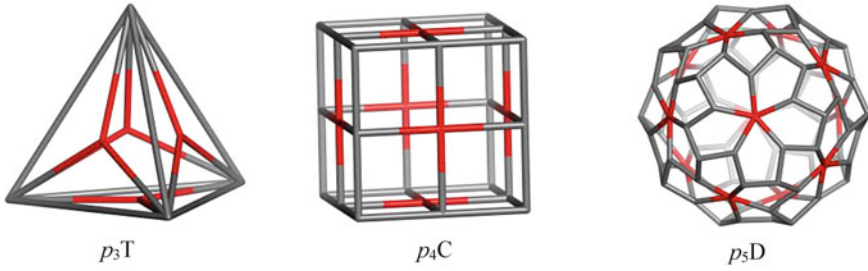


Fig. 2.5 Polygonal p_n operations on dodecahedron

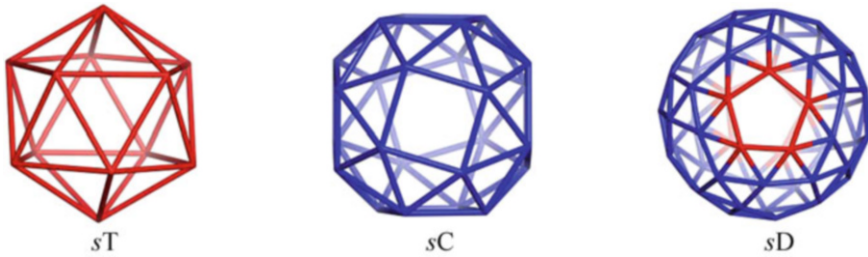


Fig. 2.6 Snub of three-connected platonic solids

p_4 —*ortho* o (Conway notation)

p_5 —*gyro* g (Conway notation)

2.5 Snub s

Snub operation is the dual of p_5 operation: $sM = dp_5M$. Similar to the medial operation, $sM = sdM$. The transformed polyhedron figure sequence is: $\{2e, 5e, 3e + \chi\}$. For $M = T$, the transformed map is the icosahedron: $sT = I$ (see the examples in Fig. 2.6).

Snub is the dual of p_5 operation: $s(P) = d(p_5(P))$ and $s(P) = s(d(P))$.

2.6 Leapfrog l

Leapfrog $l(P)$ (or *tripling* or also *dual of kiss*) is a composite operation (Eberhard 1891; Fowler 1986) that can be written as: $l(P) = t(d(P)) = d(stP)$; it rotates the parent s -gonal faces by π/s . The transformed polyhedron has the figure sequence: $\{2e, 3e, e + 2\}$; the vertices of $l(P)$ are always of degree 3, since this operation involves a truncation (see above). A bounding polygon, of size $2d$, is formed around

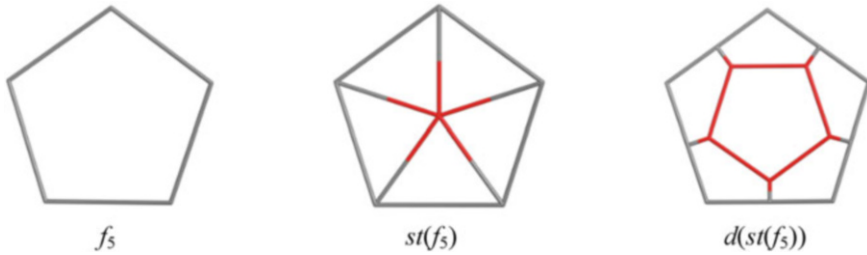


Fig. 2.7 The leapfrog l operation on a pentagonal face f_5

each parent vertex. In the most frequent cases, of 4- and 3-valent maps, the bounding polygon is an octagon and a hexagon, respectively. Leapfrog operation is illustrated, on a pentagonal face, in Fig. 2.7.

If P is a d -regular graph (d being the vertex degree) the following theorem holds (Diudea and John 2001):

Theorem 2.1 *The number of vertices in lP is dv , irrespective of the parent tessellation.*

Demonstration follows from the observation that, for each vertex of P , d vertices will newly appear in lP , that gives a multiplication ratio of $dv/v = d$. A nice example of using *leapfrog* operation is: $lD = C_{60}$; 5.6^2 .

2.7 Quadrupling q

Quadrupling (Eberhard 1891; Diudea and John 2001), also named *chamfering c* (Conway notation) can be written as: $qP = t_{sel}(stP)$, where t_{sel} is the selective truncation of the central point added by stellation st ; it is in fact an *edge truncation* that retains the parent vertices and the face orientation, as well (Fig. 2.8).

The name comes from the vertex multiplication ratio when operates on three-connected polyhedra, according to the following

Theorem 2.2 *The number of vertices in qP is $(d + 1)v$, irrespective of the parent tessellation.*

With the observation that, for each vertex of P , d new vertices appear in qP while the old vertex is preserved, the multiplication ratio is $(d + 1)v/v = d + 1$; in case of a three-connected polyhedron, the transformed figure sequence is: $\{v + 2e, 4e, f + e\}$. This operation insulates the parent faces always by hexagons; it involves two π/s rotations, so that the initial orientation of the polygonal faces is preserved. Only applied on a 3-valent map it results in a 3-regular graph (which is not the case in 4-valent maps). An example of this operation is: $qD = C_{80}$.

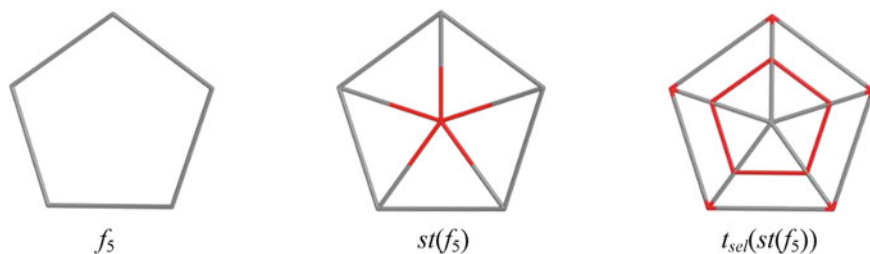


Fig. 2.8 The quadrupling Q operation on a pentagonal face f_5

2.8 Septupling s_n

Two septupling operations are known to multiply seven times the vertices of a three-connected polyhedron: s_1 and s_2 (Diudea 2004, 2005a, b; Diudea et al. 2006; Diudea and Nagy 2007). The s_1 operation is also called (Diudea 2003) *capra*—the (Romanian) goat, or *whirl* operation (Conway notation). It is achieved by truncation of vertices centered on the parent faces in p_5 : $s_1P = t_{sel}(p_5P)$. S_1 insulates any face of M by its own hexagons, which are not shared with any old face. It is an intrinsic chiral operation (it rotates the parent edges by $\pi/(3/2)s$).

The multiplication ratio comes from the Goldberg (1937) polynomial:

$$m = (a^2 + ab + b^2); \quad a \geq b; \quad a + b > 0$$

In a 3-valent map, $l(1, 1)$; $m = 3$; $q(2, 0)$; $m = 4$ and $s_1(2,1)$; $m = 7$. This is supported by the following

Theorem 2.3 *The vertex multiplication ratio in an s_1 -transformed map is $2d + 1$ irrespective of the original map tiling.*

For demonstration, observe that, for each old vertex, $2d$ new vertices appear (Fig. 2.9) and the old vertex is preserved in the transformed map. Thus, $(2d + 1)v/v = 2d + 1$. The figure sequence of the transformed by s_1 operation is: $\{v + 4e, 7e, f + 2e\}$.

Since p_5 operation can be done either clockwise or counter-clockwise, it results in an enantiomeric pair of objects: $s_{1S}P$ and $s_{1R}P$, the subscript letter referring to *sinister/rectus* stereochemical isomers. An example of s_1 realization is: $s_1D = C_{140}$.

S_1 can continue with the *open o* operation: $o_n s_i M$, where n represents the number of points added on the boundary of a parent face to become a window (i.e., an *open* face). The resulting open objects have all the polygons of the same $(6 + n)$ size. The above operation sequence enables the construction of negatively curved networks. Fig. 2.8 gives the steps of its realization on a square face in a trivalent lattice, up to the open structure.

The s_2 operation (Diudea 2005a) (Fig. 2.10) can be achieved by putting four vertices on each edge of the parent polyhedron P (e_4 operation) and next join these new vertices in order $(-1, +3)$: $s_2 = j(-1, +3)e_4P$.

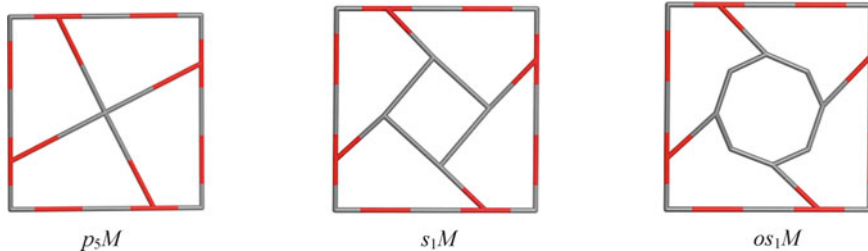


Fig. 2.9 Septupling s_1 operation on a square face, up to the open structure

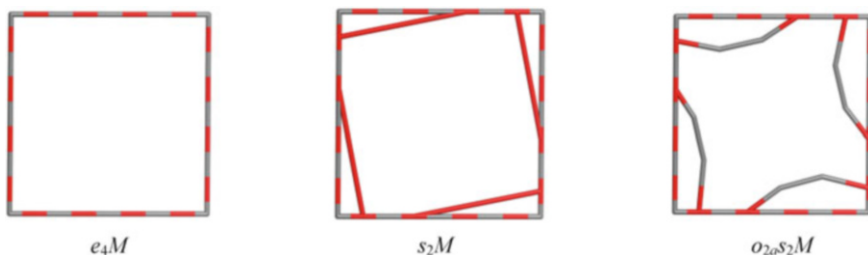


Fig. 2.10 Septupling s_2 operation on a square face, up to the open structure

It insulates the double sized parent faces by pentagons and parent vertices by pentagon n -multiples; the transformed objects are non-chiral. The transformed figure sequence is the same as for s_1 .

Chirality in s_2 can be induced by the operation o_{2a} , achieved by adding two points on alternative edges of the double sized boundary (Fig. 2.8). An example of this operation realization is: $s_2T = C_{28}$.








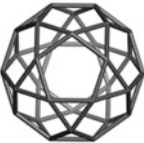

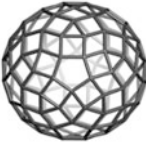




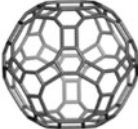



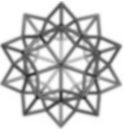




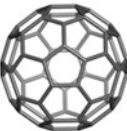

Peter John (Diudea et al. 2006) has proposed a generalization of operations on maps, inspired from the work of Goldberg (1937) and the representation of polyhedra in the (a, b) “inclined coordinates” (60° between axes).

TOPO GROUP CLUJ has developed several software programs dedicated to polyhedral tessellation and embedment in surfaces of various genera, either as finite or infinite structures: Torus, CageVersatile_CVNET, JSCEM, and NANO-Studio (Diudea et al. 2003; Stefu and Diudea 2005; Nagy and Diudea 2005, 2009).


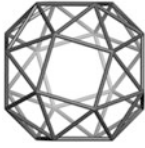
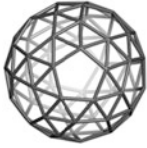
















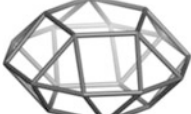
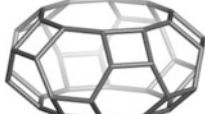
There are known different operations that enable the design/decoration of polyhedral structures, such as inflation–deflation operation, matching rules, the grid method, strip projection, cut projection or generalized dual method (de Bruijn 1981; Kramer 1982; Bak 1986; Socolar et al. 1986).

In the following, the most frequent small cages, encountered as cells/shapes within multi-shell clusters, are illustrated.

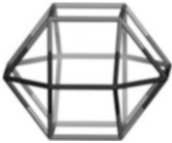














Chapter 2 Atlas: Single Shell Clusters

				
T.4	C.8	O.6	D.20	I.12
				
$mT.6=O.6$	$mC.12=mO.12=CO.12$	$mD.30=mI.30=ID.30$		
				
$m^2(D).60$	$m^3(D).120$	$m^4(D).240$		
				
RCO.24	RID.60	TCO.48	TID.120	
				
Rh ₁₂ $dmC.14$	Rh ₂₄ $dRCO.26$	Rh ₃₀ $dmD.32$	Rh ₆₀ $dRID.62$	Rh ₉₀ $d(m(C_{60})).92$
				




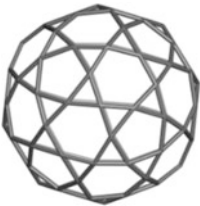
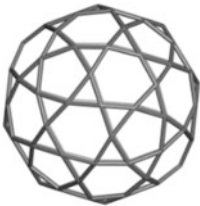
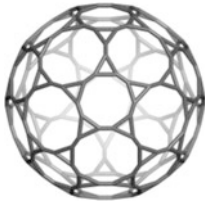
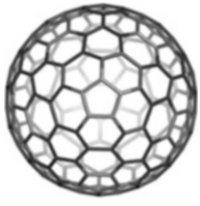
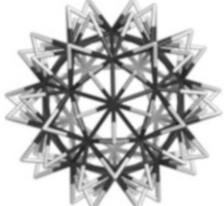
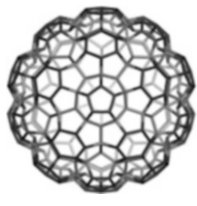
(continued)

$tT.12$	$tC.24$	$tO.24$	$tD.60$	$tI.60$
$rT.12$	$rO.24$	$rC.24$	$rI.60$	$rD.60$
$TT.12$	$TO.24$	$TC.24$	C_{60}	3.10^2
				
$sT.12=I.12$	$sC.24= sO.24$	$sI.60= sD.60$		
				
$srT.8$	$srC.14$	$srO.14$	$srD.32$	$srI.32$
				
$mP_3.9$	$mP_4.12$	$mP_5.15$	$mP_6.18$	
				
Rh_9 $d(mP_3).11$	Rh_{15} $d(mP_5).17$	Rh_{18} $d(mP_6).20$		
				
$A_3.6=O.6$	$A_4.8$	$A_5.10$		
				
$dA_5.12$	$mA_5.20$	$tA_5.40$		

(continued)

		
$m(mP_3X_9).16$ $m(dmP_4).16$ J_{28}	$mA_4.16$ J_{29}	$mA_5.20$ J_{31}
		
$t(D).60$	$m(D).30$	$m(tD).90$
		
$Py_{3,4}=T.4$	$Py_{4,5}$	$Py_{5,6}$
		
$tPy_{3,12}=TT.12$	$tPy_{4,16}$	$tPy_{5,20}$
		
C_{12} $6(3.5^2);6(5^3)$	C_{16} $8(4.5^2);8(5^3)$	C_{20} 5^3

(continued)

		
$t_{set}(p_4T).22$	$t_{set}(P_4(C)).44$	$t_{set}(p_4(D)).110$
		
$d(C_{60}).32$	$mC_{60}.90$	$tC_{60}.180$
		
$l(C_{60}).180$	$st(dC_{60}).92$	$t_{set}(p_4(C_{60})).330$

References

- Bak P (1986) Icosahedral crystals: where are the atoms? *Phys Rev Lett* 56:861–864
- Conway JH, Burgiel H, Goodman-Strauss C (2008) *The symmetries of things*. ISBN: 978-1-56881-220-5
- Coxeter HSM (1973) Petrie polygons; the generalized petrie polygon. In: *Regular polytopes*, 3rd edn. Dover, New York
- Coxeter HSM (1974) *Regular complex polytopes*. Cambridge University Press, Cambridge (Section 11.3 Petrie polygons)
- de Bruijn NG (1981) Algebraic theory of penrose's non-periodic tilings of the plane, I, II. *Proc Nederl Acad Wetensch Proc Ser A* 84:39–66
- Diudea MV (2003) Capra-a leapfrog related operation on maps. *Stud Univ Babeş-Bolyai* 48:3–16
- Diudea MV (2004) Covering forms in nanostructures. *Forma (Tokyo)* 19:131–163
- Diudea MV (2005a) Nanoporous carbon allotropes by septupling map operations. *J Chem Inf Model* 45:1002–1009
- Diudea MV (2005b) Covering nanostructures. In: Diudea MV (ed) *Nanostructures-novel architecture*. Nova, New York, pp 203–242

- Diudea MV (2010) Nanomolecules and nanostructures – polynomials and indices, MCM, No 10, Univ Kragujevac, Serbia
- Diudea MV, John PE (2001) Covering polyhedral tori. *MATCH Commun Math Comput Chem* 44:103–116
- Diudea MV, Nagy CL (2007) *Periodic nanostructures*. Springer, Dordrecht
- Diudea MV, Parv B, Ursu O (2003) *TORUS*. University Babes-Bolyai, Cluj
- Diudea MV, Ștefu M, John PE, Graovac A (2006) Generalized operations on maps. *Croat Chem Acta* 79:355–362
- Eberhard V (1891) *Zur morphologie der polyeder*. B. G. Teubner, Leipzig
- Fowler PW (1986) How unusual is C_{60} ? magic numbers for carbon clusters. *Chem Phys Lett* 131:444–450
- Goldberg M (1937) A class of multi-symmetric polyhedral. *Tôhoku Math J* 43:104–108
- Grünbaum B, Shephard GC (1987) *Tilings and patterns*. W. H. Freeman, New York
- Hart G (2015) www.georgehart.com/virtual-polyhedra/vp.html
- Johnson NW (1966) *The theory of uniform polytopes and honeycombs*, Ph.D. Dissertation, University of Toronto
- Kramer P (1982) Non-periodic central space filling with icosahedral symmetry using copies of seven elementary cells. *Acta Cryst A* 38:257–264
- Nagy CL, Diudea MV (2005) *JSchem*. University Babes–Bolyai, Cluj
- Nagy CL, Diudea MV (2009) *Nano studio*. University Babes–Bolyai, Cluj
- Pisanski T, Randić M (2000) Bridges between geometry and graph theory, geometry at work. *MAA Notes* 53:174–194
- Schläfli L (1901) *Theorie der vielfachen Kontinuität* Zürcher und Furrer, Zürich (Reprinted in: Ludwig Schläfli, 1814–1895, *Gesammelte Mathematische Abhandlungen*, Band 1, 167–387, Verlag Birkhäuser, Basel, 1950)
- Socolar JES, Steinhardt PJ, Levine D (1986) Quasicrystals with arbitrary orientational symmetry. *Phys Rev B* 32:5547–5551
- Ștefu M, Diudea MV (2005) *CageVersatile_CVNET*. Babes–Bolyai University, Cluj

Chapter 3

Definitions in Polytopes

Multi-shell clusters represent complex structures, the study of which needs appropriate theoretical information. In this respect, rigorous definitions in graph theory, geometry, set theory and others are claimed in the effort of counting structural elements, naming and properties description of such entities.

3.1 Polyhedra

A *regular polyhedron* is a polyhedron with congruent regular polygons as faces, arranged in the same way around identical vertices. Also, it is a polyhedron whose symmetry group acts transitively on its flags; a regular polyhedron is a highly symmetric structure, being vertex-transitive, edge-transitive and face-transitive (Coxeter 1973; Schulte 2014).

The property of having a similar arrangement of faces around each vertex is equivalent with the following conditions: the vertices of the polyhedron all lie on a sphere; all the dihedral angles of the polyhedron are equal; all its vertex figures are regular polygons; all the solid angles are congruent (Cromwell 1997).

The regular polyhedra have the highest symmetry of all the polyhedra. They show three symmetry groups: *tetrahedral*; *octahedral* (or cubic) and *icosahedral* (or dodecahedral). Any shapes with icosahedral or octahedral symmetry will also include the tetrahedral symmetry.

There are five regular polyhedra, known as Platonic polyhedral solids (Fig. 3.1): tetrahedron, cube, octahedron, dodecahedron and icosahedron can be written as $\{3,3\}$; $\{4,3\}$; $\{3,4\}$; $\{5,3\}$ and $\{3,5\}$ by using the basic Schläfli (1901) symbols $\{p,q\}$ where p is the number of vertices in a given face while q is the number of faces containing a given vertex. Their pair duals are (cube & octahedron) and (dodecahedron & icosahedron) while the tetrahedron is selfdual.

The ancient Greeks had good knowledge on the Platonic solids. Theaetetus, an Athenian contemporary of Plato, gave a mathematical description of all the five



Fig. 3.1 The Platonic solids, their symbol, vertex configuration and point group

regular solids and may be the first known proof that no other convex regular polyhedra exist. Plato wrote about the five regular solids in the dialogue *Timaeus*, about 360 B.C. Euclid gave a complete mathematical description of the Platonic solids in his *Elements* (Heath 1981).

Any convex polyhedron can be represented in the plane (or on the sphere surface) by a 3-connected [planar graph](#) (also called a [polyhedral graph](#)). The number of vertices v , edges e , and faces f of a convex polyhedron are related by the [polyhedral formula](#) (Euler 1752–1753).

$$v - e + f = \chi = 2(1 - g) \quad (3.1)$$

where χ is the Euler characteristic and g is the genus (i.e., the number of tori in a connected sum decomposition of an orientable surface on which the polyhedral graph is embedded, or the number of holes performed in a plastic sphere to make it homeomorphic to that surface). A surface is orientable, when it has two sides, or it is non-orientable, when it has only one side, like the Möbius strip.

Euler characteristic is a topological invariant that describes the shape of a structure regardless of the way it is bent. Positive/negative χ values indicate positive/negative curvature of the polyhedral structure.

A topological proof, showing that no other (out of the five Platonic) convex regular polyhedra exist, can be derived from the Euler (1736, 1752–1753) relations

$$pf = qv = 2e \quad (3.2)$$

$$v - e + f = 2 \quad (3.3)$$

Combining these equations one obtains: $2e/q - e + 2e/p = 2$. Then, $1/q + 1/p = 1/e + 1/2$ and, since e is strictly positive, the following condition comes out:

$$1/q + 1/p > 1/2 \quad (3.4)$$

Because p and q must be at least three, then (3.4) accepts only five solutions for the pair $\{p, q\}$: $\{3, 3\}$, $\{4, 3\}$, $\{3, 4\}$, $\{5, 3\}$, $\{3, 5\}$.

The five Platonic solids can be drawn by using operations on maps (see Chap. 2), starting from the tetrahedron T

Dodecahedron: $p_5T = dI$

Icosahedron: $dp_5T = sT$

Cube: $dO = dmT$

Octahedron: mT

Tetrahedron: T

Geometrically, a convex polyhedron can be defined as a polyhedron for which a line, connecting any two non-coplanar points on the surface, always lies in the interior of the polyhedron. There are 92 convex polyhedra, called the Johnson solids (Johnson 1966), having only regular polygons as faces; they include the Platonic solids and Archimedean solids.

Archimedean solids are highly symmetric, semi-regular convex polyhedra, showing two (or more) types of regular polygons meeting in identical vertices. They differ from the Platonic solids, which have only one type of polygon meeting in identical vertices, and from the Johnson’s solids, whose regular polygonal faces do not meet in identical vertices. Since there were some inconsistencies in considering or not as Archimedean the Johnson’s solid pseudo-rhombicuboctahedron, Grünbaum (2009) has suggested that an Archimedean solid must have the same vertex figure at each vertex. The 13 Archimedean solids, of two type polygonal faces (de La Vaissière et al. 2001) and their design from the Platonic solids, by operations on maps, are listed in Table 3.1.

A *Catalan solid* (Catalan 1865) is a dual polyhedron of an Archimedean solid. The Catalan solids are all face-transitive but not vertex-transitive (because their duals are vertex-transitive but not face-transitive). Their faces are not regular polygons, however their vertex figures are regular and have constant dihedral angles (Wenninger 1983).

A *uniform polyhedron* is a polyhedron of which faces are regular polygons and is vertex-transitive, meaning all the vertices are congruent and the polyhedron has a high degree of reflectional and rotational symmetry. Uniform polyhedra may be

Table 3.1 Archimedean solids as related by operations on maps

	Symbol	Archimedean	Map operation relation
1	TT	Truncated tetrahedron	tT
2	TO	Truncated octahedron	$tO = tmT$
3	TC	Truncated cube	$tC = tdmT$
4	TI	Truncated icosahedron	$tI = tdp_5T$
5	TD	Truncated dodecahedron	$tD = tp_5T$
6	CO	Cuboctahedron	$mC = mO = mmT$
7	ID	Icosidodecahedron	$mI = mD = msT$
8	RCO	Rhombicuboctahedron	$mCO = mmC = dp_4C$
9	RID	Rhombicosidodecahedron	$mID = mmI = dp_4I$
10	TCO	Truncated cuboctahedron	$tCO = tmmT$
11	TID	Truncated icosidodecahedron	$tID = tmsT$
12	SC	Snub cube	$sC = dp_5C$
13	SD	Snub dodecahedron	$sD = dp_5D$

regular (if is also edge- and face- transitive), *quasi-regular* (if is edge-transitive but not face-transitive) or *semi-regular* (if is neither edge- and face-transitive). The faces and vertices need not be convex, so that many of the uniform polyhedra are star polyhedra (Coxeter and Miller 1954; Sopov 1970; Wenninger 1974).

There are 75 finite uniform polyhedra (or 76 if edges are allowed to coincide): 5 Platonic solids (regular convex polyhedra), 13 Archimedean solids (2 quasi-regular and 11 semi-regular convex polyhedra), and 58 star polyhedra (4 Kepler-Poinsot polyhedra, which are regular nonconvex polyhedra, 53 uniform star polyhedra—5 quasi-regular and 48 semi-regular and 1 star polyhedron—the Skilling’s (1975) object, of which pairs of edges coincide). There are also two infinite sets of uniform prisms and antiprisms, including convex and star forms.

Dual polyhedra to uniform polyhedra are **face-transitive** and have regular vertex figures; the dual of a regular polyhedron is regular, while the dual of an Archimedean solid is a Catalan solid. A polyhedron which is vertex-transitive is also called isogonal, which is edge-transitive is also called isotoxal and is isohedral if it is face-transitive. A noble polyhedron is both isohedral and isogonal.

The concept of uniform polyhedron is a special case of the concept of **uniform polytope**, which also applies to shapes in higher-dimensional space.

In polyhedral combinatorics, according to the Steinitz theorem (Steinitz 1922; Ziegler 1995), to every convex polyhedron a 3-connected planar graph (i.e., a polyhedral graph) can be associated, and every 3-connected planar graph can be represented as the graph of a convex polyhedron. Generalization of this theorem, by Balinski (1961), states that the graph of any k -dimensional convex polytope is k -connected (see Sect. 3.2)

3.2 n -Dimensional Structures

Generalization of a polyhedron to n -dimensions is called a polytope (Grünbaum and Shephard 1988; Grünbaum 2003; Coxeter 1973, 1974). Let us introduce the most important n -dimensional structures.

Regular 4-polytopes, written as $\{p,q,r\}$, have cells of the type $\{p,q\}$, faces $\{p\}$, edge figures $\{r\}$ and vertex figures $\{q,r\}$. It can also be read as: r -polyhedra (of the type $\{p,q\}$) meet at any edge of the polytope. In case of a 4-polytope, the vertex figure is a polyhedron formed by the neighboring vertices around a given vertex; the edge figure is a polygon.

A 3-polytope is convex if any of its edges shares no more than two polygons; next, a 4-polytope is convex if any polygon shares no more than two cells. Each convex 4-polytope is bounded by a set of 3-faces (i.e., cells). If its cells are all regular, of the same type and size, the 4-polytope is called regular.

The existence of a regular 4-polytope $\{p,q,r\}$ is constrained by the existence of regular polyhedra $\{p,q\}$ and $\{q,r\}$, which are its cells; if p,q,r , are integers, the following relation is obeyed (Coxeter 1974)

$$p + 2q + r - 4/p - 4/r < 12 \tag{3.5}$$

The six regular 4-polytopes, also called polychora, are: 5-Cell {3,3,3}; 8-Cell {4,3,3}; 16-Cell {3,3,4}; 24-Cell {3,4,3}; 120-Cell {5,3,3} and 600-Cell {3,3,5}. Five of them can be associated to the Platonic solids but the sixth, the 24-Cell has no close 3D equivalent. Among them, 5-Cell and 24-Cell are selfduals while the other are pairs: (8-Cell & 16-Cell); (120-Cell & 600-Cell). The symmetry groups of these 4-polytopes are all finite Coxeter groups (Coxeter 1934, 1940, 1973; Davis 2007).

In *five dimensions*, a regular 5-polytope is written as {*p,q,r,s*}, where {*p,q,r*} is a 4-face type, {*p,q*} is the cell type, {*p*} is the face type; {*s*} is the face figure, {*r,s*} is the edge figure and {*q,r,s*} is the vertex figure. The vertex figure is a 4-polytope (arrangement of neighboring vertices to each vertex), the edge figure is a polyhedron (seen as the arrangements of faces around each edge) while the face figure is a polygon (seen by the arrangements of cells around each face).

A regular 5-polytope {*p,q,r,s*} exists within the conditions: {*p,q,r*} and {*q,r,s*} are regular 4-polytopes and the space in which a 5-space polytope exists is constrained by the expression

$$\begin{aligned} \cos^2\left(\frac{\pi}{q}\right) \cos^2\left(\frac{\pi}{r}\right) < 1 &: \text{Spherical 4 - space tessellation or 5 - polytope} \\ \frac{\cos^2\left(\frac{\pi}{q}\right)}{\sin^2\left(\frac{\pi}{p}\right)} + \frac{\cos^2\left(\frac{\pi}{r}\right)}{\sin^2\left(\frac{\pi}{s}\right)} = 1 &: \text{Euclidean 4 - space tessellation} \\ \frac{\cos^2\left(\frac{\pi}{q}\right)}{\sin^2\left(\frac{\pi}{p}\right)} + \frac{\cos^2\left(\frac{\pi}{r}\right)}{\sin^2\left(\frac{\pi}{s}\right)} > 1 &: \text{hyperbolic 4 - space tessellation} \end{aligned} \tag{3.6}$$

Enumeration of these constraints provides *three convex polytopes*, zero non-convex polytopes, three 4-space tessellations and five hyperbolic 4-space tessellations. There are no non-convex regular polytopes in five dimensions or higher. The three types of convex regular polytopes in dimensions five and higher, are as follows.

The *n-simplex* (Coxeter 1973; Buekenhout and Parker 1998), with the Schläfli symbol { 3^{n-1} }, and the number of its *k*-faces $\binom{n+1}{k+1}$, is a generalization of the [triangle](#) or [tetrahedron](#) to *n-dimensions*. For example, a 0-simplex is a point, a 1-simplex is a line segment, a 2-simplex is a triangle, a 3-simplex is a tetrahedron, and a 4-simplex is a [5-cell](#). The simplex represents the simplest possible polytope in any given space. A simplex may be defined as the smallest convex set containing the given vertices.

A regular *n-simplex* may be constructed from a regular (*n - 1*)-simplex by connecting a new vertex to all original vertices by the common edge length. The simplex is so-named because it represents the simplest possible polytope in any given space. The convex hull of any nonempty subset of *k + 1* points that define an *n-simplex* is called a face of the simplex; faces are simplexes themselves. In particular, the convex hull of a subset of size *k + 1* (of the *n + 1* defining points) is a *k-simplex* and is called a *k-face* of the *n-simplex*. The 0-faces (i.e., the points themselves) are called the vertices, the 1-faces are called the edges, the (*n-1*)-faces are called the *k-faces* (or facets), and the unique *n-face* is the whole *n-simplex* itself.

The **hypercube** is a generalization of the 3-cube to n -dimensions; it is also called an n -cube and commonly denoted Q_n . It is a regular polytope with mutually perpendicular sides, thus being an orthotope. It has the Schläfli symbol $\{4, 3^{n-2}\}$ and k -faces given by $2^{n-k} \binom{n}{k}$. The hypercube can be constructed by the Cartesian product graph of n edges: $(P_2)^{\square n} = Q_n$. Figure 3.2 illustrates the 4-Cube, i.e., 8-Cell or Tesseract, as painted by the Italian painter Juseppe Zaccuri, Milano.

The **n -orthoplex or cross-polytope** (Coxeter 1973) has the Schläfli symbol $\{3^{n-2}, 4\}$ and k -faces $2^{k+1} \binom{n}{k+1}$; it exists in any number of dimensions and is the dual of n -cube. The cross-polytope is the convex hull of its vertices; its facets are simplexes of the previous dimensions, while its vertex figures are other cross-polytopes of lower dimensions.

A **convex hull** (envelope) (Coxeter 1973; Grünbaum 2003) of a set X of points in the Euclidean space is the smallest convex set that contains X . A set of points is called convex if it contains all the line segments connecting each pair of its points. The convex hull of a finite set S of points is the set of all its convex combinations; in a convex combination, each point x_i is weighted by a coefficient α_i such that the coefficients are all non-negative and their sum is one. For each choice of coefficients, the resulting convex combination is a point in the convex hull, and the whole convex hull can be generated by choosing coefficients in all possible ways. One can write the convex hull as the set:

$$\left\{ \sum_{i=1}^{|S|} \alpha_i x_i \mid (\forall_i : \alpha_i \geq 0) \wedge \sum_{i=1}^{|S|} \alpha_i = 1 \right\} \quad (3.7)$$



Fig. 3.2 HyperCube by Giuseppe Zaccuri, Milano

The convex hull of a finite point set $S \in \mathbb{R}^n$ forms a convex polytope; for $n = 2$, it is a convex polygon. Every convex polytope in \mathbb{R}^n is the convex hull of its vertices (Lyusternik 1963).

Polyhedra are associated into pairs called duals, the vertices of one being the faces of the other; the dual of its dual is the original polyhedron (see Chap. 2). The concept of *duality* is closely related to the duality in the projective geometry (Grünbaum and Shephard 1988; Wenninger 1983).

Duality can be generalized to n -dimensional space and dual polytopes. The vertices of one polytope correspond to the $(n - 1)$ -dimensional elements, or facets, of the other, and the j points that define a $(j - 1)$ -dimensional element will correspond to j hyperplanes that intersect to give an $(n - j)$ -dimensional element.

In general, the facets of a polytope's dual will be the topological duals of the polytope's vertex figures. For regular and uniform polytopes, the dual facets will be the polar reciprocals of the original's vertex figure. For example, in four dimensions, the vertex figure of the 600-Cell is the icosahedron; the dual of the 600-Cell is the 120-Cell, whose facet is a dodecahedron, which is the dual of the icosahedron.

For general surfaces, Euler characteristic χ can be calculated as an alternating sum of figures of rank k (Euler 1752–1753; Schläfli 1901; Schulte 1985, 2014)

$$\chi(S) = f_0 - f_1 + f_2 - f_3 + \dots, \quad (3.8)$$

Euler characteristic is a dimensionless quantity associated with an object, in essence, a generalization of cardinality (Leinster 2008).

Structures herein discussed are represented by simple, non-directed graphs. Their design is based on “operations on maps”, merely applied on the Platonic solids.

3.3 Abstract Structures

An *abstract polytope* is a structure which considers only the combinatorial properties of a traditional polytope: properties like angles, edge lengths, etc. are disregarded. No space, such as Euclidean space, is required to contain an abstract polytope. Its combinatorial properties are expressed as a partially ordered set or a “poset”. The poset theory originates in the PhD thesis of Schulte (1980, 1983a, b, c, 1985), based on the early results of Grünbaum (Grünbaum and Shephard 1988), Coxeter (1973, 1974, 1982, 1984); Petri or Tits (Tits 1964; Tits and Weiss 2002) and next developed by McMullen and Schulte (2002).

3.3.1 Posets

Polytopes have a dimensional hierarchy of their structural elements, also called figures, or facets or simply faces, of dimension 0 (vertices), 1 (edges) 2 (faces), etc. In the posets theory, the *dimension* concept is replaced by that of *rank*. An element of rank k is called a k -face.

Every polytope has a *least* face (also called a *null* face, since it has no vertices or any other faces) and a *greatest* face, of which all the others are subfaces. The least and greatest faces are called *improper* faces while all the others are *proper* faces.

The *order* relation $<$ is defined as set of pairs and it induces the rank of the poset and its subfaces

$$F_{-1} < F_0 < F_1, \dots, F_{n-1} < F_n.$$

The *rank* of a face F is defined as the integer $(m - 2)$, where m is the maximum number of faces in the hierarchical string $F' < F'' < \dots < F$.

The rank of a *poset* P is the maximum rank n of any face, i.e., that of the greatest face (if required). It follows that the least face has the rank -1 while the greatest face has the rank n ; the two faces are often denoted as F_{-1} and F_n respectively. The *rank* of a face or a polytope usually corresponds to the *dimension* in traditional theory, but not always.

A flag φ is a maximal string of faces, a set totally ordered, such that each face is a subface of the successor (if any) and φ is not a subset of any larger string. If F and G are any two distinct faces in a flag, either $F < G$ or $F > G$.

Order relations are transitive, i.e., $F < G$ and $G < H$ implies $F < H$. Therefore, to specify the hierarchy of faces, only the order of pairs (the actual face and its successor) suffices.

A polytope is often represented by its graph $G(V,E)$ but the higher rank faces cannot be deduced from the graph. A Hasse diagram fully describes a poset, in particular, a polytope; all the substructures/faces of the polytope are captured in such a diagram, where the faces of equal rank are placed on the same horizontal level, starting from -1 up to n , on the vertical. Isomorphic polytopes provide isomorphic Hasse diagrams, and vice versa. Figure 3.3 shows a triangle and its Hasse diagram.

Any subset P' of a poset P is a poset. Given any two faces F, H of P with $F \leq H$, the set $\{G|F \leq G \leq H\}$ is called a “section” of P , and is denoted H/F . A k -section is a section of rank k .

A polytope that is the subset of another polytope is not necessarily a section. The square $abcd$ is a subset of the tetrahedron $abcd$, but is not a section of it. The concept is different from that in traditional geometry.

A poset P is connected if any two successive faces F_k and F_{k+1} are incident to each other; it is strongly connected if every section of P (including P itself) is connected. It is equivalent to saying that any flag can be changed into any other by changing just one face at a time.

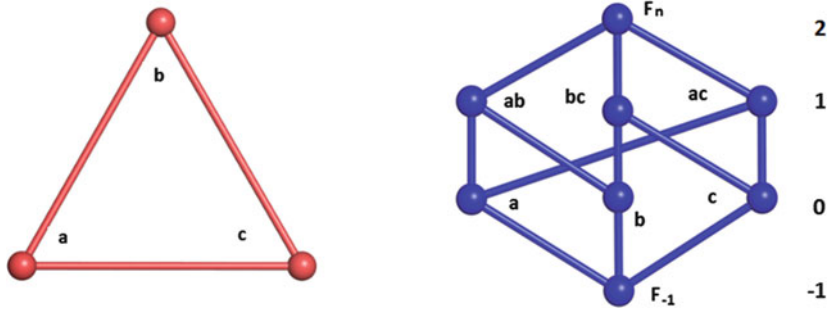


Fig. 3.3 A triangle (left) and its Hasse diagram (right)

3.3.2 Vertex Figure

The *vertex figure* at a given vertex V is the $(n-1)$ -section F_n/V , where F_n is the greatest face. Formal definitions of vertex figure can vary, according to circumstances. In one of the most simple procedure, one makes a slice through the corner of the polyhedron, cutting through all the edges connected to the vertex. The cut surface is the vertex figure. Different authors make the slice in different places: at the unit distance from the given vertex, at the midpoints of the connected edges or at the other end of each edge.

In an abstract n -polytope, the vertex figure at a given vertex is an $(n-1)$ -polytope (Schulte 1985, 2004); it includes all the elements incident to the vertex; edges, faces, etc. For example, the vertex figure of the cube is a triangle; for the tesseract, it is a tetrahedron.

By considering the neighborhood connectivity in an $(n-1)$ -polytope, the vertex figure can be constructed for each vertex of a polytope, so that: (i) each vertex of the vertex figure coincides with a vertex of the original polytope and (ii) each f_k face of the vertex figure exists on or inside of an f_{k+1} face of the original n -polytope (for $n > k+1$). Thus, the vertex figure encodes the structure of entire polytope. In polyhedra, the vertex figure can be represented by the vertex configuration, that lists the sequence of faces around that vertex. In uniform polyhedra, there is only one vertex type and therefore the vertex configuration fully defines the polyhedron. For example, 5.6^2 is a vertex in the fullerene C_{60} . Order is important, so that $3.5.3.5$ is different from $3.3.5.5$.

If the polytope is vertex-transitive, the vertex figure (an $(n-1)$ -polytope) will exist in a hyperplane surface of the n -space. In general, the vertex figure not needs to be planar. In case of a uniform polyhedron, the face of the dual polyhedron may be found from the vertex figure of the original polyhedron.

If a polytope is regular, with the Schläfli symbol $\{a,b,c, \dots ,y,z\}$, its vertex figure will be $\{b,c, \dots ,y,z\}$.

An edge figure is the vertex figure of a vertex figure; in case of an n -polytope, it will be an $(n-2)$ -polytope, representing the arrangement of facets around a given edge. Regular polytopes, with the symbol $\{a,b,c, \dots ,y,z\}$ have a single edge figure $\{c, \dots ,y,z\}$ which is also regular.

3.3.3 Abstract Polytope

An abstract polytope is a partially ordered set (poset) whose faces satisfy the following four axioms: (1) It has a least face and a greatest face; (2) All the flags contain the same number of faces; (3) It is strongly connected; (4) Every 1-section is a line segment. Axiom 2 is equivalent to saying that the poset is a graded poset (see below). Axiom 3 is equivalent to strong flag-connectedness, (see above). Axiom 4 is known as the “diamond property”, since the Hasse diagram of a line segment is diamond-shaped. From these axioms it results that every section is a polytope, and that $\text{rank } k(G/F) = k(G) - k(F) - 1$. Finally, an n -polytope is a polytope of rank n ; it can be fully described using vertex notation if every face has a unique set of vertices (such a polytope is called atomistic). In case of the null polytope, the least and greatest faces are the same single element.

A graded poset is a poset P with a rank function ρ satisfying the following two properties: (i) The rank function is compatible with the ordering, meaning that for every x and y , with $x < y$, implies $\rho(x) < \rho(y)$ and (ii) The rank is consistent with the covering relation of the ordering, meaning that for every x and y for which y covers x , it implies $\rho(y) = \rho(x) + 1$. The value of the rank function for an element of the poset is called its rank.

A poset is “bounded” if it has smallest and largest elements, called 0 and 1. The Euler characteristic of such a poset is defined as the integer $\mu(0,1)$, where μ is the Möbius function in the poset incidence algebra (Leinster 2008).

Every polytope has a dual, a polytope in which the partial order is reversed: the Hasse diagram of the dual is that of the original turned upside-down. In an n -polytope, each of the original k -faces maps to an $(n - k - 1)$ -face in the dual; the n -face maps to the (-1) -face. The dual of a dual is isomorphic to the original.

A polytope is self-dual if it is the same as (i.e., isomorphic to) its dual. Hence, the Hasse diagram of a self-dual polytope must be symmetrical about the horizontal axis half-way between the top and bottom. The vertex figure at a vertex V is the dual of the facet to which V maps in the dual polytope.

An abstract polytope is regular if its automorphism group acts transitively on the set of its flags. In particular, any two k -faces F, G of an n -polytope are “the same”, since there is an automorphism which maps F to G . All abstract polytopes of rank ≤ 2 are regular. This condition implies that any regular abstract polytope has isomorphic regular $(n - 1)$ -faces and isomorphic regular vertex figures. This is a weaker condition than the regularity for traditional polytopes, since the (combinatorial) automorphism group is achieved easier than the (geometric) symmetry group. For example, any abstract polygon is regular, since angles, edge-lengths, edge curvature, skewness etc. don’t exist for abstract polytopes.

Any abstract polytope may be realized as a geometrical polytope having the same topological structure. This structure has at least the same symmetry as the original abstract polytope, meaning that all the combinatorial automorphisms of the abstract polytope have been realized by geometric symmetries.

Note that the regular abstract polytopes are just special cases in the multitude of irregular polytopes. An irregular polyhedron has at most one automorphism, namely that provided by the identity permutation.

3.4 Polytope Realization

3.4.1 *P-Centered Clusters*

Body centered clusters derived from the Platonic solids are easily drawn, as shown in Fig. 3.4; their figure count is given in Table 3.2 (Parvan-Moldovan and Diudea 2015). These small clusters, excepting DP.21, were next transformed, by operations on maps (see Chap. 2), in 2-face-dual, medial and truncated derivatives (Figs. 3.5, 3.6, 3.7, and 3.8). P-centered clusters represent cell-duals of polyhedra with the same number of cells around a central one; they are objects of Euclidean 4D-space, as shown by the figure count (Tables 3.3, 3.4, 3.5, and 3.6) cf. (3.8). This idea can be extended to objects other than Platonics.

The name of clusters can be made in at least three ways, as shown in the bottom of figures and tables; the “endohedral” @ symbol was used, starting from the core and going radially, to the exterior; the suffix number counts the points/atoms in the whole structure.

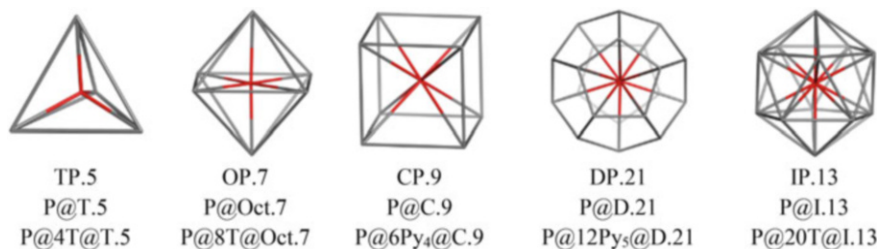


Fig. 3.4 Body centered clusters derived from the Platonic solids

Table 3.2 Figure count for clusters in Fig. 3.4

	v	e	f_3	f_5	f_6	f	c_1	c_2	c_3	M	c	χ	k	$c_n; (M)$
TP	5	10	10	0	0	10	4	0	0	1	5	0	4	T; 0; 0 (T)
OP	7	18	20	0	0	20	8	0	0	1	9	0	4	T;0;0 (O)
CP	9	20	12	6	0	18	0	6	0	1	7	0	4	0;Py ₄ ; 0 (C)
DP	21	50	30	0	12	42	0	12	0	1	13	0	4	0;Py ₅ ;0 (D)
IP	13	42	50	0	0	50	20	0	0	1	21	0	4	T; 0; 0 (I)

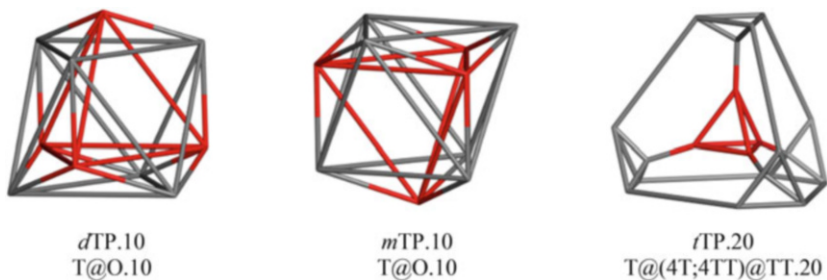


Fig. 3.5 TP-derived structures

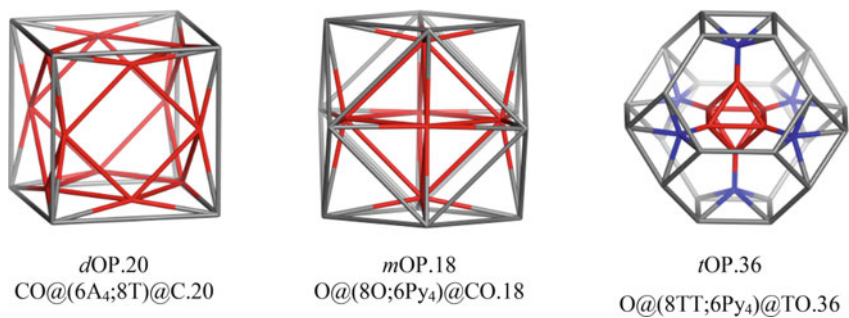


Fig. 3.6 OP-derived structures

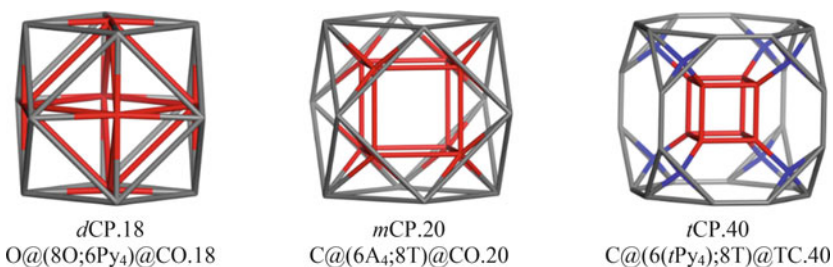


Fig. 3.7 CP-derived structures

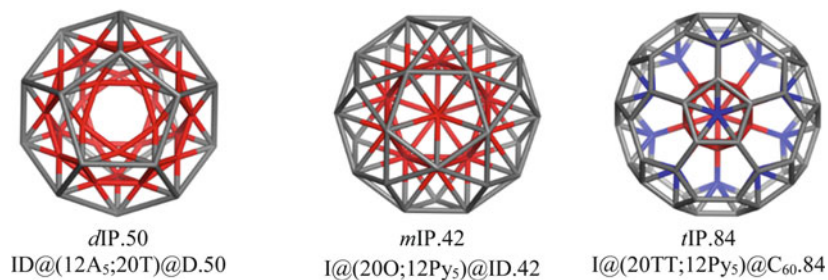


Fig. 3.8 IP-derived structures

Table 3.3 Figure count for clusters derived from TP cluster

T-structure	v	e	f	c_1	c_2	c_3	M	c	χ	k	$c_k; (M)$
TP.5	5	10	10	4	0	0	1	5	0	4	T; 0; 0 (P;T)
d TP.10	10	30	30	4	4	0	2	10	0	4	T; O = A ₃ ; 0;(T;O)
m TP.10	10	30	30	4	4	0	2	10	0	4	T; O = A ₃ ; 0 (T;O)
t TP.20	20	40	30	4	4	0	2	10	0	4	T;TT; 0; (T;TT)

Table 3.4 Figure count for clusters derived from OP cluster

O-structure	v	e	f	c_1	c_2	c_3	M	c	χ	k	$c_n; (M)$
OP.7	7	18	20	8	0	0	1	9	0	4	T;0;0 (P;O)
d OP.20	20	60	56	8	6	0	2	16	0	4	T;A ₄ ;0 (CO;C)
m OP.18	18	60	58	8	6	0	2	16	0	4	O; Py ₄ (O;CO)
t OP.36	36	78	58	8	6	0	2	16	0	4	TT;Py ₄ ;0 (O;TO)

Table 3.5 Figure count for clusters derived from CP cluster

C-structure	v	e	f	c_1	c_2	c_3	M	c	χ	k	$c_n; (M)$
CP.9	9	20	18	0	6	0	1	7	0	4	0;Py ₄ ; 0 (P;C)
d CP.18	18	60	58	8	6	0	2	16	0	4	O; Py ₄ (O;CO)
m CP.20	20	60	56	8	6	0	2	16	0	4	T;A ₄ ;0 (C;CO)
t CP.40	40	80	56	8	6	0	2	16	0	4	T; t Py ₄ ;0 (C;TC)

Table 3.6 Figure count for clusters derived from IP cluster

I-structure	v	e	f	c_1	c_2	c_3	M	c	χ	k	$c_k; (M)$
IP.13	13	42	50	20	0	0	1	21	0	4	T; 0; 0 (P; I)
d IP.50	50	150	134	20	12	0	2	34	0	4	T;A ₅ ;0 (ID.30;D.20)
m IP.42	42	150	142	20	12	0	2	34	0	4	O; Py ₅ ;0 (I;ID.30)
t IP.84	84	192	142	20	12	0	2	34	0	4	TT; Py ₅ ; 0 (I;C ₆₀)

3.4.2 Cell-in-Cell Clusters

Let now make the selective truncation of the central point in the P-clusters (see Chap. 2): it leaves unchanged the non-marked points/atoms. In this simple way, *cell-in-cell* clusters (Parvan-Moldovan and Diudea 2015) can be designed (Fig. 3.9); the figure count for these structures is listed in Table 3.7. More examples are given in Fig 3.10.

It is the time to show a lower bound for the existence of clusters in dimensions/ranks higher than three:

Theorem 3.1 A cluster of points/atoms with at least two (concentric) shells belongs to n -spaces (i.e., has a rank) of $n > 3$.

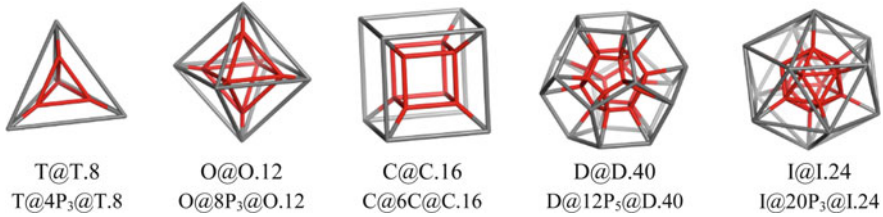


Fig. 3.9 Selectively truncated body centered clusters of the Platonic solids

Table 3.7 Figure count for selectively truncated body centered clusters $t(P@M)$; $M =$ Platonic solids

$t(P@M)$	v	e	f	c_k	M	c	χ	k	Sym	$c_n; (M)$
T@T.8	8	16	14	4	2	6	0	4	3	P ₃ (T;T)
O@O.12	12	30	28	8	2	10	0	4	4	P ₃ (O;O)
C@C.16	16	32	24	6	2	8	0	4	4	P ₄ (C;C)
D@D.40	40	80	54	12	2	14	0	4	5	P ₅ (D;D)
I@I.24	24	72	70	20	2	22	0	4	5	P ₃ (I;I)

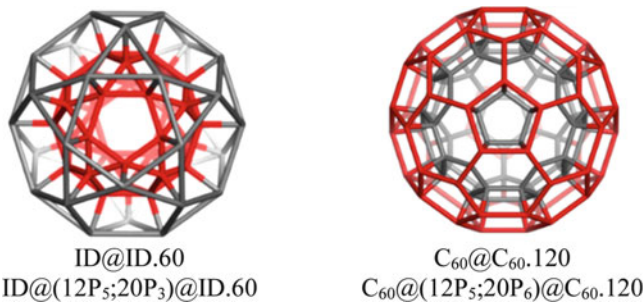


Fig. 3.10 Other “cell-in-cell” structures

Proof A polytope is convex if any of its k -facets is shared by at least two $k + 1$ -facets. In particular, for $n = 4$, $k = 2$ while $k + 1$ is a 3-facet, i.e., a cell. In other words, any 2-facet must share at least two 3-facets: the actual cell and the whole envelope. Next, the cluster is bound by 3-facets, thus the polytope is of dimension/rank $3 + 1 = 4$. This condition is already reached in P-centered clusters (Fig. 3.4; Table 3.2), as much as in the “cell-in-cell” double-shell clusters (Fig. 3.9; Table 3.7). This is a lower bound condition and the theorem is demonstrated.

At the end, two pairs of clusters are presented: $mCP.20$ & $dOP.20$ (Fig. 3.11, left) and $mDP.50$ & $dIP.50$ (Fig. 3.11, right); they illustrate the “sphere inversion” event that is equivalent to tesseract moving on the fourth dimension (i.e., the time).

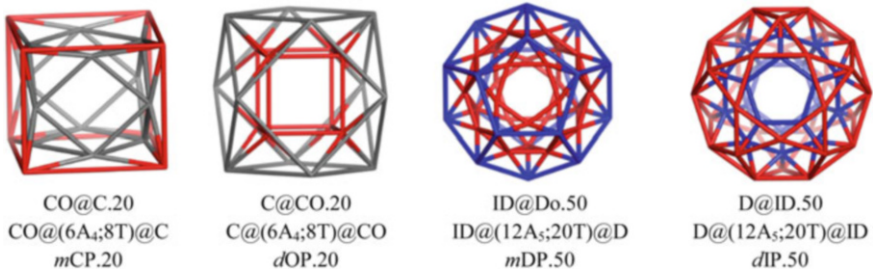


Fig. 3.11 Sphere inversion by 4D-clusters: moving on the fourth dimension

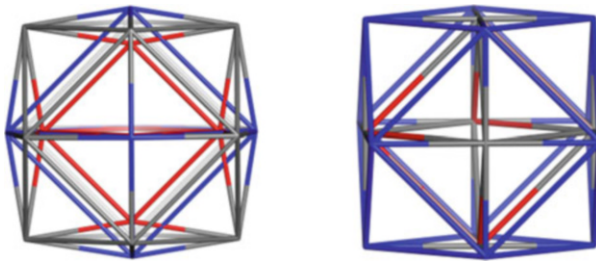


Fig. 3.12 24-Cell, realized by $d(8\text{-Cell}).24$ (left) and $m(16\text{-Cell}).24$ (right)

3.4.3 24-Cell and Its Derivatives

The regular 24-Cell 4-polytope, also known as the hyperdiamond or octaplex, consists of 24 octahedral cells, six cells meeting at each vertex; it is self-dual and has no analogue among the five Platonic solids of 3D-space.

Keeping in mind that 24-Cell has only octahedral cells and that, by operations on maps, the octahedron O may be obtained from the cube C by *dualization* dC while from the tetrahedron by the medial operation mT , this polychoron was realized starting from 8-Cell; $\{4,3,3\}$, and from 16-Cell; $\{3,3,4\}$, respectively: $d(8\text{-Cell}).24$ and $m(16\text{-Cell}).24$ (Fig. 3.12);

The 4-polytope 24-Cell is a three-colored graph and thus has a chromatic number 3 (Fig. 3.13). Its 2-face-dual (see Chap. 2): $d(24\text{-Cell}).96 = d(d(8\text{-Cell}).24).96 = (C@(6CO;8C))_2@(12CO;6C).96$ is identical to the medial transform $m(24\text{-Cell}).96 = m(d(8\text{-Cell}).24).96 = (CO@(6C;8CO))_2@(12C;6CO).96$ acting on the edges of 24-Cell, but showing a different projection (Fig. 3.14). C_{96} is a uniform 4-polytope, vertex-transitive and edge-transitive (but not faces-transitive); also it is a four-colored graph (with the chromatic number 4—Fig. 3.14). The figure count in these 4-polytopes is given in Table 3.8.

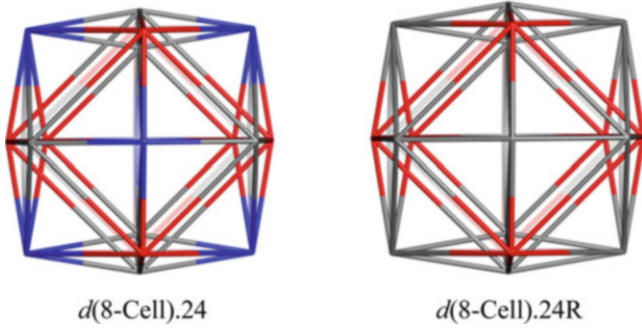


Fig. 3.13 Coloring C_{24} , a 4-polyhedral *three-colored* graph (left) and its single red-color representations (right)

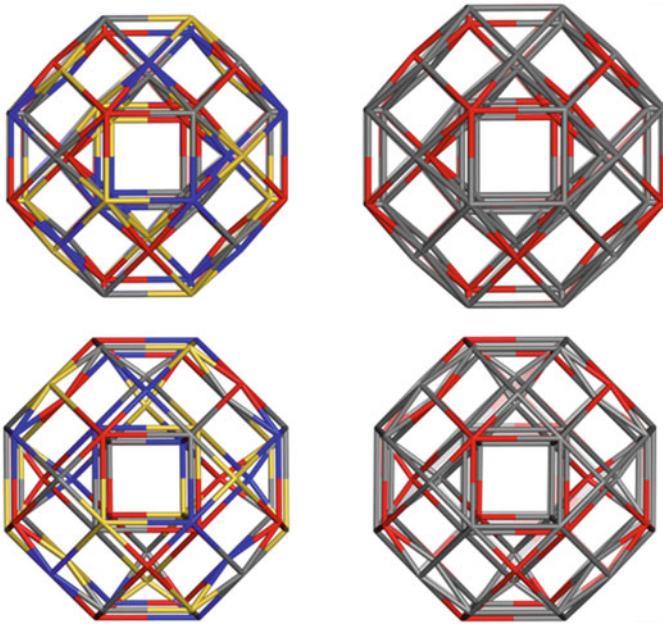


Fig. 3.14 Coloring C_{96} , a 5-polyhedral *four-colored* graph in two of its projections: $d(d(8\text{-Cell})24).96 = (C@(6CO;8C))_2@(12CO;6C).96$ (top). $m(d(8\text{-Cell})24).96 = (CO@(6C;8CO))_2@(12C;6CO).96$ (bottom) and their single red-color representations (right column)

Table 3.8 Figure count for clusters in Figs. 3.12 and 3.14 and their vertex classes

Structure	v	e	f_2	f_3	χ	k	Class
$m(16\text{-Cell}).24$	24	96	96	24^a	0	4	$1\{24\}$
$d(8\text{-Cell}).24$	24	96	96	24^a	0	4	$1\{24\}$
$m(24\text{-Cell}).96$	96	288	240	48^b	0	4	$1\{96\}$
$d(24\text{-Cell}).96$	96	288	240	48^b	0	4	$1\{96\}$

^aO
^b $24C+24CO$

References

- Balinski ML (1961) On the graph structure of convex polyhedra in n -space. *Pac J Math* 11(2): 431–434
- Buekenhout F, Parker M (1998) The number of nets of the regular convex polytopes in dimension ≤ 4 . *Discret Math* 186:69–94
- Catalan E (1865) Mémoire sur la Théorie des Polyèdres. *J de l'École Polytechnique (Paris)* 41: 1–71
- Coxeter HSM (1934) Discrete groups generated by reflections. *Ann Math* 35(3):588–621
- Coxeter HSM (1940) Regular and semi-regular polytopes. *J Math Zeit* 46:380–407
- Coxeter HSM (1973) Regular polytopes, 3rd edn. Dover, New York, NY
- Coxeter HSM (1974) Regular complex polytopes. Cambridge University Press, Cambridge
- Coxeter HSM (1982) Ten toroids and fifty-seven hemi-dodecahedra. *Geom Dedicata* 13:87–99
- Coxeter HSM (1984) A symmetrical arrangement of eleven hemi-icosahedra. *Ann Discrete Math* 20:103–114
- Coxeter HSM, Longuet-Higgins MS, Miller JCP (1954) Uniform Polyhedra. *Phil Trans A*, 403–439.
- Cromwell PR (1997) Polyhedra. Cambridge University Press, Cambridge
- Davis MW (2007) The geometry and topology of coxeter groups, London Mathematical Society monographs series, vol 32. Princeton University Press, Princeton, NJ
- de la Vaissière B, Fowler PW, Deza M (2001) Codes in Platonic, Archimedean, Catalan, and related polyhedra: a model for maximum addition patterns in chemical cages. *J Chem Inf Comput Sci* 41:376–386
- Euler L (1736) Solutio problematis ad geometriam situs pertinentis. *Comment Acad Sci I Petropolitanae* 8:128–140
- Euler L (1752–1753) Elementa doctrinae solidorum. *Novi Comment Acad Sci I Petropolitanae* 4:109–160
- Grünbaum B (2003) Convex polytopes. In: Kaibel V, Klee V, Ziegler GM (eds) Graduate texts in mathematics, vol 221, 2nd edn. Springer, New York, NY
- Grünbaum B (2009) Elemente der Mathematik 64 (3):89–101; Reprinted in Pitici M (ed) (2011) The best writing on mathematics 2010. Princeton University Press, pp 18–31
- Grünbaum B, Shephard GC (1988) Duality of polyhedra. In: Senechal M, Fleck GM (eds) Shaping space – a polyhedral approach. Birkhäuser, Boston, MA, pp 205–211
- Heath TL (1981) A history of Greek mathematics. Dover, New York, NY
- Johnson NW (1966) Convex solids with regular faces. *Can J Math* 18:169–200 (The theory of uniform polytopes and honeycombs. Ph.D. Dissertation, University of Toronto)
- Leinster T (2008) The Euler characteristic of a category. *Doc Math* 13:21–49
- Lyusternik LA (1963) Convex figures and polyhedra. Dover, New York, NY
- McMullen P, Schulte P (2002) Abstract regular polytopes, 1st edn. Cambridge University Press, Cambridge
- Parvan-Moldovan A, Diudea MV (2015) Cell@cell higher dimensional structures. *Stud Univ Babeş-Bolyai Chem* 60(2):379–388
- Schläfli L (1901) Theorie der vielfachen Kontinuität Zürcher und Furrer, Zürich (Reprinted in: Ludwig Schläfli, 1814–1895, Gesammelte Mathematische Abhandlungen, Band 1, 167–387, Verlag Birkhäuser, Basel, 1950)
- Schulte E (1980) Regular incidence complexes. PhD Dissertation, Dortmund University
- Schulte E (1983a) Reguläre Inzidenzkomplexe, II. *Geom Dedicata* 14:33–56
- Schulte E (1983b) Reguläre Inzidenzkomplexe, III. *Geom Dedicata* 14:57–79
- Schulte E (1983c) On arranging regular incidence-complexes as faces of higher-dimensional ones. *Eur J Comb* 4:375–384
- Schulte E (1985) Regular incidence-polytopes with Euclidean or toroidal faces and vertex-figures. *J Comb Theory Ser A* 40(2):305–330

- Schulte E (2004) Symmetry of polytopes and polyhedra. In: Goodman JE, O'Rourke J (eds) Handbook of discrete and computational geometry, 2nd edn. Chapman & Hall, New York, NY
- Schulte E (2014) Polyhedra, complexes, nets and symmetry. *Acta Crystallogr A* 70:203–216
- Skilling J (1975) The complete set of uniform polyhedra. *Philos Trans R Soc Lond Ser A Math Phys Sci* 278(1278):111–135
- Sopov SP (1970) Proof of the completeness of the enumeration of uniform polyhedra. *Ukrain Geom Sbornik* 8:139–156
- Steinitz E (1922) Polyeder und Raumeinteilungen, *Encyclopädie der mathematischen Wissenschaften*, Band 3 (Geometries) (IIIAB12), pp 1–139, Abgeschlossen am 31 August 1916
- Tits J (1964) Algebraic and abstract simple groups. *Ann Math 2nd Ser* 80(2):313–329
- Tits J, Weiss RM (2002) Moufang polygons. Springer monographs in mathematics. Springer, Berlin
- Wenninger M (1974) Polyhedron models. Cambridge University Press, Cambridge
- Wenninger M (1983) Dual models. Cambridge University Press, Cambridge
- Ziegler GM (1995) Lectures on polytopes, graduate texts in mathematics 152. Chap. 4 “Steinitz’ theorem for 3-polytopes”. Springer, Berlin, p 103

Chapter 4

Symmetry and Complexity

Symmetry (from Greek *συμμετρία* *symmetria* “agreement in dimensions, due proportion, arrangement”) commonly refers to harmony of proportions in realization of a composition (Hargittai and Hargittai 2010). The simplest symmetry is the mirror symmetry. In Mathematics, symmetry refers to some operations acting on geometric or other regularities of a mathematical object that leave the object invariant.

While the classical, geometric symmetry is involved/reflected in several molecular properties, such as dipole moments, IR vibrations, ^{13}C -NMR signals etc., *topological symmetry*, defined in terms of *connectivity*, is addressed to constitutive aspects of a molecule and is involved in its synthesis and/or its structure elucidation.

Complexity refers to the state or quality of being complex/intricate/complicated, or being the union/organization of some interacting (by some rules) parts/organs. There is no unique definition of complexity, the notion being conveyed rather by using particular examples. It is popular the computational complexity, looked on the ground of working time, memory or other resources involved in solving a given problem. Time and space are two of the most important criteria when problems of complexity are analyzed.

A hierarchical complexity is also considered; it is orthogonal to the usual forms of complexity, which may be called horizontal complexity.

Structural complexity is addressed to the organization of matter. It is studied by the aid of graphs associated to molecules/ions/crystals, on which basis several descriptors are calculated. Among these, entropy, information measures and topological indices are the most popular (Dehmer et al. 2011, 2013; Dehmer and Mowshowitz 2011; Dehmer and Grabner 2013; Diudea et al. 2010).

Topological symmetry speaks about structural complexity by considering the type of atoms/vertices and their reciprocal distribution. Other characteristics, including metrics, posets, packing, etc. may give information about the complexity of matter (or abstract graphs, in general).

Genus and rank (or space dimension) of a structure are parameters of complexity acting by means of Euler characteristic of the embedding surface.

This chapter gives a summary introduction to: (i) Euler characteristic; (ii) Topological symmetry; (iii) Centrality index; (iv) Ring signature index and (v) Euler characteristic, as reflected in pairs of map operations.

4.1 Euler Characteristic

An embedding is a representation of a graph on a surface such that no edge-crossing occurs (Harary 1969). A polyhedral graph, embedded in an orientable surface S obeys the Euler's formula (Euler 1752–1753)

$$v - e + f = \chi(S) \quad (4.1)$$

where $\chi(S)$ is the Euler characteristic. It can be calculated from the genus g (i.e., the number of simple tori composing that surface) by Poincaré formula

$$v - e + f = \chi(S) = 2(1 - g) \quad (4.2)$$

The Euler characteristic of a closed non-orientable surface can be calculated from its non-orientable genus n (the number of real projective planes in a connected sum decomposition of the surface or the number of cross-caps needed to be attached to the sphere to make it homeomorphic to that surface) as

$$\chi = 2 - n \quad (4.3)$$

A surface is orientable, when it has two sides, or it is non-orientable, when it has only one side, like the Möbius strip. Positive/negative χ -values indicate positive/negative curvature of that embedding. Curvature (see Diudea and Nagy 2007) is the amount by which a geometric object deviates from the planarity; it is usually measured as the Gaussian curvature K (*Gauss–Bonnet* theorem—Bonnet 1853)

$$\int_S K dS = 2\pi\chi \quad (4.4)$$

A combinatorial curvature was also proposed (Higuchi 2001; Klein 2002; Devos and Mohar 2007).

A discrete analog of the Gauss–Bonnet theorem is due to Descartes; it shows that the overall angular defects (i.e., disclinations), measured in full circles, equals the Euler characteristic of the polyhedron P

$$\sum_p \varphi_p = 2\pi\chi \quad (4.5)$$

Euler characteristic is a topological invariant, a single number that describes the shape of a structure regardless of its tiling; it is denoted by χ (small Greek “chi”)

and makes the subject of study in algebraic topology, polyhedral combinatorics, crystallography and many other mathematical fields (Epstein 2016).

Euler characteristic, named after Leonhard Euler, was originally defined for polyhedra and used to check the consistency of a proposed structure. Any convex polyhedron can be represented in the plane by a 3-connected [planar graph](#) (also called a [polyhedral graph](#)). The number of vertices v , edges e , and faces f of a convex polyhedron are related by the Euler's [polyhedron formula](#) (4.1) in which case $\chi = 2$ (Euler characteristic of the sphere). The surface of nonconvex polyhedra may have various χ -values.

Euler characteristic can be calculated for general surfaces as the alternating sum of figures of dimension/rank k (Schulte 1985, 2014)

$$\chi(S) = f_0 - f_1 + f_2 - f_3 + \dots, \quad (4.6)$$

by finding a polygonization of the surface; in (4.6) f_0 is a vertex, f_1 is an edge, f_2 is a face, f_3 is a cell $\dots f_k$ being a facet of rank k ; a structure will have the rank k if it is closed by substructures/facets of rank $k - 1$ and obey relation (4.6); in case $S = \text{sphere}$, 2 and 0 alternates for odd and even ranks, respectively.

4.2 Topological Symmetry

Let $G = (V, E)$ and $G^\wedge = (V^\wedge, E^\wedge)$ be two graphs and a function f , mapping the vertices of V onto the vertices belonging to the set V^\wedge , $f: V \rightarrow V^\wedge$. That is, the function f makes a one-to-one correspondence between the vertices of the two sets. The two graphs are called *isomorphic*, $G \approx G^\wedge$, if there exists a mapping f that preserves the graph adjacency (i.e., if $(i, j) \in E$, then $(f(i), f(j)) \in E^\wedge$). An isomorphism of a graph with itself is called an automorphism.

Let the mapping be a permutation P ; the permutation that leaves the graph unchanged is called the *permutation identity*. There exists at least one automorphism, namely that provided by the permutation identity.

An *isomorphism* can be expressed as $A(G) = P^{-1}A(G^\wedge)P$; since P is orthogonal, one can write the transpose instead of the inverse matrix $A(G) = P^T A(G^\wedge)P$; in case of an *automorphism*, relation becomes: $A(G) = P^T A(G)P$. The all automorphisms of a graph form a group $Aut(G)$ (Razinger et al. 1993; Balasubramanian 1994). Given a graph $G = (V, E)$ and a group $Aut(G)$, two vertices, $i, j \in V$ are called *equivalent* if there is a group element, $aut(v_i) \in Aut(G)$, such that $j = aut(v_i)(i)$ (in other words, there exists an automorphic permutation that transforms one vertex to the other). The set of all vertices j obeying the *equivalence relation* is called the *orbit of vertex i* , V_i (or automorphic partition, or also, class of equivalence). Vertices belonging to the same equivalence class cannot be differentiated by graph-theoretical parameters. If V_1, V_2, \dots, V_m are the m disjoint *automorphic partitions* of the vertex set $|V(G)| = v_1 + v_2 + \dots + v_m$, then: $V = V_1 \cup V_2 \cup \dots \cup V_m$ and $V_i \cap V_j = \emptyset$.

Consider a vertex invariant, $In = In_1, In_2, \dots$ which assigns a value In_u to vertex u . Two vertices, u and v , with $In_u = In_v$, belong to the same *invariant class IC*. However, the invariant classes may differ to the orbits of automorphism since no vertex invariant is known so far to discriminate any two non-equivalent vertices in any graph. The classes of vertices are eventually *ordered* according to some rules (e.g., according to their centrality).

4.3 Centrality Index

A layer matrix (Diudea 1994) is built up on layer $(H(i)_j)$ partition of a vertex i in the graph $H(V,E)$:

$$H(i) = \left\{ H(i)_j, j \in [0, 1, \dots, ecc_i] \text{ and } v \in H(i)_j \Leftrightarrow d_{iv} = j \right\}$$

where ecc_i is the eccentricity of i (i.e., the largest distance from i to the other vertices of the graph).

The entries in a layer matrix, LM , collect the vertex property p_v (a topological, chemical, or physical property) for all the vertices v belonging to the layer $H(i)_j$, located at distance j from vertex i .

$$[LM]_{ij} = \sum_{v \in H(i)_j} p_v$$

The matrix LM is defined as a collection of these entries, over the diameter of the graph $d(H)$:

$$LM(H) = \left\{ [LM]_{ij}; i \in V(H); j \in [0, 1, \dots, d(H)] \right\}$$

The dimensions of the matrix are $n \times (d(H) + 1)$; the zero-distance column is just the column of vertex properties. The most simple property collected in a layer matrix is the vertex counting. Other topological properties, like distances in the graph or the number of rings around each vertex are more informative.

Similarly, the entries in the shell matrix, ShM , collect the property of a vertex pair (e.g., that given by the square info matrix M):

$$[ShM]_{ij} = \sum_{v \in H(i)_j} [M]_{i,v}$$

The shell matrix is the collection of the above defined entries:

$$ShM(H) = \left\{ [ShM]_{ij}; i \in V(H); j \in [0, 1, \dots, d(H)] \right\}$$

A shell matrix ShM will partition the entries of the square matrix according to the vertex (distance) partitions in the graph. The zero column entries $[ShM]_{i,0}$ may be the diagonal entries in the info matrix.

Layer (and Shell) matrices are used to derive the indices of centrality $C(LM)$, that quantify the centrality of vertices (Diudea and Ursu 2003).

$$c_i(LM) = \left[\sum_{k=1}^{ecc_i} \left([LM]_{ik}^{2k} \right)^{1/(ecc_i)^2} \right]^{-1} \quad (4.7)$$

4.4 Ring Signature Index

Ring Signature Index RSI collects the rings around the vertices of a network, and is defined (Nagy and Diudea 2017) as follows:

$$P(x)_i = \sum_s s \cdot x^{k_s} \quad (4.8)$$

$$RS_i = P'_i(1)/P_i(1) \quad (4.9)$$

$$RSI = (1/qv) \sum_i RS_i \quad (4.10)$$

In the above Eq. (4.8), $P(x)_i = \sum_s s \cdot x^{k_s}$ is the polynomial of “ring occurrence” or the ring signature, with s being the size of a “strong” ring (Blatov et al. 2010) occurring k_s -times around each vertex i . Then, RS_i calculates a “mean ring signature” as the ratio (in $x = 1$) of the first derivative to the “zero” derivative of the ring occurrence polynomial [see (4.9)]. The summation of RS_i over all vertices i is further mediated (4.10) to the number of vertices and to the number of vertex equivalence classes q of the whole structure. A descriptor involving vertex equivalence classes was earlier proposed by Graovac and Pisanski (1991).

The ring notion may be extended to “circuit” notion, to get a “zoom” on the topology of the network.

Proposition 4.1 At the same occurrence k , the mean ring signature RS_i is an integer number, irrespective of the ring size.

The proof comes from the RS_i definition, as follows: denote by k_{s1} and k_{s2} the (integer number) occurrence of two rings around a vertex, of size s_1 and s_2 ; since $k_{s1} = k_{s2} = k$ (same occurrence), then:

$$RS_i = (s_1 \cdot k_{s1} + s_2 k_{s2}) / (s_1 + s_2) = k(s_1 + s_2) / (s_1 + s_2) = k \quad (4.11)$$

Proposition 4.2 Isohedral graphs show integer RS_i since they have a single ring type (i.e., are face transitive) and a single occurrence number:

$$RS_i = sk/s = k \quad (4.12)$$

Proposition 4.3 There exist graphs that show different occurrence for the same ring size; in such a case, RS_i may be non-integer, according to the parity of occurrence numbers sum:

$$RS_i = (s \cdot k_1 + s \cdot k_2)/2s = s(k_1 + k_2)/2s = (k_1 + k_2)/2 \quad (4.13)$$

The statements (4.11, 4.12, and 4.13) were formulated for isohedral (and isogonal, i.e., vertex transitive) graphs, where $q = 1$ and $RS_i = RSI$. However, isohedral graphs are not always isogonal: the Catalan solid graphs (which are duals to Archimedean) are all face-transitive but not vertex-transitive. In vertex non-transitive structures, $q > 1$ and the global index RSI may be a non-integer number, according to the numbers parity.

Theorem 4.4 *The upper bound of ring signature index RSI can be combinatorially calculated from the vertex degree by $\binom{Deg}{2}$; this is reached in isohedral and isogonal graphs with no self-intersection of strong rings.*

Demonstration comes from the above propositions, basically from proposition 4.2. It is well-known that the maximum number of rings around a vertex equals the combination of the number of its connections (i.e., degrees, Deg - Harary 1969; Diudea et al. 2002) taken two. This is the case described by Eq. (4.12): $RS_{i,max} = k_{max} = \binom{Deg}{2}$. However, some isohedral graphs can be seen as “networks” (i.e., with rings that intersect to each other), like Icosahedron I, Octahedron O, 16-Cell, 24-Cell, etc.; in such cases, the set of connections is split, at least in two subsets (for which, e.g., $Deg = Deg_1 + Deg_2$) and, because $\binom{Deg}{2} > \binom{Deg_1}{2} + \binom{Deg_2}{2}$, the maximum value of RS_i is less than k_{max} (see Table 4.1, e.g., 24-Cell_net). The case $Deg_1 = Deg_2$ recovers the case of Eq. (4.11), with $RS_i = k < k_{max}$. Since the isogonal graphs have only one vertex orbit ($q = 1$), it means that $RS_i = RSI$ and the theorem is demonstrated. Maximal RSI values are found in Dodecahedron D, Tetrahedron T or the Hypercube Q_n . The case (4.13) is found in the “spongy-hypercube” (Sect. 11.4): since here $k_1 + k_2 = k_{max}$, then $RS_i = \binom{Deg}{2}/2$, in words, RS_i equals the half of the upper bound value. Data in Table 4.1 and in the following ones support the above theorem.

Table 4.1 Ring signature index RSI in some cells and nets

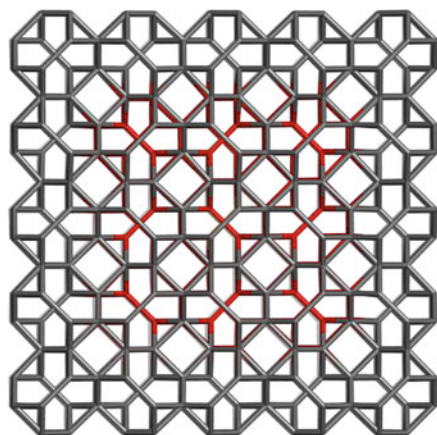
Structure	v	v_i	q	Deg	Ring signature	RSI	$\binom{Deg}{2}$
D	20	20	1	3	5^3	3	3
I	12	12	1	5	3^5	5	10
C	8	8	1	3	4^3	3	3
O	6	6	1	4	3^4	4	6
T	4	4	1	3	3^3	3	3
I_net	12	12	1	5	$3^5.5^5$	5	10
O_net	6	6	1	4	$3^4.4^2$	2.857	6
16-Cell	8	8	1	6	3^{12}	12	15
16-Cell_net	8	8	1	6	$3^{12}.4^3$	6.857	15
24-Cell	24	24	1	8	3^{12}	12	28
24_Cell_net	24	24	1	8	$3^{12}.4^{12}$	12	28
C ₆₀	60	60	1	3	$5^1.6^2$	1.546	3

4.4.1 Ring Signature in a Translational Network

Structure elucidation in Chemistry in general, and particularly in Crystallography, makes appeal of instrumental techniques but also of theoretical tools. In this respect, RSI would be of real interest in classification of networks, both radial and translational and in an accurate description of complex molecular/ionic structures.

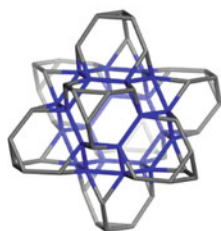
The network focused on hereafter was built starting from the Octahedron by stellation st , followed by truncation t , operations resulted in the cluster $C_{72}A = 24@TT.222.72$, of which shapes are detailed as $TO@(8TT;6HCO).72$ (see Fig. 4.1). (For map operations, the reader is invited to consult Chap. 2, this book). The name of clusters is written in a “shell-in-shell” manner (Diudea 2013; Diudea et al. 2014), starting with the core (symbolized either by the shortened names of the consisting shape: TT = truncated Tetrahedron; TO = truncated Octahedron; CO = Cuboctahedron, or by the number of atoms of that shape) endohedrally @ included into the next (outer) shell(s), then suffixed by the number of atoms in the whole structure. The net is made by self-assembly of TT (by “face-to-face” gluing/identification), which is reflected in the name we gave to this net: $C_{72}@TT$, delimited as a cubic domain, e.g., $C_{72}@TT.222.72$, where “222” means $2 \times TT$ along the directions of translation. According to the map operations used to draw this network, it is named: $t(st(O))72@TT$. The letter “A” in the name specifies the “net” while “B” denotes the “co-net”, net/co-net being interchangeable; the letter “H” in the front of shape symbols means “half”, used to avoid fractional numbers in the name of clusters.

The network $C_{72}@TT$ (crystallographic synonyms: UB12, sqc7309, 5/3/c4; Tiling: $2TT + CO + TO$; Space Group: $Fm\bar{3}m$ (<http://rcsr.net/nets/ubt>), is a

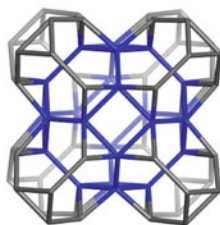


$C_{216}@TT.555.900$

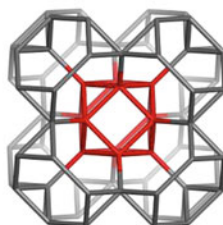
Class 1: $3^2.4^2.6^6$; | {216} | deg = 5 |; RSI=3.84615
(uninodal); (Selection 216/900)



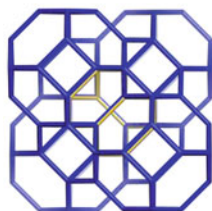
$24@8TT.72$
 $t(st(O)).72$



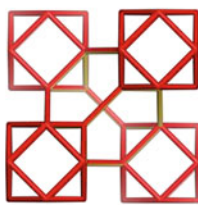
$C_{72}A=24@TT.222.72$
 $TO@(8TT;6HCO).72$



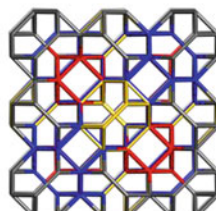
$C_{72}B=12@TT.222.72$
 $CO@(8TT;6HTO).72$



$TT@4TO.84$



$TT@4CO.48$



$C_{216}=C_{72}@TT.333.216$
 $TT@(4TO;4CO;6TT)@(8TT;12T)$

Fig. 4.1 Network $C_{72}@TT$ with a selection $C_{216}@TT.555.900$ and its substructures (*bottom*). Its three shapes are: TT (truncated Tetrahedron) = $[3^4.6^4]$; TO (truncated Octahedron) = $[4^6.6^8]$ and CO (Cuboctahedron) = $[3^8.4^6]$; “H” means “half”. Tiling signature: $TT@(4TO;4CO;6TT)$; $TO@(6CO;8TT)$; $CO@(6TO;8TT)$

Table 4.2 Ring signature index RSI in $C_{72}A = 24@TT.222.72$ and $C_{72}B = 12@TT.222.72$ clusters

	Structure	v	v_i	q	Deg	Ring signature	RSI
1	$TO_{sel}@TT.444.480$	24	24	1	5	$3^2.4^2.6^6$	3.846
2	$C_{72}A_{sel}@TT.444.480$	72	72	1	5	$3^2.4^2.6^6$	3.846
3	$C_{72}A$	72	24 48	2	5 3	$3^2.4.6^4$ 3.6^2	0.992
4	$C_{72}A@TT.480$	480	24 168 96 192	4	5 5 5 3	$3^2.6^4$ $3^2.4^2.6^6$ $3^2.4.6^4$ 3.6^2	0.676
5	$CO_{sel}@TT.444.480$	12	12	1	5	$3^2.4^2.6^6$	3.846
6	$C_{72}B_{sel}@TT.444.480$	72	72	1	5	$3^2.4^2.6^6$	3.846
7	$C_{72}B$	72	12 12 48	3	5 5 3	$3^2.6^4$ $3^2.4^2.6^6$ 3.6^2	0.769
8	$C_{72}B@TT.480$	480	12 156 120 192	4	5 5 5 3	$3^2.6^4$ $3^2.4^2.6^6$ $3^2.4.6^4$ 3.6^2	0.664

uninodal one, of degree five, with the topology (ring signature): $3^2.4^2.6^6$; we added the value of RSI corresponding to this vertex symbol ($RSI = 3.846$, see Table 4.2), that reflects its high topological symmetry (e.g., a single vertex/atom equivalence class—Nagy and Diudea 2017; Diudea et al. 2013; Ştefu et al. 2015). The ring signature was obtained by selecting the $C_{72}@TT.333.216$ (that contains the three shapes of the net: TT, TO and CO) within a larger domain, e.g., $C_{216}@TT.555.900$.

4.4.2 Ring Signature in Spongy Structures of Higher Rank

In describing the network $C_{72}@TT$ (i.e., sqc7309, <http://rcsr.net/nets/ubt>) assumed E_2 for the two classes of edges and no specification about faces/rings. To verify this result, we applied to $C_{72}@TT$ the “medial” m operation thus resulting the net $m(C_{72})132@mTT$ (Fig. 4.2, left). A “spongy” version $m(C_{72})132X@mTTX$ (Fig. 4.2, right) was obtained by the “Open” op map operation applied to the initial medial. The both nets show two classes of vertices, corresponding to the parent edges; RSI data and the tiling signatures are given in Fig. 4.2.

Then, the face-dual operation applied to $C_{72}@TT$ resulted in $d(C_{72})70@dTT$ net (Fig. 4.3). This new net consists in three classes of vertices with the populations: $\{36\}$; $\{108\}$ and $\{108\}$, in the selection $dC_{216}.252@dTT.555.1240$, the same as the faces in the parent cluster C_{216} (squares, triangles and hexagons, respectively).

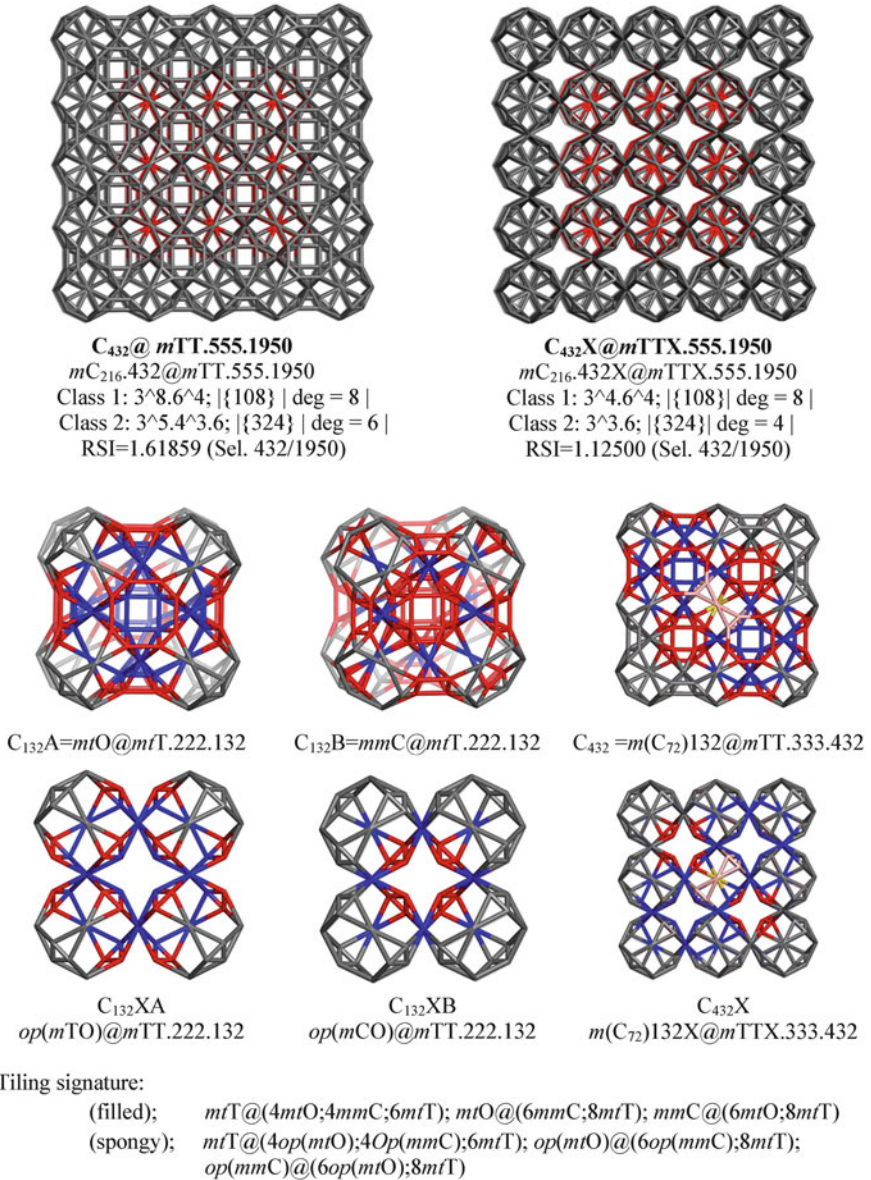
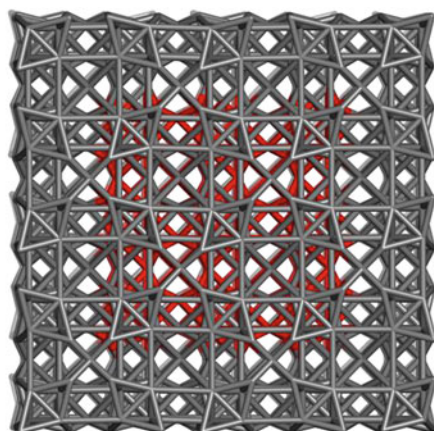


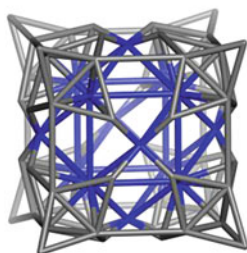
Fig. 4.2 Medial nets $m(C_{72})132@mTT$ of the parent $C_{72}@TT$ net, with their selections $C_{432}X@mTTT.555.1950$ ($X = op$, for the spongy medial net) and their substructures (*bottom*)

Figure count in the clusters C_{216} and C_{432} (and their substructures) confirmed their assigned structure and the rank $k = 4$ (Tables 4.3 and 4.4). Interestingly, the cluster $C_{432}X$ accounts for the rank $k = 5$, being bound by eight subunits of $k = 4$ (Table 4.5).

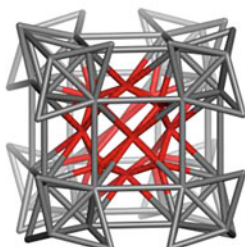


$dC_{216.252}@dTT.555.1240$

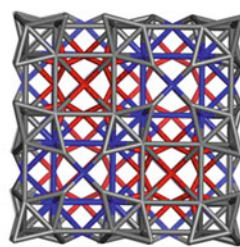
Class 1: $3^8.4^4$; $\{36\}$ (squares) | deg = 8 |
 Class 2: $3^6.4^3$; $\{108\}$ (triangles) | deg = 6 |
 Class 3: $3^4.18.4^6$; $\{108\}$ (hexagons) | deg = 12 |
 RSI=2.47619 (Selection 252/1240)



C_{70A}
 $dC72A=dTO@dTT.222.70$



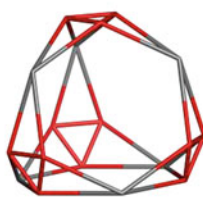
C_{70B}
 $dC72B=dCO@dTT.222.70$



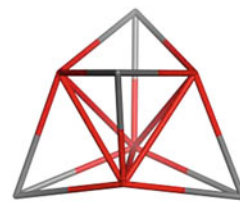
C_{252}
 $dC216.252=dTT.333.252$



$TT.12$
 $[12(3.6^2)]$



$mTT.18$
 $[12(3^3.6)+6(3^2.6^2)]$



$dTT.8 = stT.8$
 $[4(3^3)+4(3^9)]$

Fig. 4.3 Network $d(C_{72})70@dTT$ with a selection $C_{252}@dTT.555.1240$ and its substructures (bottom)

Table 4.3 Figure count in C_{216} and its relatives

Structure	v	e	3(2)	4(2)	6(2)	2	3	χ	k
C_{216}	216	432	108	36	108	252	36	0	4
C_{72A}	72	132	32	6	32	70	10	0	4
C_{72B}	72	132	32	6	32	70	10	0	4

Table 4.4 Figure count in $mC_{216} = C_{432}$ and its relatives

Structure	v	e	3(2)	4(2)	6(2)	2	3	χ	k
mC_{216}	432	1188	648	144	108	900	144	0	4
C_{132A}	132	336	176	30	32	238	34	0	4
C_{132B}	132	336	176	30	32	238	34	0	4

Table 4.5 Figure count in $mC_{216}X$ and its spongy relatives

Structure	v	e	3(2)	6(2)	2	3	4	χ	g	k
$mC_{216}X$	432	972	432	108	540	28	8	-20	11	5
C_{132A}	132	288	128	32	160	8	0	-4	3	4
C_{132B}	132	288	128	32	160	8	0	-4	3	4

4.4.3 Ring Signature in Spongy Hypercubes

Hypercube Q_n is an n -dimensional analogue of the Cube C ($n = 3$), also called an n -cube. It is a regular graph of degree n , according to Balinski (1961) theorem. The graph of Hypercube may be drawn by the Cartesian product of n edges: $(P_2)^{\square n} = Q_n$. The n -cube is written by the Schläfli (1901) symbols as $\{4, 3^{n-2}\}$.

Let now take a graph $G(v)$ of a 3-connected polyhedron on v -vertices and make n -times the Cartesian product with an edge; the operation results in a “spongy hypercube” $G(v, Q_n) = G(v) \square^n P_2$. On each edge of the original polyhedral graph, a local hypercube Q_n will evolve; it means that, in a spongy hypercube, the original 2-faces will not be counted. Figure 4.4 illustrates such spongy hypercubes, embedded in the Cube and Dodecahedron, respectively. More precisely, the “spongy hypercube” is the union of the original polyhedron and the hypercubes developed on each edge of the parent polyhedral graph $G(v)$.

The RSI descriptor can be calculated both in hypercube Q_n and in spongy-hypercube $C(Q_n)$, as shown in Table 4.6. For spongy hypercubes, embedded in Platonic polyhedral and in C_{60} , the values of this index are given in Table 4.7.

4.4.4 Truncation Operation

Let $H = (V, E)$ be a simple graph with the vertex set V and edge set E . A perfect matching M of a simple graph H having an even number of vertices $|V(H)| = 2h$ is a

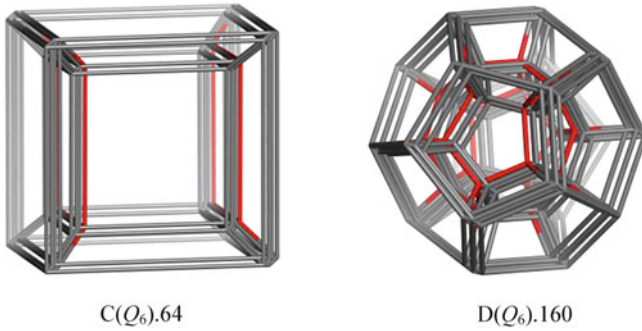


Fig. 4.4 Spongy hypercubes: cubic $C(Q_6)$ (top, left) and dodecahedral $D(Q_6)$ (top right) and their parents (bottom)

Table 4.6 Ring signature index RSI in Hypercube Q_n and its spongy view $C(Q_n)$

v	Deg	n	Q_n			$C(Q_n)$	
			Ring signature	RSI	$\binom{Deg}{2}$	Ring signature	RSI
8	3	3	4^3	3	3	4^3	3
16	4	4	4^6	6	6	$4^3 \cdot 4^3$	3
32	5	5	4^{10}	10	10	$4^7 \cdot 4^3$	5
64	6	6	4^{15}	15	15	$4^{12} \cdot 4^3$	7.5
128	7	7	4^{21}	21	21	$4^{18} \cdot 4^3$	10.5
256	8	8	4^{28}	28	28	$4^{25} \cdot 4^3$	14

subset $E(M) \subset E(H)$ of its h pairwise nonincident edges covering all vertices of H . Similarly, a cycle cover C is a set of disjoint cycles covering all vertices of H , $E(C) \subset E(H)$. Note that, in general, not every graph has M and/or C . In a simple cubic graph, the two subsets of edges are disjoint and complementary: $E(M) \cap E(C) = \emptyset$ and $E(M) \cup E(C) = E(H)$, meaning their union contains all the edges of H . These notions are illustrated in Fig. 4.5.

There is a result (Diudea and Rosenfeld 2017), stating that: a necessary and sufficient condition for a simple cubic graph G to be isomorphic to the truncation $t(H)$ of a simple cubic graph H is that G to have a cyclic cover C of which all components are triangles (Fig. 4.5). The above result may be extended to a simple graph with all the vertices of degree d : the cyclic cover will consist of disjoint d -fold cycles. If the graph has vertices of different degree d_k , the cyclic cover will be the union of d_k -fold cycles.

In a multi-shell polyhedral graph, the internal vertices of degree four are transformed by truncation in tetrahedra. When applied on hypercubes Q_n , truncation replaces any parent vertex in Q_n by a simplex S_{n-1} (Coxeter 1973, 1974; Buekenhout and Parker 1998) and these all trigonal substructures are disjoint while

Table 4.7 Ring signature RSI in Platonic polyhedral and C_{60} spongy hypercube

Structure: [n]	v	Deg	Ring signature	RSI	$\binom{Deg}{2}$
$D(Q_n)$;	20	3	$5^{\wedge}3$	3	3
[2]	40	4	$4^{\wedge}3.5^{\wedge}3$	3	6
[3]	80	5	$4^{\wedge}7.5^{\wedge}3$	4.777778	10
[4]	160	6	$4^{\wedge}12.5^{\wedge}3$	7	15
[5]	320	7	$4^{\wedge}18.5^{\wedge}3$	9.666667	21
$I(Q_n)$;	12	5	$3^{\wedge}5$	5	10
[2]	24	6	$3^{\wedge}5.4^{\wedge}5$	5	15
[3]	48	7	$3^{\wedge}5.4^{\wedge}11$	8.428571	21
[4]	96	8	$3^{\wedge}5.4^{\wedge}18$	12.428571	28
[5]	192	9	$3^{\wedge}5.4^{\wedge}26$	17	36
$C(Q_n)$;	8	3	$4^{\wedge}3$	3	3
[2]	16	4	$4^{\wedge}3.4^{\wedge}3$	3	6
[3]	32	5	$4^{\wedge}7.4^{\wedge}3$	5	10
[4]	64	6	$4^{\wedge}12.4^{\wedge}3$	7.5	15
[5]	128	7	$4^{\wedge}18.4^{\wedge}3$	10.5	21
$O(Q_n)$;	6	4	$3^{\wedge}4$	4	6
[2]	12	5	$3^{\wedge}4.4^{\wedge}4$	4	10
[3]	24	6	$3^{\wedge}4.4^{\wedge}9$	6.857143	15
[4]	48	7	$3^{\wedge}4.4^{\wedge}15$	10.285714	21
[5]	96	8	$3^{\wedge}4.4^{\wedge}22$	14.285714	28
$T(Q_n)$	4	3	$3^{\wedge}3$	3	3
[2]	8	4	$3^{\wedge}3.4^{\wedge}3$	3	6
[3]	16	5	$3^{\wedge}3.4^{\wedge}7$	5.28571	10
[4]	32	6	$3^{\wedge}3.4^{\wedge}12$	8.14286	15
[5]	64	7	$3^{\wedge}3.4^{\wedge}18$	11.57143	21
$C_{60}(Q_n)$;	60	3	$5.6^{\wedge}2$	1.545455	3
[2]	120	4	$4^{\wedge}3.5.6^{\wedge}2$	1.933333	6
[3]	240	5	$4^{\wedge}7.5.6^{\wedge}2$	3	10
[4]	480	6	$4^{\wedge}12.5.6^{\wedge}2$	4.333331	15
[5]	960	7	$4^{\wedge}18.5.6^{\wedge}2$	5.933338	21

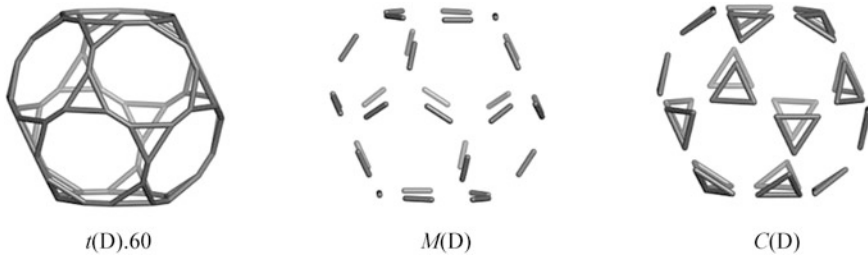


Fig. 4.5 Truncation of the dodecahedron D

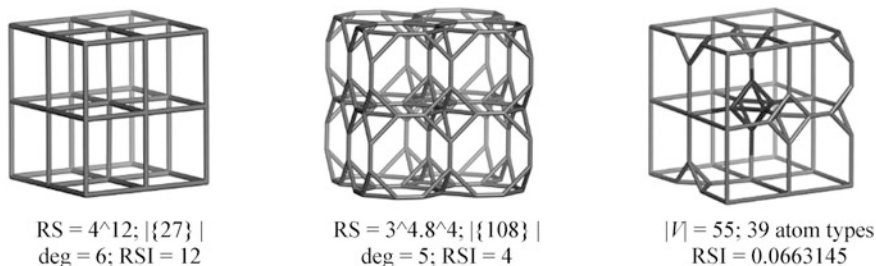


Fig. 4.6 Truncation of the cubic net (*left*): fully truncated (*middle*) and with defects (*right*)

their union covers all the vertices in the truncated transform $t(Q_n)$ (see Chap. 10, Sect. 10.5).

Truncation may be seen as a defect occurring in a crystal network, like that envisaged in Fig. 4.6. While the full realization of truncation leads to a uninodal (i.e., single atom type) net, the defects induce a variety of atom types (Fig. 4.6, right). RSI was calculated by embedding the 8-unit structures in a larger corresponding net.

RSI was created to investigate translational networks; since the centrality index $C(LM)$ gives vertex “topological” classes function of the “sample” size, RSI provides “chemical”-vertex classes, not influenced by the sample size. A structural sample is embedded in a large network, such as the external vertices will take the connectivity of the bulk vertices; then RSI is calculated as in the infinite network.

This could be useful for a network synthesis and also in theoretical Crystallography.

4.5 Pairs of Map Operation

Euler characteristic χ is calculated as the alternating sum of figures of rank k of an n -polytope, as shown in (4.6). Also, it is related to the genus g by Poincaré formula (4.2); in case of the sphere, $\chi = 2$ and $g = 0$; for the torus, $\chi = 0$ and $g = 1$ while in case $\chi < 0$, the surface shows a negative curvature.

Theorem 4.5 *Let $\{v, e, f\}$ and $\{n_1e + \delta, n_2e, n_3e\}$ be types of a parent polyhedron and its derivative polyhedron $o(P)$ (obtained by a map operation o). Also, let both P and $o(P)$ have the same Euler characteristic χ . Then, $\delta = \chi$ if and only if $(n_1 + n_3) = n_2$.*

Proof Assuming that the transformed polyhedron $o(P)$ has the same χ -characteristic as the parent polyhedron P , the Euler formula (4.1) can be re-written, in case of $o(P)$ (Pirvan-Moldovan and Diudea 2016) as:

Table 4.8 Operations on maps and pair of operations providing the Euler characteristic

Operation	$o(P)$	$d(o(P))$
<i>leapfrog</i> (l)	$\{2e, 3e, e + \chi\}$	$\{e + \chi, 3e, 2e\}$
<i>medial</i> (m)	$\{e; 2e; e + \chi\}$	$\{e + \chi; 2e; e\}$
$medial^k = 1, 2, \dots (m^k)$	$\{2^{k-1}e, 2(2^{k-1})e, 2^k(k-1)e + \chi\}$	–
$p_4 = dm^2$	$\{2e + \chi, 4e, 2e\}$	$\{2e, 4e, 2e + \chi\} = m^2$
<i>truncation</i> (t)	$\{2e, 3e, e + \chi\}$	$\{e + \chi, 3e, 2e\}$
$ V(o_1(P)) - V(o_2(P)) = \chi$	o_1	o_2
	dm	m
	dl	m
	dt	m
	p_4	$d(p_4) = mm$
	p_4	l
	p_4	t
$ V(t(P)) = V(l(P)) = V(mm(P)) = 2 V(m(P)) $	(Different edges and faces)	
$ V(p_4(P)) = V(dmm(P)) $	(Identical edges and faces)	

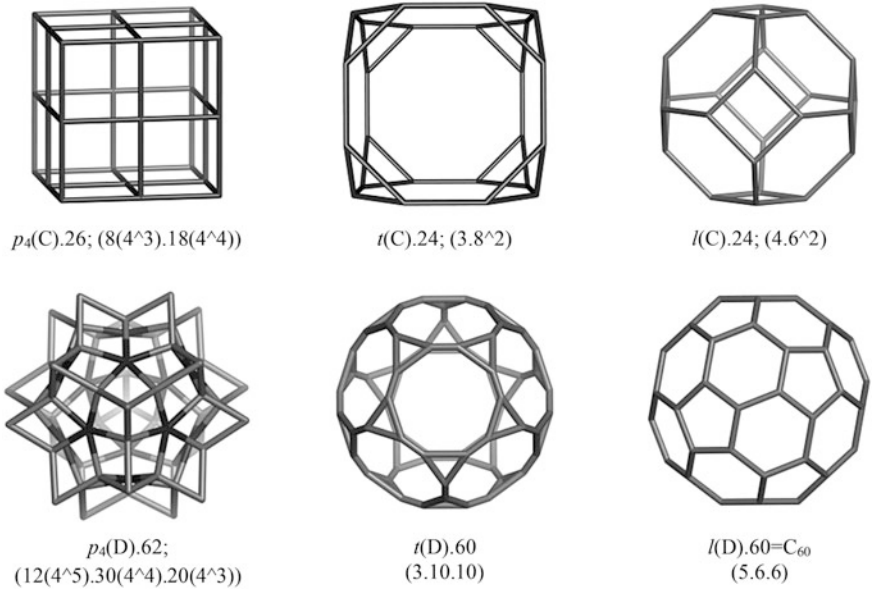


Fig. 4.7 Operations: $o_1 = p_4$ (left); $o_2 = t$ (truncation, middle); and $o_2 = l$ (leapfrog, right), applied on Cube C (top) and Dodecahedron D (bottom); vertex number difference: $\chi = 2$, the Euler characteristic of the sphere

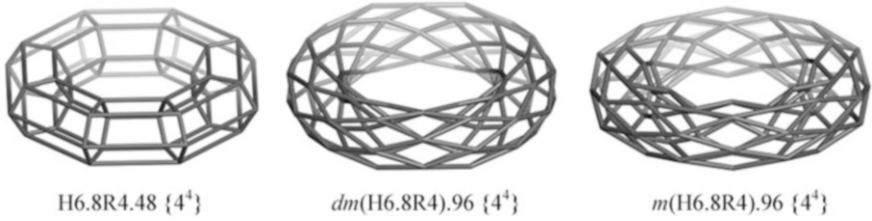


Fig. 4.8 Operations acting on a square-tiled torus (*left*): $o_1 = dm$ (dual of medial, *middle*) and $o_2 = m$ (*right*); vertex number difference: $\chi = 0$; $g = 1$ (Euler characteristic of the torus)

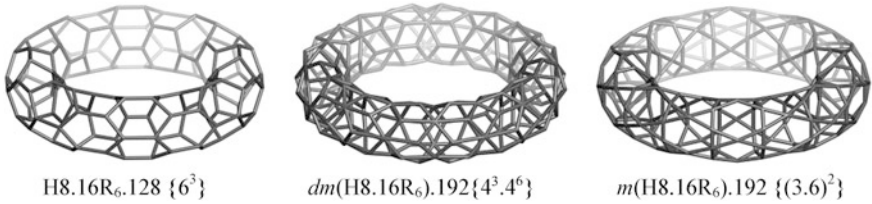


Fig. 4.9 Operations acting on a polyhex torus (*left*): $o_1 = dm$ (dual of medial, *middle*) and $o_2 = m$ (*right*); vertex number difference: $\chi = 0$; $g = 1$ (Euler characteristic of the torus)

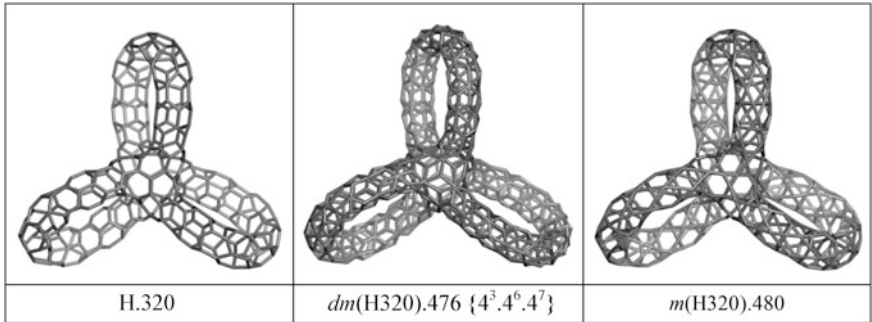


Fig. 4.10 Operations acting on a triple torus (*left*): $o_1 = dm$ (dual of medial, *middle*) and $o_2 = m$ (*right*); vertex number difference: $\chi = -4$; $g = 3$

$$(n_1e + \delta) - (n_2e) + (n_3e) = \chi \tag{4.14}$$

and rearrange it as:

$$e(n_1 - n_2 + n_3) + \delta = \chi \tag{4.15}$$

It is clear that equality $\delta = \chi$ holds only if

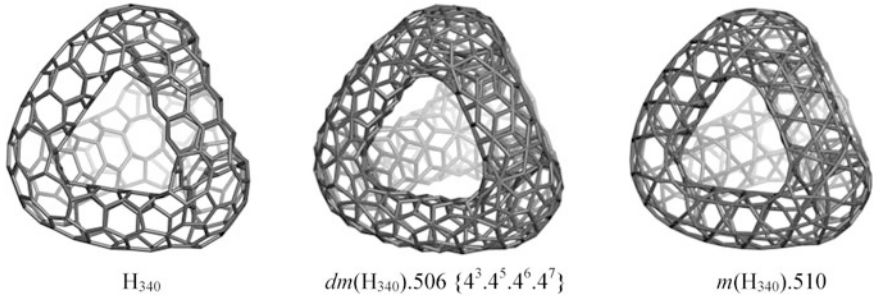


Fig. 4.11 Operations acting on a triple torus (left): $o_1 = dm$ (dual of medial, middle) and $o_2 = m$ (right); vertex number difference: $\chi = -4$; $g = 3$

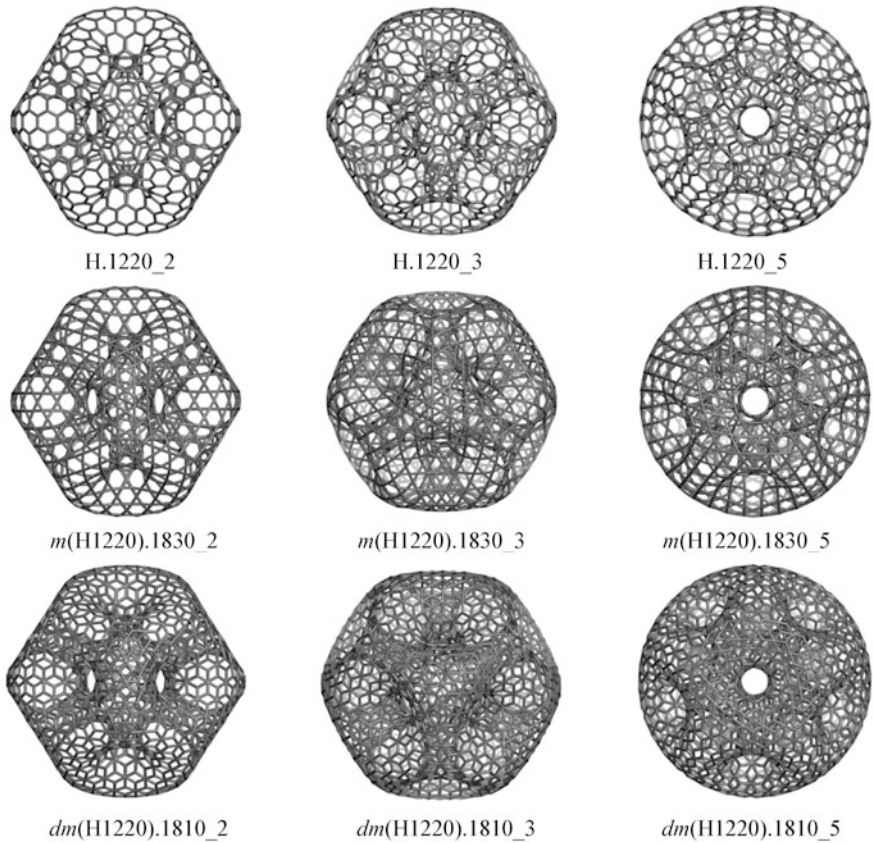


Fig. 4.12 Operation sequence dm acting on a dodecahedron-shaped torus; $\chi = -20$; $g = 11$

Table 4.9 Figure count for the objects in Figs. 4.8, 4.9, 4.10, 4.11, and 4.12

Structure	v	e	f_3	f_4	f_5	f_6	f_7	f	χ	g	$Diff$
H6.8R4	48	96	0	48	0	0	0	48	0	1	–
$m(H6.8R4)$	96	192	0	96	0	0	0	96	0	1	–
$dm(H6.8R4)$	96	192	0	96	0	0	0	96	0	1	0
H8.16R6	128	192	0	0	0	64	0	64	0	1	–
$m(H8.16R6)$	192	384	128	0	0	64	0	192	0	1	–
$dm(H8.16R6)$	192	384	0	192	0	0	0	192	0	1	0
H_{320}	320	480	0	0	0	132	24	156	–4	3	–
$m(H_{320})$	480	960	320	0	0	132	24	476	–4	3	–
$dm(H_{320})$	476	960	0	480	0	0	0	480	–4	3	–4
H_{340}	340	510	0	0	12	118	36	166	–4	3	–
$dm(H_{340})$	506	1020	0	510	0	0	0	510	–4	3	–
$m(H_{340})$	510	1020	340	0	12	118	36	506	–4	3	–4
H1220	1220	1830	0	0	0	470	120	590	–20	11	–
$m(H1220)$	1830	3660	1220	0	0	470	120	1810	–20	11	–
$dm(H1220)$	1810	3660	0	1830	0	0	0	1830	–20	11	–20

Table 4.10 Topological data for the Petrials of Platonic polyhedra

Platonic	Petrial type	v	e	f	χ	Skew polygon	Embedding	Tiling
Tetrahedron	$\{3,3\}^\pi$	4	6	3	1	Square	Hemi-cube	$\{4,3\}/2$
Cube	$\{4,3\}^\pi$	8	12	4	0	Hexagon	Toroidal	$\{6,3\}_{(2,0)}$
Octahedron	$\{3,4\}^\pi$	6	12	4	–2	Hexagon	Hyperbolic	$\{6,4\}_3$
Dodecahedron	$\{5,3\}^\pi$	20	30	6	–4	Decagon	Hyperbolic	$\{10,3\}_5$
Icosahedron	$\{3,5\}^\pi$	12	30	6	–12	Decagon	Hyperbolic	$\{10,5\}_3$

$$(n_1 + n_3) = n_2 \tag{4.16}$$

Thus, (4.16) is both a necessary and sufficient condition for Theorem 4.5 to be true.

Corollary 4.5 (6) The dual of the generalized transform $d(o(P))$ will have the type: $\{n_3e, n_2e, n_1e + \chi\}$. This comes out from the property of Schläfli symbol that its reversal gives the symbol of the dual polyhedron.

Corollary 4.5 (7) Difference in the number of vertices of the transformed polyhedral graphs by selected pairs of map operations, o_1 and o_2 , equals the Euler characteristic of the embedding surface (Table 4.8): $|V(o_1(P))| - |V(o_2(P))| = \chi$.

Difference may also be done with respect to the polyhedron faces but the counting of faces is more expensive. Such pairs of map operations will be illustrated in the following (Figs. 4.7, 4.8, 4.9, 4.10, 4.11, and 4.12). The figure count data for the structures in Figs. 4.8, 4.9, 4.10, 4.11, and 4.12 are given in Table 4.9. Note that the number of points/atoms suffixes the name of structures.

Euler characteristic can also be calculated for Petrie duals of polyhedral. Table 4.10 gives data about the Petrie duals of Platonic polyhedra and their embedding surfaces.

Figures were designed and computed by CVNET (Stefu and Diudea 2005) and Nano Studio (Nagy and Diudea 2009).

References

- Balasubramanian K (1994) Computer generation of automorphism graphs of weighted graphs. *J Chem Inf Comput Sci* 34:1146–1150
- Balinski ML (1961) On the graph structure of convex polyhedra in n -space. *Pac J Math* 11:431–434
- Blatov VA, O’Keeffe M, Proserpio DM (2010) Vertex-, face-, point-, Schläfli-, and Delaney-symbols in nets, polyhedra and tilings: recommended terminology. *CrystEngComm* 12:44–48
- Bonnet O (1853) Note sur la theorie generale des surfaces. *C R Acad Sci Paris* 37:529–532
- Buekenhout F, Parker M (1998) The number of nets of the regular convex polytopes in dimension ≤ 4 . *Disc Math* 186:69–94
- Dehmer M, Emmert-Streib F, Tsoy RY, Varmuza K (2011) Quantifying structural complexity of graphs: information measures in mathematical chemistry. In: Putz M (ed) *Quantum frontiers of atoms and molecules*. Nova Publishing House, New York, NY, pp 479–497
- Dehmer M, Grabner M (2013) The discrimination power of molecular identification numbers revisited. *MATCH Commun Math Comput Chem* 69(3):785–794
- Dehmer M, Grabner M, Mowshowitz A, Emmert-Streib F (2013) An efficient heuristic approach to detecting graph isomorphism based on combinations of highly discriminating invariants. *Adv Comput Math* 39(2):311–325
- Dehmer M, Mowshowitz A (2011) Generalized graph entropies. *Complexity* 17(2):45–50
- Dehmer M, Mowshowitz A, Emmert-Streib F (2013) *Advances in network complexity*. Wiley-Blackwell, Weinheim
- Devos M, Mohar B (2007) An analogue of the Descartes-Euler formula for infinite graphs and Higuchi’s conjecture. *Trans Am Math Soc* 359(7):3287–3300
- Diudea MV (1994) Layer matrices in molecular graphs. *J Chem Inf Comput Sci* 34:1064–1071
- Diudea MV (2013) Quasicrystals: between spongy and full space filling. In: Diudea MV, Nagy CL (eds) *Diamond and related nanostructures*. Springer, Dordrecht, pp 335–385
- Diudea MV, Bende A, Nagy CL (2014) Carbon multi-shell cages. *Phys Chem Chem Phys* 16:5260–5269
- Diudea MV, Bucila VR, Proserpio DM (2013) 1-periodic nanostructures. *MATCH Commun Math Comput Chem* 70:545–564
- Diudea MV, Gutman I, Jäntschi L (2002) *Molecular topology*. NOVA, New York, NY
- Diudea MV, Ilić A, Varmuza K, Dehmer M (2010) Network analysis using a novel highly discriminating topological index. *Complexity* 16(6):32–39
- Diudea MV, Nagy CL (2007) *Periodic nanostructures*. Springer, Dordrecht
- Diudea MV, Rosenfeld VR (2017) The truncation of a cage graph. *J Math Chem* 55:1014–1020
- Diudea MV, Ursu O (2003) Layer matrices and distance property descriptors. *Indian J Chem A* 42(6):1283–1294
- Epstein D (2016) Euler’s formula references (The geometry Junkyard, Theory Group, ICS, UC Irvine). <https://www.ics.uci.edu/~eppstein/junkyard/euler/refs.html>
- Euler L (1752–1753) *Elementa doctrinae solidorum-Demonstratio nonnullarum insignium proprietatum, quibus solida hedris planis inclusa sunt praedita*. *Novi Comment Acad Sci I Petropolitanae* 4:109–160
- Graovac A, Pisanski T (1991) On the Wiener index of a graph. *J Math Chem* 8:53–62

- Harary F (1969) Graph theory. Addison-Wesley, Reading, MA
- Hargittai M, Hargittai I (2010) Symmetry through the eyes of a chemist. Springer, Dordrecht
- Higuchi Y (2001) Combinatorial curvature for planar graphs. *J Graph Theory* 38:220–229
- Klein DJ (2002) Topo-combinatoric categorization of quasi-local graphitic defects. *Phys Chem Chem Phys* 4:2099–2110
- Nagy CL, Diudea MV (2009) Nano-studio. Babes-Bolyai Univ, Cluj
- Nagy CL, Diudea MV (2017) Ring signature index. *MATCH Commun Math Comput Chem* 77(2):479–492
- Pirvan-Moldovan A, Diudea MV (2016) Euler characteristic of polyhedral graphs. *Croat Chem Acta* 89(4):471–479
- Razinger M, Balasubramanian K, Munk ME (1993) Graph automorphism perception algorithms in computer-enhanced structure elucidation. *J Chem Inf Comput Sci* 33:197–201
- Schläfli L (1901) Theorie der vielfachen Kontinuität Zürcher und Furrer, Zürich (Reprinted in: Ludwig Schläfli, 1814–1895, *Gesammelte Mathematische Abhandlungen*, Band 1, 167–387, Verlag Birkhäuser, Basel, 1950)
- Schulte E (1985) Regular incidence-polytopes with Euclidean or toroidal faces and vertex-figures. *J Comb Theory Ser A* 40(2):305–330
- Schulte E (2014) Polyhedra, complexes, nets and symmetry. *Acta Crystallogr A* 70:203–216
- Ştefu M, Diudea MV (2005) CageVersatile_CVNET. Babes-Bolyai University, Cluj
- Ştefu M, Parvan-Moldovan A, Kooperazan-Moftakhar F, Diudea MV (2015) Topological symmetry of C_{60} -related multi-shell clusters. *MATCH Commun Math Comput Chem* 74:273–284

Chapter 5

Small Icosahedral Clusters

Dodecahedron (Greek δωδεκάεδρου), the fifth Platonic solid, has been associated to the ether (or the universe) by ancient Greeks, as described by Platon in its *Timaeus* dialogue (Papacostea 1930–1935; Taylor 1928); the remaining Platonics have been used as symbols for the four other elements: tetrahedron—fire; icosahedron—water; octahedron—air and cube—earth. In geometry, any polyhedron with 12 faces can be named a dodecahedron, among which only one is the regular dodecahedron (i.e., the Platonic solid), composed of 12 regular pentagonal faces, three of which meeting at each vertex; it has the symbol $\{5,3\}$ (Schläfli 1901) and icosahedral (point group) symmetry, I_h . The dual of a dodecahedron is an icosahedron, referring to shapes (with the disregard of angles and bond length—Schulte 1985) rather than to regular polyhedra.

5.1 Small Cages: Source of Complex Clusters

In the introductory chapters of this book (Chaps. 2 and 3) there were mentioned “point centered polyhedra”, symbolized MP (Parvan-Moldovan and Diudea 2015); these represent the most simple structures of rank four ($k = 4$) and, as will be shown, a source for deriving a plethora of complex structures/clusters. As starting structures for the operations on maps, “cell-in-cell” clusters, with the same or different units, were also used.

The pair dual polyhedral graphs (both of icosahedral symmetry—Fig. 5.1): Dodecahedron and Icosahedron often coexist in these complex structures. The symbol for hyper-structures is either DY (i.e., $C_{20}Y$) or IY (i.e., $C_{12}Y$) depending which topology is aimed to be evidenced.

Figure count of the herein studied clusters are included in the following tables; data are used for checking the consistency of attributed structures; along with the topological structural parameters (vertices, edges, facets of various rank), Euler

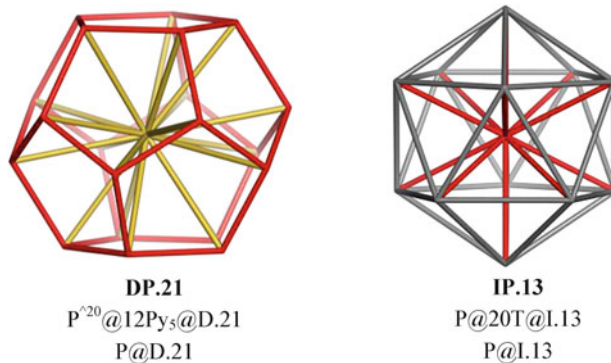


Fig. 5.1 Platonic dual pair: dodecahedron (*left*) and icosahedron (*right*), as “point centered polyhedra”

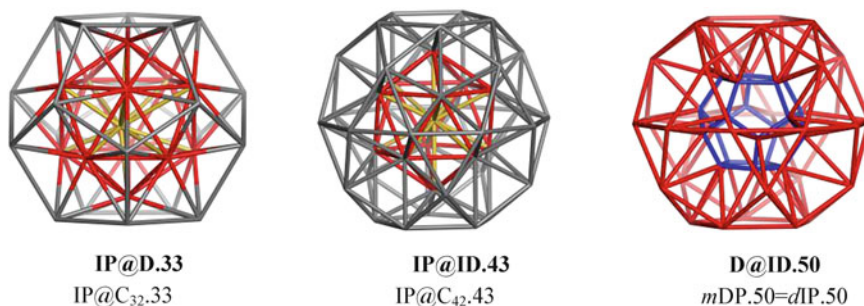


Fig. 5.2 Small clusters used as starting structures in the design of more complex clusters

characteristic χ , the rank k and the genus g represent the main results of this kind of calculation, also helpful in the classification of clusters.

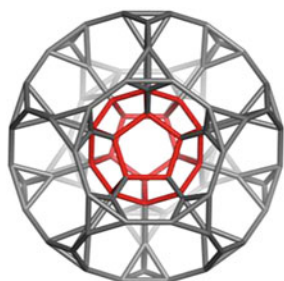
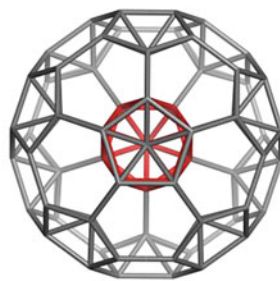
Figures 5.1 and 5.2 illustrate some small cages useful in the generation of more complex clusters by means of map operations; they will be detailed in the Atlas of this chapter. Their figure count is given in Table 5.1.

5.2 Truncated MP Icosahedral Clusters

Truncation t cuts off the neighborhood of each vertex by a plane, such that it intersects each edge incident in that vertex. The truncated polyhedron has the figures (vertices, edges and faces, respectively): $\{2e, 3e, e + 2\}$, with e being the number of edges in the parent polyhedron; the truncated transform is always a three-connected graph (Diudea et al. 2006; Pisanski and Randić 2000; Diudea and Nagy 2007), (see Fig. 5.3).

Table 5.1 Figure count in the smallest clusters of icosahedral symmetry

Cluster	v	e	3(2)	5(2)	2	1(3)	2(3)	3(3)	(M)	3	4	χ	k	$n(3);(M)$
DP	21	50	30	12	42	0	12	0	1	13	0	0	4	T;Py ₅ (P;D)
IP	13	42	50	0	50	20	0	0	1	21	0	0	4	T;Py ₅ (P;I)
I@D	32	120	140	12	152	50	12	0	2	64	0	0	4	T;Py ₅ (I;D)
IP@D	33	132	170	12	182	70	12	0	1	83	2	2	5	T;Py ₅ (P;D)
dDP	42	150	130	12	142	0	12	20	2	34	0	0	4	Py ₅ ;O(I;ID)
IP@ID	43	162	160	12	172	20	12	20	1	53	2	2	5	T; Py ₅ ;O(P;ID)

 $tDP.100$ (5A1.1) $tIP.84$ (5A2.1)**Fig. 5.3** Truncated clusters derived from the smallest icosahedral MP clusters**Table 5.2** Figure count in the truncated smallest clusters of icosahedral symmetry

Cluster	v	e	3(2)	5(2)	6(2)	2	3(T/TT)	3(A ₅)	3(Py _k)	(M)	3	4	χ	k
tIP (5A2.1)	84	192	80	12	50	142	20	0	12	2	34	0	0	4
tDP (5A1.1)	100	230	96	12	62	170	24	0	14	2	40	0	0	4

Truncation of the smallest icosahedral MP ($M = D; I$) clusters results in two structures: $C_{100} = tDP = D@(12tPy_5;20Py_3).100$ and $C_{84} = tIP = I@(20tPy_3; 12Py_5).84$, detailed in the Atlas 5A (5A1.1 and 5A2.1, respectively). These clusters have the rank 4, as shown in Table 5.2. Vertex configuration for truncated pyramids is: $tPy_k = k\{k.6.6.\};k\{3.6.6\};2k\{3.6.2k\}; |V(tPy_k)| = 4k; k = 3, 4, \dots$; in case $k = 3$, one recovers the tetrahedron T and its truncated object TT.

The cluster C_{84} was further transformed (or exists as a subgraph) in: 5A2.1.1; 5A2.1.2; 5A4.2; 5A6.3; 6A6.2.

5.3 Clusters by Medial Operation

Medial m is achieved by marking the midpoints of parent edges and next joining two such points if the edges span an angle; the parent vertices are cut off. Medial is a 4-connected graph, symmetric between the parent and its dual, that is $mdM = mM$.

By medial, edges of the parent polyhedron are reduced to a point (Diudea and Nagy 2007).

If medial is succeeded by dual d operation, the transformed structure will have all 4-rings, and are called “rhombic figures”. Dual is made by setting a point in the center of each face of a map and then joining two such points if their corresponding faces share a common edge. In a polyhedral graph, the points of the dual represent faces in the parent graph; dual of the dual returns the original map: $dd(M) = M$. For the medial and dual of medial of the small structures herein discussed, the figure count is shown in Table 5.3; structures are detailed in the Atlas of this chapter.

Note that, the rhombic clusters have only 4(2) faces (last row in Table 5.3). Also note that in case of spongy structures (with the name suffixed by the subscript “ sp ”) the windows faces (e.g., 2(5) faces) and M (the core and hull, respectively) are counted empty (i.e., zero, Table 5.3)

There is an interesting case: rhombic icosahedron Rh_{20} is assumed (Wikipedia 2016) to have as dual the *pentagonal gyrobicupola* (the Johnson solid J_{31} —Johnson 1966) that is not true. We bring proofs here about the correct dual of Rh_{20} , that is $d(Rh_{20}).20$ (Fig. 5.4). The structure Rh_{20} was drawn by cutting the equatorial ten rhombi of the rhombic triacontahedron $Rh_{30} = d(mD30).32$ (5A8) designed as the dual of icosidodecahedron $ID = mD.30$. Retro-medial rm operation was applied to both $d(Rh_{20}).20$ and $J_{31}.20$; the data in Table 5.4 (particularly, the vertex centrality signature $c(LR)$ —Nagy and Diudea 2017) clearly demonstrate that the two columns in Fig. 5.4 represent two different series and J_{31} (i.e., $mA_5.20$, by map operations) is not the dual of Rh_{20} . In the name of structures, the last number counts all their vertices.

5.4 Clusters of Higher Rank

Let apply a map operation on a small cluster, e.g., $o(M_1@M_2)$ and then make $o(M_1P@M_2)$, on the point-centered map M_1P ; the transformed map in the second case will include the product of the first case identified on a common facet with the product of $o(M_1P)$ operation. Then, one can write a complex operation as:

$$o(M_1P)@o(M_1@M_2) = o(M_1P@M_2)$$

The shared facet, in case of 4-polytopes (Coxeter 1973), is a 3-facet (a cell or a polyhedron). It means that $o(M_1P@M_2)$ is a cluster bonded by two 4-facets while such a cluster is a 5-polytope. It is the lower bound for the existence of a 5-polytope (cf. Euler (1752–1753) formula). Not any 4-polytope can be split by the above rule (e.g., M_1P , the simplest 4-polytope—Parvan-Moldovan and Diudea 2015), that is the rule is not trivial. The “core” $o(M_1P)$ can vary, i.e., it is not necessary to start from M_1P .

Structures of rank 5 (Schulte 2014) and their substructures are listed in Tables 5.5, 5.6 and 5.7 and detailed in the Atlas. Equivalence classes for the vertices of the studied clusters were calculated by Nano Studio software program (Nagy and Diudea 2009) and confirmed by Mathematica (Wolfram 2016).

Table 5.3 Figure count in some clusters generated by the medial m and dual of medial dm operations

Structure	v	e	3(2)	4(2)	5(2)	2	$c_1(3)$	$c_2(3)$	M	3	4	χ	$g(k)$	$c_1(3)$	M	4
$m(l@d32)$ (5A3.2)	120	420	340	0	24	364	50	12	2	64	0	0	0(4)	$O;A_5$	(ID;...)	—
$m(l@d32)sp$	120	420	340	0	0	340	50	0	0	50	0	-10	6(4)	$O;...$	\emptyset	—
$m(l@d33)$ (5A4.1)	132	510	450	0	24	474	70	24	2	96	2	2	0(5)	$O;(A_5;Py_5)$	(I;...)	$C_{42}@C_{120}$
$m(D@ID50)$ (5A7.2)	150	450	210	150	24	384	70	12	2	84	0	0	0(4)	mA_5	(O;P3)	(ID; mID)
$m(m(l@d32))$ (5A3.2.1)	420	1020	340	300	0	640	50	0	0	50	0	-10	6(4)	CO	0	—
$m(m(l@d33))$ (5A4.1.1)	510	1350	450	420	84	954	70	42	2	114	0	0	0(4)	$CO;P_5$	ID	—
$m(m(l@d33))sp$	510	1350	450	420	0	870	70	0	0	70	0	-40	21(4)	CO	0	—
$d(m(m(l@d33)))sp$ (5A4.1.4)	870	1680	0	840	0	840	70	0	0	70	0	-40	21(4)	Rh12.14	0	—

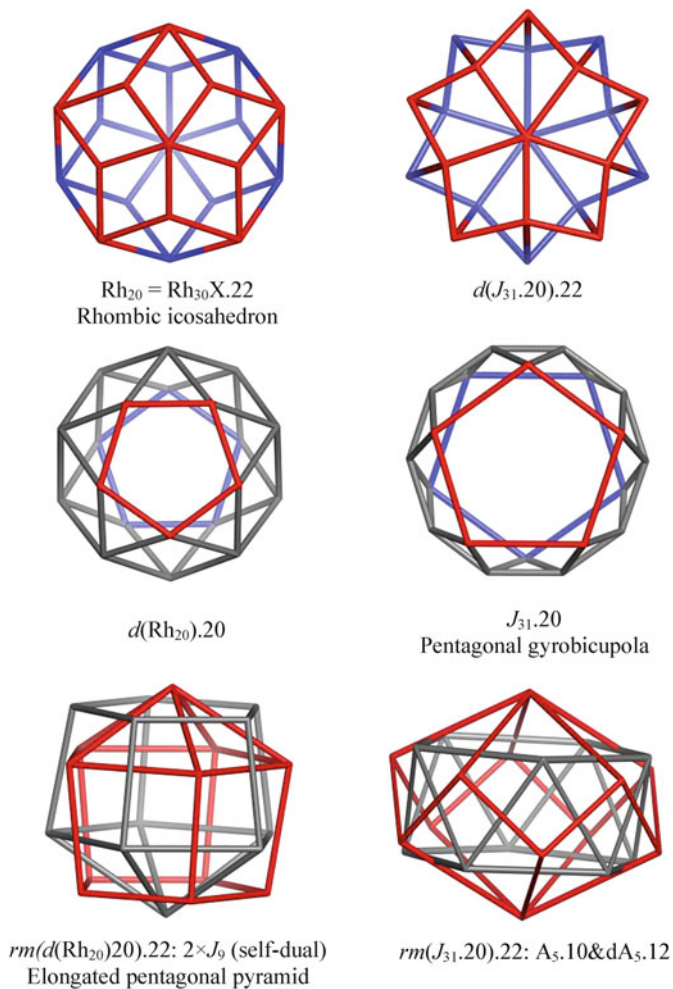


Fig. 5.4 Structures related to the rhombic icosahedron Rh_{20}

Table 5.4 Vertex classes of rhombic icosahedron related structures

Structure	v/elf -class	v -Signature ($c(LR)$)	No	Deg	Rings
$Rh_{20}.22$	$3/3/2$	0.112882	10	3	4^3
		0.110588	10	4	4^4
		0.108795	2	5	4^5
$d(J_{31}.20).22$	$3/3/2$	0.109819	2	5	4^5
		0.095588	10	4	4^4
		0.091812	10	3	4^3
$d(Rh_{20}).20$	$2/3/3$	0.115289	10	4	3.4.3.5
		0.112052	10	4	3.4.4.4
$J_{31}.20$	$2/3/3$	0.116139	10	4	3.4.5.4
		0.099553	10	4	3.4.3.4

Table 5.5 Figure count in some clusters of rank $k = 5$ and their substructures (a)

Structure	v	e	3(2)	4(2)	5(2)	6(2)	2	U(3)	M	3	4	χ	k	$n(3);(M);4$
$d(IIP)$ (5A2.1.1)	130	450	410	0	36	30	476	54	100	2	156	2	5	$(2A_5;P_6;T;(D..);C_{50}@C_{110}$
$d(IIP)X$ (5A2.1.2)	110	360	320	0	24	30	374	42	80	2	124	0	4	$(A_5;Py_6;T;(ID;C_{80})$
mDP (5A7)	50	150	110	0	24	0	134	12	20	2	34	0	4	$A_5;T;(D;ID)$
$d(IP@ID)$ (5A6.1)	160	450	200	120	36	0	356	24	40	2	66	2	5	$(A_5;mP_3;(T;C);(ID..);C_{50}@C_{130}$
$d(m(IP)42)$ (5A5.1)	130	330	90	120	24	0	234	12	20	2	34	0	4	$mP_3;20C;(D..)$
$d(d(IP))$ (5A7.1)	134	450	250	150	0	0	400	12	70	2	84	2	5	$Rh_{10};(mP_3;T);(t;Rh_{30})$
$C_{122}(5A7.1b)$	122	360	200	90	0	0	290	30	20	2	52	0	4	$mP_3;T;(.;Rh_{30})$
$C_{114}(5A7.1b)$	114	330	130	120	0	0	250	12	20	2	34	0	4	$Rh_{10};mP_3;(I..)$

Table 5.6 Figure count in some clusters of rank $k = 5$ and their substructures (b)

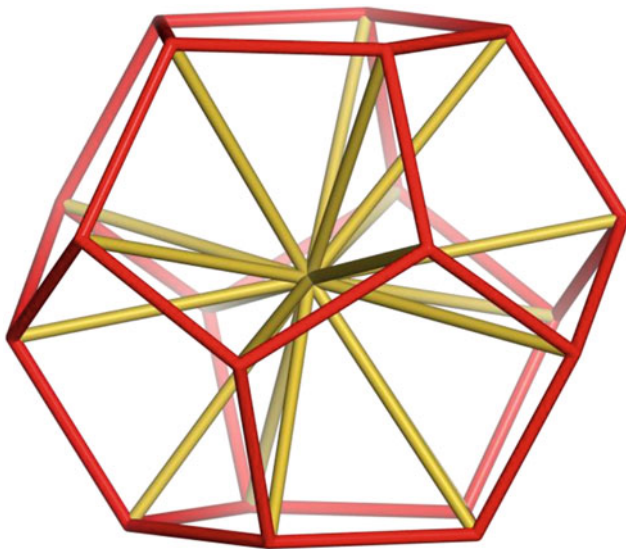
Structure	v	e	3(2)	4(2)	5;10*(2)	6(2)	2	U(3)	$n(3)$	M	3	4	χ	$g(k)$	$n(3);(M);4$
$d(l@D)$ (5A3.1)	140	390	200	90	24	20	334	32	50	2	84	2	2	0(5)	$(mA_5;hCO);T;(D;C_{60});C_{80}@C_{120S}$
$r(l@D)$ (5A3.1b)	120	300	140	60	24*	20	244	32	30	2	64	0	0	0(4)	$(mA_5;hCO);T;(ID;C_{60})$
$D@ID$ (5A3.1b)	80	180	80	30	24*	0	134	20	12	2	34	0	0	0(4)	$rPy_5;T;(D;rD)$
$m(IP@ID)$ (5A6.2)	162	480	240	120	12	0	372	40	12	2	54	2	2	0(5)	$(CO;O);P_5;(L.);C_{42}@C_{150}$
$m(l@ID)$ (5A5.2)	150	390	130	120	24	0	274	20	12	2	34	0	0	0(4)	$CO;P_5;(ID.)$
$l@ID$ (5A5)	42	150	130	0	12	0	142	20	12	2	34	0	0	0(4)	$T;Py_5;O(l;ID)$
$r(IP@ID)$ (5A6.3)	324	642	80	120	24	160	384	40	24	2	66	2	2	0(5)	$(TO;TT);(Py_5;P_5);(L.);C_{84}@C_{300}$
$r(l@ID)$ (5A5.6)	300	540	0	120	24	130	274	20	12	2	34	0	0	0(4)	$TO;P_5;(C_{60..})$
rIP (5A2.1)	84	192	80	0	12	50	142	20	12	2	34	0	0	0(4)	$TT;Py_5;(l;C_{60})$

Face $f = 10$ when *

Table 5.7 Figure count in some clusters of rank $k = 5$ and their substructures (c)

Structure	v	e	3(2)	5(2)	2(6)	2	U(3)	$n(3)$	M	3	4	χ	$g(k)$	$n(3);(M);4$
$I(IP@D)$ (5A.4.2)	264	642	280	24	170	474	70	24	2	96	2	2	0(5)	TT; (A ₅ ; P ₅); (I ₁); C ₈₄ @C ₂₄₀
$I(I@D32)$ (5A.3.3)	240	540	200	24	140	364	50	12	2	64	0	0	0(4)	(TT@3TT); A ₅ ; (C ₆₀ ..)
IP (5A.2.1)	84	192	80	12	50	142	20	12	2	34	0	0	0(4)	TT; P ₅ ; (I; C ₆₀)
$I(IP@D)$ (5A.4.3)	510	930	170	42	280	492	70	0	2	72	2	2	0(5)	TT; (C ₆₀ ..); (C ₁₅₀ @C ₄₂₀)
$I(IP@D)_{sp}$	510	930	170	0	280	450	70	0	0	70	0	-40	21(4)	TT
$I(I@D)$ (5A.3.4)	420	720	140	0	200	340	50	0	0	50	0	-10	6(4)	TT
$I(IP)$ (5A.2.2)	150	270	50	12	80	142	20	0	2	22	0	0	0(4)	TT; (C ₆₀ ..)

Chapter 5 Atlas: Small Icosahedral Clusters



IY(12Py₅; f₃).21

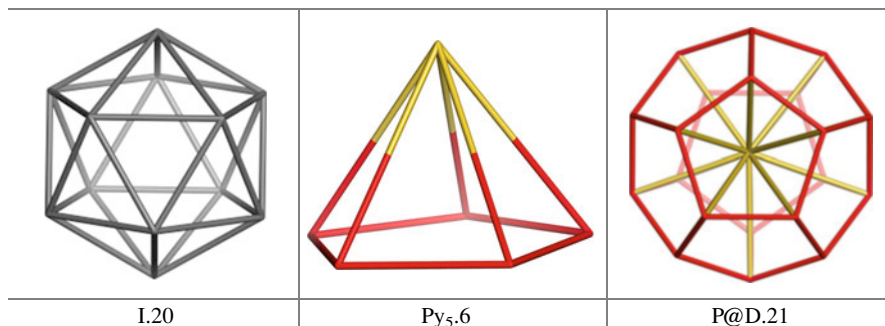
DP.21

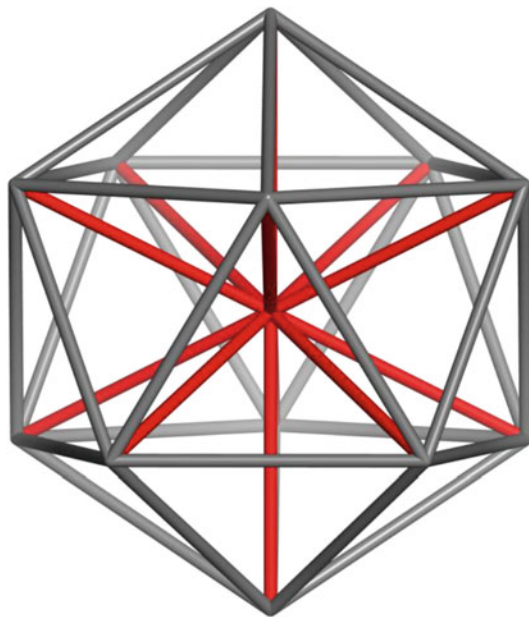
P²⁰@12Py₅@D.21

P@D.21

C₂×A₅; classes 2: |{1}|; {20}|

5A1





DY(20T; f_3).13

IP.13

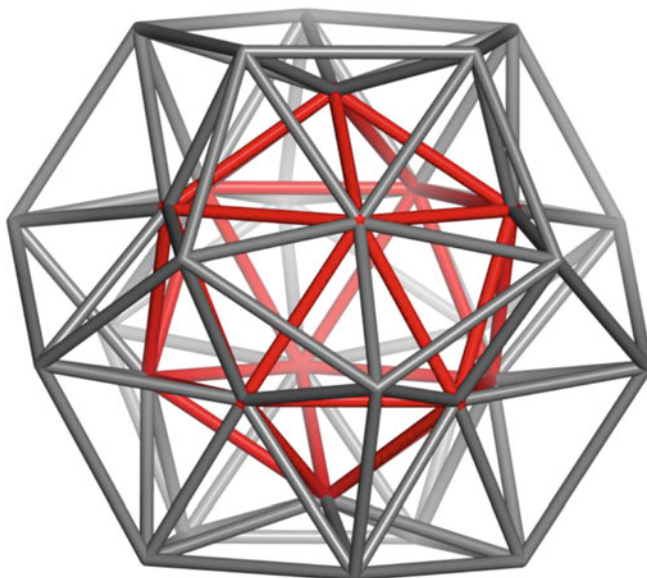
P@I.13

P@T₂₀@I.13

$C_2 \times A_5$; classes 2: $\{1\}; \{12\}$

5A2

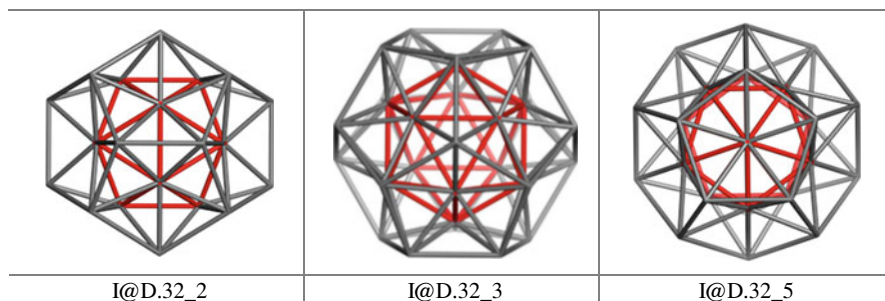
<p>D.20</p>	<p>T.4</p>	<p>IP.13 P@T₂₀@I.13</p>

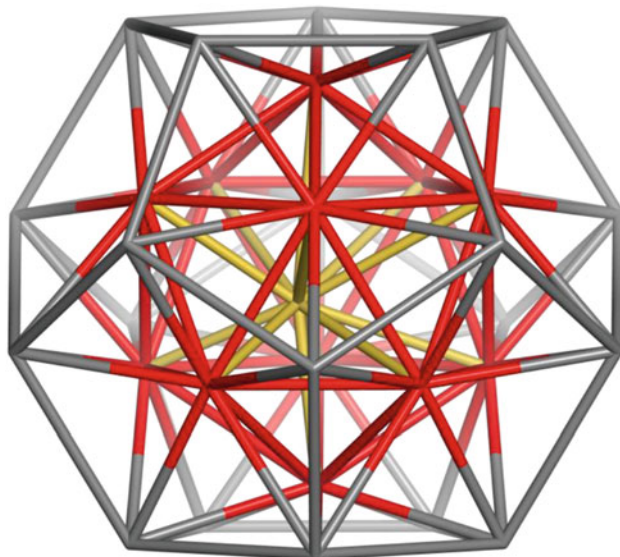


DY(20T;T).32
IY(12Py₅;T).32

I@(20T;12Py₅;30T)@D.32
 I@D.32
 C₂×A₅; classes 2: |{20};{12}|

5A3



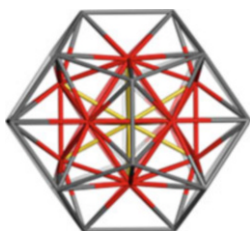


IP@D.33

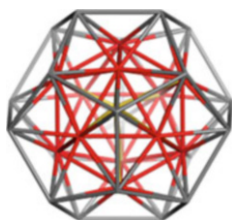
IP@C₃₂.33

C₂ × A₅; classes 3: |{20}; {12}; {1}|

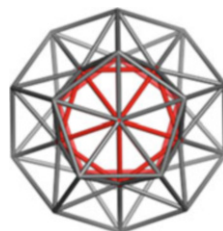
5A4



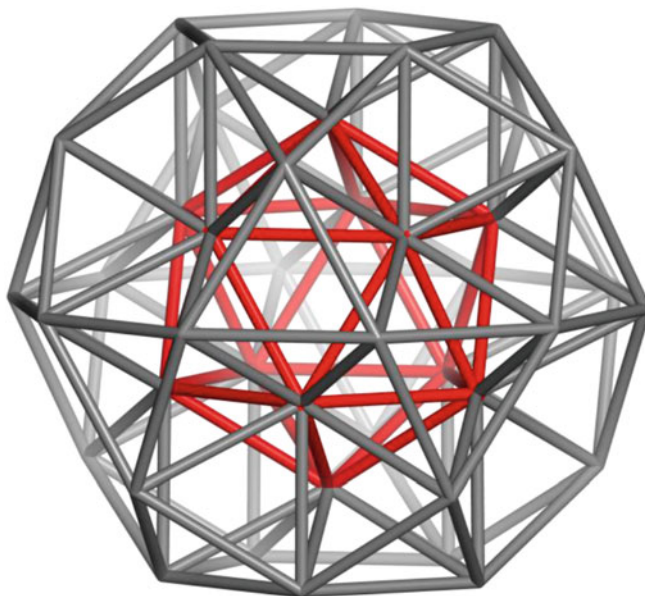
IP@D.33_2



IP@D.33_3



I@D.32_5



DY(200; f_3).42

I@(200;12Py₅).42

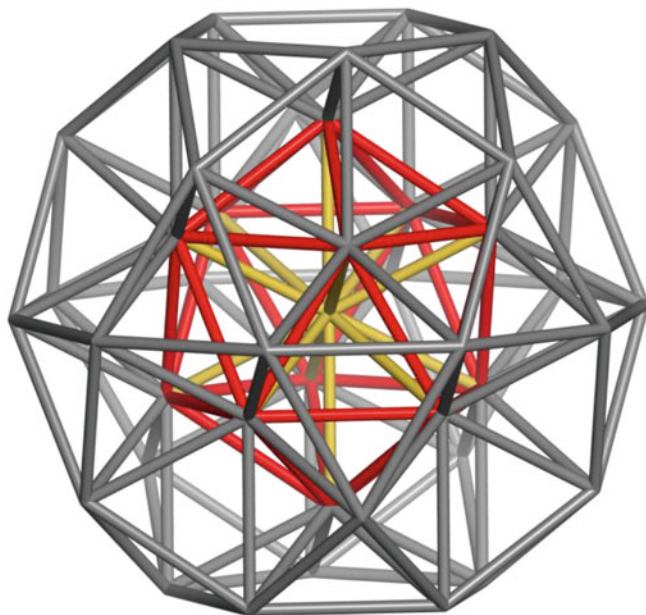
I@ID.42

$dDP.42 = mIP.42$

$C_2 \times A_5$; classes 2: $|\{12\}; \{30\}|$

5A5

I.12	ID.30 = mI.30	mIP.42_5



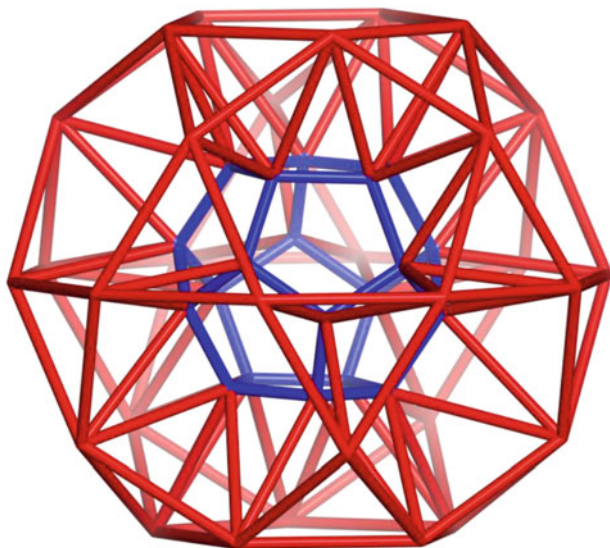
IP@ID.43

IP@C₄₂.43

C₂×A₅; classes 3: |{12};{30};{1}|

5A6

IP.13	ID.30	I@ID.42



DY(20T;P).50

D@(20T;12A₅)@ID.50
 D@ID.50
mDP.50 = dIP.50
 C₂×A₅; classes 2: |{20};{30}|

5A7

D@ID.50_2	D@ID.50_3	ID@D.50_5



Rh₃₀

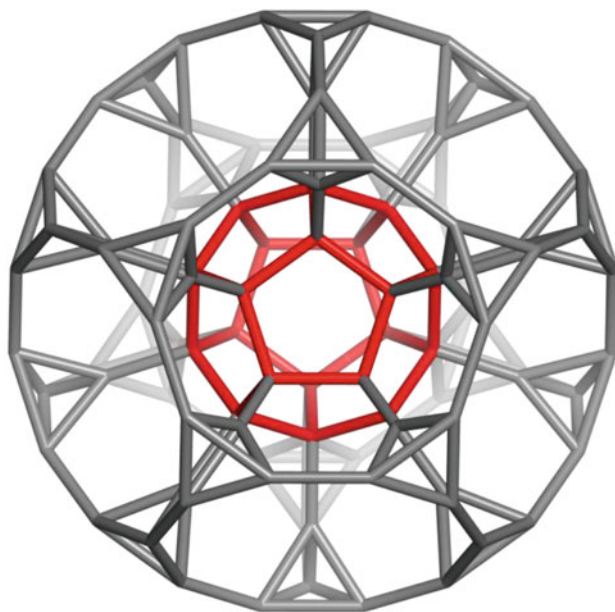
d(mD30).32

Triacontahedron.32

$C_2 \times A_5$; classes 2: $|\{20\}; \{12\}|$

5A8

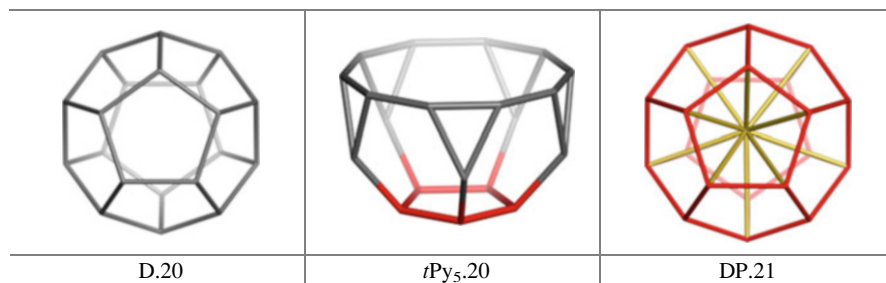
<p>D.20</p>	<p>I.12</p>	<p><i>mD.30 = ID.30 = d(Rh₃₀).30</i></p>

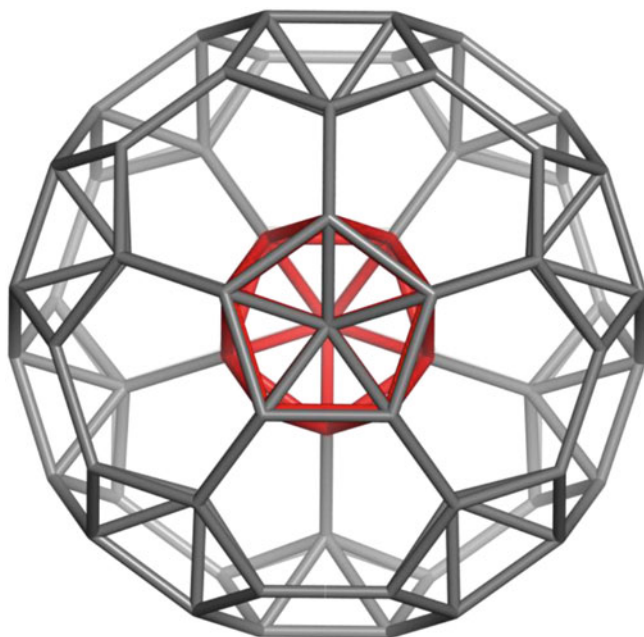


IY(12*t*Py₅; *f*₆).100

D@(12*t*Py₅;20T)@*t*D.100
*t*DP.100

C₂ × A₅; classes 3: |2{20};{60}|
 5A1.1





$C_{20}Y(20TT; f_6).84$

DY(20TT; f_6).84

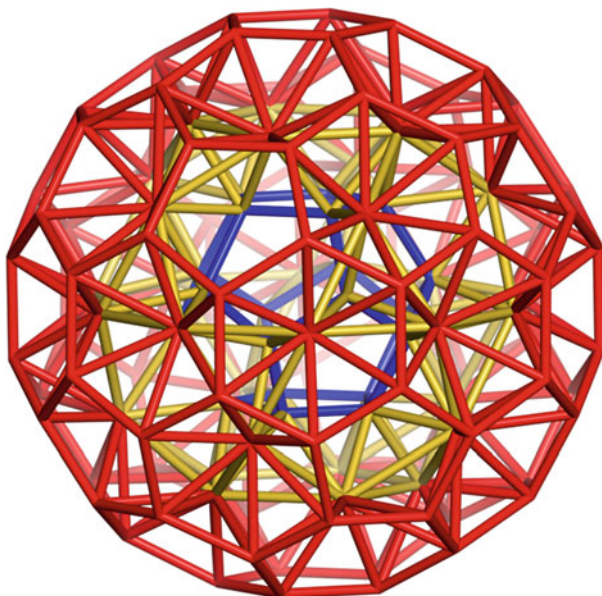
I@(20TT; 12Py₅)@C₆₀.84

tIP13.84

$C_2 \times A_5$; classes 3: $\{60\}, 2\{12\}$

5A2.1

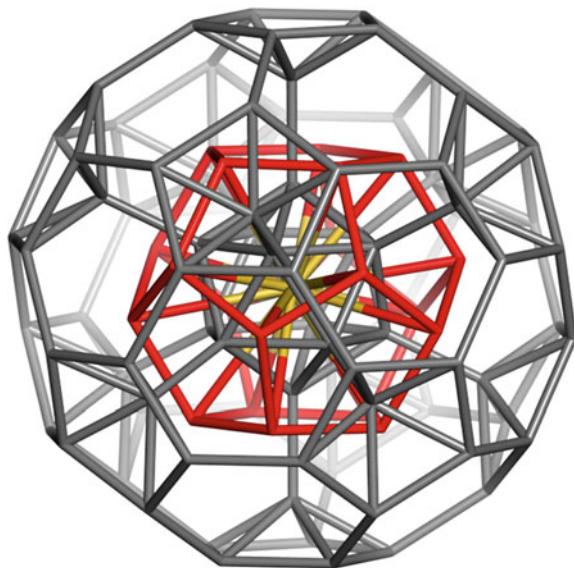
I.12	$tPy_{3.12} = TT.12$	IP.13



$D@(12(2A_5);30Py_6;100T).130$

$d(C_{84}).130$
 $C_{50}@C_{110}.130$
 $C_2 \times A_5$; classes 4: $|\{60\}; 2\{20\}; \{30\}|$
 5A2.1.1

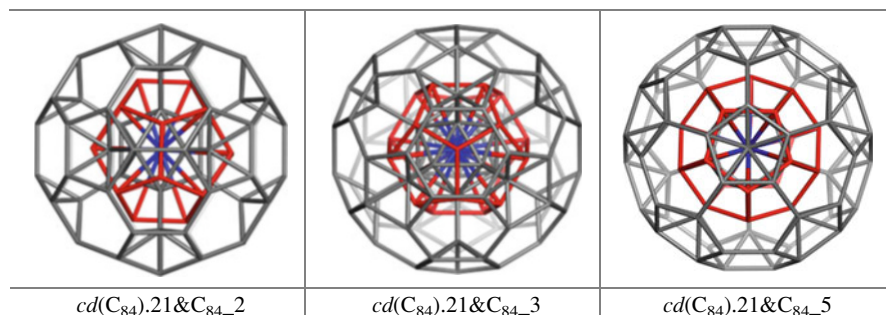
<p>$D@ID.50$</p>	<p>$ID@C_{80-110}$</p>	<p>$C_{50}@C_{110-130}_5$ $d(C_{84}).130$</p>

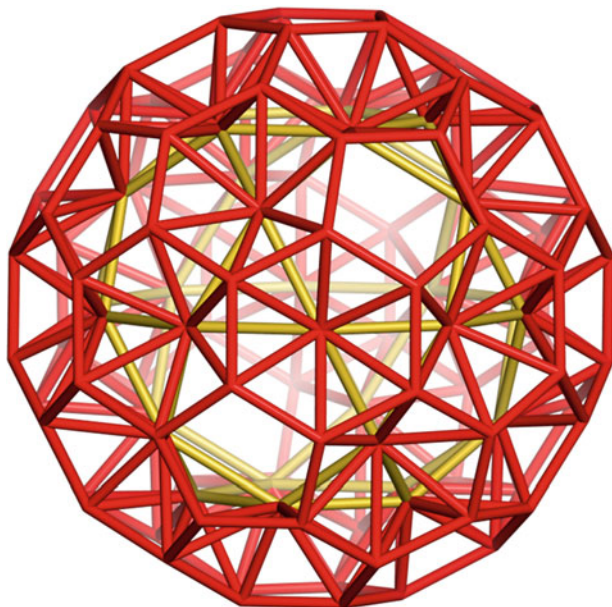


$cd(C_{84}).21 \& C_{84}$

$cd(C_{84}) = P^{20} @ D.21 = DP.21$

5A2.1.1a



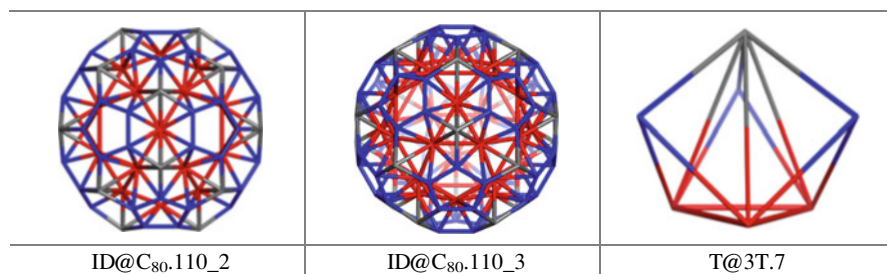


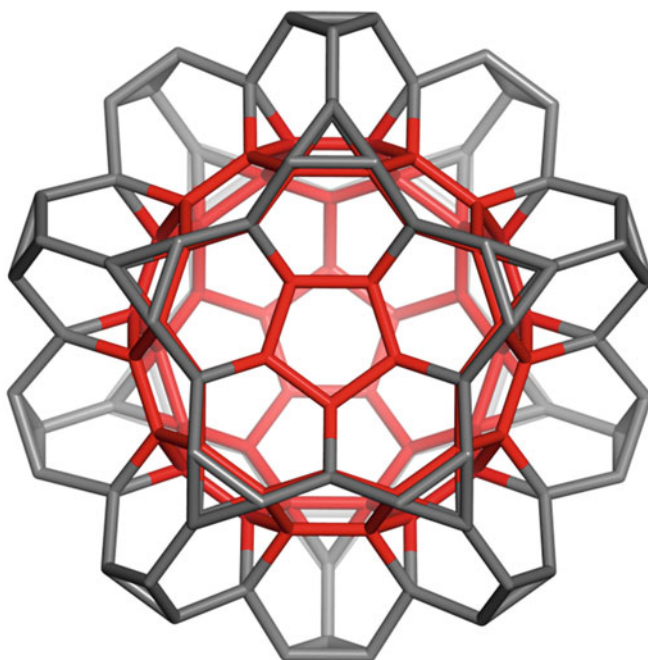
ID@C₈₀.110

ID@(20(T@T₃);12A₅;30Py₆)@C₈₀.110

C₂×A₅; classes 3: |{60};{30};{20}|

5A2.1.2





DY(20TT; f_3).150

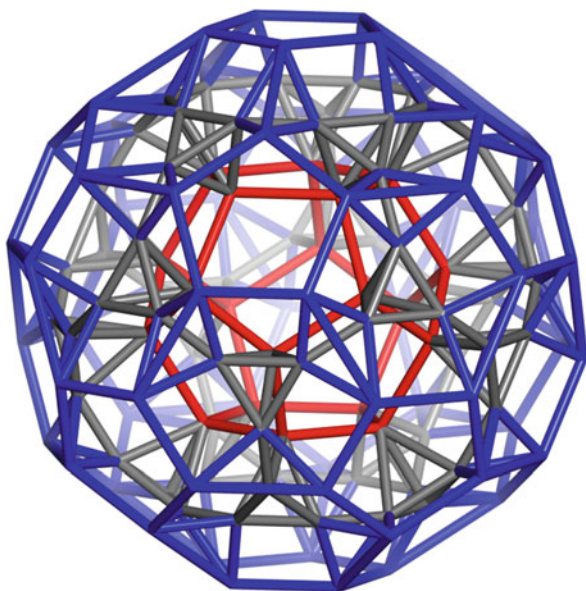
$C_{60}@20TT.150$

$I(IP).150$

$C_2 \times A_5$; classes 3: $|2\{60\}; \{30\}|$

5A2.2

<p>$I(IP).150_2$</p>	<p>$I(IP).150_3$</p>	<p>IP.13 $P@T_{20}@I.13$</p>



IY(12mA₅; f₄).140

D@(12mA₅;20hCO;50T)@C₆₀.140

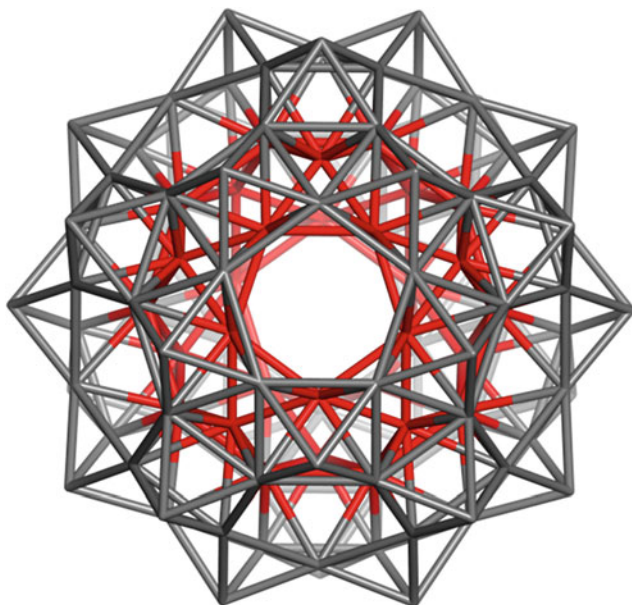
d(I@D32).140

C₈₀@C₁₂₀.140

C₂×A₅; classes 3: |2{60};{20}|

5A3.1

<p>D@tD.80 D@(12hmA₅;20T)@tD.80</p>	<p>C₆₀@tD.120 C₆₀@(12hmA₅;20hCO;30T) @tD.120</p>	<p>d(I@D32).140_5</p>



DY(20(O@(3/2)O);f₃).120

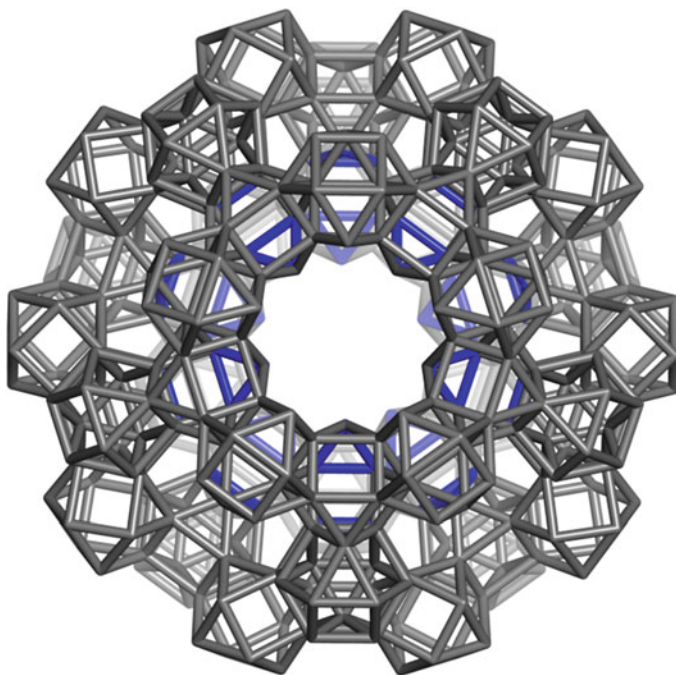
ID@(12A₅;20O;30O).120

m(I@D32).120

C₂ × A₅; classes 3: |2{30};{60}|

5A3.2

A ₅ .10	ID.30	I@D.32



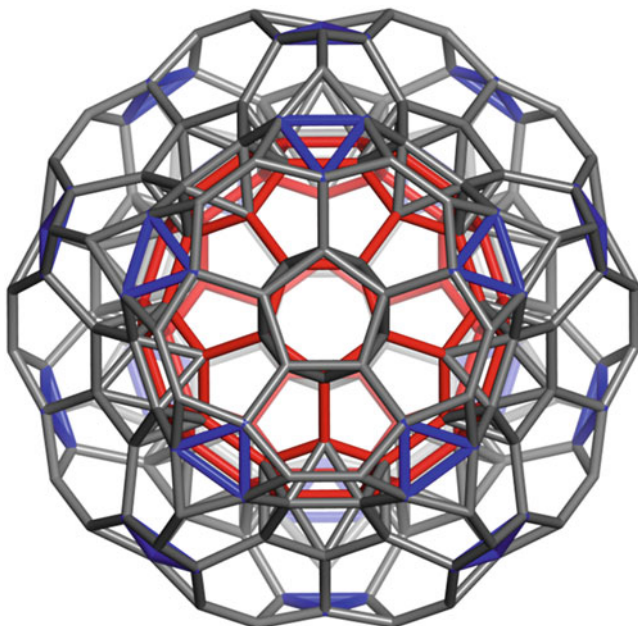
DY(20(CO@3CO/2); f_3).420

m(m(I@D32)120).420

$C_2 \times A_5$; classes 5: |2{120}; 3{60}|

5A3.2.1

I.12	ID.30	<i>m(I@D32).120</i>



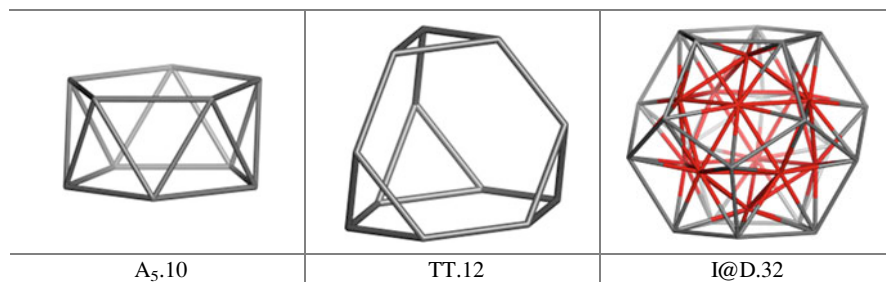
DY(20(TT@3TT/2); f_6).240

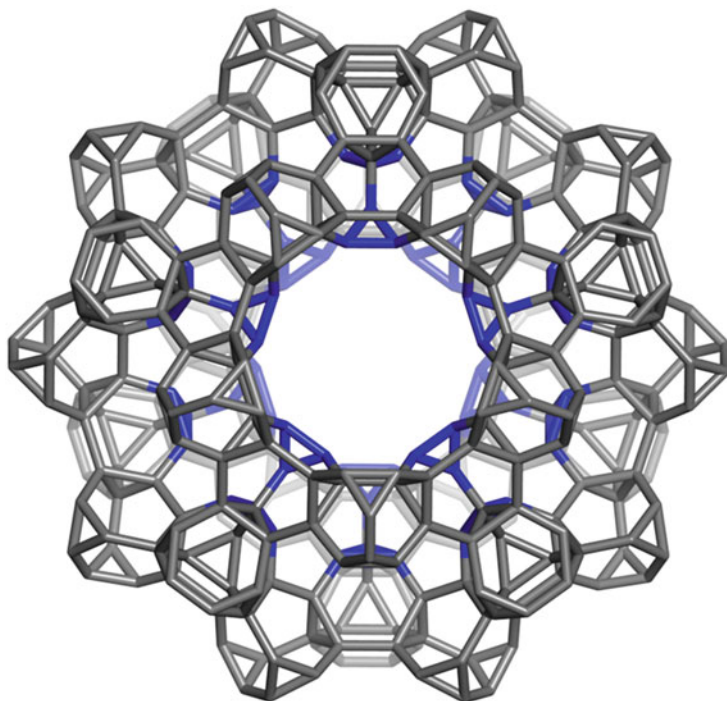
$C_{60}@ (12A_5; 50TT).240$

$t(I@D32).240$

$C_2 \times A_5$; classes 4: $|4\{60\}|$

5A3.3



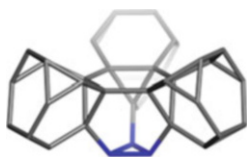


DY(20TT@(3TT/2); f_3).420

$I(I@D32).420$

$C_2 \times A_5$; classes 5: $|3\{60\}; 2\{120\}|$

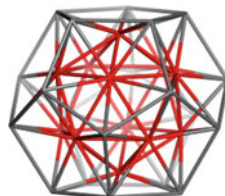
5A3.4



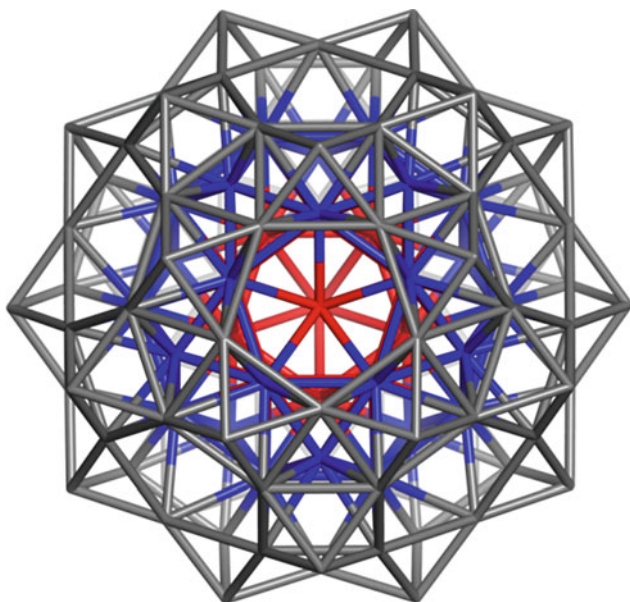
TT@3TT.39



TT.12 = t T.12



I@D.32



(I@20O)@ID@(12A₅;50O).132

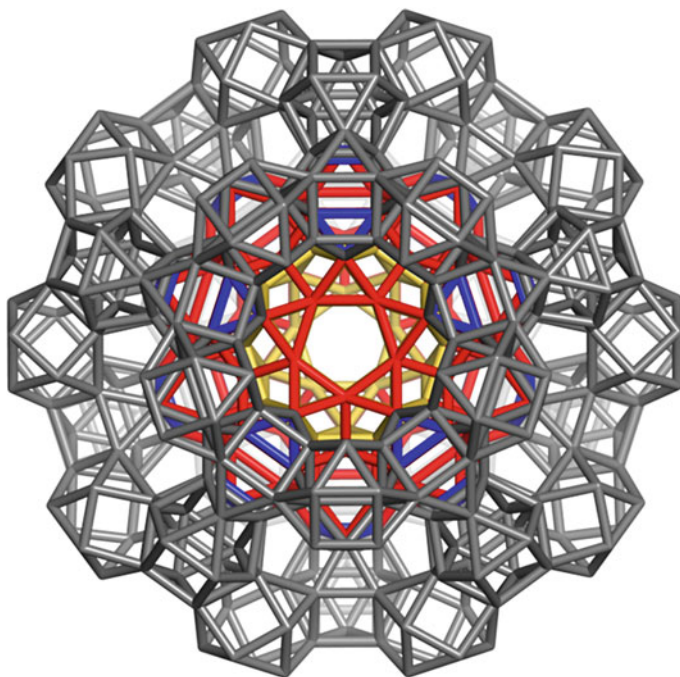
$C_{42}@C_{120}.132$

$m(IP@D_{33}).132$

$C_2 \times A_5$; classes 4: $|\{12\}; 2\{30\}; \{60\}|$

5A4.1

I@ID.42	m(IaD32).120	P ¹² @I@D.33



(ID@20CO150)@(m(m(I@D32)120)420).510

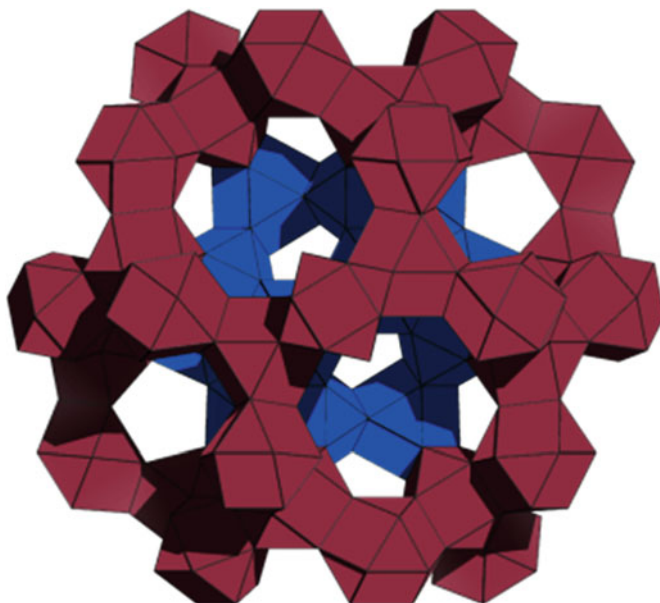
ID@20CO@50CO.510

m(m(IP@D33)132).510

$C_2 \times A_5$; classes 7: $|4\{60\}; \{30\}; 2\{120\}|$

5A4.1.1

I.12	<i>m(IP@D33)132</i>	ID@20CO.150

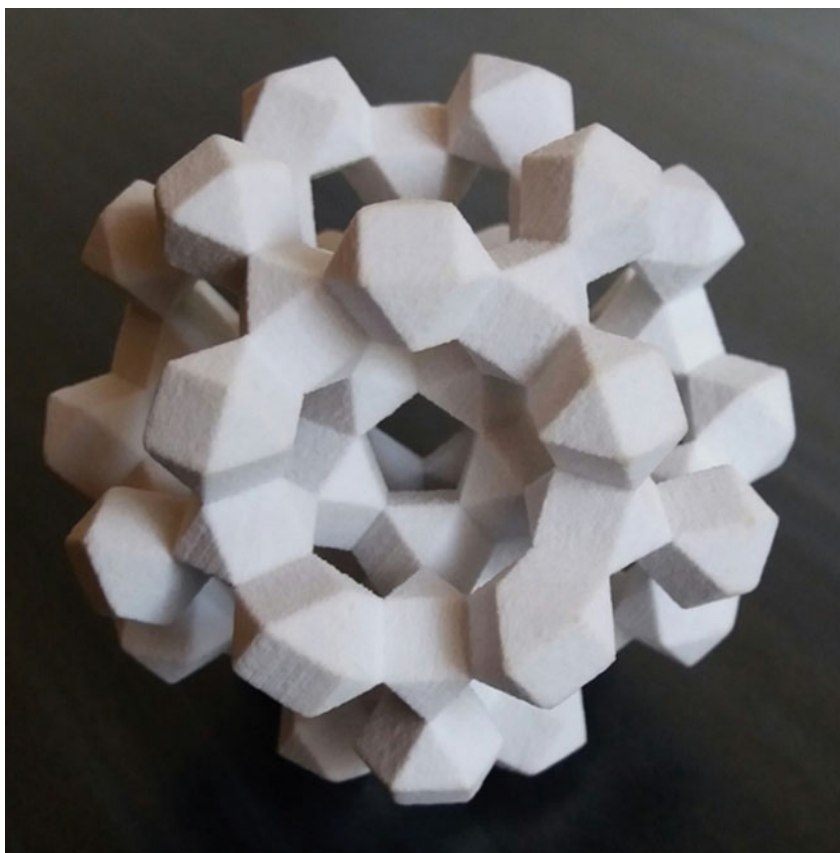


ID@20CO@50CO.510

$m(m(\text{IP@D33})132).510$
 $C_2 \times A_5$; classes 7: $|4\{60\}; \{30\}; 2\{120\}|$

5A4.1.2

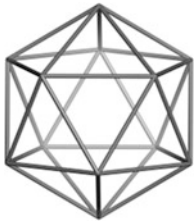
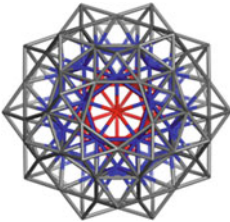
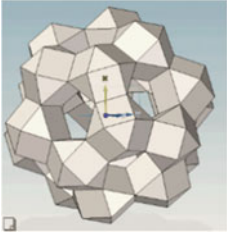
I.12	$m(\text{IP@D33})132$	ID@20CO.150

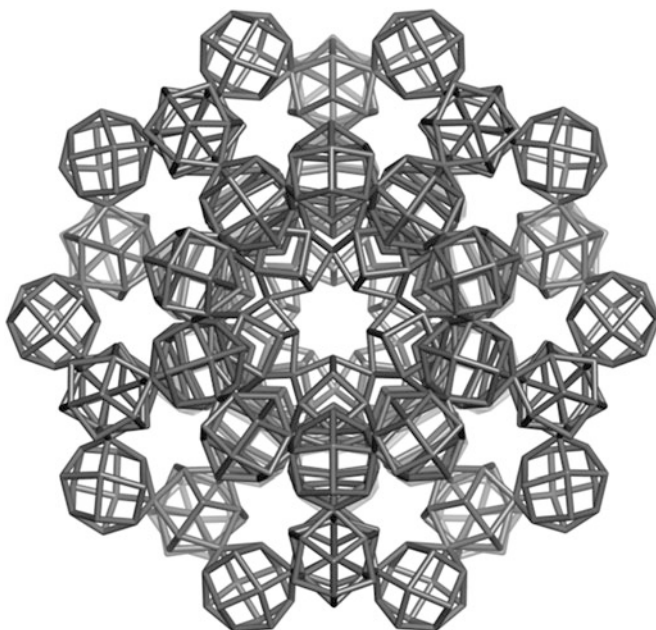


ID@20CO@50CO.510

$m(m(\text{IP}@\text{D}33)132).510$
 $\text{C}_2 \times \text{A}_5$; classes 7: $|4\{60\}; \{30\}; 2\{120\}|$

5A4.1.3

		
I.12	$m(\text{IP}@\text{D}33)132$	ID@20CO.150



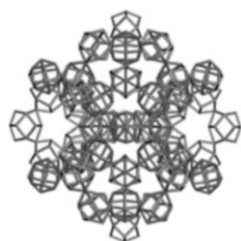
$20dCO@50dCO.870$

$d(m(m(IP@D)132)510).870$

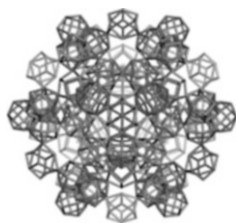
$d(510).870$

$C_2 \times A_5$; classes 17: $\{3\{30\}; 10\{60\}; 3\{20\}; \{120\}$

5A4.1.4



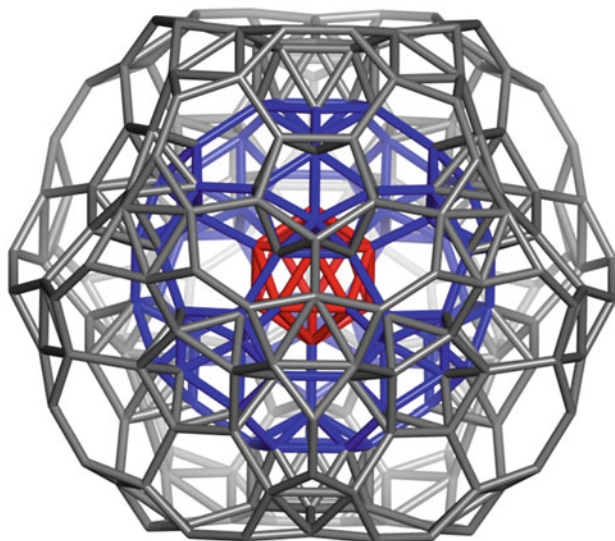
$d(510).870_2$



$d(510).870_3$



$dCO.14 = Rh12.14$



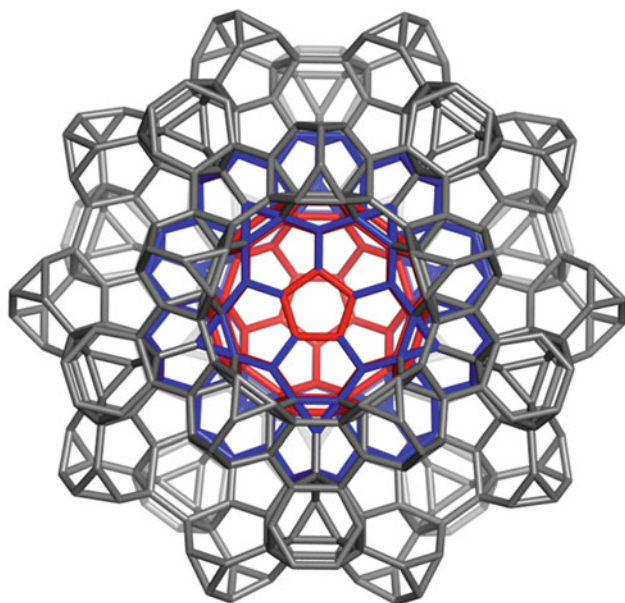
$(t(IP)84)@(t(I@D32)240).264$

$t(IP@D33).264$

$C_2 \times A_5$; classes 6: $|4\{60\}; 2\{12\}|$

5A4.2

<p>$t(IP@D33).264$</p>	<p>TT.12</p>	<p>$I@D.33$</p>



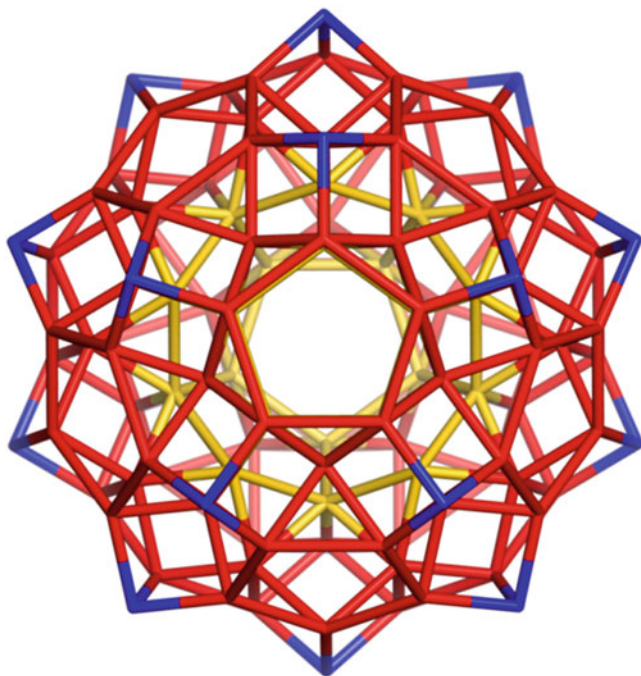
$(I(IP)150)@(I(I@D32)420).510$

$I(IP@D.33).510$

$C_2 \times A_5$; classes 7: $|\{30\}; 4\{60\}; 2\{120\}|$

5A4.3

<p>TT@3TT.39</p>	<p>TT.12 = iT.12</p>	<p>IP@D.33</p>



IY(12mP₅; f₃).130

D@(12mP₅; 20C).130

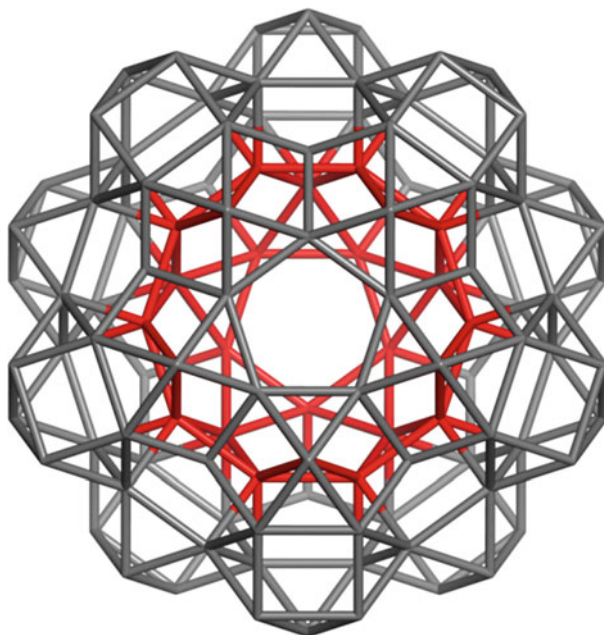
d(I@ID42).130

d(mIP42).130

C₂ × A₅; classes 4: |2{20}; {30}; {60}|

5A5.1

C	mP ₅ .15	I@ID.42



$C_{20}Y(20CO; f_3).150$

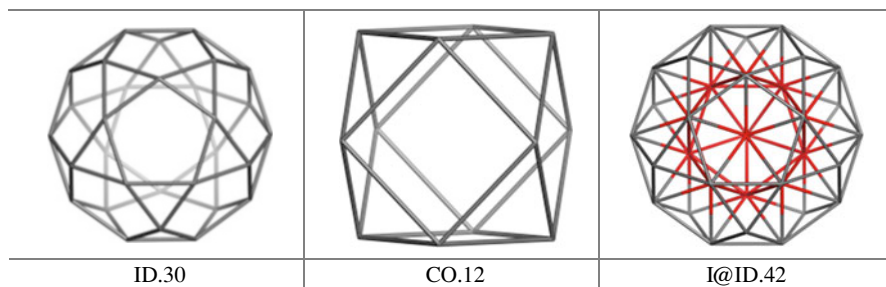
ID@20CO.150

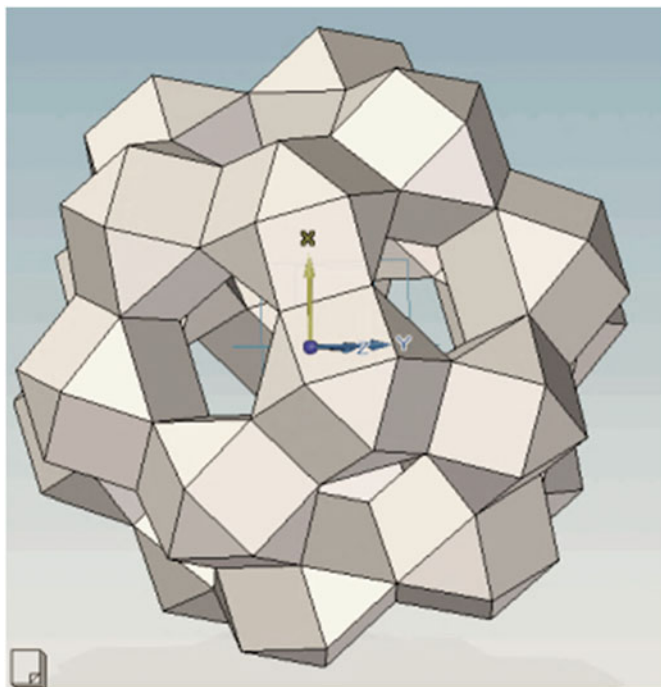
ID@(20CO;12P₅).150

m(mIP42).150

$C_2 \times A_5$; classes 3: |{30};2{60}|

5A5.2

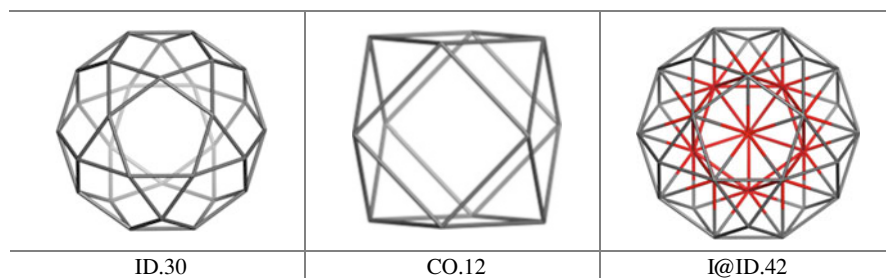




DY(20CO; f_3).150

ID@20CO.150
 $m(I@ID.42).150$
 $C_2 \times A_5$; classes 3: $\{|30\}; 2\{60\}$

5A5.3

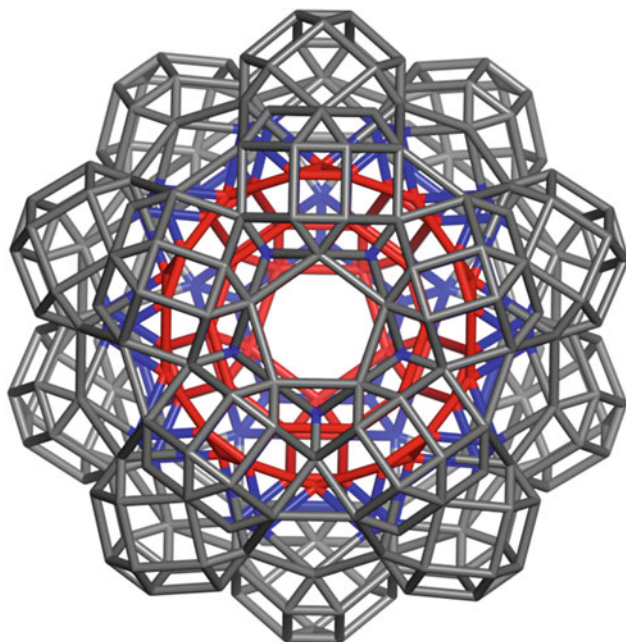




ID@20CO.150

m(I@ID.42).150
5A5.4

Apahida, Cluj, Romania, 2009



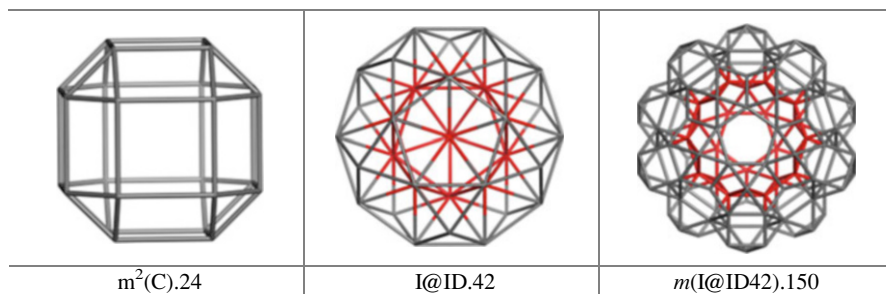
DY(20(m^2C);(f_3 ;P₃)).390

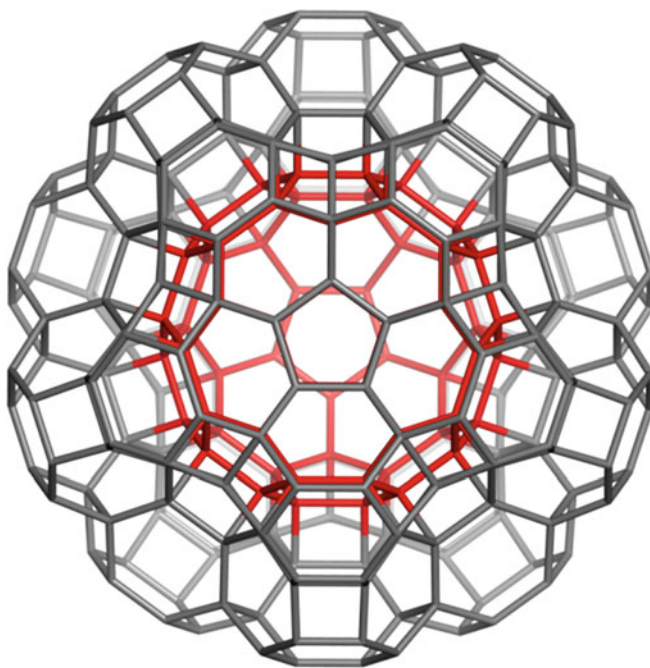
(m^2D)@(20 m^2C ;12 mP_5 ;30 P_3).390

$m(m(I@ID42)150).390$

$C_2 \times A_5$; classes 6|4{60};{30};{120}|

5A5.5





DY(20TO; f_6).300

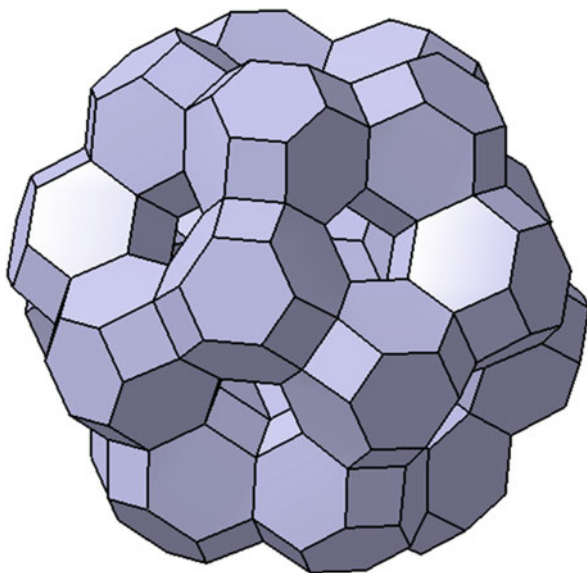
$C_{60}@$ (20TO;12P₅).300

$t(mIP42).300$

$C_2 \times A_5$; classes 4: $|\{120\}; 3\{60\}|$

5A5.6

P ₅ .10	TO.24	$mIP.42$



$C_{20}Y(20C_{24}; f_6).300$

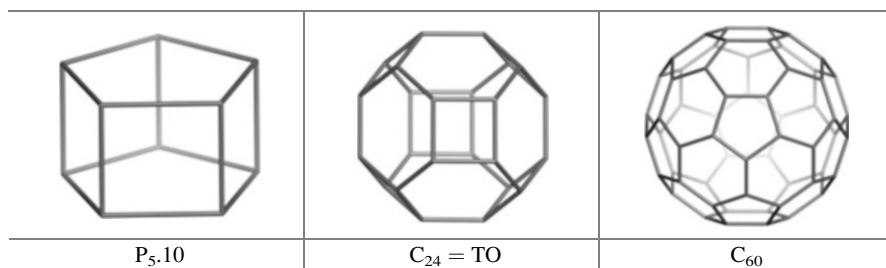
$DY@(20TO).300$

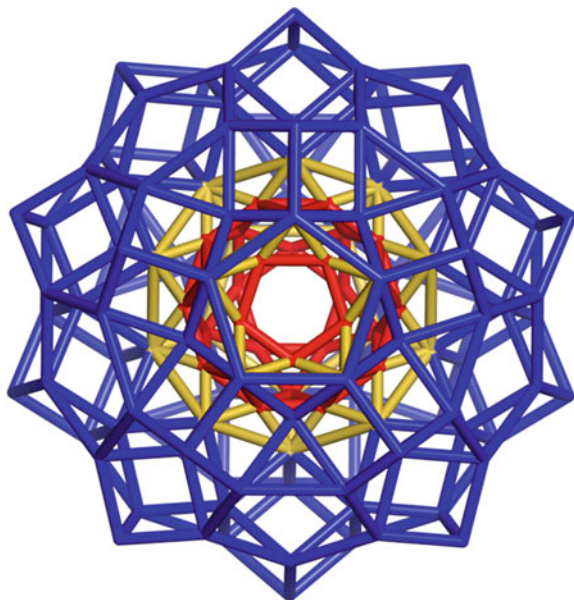
$C_{60}@(12P_5; 20TO).300$

$I(I@ID.42).300$

$C_2 \times A_5$; classes 4: $|\{120\}; 3\{60\}|$

5A5.7





d(IP50)@d(mIP42).160

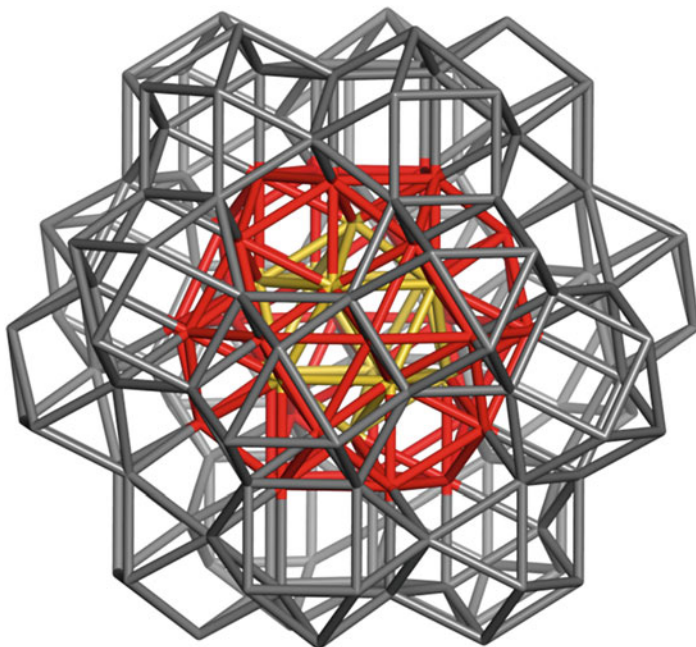
C50@C130.160

d(IP@ID43).160

$C_2 \times A_5$; classes 5: |2{20}; 2{30}; {60}|

5A6.1

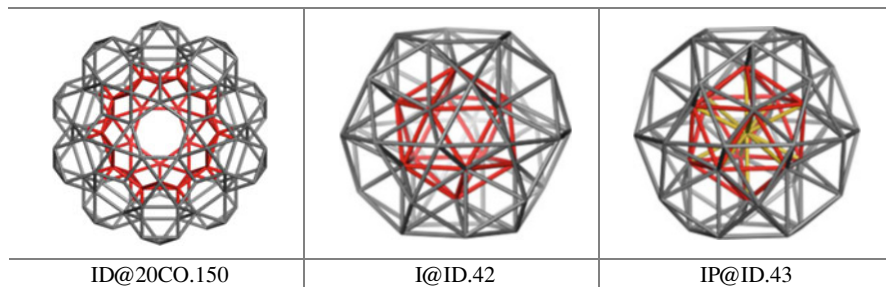
<p>d(IP@ID).160_2</p>	<p>d(IP@ID).160_3</p>	<p>IP@ID.43</p>

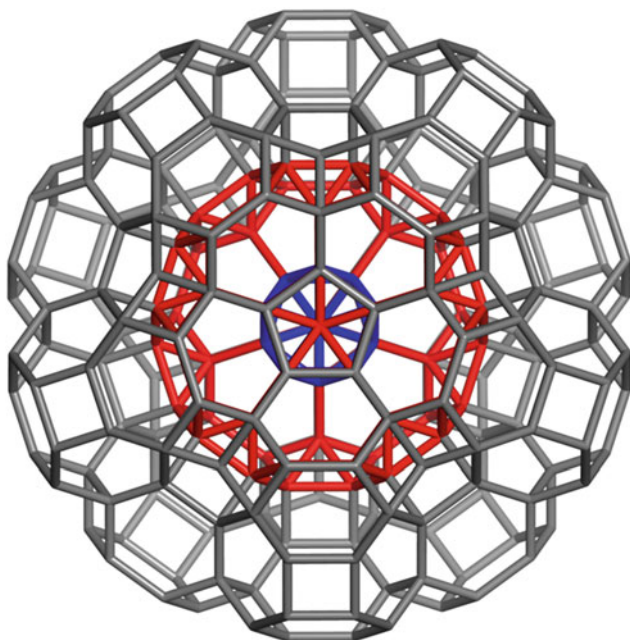


I@ID@20CO.162

(I@ID42)@(m(I@ID42)150).162
 $C_{42}@C_{150}.162$
 $m(IP@ID43).162$
 $C_2 \times A_5$; classes 4: |{30}; 2{60}; {12}|

5A6.2





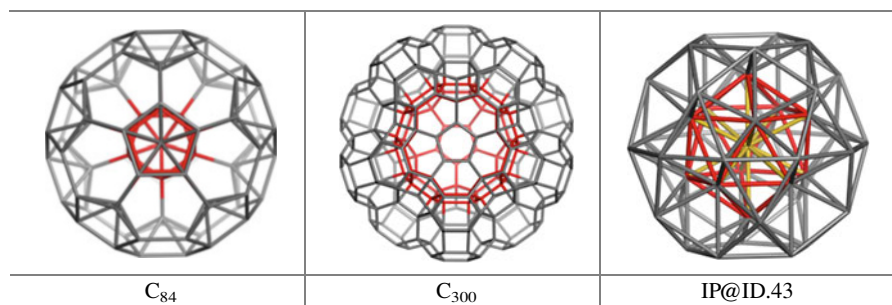
$C_{84}@C_{300}.324$

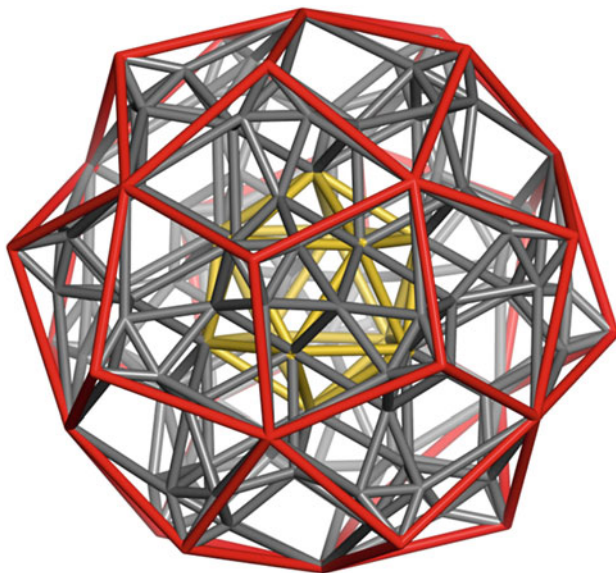
$I(IP@ID43).324$

$C_{84}@C_{300}.324$

$C_2 \times A_5$; classes 6: $|3\{60\}; 2\{12\}; \{120\}|$

5A6.3





$I@(12Rh_{10};20(mP_3;T))@(Rh_{30}).134$

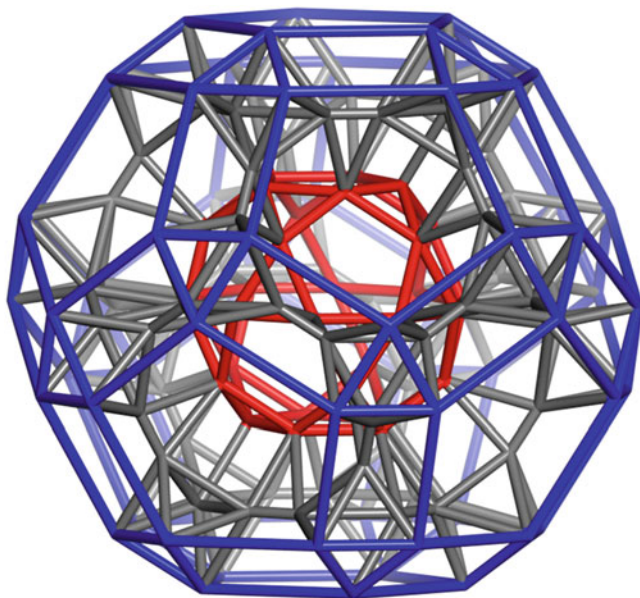
$C_{114}@C_{122}.134$

$d(D@ID50).134$

$C_2 \times A_5$; classes 5: $|\{60\}; \{30\}; \{20\}; 2\{12\}|$

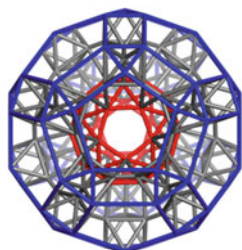
5A7.1

<p>C_{114} $I@(12(Rh_{10});20mP_3).114$</p>	<p>C_{122} $(Rh_{30})@(20T;30mP_3).122$</p>	<p>$d(D@ID50).134_5$</p>

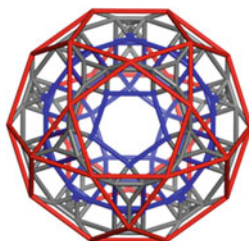


ID@(12m A_5 ;20(P $_3$;O);30P $_3$)@(mID).150

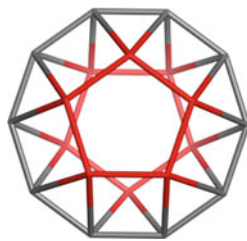
$m(D@ID50).150$
 $C_2 \times A_5$; classes 3: |{30};2{60}|
 5A7.2



$m(D@ID50).150_5a$



$m(D@ID50).150_5b$



mA_5

References

- Coxeter HSM (1973) *Regular polytopes*, London, 1948. Dover, New York, NY
- Diudea MV, Nagy CL (2007) *Periodic nanostructures*. Springer, Dordrecht
- Diudea MV, Ştefu M, John PE, Graovac A (2006) Generalized operations on maps. *Croat Chem Acta* 79:355–362
- Euler L (1752–1753) *Elementa doctrinae solidorum*. *Novi Comment Acad Sci I Petropolitanae* 4:109–160
- Johnson NW (1966) Convex solids with regular faces. *Can J Math* 18:169–200
- Nagy CL, Diudea MV (2009) *Nano Studio*. Univ Babeş–Bolyai, Cluj
- Nagy CL, Diudea MV (2017) Ring signature index. *MATCH Commun Math Comput Chem* 77 (2):479–492
- Papacostea C (1930–1935) *Platon*. *Opere*, 1–11 (Roum. translation), Casa Şcoalelor, Bucureşti
- Parvan-Moldovan A, Diudea MV (2015) Cell@cell higher dimensional structures. *Stud Univ Babeş-Bolyai Chem* 60(2):379–388
- Pisanski T, Randić M (2000) Bridges between geometry and graph theory, geometry at work. *MAA Notes* 53:174–194
- Schläfli L (1901) *Theorie der vielfachen Kontinuität* Zürcher und Furrer, Zürich (Reprinted in: Ludwig Schläfli, 1814–1895, *Gesammelte Mathematische Abhandlungen*, Band 1, 167–387, Verlag Birkhäuser, Basel, 1950)
- Schulte E (1985) Regular incidence-polytopes with Euclidean or toroidal faces and vertex-figures. *J Combin Theory Ser A* 40(2):305–330
- Schulte E (2014) *Polyhedra, complexes, nets and symmetry*. *Acta Cryst A* 70:203–216
- Taylor AE (1928) *A commentary on Plato's Timaeus*. Clarendon, Oxford
- Wikipedia (2016) https://en.wikipedia.org/wiki/Pentagonal_gyrobicupola. Accessed 12 Dec 2016
- Wolfram Research, Inc. (2016) *Mathematica*, Version 10.4. Champaign, IL

Chapter 6

Large Icosahedral Clusters

Dodecahedron, the fifth Platonic “element”, has been thought as the “quintessence” of universe (“God used this solid for the whole universe, embroidering figures on it”—Plato, *Timaeus* dialogue —Papacostea 1930–1935; Taylor 1928).

Together with the four others: Tetrahedron—fire; Icosahedron—water; Octahedron—air, and Cube—earth, the five shapes based the Plato’s “theory of everything”.

Dodecahedron is composed of twelve regular pentagonal faces, three of which meeting at each vertex (symbol $\{5,3\}$, Schläfli 1901), within the icosahedral symmetry; however, at the Plato’s time, it was not clear that its faces are all regular, that later was demonstrated by Euclid (“*Elements*”, Book XIII—Heath 1981).

The dual polyhedron of the Dodecahedron is the Icosahedron. Recall that, within this book, only the shapes of polyhedra are considered while the angles and bonds length are disregarded.

6.1 Small Complex Clusters

In the introductory Chap. 3 of this book, there were mentioned “point centered polyhedra”, symbolized MP or P@M (see Fig. 6.1); these represent the most simple structures of rank $k = 4$ and a source for deriving a plethora of complex structures/clusters by means of operations on maps. Also, the MP clusters represent “cell-dual” of some important complex structures (e.g., $C_{60}P.61$ & C_{750} , Sect. 9.3). The number of connections of the central vertex is written as an exponent number $P^{n}@$ while the “endo” symbol is used to recall that the point/atom P lies inside the cage. The last number in the name of a cluster represents the total number of points/atoms.

P-centered polyhedra, as real structures, are found in endohedral fullerenes (Saunders et al. 1993; Koltov 2007; Popov et al. 2013). P@M are models for



Fig. 6.1 P-centered cluster graphs

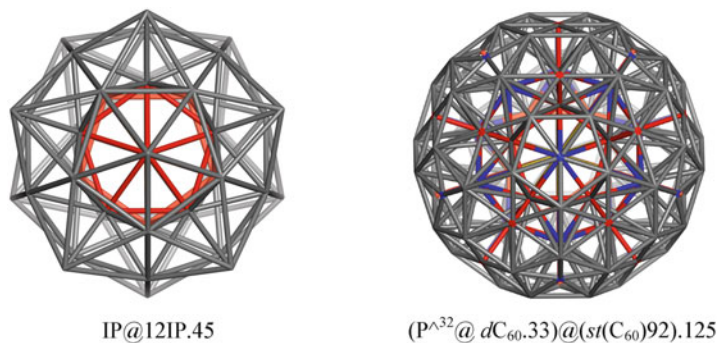


Fig. 6.2 P@M clusters: Bergman's cluster C_{45} (left) and C_{125} (right)

Table 6.1 Figure count in C_{45} and IP structures

Cluster	v	e	3(2)	5(2)	6(2)	2	T(3)	U(3)	M	3	χ	k
IP (6A2)	13	42	50	0	0	50	20	0	1	21	0	4
C_{45} (6A3)	45	204	290	0	0	290	130	0	1	131	0	4
C_{125} (9A1.3.1)	125	604	870	12	20	902	390	32	1	423	0	4

metallic clusters $M@M_{12}$, with $M = Ru, Rh, Pd, Fe$; such clusters have been predicted to exhibit outstanding magnetic properties (Reddy et al. 1993).

Here, two new MP clusters are introduced: Bergman's cluster C_{45} (Bergman et al. 1952; Duneau and Gratias 2002) and C_{125} , a cluster inspired from C_{45} (Fig. 6.2). Figure count of the two clusters and additional IP.13 is given in Table 6.1; all these clusters have the rank $k = 4$.

Dodecahedron and Icosahedron, as a dual pair, often coexist within a same complex structure. The symbol for hyper-structures is either DY (i.e., $C_{20}Y$) or IY (i.e., $C_{12}Y$) depending which topology is aimed to be evidenced. The number, variety and size of clusters with icosahedral symmetry being higher than to be included in only two chapters (Chaps. 5 and 6), a new chapter was needed to discuss the relatives of $C_{60}I_h$ fullerene; that is why several structures are treated both here and in the following Chap. 9.

6.2 Icosahedral Clusters Derived from the C_{45} Seed

The above small clusters can be used as seeds in two operation sequences:

- (a) medial: (1) $m(IP_{13}).42$; $d(C_{42}).130a$; (2) $m(C_{45}).204(6A3.1)$; $d(C_{204}).810a$ (6A3.1.1).
 (b) truncation: (1) $t(IP_{13}).84$; $d(C_{84}).130b$; (2) $t(C_{45}).408(6A3.2)$; $d(C_{408}).810b$ (6A3.2.1); (3) $t(C_{125}).1208$; $d(C_{1208}).2430$.

Figure 6.3 illustrates the clusters obtained from $IP@12IP.45$ (6A3) (Bergman's cluster) by medial and truncation, respectively, while their duals are shown in Fig. 6.4. Figure count for these structures is listed in Tables 6.2, 6.3, and 6.4.

By using the Y-symbol for a hyper-structure, the names of the above clusters are: $IP = P^{12}@I.13$ (6A2); $(IP)Y(13IP).45$ (6A3); $(IP)Y(13C_{42}).204$ (6A3.1); $(IP)Y(13C_{84}).408(6A3.2)$; $(IP)Y(13C_{130a}).810a$ (6A3.1.1) and $(IP)Y(13C_{130b}).810b$ (6A3.2.1). From these names, it is clear that all these clusters preserve the Icosahedralsymmetry group ($C_2 \times A_5$; order 120) of the parent IP cluster.

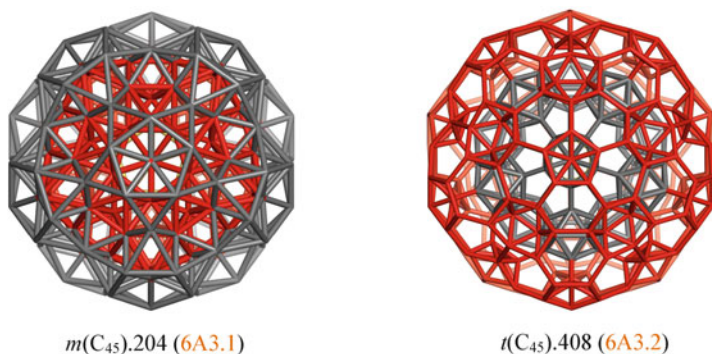


Fig. 6.3 Clusters designed by medial and truncation

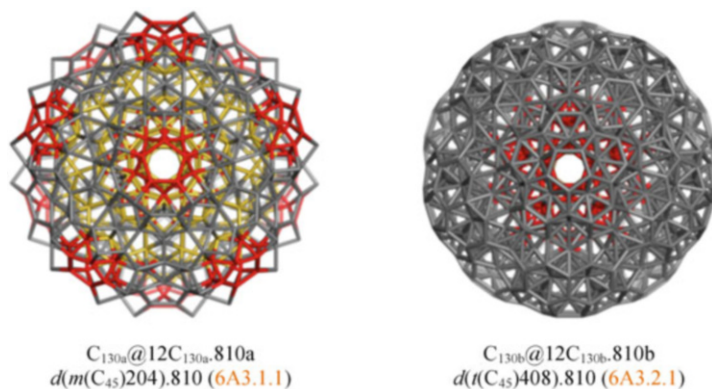


Fig. 6.4 Icosahedral clusters derived by dual operation

Table 6.2 Figure count in $d(C_{204}), 810a$ (6A3.1.1) and related structures

v	e	3(2)	4(2)	5(2)	2	U(3)	C(3)	Py ₅ (3)	mP ₅ (3)	O(3)	M	3	χ	k	U(M)
1	810	690	780	228	1698	12	130	0	114	0	2	258	0	4	D(D;E)
2	130	90	120	24	234	0	20	0	12	0	2	34	0	4	(D;C ₈₀)
3	204	870	810	0	12	822	0	12	0	130	2	156	0	4	I(I;mC ₆₀)
4	42	150	130	0	12	142	0	12	0	20	2	34	0	4	(I;ID)

1 = $d(m(C_{45})204), 810$ (6A3.1.1); 2 = $d(m(IP)42), 130a$ (6A3.1.1b); 3 = $m(C_{45}), 204$ (6A3.1); 4 = $m(IP), 42$ (5A5)

Table 6.3 Figure count in $d(C_{408}), 810b$ (6A3.2.1) and related structures ($k = 4-6$)

V	e	3(2)	5(2)	6(2)	2	T/TT	U	A_5	Py_k	M	3	4	5	6	U(M)	4;5
1	810	3030	2770	342	120	3232	650	12	228	2	1012	13	13	0	D(D;E)	$C_{110}; C_{130}$
2	130	450	410	36	30	476	100	0	24	2	156	2	2	-	(D; C_{80})	
3	110	360	320	24	30	374	80	0	12	2	124	0	-	-	(ID; C_{80})	
4	50	150	110	24	0	134	20	0	12	2	34	0	-	-	(D; ID)	

1 = $d(r(C_{45})408), 810b$ (6A3.2.1); 2 = $d(C_{84}), 130b$ (6A3.2.1b); 3 = $d(C_{84}), 130bX, 110$; 4 = $dIP, 50$ (5A7)

Table 6.4 Figure count in C_{408} (6A3.2) relatives

	v	e	3(2)	5(2)	6(2)	2	U	TT	Py ₅	C ₆₀ (3)	3	4	χ	k	U
1	408	1074	520	12	290	822	12	130	12	13	167	13	2	5	I
2	143	490	390	114	0	504	12	0	156	0	168	13	2	5	D
3	84	192	80	12	50	142	1	20	12	1	34	0	0	4	I
4	21	50	30	12	0	42	1	0	12	0	13	0	0	4	–
5	13	42	50	0	0	50	1	20	0	0	21	0	0	4	–

1 = $t(C_{45})_{408}$ (6A3.2); 2 = $cd(C_{408})_{143}$ (6A3.3); 3 = $t(IP)_{84}$ (5A2.1); 4 = DP.21 (6A1); 5 = IP (6A2)

Cluster tIP_{84} (5A2.1) is related to the Samson cluster, that consists of 20 truncated tetrahedra TT (i.e., Friauf polyhedra), icosahedrally arranged, with a central atom inside each TT, all together counting 104 points/atoms (de Boiesieu et al. 1991; Samson 1965, 1972); the central shell forms an icosahedron. It was found in Al-Cu-Li intermetallics, which represent compounds involving two or more metals, such as Frank and Kasper (1958) phases, etc. They can display desirable magnetic, superconducting and chemical properties, due to their strong internal order and mixed (metallic and covalent/ionic bonding, respectively).

Note that any cluster may be decomposed in several ways, some key-substructures being illustrated, in the Atlas, at the bottom of figures; accordingly, several names are used for a same structure, with the aim of a better detailing its composition. However, the fragment union (i.e., re-construction) finally will provide a single structure, the figures/substructures of which are counted to find its rank. Here, the term “rank” (Schulte 1985, 2014) is preferred to “(space) dimension” since our description is a topological one, the geometric aspects (angles and bond length) being disregarded.

By truncating C_{45} (6A3) one obtains the cluster $t(C_{45})_{408}$ (Figs. 6.2 and 6A3.2) of which (all face) dual is $d(t(C_{45})_{408})_{810b} = C_{130b}@12C_{130b}_{810}$ (Figs. 6.4, right and 6A3.2.1), a cluster of rank 6 (Table 6.3). As shown in Sect. 5.4, if there is a 3-facet within a cluster that is shared by two 4-facets, the cluster is of rank $k = 5$; it is the case of C_{130b} (6A3.2.1, bottom) (Coxeter 1973; Euler (1752–1753), which is, in turn, a 5-facet (among the 13 ones) of C_{810b} , this being thus of rank $k = 6$. In addition, Table 6.5 provides data about its topological symmetry (Nagy and Diudea 2017).

Searching for the atom classes by face/ring count provides the “chemical vertex type” if the rings around each vertex/atom (counted by RSI) are „strong rings” (Blatov et al. 2010); however, by enlarging the rings to “circuits” of various length (the upper bound involves the counting of circuits of length $2d + 1$, d being the diameter of the graph), then “topological vertex type” is obtained [finally correctly discriminating all the classes of a graph, as proved by performing the permutations within the adjacency matrix, by Mathematica and GAP software (Groups, Algorithms and Programming, <http://www.gap-system.org>)]. If the “ring signature” is collected in a layer matrix (Diudea 1994; Diudea and Ursu 2003), the centrality index calculated on it (see Chap. 4), will distinguish all the distinct vertices, at the early level of strong rings (see Table 6.5). The same vertex classes are obtained with

Table 6.5 Topological symmetry by ring count and centrality C-index (see Chap. 4), in non-increasing order of centrality, in C_{810b} (6A3.2.1) and its relatives

	(RSI)	R_{\min}	R_{\max}	Deg	Signature ($C_{\min}; C_{\max}$)	Classes {elements}
2	C_{84} (5A2.1)	3	6	6	$3^5.5^5.6^5.25$	3 : {12};
				6	$3^5.6^5$	{12};
				4	$3^2.5.6^3$	{60}
	LM(C_{84})	3	6	6	(0.149447)	3 : {12};
				6	(0.118464)	{12};
4				(0.097012)	{60}	
4	C_{408} (6A3.2)	3	6	6	$3^5.5^5.6^5.25$	6 : {156};
				6	$3^5.5^2.6^6$	{60};
				5	$3^3.5^2.6^8$	{60};
				6	$3^5.6^5$	{12};
				4	$3^2.5.6^6$	{60};
				4	$3^2.5.6^3$	{60}
	LM(C_{408})	3	6	4; 5; 6	(0.095120)	10 :4 × {12};
					(0.057074)	6 × {60}
5	$C_{810b} = d$ (C_{408})	3	6	12	$3^2.1.5^3.6^6$	7 : {110};
				12	$3^2.1.5^2.6^4$	{60};
				12	$3^2.1.5^2.6^4$	{60};
				6	$3^6.5^3.6^3$	{280};
				6	$3^6.5^2.6^4$	{60};
				6	$3^9.6^3$	{60};
				5	$3^5.5.6^3$	{180}
LM(C_{810b})	3	6	(5;6;12)	(0.104546) (0.065660)	15 : 3 × {20}; {30};10 × {60} {120}	

the layer matrix of topological distances, an even faster procedure, compared to the ring counting. These theoretical tools, implemented in the Nano Studio software (Nagy and Diudea 2009), developed at TOPO GROUP, “Babes-Bolyai” University, Cluj, Romania, enable the study of topological symmetry of rather complex structures.

Resuming to C_{408} , its cell dual (realized by changing a cell by a point/vertex) cd (C_{408}) = (IP)Y(13DP; f_5).143 = 13(P²⁰@D21).143 consists of 13 DP.21 units; it is illustrated in Fig. 6A3.3 and figure count listed in Table 6.4. Further, cd (C_{84}) = DP.21 (5A2.1.1a) and cd (D@12D.130) = IP.13 (6A6.3).

6.3 Clusters of Dodecahedral Topology

Structures decorated with dodecahedral shapes D (i.e., C_{20}) can be designed by the following sequence of operations (Diudea 2013): $t_{sel}(p_4(P))$; $s_2(P)$; $t_{sel}(p_4(P)) @s_2(P)$, where t_{sel} stands for the selected vertices truncation while the “endo” symbol @ means “inside”. Formally, every point in the parent polyhedron P was changed by a C_{20} cell; the resulted structure $PY(nD;f_5)$ is a “hyper” and a “spongy” structure, with the central hollow of exact topology of $t_{sel}(p_4(P))$. If this hollow is filled, by connecting inside the parent P , a double-shell cluster will result, which is no more a spongy structure.

In case $P = D$, the topology of both parent polyhedron and decoration is dodecahedral: $DY(20M)$, M being D or $o(D)$ transforms; the structures are shown in the Atlas (Figs. 6A4*n* and 6A5*n*) while the figure count is given in Table 6.6.

The cluster $DY(20D;f_5).250$ (6A4), consisting of 20 dodecahedral shapes, is a spongy hyper-dodecahedron, of genus $g = 11$, its core being the 110-keplerate. The packing fraction $\phi = 20/33 \approx 0.6060$ is calculated with respect to the 33 dodecahedra needed for the radial space filling, as is the case of cluster $D@12D@20D.270$ (6A5). Compared with the spheres maximum fraction [0.7405, see Ulam conjecture (Gardner 2001, Hales 1992, 2005)] clearly it is a spongy, non-convex structure. Its five-fold symmetry ($C_2 \times A_5$; order 120) is also clear, even pentagons show some distortion (and strain) to the regular pentagon.

In structures of the type $PY(nD)$; $P:n = D:20, C:8, T:4$, decorated with dodecahedral shapes D , the number of faces is counted as follows ($P = D$; Table 6.6):

$$l2\text{-faces}l = 5(2) + w(s) \text{ if } s \neq 5$$

$$l2\text{-faces}l = 5(2) \text{ if } s = 5$$

$$l3\text{-faces}l = U(3) + M$$

The number of 3-faces (i.e., cells) equals the number of U-shapes plus M (including the “core” (i.e., the central hollow seen as a “cell”) and the “envelope” (or 4-embedding), thus its maximum value being 2). The column heads in tables of “figure count” (such as Table 6.6) are to be read as “cardinality of x -type sets”.

In spongy *spa* the number of 2-faces equals the sum of pentagons $5(2)$; thus $w(5) = 0$; $M = 0$; $g = w/2$, with w being the window-faces. The cells $U(3)$ are only dodecahedra D while the “core” is seen “empty” (and the envelope, as well).

Spongy *spb* represents a (discretized) continuous surface, forming the envelope (of rank $k = 3$ and genus g equals the number of windows minus one: $g = w - 1$).

Table 6.6 Figure count in hyper-dodecahedra DY decorated with dodecahedral shapes D

Structure	v	e	$5(2)$	$w(s)$	2	$U(3)$	M	3	χ	$k(g)$
$DY(20D)$ (6A4)	250	450	222	$12(5)$	222	20	2	22	0	$4(0)$
$DY(20D)_{spa}$	250	450	222	$12(5)$	210	20	0	20	-10	$4(6)$
$DY(20D)_{spb}$	250	450	180	$12(5)$	180	0	0	0	-20	$3(11)$
$D@DY(20D)$ (6A5)	270	500	264	$24(5)$	264	32	2	34	0	$4(0)$

Table 6.7 Figure count in clusters of dodecahedral topology

	v	e	3(2)	4(2)	5;10(2)	6(2)	2	U(3)	$c_h(3)$	M	3	χ	$k(g)$
1	210	600	400	0	0	0	400	20	0	0	20	-10	4(6)
2	400	750	0	150	240	0	390	20	30	0	50	-10	4(6)
3	450	1110	520	0	222	0	742	20	60	2	82	0	4(0)
3 _{sp}	450	1050	400	0	210	0	610	20	0	0	20	-10	4(6)
4	610	1200	0	600	0	0	600	20	0	0	20	-10	4(6)
5	500	1320	720	0	264	0	984	32	130	2	164	0	4(0)
6	900	1650	700	0	222	0	922	20	150	2	172	0	4(0)
6 _{sp}	900	1650	700	0	210	0	910	20	150	0	170	-10	4(6)
7	1050	1650	0	0	210	400	610	20	0	0	20	-10	4(6)
8	1200	1950	0	150	240	400	790	20	30	0	50	-10	4(6)
9	1200	1860	0	30	240	400	670	20	0	0	20	-10	4(6)

1 = $d(C_{250}).210sp$ (6A4.3); 2 = $d(d(C_{250})J).400sp$ (6A4.3.3); 3 = $m(C_{250}).450$ (6A4.4); 3_{sp} = (6A4.4.1); 4 = $d(m(C_{250})).610 sp$ (6A4.4.2); 5 = $m(C_{270}).500$ (6A5.1); 6 = $t250.900$ (6A4.5); 6_{sp} (6A4.5); 7 = $l(C_{250}).1050$ (6A4.6); 8 = $DY(20C_{60};P_5).1200$ (6A4.3.1); 9 = $DY(20C_{60};hh[2 + 2]).1200$ (6A4.3.2)

Filled structures are basic structures with the core same as the parent polyhedron P (of which points were replaced by D-shapes) while U(3) includes, besides D-units, some shapes with 2-faces pentagons and two non-pentagonal faces (coming from P); the number of such shapes equals the number of 2-faces in P; the number of windows in filled clusters is twice that in the basic spongy ones.

When C_{250} or C_{270} clusters were taken as seeds for map operations, the resulting objects were decorated with the C_{60} cluster (6A4.3.1; 6A4.3.2; 6A4.6) or its transforms; structures are illustrated in the Atlas; the figure count is listed in Table 6.7. Some of these clusters show higher genus g , being spongy structures (6A4.3; 6A4.4.1; 6A4.4.2). The structures could be used to build monumental constructions.

6.4 Clusters of Icosahedral Topology

When a hyper-structure has the topology of icosahedron, either 13 cells, of formula (IP)Y(13M) or 12 cells, of formula IY(12M) can be seen, M being D or \circ (D) transforms; this is because the 13 cells are in fact 12 cells with the hollow inside of the same topology as the other 12 cells; it is clear that “spongy” structures will have the formula IY(12M).

Starting from the cluster $D@12D.130 = C_{20}@12C_{20}.130$ (6A6), a series of new clusters can be derived by map operations; these derivatives are illustrated in the Atlas (Figs. 6A6n) while their figure count is listed in Table 6.8. Note that sequences $t(d(C_{130}))$ and $l(C_{130})$ lead to C_{60} -decorated structures (6A6.1.1; 6A6.1.2; 6A6.1.3; 6A6.6).

Table 6.8 Figure count in clusters of icosahedral topology

v	e	3:4(2)	5(2)	6(2)	2	U	$c_1(3)$	$c_2(3)$	M	3	χ	$k(g)$	$U; c_n(M)$
1	130	230	114	0	114	12	0	0	2	14	0	4	D(D..)
2	114	390	0	0	310	12	20	0	2	34	0	4	I;O;(L..)
2 sp	114	360	240	0	240	12	0	0	0	12	-18	4(10)	I;(ID..)
3	230	570	280	114	394	12	40	0	2	54	0	4	ID;(ID..)
4	460	830	340	114	454	12	70	0	2	84	0	4	rD;T;(rD..)
5	570	1020	110	114	504	12	40	0	2	54	0	4	C ₆₀ ;TT;(C ₆₀ ..)
5 sp	570	930	0	114	354	12	0	0	0	12	-18	4(10)	C ₆₀ ;()
6	780	1380	210	156	676	12	42	20	2	76	0	4	C ₆₀ ;TO;P ₅ ;(C ₆₀ ..)
6 sp	720	1230	150	144	534	12	30	0	0	42	-18	4(10)	C ₆₀ ;P ₅ ()
6 sp_2	720	1140	0	144	414	12	0	0	0	12	-18	4(10)	C ₆₀ ;()

1 = C₁₃₀(6A6); 2 = C₁₁₄(6A6,1); 2 sp = C₁₁₄ sp (6A6,2); 3 = m(C₁₃₀),230(6A6,4); 4 = r(C₁₃₀),460(6A6,5); 5 = l(C₁₃₀),570(6A6,6); 6 = t(C₁₃₀),780(6A6,1.1); 6 sp = r(C₁₃₀),720 sp (6A6,1.2); 6 sp_2 = r(C₁₃₀),720 sp (6A6,1.3)

6.5 Rhomb Decorated Clusters

Rhombic prototiles have been used in the aperiodic Penrose tessellation (Penrose 1974; Ammann et al. 1992; Grünbaum and Shephard 1987). A prototile is one of the shapes of a tile in a tiling/tessellation. A tiling is a covering of the plane by tiles, with no overlaps or gaps.

Rhombic tiling may be realized by performing the medial operation followed by the dualization: $dm(M)$. Medial may be repeated iteratively, as in the sequence $dm^k(M)$. The rhombic tiling may also be realized by the $p_4(M)$ operation (see Chap. 2).

Within this chapter, attention is focused only on the cluster $Rh_{30}@12Rh_{30},374$ (or $d(m(D@12D.130)230),374$) (6A6.4.1); it was built up by applying the sequence dm to the cluster $D@12D.130$, representing 12 dodecahedra surrounding a hollow with the same shape of the dodecahedron. All the 13 dodecahedra are recovered in C_{374} transformed in the rhombic triacontahedron shape Rh_{30} . The envelope E is considered as the “embedding cell” into the fourth dimension space or as an abstract 4-rank figure. The alternating sum of all figures, cf. Euler (1752–1753) formula equals zero, thus the structure has the rank 4. Table 6.9 lists the figure count for some related clusters of C_{374} ; its spongy version C_{354} (6A6.4.2 and Table 6.9, #2) is a hyper-structure $IY(12Rh_{30};P)$, a multi-torus of genus $g = 10$, equaling half the number of windows $w(6)$. Another rhombic spongy cluster, $d(m(DY(20D;f_5)250)),610$, of genus $g = 6$; its structure is detailed in Fig. 6A4.4.2 and Table 6.7 (#4).

A special attention needs the cluster C_{152} (6A6.4.3 and Table 6.9, #3), a relative of C_{374} ; it includes the smallest rhombic $Rh_{3,5}$ substructure, which is not a polyhedron cf. Steinitz (1922) theorem but a tile (Blatov et al. 2010); Rh_3 is the skeleton of a molecule, named [1,1,1]-propellane. C_{152} was designed by identifying (32 points of) Rh_{60} (6A7.1) inside of $Rh_{120} = dm^3D.122$ (6A7.2), see Fig. 6.5.

The vertices of C_{152} form five classes; there is no connection within the vertices of a same class, the cluster being a five-partite graph and consequently its chromatic

Table 6.9 Figure count for some clusters related to C_{374} (6A6.4.1)

	v	e	3(2)	4(2)	5(2)	2	3i	3ii	3iii	3iv	M	3	$\chi(g)$	k
1	374	960	280	390	0	670	20	0	50	12	2	84	0	4
2	354	720	0	360	0	360	0	0	0	12	0	12	18(10)	4
3	152	360	0	300	0	300	60	0	0	30	2	92	0	4
4	122	240	0	180	0	180	60	0	0	0	2	62	0	4
5	360	1020	400	360	24	784	60	12	30	20	2	124	0	4
6	610	1200	0	600	0	600	0	0	0	20	0	20	-10(6)	4

1 = C_{374} ; $d(m(D@12D).130)$; (6A6.4.1); 3i(T); 3iii(mP_3X); 3iv($Rh_{30},32$); M($Rh_{30},32$); E); 2 = C_{354} ($C_{374}sp$); (6A6.4.2); 3iv ($Rh_{30},32$); 3 = C_{152} (6A6.4.3); 3i($Rh_{3,5}$); 3iv($Rh_8,10$); M($Rh_{60},62$); $dm^3D.122$); 4 = C_{122} (6A6.4.4); 3i($Rh_{3,5}$); M($Rh_{60},62$); E); 5 = $mC_{152},360$ (6A6.4.5); 3i(P_3); 3ii(A_5); 3iii($mA_4,16$); 3iv(O); M($m^3D.120$); E); 6 = $d(m(DY(20D;f_5)250)),610$ sp (6A4.4.2). 3iv ($Rh_{30},32$)

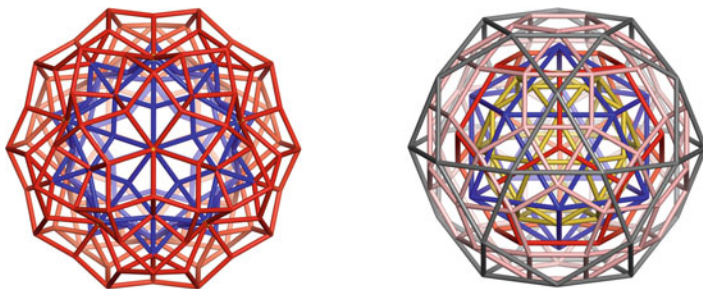


Fig. 6.5 Building C_{152} (6A6.4.3): $Rh_{60}@Rh_{120}$ (left) and superposing the five (inside connected) classes, distinctly colored (right); for details see text

Table 6.10 Topology of C_{152} (6A6.4.3) ($ppl(C_{152}).122$ (6A6.4.4)): vertex classes by centrality (non-increasing order)

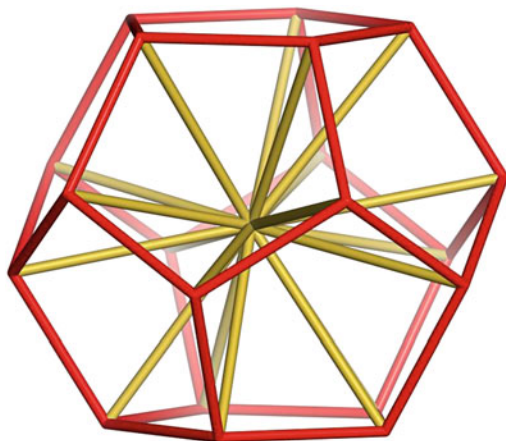
Class	Centrality signature	Elements	Vertex degree	Ring signature
1	0.122077 (0.127515)	{12}	10 (10)	4^{20} (4^{15})
2	0.121176 (0.127072)	{30}	4 (4)	4^8 (4^8)
3	0.105571 (0.123826)	{20}	6 (6)	4^{12} (4^9)
4	0.104829 (0.109943)	{60}	4 (2)	4^6 (4^2)
5	0.104090	{30}	4	4^4
RSI	1.578947 (1.475410)			

number is five. If the vertices inside each class are connected, the following shapes are obtained: icosahedron (class {12}); dodecahedron (class {20}); icosidodecahedron $mD.30$ (two classes {30}) and rhombicosidodecahedron $m^2D.60$ (class {60}), all of icosahedral symmetry. Superposition of these substructures, each distinctly colored, is suggested in Fig. 6.5 (right). Note that atom-vertex classes superimpose over topological/central-vertex classes (a consequence of vertex five-partity); vertex ring signature, centrality index and RSI are given in Table 6.10. Further, all the 300 4(2) faces of C_{152} are rhombic (Table 6.9; #3); they are distributed in four equivalence classes, of composition: $\{60^3;120\}$.

If the 30 external points in C_{152} are deleted, the remaining structure is still a cluster, of rank $k = 4$ (and a four-partite graph), the only “cell” of which being the propellane; again the atom-vertex classes superimpose over topological/central-vertex classes. It was named $ppl(C_{152}).122$ (6A6.4.4 and Table 6.9, #4); a new class of structures, called propellanes, was thus discovered.

A relative of C_{152} , made by the medial operation, is the cluster C_{360} ; its main substructure is the square gyrobicupola = J_{29} (see the discussion in Sect. 5.3) along with antiprism A_5 (see 6A6.4.5 and Table 6.9, #5), prism P_3 and octahedron O .

Chapter 6 Atlas: Large Icosahedral Clusters



IY(12Py₅; f₃).21

DP.21

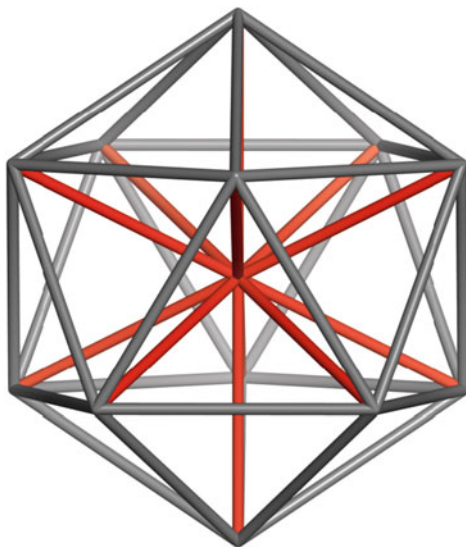
P²⁰@12Py₅@D.21

P@D.21

C₂ × A₅; classes: 2 |{1}; {20}|

6A1

I.20	Py _{5,6}	P@D.21



DY(20T; f_3).13

IP.13

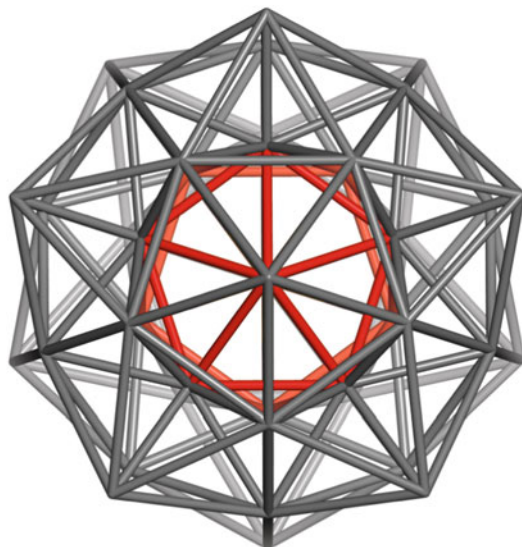
P@I.13

P@T₂₀@I.13

C₂×A₅; classes: 2 |{1};{12}|

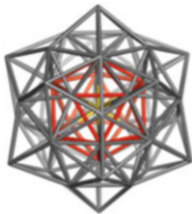
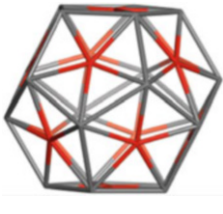
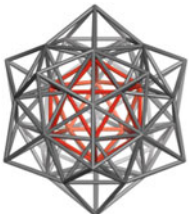
6A2

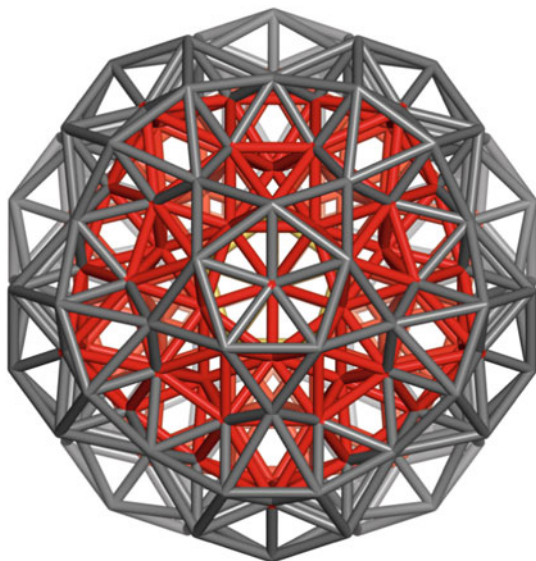
D.20	T.4	IP.13 = P@T ₂₀ @I.13



(IP)Y(13IP;(e@5T)).45

IP@C₄₄.45
 IP@12IP.45
 (P¹²@I)@st(D).45
 20T@(20T;30T)@60T.45
 C₂×A₅; classes: 4{|1};2{|12};{20}|
 6A3

		
IP@C ₄₄ .45	st(D).32	I@st(D).44




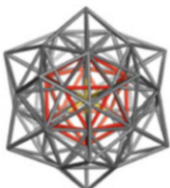

(IP)Y(13(I@ID);(P@5O)).204

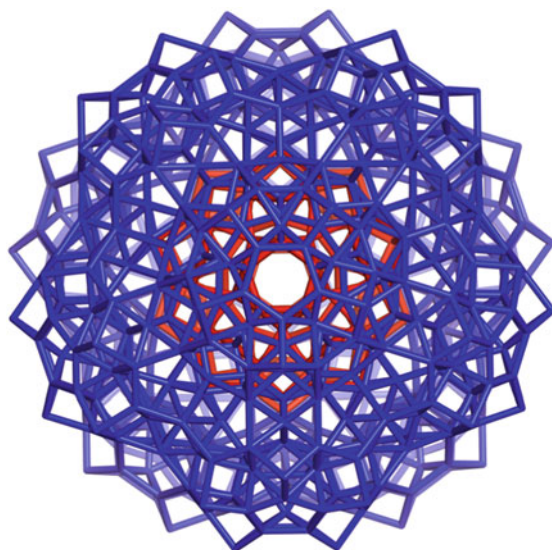
(I@ID)@12(I@ID).204

$m(C_{45}).204$

$C_2 \times A_5$; classes: 6 |2{12}; 2{30};2{60}|

6A3.1

		
I@ID.42	IP@12IP.45	$f_5(C_{204}) = P@5O.16$



(IP)Y(13C₁₃₀;(mP₅@5C)).810a

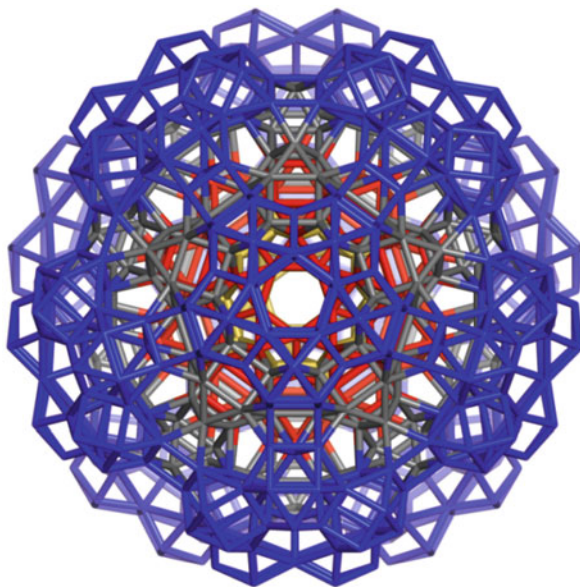
C_{130a}@12C_{130a}.810

d(m(C₄₅)204).810

C₂×A₅; classes: 15 |3 {20}; {30}; 10 {60}; {120}|

6A3.1.1

<p>mP₅@5C.32</p>	<p>C₄₅ IP@12IP.45</p>	<p>C₁₃₀ = d(I@ID).130a d(m(IP)42).130</p>



IY(12(DY(20CO; f_3).150);(P₅@5CO.45)).870

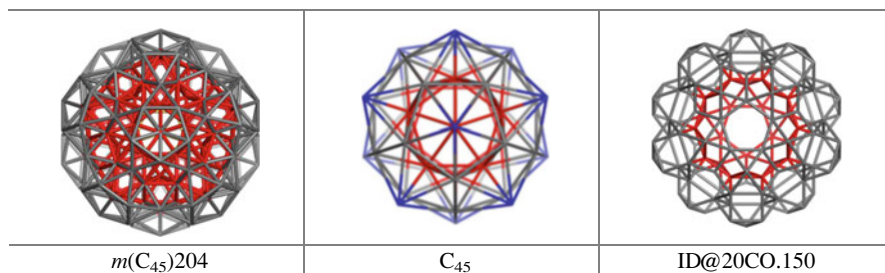
(ID@20CO)@12(ID@20CO).870

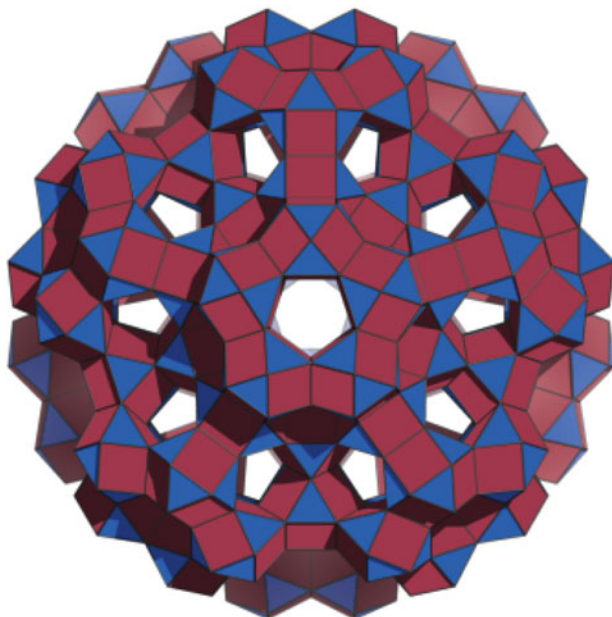
ID@(20CO;50CO)@60CO.870

$m(m(C_{45})204).870$

$C_2 \times A_5$; classes: 12 |{30}; 8 {60}; 3 {120}|

6A3.1.2

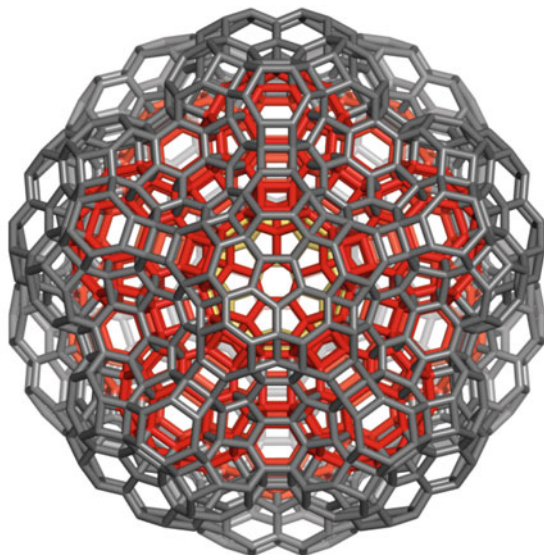




IY(12(DY(20CO; f_3).150);(P₅@5CO.45)).870

ID@(20CO;50CO)@60CO.870
 (ID@20CO)@12(ID@20CO).870
 $m(m(C_{45})204).870$
 $C_2 \times A_5$; classes: 12 |{30}; 8 {60}; 3 {120}|
 6A3.1.3

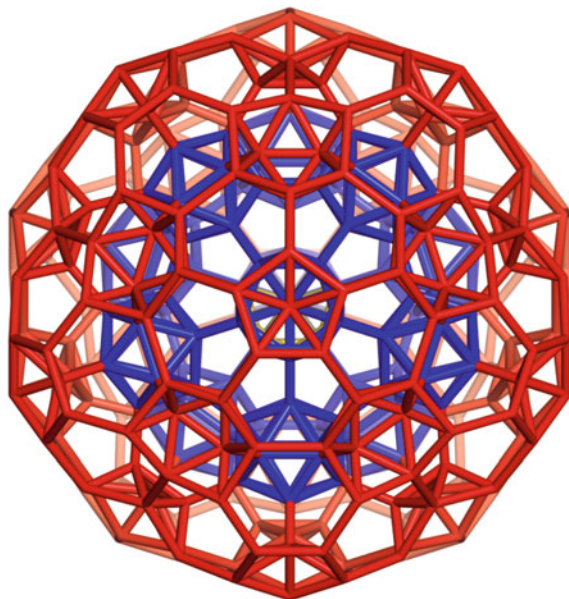
$f_3 Y_{870} = P_5 @ 5CO.45$	ID@20CO.150	$m(m(C_{45})204).870$



IY(12(DY@(20TO).300);(P₅@5TO.90)).1740

$t(m(C_{45})204).1740$
 $C_2 \times A_5$; classes: 19 {9{60};10{120}}|
 6A3.1.4

$f_5 Y_{1740} = P_5 @ 5TO.90$	$I @ ID.42$	$DY @ (20TO).300$ $t(I @ ID.42).300$



(IP)Y(13(*t*(IP)84);(*e*@5TT32)).408

t(IP)@12*t*(IP).408

$C_{84}@12C_{84}@C_{180}$.408

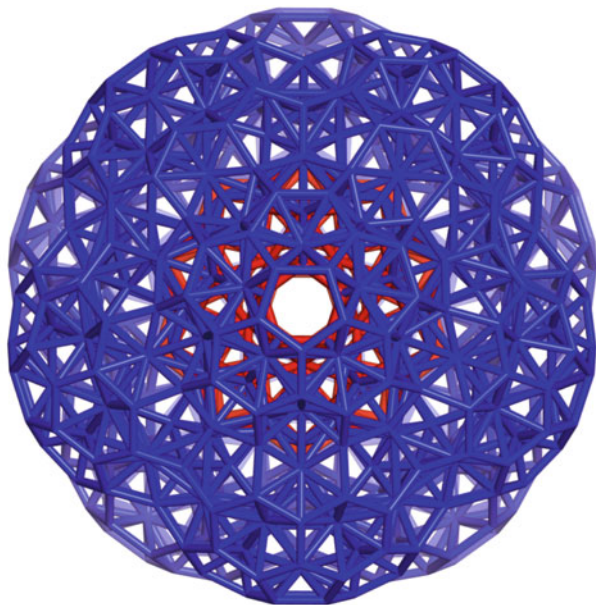
t(IP@12IP.45).408

t(C_{45}).408

$C_2 \times A_5$; classes: 10 |4{12};6{60}|

6A3.2

$f_5 Y_{408} = e@5TT.32$	$t(C_{45}).408_3$	$Hull(C_{408}).180 = C_{180}(I_h)$



(IP)Y(13($d(t(\text{IP}))$ 130);(2A₅@(5(2Py₆;5T)35)).810b

$C_{130b}@12C_{130b}.810$

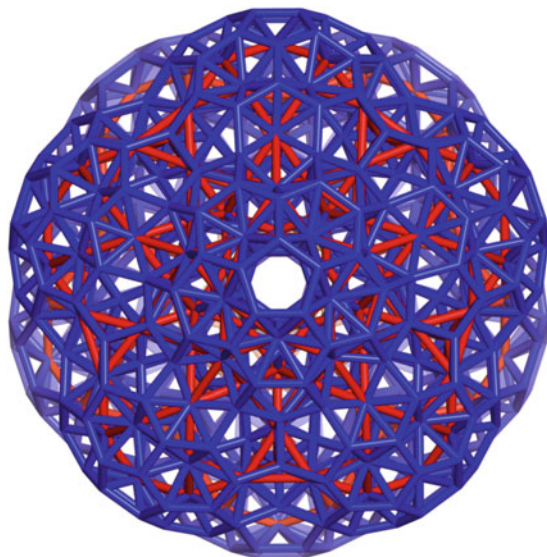
$d(C_{408}).810$

$d(t(C_{45})408).810$

$C_2 \times A_5$; classes: 15 |3 {20}; {30}; 10 {60}; {120}; |

6A3.2.1

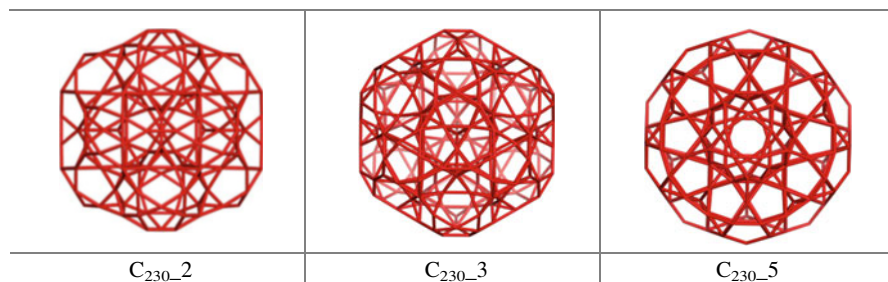
$f_5 Y_{810} = 2A_5 @ 5(2Py_6; 5T).35$	C_{810-3}	$d(C_{84}).130b$ $d(t(\text{IP})84).130$

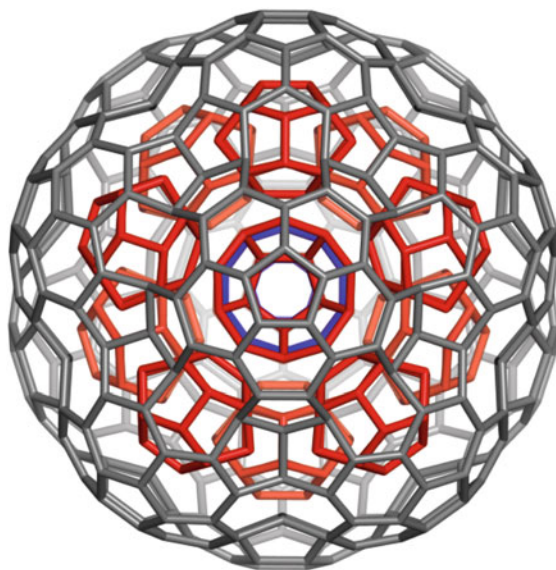


$$C_{230}@C_{810}$$

$$d(C_{408}).810$$

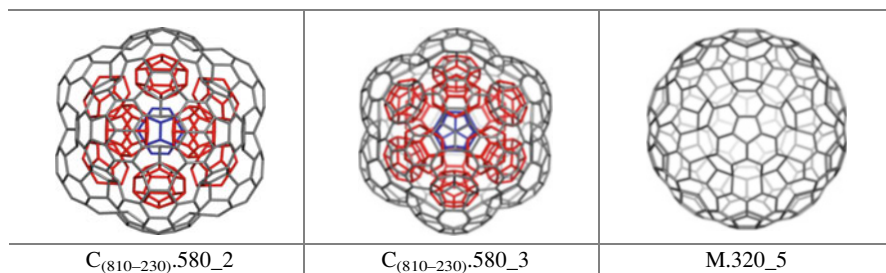
$$C_2 \times A_5; \text{ classes: } 15 \{3\{20\};\{30\};10\{60\};\{120\}\}$$

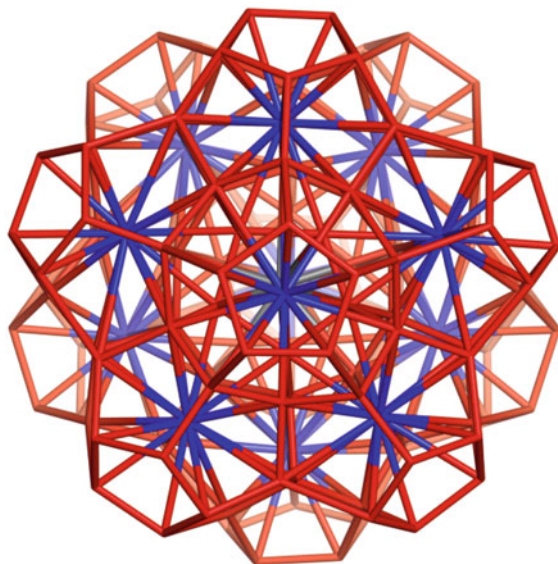
$$6A3.2.2$$




$C_{(810-230)}.580$

13D@M.580
(disjoint D)
6A3.2.3



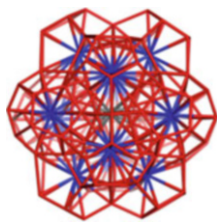


(IP)Y(13DP; f_5).143

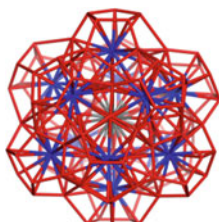
$13(P^{20}@D_{21}).143$

$cd(C_{408}).143$

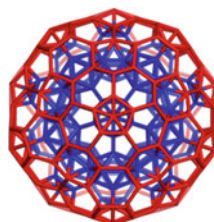
$C_2 \times A_5$; classes: $6 \{ \{1\}; \{12\}; 2\{20\}; \{30\}; \{60\} \}$
 $6A3.3$



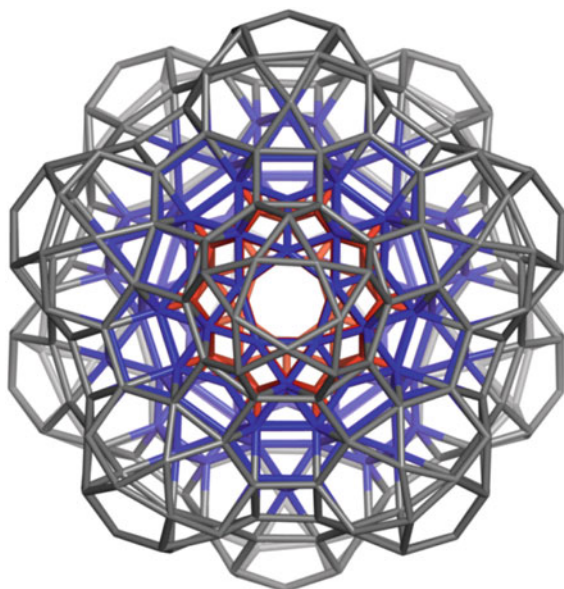
$cd(C_{408}).143-2$



$cd(C_{408}).143-3$



C_{408}



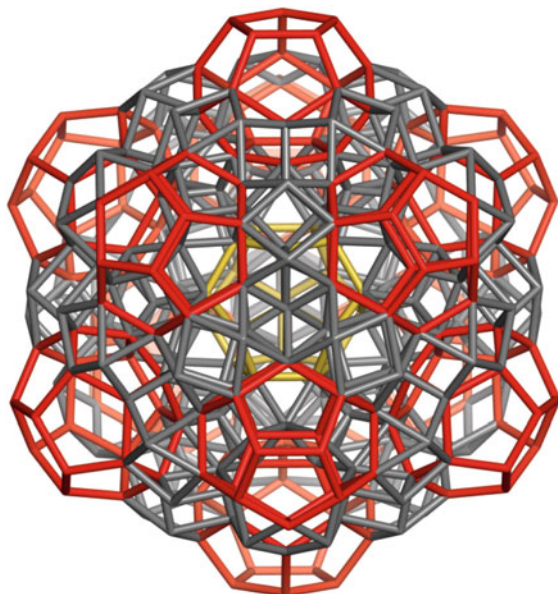
$d(cd(C_{408}), 143), 390$

$d(cd(t(C_{45})), 390)$

$C_2 \times A_5$; classes: $6 \{30\}; 4\{60\}; \{120\}$

6A3.3.1

<p>$d(cd(C_{408}), 143), 390_3$</p>	<p>$cd(C_{408}), 143-5$</p>	<p>$t(C_{45}) = C_{408}$</p>



(IP)Y(13D; (I)).370

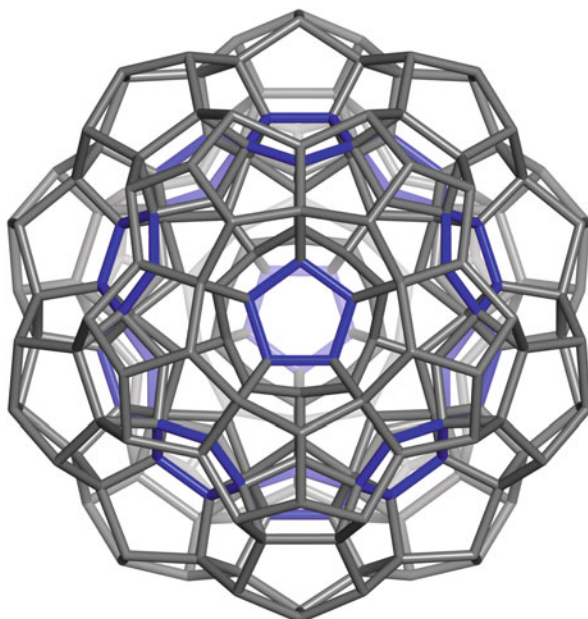
$D@(12D;20C;42mP_5).370$

$m(cd(t(C_{45}))).370$

$C_2 \times A_5$; classes: $8 | 2\{20\}; \{30\}; 5\{60\} |$

6A3.3.2

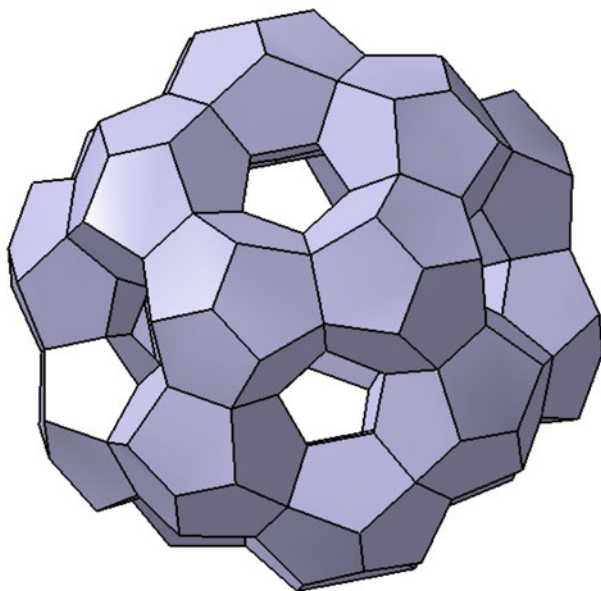
<p>$m(cd(t(45))).370_2$</p>	<p>$m(cd(t(45))).370_5$</p>	<p>$cd(C_{408}).143-5$</p>



DY(20D).250

$C_{20}Y(20C_{20}).250$
 $C_2 \times A_5$; classes: $6 \{2\{20\};\{30\};3\{60\}\}$
 $6A_4$

$t_{sel}(p_4(D)).110$	$s_2(D).140$	$t_{sel}(p_4(D))@s_2(D).250$

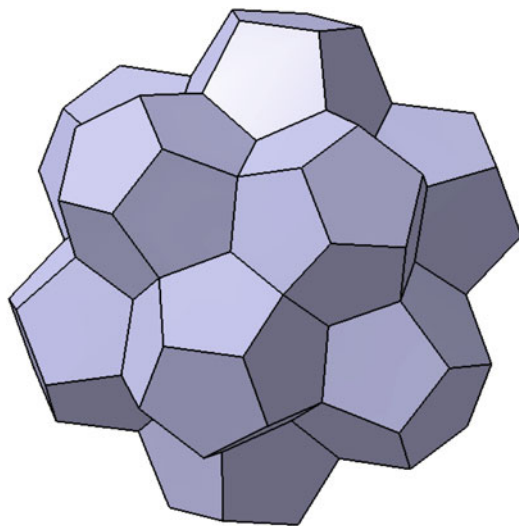


$C_{20}Y(20C_{20}; f_5).250$

DY(20D; f_5).250

$C_2 \times A_5$; classes: 6 | 2 {20}; {30}; 3 {60}|
6A4.1

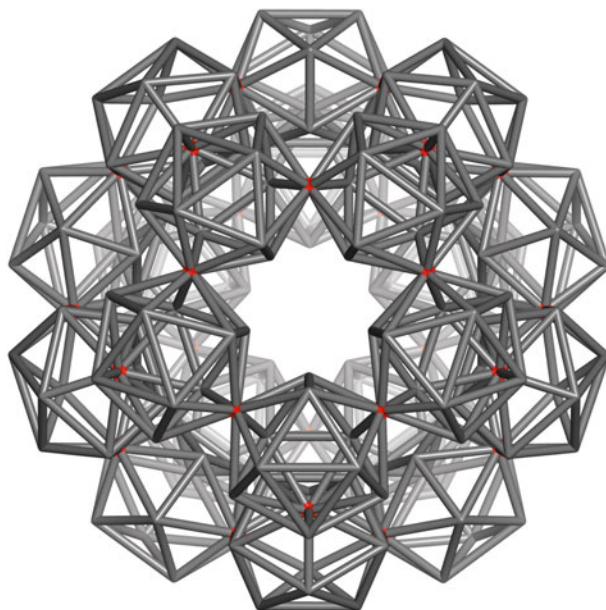
<p>$t_{sel}(p_4(D)).110$</p>	<p>$s_2(D).140$</p>	<p>$(D@12D)@20D.270$</p>



$t_{sel}(p_4(\mathbf{D})).110$

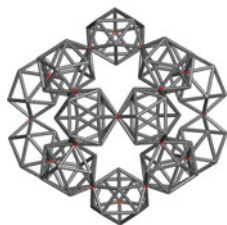
$C_2 \times A_5$; classes: 3 | {20}; {30}; {60} |
6A4.2

D.20	$t_{sel}(p_4(\mathbf{D})).110$	DY(20D; f_5).250

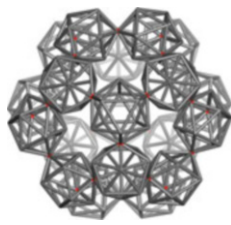


DY(20I;P).210

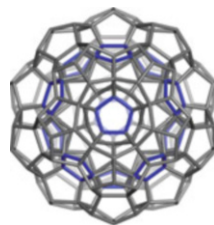
$d(C_{250}).210$ sp
 $C_2 \times A_5$; classes: 4 |{30}; 3 |{60}|
 6A4.3



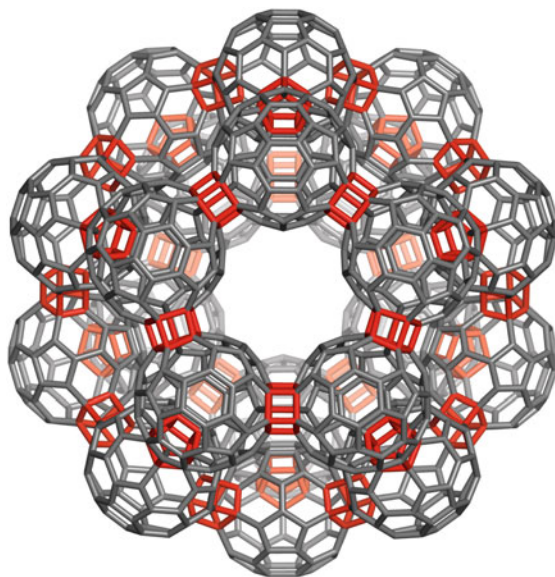
$d(C_{250}).210_2$



$d(C_{250}).210_3$



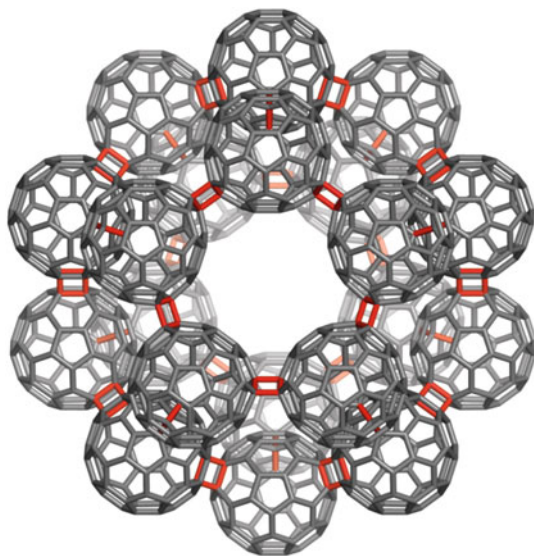
DY(20D; f_3).250



DY(20C₆₀;P₅).1200

$t(d(C_{250})).1200$
 $C_2 \times A_5$; classes: 12 |4{60};8{120}|
 6A4.3.1

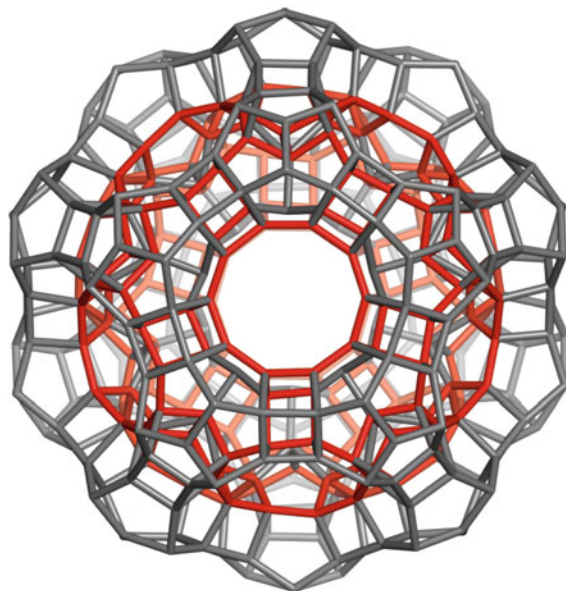
$td(C_{250}).1200_2$	$td(C_{250}).1200_3$	$DY(20D; f_5).250$



$C_{20}Y(20C_{60};hh[2+2]).1200$

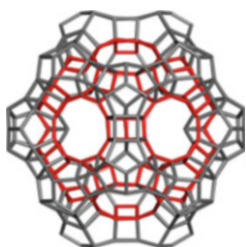
$C_2 \times A_5$; classes: $12 |4\{60\};8\{120\}|$
6A4.3.2

<p>$C_{20}Y(20C_{60};hh[2+2]).1200$</p>	<p>$C_{20}Y(20C_{60};ph[2+2]).1200$ $l(C_{400})X.1200$</p>	<p>$C_{20}Y(20C_{20};P_5).1200$ $t(d(C_{250})).1200$</p>

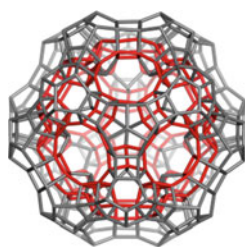


$C_{20}Y(20C_{20};P_5).400$

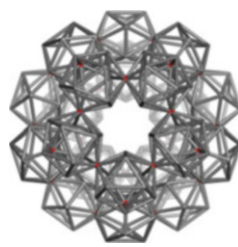
$d(d(C_{250}),210).400J$
 $C_2 \times A_5$; classes: $6 | 2 \{20\}; 2 \{60\}; 2 \{120\} |$
 $6A4.3.3$



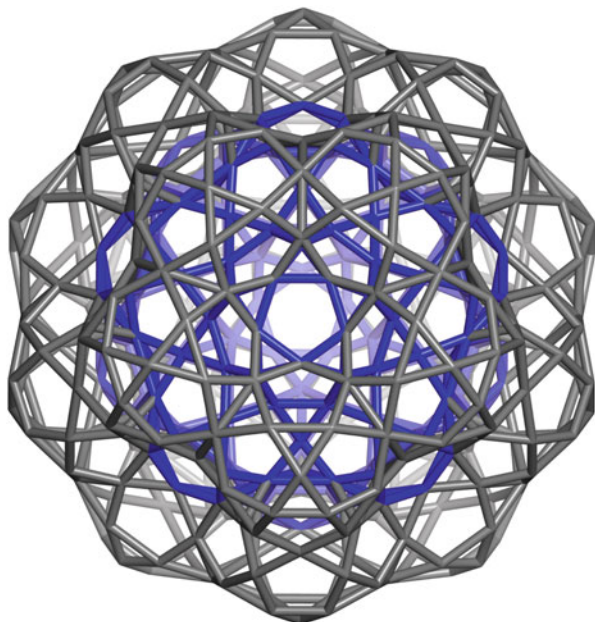
$C_{20}Y(20C_{20};P_5).400_2$



$C_{20}Y(20C_{20};P_5).400_3$



$d(C_{250}).210 \text{ sp}$



DY(20ID; f_3).450

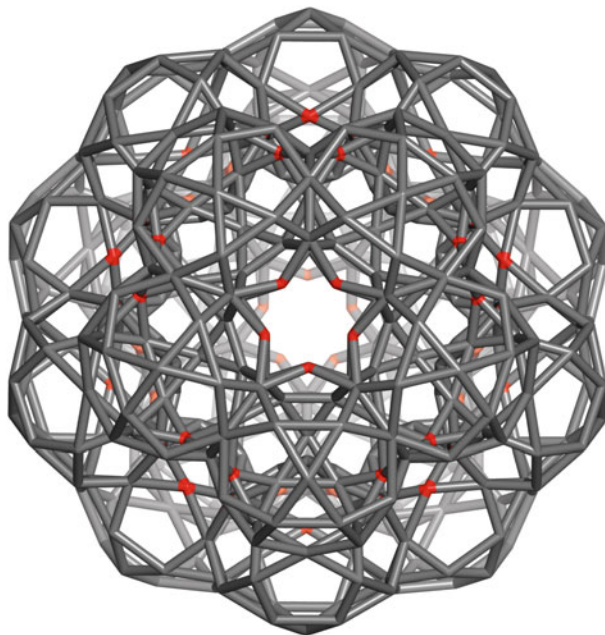
$m(\text{DY}(20\text{D}; f_3).450$

$m(\text{C}_{250}).450$

$\text{C}_2 \times \text{A}_5$; classes: 7 | {30}; 5 {60}; {120} |

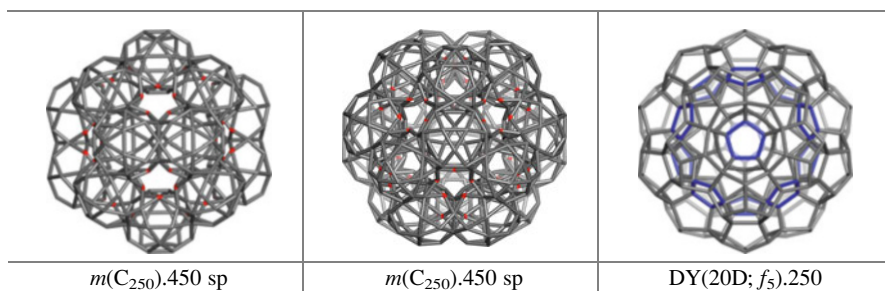
6A4.4

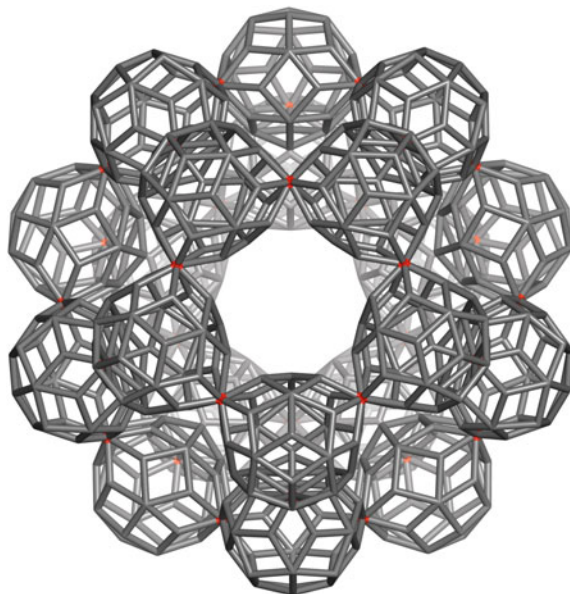
D.20	ID.30= m I.30	DY(20D; f_3).250



DY(20ID; f_5).450

$m(\text{DY}(20\text{D}; f_5).450$
 $m(\text{C}_{250}).450 \text{ sp}$
 $\text{C}_2 \times \text{A}_5$; classes 7: $|\{30\}; 5\{60\}; \{120\}|$
 6A4.4.1

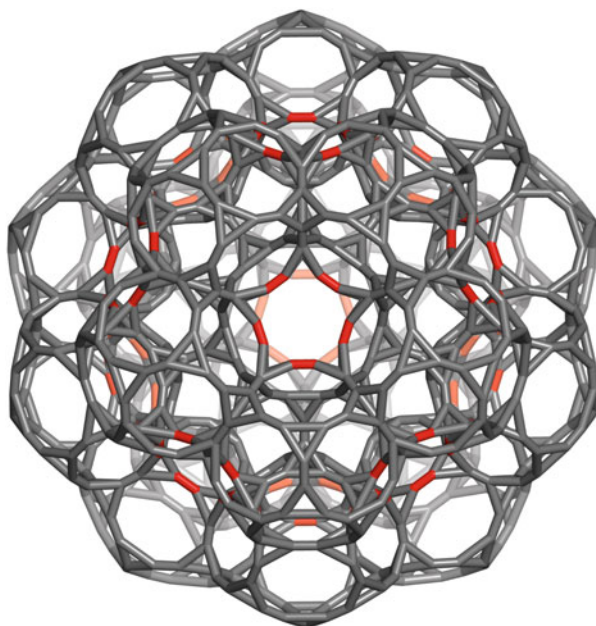




DY(20Rh₃₀;P).610

$d(m(C_{250})).610_{sp}$
 $C_2 \times A_5$; classes: 10 $|2\{20\};\{30\};5\{60\};2\{120\}|$
 6A4.4.2

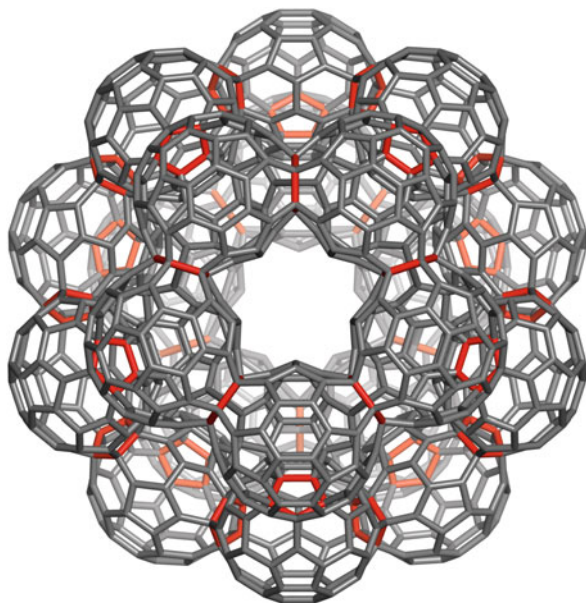
$d(m(C_{250})).610_2 sp$	$d(m(C_{250})).610_3 sp$	DY(20D; f_3).250



DY(20tD; f_{10}).900

$t(C_{250}).900$
 $C_2 \times A_5$; classes: 12 |9 {60}; 3 {120}|
 6A4.5

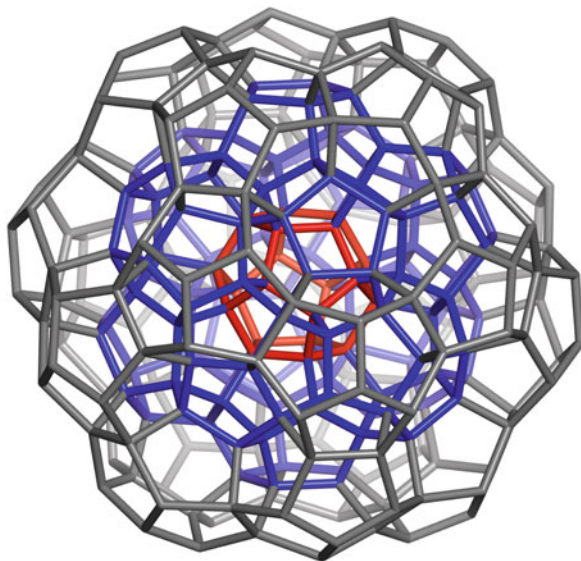
$t(C_{250}).900$	$t(C_{250}).900$	DY(20D; f_3).250



DY(20C₆₀; *f*₅).1050

$I(C_{250}).1050$
 $C_2 \times A_5$; classes: 12 |{30}; 5 {60}; 6 {120}|
 6A4.6

<p>$I(C_{250}).1050_2$</p>	<p>$I(C_{250}).1050_3$</p>	<p>DY(20D; <i>f</i>₅).250</p>



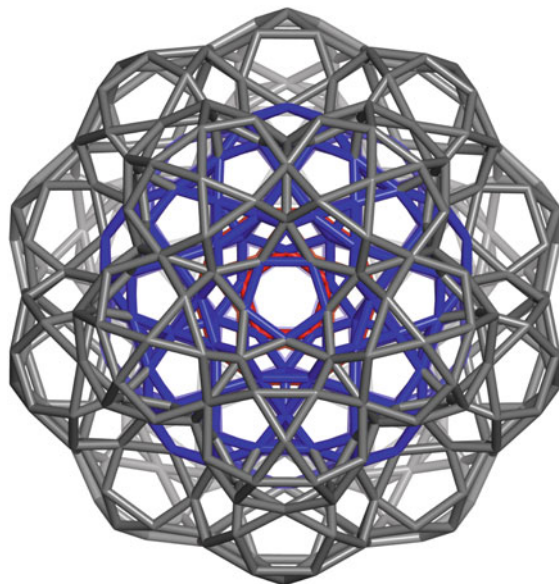
$C_{20}@(12C_{20};20C_{20}).270$

$(D@12D)@DY(20D; f_5).270$

$D@12D@20D.270$

$C_2 \times A_5$; classes: $7 [3\{20\};\{30\};3\{60\}]$
 $6A_5$

<p>$P^{12}@I@D.33$</p>	<p>$D@12D.130$</p>	<p>$DY(20D; f_5).250$</p>



ID@(32ID).500

ID@(12ID;20ID).500

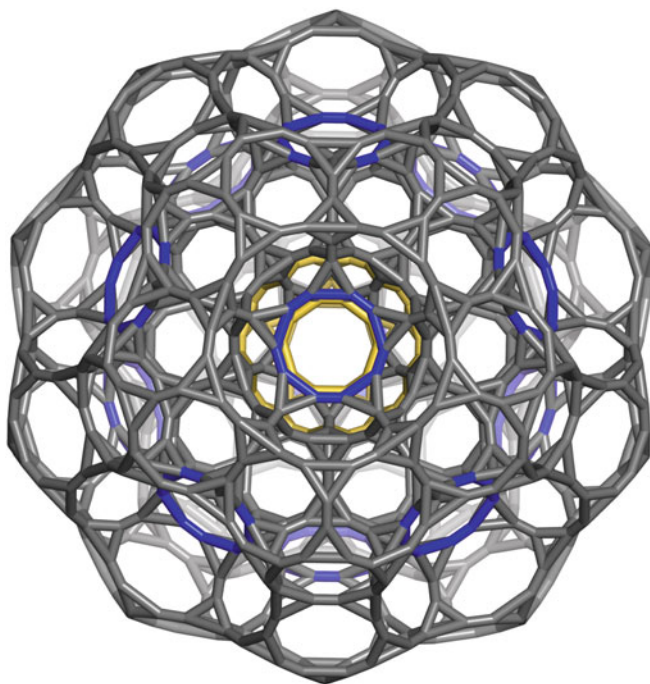
$m(D@(32D)270).500$

$m(C_{270}).500$

$C_2 \times A_5$; classes: $9 \{|20\}; 2\{30\}; 5\{60\}; \{120\}$

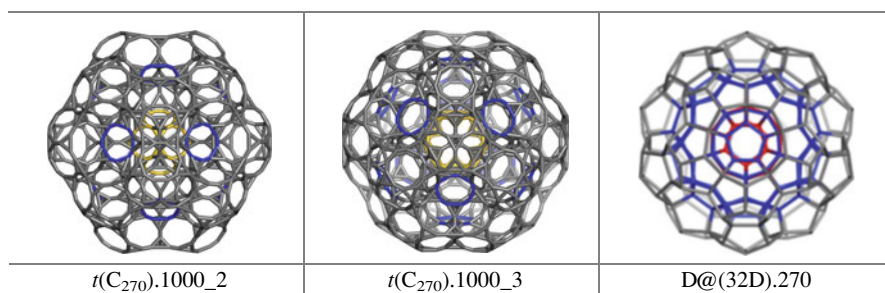
6A5.1

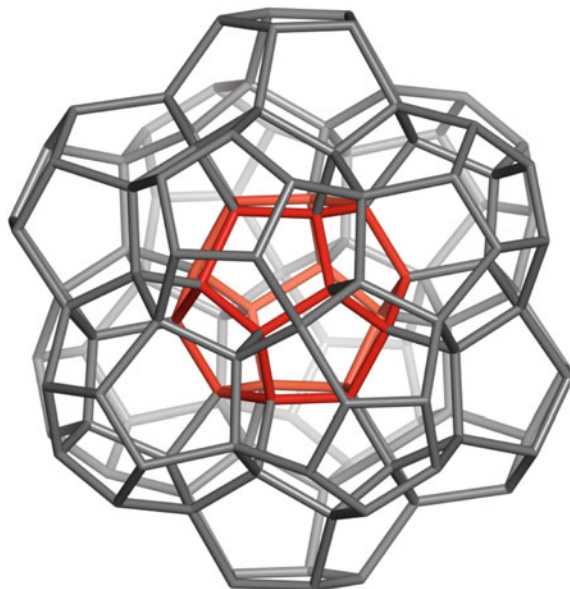
ID_30	$m(D@12D130).230$	$D@(32D).270$



$t(C_{270}).1000$

$C_2 \times A_5$; classes: 15 $|2\{20\}; 10\{60\}; 3\{120\}|$
6A5.2





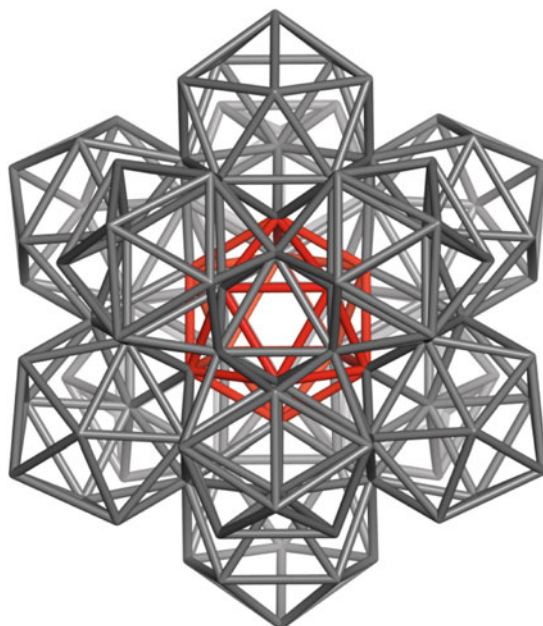
(IP)Y(13D; f_5).130

D@12D.130

$C_2 \times A_5$; classes: 4 |2{20};{30};{60}|

6A6

D.20	I.12	D@12D.130



(IP)Y(13I;P).114

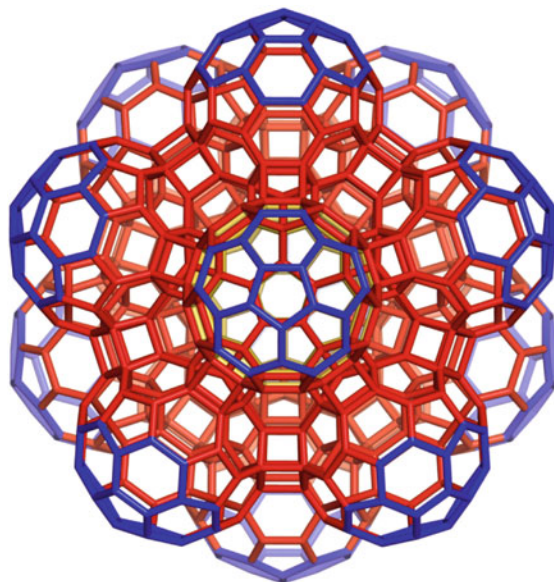
I@12I.114

$d(C_{130}).114$

$C_2 \times A_5$; classes: 4 |2{12};{30};{60}|

6A6.1

<p>$d(D@12D).114_5$</p>	<p>I.12</p>	<p>D@12D.130</p>



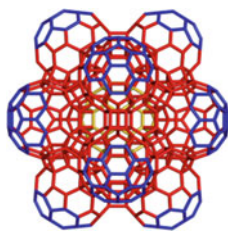
(IP)Y(13C₆₀;P₅).780

C₆₀@(12C₆₀;20T_O;42P₅).780

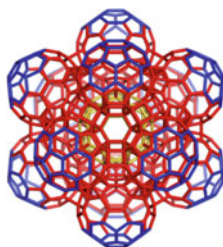
t(*d*(C₁₃₀)).780

C₂×A₅; classes: 9 |5 {60};4 {120}|

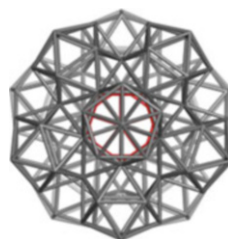
6A6.1.1



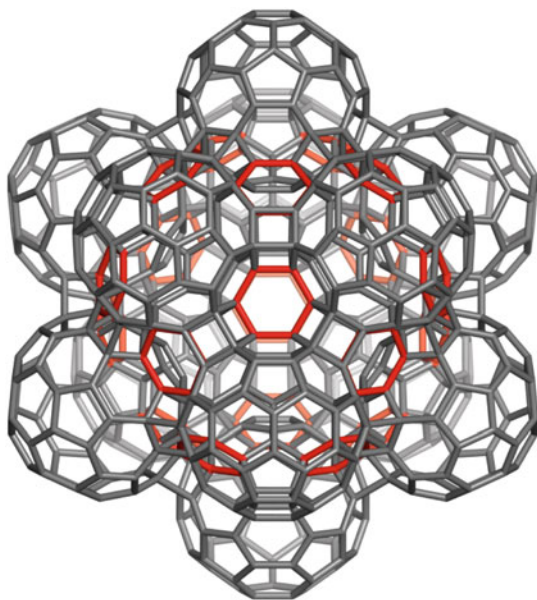
t(*d*(C₁₃₀))₂



t(*d*(C₁₃₀))₃



d(C₁₃₀).114_5



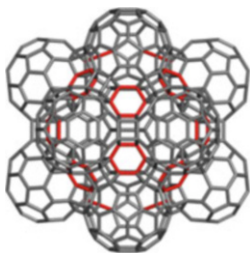
IY(12C₆₀;P₅).720

(12C₆₀;30P₅).720_{sp}

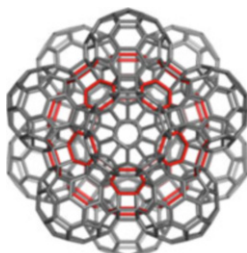
t(d(C₁₃₀).720_{sp})

C₂ × A₅; classes: 8|4{60};4{120}|

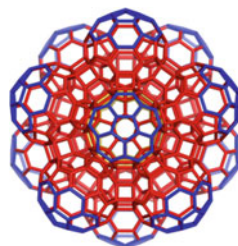
6A6.1.2



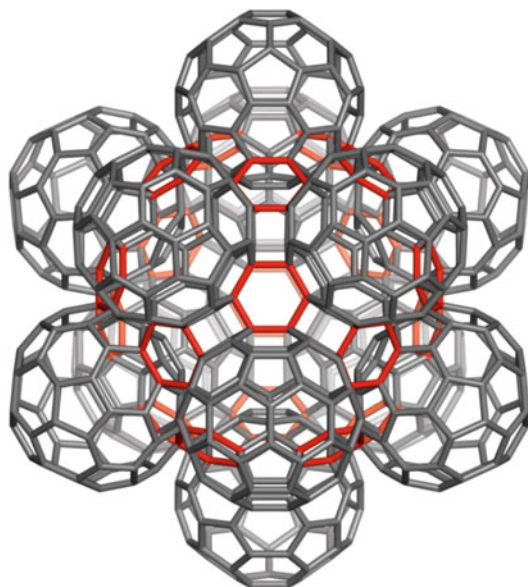
t(d(C₁₃₀).720_2)



t(d(C₁₃₀).720_5)



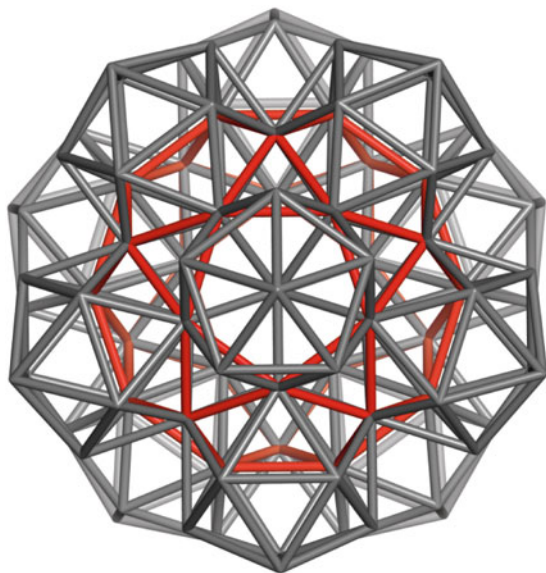
t(d(C₁₃₀).780_5)



IY(12C₆₀;e).720X

C₂₄₀@12C₆₀.720X sp
t(d(C₁₃₀)).720X sp
 C₂×A₅; classes: 8 |4{60};4{120}|
 6A6.1.3

C ₂₄₀ -5	C ₂₄₀ -5 disjoint polygons	C ₂₄₀ -2 disjoint corannulenes



IY(12I;P).114

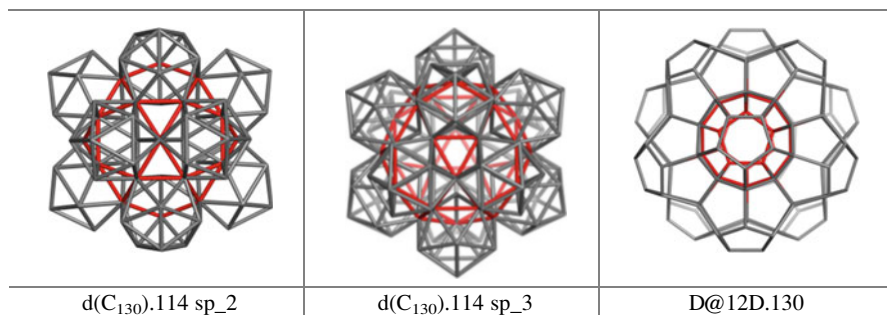
(12I).114_{sp}

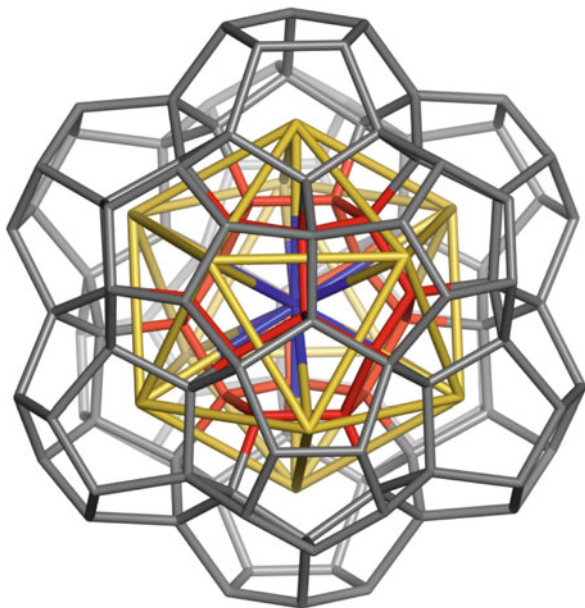
$d(D@12D)$.114_{sp}

$d(C_{130})$.114_{sp}

$C_2 \times A_5$; classes: 4 | 2{12}; {30}; {60} |

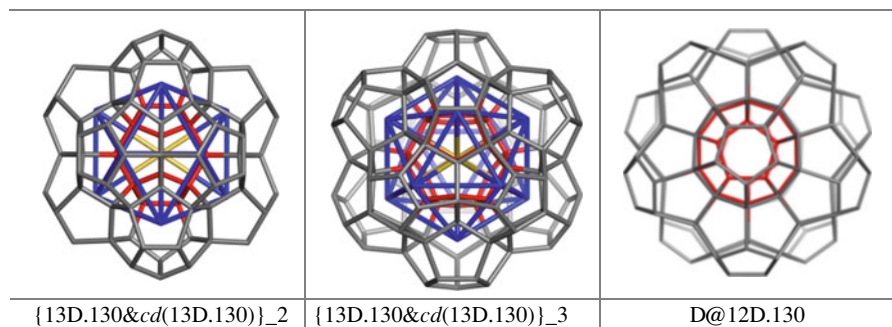
6A6.2

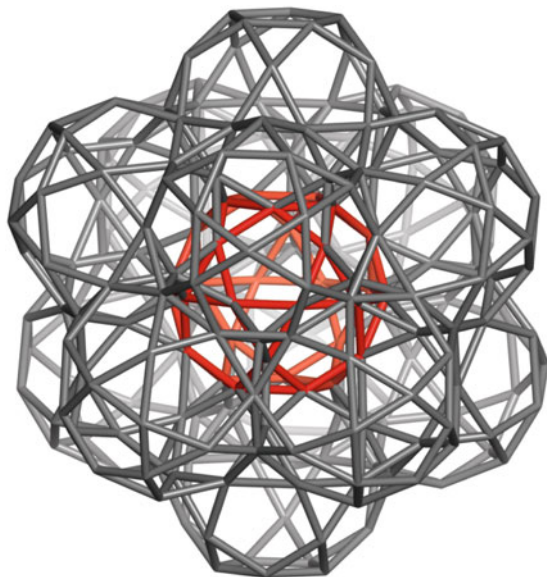




$(cd(D@12D).13)\&(D@12D.130)$

$cd(D@12D) = P@I.13$
6A6.3





(IP)Y(13ID; f_5).230

ID@(12ID;20(2T);30T).230

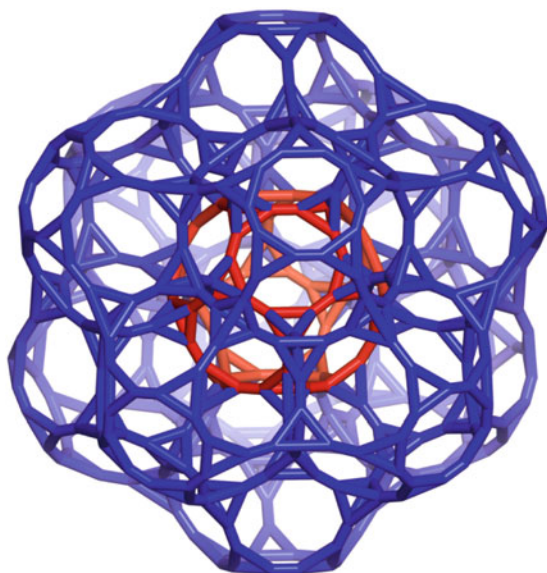
ID@12ID.230

$m(D@12D).230$

$C_2 \times A_5$; classes: 5 $\{20\}$; $\{30\}$; 3 $\{60\}$

6A6.4

ID.30	D@12D.130	ID@12ID.230_5



(IP)Y(13*t*D; *f*₁₀).460

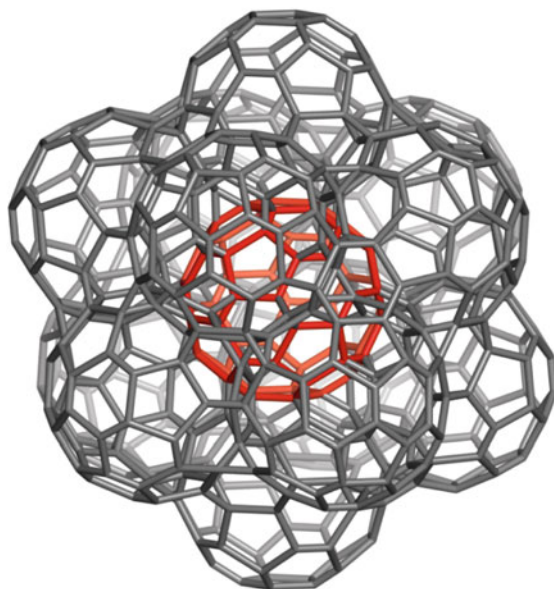
*t*D@12*t*D.460

t(C₁₃₀).460

C₂ × A₅; classes: 8 |2{20};5{60};{120}|

6A6.5

D.20	<i>t</i> D.60	<i>t</i> (C ₁₃₀).460_5



(IP)Y(13C₆₀; f₅).570

C₁₂Y(12C₆₀; f₅).570

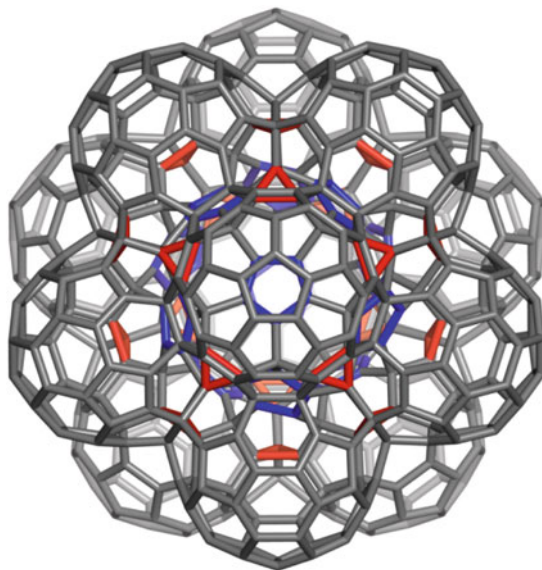
C₆₀@(12C₆₀; 20(2×TT)).570

I(D@12D).570

C₂×A₅; classes: 8 |{30}; 5 {60}; 2 {120}|

6A6.6

TT.12	D@12D.130	I(D@12D).570



IY(12C₆₀; f₅).570_{sp}

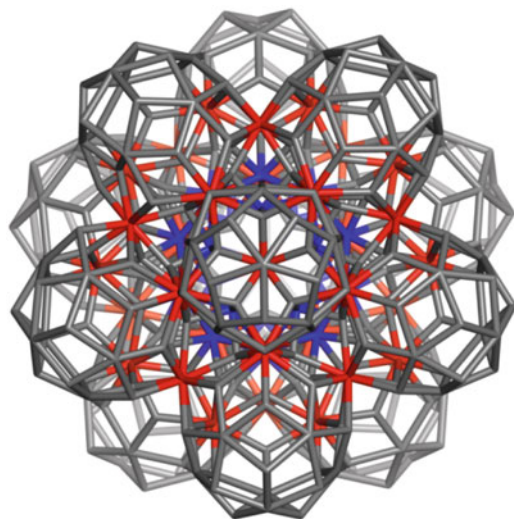
C₁₂Y(12C₆₀;f₅).570_{sp}

I(D@12D).570_{sp}

C₂×A₅; classes 8: |{30};5{60};2{120}|

6A6.6.1

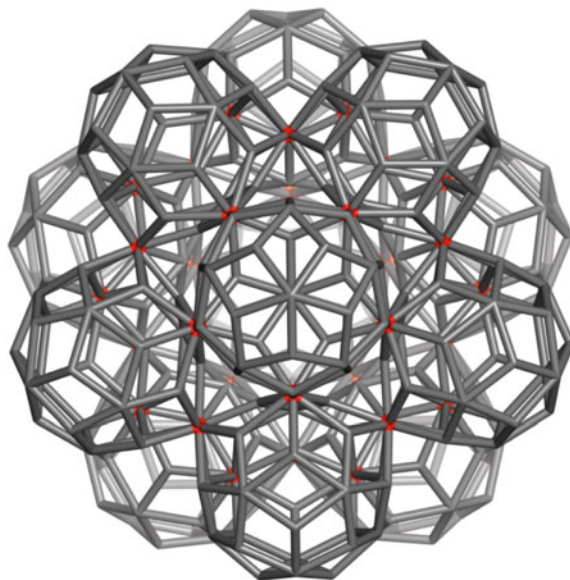
TT.12	D@12D.130	I(D@12D).570



Rh₃₀@(12Rh₃₀).374

Rh₃₀@(12Rh₃₀;30m(P₃)).374
d(m(D@12D)).374
 6A6.4.1

Rh ₃₀ = <i>d(mD30).32</i>	<i>mP_{3,9}</i>	ID@12ID.230



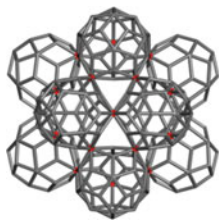
IY(12Rh₃₀;P).354

$d(m(D@12D)230).354_{sp}$

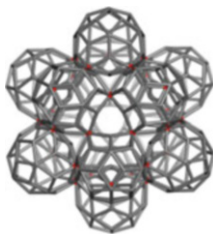
$d(m(C_{130})230).354$

$C_2 \times A_5$; classes: 8 |2{12}; {30}; 5{60}|

6A6.4.2



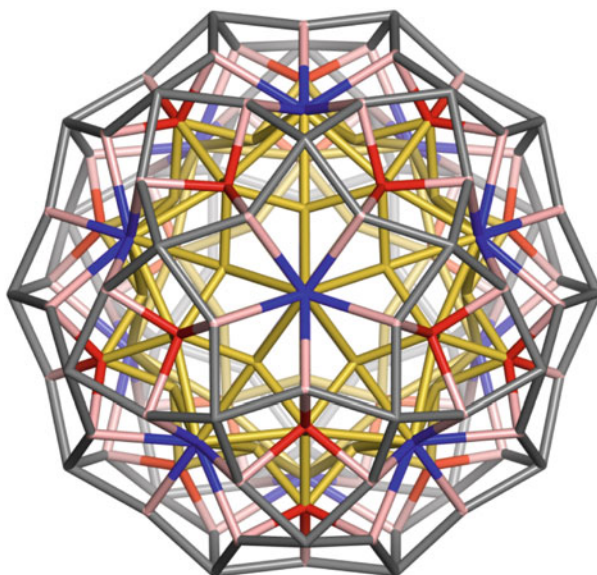
$d(m(C_{130}).354_2$



$d(m(C_{130}).354_3$



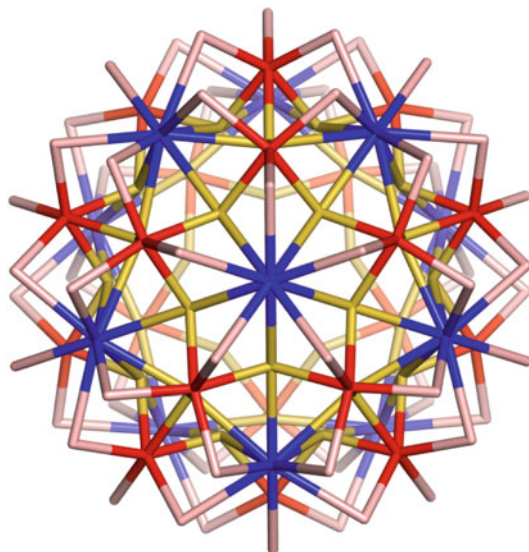
$dID.32 = Rh_{30}$



Rh₆₀@(Rh₁₂₀).152

Rh₆₀@(60Rh₃;30Rh₈)@(Rh₁₂₀).152
 $C_2 \times A_5$; classes: 5 | {12}; {20}; 2{30}; {60}|
 6A6.4.3

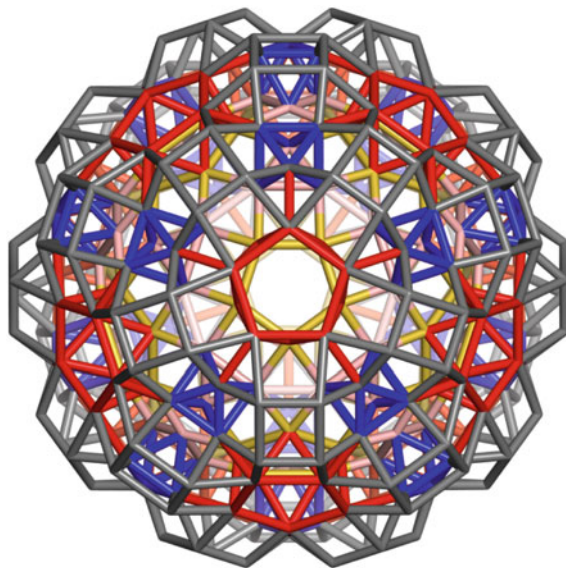
Rh3.5	Rh8.10	$d(m^2D60).62$



ppl(C₁₅₂).122

Rh₆₀@(60Rh₃).122
 $C_2 \times A_5$; classes: 4 | {12}; {20}; {30}; {60}|
 6A6.4.4

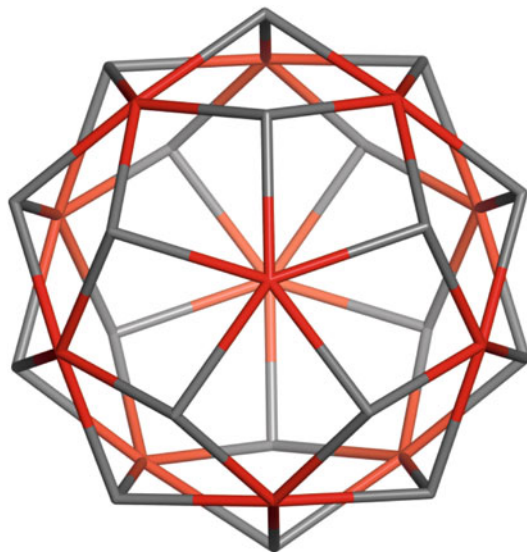
ppl(C ₁₅₂).122_2	ppl(C ₁₅₂).122_3	Rh ₃ .5 [1,1,1]-Propellane



$m^3D@(30J_{29};20O;12A_5;60P_3).360$

$m(C_{152}).360$
6A6.4.5

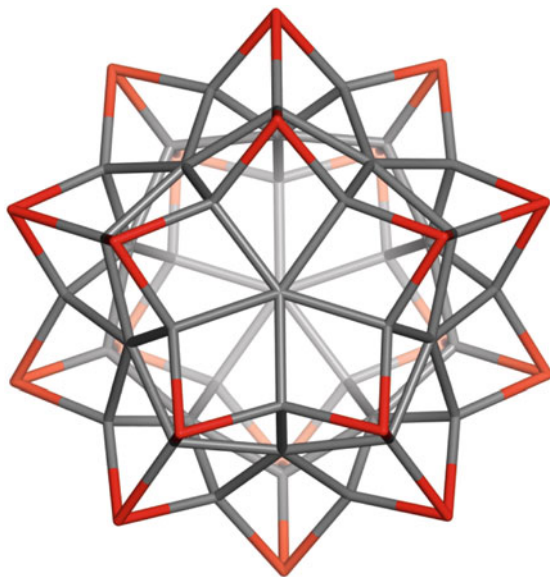
<p>$A_5.10$</p>	<p>$m(A_4).16$ Square gyrobicupola = J_{29}</p>	<p>$m^3D.120$</p>



Rh₃₀-32

d(mD.30).32
Triacontahedron
6A7

D.20	I.12	<i>mD.30 = ID.30</i>



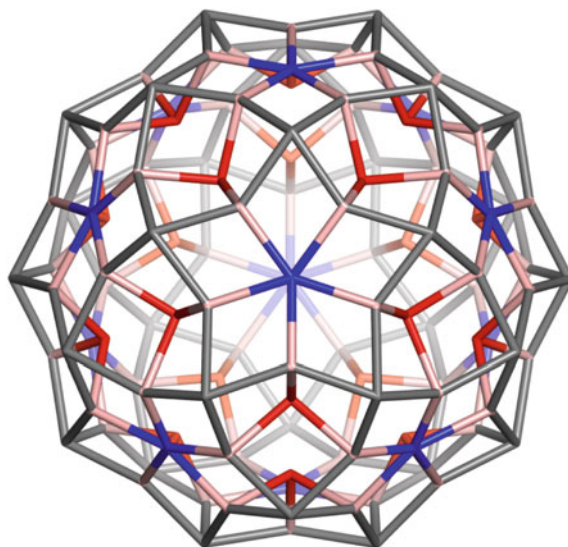
Rh₆₀-62

$d(m^2D_{60}).62 = p_4D.62$

Hexecontahedron

6A7.1

D.20	I.12	$m^2D.60$



Rh₁₂₀.122

d(m³D).122
6A7.2

<p><i>m²D.60</i></p>	<p>Rh₆₀.62 <i>d(m²D.60).62</i></p>	<p><i>m³D.120</i></p>

References

- Ammann R, Grünbaum B, Shephard GC (1992) Aperiodic tiles. *Discret Comp Geom* 8:1–25
- Bergman G, Waugh JLT, Pauling L (1952) Crystal structure of the intermetallic compound Mg₃₂(Al, Zn)₄₉ and related phases. *Nature* 169:1057–1058
- Blatov VA, O’Keeffe M, Proserpio DM (2010) Vertex-, face-, point-, Schläfli-, and Delaney-symbols in nets, polyhedra and tilings: recommended terminology. *Cryst Eng Comm* 12:44–48

- de Boisieu M, Dubois JM, Audier M, Dubost B (1991) Atomic structure of the icosahedral AlLiCu quasicrystal. *J Phys Condens Matter* 3:1–25
- Coxeter HSM (1973) *Regular polytopes*, 3rd edn. Dover, New York, NY
- Diudea MV (1994) Layer matrices in molecular graphs. *J Chem Inf Comput Sci* 34:1064–1071
- Diudea MV (2013) Quasicrystals, between spongy and full space filling. In: Diudea MV, Nagy CL (eds) *Carbon materials: chemistry and physics*, vol 6. *Diamond and related nanostructures*. Springer, Dordrecht, Chap. 19, pp 333–383
- Diudea MV, Ursu O (2003) Layer matrices and distance property descriptors. *Indian J Chem A* 42(6):1283–1294
- Duneau M, Gratias D (2002) Covering clusters in icosahedral quasicrystals. In: *Coverings of discrete quasiperiodic sets*, vol 180 of the series *Springer tracts in modern physics*, pp 23–62
- Euler L (1752–1753) *Elementa doctrinae solidorum*. *Novi Comment Acad Sci Imp Petropolitanae* 4:109–160
- Frank FC, Kasper JS (1958) Complex alloy structures regarded as sphere packings. Definitions and basic principles. *Acta Crystallogr* 11:184–190
- Gardner M (2001) *Packing spheres*. Ch10 in *The colossal book of mathematics: classic puzzles, paradoxes, and problems*. WW Norton, New York, NY, pp 128–136
- Grünbaum B, Shephard GC (1987) *Tilings and patterns*. W. H. Freeman, New York, NY
- Hales TC (1992) The sphere packing problem. *J Comput Appl Math* 44:41–76
- Hales TC (2005) A proof of the Kepler conjecture. *Ann Math* 162:1065–1185
- Heath TL (1981) *A history of Greek mathematics*. Dover, New York, NY
- Koltover VK (2007) Endohedral fullerenes: from chemical physics to nanotechnology and nanomedicine. In: Lang M (ed) *Progress in fullerene research*. Nova Science Publishers, New York, NY, pp 199–233
- Nagy CL, Diudea MV (2009) Nano studio software. “Babes-Bolyai” Univ, Cluj
- Nagy CL, Diudea MV (2017) Ring signature index. *MATCH Commun Math Comput Chem* 77(2): 479–492
- Papacostea C (1930–1935) P1 aton. *Opere*, 1–11 (Roum. translation), Casa Școalelor, București
- Penrose R (1974) The role of aesthetics in pure and applied mathematical research. *Bull Inst Math Appl* 10:266–271
- Popov AA, Yang S, Dunsch L (2013) Endohedral fullerenes. *Chem Rev* 113(8):5989–6113
- Reddy BV, Khanna SN, Dunlap BI (1993) Giant magnetic moments in $4d$ clusters. *Phys Rev Lett* 70(21):3323–3326
- Samson S (1965) The crystal structure of the phase β of Mg_2Al_3 . *Acta Crystallogr* 19:401–413
- Samson S (1972) Complex cubic A6B compounds. II. The crystal structure of Mg_6Pd . *Acta Crystallogr B* 28:936–945
- Saunders M, Jiménez-Vázquez HA, Cross RJ, Poreda RJ (1993) Stable compounds of helium and neon. $\text{He}@C_{60}$ and $\text{Ne}@C_{60}$. *Science* 259(5100):1428–1430
- Schläfli L (1901) *Theorie der vielfachen Kontinuität* Zürcher und Furrer, Zürich (Reprinted in: Ludwig Schläfli, 1814–1895, *Gesammelte Mathematische Abhandlungen*, Band 1:167–387, Verlag Birkhäuser, Basel, 1950)
- Schulte E (1985) Regular incidence-polytopes with Euclidean or toroidal faces and vertex-figures. *J Combin Theory Ser A* 40(2):305–330
- Schulte E (2014) Polyhedra, complexes, nets and symmetry. *Acta Cryst A* 70:203–216
- Steinitz E (1922) *Polyeder und Raumeinteilungen*, *Encyclopädie der mathematischen Wissenschaften*, Band 3 (Geometries) (IIIAB12), pp 1–139, Abgeschlossen am 31 August 1916
- Taylor AE (1928) *A commentary on Plato’s Timaeus*. Clarendon, Oxford

Chapter 7

Clusters of Octahedral Symmetry

Cube was associated to the earth, by ancient Greeks and is one of the five Platonic solids (along with Tetrahedron—fire; Icosahedron—water; Octahedron—air and Dodecahedron—universe), as Plato exposed in its “theory of everything” (Papacostea 1930–1935; Taylor 1928). Also called “hexahedron” in geometry, its six regular square faces follow the direction of rectangle coordinates. Its dual is the octahedron. Cube and its dual exist in any multi-dimensional space.

In algebra, cube is the third power function; it is associated to the volume calculation in the Euclidean space.

7.1 Small Clusters as Seeds for Complex Structures

In Sect. 3.4.1, P-centered clusters have been introduced, as the smallest clusters of rank higher than three and a source of seeds for vary multi-shell clusters (Parvan-Moldovan and Diudea 2015). In the same idea, we start here with centered clusters of the Platonic regular polyhedra, namely CP.9 (7A1) and O.7 (7A2) (see also Fig. 7.1). As hyper-structures, they can be written as OY(6Py4; f_3).9 and CY(8T; f_3).7, respectively, thus reminding the duality of their parent objects. They belong to the symmetry group $C_2 \times S_4$, of order 48.

Other small clusters used in the same respect (named by the map operation used in their design) are: $mCP.20 = dOP.20$ (7A3), $tCP.40$ (7A4) and $dCP.18 = mOP.18$ (7A5).

A double shell cluster can be designed by joining a polyhedron P in its dual, P@dP; the two objects can be scaled so that is no matter which one is “endo” or “exo”, by fullerenes terminology. It is also the case of a polyhedral dual pair, differently operated but resulting the same cluster, e.g., $mCP.20 = dOP.20$, as shown in Fig. 7.2.

These clusters and their derivatives are detailed in the Atlas of the chapter; the figure count for them is given in Table 7.1.

Fig. 7.1 The smallest clusters of octahedral PG symmetry used as seeds in map operations

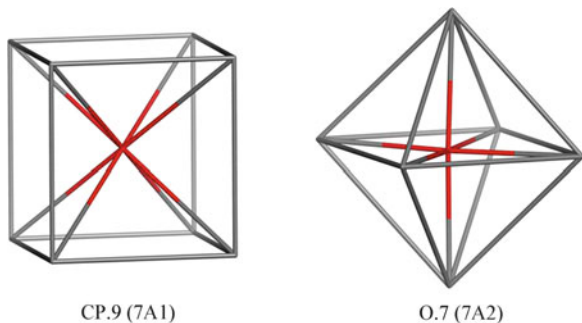


Fig. 7.2 Endo-exo positioning of components of the $mCP.20 = dOP.20$ cluster

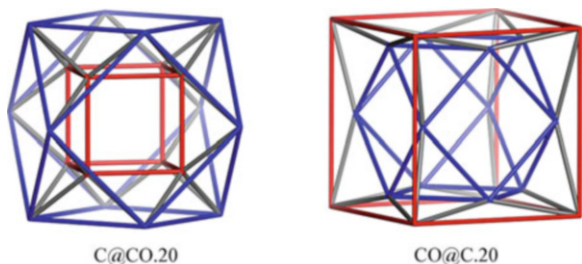


Table 7.1 Figure count for derivatives of CP.9 (7A1) and OP.7 (7A2) clusters

	v	e	3(2)	4(2)	6/8(2)	2	1(3)	2(3)	3(3)	M	3	χ	k	$n(3);(M);(4)$
1	9	20	12	6	0	18	0	6	0	1	7	0	4	0;Py ₄ ;0(C)
2	7	18	20	0	0	20	8	0	0	1	9	0	4	T;0;0(O)
3	20	60	44	12	0	56	8	6	0	2	16	0	4	T;A ₄ ;(C;CO)
4	56	180	100	60	0	160	8	20	6	2	36	0	4	T;mP ₃ ;Rh ₈ ;(Rh ₁₂ ..)
5	60	180	84	72	0	156	20	8	6	2	36	0	4	P ₃ ;O;mA ₄ ;(CO..)
6	120	240	40	60	56	156	20	6	8	2	36	0	4	P ₃ ;C ₃₂ ;TT;(TC..)
7	40	80	32	6	18	56	8	6	0	2	16	0	4	T;TC;(C;TC)
8	18	60	52	6	0	58	8	6	0	2	16	0	4	O;Py ₄ ;(O;CO)
9	52	132	36	60	0	96	8	6	0	2	16	0	4	C;CO;(C..)
10	60	156	52	60	0	112	8	6	0	2	16	0	4	CO;C;(CO..)
11	120	216	0	60	52	112	8	6	0	2	16	0	4	TO;C;(TO..)

1 = CP.9 (7A1); 2 = OP.7 (7A2); 3 = $mCP.20$ (7A3); 4 = $d(mCP).56$ (7A3.1); 5 = $m(mCP).60$ (7A3.2); $C_{32} = 16(4.6.8)$; $16(4.6^2)$; 6 = $t(mCP).120$ (7A3.3); 7 = $tCP.40$ (7A4); 8 = $O@CO.18$ (7A5); 9 = $d(O@CO).52$ (7A5.1); 10 = $m(O@CO).60$ (7A5.2); 11 = $t(O@CO).120$ (7A5.3)

7.2 Clusters Decorated by Octahedra

The seeds of the considered clusters decorated by octahedra are $CO@dCO.26$ (7A6) and its centered pair $COP@dCO.27$ (7A7); the medial of these clusters provides $m(COP@dCO.26).96$ (7A6.1) and $m(COP@dCO.27).108$ (7A7.1), respectively.

Table 7.2 Figure count for clusters decorated by octahedra

	v	e	3(2)	4(2)	5/6/ 8(2)	2	1(3)	2(3)	3(3)	M	3	4	χ	$k(g)$	$n(3);(M);(4)$
1	26	96	104	18	0	122	32	18	0	2	52	0	0	4(0)	T;Py4;(Rh ₁₂ ; CO)
2	27	108	128	18	0	146	40	24	0	1	65	0	0	4(0)	T;Py4;Rh ₁₂ ; (P;CO)
3	60	168	88	36	0	124	8	6	0	2	16	0	0	4(0)	O;CO;(CO..)
4	96	312	232	18	0	250	32	0	0	2	34	0	0	4(0)	O;()
4 _{sp}	96	312	232	0	0	232	32	0	0	0	32	0	-16	4(9)	O;(); $g = w/2$
5 (4)	108	384	288	48	0	336	40	6	12	2	60	0	0	4(0)	O;CO; mP_3 ; (CO..)
5 (5)	108	384	288	48	0	336	40	6	12	2	60	2	2	5(0)	O;CO; mP_3 ; (CO..);(C ₉₆ ; C ₆₀)

1 = CO@dCO.26 (7A6); 2 = COP@dCO.27 (7A7); 3 = C₁₀₈X.60 (7A7.1b); 4 = m (CO@dCO).96_{sp} (7A6.1); 5 = C₆₀@C₉₆.108 (7A7.1)

C₉₆ is a hyperstructure, CY(8(O@3O);P).96 (7A6.1) (the repeating substructure being a triple of octahedral shapes around a fourth one, O@3O.15 (7A6.2b)) and, in the whole, it is a hyper structure, entirely decorated by octahedra.

C₁₀₈ (7A7.1) is a cluster of rank $k = 5$, consisting of two sub-clusters of rank $k = 4$, namely C₉₆ and C₆₀ (7A7.1b). The figure count of these clusters is given in Table 7.2. About rank 5 in double shell clusters, see the discussion in Sect. 5.4.

7.3 Clusters Decorated by Dodecahedra

Structures decorated with dodecahedral shapes D (i.e., C₂₀), can be drawn, as shown in Sect. 6.3, by the sequence of operations (Diudea 2013): $t_{sel}(p_4(P))$; $s_2(P)$; $t_{sel}(p_4(P))@s_2(P)$, where t_{sel} stands for the selected vertices truncation while the “endo” symbol @ means “inside”. Formally, every point in the parent polyhedron P was changed by a C₂₀ cell; the resulted structure PY(nD ;f₅) is a “hyper” and a “spongy” structure, with a central hollow of $t_{sel}(p_4(P))$ topology; if this hollow is filled, by connecting inside the parent P, a double-shell cluster will result.

In case P = C, CY(8D).100 (7A8) and the other the structures involved in the above sequence are illustrated in the Atlas (Figs. 8n and 9n), while the figure count is given in Table 7.3.

In spongy *spa* the genus number of 2-faces equals the sum of pentagons 5(2); thus $w(4) = 6$; M = 0; $g = w/2 = 3$, with w being the window-faces. Spongy *spb* represents only the envelope (of rank $k = 3$ and genus g equals the number of windows minus one: $g = w - 1 = 5$).

Table 7.3 Clusters decorated with dodecahedral shape $D = C_{20}$

Structure	v	e	5(2)	$w(s)$	2	U(3)	M	3	χ	$k(g)$
CY(8D) (7A8)	100	180	84	6(4)	90	8	2	10	0	4(0)
CY(8D) _{spa}	100	180	84	6(4)	84	8	0	8	-4	4(3)
CY(8D) _{spb}	100	180	72	6(4)	72	0	0	0	-8	3(5)
C@CY(8D) (7A9)	108	200	96	12(4)	108	14	2	16	0	4(0)

In the filled structure C@CY(8D).108 (7A9) the core is just a cube while U (3) includes, besides D-units, some shapes with 2-faces pentagons and two squares (coming from C); the number of such shapes is 6, as the number of C-faces; the number of windows is twice that in the spongy CY(8D).100.

When C_{100} or C_{108} clusters are further subjects of map operations, the resulting structures are decorated with the C_{60} cluster (7A8.2.5; 7A9.2) or its transforms; structures are illustrated in the Atlas; the figure count is listed in Table 7.4.

Some of these clusters show higher genus g , being spongy structures (7A8.2.1–5). Two clusters: $t(C_{108}).400$ (7A9.1) and $l(C_{108}).528$ (7A9.2) are counted as clusters of rank $k = 5$ (see the discussion in Sect. 5.4).

7.4 Rhomb Decorated Octahedral Clusters

Applying the pair dm of map operations to the hypercube Q_4 resulted in a cluster named $dm(Q_4).88 = Rh_{12}@(32mP_3;16T;6Rh_{12})@Rh_{12}.88$ (7A10.1), basically decorated by rhombic dodecahedra Rh_{12} and medial of trigonal prisms mP_3 , keeping the octahedral/cubic symmetry of the parent Q_4 but raising its rank from 4 to 5 (Table 7.5); there are two identical $n - 1$ faces of rank $k = 4$ (actually $Rh_{12}@(12mP_3;8T).50$ (7A10.1b), thus the whole structure will have the rank $k = 5$ (Coxeter 1973; Schulte 2014). Analogously was done for the precursor $m(Q_4).32$ (7A10 and Table 7.5). By face-identification, the unit C_{50a} (for “b” see below) can be translated in the three directions of the Euclidean space to generate a network, shown in Fig. 7A10.2; its topological symmetry is given in Table 7.7.

Two units were embedded in a large domain ($C_{50a}.444.2156$) of the network: $C_{50a}.111.50$ (7A10.1b) and $C_{50a}.222.310$ (7A10.2); both of these units show the same four atom-vertex classes (ring signature is listed in the last column); the smallest unit showing all the atom-vertex types is $C_{50a}.111.50$ (7A10.1b), that is the repeating unit enabling the building (and fully characterizing) of the network, shortened hereafter as “ C_{50a} -net”. Centrality vertex classes differ function of the size of unit considered; this will be used to discriminate different network-types within the same size (given here as the number of smallest units along the three coordinates).

The second network and the series of related clusters are as follows. An isomer of the 24-cell, $O@14O.24$ (7A11b) was submitted to the medial and then dual operations. The resulting structure, $d(m(C_{24})84).166$ (7A11), is tessellated by

Table 7.4 Figure count in clusters decorated by dodecahedra and its derivatives

v	e	3(2)	4(2)	5/6/8/10(2)	2	1(3)	2(3)	3(3)	M	3	4	χ	$k(g)$	$n(3);(M);(4)$
1	84	240	160	0	0	160	8	0	0	8	0	-4	4(3)	I;(0)
2	180	420	160	0	84	244	8	0	0	8	0	-4	4(3)	ID;(0)
3	244	480	0	240	0	240	8	0	0	8	0	-4	4(3)	Rh ₃₆ ;(0)
4	184	332	136	0	48	184	6	28	0	36	0	0	4(0)	$tC_{16};T(tC_{..})$
5	360	600	160	0	84	244	8	0	0	8	0	-4	4(3)	tD ;(0)
6	400	752	336	0	108	444	14	76	0	92	2	2	5(0)	$(tC_{20};tC_{16});T;(tC_{..});(C_{184};C_{360})$
7	204	372	68	6	124	198	0	0	28	30	0	0	4(0)	$C_{60};hC_{48};TT;(TO_{..})$
8	420	660	0	0	244	244	8	0	0	8	0	-4	4(3)	C_{60} ;(0)
9	528	972	116	12	384	512	8	6	52	68	2	2	5(0)	$C_{60};C_{48};TT;(TO_{..});(C_{204};C_{420})$

1 = $d(C_{100},84sp)$ (7A8.2.1); 2 = $m(C_{100},180sp)$ (7A8.2.2); 3 = $dm(C_{100},244sp)$ (7A8.2.3); 4 = $t(C_{108},400X,184)$ (7A9.1.1); 5 = $t(C_{100},360sp)$ (7A8.2.4); 6 = $t(C_{108},400)$ (7A9.1); 7 = $t(C_{108},528X,204)$ (7A9.2); 8 = $t(C_{100},420sp)$ (7A8.2.5); 9 = $t(C_{108},528)$ (7A9.2); 0 = no cell; $(C_{n..})$ = in pair "M", only one cell is well-defined; C_{16} = $(8(4,5,5),8(5,5,5))$ -vertex figure; C_{48} = $(4,6^4,4,5,6)^4$; $(6,5)^4$; $(6,5)^4$; $(6,5)^4$; $(6,5)^4$ -spiral code

Table 7.5 Figure count in the clusters derived from the hypercube Q_4

	v	e	3(2)	4(2)	2	1(3)	2(3)	3(3)	M	3	4	χ	k	$n(3);(M)$	(4)
1	32	96	64	24	88	6	16	0	2	24	2	2	5	CO;T;(CO;CO)	(C ₂₀ ; C ₂₀)
2	20	48	32	6	38	0	8	0	2	10	0	0	4	CO;T;(CO..)	–
3	88	288	160	96	256	6	16	32	2	56	2	2	5	Rh ₁₂ ;T;mP ₃ ; (2 × Rh ₁₂)	(C _{50a} ; C _{50a})
4	50	144	80	36	116	0	8	12	2	22	0	0	4	();T;mP ₃ ;(Rh ₁₂ ..)	–

1 = $m(Q_4)$.32 (7A10); 2 = $m(Q_4)$ X.20 (7A10b); 3 = $m(Q_4)$.88 (7A10.1); 4 = $m(Q_4)$ X.50 = C_{50a} (7A10.1b)

Table 7.6 Figure count in the clusters derived from O@14O.24 (7A11b)

	v	e	3(2)	4(2)	2	1(3)	2(3)	3(3)	M	3	4	χ	k	$n(3);(M)$	(4)
1	166	492	204	180	384	6	36	14	2	52	2	8	5	O;mP ₃ ;Rh ₁₂ ; (Rh ₁₂ ..)	(C _{50b} ; C ₁₅₂)
2	152	420	156	150	306	6	24	6	2	38	0	0	4	Py ₄ ;mP ₃ ;Rh ₁₂ ; (Rh ₁₂ ..)	–
3	50	144	72	42	114	6	12	0	2	20	0	0	4	Py ₄ ;mP ₃ ;(Rh ₁₂ ..)	–
4	98	288	144	84	228	12	24	0	2	38	0	0	4	Py ₄ ;mP ₃ ; (Rh ₂₄ ..)	–

1 = $d(m(C_{24})84)$.166 (7A11); 2 = C₁₆₆X.152 (7A11b); 3 = C_{50b} (7A11.2); 4 = C_{50b} (co-net) (7A11.3)

rhombic substructures; it can be split into two clusters of $k = 4$: C₁₅₂ and C_{50b}, (inside/outside position being relative), from which the re-combined cluster: C_{50b}@C₁₅₂.166 (7A11) has the rank $k = 5$ (Table 7.6). The unit C_{50b} = R₁₂@(12mP₃;6Py₄).50 (7A11.2) can be translated over the three coordinate directions to generate a “C_{50b}” (7A11.1) network, analogous to “C_{50a}” above discussed; the co-net unit, Rh₂₄@24mP₃.98 (7A11.3), with a larger rhombic cell Rh₂₄ is well defined. Topological symmetry of the “C_{50b}” network is detailed in Table 7.7. One can see that atom-vertex types are only three, compared to four, for the “C_{50a}” net; nevertheless, the spatial distribution of points/atoms is similar: there are 15 classes (by centrality) vertices in the “444.2156” domain, all of the same number of elements, only the position with respect to the center of domain being somehow changed. The close RSI values argue in addition for the similarity of these networks and their substructures.

Another rhomb-decorated structures is CY(8Rh₃₀;P).244 (7A8.2.3), the vertices of cube being changed by triacontahedra R₃₀.

Ring signature index RSI and centrality index were computed by the original Nano Studio software (Nagy and Diudea 2009) developed at TOPO GROUP.

Table 7.7 Topological symmetry by RSI and centrality index of C_{50} (a;b) networks

	Structure	Centrality classes {elements}	Deg	Atom-vertex classes {elements}	RSI signature
1	$C_{50a.111.50}$ (7A10.1b)	4	6	{8}	$3^6.4^3$
	sel@	{8.6.24.12}	8	{6}	$3^4.4^4$
	$C_{50a.444.2156}$		10	{24}	$3^4.2.4^9$
			8	{12}	$3^8.4^8$
				{50}	2.177143
2	$C_{50b.111.50}$ (7A13.2)	4	8	{30}	$3^8.4^6$
	sel@	{8.6.24.12}	8	{12}	$3^4.4^8$
	$C_{50b.444.2156}$		6	{8}	$3^3.4^6$
				{50}	2.125714
3	$C_{50a.222.310}$ (7A10.2)	15	6	{64}	$3^6.4^3$
	sel@	{12.6.8.24.24.24.12.	8	{48}	$3^4.4^4$
	$C_{50a.444.2156}$	24.24.24.24.48.	10	{144}	$3^4.2.4^9$
		8.24.24}	8	{54}	$3^8.4^8$
				{310}	2.140092
4	$C_{50b.222.310}$ (7A11.1)	15	8	{192}	$3^8.4^6$
	sel@	{6.12.24.8.24.12.	8	{54}	$3^4.4^8$
	$C_{50b.444.2156}$	24.24.24.24.24.48.	6	{64}	$3^3.4^6$
		8.24.24}			
				{310}	2.105069

7.5 Cubic Net Transforming

A space-filling polyhedron is a polyhedron which can tessellate the 3D space (Grünbaum and Shephard 1980). The cube is the only Platonic solid showing this property (Gardner 1984). There are only five space-filling convex polyhedra with regular faces: triangular prism, hexagonal prism, cube, truncated octahedron (Steinhaus 1999), and gyrobifastigium, (J_{26} , Johnson 1966). The rhombic dodecahedron Rh_{12} is also a space-filler (Steinhaus 1999). Combinations of two or more polyhedra may also fill the space (Goldberg 1979).

Our attention was focused on two space fillers: the cube C and the rhombic dodecahedron, $Rh_{12.14}$ (i.e., $d(mC).14$, or dual of cuboctahedron DCO) (Fig. 7.3) and to their networks, *pcu* and *flu*, respectively. By applying some map operations, like dual, medial, truncation or leapfrog, directly on networks, a variety of periodic structures could be drawn; some of the most interesting and aesthetical networks thus designed are illustrated and characterized in the Atlas, Figs. 7A12 n –7A13 n .

Centrality topological index (Diudea and Ursu 2003), computed on the layer matrix of all rings around atoms refers to a given domain cut-off from a network

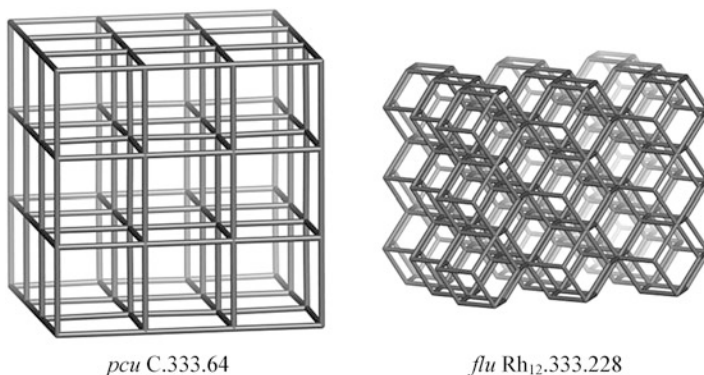


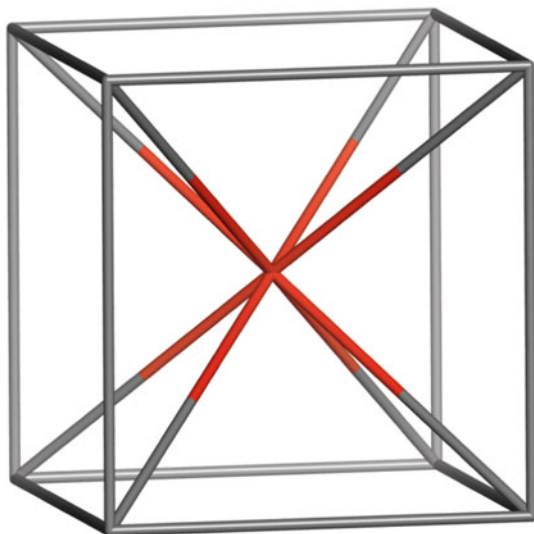
Fig. 7.3 Basic networks filling the 3D space

and is dependent of the size and shape of the considered domain, thus being here less informative. That's why, in networks characterization, the simple ring signature (given in the Atlas as the number of vertex types, v , and vertex symbol, vs) is more useful. The type of tiles characterizes the space filling; it is described focused on the larger tile, surrounded by smaller ones, according to face homology; face-tiling of these tiles is given at the bottom of figures.

For a better identification of structural features, both the “net” and “co-net” appearances of a network were illustrated, keeping the information on their particular drawing, despite the net/co-net view is interchangeable. Also, a name to remind the map operation used for drawing was added to the (known) name of networks (by capitals, e.g., *flu* = DCO; *lta* = TMC, etc.). For the crystallographic name and additional information on these networks, the reader is invited to consult Reticular Chemistry Structure Resource, <http://rcsr.anu.edu.au>.

Among the herein discussed networks, *pcu* (primitive cubic lattice), *flu* (fluorite) and *sod* (sodalite) possess a single tile in filling the 3D space; the others have two or three tiles (see the Atlas 7). The number of vertex types, expressed as vertex symbol, is more important in the evaluation of net feasibility by chemical reactions; in this respect, the uninodal networks could appear more promising.

Chapter 7 Atlas: Octahedral Clusters



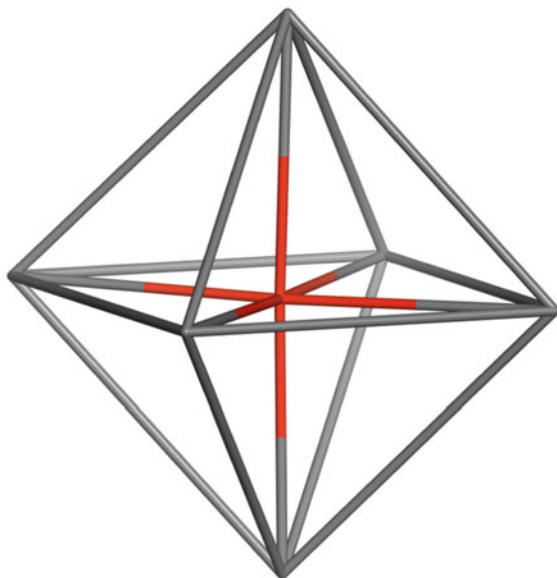
OY(6Py₄; f₃).9

CP.9

$C_2 \times S_4$; $|C_2 \times S_4| = 48$; Classes: 2 $|\{1\}; \{8\}|$

7A1

C.8	O.6	OP.7



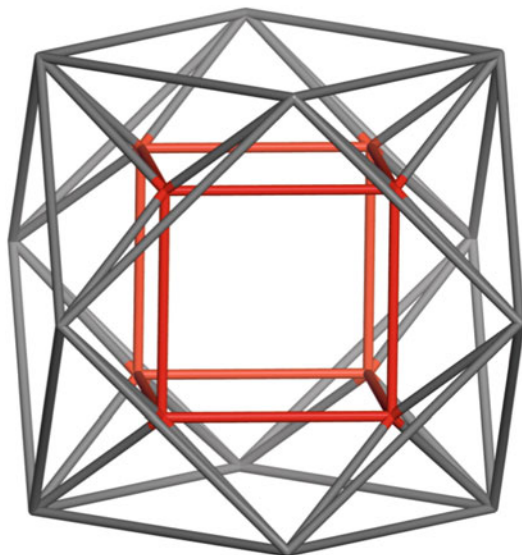
CY(8T; f_3).7

OP.7

$C_2 \times S_4$; classes: 2 | {1}; {6} |

7A2

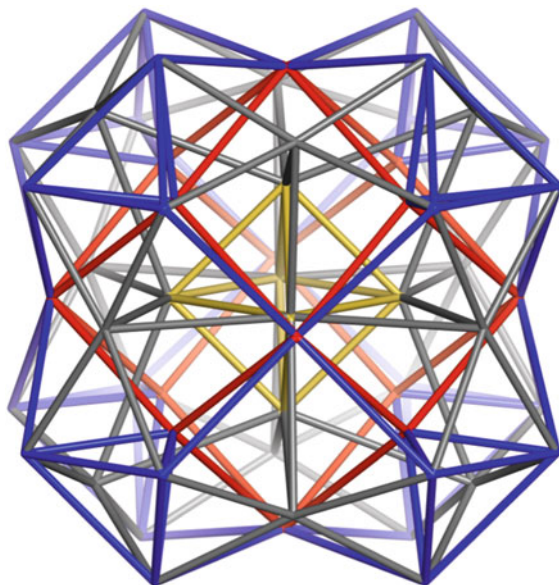
O.6	C.8	CP.9



C@CO.20

$C@(6A_4;8T)@CO.20$
mCP.20
 $C_2 \times S_4$; classes: $2 \{ \{8\}; \{12\} \}$
 $7A_3$

C ₈	A ₄ .8	CP.9

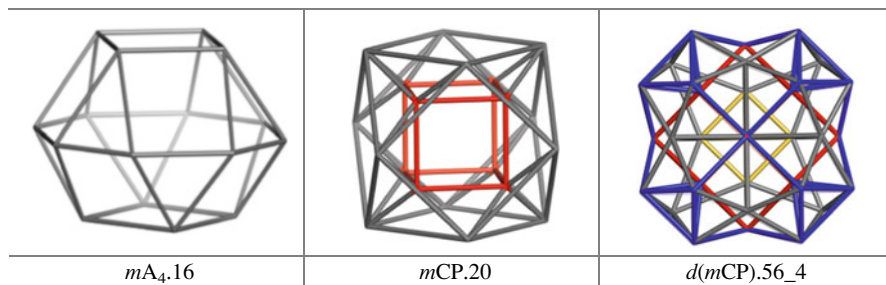


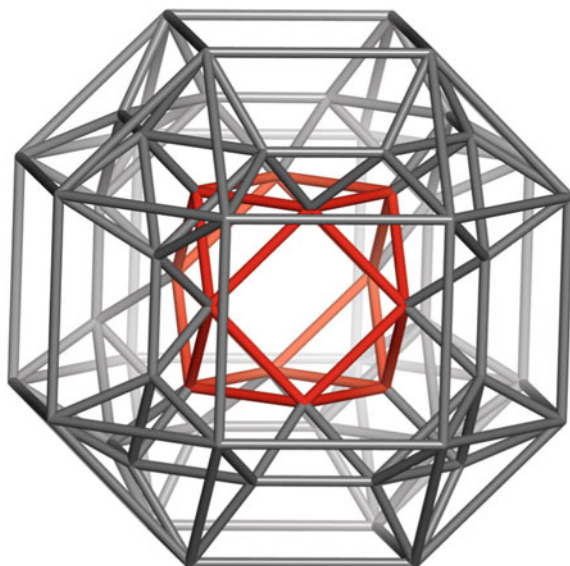
$O@(8mP_3;6Rh_{10})@(8T;12mP_3)@dCO.56$

$d(mCP).56$

$C_2 \times S_4$; classes: 5 | 2{6};{8};{12};{24}|

7A3.1



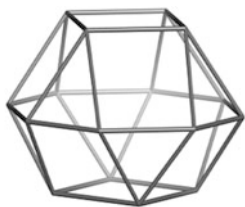


$CO@(6mA_4;8O;8P_3;12P_3).60$

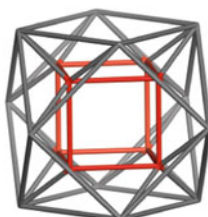
$m(mCP).60$

$C_2 \times S_4$; classes: 3 $\{12\}$; 2 $\{24\}$ |

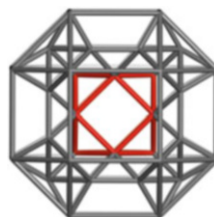
7A3.2



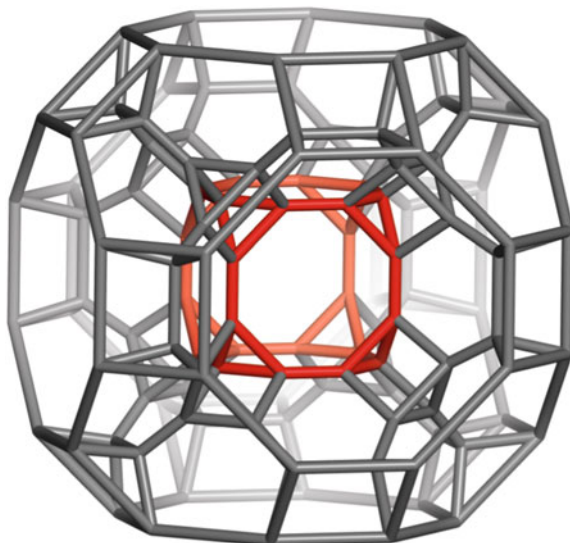
$mA_4.16$



$mCP.20$



$m(mCP).60_4$



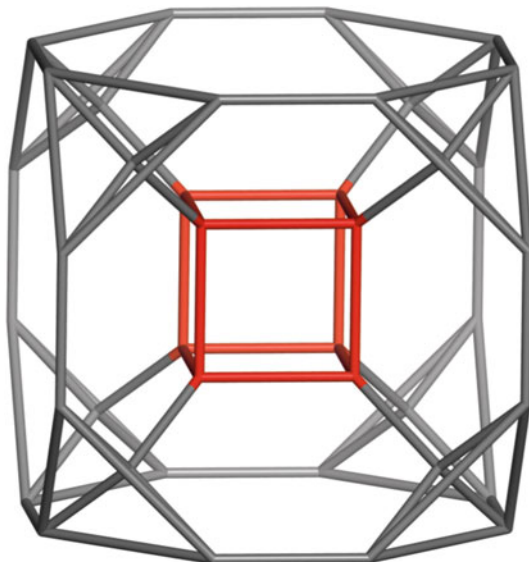
$tC@(6htCO;8TT;8P_3;12P_3)@tCO.120$

$t(mCP).120$

$C_2 \times S_4$; classes 4 |{3 {24}; {48}}|

7A3.3

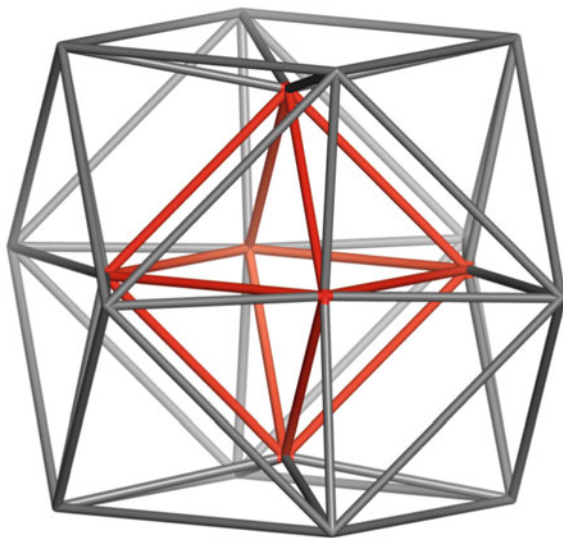
TC.24	mCP.20	$t(mCP).120_4$



C@TC.40

C@(6hTO;8T)@iC.40
 iCP.40
 $C_2 \times S_4$; classes 3 |2{8};{24}|
 7A4

C.8	TO.24	CP.9



CY(8O; f_3).18

O@(8O;6Py4)@CO.18

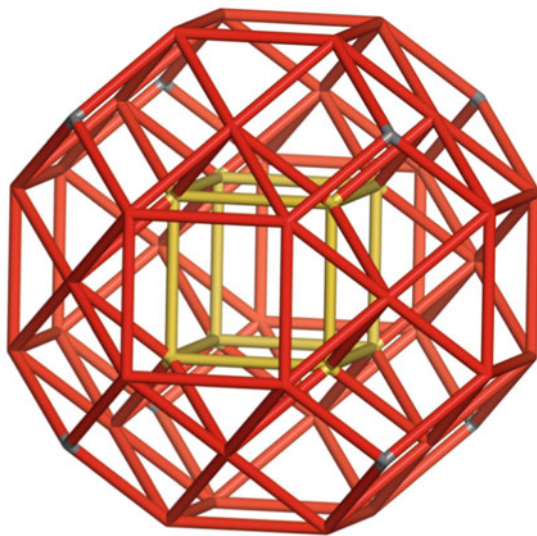
O@CO.18

d CP.18= m OP.18

$C_2 \times S_4$; classes 2 |{6};{12}|

7A5

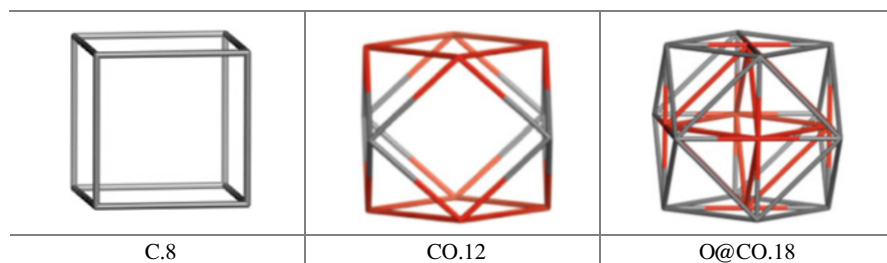
O ₆	C ₈	CP ₉

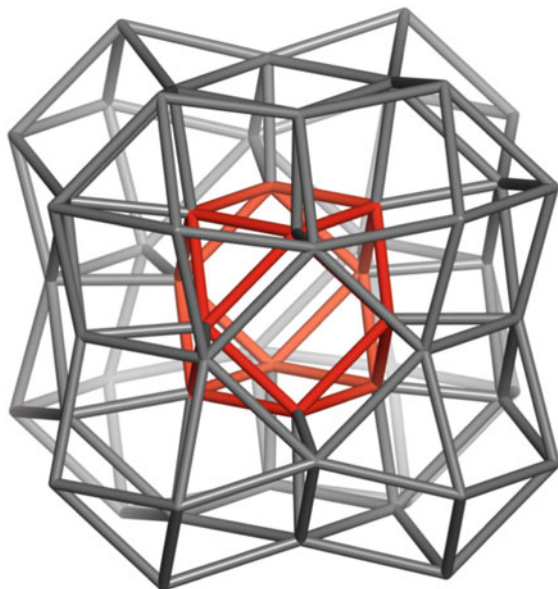


C@(6CO; 8C).52

d(O@CO18).52

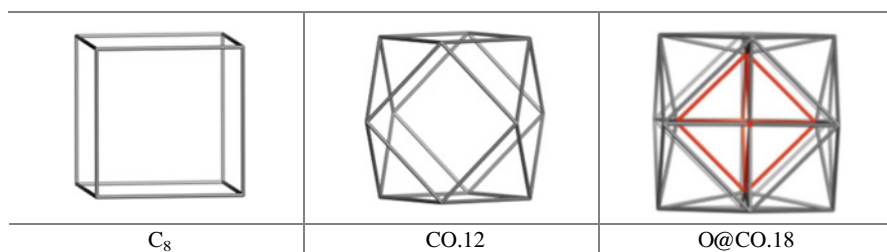
$C_2 \times S_4$; classes: 4 |2{8}; {12}; {24}|
7A5.1

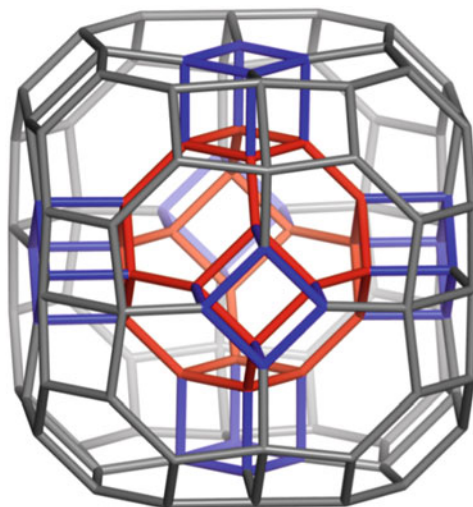




CY(8CO; f_3).60

CO@(8CO;6C).60
mmOP.60=mdCP.60
m(O@CO).60
 $C_2 \times S_4$; classes: 3 |{12}; 2 |{24}|
 7A5.2





TO@(8TO;6C).120

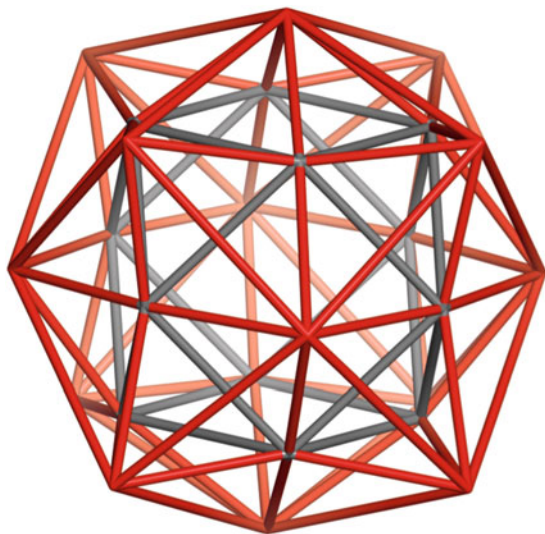
$t(\text{O@CO}).120$

$t(m\text{OP}).120$

$C_2 \times S_4$; classes: 4 | 3 {24}; {48} |

7A5.3

O.6	TO.24	O@CO.18=mOP.18

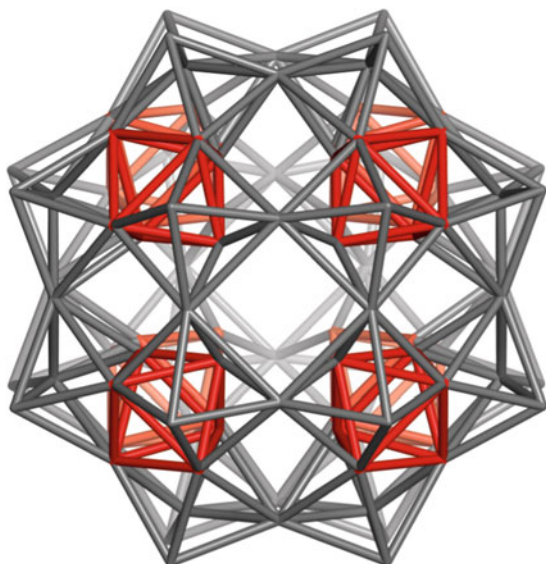


CO@dCO.26

$C_2 \times S_4$; classes: 3 | {6}; {8}; {12} |

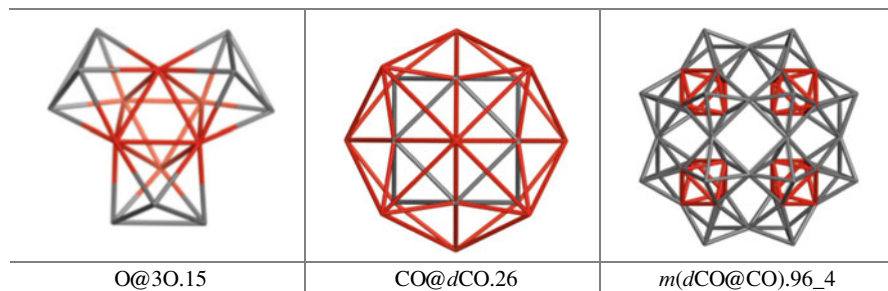
7A6

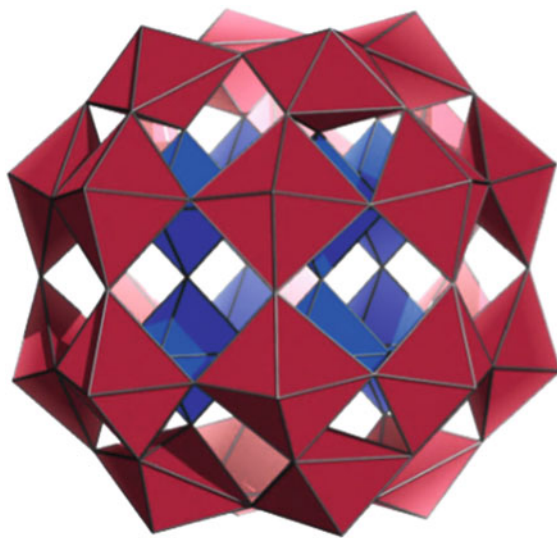
<p>O@3O.15</p>	<p>dCO@CO.26</p>	<p>COP@dCO.27</p>



CY(8(O@3O);P).96

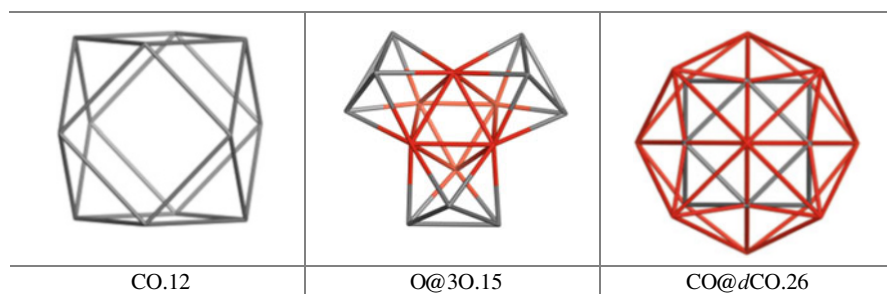
m(dCO@CO).96
 $C_2 \times S_4$; classes: 4 |4{24}|
 7A6.1

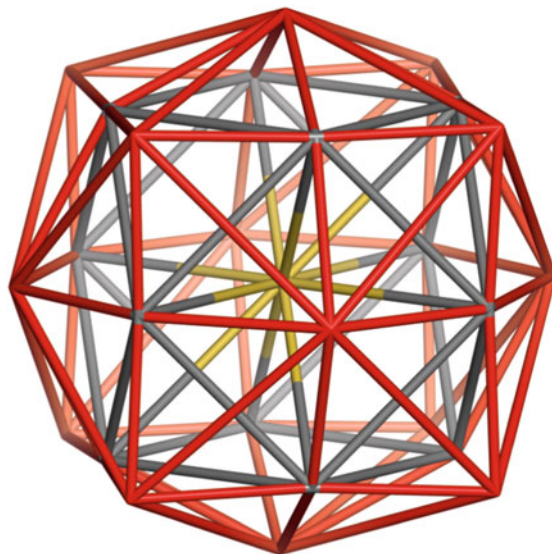




CY(8(O@3O);P).96

m(CO@dCO).96
 $C_2 \times S_4$; classes: 4 |4{24}|
 7A6.2

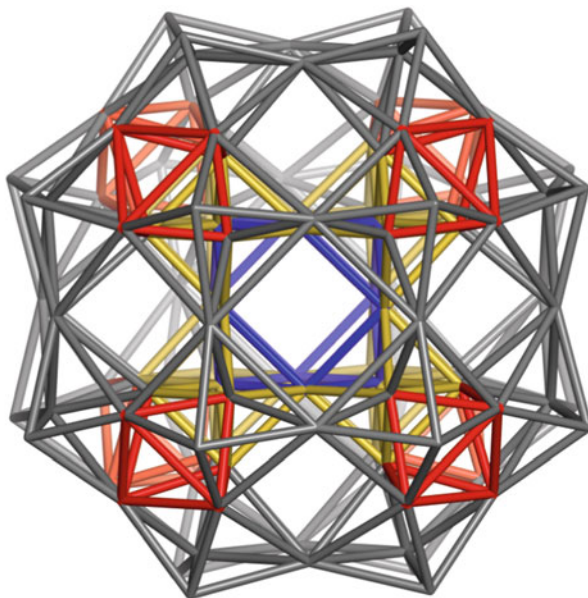




COP@dCO.27

$C_2 \times S_4$; classes: 4 | {1}; {6}; {8} | {12} |
7A7

O@3O.15	<i>dCO@COP.27</i>	CO@dCO.26



$\text{CO}@(\text{m}(\text{dCO}@\text{CO})96).108$

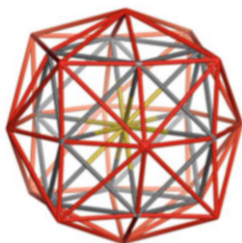
$\text{CO}@(\text{6CO};8\text{O})@(\text{12mP}_3;8(\text{O}@3\text{O})).108$

$\text{C}_{60}@C_{96}.108$

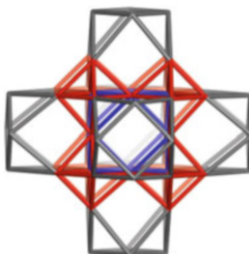
$\text{m}(\text{COP}@d\text{CO}27).108$

$\text{C}_2 \times \text{S}_4$; classes: 5 $\{|12\}; 4\{24\}$

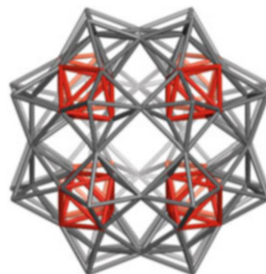
7A7.1



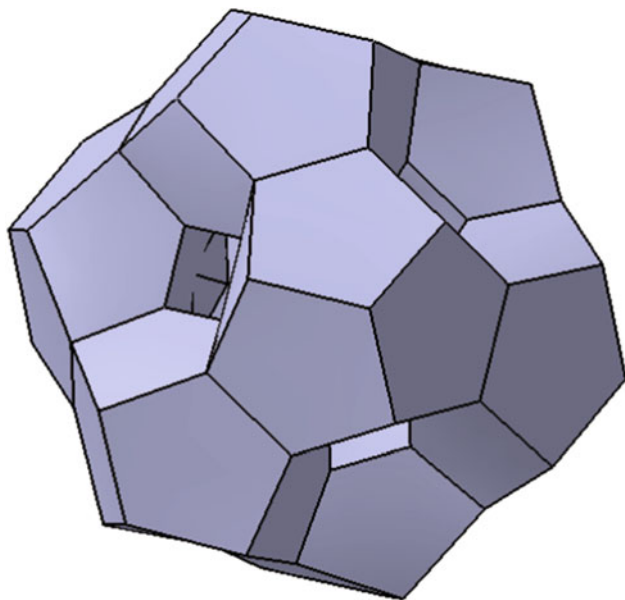
$\text{COP}@d\text{CO}.27$
 $\text{P}^{12}@CO@dCO.27$



$\text{C}_{108}\text{X}.60$



$\text{m}(\text{CO}@d\text{CO}27).96$



CY(8D; f_5).100

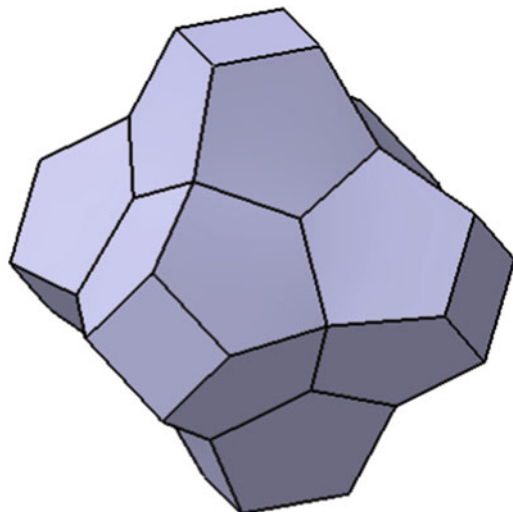
$t_{sel}(p_4(C))@(8D).100$

$t_{sel}(p_4(C))@s_2(C).100$

$C_2 \times S_4$; classes: 6 | 2 {8}; {12}; 3 {24} |

7A8

<p>$t_{sel}(P_4(C)).44$</p>	<p>$s_2(C).56$</p>	<p>$t_{sel}(P_4(C))@(8D).100$</p>

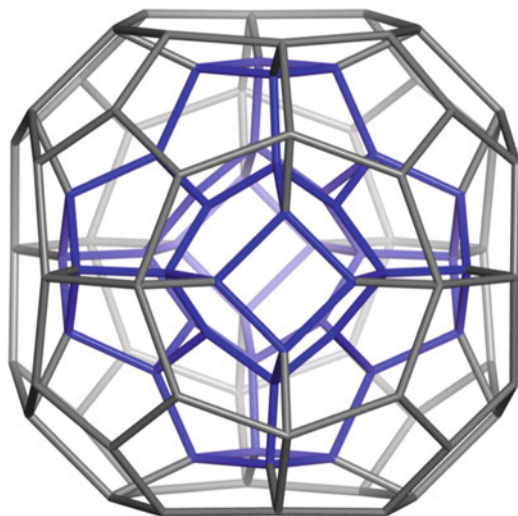


$t_{sel}(p_4(C)).44$

$C_2 \times S_4$; classes: 3 | {8}; {12}; {24} |

7A8.1

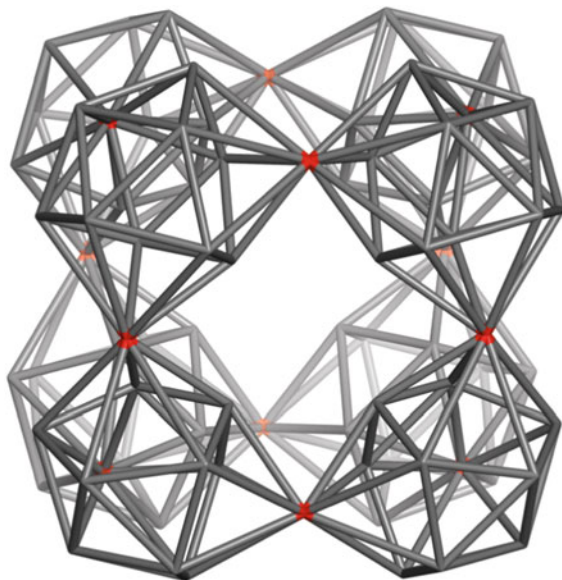
D.20	$t_{sel}(P_4(C)).44$	$t_{sel}(P_4(C))@(8D).100$



CY(8D; f_5).100

$C_2 \times S_4$; classes: 6 $[2\{8\};\{12\};3\{24\}]$
7A8.2

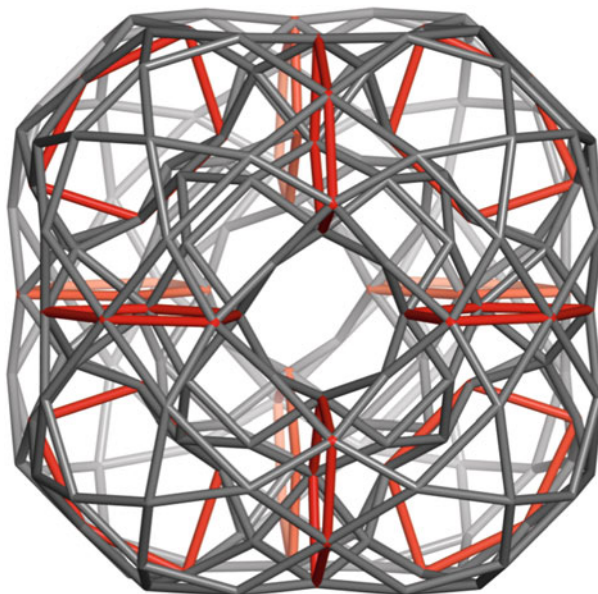
$t_{set}(P_4(C))@(8D).100_2$	$t_{set}(P_4(C))@(8D).100_3$	$t_{set}(P_4(C))@(8D).100_4$



CY(8I;P).84

$d(C_{100}).84$
 $C_2 \times S_4$; classes: 4 |{12}; 3 {24}|
 7A8.2.1

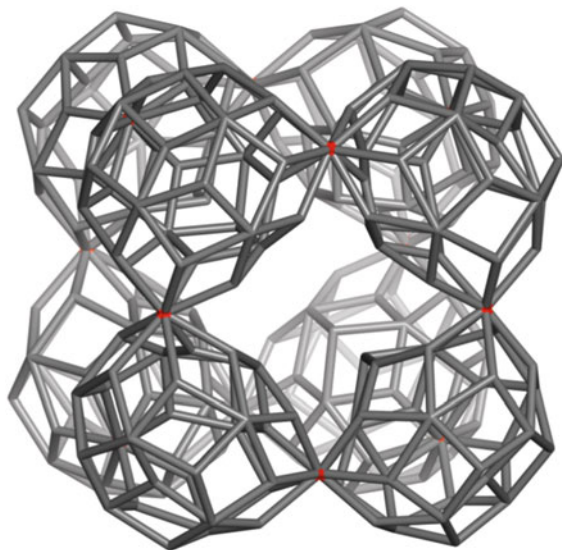
$d(C_{100}).84_2$	$d(C_{100}).84_3$	$t_{sel}(P_4(C))@(8D).100_4$



CY(8ID; f_5).180

$m(C_{100}).180$ *sp*
 $C_2 \times S_4$; classes: 7 | {12}; 5 {24}; {48} ||
 7A8.2.2

<p>$m(C_{100}).180_2$</p>	<p>$m(C_{100}).180_3$</p>	<p>$t_{sel}(P_4(C))@(8D).100$</p>

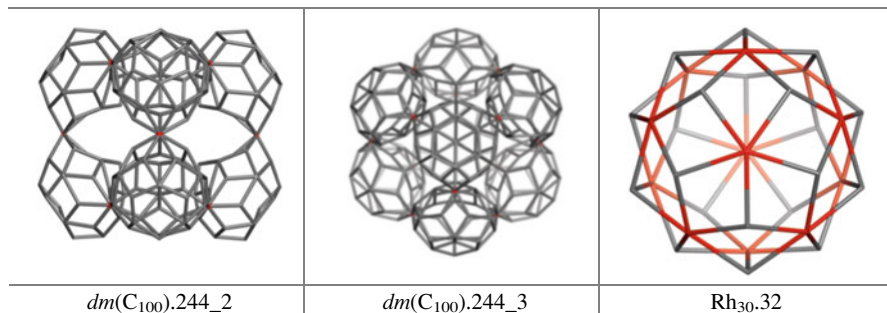


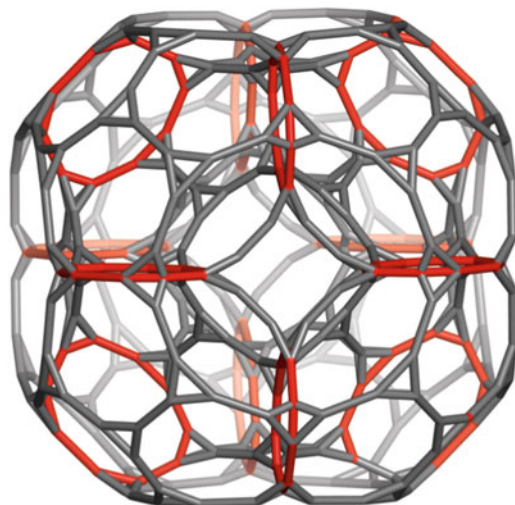
CY(8Rh₃₀;P).244

dm(C₁₀₀).244

C₂×S₄; classes: 10 | 2{8}; {12}; 5{24}; 2{48} ||

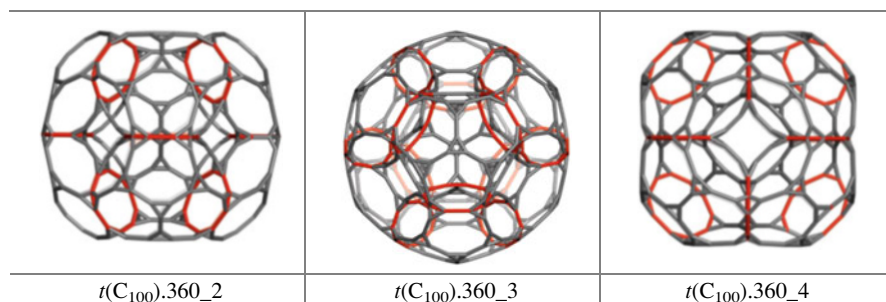
7A8.2.3

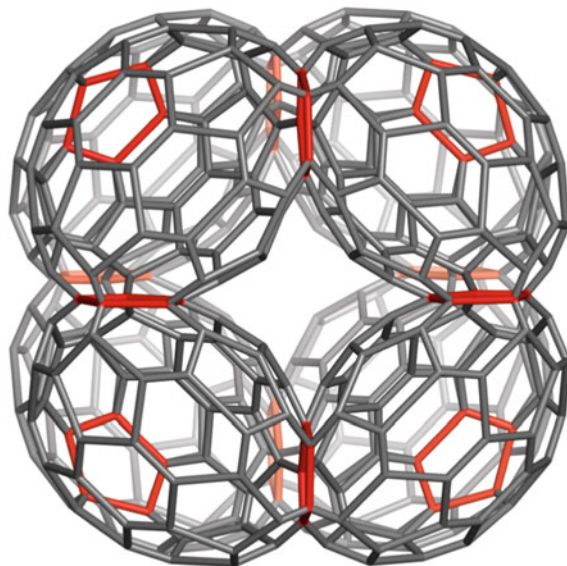




CY(8*t*D; *f*₁₀).360

t(C₁₀₀).360 *sp*
 C₂×S₄; classes: 12 |9 {24};3 {48}||
 7A8.2.4

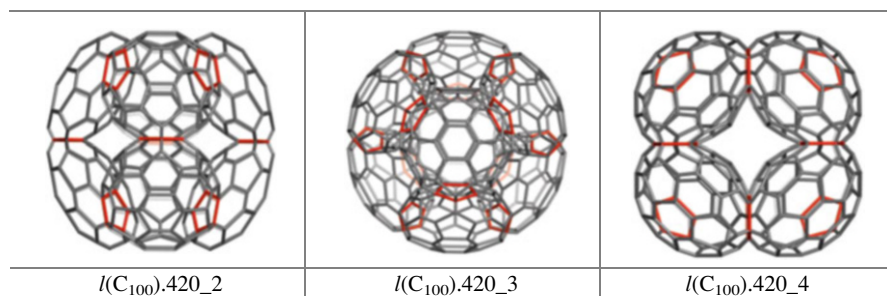


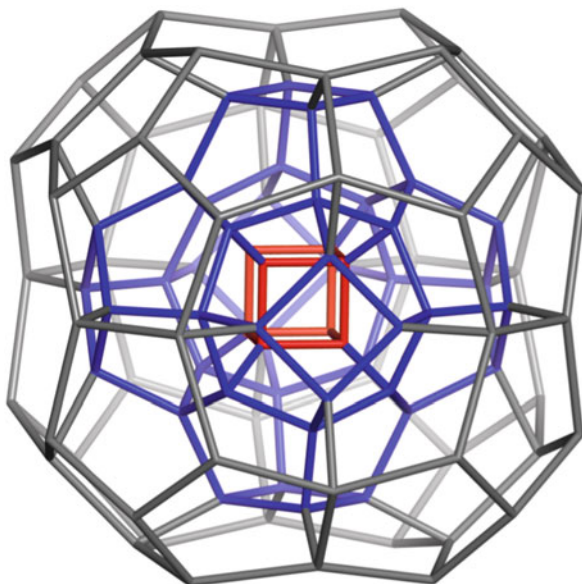


CY(8C₆₀; f₅)-420

$I(C_{100}).420_{sp}$
 $C_2 \times S_4$; classes: 12 | {12}; 5 {24}; 6 {48} ||

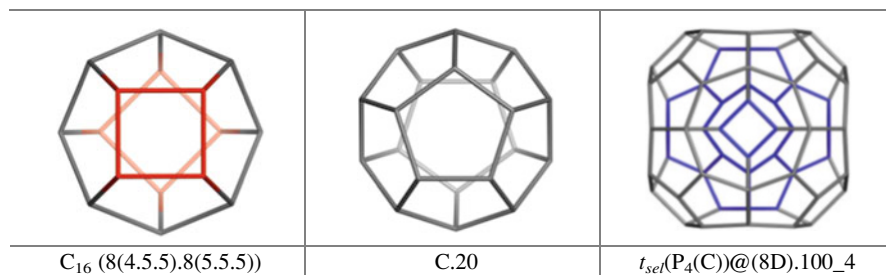
7A8.2.5

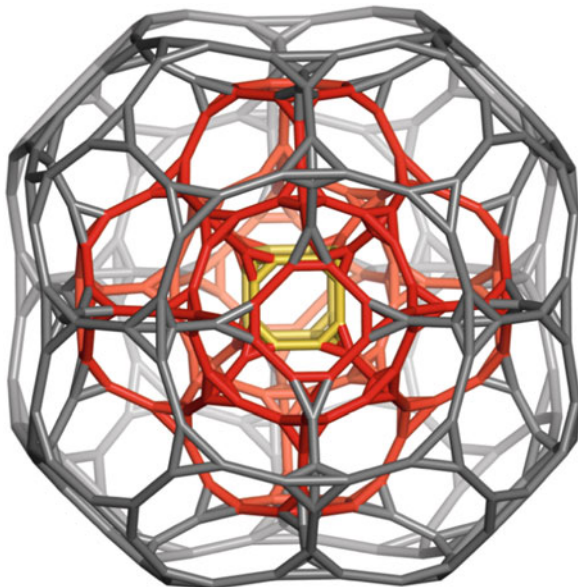




$C@6C_{16}@8C_{20}\cdot 108$

$C_2 \times S_4$; classes: $7 \{3\{8\};\{12\};3\{24\}$
 $7A_9$

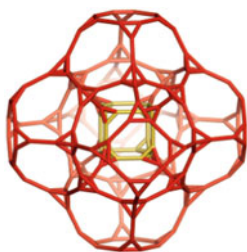




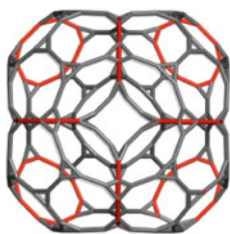
$C_{184}@C_{360}\cdot 400$

$t(C_{108})\cdot 400$

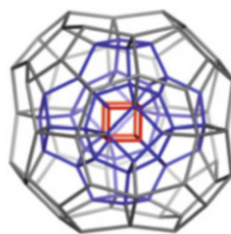
$C_2 \times S_4$; classes: 15 {2{8}}; 10 {24}; 3 {48} ||
7A9.1



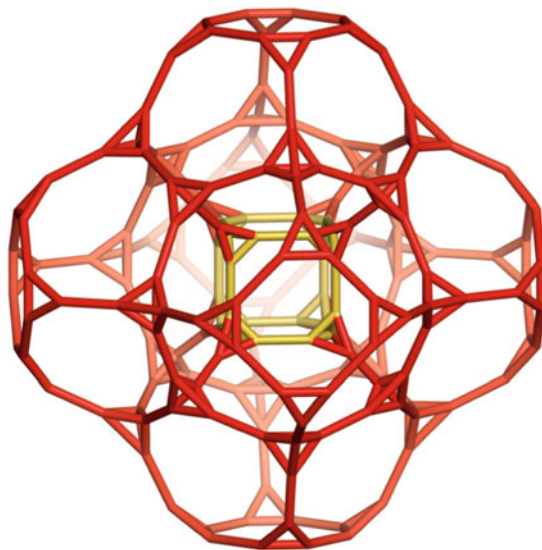
$t(C_{108})X\cdot 184$



$t(C_{100})\cdot 360$

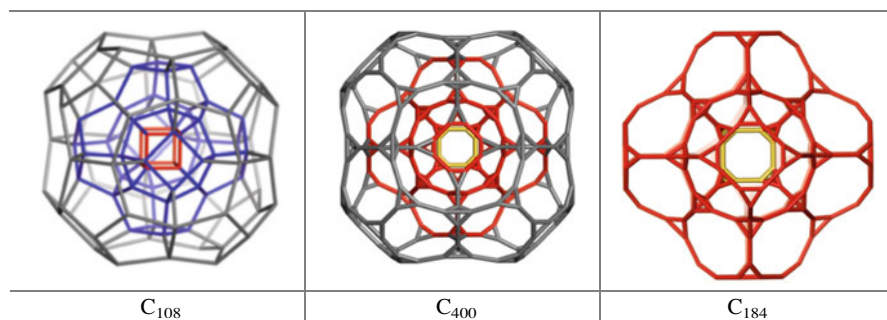


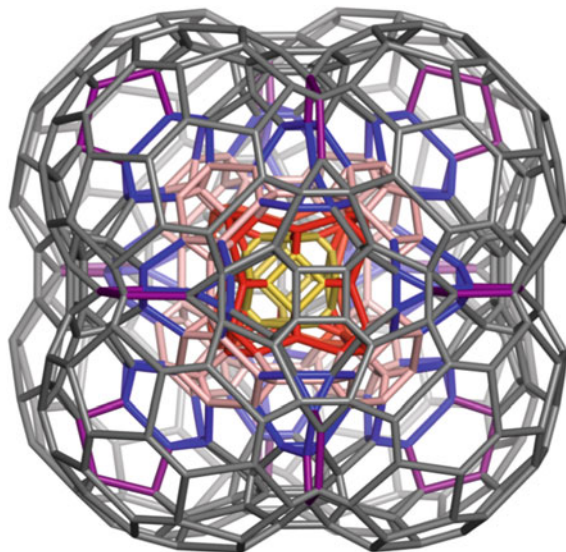
C_{108}



TC@6TC.184

$t(C_{108})400X.184$
7A9.1.1

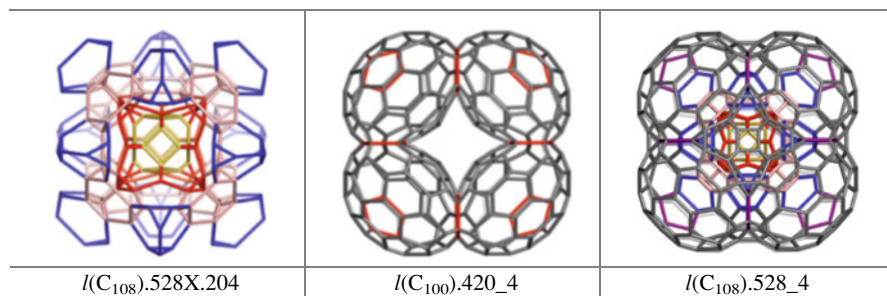


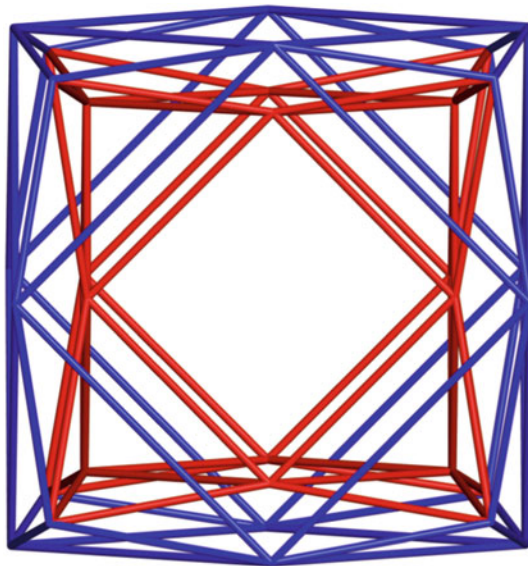


$$C_{204}@C_{420}.528$$

$$I(C_{108}).528$$

$$C_2 \times S_4; \text{ classes: } 17 \{2\{12\}; 9\{24\}; 6\{48\}\} ||$$

$$7A9.2$$




CO@(6CO;16T)@CO.32

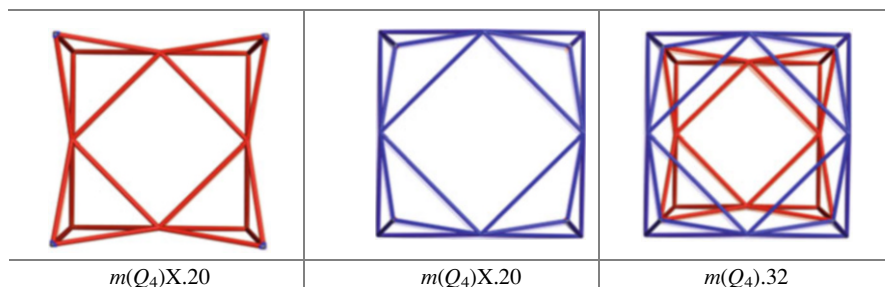
$C_{20}@C_{20}.32$

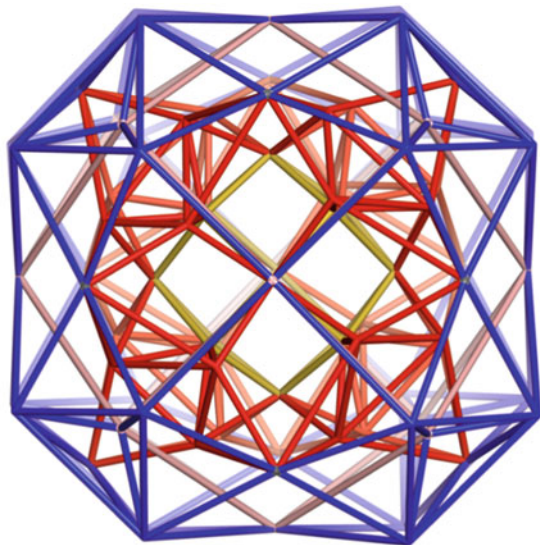
$m(Q_4).32$

$((((C_2 \times D_8): C_2): C_3): C_2): C_2$; Order 384

Classes: 1 | {32}|

7A10





(Rh₁₂@((32mP₃);16T;6Rh₁₂)@(Rh₁₂)).88

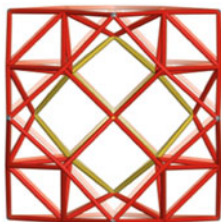
$C_{50a}(r)@C_{50a}(b).88$

$dm(Q_4).88$

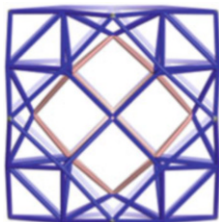
(((C₂×D₈): C₂): C₃): C₂: C₂; Order 384

Classes: 2 |{24};{64}|

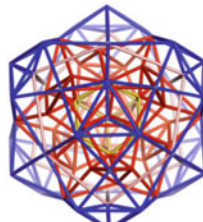
7A10.1



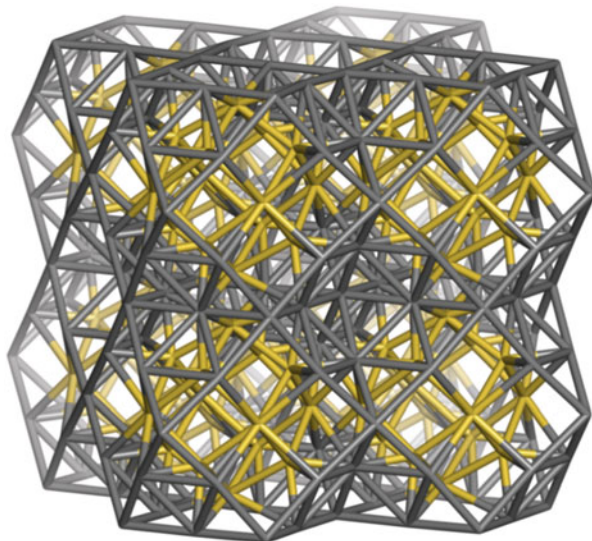
$dm(Q_4)X.50a(r)$
Rh₁₂@(12mP₃;8T).50
C₂ × S₄; Order 48;
|{6};{8};{12};{24}|



$dm(Q_4)X.50a(b)$
Rh₁₂@(12mP₃;8T).50
C₂ × S₄; Order 48;
|{6};{8};{12};{24}|



$dm(Q_4).88_3$



$(dm(Q_4)88X50).222.310$

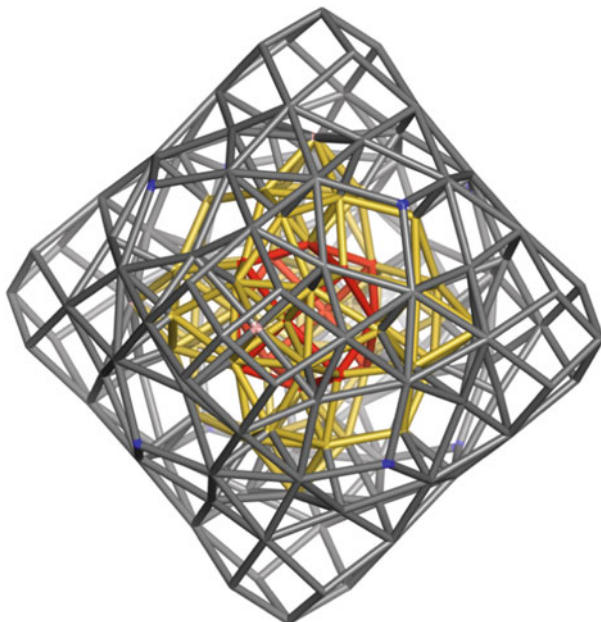
$C_{50a}.222.310$

$C_2 \times S_4$; Order: 48

Classes: 15 |{6};2{8};2{12};9{24};{48}|

7A10.2

<p>$d(m(Q_4)88)X.50$ C_{50a}</p>	<p>$(d(mQ_4)88)X50.222.310$ $C_{50a}.222.310$</p>	<p>$d(m(C_{24})84)166X50.222.310$ $C_{50b}.222.310$</p>



$Rh_{12}@ (14Rh_{12}; 6O; 36mP_3).166$

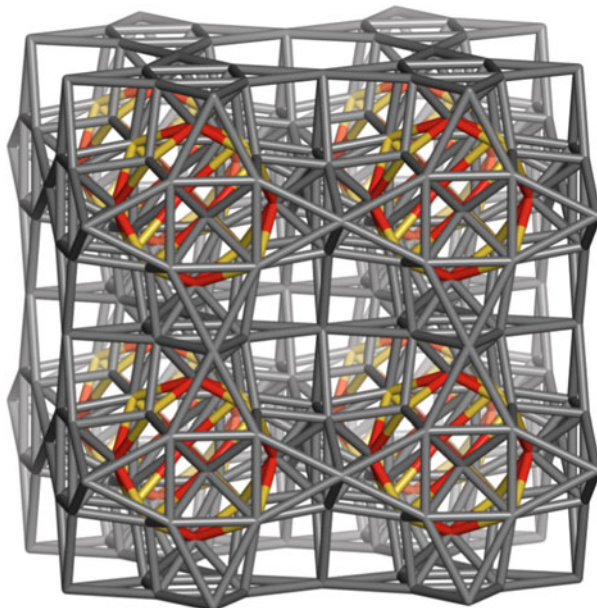
$d(m(C_{24})84).166$

$C_2 \times S_4$; Order 48;

Classes: 11 | 3 {6}; 2 {8}; {12}; 5 {24}|

7A11

<p>$O@14O.24$ $C_2 \times S_4$ Classes: 2 {6}; {12} </p>	<p>$d(m(C_{24})84).166X.50$ $Rh_{12}@12mP_3.50$</p>	<p>$d(m(C_{24})84).166$</p>



$d(m(C_{24})84)166X50.222.310$

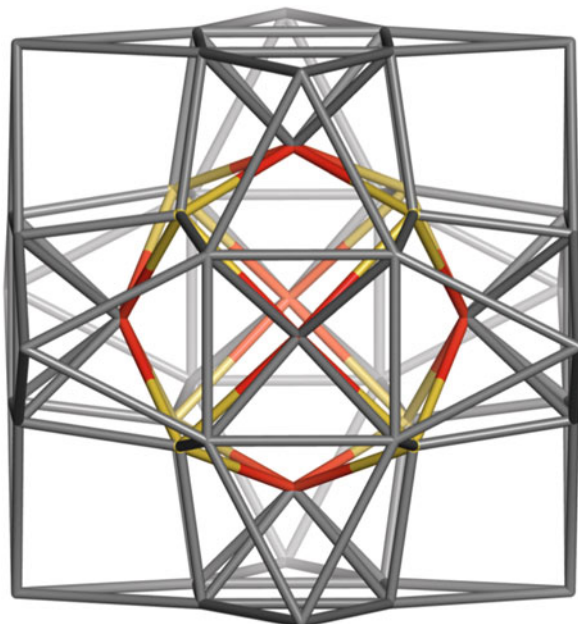
$C_{50b}.222.310$

$C_2 \times S_4$; Order: 48

Classes: 15 |{6};2{8};2{12};9{24};{48}|

7A11.1

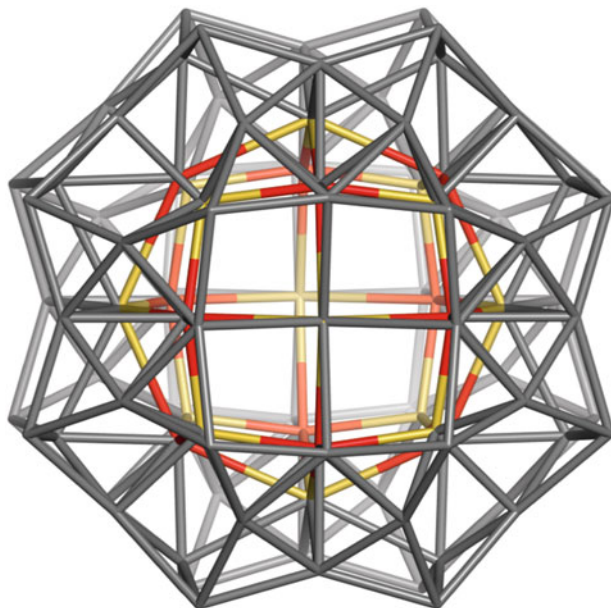
<p>$Rh_{12}@12mP_3.50$ C_{50b}</p>	<p>$d(m(C_{24})84)166X50.222.310$ $C_{50b}.222.310$</p>	<p>$(d(mQ_4)88)X50.222.310$ $C_{50a}.222.310$</p>



$Rh_{12}@12mP_3.50$ (b)

$Rh_{12}@12mP_3;6Py4).50$
 $d(m(C_{24})84)166X.50$
 $C_2 \times S_4$; Order 48;
 Classes 4 {6}; {8}; {12}; {24}|
 7A11.2

<p>$Rh_{24}@24mP_3.98$ C_{50b} co-net</p>	<p>$Rh_{12}@12mP_3.50_3$</p>	<p>$Rh_{12}@12mP_3.50$ C_{50b} net</p>

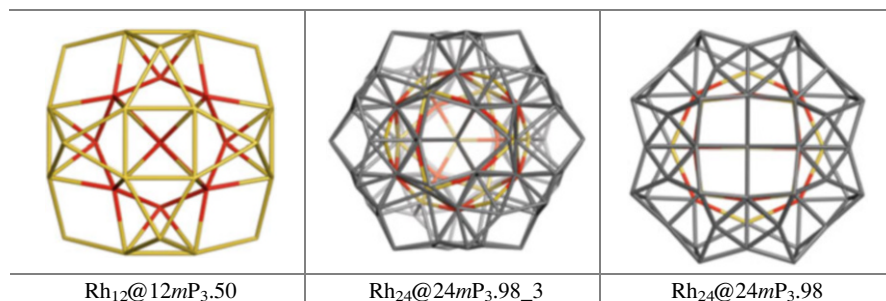


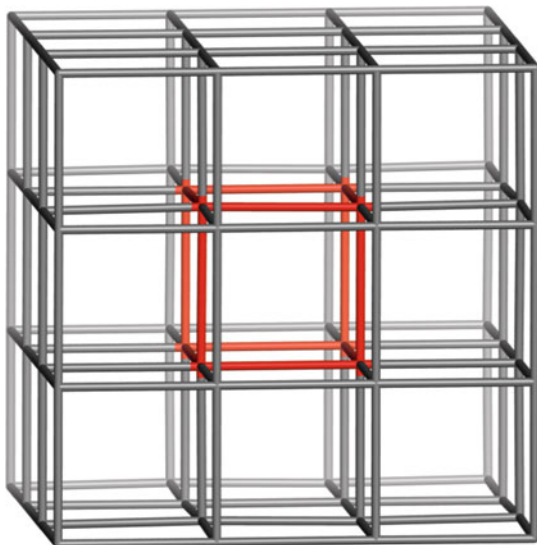
$Rh_{24}@24mP_3.98$

50 Co-net.98

$C_2 \times S_4$; Order: 48

Classes: 6 | {6}; {8}; {12}; 3 {24} |
7A11.3

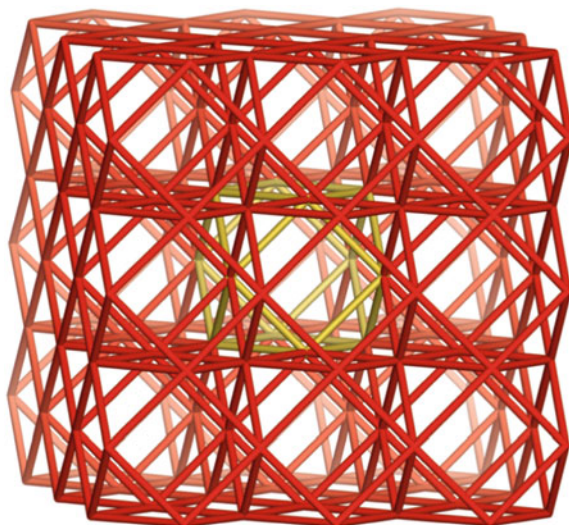




$$pcu = C$$

Space group: $Pm-3m$
 $v = 1$ (vs: 4^{12} ; deg=6)
 $t = 1$; $C@(6C)$
 C.333.64
 7A12

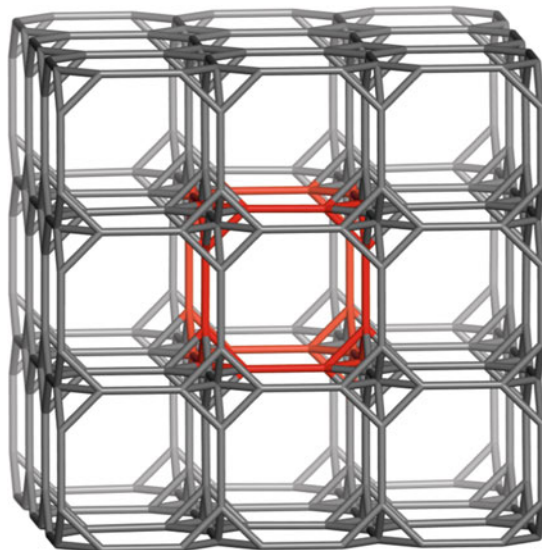
C.8	O.6	C.222.27



$$m(pcu) = reo = MC$$

Space group: $Pm-3m$
 $v = 1$ (vs: $(3^8.4^4)$; deg=8)
 $t = 2$; $CO@(6CO + 8O)$
 $m(pcu) = d(pcu) = d(flu)$
 $m(C.333).144$
 7A12.1

C.222.27	O.6	CO.12



$$t(\text{pcu}) = \text{cab} = \text{TC}$$

Space group: $Pm-3m$

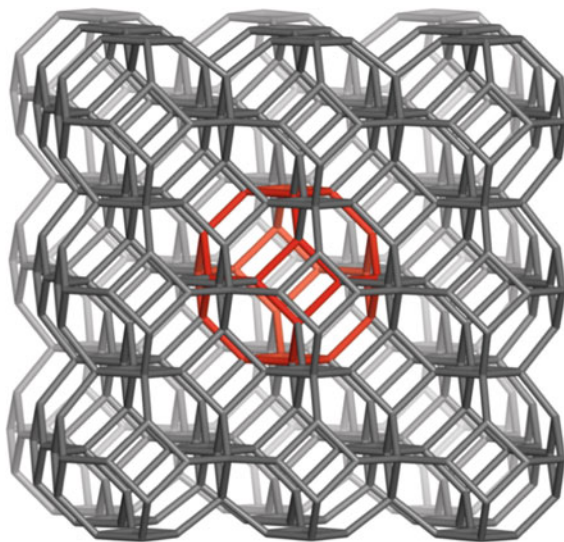
$v = 1$ (vs: $(3^4 \cdot 4^4 \cdot 2 \cdot 8^4)$; deg=5)

$t = 2$; TC@(6TC + 8O)

$t(\text{C}.333).288$

7A12.2

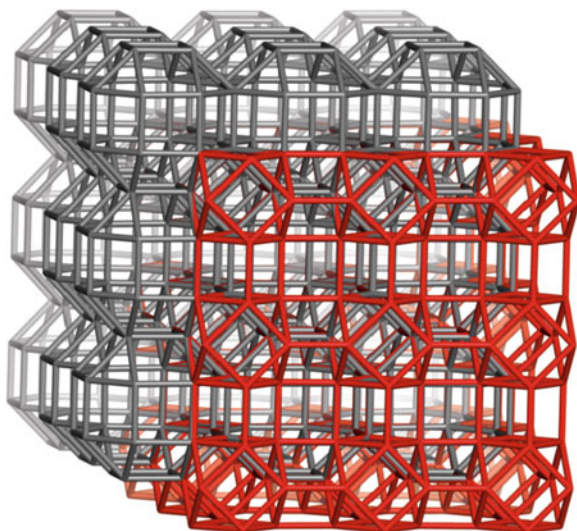
C.222.27	O.6	TC.24



$I(pcu) = sod = TO$

Space group: $Im-3m$
 $v = 1$ (vs: $(4^2.6^4)$; deg=4)
 $t = 1$; $TO@(14TO)$
 $I(C.333).432$
 7A12.3

$I(C.222).144$	O.6	TO.24



$mm(pcu) = reo-e = MMC$

Space group: $Pm-3m$

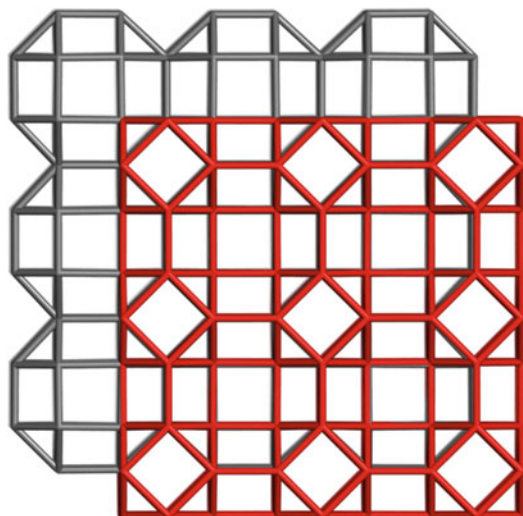
$v = 1$ (vs: $(3^2 \cdot 4^7 \cdot 6^2 \cdot 8^4)$; deg=6)

$t = 3$; RCO@(6RCO + 8CO + 12C)

$m(m(C.333)).432$ net / $m(d(C.333)).324$ co-net

7A12.4

C.8	CO.12	RCO.24= $mmC.24$



$$mm(pcu) = reo-e = MMC$$

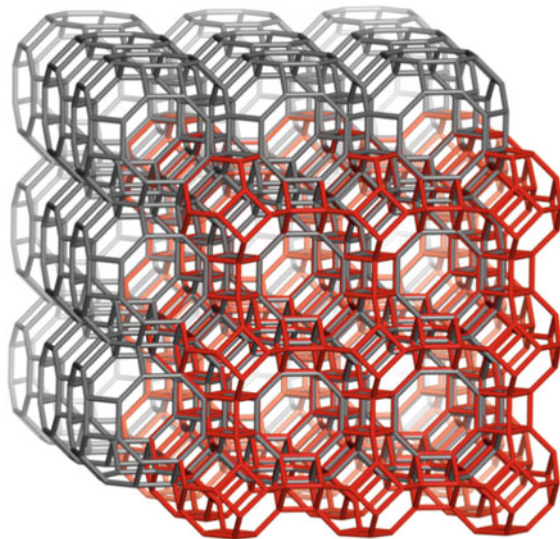
Space group: $Pm-3m$

$v = 1$ (vs: $(3^2 \cdot 4^7 \cdot 6^2 \cdot 8^4)$; $\text{deg}=6$)

$t = 3$; $RCO@(6RCO + 8CO + 12C)$

$m(m(C.333)).432 \text{ net} / m(d(C.333)).324 \text{ co-net}$
 $7A12.5$

RCO.24= $mmC.24$	CO.12	C.8



$$tm(pcu) = lta = TMC$$

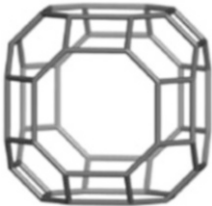
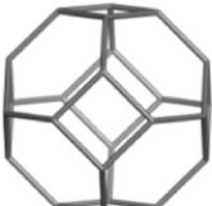

Space group: $Pm-3m$

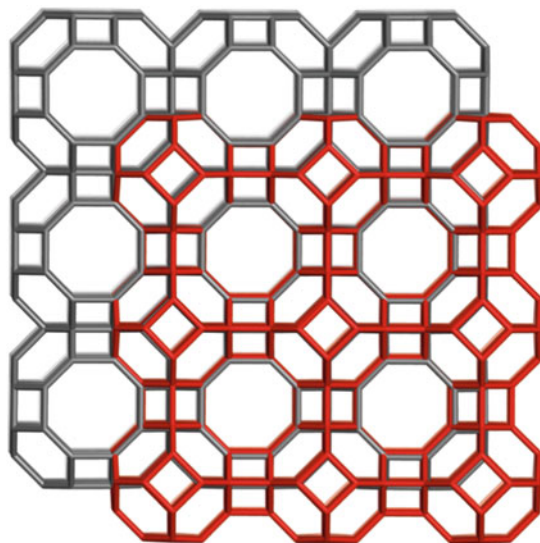
$v = 1$ (vs: $(4^3.6^2.8)$; deg=4)

$t = 3$; TCO@(6TCO + 8TO + 12C)

$t(m(C.333)).864$ net / $t(d(C.333)).648$ co-net

7A12.6

		
TCO.48	TO.24	C.8



$$tm(pcu) = lta = \text{TMC}$$

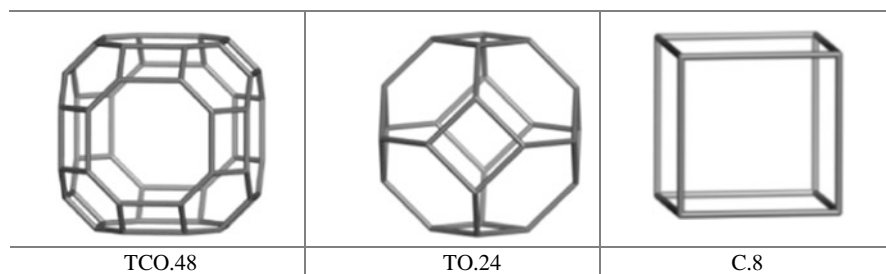
Space group: $Pm-3m$

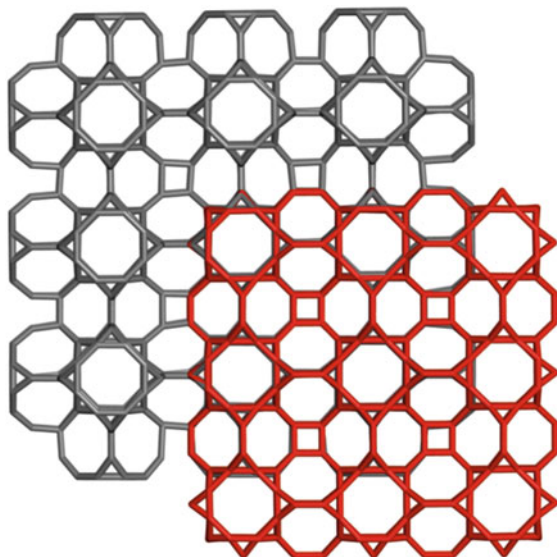
$v = 1$ (vs: $(4^3.6^2.8)$; deg=4)

$t = 3$; $\text{TCO}@(\text{6TCO} + \text{8TO} + \text{12C})$

$t(m(\text{C.333})).864$ net / $t(d(\text{C.333})).648$ co-net

7A12.7





$$l(m(C)) = LMC$$

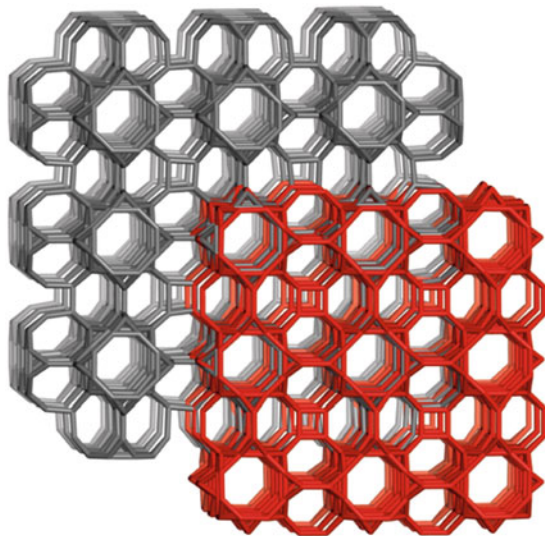
$v = 2$ (vs: $(3^2.8^4)$; deg=4); $(3.4.8^4)$; deg=4))

$t = 2$; DSCO @ (6DSCO + 20TC)

$l(mC333.144).1080$ net / $l(CP333.91).936$ co-net

7A12.8

DSCO= $d(stCO)$.48	TC.24	CP.9



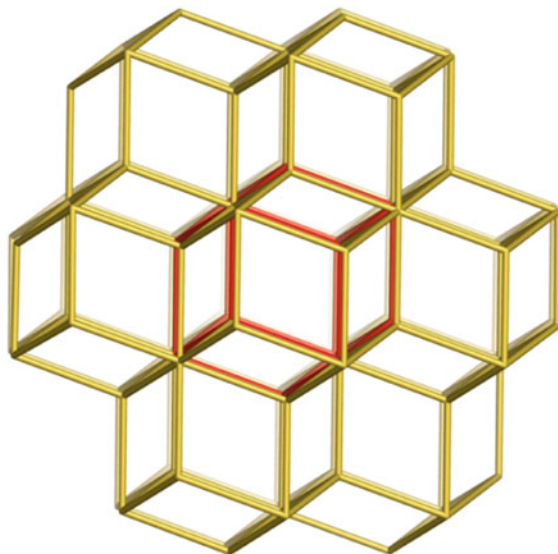
$$l(m(C)) = \text{LMC}$$

$v = 2$ (vs: $(3^2.8^4)$; $\text{deg}=4$); $(3.4.8^4)$; $\text{deg}=4$)

$t = 2$; DSCO @ (6DSCO + 20TC)

$l(mC333.144).1080$ net / $l(CP333.91).936$ co-net
7A12.9

DSCO= $d(stCO)$.48	TC.24	CP.222.35



***flu* = DCO**

Space group: *Fm-3m*

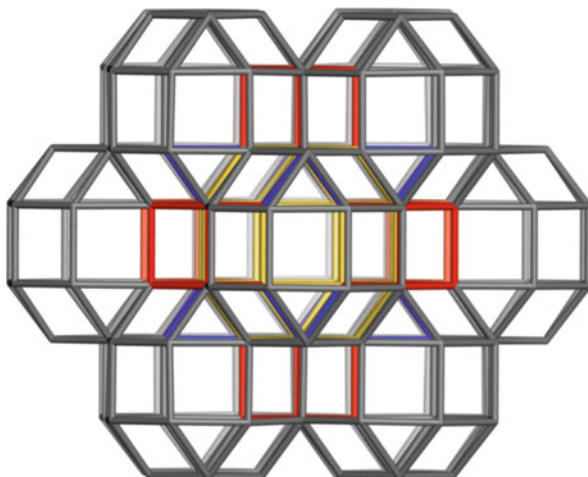
$v = 2$ (vs: $(4^6; \text{deg}=4)$; $(4^{12}; \text{deg}=8)$)

$t = 1$; DCO@(12DCO); DCO = Rh₁₂.14

Rh₁₂@12Rh₁₂.94

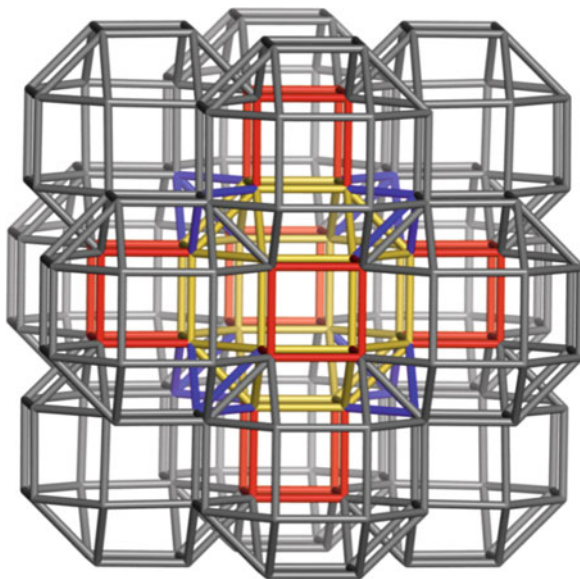
7A13

Rh ₁₂ @12Rh ₁₂ .94	Rh ₁₂ .14 = <i>d</i> (CO).14 [4 ¹²]	<i>l</i> ((Rh ₁₂ @12Rh ₁₂).480



Space group: $Fm-3m$
 $v = 1$ (vs: $(3^4 4^6 8^6)$; $deg=6$)
 $t = 3$; $RCO@(12RCO + 6C + 8T)$
 $m(Rh_{12}.333).504$
 7A13.1

RCO.24= $mmC.24$	C.8	T.4



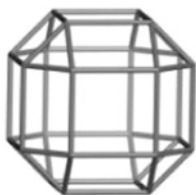
Space group: $Fm-3m$

$v = 1$ (vs: $(3^3 \cdot 4^6 \cdot 8^6)$; deg=6)

$t = 3$; RCO@(12RCO + 6C + 8T)

$m(Rh_{12}.333).504$

7A13.2



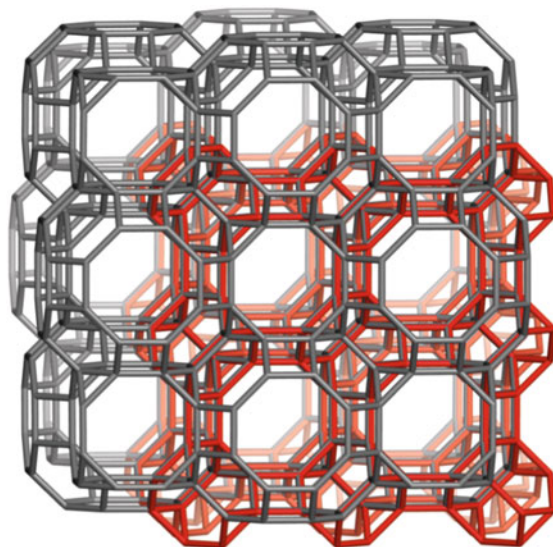
RCO.24 = $mmC.24$



C.8



T.4



Space group: $Fm-3m$

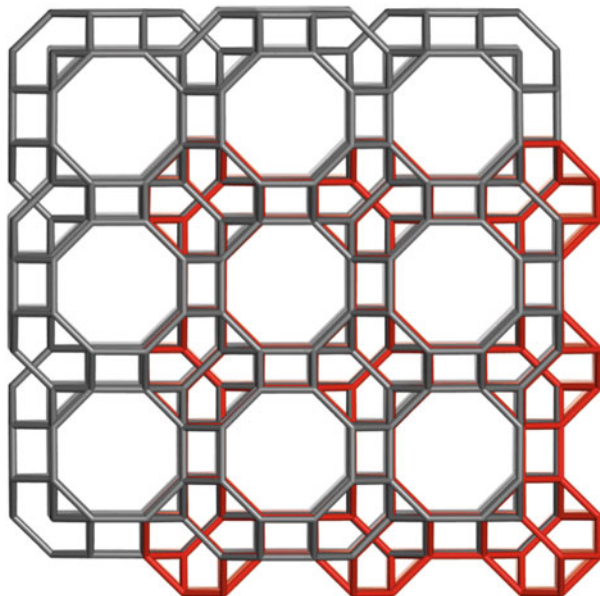
$\nu=1$ (vs: $(3.4.6^2.8^2)$; deg=4)

$t=3$; TCO @ (12TCO + 6TC + 8TT)

$I(Rh_{12}).333.528$ net / $I(Rh_{12}).333.324$ co-net

7A13.3

<p>$Rh_{12}.14 = p_4(T).14$ $d(mC).14 = d(CO).14$</p>	<p>TCO.48</p>	<p>$I((DCO).333.324$ co-net</p>



$I\text{Rh}_{12} = \text{hal} = \text{LDCO}$

Space group: $Fm-3m$

$v=1$ (vs: $(3.4.6^2.8^2)$; $\text{deg}=4$)

$t=3$; TCO @ (12TCO + 6TC + 8TT)

$I(\text{Rh}_{12}).333.528$ net / $I(\text{Rh}_{12}).333.324$ co-net

7A13.4

TCO.48 [$4^2.12.6^8.8^6$]	TC.24 [$3^8.8^6$]	TT.12 [$3^4.6^4$]

References

- Coxeter HSM (1973) *Regular polytopes*, 3rd edn. Dover, New York
- Diudea MV (2013) Quasicrystals: between spongy and full space filling. In: Diudea MV, Nagy CL (eds) *Diamond and related nanostructures*. Springer, Dordrecht, pp 335–385
- Diudea MV, Ursu O (2003) Layer matrices and distance property descriptors. *Indian J Chem A42* (6):1283–1294
- Gardner M (1984) *The sixth book of mathematical games from scientific American*. University of Chicago Press, Chicago
- Goldberg M (1979) Convex polyhedral space-fillers of more than twelve faces. *Geom Dedicata* 8:491–500
- Grünbaum B, Shephard GC (1980) Tilings with congruent tiles. *Bull Am Math Soc* 3:951–973
- Johnson NW (1966) Convex solids with regular faces. *Can J Math* 18:169–200
- Nagy CL, Diudea MV (2009) Nano studio software program. Babes-Bolyai University, Cluj
- Papacostea C (1930–1935) *Platon. Opere*, 1–11 (Roum. translation), Casa Școalelor, București
- Parvan-Moldovan A, Diudea MV (2015) Cell@cell higher dimensional structures. *Stud Univ Babes-Bolyai Chem* 60(2):379–388
- Schulte E (2014) Polyhedra, complexes, nets and symmetry. *Acta Cryst A70*:203–216
- Steinhaus H (1999) *Mathematical snapshots*, 3rd edn. Dover, New York
- Taylor AE (1928) *A commentary on Plato's Timaeus*. Clarendon, Oxford

Chapter 8

Tetrahedral Clusters

Tetrahedron, the first Platonic solid, has been used as a symbol for the fire, in the ancient Greece, as Platon noted in its *Timaeus* dialogue (Papacostea 1930–1935; Taylor 1928); the remaining Platonics have been associated to: icosahedron—water; octahedron—air, cube—earth and dodecahedron—ether (or the cosmos). The regular tetrahedron (i.e., the Platonic solid) has its four faces regular triangles, three of which meeting in each vertex. Tetrahedron is self-dual; recall that within chapter (also within the whole book) we refer to shapes (with the disregard of angles and bond length—Schulte 2014) rather than to regular polyhedra.

Higher dimensional analogues are called simplex/simplices (see Chap. 3).

8.1 Small Tetrahedral Clusters

Small tetrahedral clusters, on which this chapter is focused, include the P-centered cluster TP.5 (Sect. 3.4) and two “cell-in-cell” clusters: T@O.10 and T@TT.16, as illustrated in Fig. 8.1 and detailed in the Atlas of this chapter. These small clusters were used as inputs for map operations in developing more complex, multi-shell clusters. Some clusters, derived from TP.5 by medial (8A1.1; 8A1.1.2), or truncation (8A1.1.3; 8A1.2) operations, are self-centered graphs, i.e., all the vertices form a single orbit, being the multi-center of graph; they belong to the symmetry group S_5 , of order 120. Self-centered graphs have extensively been studied (Buckely 1979, 1989; Janakiraman and Ramanujan 1992; Negami and Xu 1986; Nazeer et al. 2016).

Figure count in small tetrahedral clusters is given in Table 8.1.

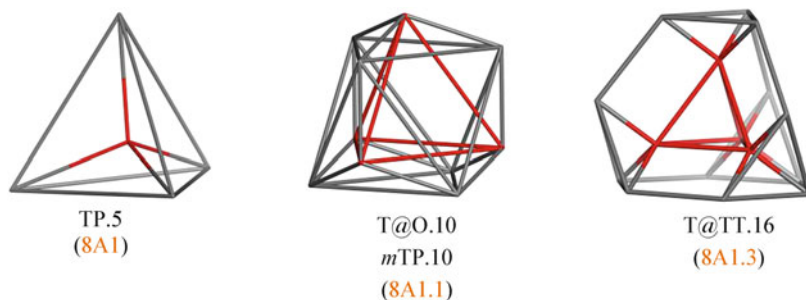


Fig. 8.1 Small tetrahedral clusters

8.2 Tetrahedral Clusters of Higher Rank

As described in Sect. 5.4, complex clusters can be decomposed in components of rank higher than 3; the simplest case is when two components, $M_1@M_2$, can be defined, of rank $k = 4$ and with a common/shared facet, of rank $k = 3$. It follows that the parent cluster is bonded by two 4-facets while such a cluster is a 5-polytope (Coxeter 1973; Schulte 2014).

Structures of rank 5 ($C_{22}@C_{26}.30$ (8A1.1.1) and t TP.20 (8A1.2)) and their substructures are listed in Tables 8.2 (#1 and #4, respectively) and detailed in the Atlas. Equivalence classes for the vertices of the studied clusters were calculated by Nano Studio software program (Nagy and Diudea 2009) and confirmed by Mathematica (Wolfram 2016).

8.3 Tetrahedral Clusters Derived From Ada20

The so-called “diamond D_5 ” (Diudea 2010; Diudea and Nagy 2012; Szefer and Diudea 2012; Nagy and Diudea 2013) is a complex hyper-structure, based on adamantane-like “Ada” and diamantane-like “Dia” substructures; these both can be identified in the zeolite MTN-type (or ZSM-39—see First et al. 2011; Karttunen et al. 2011) and may be designed either starting from C_{20} or from C_{28} . Within this section, the structures originate in C_{20} , that’s why the name “Ada20”; more details the reader will find in Chap. 12.

Ada20 (8A2) is a hyper-tetrahedron, a tetrahedron of which points were changed by four tetrahedral units $P@4C_{20}$ (where P is the shared/common point) and joined by a pentagonal face; the central hollow has exactly the topology of small fullerene C_{28} . Thus its name in the Atlas: TY(4(P@ C_{20}); f_5).198 (8A2) reflects the state of hyper-structure (TY—built on the tetrahedron topology) and the main features

Table 8.1 Figure count in tetrahedral clusters

Cluster	v	e	3(2)	4/8*(2)	6(2)	2	1(3)	2(3)	3(3)	4(3)	M	3	χ	k	$n(3);(M)$
1	5	10	10	0	0	10	4	0	0	0	1	5	0	4	T(1;T)
2	10	30	30	0	0	30	4	4	0	0	2	10	0	4	T;O;(T;O)
3	16	36	20	6	4	30	4	4	0	0	2	10	0	4	T;hCO;(T;TT)
4	20	40	20	0	10	30	4	4	0	0	2	10	0	4	T;TT;(T;TT)
5	36	108	76	18	4	98	12	4	4	4	2	26	0	4	T;O;P ₃ ;hmCO ₂ (O;mTT)
6	60	120	20	30	30	80	4	4	10	0	2	20	0	4	TT;TO;P ₃ ;(P ₃ ;M)
7	90	180	60	30*	20	110	4	4	10	0	2	20	0	4	TT;TC;TP ₃ (TT;TC)

1 = TP.5 (8A1); 2 = mTP.10 (8A1.1); 3 = T@TT.16 (8A1.3); 4 = tTP.20 (8A1.2); 5 = m(T@TT)16.36 (8A1.3.1); 6 = t(mTP).60 (8A1.1.3); 7 = l(mTP).90 (8A1.1.4)

Table 8.2 Figure count in tetrahedral clusters of rank $k = 5$

Cluster	v	e	3(2)	4(2)	6(2)	2	$c_1(3)$	$c_2(3)$	$c_3(3)$	M	3	4	χ	k	$c_n(M);(4)$
1	30	90	50	30	0	80	4	4	10	2	20	2	2	5	T;C; mP_3 (T;C);(C ₂₂ ;C ₂₆)
2	22	54	26	12	4	42	0	4	4	2	10	0	0	4	hC ; mP_3 (T; mTT)
3	26	72	40	18	4	62	4	4	6	2	16	0	0	4	T; hC ; mP_3 (C; mTT)
4	30	90	50	30	0	80	4	4	10	2	20	2	2	5	CO;O; P_3 (O;CO);(C ₁₈ ;C ₂₄)
5	18	42	18	12	4	34	0	4	4	2	10	0	0	4	hCO ; P_3 (O;TT)
6	24	66	36	18	4	58	4	4	6	2	16	0	0	4	O; $6P_3$ (CO;TT)

1 = C₂@C₂₆30 (8A1.1.1); 2 = T@(4mP₃;4hC)@(mTT).22 (8A1.1.1b); 3 = C@(4T;4hC;6mP₃)@(mTT).26 (8A1.1.1b); 4 = C₁₈@C₂₄30 (8A1.1.2);

5 = O@(4P₃;4hCO)@TT.18 (8A1.1.2b); 6 = TT@(4O;4hCO;6P₃)@CO.24 (8A1.1.2b)

(substructure $(P@C_{20})$, counted $4\times$, and the joining manner f_5); the number suffixing the name counts the all points/atoms in a structure.

By performing the dual operation on Ada20 one obtains the spongy structure d (Ada20).162sp (8A2.1). The icosahedral shapes are joined sharing an octahedral shape $O@4I$ while two such units share a point P located on the edges of a tetrahedron; this cluster has a “spongy” structure, as counted in Table 8.3 (entry 7). The same spongy can be seen for Ada20 (8A2) if neglect (i.e., consider “empty”) the core (Table 8.3, entry 6sp); the genus g equals here half of the number of window faces of the tetrahedron.

Other operations (medial m , truncation t and leapfrog l) were applied to Ada20 (8A2) or to its dual, the resulting clusters being detailed in the Atlas; spongy structures were obtained by cutting off the core of filled structures. Note that truncation and leapfrog operation provide tetrahedral hyper-structures decorated by C_{60} fullerene (Figs. 8A2.1.1; 8A2.1.2; 8A2.4; 8A2.5; 8A2.6 and 8A2.7) arranged in tetrahedral substructures, often including some “bonding” cells, with the shape of pentagonal prisms P_5 , octahedron, tetrahedron and their truncates; we consider such clusters as candidates to the C_{60} aggregation (see Chap. 12).

8.4 Tetrahedral Hyper-structures Decorated with Only Dodecahedra

As mentioned within this book (Sects. 6.3, 7.4 and 9.3), structures decorated with dodecahedral shapes D (i.e., C_{20}) can be designed by the following sequence of operations (Diudea 2013): $t_{sel}(p_4(P))$; $s_2(P)$; $t_{sel}(p_4(P))@s_2(P)$, where t_{sel} stands for the selected vertices truncation while the “endo” symbol $@$ means “inside”. Formally, every point in the parent polyhedron P was changed by a C_{20} cell; the resulted structure $PY(nC_{20})$ is a “hyper” and “spongy” structure, with the central hollow of exact topology of $t_{sel}(p_4(P))$. If this hollow is filled, by connecting inside the parent P , a double-shell cluster will result, which is no more a spongy structure. In case $P = T$, the corresponding structures are shown in Figs. 8A4; 8A4.1; 8A4.2 and 8A5 while the figure count is given in Table 8.4 (details and explanations were given in Sect. 6.3).

Structures TY(4D).50 (8A4) and T@TY(4D).54 (8A5) have been derived by map operations, as illustrated in the Atlas of this chapter (Figs. 8A4.2.1 to 8A4.2.3 and 8A5.1). Design of higher rank and genusmulti-shell clusters was performed at TOPO GROUP CLUJ by the original CVNET (Stefu and Diudea 2005) and Nano Studio (Nagy and Diudea 2009) software programs.

Table 8.3 Figure count in C_{60} and C_{20} tetrahedral hyper-clusters derived from Ada20

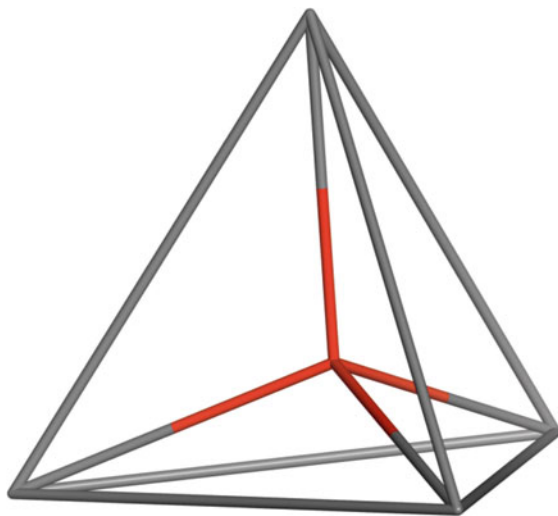
Cluster	v	e	3(2)	4(2)	5(2)	6(2)	2	U	TO/TT*	$P_5(+P_6)$	M	3	χ	g
1	1212	2136	0	318	204	510	1032	16	44	42(+4)	2	108	0	0
2	960	1590	0	150	192	336	678	16	4	30	0	50	-2	2
3	834	1440	118	0	162	388	668	16	44*	0	2	62	0	0
3 $_{sp}$	810	1290	16	0	162	320	498	16	4*	0	0	22	-2	2
4	654	1116	82	0	126	300	508	12	32*	0	2	46	0	0
5+	630	1014	28	0	126	248	402	12	8*	0	0	22	-2	2
5 $_{sp}$	630	990	4	0	126	240	370	12	0	0	0	12	-2	2
6	198	346	0	0	162	4	166	16	0	0	2	18	0	0
6 $_{sp}$	198	346	0	0	162	0	162	16	0	0	0	16	-2	2
7	162	480	336	0	0	0	336	16	4	0	0	20	-2	2

1 = $r(d(\text{Ada}20.198)162)1212$ (8A2.1.1); 2 = $(16C_{60};4TO;30P_3)960_{sp}$ (8A2.1.2); 3 = $l(\text{Ada}.198)834$ (8A2.4); 3 $_{sp}$ = $l(\text{Ada}20.198)834X.810_{sp}$ (8A2.5);
4 = $C_{84}@(12C_{60};4TT).654$ (8A2.6); 5+ = $TTY(4C_{165};f_5).630$ (8A2.7); 5+ counts double TT at corners; 5 $_{sp}$ = $TTY(4(3C_{60});f_5).630_{sp}$ (8A2.7); 6 = $TY(4(P@4C_{20});f_5).198$ (8A2); 6 $_{sp}$ = $\text{Ada}20.198_{sp}$ (8A2); 7 = $TY(4(O@4I);P).162_{sp}$ (8A2.1)

Table 8.4 Figure count in C_{20} tetrahedral hyper-clusters


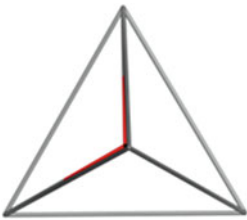

Structure	v	e	$5(2)$	$w(s)$	2	$U(3)$	M	3	χ	$k(g)$
TY(4D) (8A4)	50	90	42	4(3)	46	4	2	6	0	4(0)
TY(4D) _{spa}	50	90	42	4(3)	42	4	0	4	-2	4(2)
TY(4D) _{spb}	50	90	36	4(3)	36	0	0	0	-4	3(3)
T@TY(4D) (8A5)	54	100	48	8(3)	56	8	2	10	0	4(0)

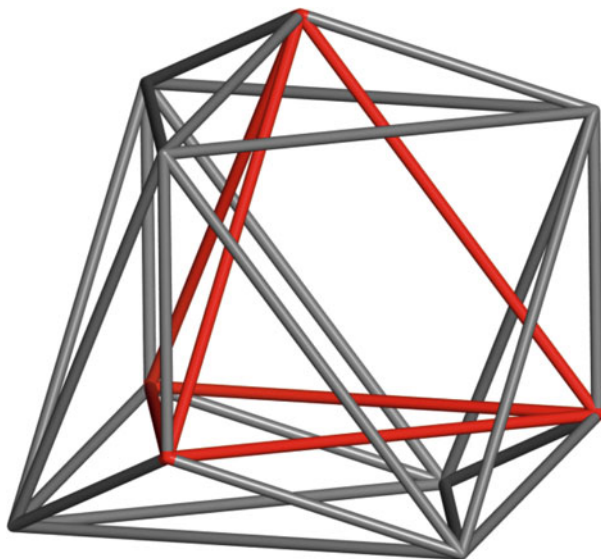
Chapter 8 Atlas: Tetrahedral Clusters



TY(4T; f_3).5

P@T.5
P@4T@T.5
TP.5
 S_5 classes 1:|{5}|
8A1

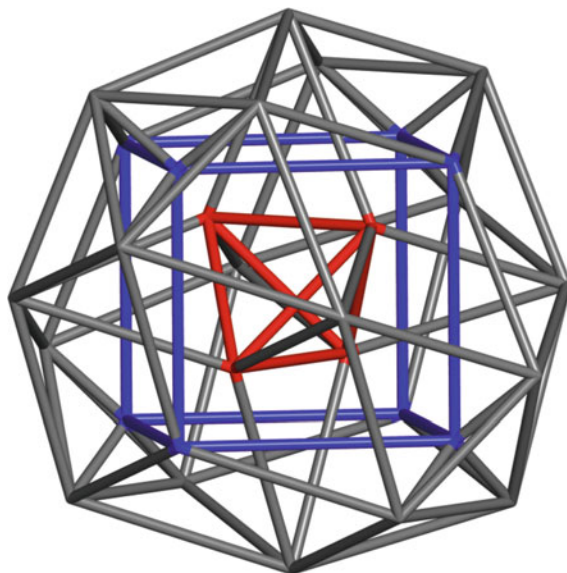
		
P@T.5_2	P@T.5_3	T.4



TY(4T;P).10
TY(4O; f_3).10

T@O.10
 T@(4T;4O)@O.10
 $mTP.10$
 S₅ classes 1:|{10}|
 8A1.1

T.4	O.6	$mTP.10=T@O.10$



$C_{22}@C_{26}\cdot 30$

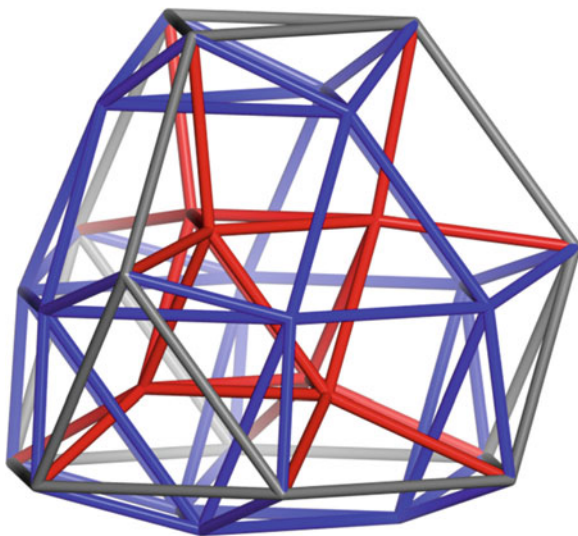
$d(T@O).30$

$d(mTP).30$

S_5 classes 2: $\{10\}; \{20\}$

8A1.1.1

<p>$T@(4mP_3;4hC@(mTT).22$</p>	<p>$C@(4T;4hC;6mP_3@(mTT).26$</p>	<p>$T@O.10=mTP.10$</p>



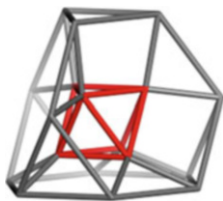
$C_{18}@C_{24}.30$

$m(T@O).30$

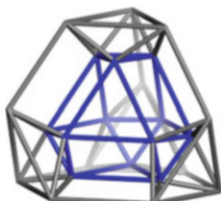
$m(mTP).30$

S_5 classes 1:|{30}|

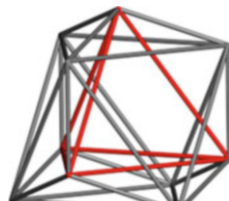
8A1.1.2



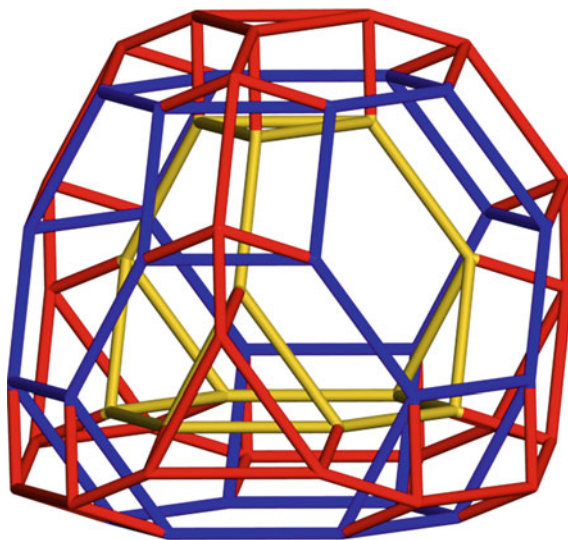
$O@(4P_3;4hCO)@TT.18$



$TT@(4O;4hCO;6P_3)@CO.24$



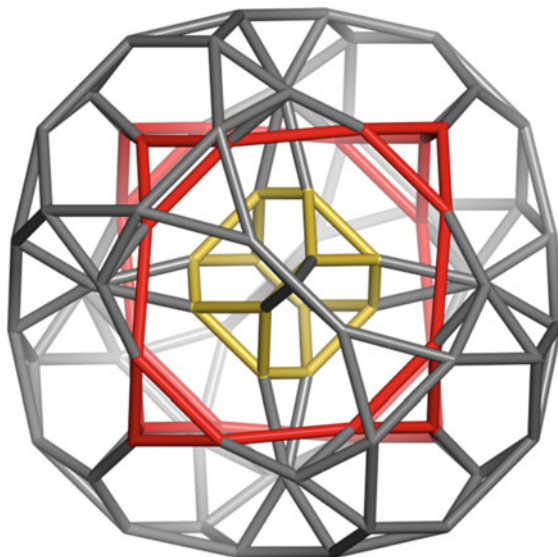
$T@4O@O.10=mTP.10$



TT@(4P₃;4TT)@(6P₃;4TO)@TO.60

t(mTP).60
 S₅ classes 1:|{60}|
 8A1.1.3

Tr(T)=TT_12	Tr(Oct)=TO_24	P ₃ @(3TO;2TO;5TT;9P ₃).60

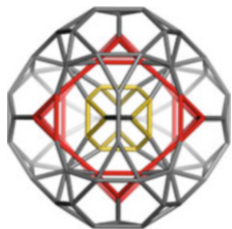


TT@(4TC;4TP₃)@(4TT;6TP₃)TC.90

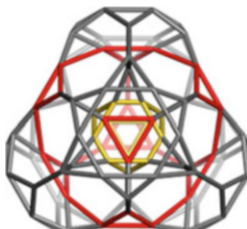
I(mTP).90

S₅ classes: 2 |{30};{60}|

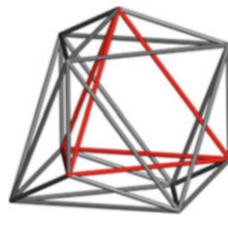
8A1.1.4



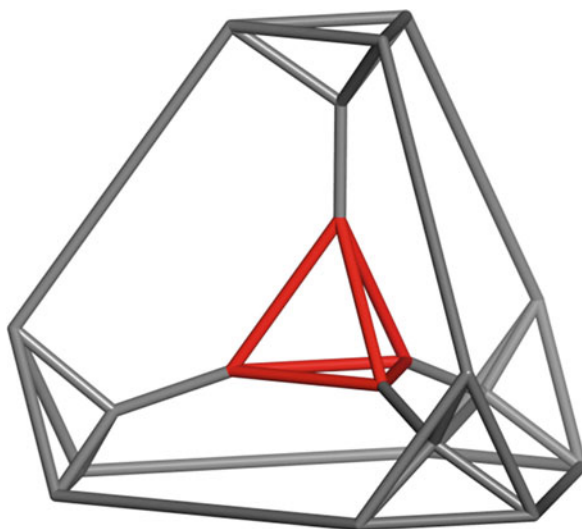
I(T@4O@O).90_2



I(T@4O@O).90_3



T@4O@O.10=mTP.10



TY(4TT; f_6).20

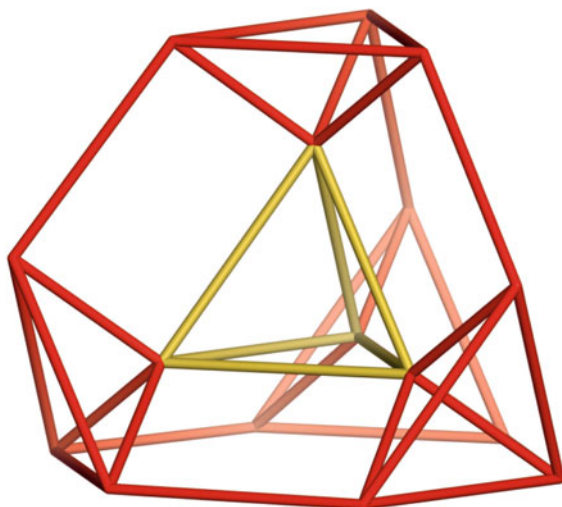
T@(4TT;4T)@TT.20

f TP.20

S₅ classes 1:|{20}|

8A1.2

T.4	TT.12	f TP.20_3



TY(4hTO; f_4).16

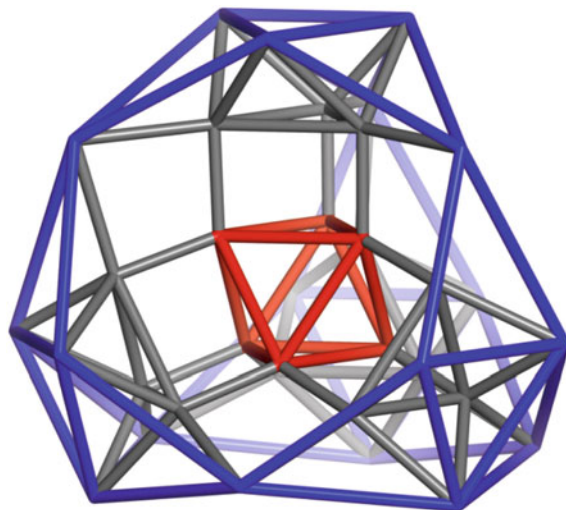
T@(4T;4hTO)@TT.16

T@TT.16

S₄ classes 5:|{4};4{12}|

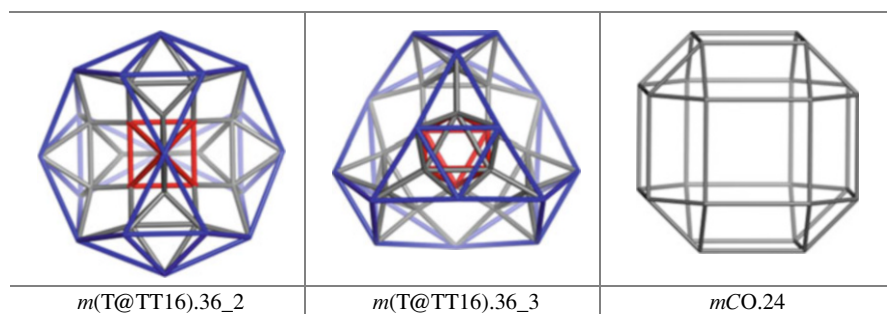
8A1.3

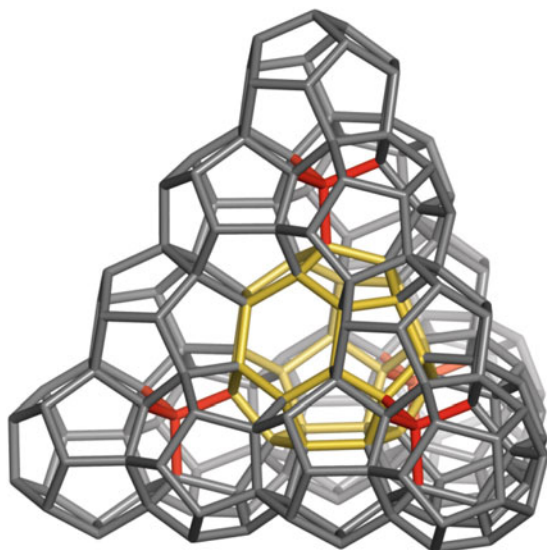
T.4	TT.12	T@TT.16_3



$O@(4P_3;4hmCO;4O;4(3T))@mT.36$

$m(T@TT16).36$
 S_4 classes: $4 [2\{6\};2\{12\}]$
 $8A1.3.1$





TY(4(P@4C₂₀);f₅).198

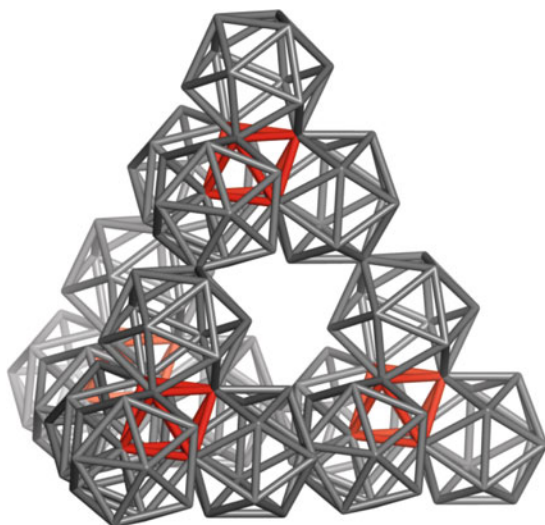
C₂₈@4(P@4C₂₀).198

Ada20.198

S₄ classes: 15 |3{4};{6};7{12};4{24}|

8A2

T.4	C ₂₀ (I _h)	C ₂₈ (T _d)

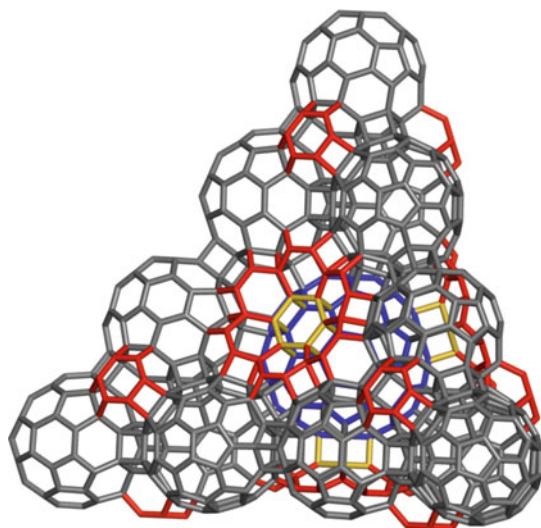


TY(4(O@4I);P).198

d(Ada20.198).162sp

S_4 classes: 39 |2{4};17{12};20{24}|
8A2.1

I.12	Ada20.198	<i>d(Ada20.198).162</i>



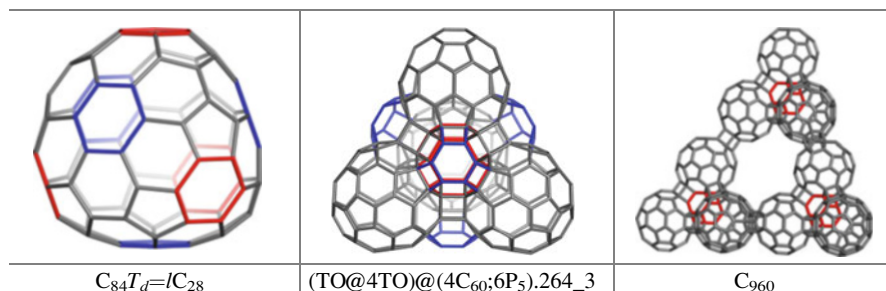
$C_{84}@ (4C_{264}; 24TO).1212$

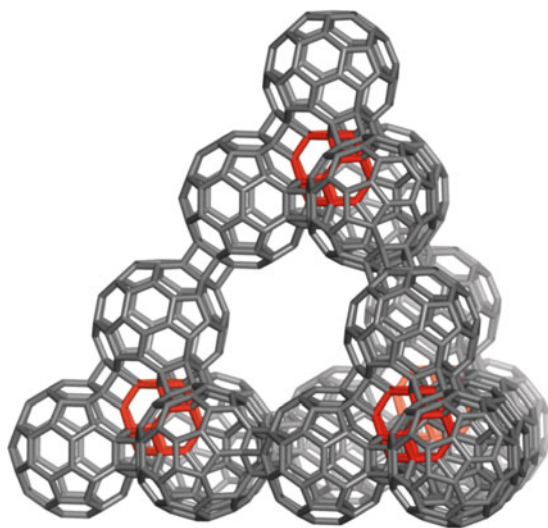
$C_{84}@ (16C_{60}; 44TO; 42P_5, 4P_6).1212$

$t(d(Ada20.198)162).1212$

S_4 classes: $55 | 9 \{12\}; 46 \{24\} |$

8A2.1.1





TY(4C₂₄₀;P₅).960

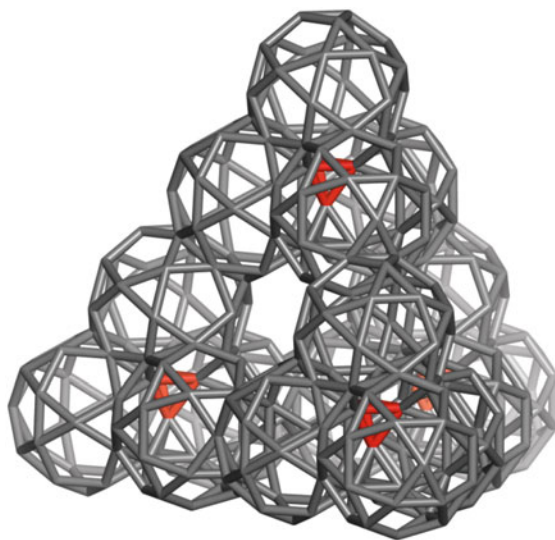
(16C₆₀;4TO;30P₅).960

C₁₂₁₂X.960

S₄ classes: 44 |8{12};36{24}|

8A2.1.2

TO@(4C ₆₀ ;6P ₅).240_3	(TO@4TO)@(4C ₆₀ ;6P ₅).264_3	C ₁₂₁₂

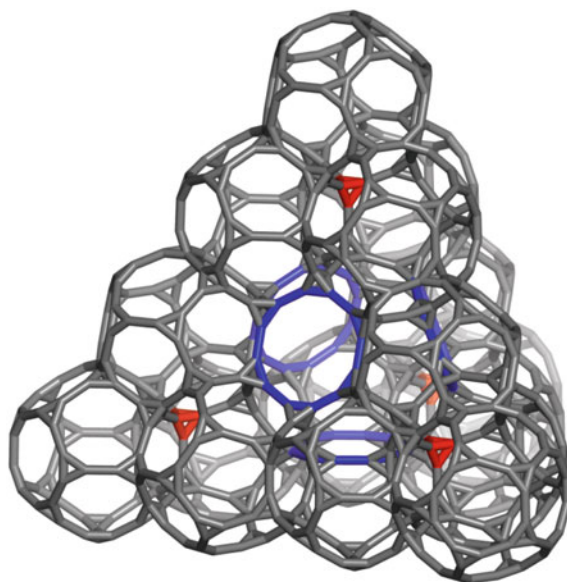


TY(4(T@4ID);f₅).346

m(Ada20).346

S₄ classes: 21 |{4};{6};10{12};9{24}|
8A2.2

T.4	ID.30	Ada20.198



$TY(4(T@4tC_{20});f_{10}).692$

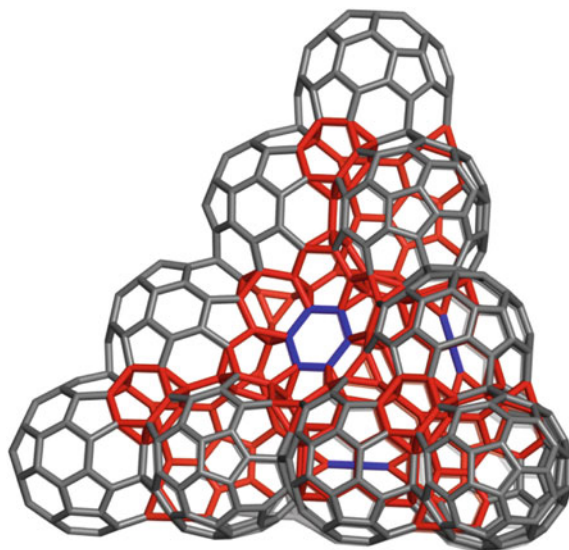
$t(C_{28})@4(T@4tC_{20}).692$

$t(Ada20).692$

S_4 classes: 39 | 2{4}; 17{12}; 20{24}|

8A2.3

<p>$t(C_{20})$</p>	<p>$t(C_{28})$</p>	<p>Ada20.198</p>



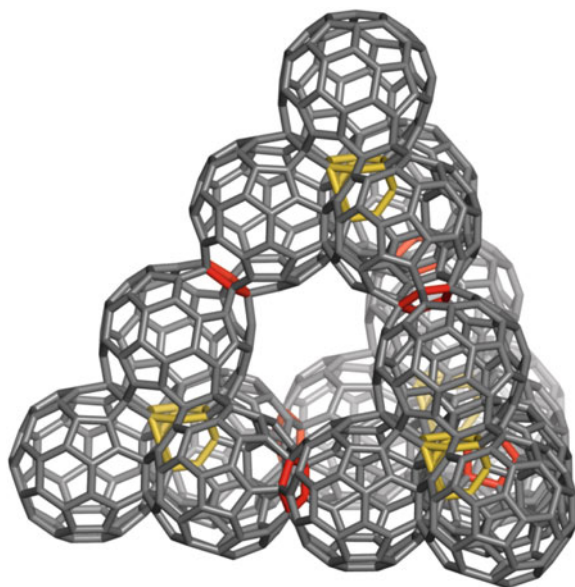
$C_{84}@ (4C_{210}; 24TT).834$

$C_{84}@ (16C_{60}; 44TT).834$

$I(Ada.198).834$

S_4 classes: $42 | \{6\}; 13 | \{12\}; 28 | \{24\} |$
8A2.4

$C_{84}T_d=IC_{28}$	$(TT@4TT)@(4C_{60}).210$	C_{810}

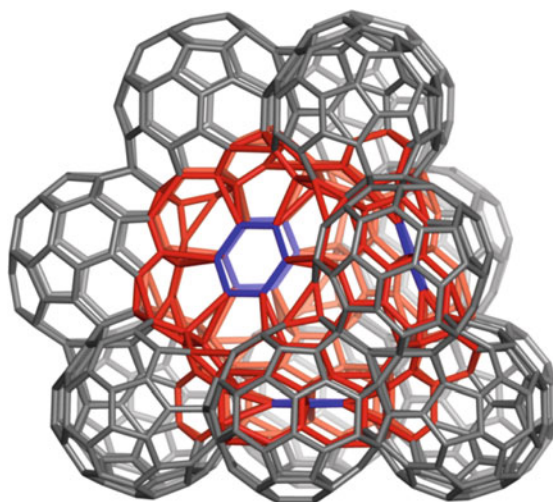


TY(4(TT@4C₆₀);f₅).810_{sp}

/(Ada20.198)834X.810_{sp}

S₄ classes 41: |{6};13{12};27{24}|
8A2.5

Ada20.198	(TT@4TT)@(4C ₆₀).210	C ₈₃₄

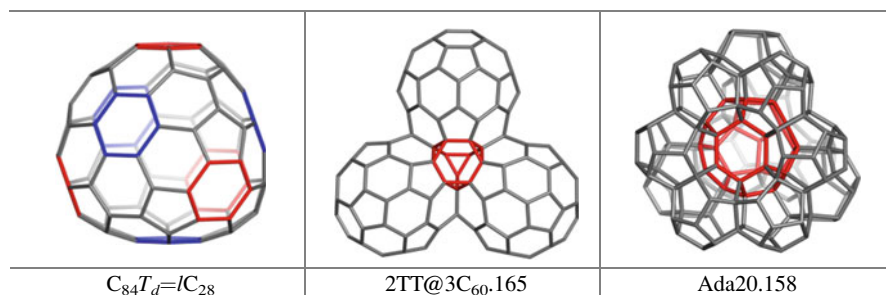


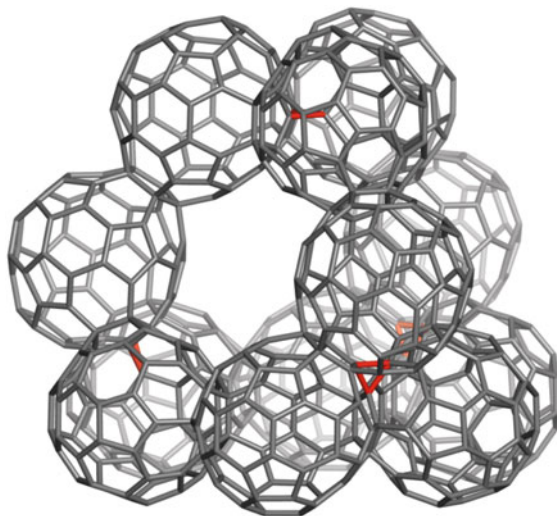
$C_{84}@(4C_{165};24TT).654$

$C_{84}@(12C_{60};4TT).654$

$I(Ada20.158).654$

S_4 classes: $33 \{ \{6\}; 10 \{12\}; 22 \{24\} |$
 $8A2.6$





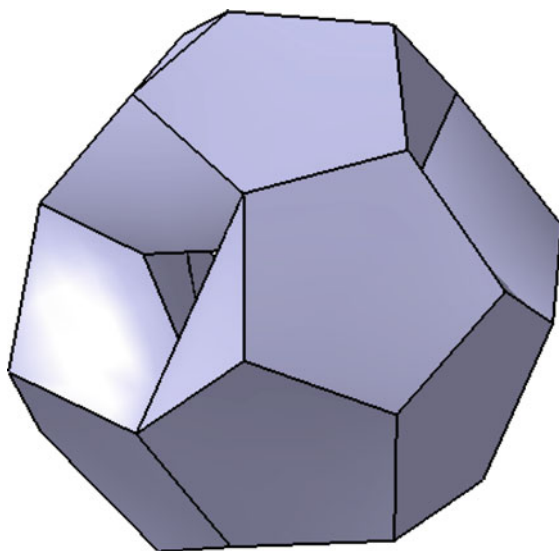
TTY(4(3C₆₀);f₅).630_{sp}

C₆₅₄X.630_{sp}

S₄ classes: 32 |{6};10{12};21{24}|

8A2.7

2TT@3C ₆₀ .165	TTY(4C ₁₆₅);f ₅).630	C ₆₅₄



TY(4D; f_5).50

$t_{sel}(p_4T)@4D.50$

$t_{sel}(p_4T)@s_2T.50$

S_4 classes: 6 | 2 {4}; {6}; 3 {12} |

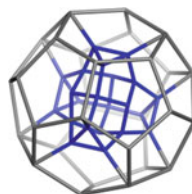
8A4



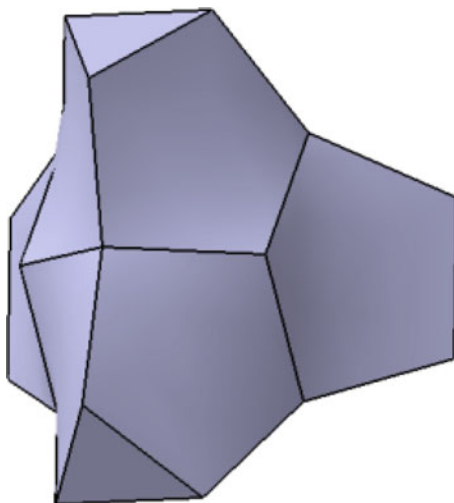
$t_{sel}(p_4T).22$



$s_2T.28$



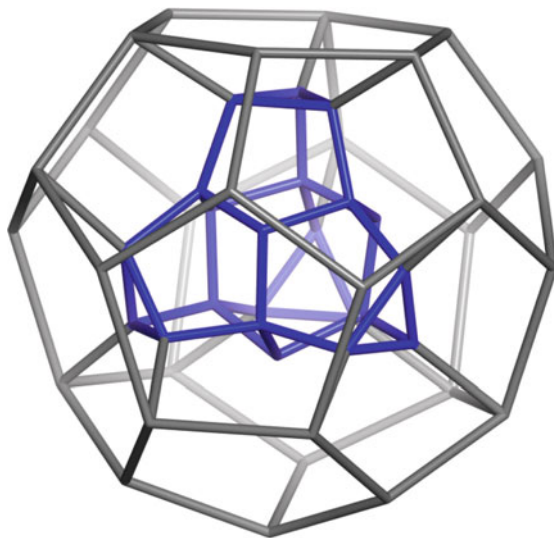
$t_{sel}(p_4T)@s_2T.50$



$t_{sel}(p_4T).22$



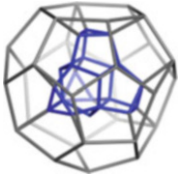
S_4 classes 3: $\{4\};\{6\};\{12\}$
8A4.1

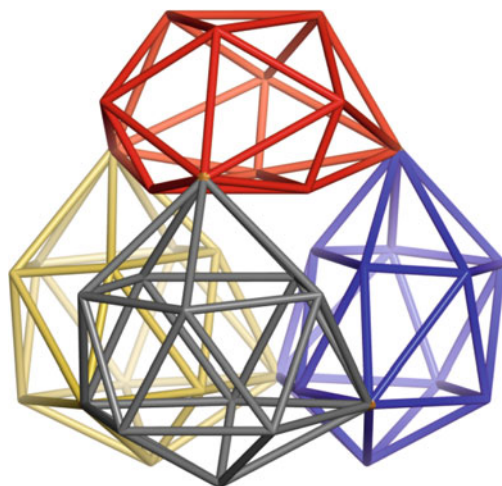
D.20	$t_{sel}(p_4T).22$	$t_{sel}(p_4T)@s_2T.50$



TY(4D; f_5).50

$t_{sel}(p_4(T))@s_2(T).50$
 S_4 classes: 6 | 2 {4}; {6}; 3 {12} |
 8A4.2

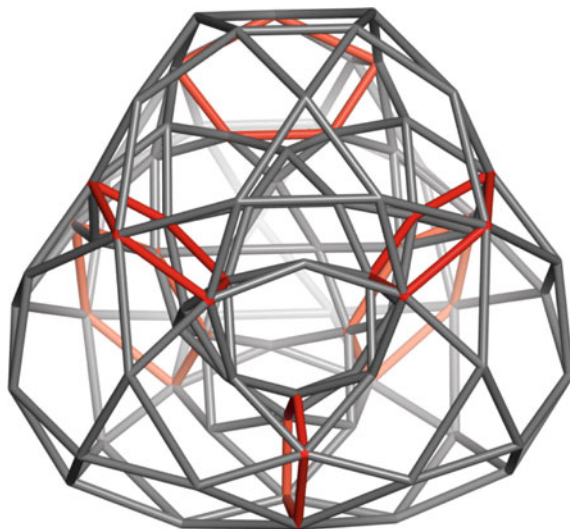
		
C _{50_2}	C _{50_3}	C _{50_4}



TY(4I;P).42

$d(C_{50}).42$
 S_4 classes: $7 \{6\}; 4 \{12\}; 2 \{24\}$
 8A4.2.1

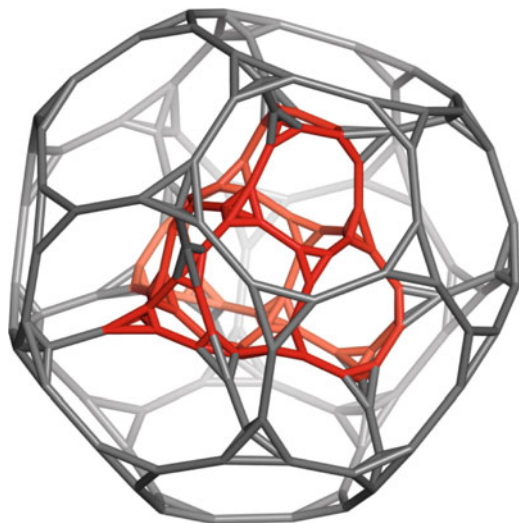
<p>$d(C_{50}).42_2$</p>	<p>$d(C_{50}).42_3$</p>	<p>$d(C_{50}).42_4$</p>



TY(4ID; f_3).90

$op(mC_{22})@4ID.90sp$
 $m(C_{50}).90$
 S_4 classes: 7 | {6}; 5 | {12}; {24} |
 8A4.2.2

<p>$m(C_{50}).90_2$</p>	<p>$m(C_{50}).90_3$</p>	<p>$m(C_{22}).36$</p>



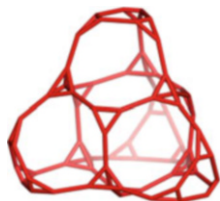
TY($4tD$; f_{10}).180

$t(C_{22})@4tD.180$

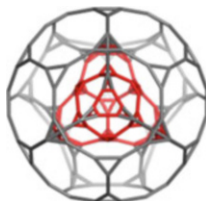
$t(C_{50}).180$

S_4 classes: 12 |9{12};3{24}|

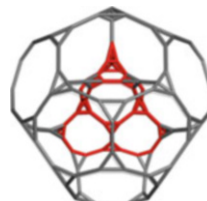
8A4.2.3



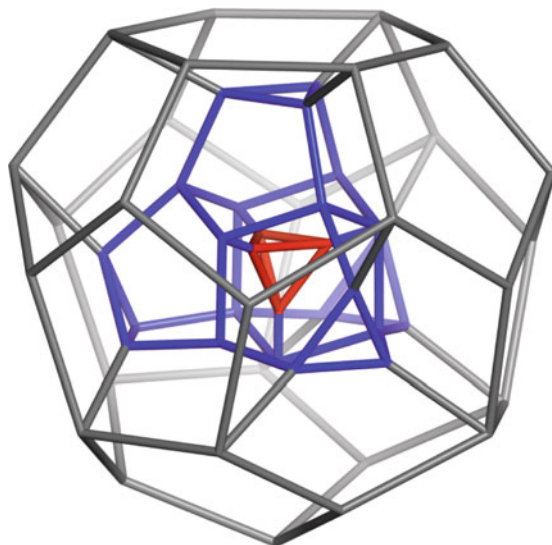
$t(C_{22}).72$



$t(C_{50}).180_3$



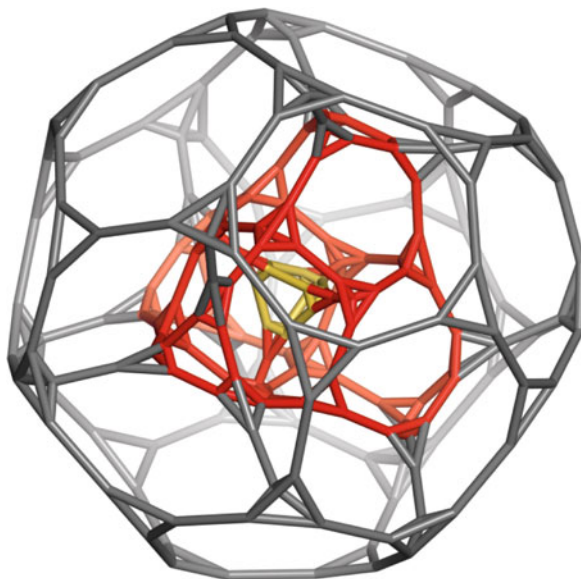
$t(C_{50}).180_4$



$T@4C_{12}@4D.54$

S_4 classes: $7 | 3\{4\}; \{6\}; 3\{12\} |$
 $8A5$

T.4	$C_{12} 6(3.5.5).6(5.5.5)$	D.20



$t(C_{54}).200$

$t(T@C_{22})@4tD.200$

S_4 classes 15: $|2\{4\};10\{12\};3\{24\}|$
8A5.1

<p>$t(C_{54}).200_2$</p>	<p>$t(C_{54}).200_3$</p>	<p>$t(T@C_{22}).92$</p>

References

- Buckley F (1979) Self-centered graph with given radius. Congr Number 23:211–215
 Buckley F (1989) Self-centered graphs. Ann NY Acad Sci 576:71–78
 Coxeter HSM (1973) Regular polytopes, 3rd edn. Dover, New York

- Diudea MV (2010) Diamond D_5 , a novel allotrope of carbon. *StudUniv Babeş-Bolyai, Chem* 55 (4):11–17
- Diudea MV (2013) Quasicrystals, between spongy and full space filling. In: Diudea MV, Nagy CL (eds) Carbon materials: chemistry and physics, Diamond and related nanostructures, vol 6. Springer, Dordrecht, pp 333–383
- Diudea MV, Nagy CL (2012) All pentagonal ring structures related to the C_{20} fullerene: diamond D_5 . *Diam Relat Mater* 23:105–108
- First EL, Gounaris CE, Wei J, Floudas CA (2011) Computational characterization of zeolite porous networks: an automated approach. *Phys Chem Chem Phys* 13(38):17339–17358
- Janakiraman TN, Ramanujan J (1992) On self-centered graphs. *Math Soc* 7:83–92
- Karttunen AJ, Fässler TF, Linnolahti M, Pakkanen TA (2011) Structural principles of semiconducting group 14 clathrate frameworks. *Inorg Chem* 50:1733–1742
- Nagy CL, Diudea MV (2009) Nano-Studio. Babeş-Bolyai University, Cluj
- Nagy CL, Diudea MV (2013) Diamond D_5 . In: Nagy CL, Diudea MV (eds) Diamond and related nanostructures. Springer, Dordrecht, pp 91–105
- Nazeer W, Kang SM, Nazeer S, Munir M, Kousar J, Sehar A, Kwun YC (2016) On center, periphery and average eccentricity for the convex polytopes. *Symmetry* 8:145–168
- Negami S, Xu GH (1986) Locally geodesic cycles in 2-self-centered graphs. *Discret Math* 58:263–268
- Papacostea C (1930–1935) Platon. *Opere*, 1–11 (Roum. translation). Casa Școalelor, București
- Schulte E (2014) Polyhedra, complexes, nets and symmetry. *Acta Cryst A* 70:203–216
- Stefu M, Diudea MV (2005) CageVersatile_CVNET. Babeş-Bolyai University, Cluj
- Szeffler B, Diudea MV (2012) On molecular dynamics of the diamond D_5 seed. *Struct Chem* 23 (3):717–722
- Taylor AE (1928) A commentary on Plato's Timaeus. Clarendon, Oxford
- Wolfram Research, Inc. (2016) Mathematica, Version 10.4, Champaign

Chapter 9

C₆₀ Related Clusters

A *hyper-structure* is a (molecular) construction resulted by replacing, in a “host” structure M, of all substructures, of the same rank k , by “guest” substructures (i.e., monomers/shapes), of rank at least $k+1$; it is named $MY(\sum_i m_i S_i; p).n$ to indicate the topology of the parent map/molecule M in the Y- “hyper”-building, the number m of monomers, the type p of shapes joining facet and the total number n of atoms in the hyper-structure. More often, there is a single type of substructure and the above formula simplifies to $MY(mS;p).n$. Note that, in the name, the eventual smaller shapes, needed to fill the space, are omitted.

Design of a hyper-structure may be achieved from “monomers”, e.g., small shapes with the topology of Platonics, Archimedean or Catalans, i.e., the duals of Archimedean, or even C₆₀ while the host structure is, within this chapter, C₆₀(I_h). In developing this subject, we kept in mind the outstanding importance of C₆₀ Buckminster fullerene in promoting the whole Nano-era.

9.1 Structures Derived from the Cluster P³²@dC₆₀.33

A point-centered cluster, as those presented in Sect. 3.4.1, is now considered in view of designing C₆₀ related structures by derivatization, mainly by dual, medial and truncation, to which leapfrog operation is sometimes added. It is the cluster C₃₃ = P³²@dC₆₀.33(9A1), made by insertion of a point/vertex inside the *dual* of C₆₀ graph dC₆₀.32 connected by all 32 vertices.

A second cluster, C₉₂=dC₆₀@C₆₀.92 (9A2) is made by joining the C₆₀ dual’s vertices with the boundary vertices of the corresponding parent faces.

Since the basic structure involved in construction of C₆₀ related clusters is the cluster C₉₂, our investigation needs its P-centered derivative C₉₃ = P³²@dC₆₀@C₆₀.93 (9A3). Cluster C₉₃ is equivalent to the union C₃₃UC₉₂ and also to P³²@(C₉₂).93; it is a filled clusters of rank $k = 5$ (having two faces/substructures

Table 9.1 Figure count for C₆₀@dC₆₀.92 (9A2) and its derivatives

Structure	v	e	3(2)	5(2)	6(2)	2	U	A ₅	A ₆	M	3	4	χ	k	U; (4)
1 (9A1)	33	122	150	0	0	150	60	0	0	1	61	0	0	4	T
2 (9A2)	92	360	420	12	20	452	150	12	20	2	184	0	0	4	T
3 (9A3)	93	392	510	12	20	542	210	12	20	1	243	0	0	4	T
3 (k=5)	93	392	510	12	20	542	210	12	20	1	243	2	2	5	T; (C ₃₃ ;C ₉₂)

$$1 = P^{32}@dC_{60}; 2 = dC_{60}@C_{60}; 3 = P^{32}@dC_{60}@C_{60}; 3(k=5) = P^{32}@dC_{60}@C_{60}$$

of $k = 4$ (C₃₃ and C₉₂, sharing a same tessellation: dC₆₀.32) that bound the basic structure; it is also true for its derivatives.

Note that C₉₃ is the cell dual of C₈₁₀ (C₆₀@(12C₂₀;20C₂₄)@(60C₂₀).810 (9A7)) while the external shell of C₈₁₀ (i.e., a C₆₀ shape) stands for the cell dual of C₇₅₀ (9A6), structures detailed in Sect. 9.3.

Derivatization by map operations of the three above clusters is illustrated in the Atlas of this chapter (Figs. 9A1 to 9A3) and their figure counts are listed in Tables 9.1, 9.2, 9.3, 9.4 and 9.5. Remark here the involvement of triplets of shapes around a fourth one, M@3M/2, that can be seen as a derivation of the trigonal sp^2 carbon atom, in Chemistry; in the above, “3M/2” means that each shape of the triplets is shared by two “three-connected hyper-vertices”.

Spongy structures provide negative values of χ and high genus (Tables 9.2, 9.4 and 9.5, entries marked by a subscript “sp”).

Remark the cluster C₂₄₄ (9A1.3) derived by truncation of P³²@dC₆₀.33; it represents the core of a more complex C₁₂₀₈ (9A1.3.2), that can be obtained directly by truncation of C₁₂₅ (9A1.3.1), a cluster inspired from the Bergman’s cluster (C₄₅, Bergman et al. 1952); figure count for these structures are listed in Table 9.3. It is expected that different map operations provide clusters with a same number of atoms but having different tessellation, as discussed in Sect. 4.5.

A last remark for this section: there are clusters composed by shapes smaller than C₂₀, e.g., TO (C₂₅₂₀ (9A2.2.2); C₉₀₀ (9A1.2.4)) or TT (C₁₂₆₀ (9A2.2.1)) and related structures, made by truncation or leapfrog operations, that have connectivity three and four; such structures (including those made by C₂₀) may appear in carbon phases produced at high pressure (and high temperature).

9.2 Stellated Clusters

There are many clusters that can serve as startin structures in map operation derivatization; it is not the aim of this book to exhaust all possibilities in this respect, thus only some “other” structures will be discussed.

Stellation of dual of C₆₀ cage, dC₆₀.32, leads to $st(dC_{60}).92$ (9A4), a cluster that can be further transformed by dualization, medial and truncation (Figs. 9A4n). Observe, in the name of hyper-structures, the manner of units binding (e.g., for TT

Table 9.2 Figure count for $P^{32}@dC_{60,33}$ and its derivatives

Structure	v	e	3(2)	4(2)	5(2)	6(2)	2	U	c_1	c_2	M	3	χ	$g(k)$	U; c_n
1 (9A1.2)	122	450	390	0	12	20	422	60	12	20	2	94	0	0(4)	O;Py ₅ ;Py ₆
2 (9A1.1)	150	450	330	0	24	40	394	60	12	20	2	94	0	0(4)	T; A ₅ ;A ₆
3 (9A1.2.1)	390	990	270	360	24	40	694	60	12	20	2	94	0	0(4)	C;mP ₅ ;mP ₆
3 _{sp}	390	720	0	360	0	0	360	60	0	0	0	60	-30	16(4)	C; ()
4 (9A1.2.2)	450	1170	390	360	24	40	814	60	12	20	2	94	0	0(4)	CO; P ₅ ;P ₆
4 _{sp}	450	1170	390	360	0	0	750	60	0	0	0	60	-30	16(4)	CO; ()
5 (9A1.2.3)	750	1440	0	720	0	0	720	60	0	0	0	60	-30	16(4)	dmC; ()
6 (9A1.2.5)	900	1620	0	360	24	430	814	60	12	20	2	94	0	0(4)	TO;P ₅ ;P ₆
6 _{sp}	900	1620	0	360	0	390	750	60	0	0	0	60	-30	16(4)	TO; ()
7 (9A1.2.4)	1170	2610	390	1080	0	0	1470	60	0	0	0	60	-30	16(4)	mmC; ()

1 = $m(P^{32}@dC_{60,33}),1,22$; 2 = $d(P^{32}@dC_{60,33}),150$; 3 = $dm(P^{32}@dC_{60}),390$; 3_{sp} = $dm(P^{32}@dC_{60}),390$ sp; 4 = $m(C_{122}),450$; 4_{sp} = $m(C_{122}),450$ sp; 5 = $d(m(C_{122}),450),750$ sp; 6 = $r(C_{122}),900$; 6_{sp} = $r(C_{122}),900$ sp; 7 = $m(m(C_{122}),450),1170$, “()” means not detailed cells c_n

Table 9.3 Figure count for C₂₄₄ and its derivatives

Structure	<i>v</i>	<i>e</i>	3(2)	5(2)	6(2)	2	M	TT	U	3	χ	<i>k</i>
1 (5A2.1)	84	192	80	12	50	142	2	20	12	34	0	4
2 (5A1.1)	100	230	96	12	62	170	2	24	14	40	0	4
3 (9A1.3)	244	572	240	12	170	422	2	60	32	94	0	4
4 (9A1.3.1)	125	604	870	12	20	902	1	390 ^a	32 ^b	423	0	4
5 (9A1.3.2)	1208	3214	1560	12	890	2462	2	390	64	456	0	4

1 = $t(\text{IP})$.84; 2 = $t(\text{P}@st(\text{A}_6))$.100; 3 = $t(\text{P}^{32}@d\text{C}_{60.33})$.244; 4 = $(\text{P}^{32}@d\text{C}_{60.33})@(st(\text{C}_{60}92))$.125; 5 = $t(\text{C}_{125})$.1208; ^aT; ^bPPY_k

Table 9.4 Figure count in $l(\text{P}^{32}@d\text{C}_{60.33})$.450 and its relatives

Struct	<i>v</i>	<i>e</i>	3(2)	5(2)	6(2)	2	M	TT	3	4	χ	<i>g</i>	<i>k</i> (4)
1 (9A1.4)	450	810	150	12	260	422	2	60	62	0	0	0	4
1 _{sp}	450	810	150	0	240	390	0	60	60	0	-30	16	4
2 (9A2.4)	1260	2160	420	0	600	1020	0	150	150	0	-30	16	4
3 ₄ (9A3.2)	1530	2790	510	102	860	1472	2	210	212	0	0	0	4
3 ₅ (9A3.2)	1530	2790	510	102	860	1472	2	210	212	2	2	0	5 (C ₄₅₀ ;C ₁₂₆₀)

1 = $l(\text{P}^{32}@d\text{C}_{60.33})$.450; 2 = $l(d\text{C}_{60}@C_{60.92})$.1260 *sp*; 3_{*n*} = $l(\text{P}^{32}@d\text{C}_{60}@C_{60.93})$.1530

shape, there are: f_6 (9A1.3); f_3 (9A1.4); e (9A4.3)). Figure count for $st(d\text{C}_{60})$.92 and its relatives is given in Table 9.6.

Icosidodecahedron $\text{ID} = m\text{D} = m\text{I}$ can also be stellated to $st\text{ID}$.50 and this unit enables, by a hypothetical self-arranging process, the construction of a hyper-cluster, C₆₀Y(60($st(\text{ID});f_5$)).1650 (9A5.1); hexagonal and pentagonal hyper-faces are shown at the bottom of Fig. 9A5.1. Figure count for this cluster, its monomer and spongy-view is given in Table 9.7 while topological symmetry in Table 9.8.

Ring counting around vertices provides “chemical vertex type” classes (if the rings are the “strong” ones) or “topological vertex type” classes (if the rings are circuits long enough), equaling the number of “centrality atom type” classes (obtained at the early strong rings stage), as shown in Table 9.8. All the vertex classes counted by C-index (Nagy and Diudea 2009) have been confirmed by symmetry calculation using the adjacency matrix permutations (Nagy 2016).

9.3 C₇₅₀ Related Structures

Design of cluster C₇₅₀ (9A6) was realized by operations on maps, by a procedure developed by Diudea (2013). For this, the following sequence of operations was used: $t_{sel}(p_4(\text{C}_{60}))$.330; $s_2(\text{C}_{60})$.420; $t_{sel}(p_4(\text{C}_{60}))@s_2(\text{C}_{60})$.750, where t_{sel} stands for the selected (i.e., marked) vertices truncation while the “endo” symbol @ means: the substructure to the left of symbol is “inside” the substructure lying to the right of this

Table 9.5 Figure count for the cluster C₆₀@dC₆₀.92 and its derivatives

Structure	v	e	3(2)	4(2)	5(2)	6(2)	2	U	A ₅	A ₆	M	3	4	χ	g(k)	U (M); (4)
1 (9A.2.1)	420	1080	420	270	24	40	754	60	12 ^a	20 ^a	2	94	0	0	0(4)	T (C ₆₀)
2 (9A.2.2)	360	1260	1020	0	24	40	1084	150	12	20	2	184	0	0	0(4)	O (mC ₆₀)
2 _{sp}	360	1260	1020	0	0	0	1020	150	0	0	0	150	0	-30	16(4)	O (mC ₆₀)
3 (9A.1.2)	122	450	390	0	12	20	422	60	12	20	2	94	0	0	0(4)	O; Py5; Py6; 0
4 (9A.3.1)	392	1530	1350	0	24	40	1414	210	24 ^b	40 ^b	2	276	2	2	0(5)	O (dC ₆₀); (C ₋₁₂₂ ; C ₃₆₀)
5 (9A.2.2.1)	1260	3060	1020	900	0	0	1920	150	0	0	0	150	0	-30	16(4)	CO 0
6 (9A.2.2.2)	2520	4320	0	900	0	1020	1920	150	0	0	0	150	0	-30	16(4)	TO 0
7 (9A.2.3)	720	1620	600	0	24	460	1084	150	12	20	2	184	0	0	0(4)	TT (C ₆₀)
7 _{sp}	720	1620	600	0	0	420	1020	150	0	0	0	150	0	-30	16(4)	TT 0

1 = d(C₆₀@d(C₆₀)).420; 2 = m(C₆₀@d(C₆₀)).360; 3 = m(P³²@dC₆₀.33).122; 4 = C₁₂₂@C₃₆₀.392; 5 = C_{1260sp} = mm(C₉₂).1260; 6 = t(m(C₉₂).360).2520_{sp}; 7 = l(C₆₀@((60)(TT@3TT/2);12A₅;20A₆);720; ^amA_k; ^bPy_k&A_k

Table 9.6 Figure count for $st(dC_{60}).92$ (9A4) and its relatives

Struct	v	e	3(2)	4(2)	5(2)	6(2)	2	M	c_1	c_2	3	χ	c_n (M)
1 (9A4)	92	270	240	0	0	0	240	2	60	0	62	0	T (C ₆₀)
2 (9A4.1)	240	540	240	90	24	40	394	2	60	32	94	0	T;hmP _k (C ₆₀)
3 (9A4.2)	270	720	480	0	12	20	512	2	60	0	62	0	O (C ₆₀)
4 (9A4.3)	540	990	240	0	12	260	512	2	60	0	62	0	TT (C ₁₈₀)

1 = $st(dC_{60}).92$; 2 = $d(st(dC_{60})).240$; 3 = $m(st(dC_{60})).270$; 4 = $t(st(dC_{60})).540$

Table 9.7 Figure count for cluster $st(ID).50$ (9A5) and its derivative

Structure	v	e	3(2)	5(2)	6(2)	2	T	M	U ₅₀	3	χ	$g(k)$
1 (9A5)	50	120	80	12	0	92	20	2	0	22	0	0(4)
2 (9A5.1)	1650	4500	3000	642	20	3662	750	2	60	812	0	0(4)
2 _{sp}	1650	4500	3000	630	0	3630	750	0	60	810	-30	16(4)

1 = $st(ID).50$; 2 = $60(st(ID)50).1650$

Table 9.8 Topological symmetry by RSI and centrality C-index of C₁₆₅₀ (9A5.1) cluster

Structure	R _{min}	R _{max}	Signature (C _{min} ; C _{max})	Classes {elements}	Deg	RSI
C ₁₆₅₀ (9A5.1)	3	6	3 ⁶ .5 ³	4: {510}	6	0.881088
	-	-	3 ⁶ .5 ² .6	{120}	6	-
	-	-	3 ⁶ .5 ²	{720}	6	-
	-	-	3 ³	{300}	3	-
LM(C ₁₆₅₀)	3	6	(0.039044) (0.033227)	21: {30}; 13 × {60}; 7 × {120}	3;6	-

symbol. Formally, every point in the graph of C₆₀(I_h) was changed by a cell C₂₀; structure C₆₀Y(60C₂₀).750 (9A6) is a “hyper” and “spongy” structure, with the central hollow of exact topology of $t_{set}(p_4(C_{60})).330$. If this hollow is “endohedrally” functionalized (a term taken from nanoscience) by connecting inside the fullerene graph C₆₀(I_h), a double-shell cluster is thus designed: C₆₀@(C₃₃₀)=C₆₀@(12C₂₀;20C₂₄).390 (9A7a). Then, all these substructures subsequently fit to each other, providing a filled cluster C₃₉₀@C₇₅₀ = C₆₀@C₇₅₀.810 = C₆₀@(12C₂₀;20C₂₄)@(60C₂₀).810 (9A7). The structures involved in the design of clusters C₇₅₀ (9A6) and C₈₁₀ (9A7) are illustrated at the bottom of these figures; their figure count is shown in Table 9.9. The procedure for spongy structures is general, working on any three-connected cage.

C₇₅₀ has its cell-dual the point-centered cluster P⁶⁰@C₆₀.61 = C₆₀P.61, (9A6.1a) with the central point of degree 60 (written as a superscript number), from which the “spongy” character of C₇₅₀ immediately comes out. It is also clear when its figures are counted as in Table 9.9, entry C_{750sp}; 12 pentagons (5(2)) and 20 hexagons (6(2)) are “seen” as “empty” faces or “windows” while the closing (internal/external) maps M are disregarded. The alternating sum of figures, according to Euler (1752-1753) formula (Chap. 4; (6)) gives $\chi = -30$ and $g = 16$, the correct values for the spongy C₆₀-derivatives.

In the opposite, C_{810} (9A7) is a filled cluster, as shown by the group of Diudea (Stefu et al. 2015); if one considers only the cells (i.e., faces/figures of rank $k = 3$), the calculated rank is $k = 4$ (as for C_{750}). However, its boundaries are closed by two faces of rank 4 (namely C_{750} and C_{390}); thus, C_{810} can be considered as a cluster of rank $k = 5$ (see Table 9.9, entry C_{810_5}). For $C_{60}P.61$ one counts $k = 4$, as shown in the bottom of Table 9.9. In the following, attention is focused on “spongy” structures, rather to the filled ones.

9.3.1 Duals of C_{750} and Related Structures

All ring dualization of C_{750} (9A6) leads to a spongy cluster $d(C_{750}) = C_{60}Y$ ($60dC_{20}$) sp , (9A6.1 and Table 9.10) with only icosahedral cells. Similarly, clusters $C_{60}Y(60C_{60};P_5).3600$ (9A6.1.1) and $C_{60}Y(60C_{60};f_5).3150$ (9A6.4) are spongy hyper-structures of C_{60} , of which atoms were replaced by C_{60} units.

Recently, the group of Klein (Bhattacharya et al. 2016) published an isomer on 3600 atoms (denoted here $C_{60}Y(60C_{60};hh[2+2]).3600$ (9A6.1.1a), in which the units are joined by two covalent bonds (coming, in Chemistry, from a 2+2 cycloaddition); in our 3600-isomer the units are joined by pentagonal prisms P_5 , while in the other hyper- C_{60} on 3150 vertices, the units are joined by identification of pentagonal faces. (In Chap. 12, on energetics associated to such structures, will be shown that such f_5 -joining of C_{60} cells could have a real chance in Nanotechnology, as a way of C_{60} fullerene aggregation).

Counting the rings around vertices provides “chemical vertex type” classes (if the rings are the “strong” ones) or the “topological vertex type” classes (if the rings are circuits long enough), equaling the number of “centrality vertex type” classes (obtained with layer matrices just from hard rings), as shown in Table 9.11. It is noticeable that the vertex equivalence classes found by our topological descriptors are confirmed by permutations performed on the adjacency matrix associated to such complex graphs (by using Mathematica software—Nagy 2016), as shown at the bottom of the most important figures, in the Atlas. When the number of classes is rather big (see Table 9.11 and others), only RSI and extreme values of the centrality index $C_{\min/\max}$ are given.

9.3.2 Medials of C_{750} and Related Clusters

Medial operation introduces tetrahedral cells to fill the space with the icosidodecahedra $ID = mD = mI$, which join pentagonal face identification. The spongy hyper-structure $C_{60}Y(60 ID;f_5).1350$ (9A6.2) is obtained starting from the spongy C_{750} cluster while the filled pair (9A7.1) is made from the filled cluster C_{810} . A further dualization of the spongy medial cluster led to the hyper-structure $C_{60}Y(60 Rh_{30}.32;P).1830$, with the units being the rhomb-tessellated triacontahedron Rh_{30} (9A6.2.1). Figure count for these three clusters is included in Table 9.10.

Table 9.9 Figure count of C₇₅₀ (9A6), C₈₁₀ (9A7) and its relatives

Struct	v	e	3(2)	5(2)	6(2)	2	c_1	c_2	M	3	4	χ	$g(k)$	C ₇₅₀ ; (M); (4)
1 (9A6)	750	1350	0	642	20	662	60	0	2	62	0	0	0(4)	C ₂₀₆ ; ()
1.sp	750	1350	0	630	0	630	60	0	0	60	0	-30	16(4)	C ₂₀₆ ; ()
2 (9A7)	810	1500	0	744	40	784	72	20	2	94	0	0	0(4)	C ₂₀₆ ; C ₂₄ ; (C ₆₀)
2.full	810	1500	0	744	40	784	72	20	2	94	2	2	2(5)	C ₂₀₆ ; C ₂₄ ; (C ₆₀); (C ₃₉₀ ; C ₇₅₀)
3 (9A7a)	390	690	0	294	40	334	12	20	2	34	0	0	0(4)	C ₂₀₆ ; C ₂₄ ; (C ₆₀)
4 (9A6.1a)	61	150	90	12	20	122	12	20	1	33	0	0	0(4)	Py ₅ ; Py ₆ ; (C ₆₀)

1 = $t_{ser}(p_4(C_{60})) @ (s_2(C_{60})420); 750; 2 = C_{60} @ (12C_{20}; 20C_{24}) @ (60C_{20}); 810; 3 = C_{60} @ (12C_{20}; 20C_{24}); 390; 4 = C_{60}P$

Table 9.10 Figure count in C₇₅₀ (9A6) cluster and its relatives

Struct	v	e	3(2)	4(2)	5/10*(2)	6/12*(2)	2	U	c ₁	c ₂	c ₃	M	3	κ	g(k)	U; c _n ; (M)
1 (9A6)	750	1350	0	0	642	20	662	60	0	0	0	2	62	0	0(4)	D
2 (9A6.1)	630	1800	1200	0	0	0	1200	60	0	0	0	0	60	-30	16(4)	I
3 (9A6.2)	1350	3600	2100	0	642	20	2762	60	450	0	0	2	512	0	0(4)	mC ₂₀ ; T
4 (9A7.1)	1500	4140	2520	0	744	40	3304	60	570	12	20	2	664	0	0(4)	mC ₂₀ , mC ₂₄ ; T
5 (9A6.2.1)	1830	3600	0	1800	0	0	1800	60	0	0	0	0	60	-30	16(4)	dmD
6 (9A6.3)	2700	4950	2100	0	642*	20*	2762	60	450	0	0	2	512	0	0(4)	rD; T
6 sp	2700	4950	2100	0	630*	0	2730	60	450	0	0	0	510	-30	16(4)	rD; T
7 (9A7.2)	3000	5640	2520	0	744*	40*	3304	60	570	12	20	2	664	0	0(4)	rD; T; (rC ₆₀)
7 sp	3000	5640	2520	0	720*	0	3240	60	570	0	0	0	630	-30	16(4)	rD; T
8 (9A6.1.1)	3600	5850	0	450	720	1200	2370	60	0	90	0	0	150	-30	16(4)	C ₆₀ ; P ₅
8 sp(9A6.1.1a)	3600	5580	0	90	720	1200	2010	60	0	0	0	0	60	-30	16(4)	C ₆₀
9 (9A6.4)	3150	4950	0	0	630	1200	1830	60	0	0	0	0	60	-30	16(4)	C ₆₀
10 (9A6.4.1)	9900	15,300	3600	0	630*	1200*	5430	60	0	0	0	0	60	-30	16(4)	t(C ₆₀); T
10 ^a	9900	15,750	4500	0	630*	1200*	6330	60	450	0	0	0	510	-30	16(4)	t(C ₆₀); T

1 = $t_{ser}(p_4(C_{60})) @ \{s_2(C_{60})420\}$.750; 2 = $d(C_{750}).630$ sp; 3 = $m(C_{750}).1350$; 4 = $m(C_{810}).1500$; 5 = $dm(C_{750}).1830$ sp; 6 = $t(C_{750}).2700$;
 7 = $t(C_{810}).3000$; 8 = $t(d(C_{750})).3600$ sp; 9 = $t(C_{750}).3150$ sp; 10 = $t(t(C_{750})).9900$; ^aTetrahedra from the inner truncated vertices
 Face f= 10 when *

Table 9.11 Topological symmetry by RSI and centrality C-index of C₇₅₀ (9A6) and its relatives

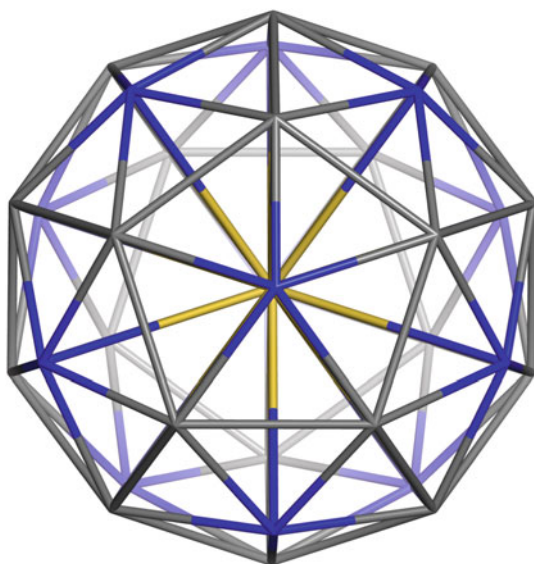
	Structure	R _{min}	R _{max}	Signature (C _{min} ; C _{max})	Classes {elements}	Deg	RSI
1	C ₇₅₀	5	6	5 ⁶	4:{60};	4	0.982727
	(9A6)	–	–	5 ⁵ .6	{120};	4	–
		–	–	5 ⁵	{270};	4	–
				5 ³	{300}	3	–
		5	12	–	12	3;4	3.461587
	LM(C ₇₅₀)	5	6	(0.042611) (0.036394)	12: {30}; 10×{60}; {120}	3;4	–
	5	12	(0.036301) (0.030290)	12: {30}; 10×{60}; {120}	3;4	–	
2	C ₃₆₀₀	4	6	4 ² .5.6 ²	2: {900}	4	0.787879
	(9A6.1.1)			5.6 ²	{2700}	3	–
	LM (C ₃₆₀₀)	4	6	(0.016690) (0.015499)	32: 4×{60} 28×{120}	3; 4	–
3	C ₃₁₅₀	5	6	5.6 ⁴	2:{450}	4	0.850649
	(9A6.4)	–	–	5.6 ²	{2700}	3	–
	LM (C ₃₁₅₀)	5	6	(0.019671) (0.018001)	32: {30}; 10×{60}; 21×{120}	3; 4	–
4	C ₉₉₀₀	3	12	3 ² .10.12 ²	3:{900}	4	0.448485
	(9A6.4.1)	–	–	3.12 ²	{3600}	3	–
		–	–	3.10.12	{5400}	3	–
	LM (C ₉₉₀₀)	3	12	(0.010474) (0.009631)	92:19×{60}; 73×{120}	3;4	–
4a	C ₉₉₀₀	3	12	3 ³ .12 ²	4:{900};	4	0.348182
	(9A6.4.1)			3 ³ .10.12 ²	{900};	4	–
				3.12 ²	{2700};	3	–
				3.10.12	{5400}	3	–
	LM (C ₉₉₀₀)	3	12	(0.010472) (0.009629)	92:19×{60}; 73×{120}	3;4	–

9.3.3 Truncated C₇₅₀ and Related Clusters

Truncation enabled us to design two spongy hyper-structures related to C₇₅₀: C₆₀Y (60 TD; f_{10}).2700 (9A6.3) and C₆₀Y(60 $t(C_{60})$; f_{10}).9900 (9A6.4.1), with the units: truncated dodecahedron TD = $t(C_{20})$.60 and truncated C₆₀, tC_{60} .180, respectively, both joined by decagonal faces. Realization by carbon of such spongy structures, containing only three- and four-connected vertices/atoms, could be possible by an adequate nanotechnology. Figure count for these structures is included in Table 9.10 while RSI and centrality data for the structure on 9900 vertices are given in Table 9.11.

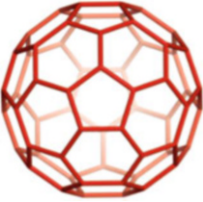


The condition (Diudea and Rosenfeld 2017) for a simple cubic graph G to be isomorphic to the truncation $t(H)$ of a simple cubic graph H , namely G to have a cyclic cover C of which all components are triangles, here is extended to include also tetrahedra (see 9A6.3), provided by four-connected inner vertices (Table 9.10, entries 7,8,11 and 12). A filled truncated structure is obtained from C_{810} , namely $t(C_{810}).3000$ (9A7.2), of which inner cells are supported by $tC_{60}.180$ cage.

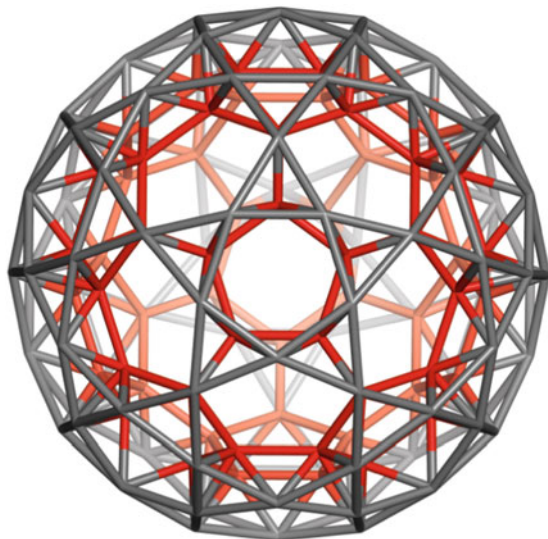
Chapter 9 Atlas: C_{60} Related Structures



$P^{32}@dC_{60}.33$

$C_2 \times A_5$; Classes: 3 $\{ \{1\}; \{12\}; \{20\} \}$
9A1

		
C_{60}	$dC_{60}.32$ $12(3^5).20(3^6)$	$P^{\wedge 32}@dC_{60}.33$



$f(C_{60})Y(12A_5; 20A_6; f_3).150$

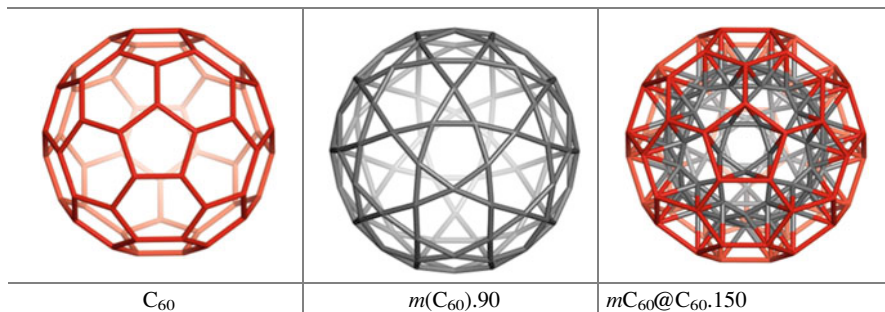
$C_{20}Y(20A_6; f_3).150$

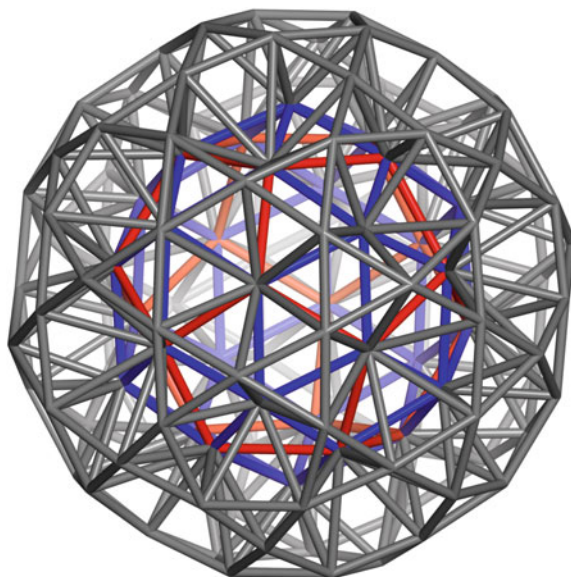
$C_{60}@((12A_5; 20A_6; 60T)@mC_{60}).150$

$d(P^{32}@dC_{60}.33).150$

$C_2 \times A_5$; Classes: 3 |{30}; 2{60}|

9A1.1





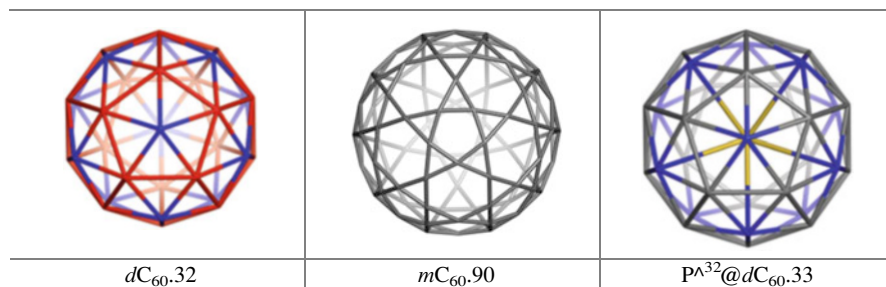
$C_{60}Y(60O; f_3).122$

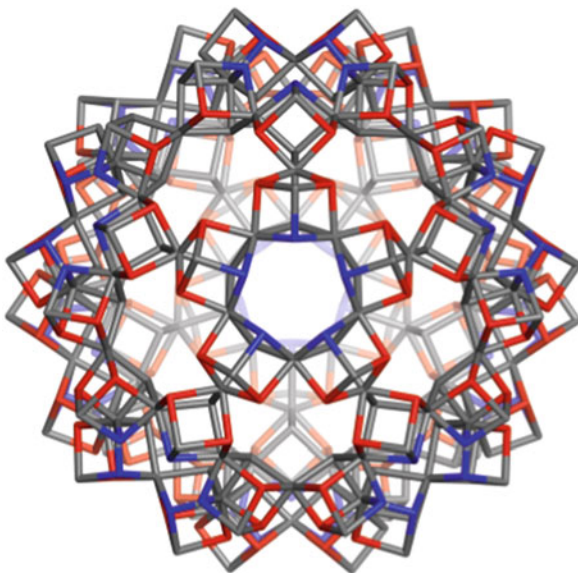
$dC_{60}@ (60O; 12Py_5; 20Py_6) @ mC_{60}.122$

$m(P^{32}@dC_{60}.33).122$

$C_2 \times A_5$; Classes: 4 $\{|12\}; \{20\}; \{30\}; \{60\}$

9A1.2





C₆₀Y(60C;P).390

(60 C.390_{sp}) (C₆₀@(12mP₅;20mP₆)330).390

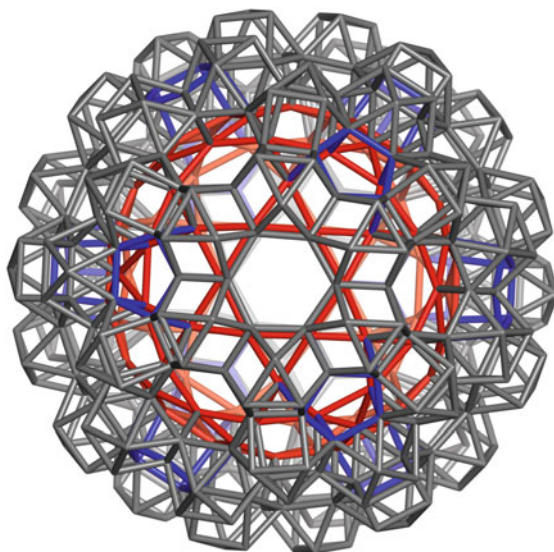
C₆₀@(12mP₅;20mP₆;60C).390_{sp}

d(C₁₂₂).390_{sp}

C₂ × A₅; Classes: 6 |{30}4{60};{120}|

9A1.2.1

<p>$m(P^{32}@dC_{60}.33).122$</p>	<p>C₆₀@(12mP₅;20mP₆).330_5</p>	<p>C₆₀@ (12mP₅;20mP₆;60C).390_5 d(C₁₂₂).390</p>



$C_{60}Y(60CO; f_3).450$

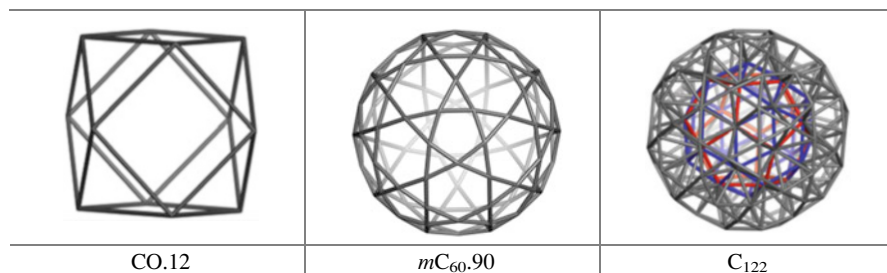
$mC_{60}@60CO.450$

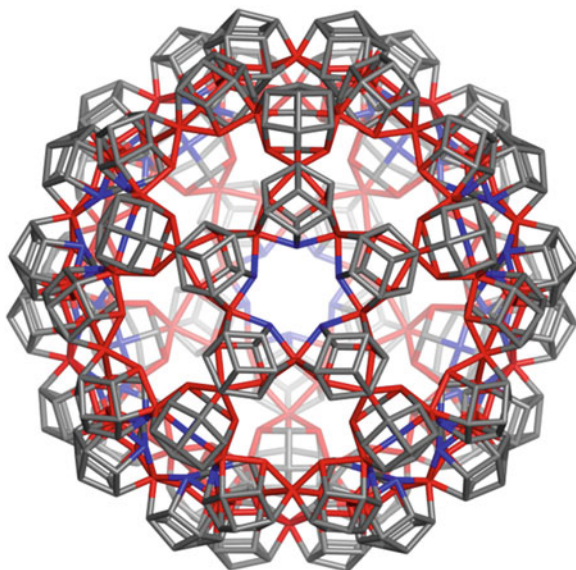
$mC_{60}@(60mC; 12P_5; 20P_6).450$

$m(C_{122}).450$

$C_2 \times A_5$; Classes: 7 $\{|30\}; 5\{60\}; \{120\}$

9A1.2.2



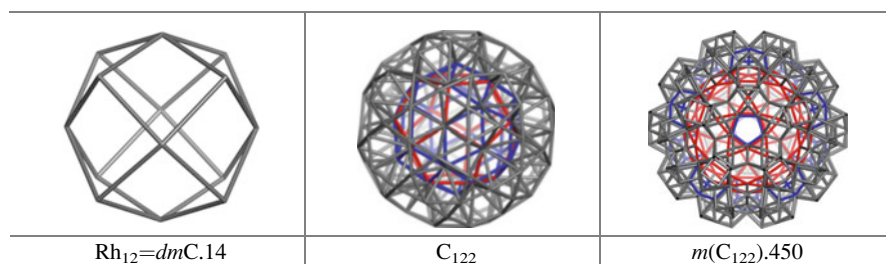


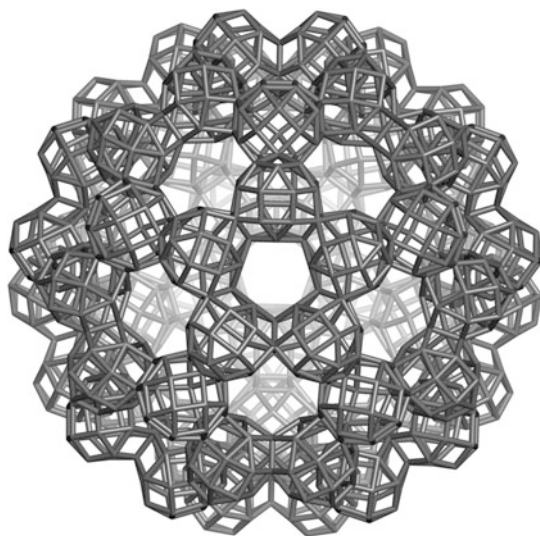
$C_{60}Y(60Rh_{12};P).750$

$d(m(C_{122})450).750$

$C_2 \times A_5$; Classes: $10 \{30\}; 6 \{60\}; 3 \{120\}$

9A1.2.3

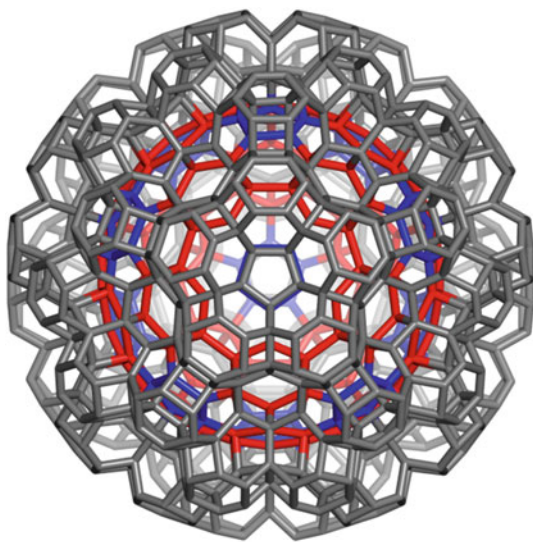




$C_{60}Y(60(m^2C); f_3).1170$

$m(m(C_{122})450).1170$
 $C_2 \times A_5$; Classes: 14 | {30}; 7 {60}; 6 {120} |
 9A1.2.4

<p>$mmC.24$</p>	<p>C_{122}</p>	<p>$m(C_{122}).450$</p>



C₆₀Y(60TO; f₆).900

C₁₈₀@(60TO; 12P₅; 20P₆).900

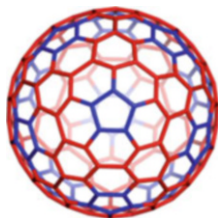
I(C₁₂₂).900

C₂ × A₅; Classes: 12 |9{60}; 3{120}|

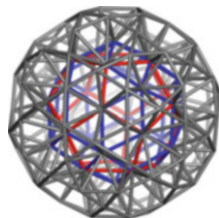
9A1.2.5



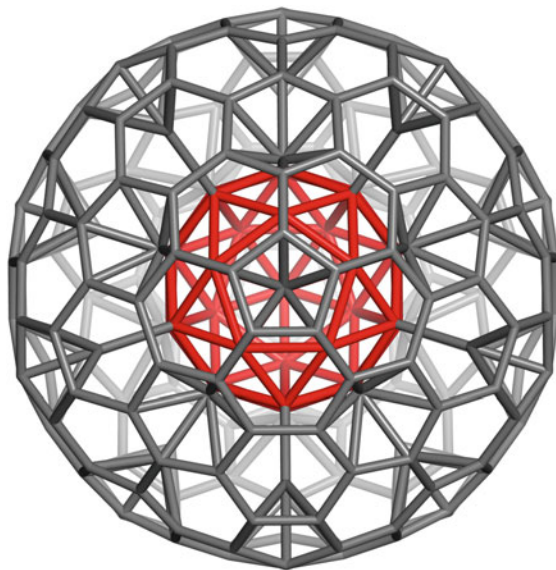
*t*O.24=TO.24



I(C₆₀).180



C₁₂₂



$C_{60}Y(60TT; f_6).244$

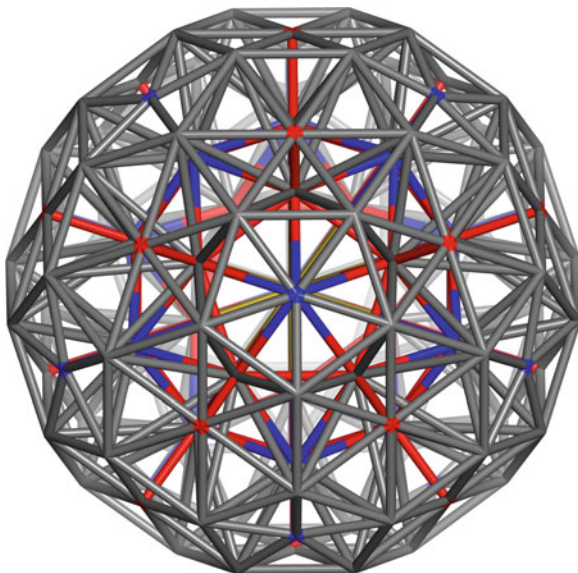
$dC_{60}@ (12Py_5; 20Py_6; 60TT)@ C_{180}(I_h).244$

$t(P^{32}@dC_{60}.33).244$

$C_2 \times A_5$; Classes: $7 | 2\{12\}; 2\{20\}; 3\{60\} |$

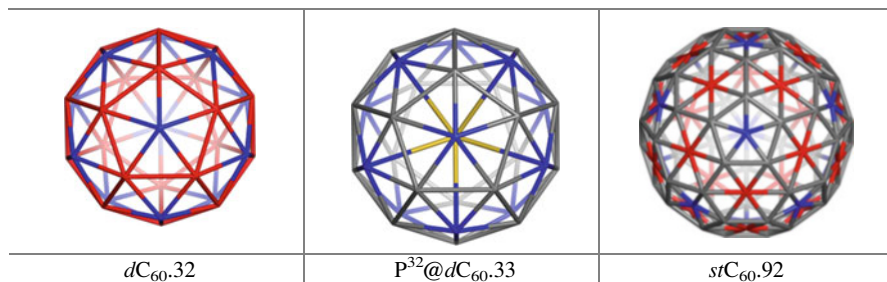
9A1.3

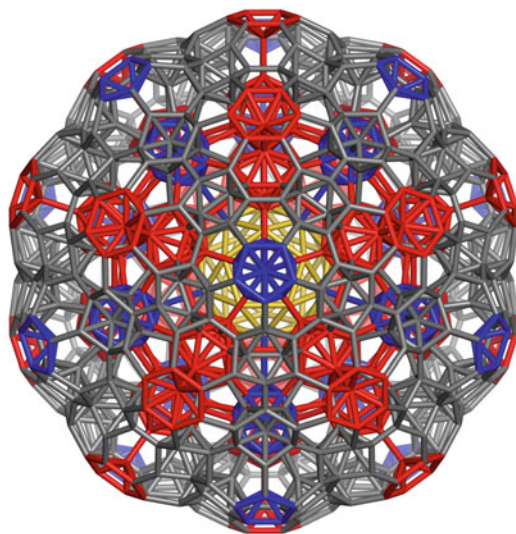
TT.12	$dC_{60}.32 = st(D).32$	$P^{32}@dC_{60}.33$



(P³²@ dC₆₀.33)@(st(C₆₀)92).125

(P³²@ dC₆₀.33)@(12PPy₅;20PPy₆;90T)@C₆₀.125
 C₂×A₅; Orbits: 6 |{1};2{12};2{20};{60}|
 9A1.3.1





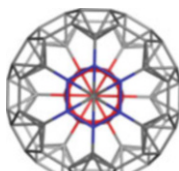
$C_{244}@(12C_{84};20C_{100})@C_{540}(I_h).1208$

$t(C_{125}).1208$

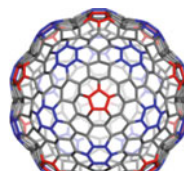
$C_2 \times A_5$; Orbits: $21 | 4\{12\}; 4\{20\}; 8\{60\}; 5\{120\} |$
9A1.3.2



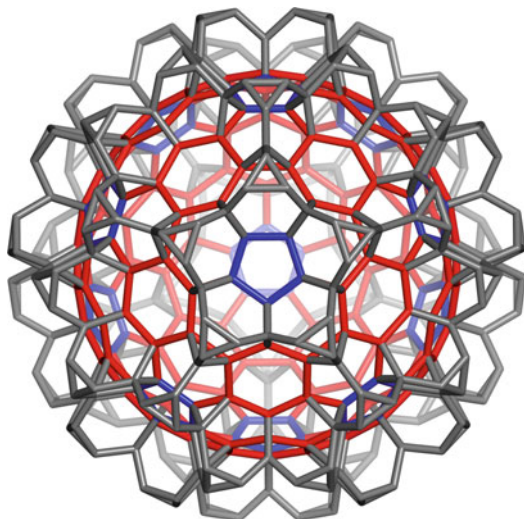
$C_{84}=t(IP).84$



$C_{100}=t(P@st(A_6)).100$



$C_{540}(I_h)$



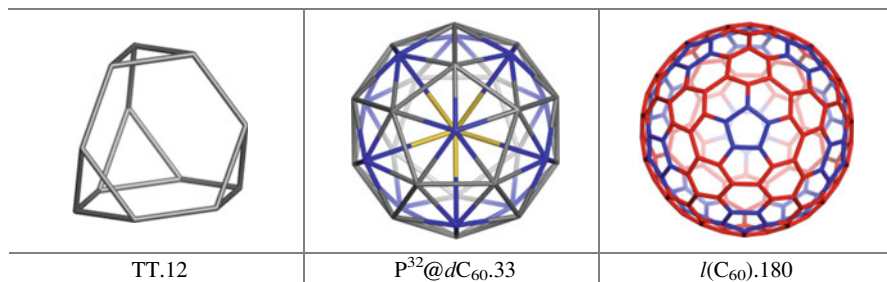
C₆₀Y(60TT; f₃)-450

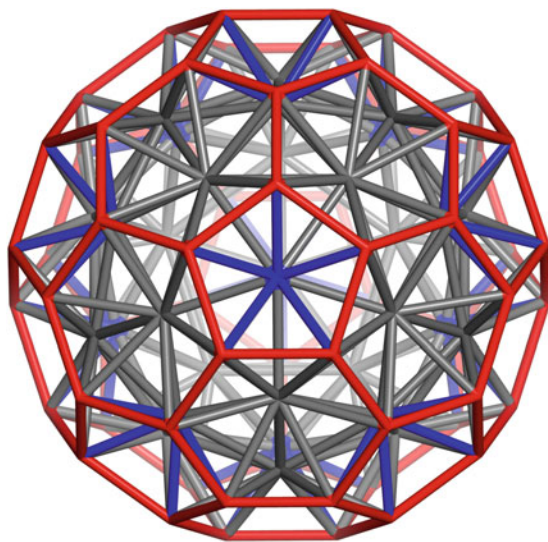
$I(C_{60})@(60TT).450$

$I(P^{32}@dC_{60}.33).450$

$C_2 \times A_5$; Orbits: 7 | {30}; 5 {60}; {120}; |

9A1.4

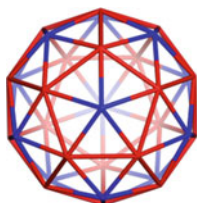




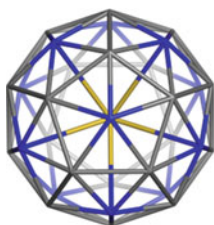
$dC_{60}@C_{60}.92$

$C_2 \times A_5$; Classes: 3: $|\{60\}; \{12\}; \{20\}|$

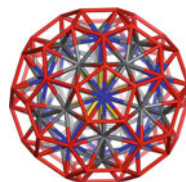
9A2



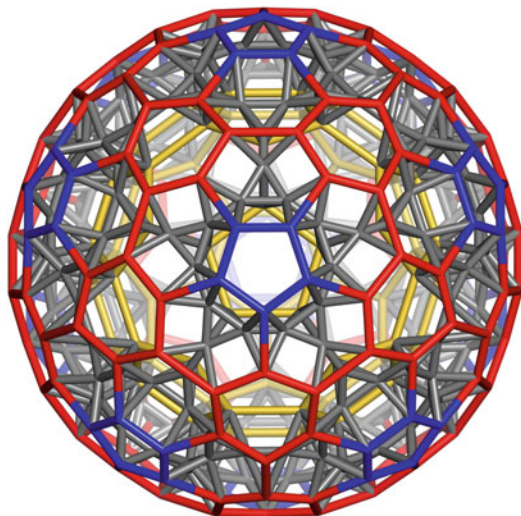
$dC_{60}.32$



$P^{32}@dC_{60}.33$



$P^{32}@dC_{60}@C_{60}.93$



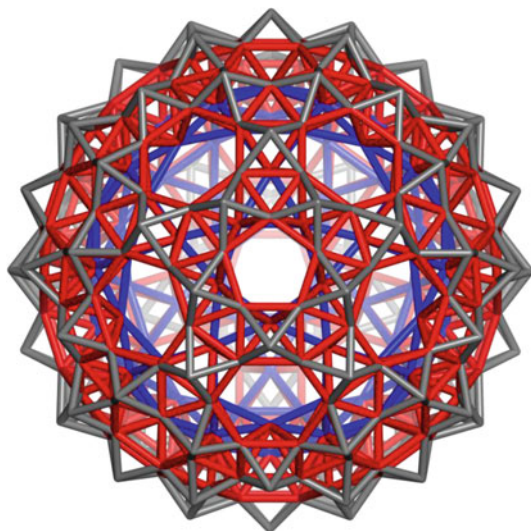
$f(C_{60})@(12mA_5;20mA_6;60T).420$

$d(C_{60}@d(C_{60})).420$

$C_2 \times A_5$; Classes: 6: $|5\{60\};\{120\}|$

9A2.1

A ₅ .10	mA ₆ .24	C ₉₂ =C ₆₀ @dC ₆₀ .92



$C_{60}Y(60(O@3O/2); f_3).360$

$mC_{60}@ (60(O@3O/2); 12A_5; 20A_6).360$

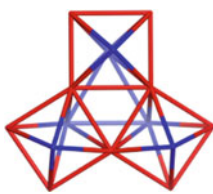
$m(C_{60}@d(C_{60})).360$

$C_2 \times A_5$; Classes 6: $|\{120\}; 3\{60\}; 2\{30\}|$

9A2.2



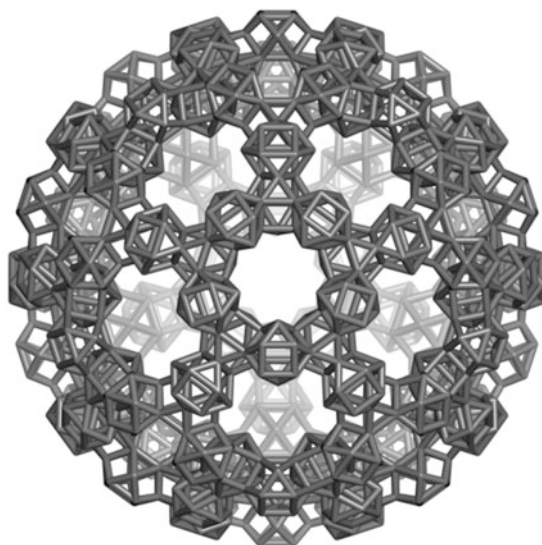
$d(C_{60}).32$



$O@3O.15$



$m(C_{60}).90$



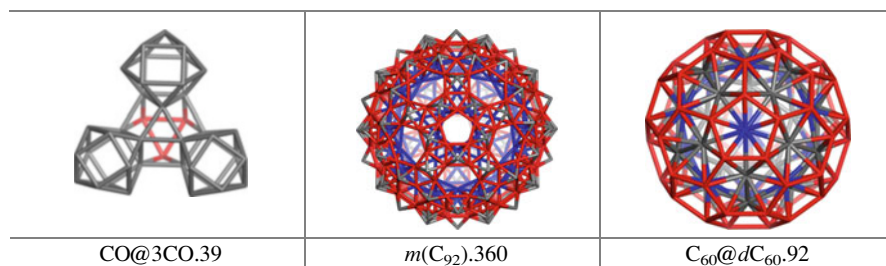
C₆₀Y(60(CO@3CO/2); f₃).1260

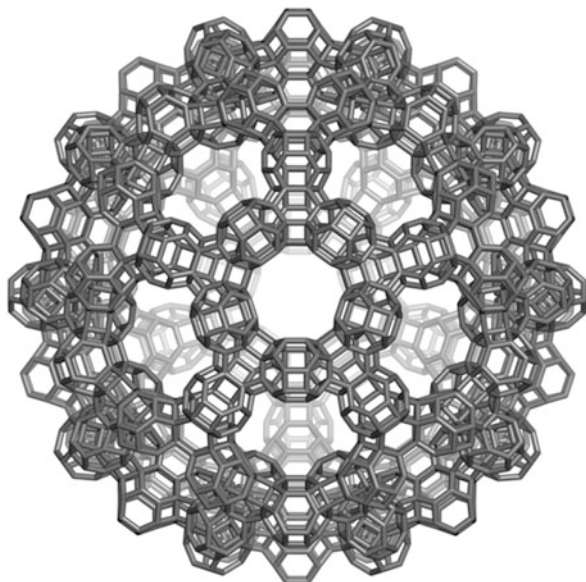
m(C₃₆₀).1260

mm(C₉₂).1260

C₂ × A₅; Classes 13: |8{120};5{60}|

9A2.2.1





$C_{60}Y(60(TO@3TO/2); f_6).2520$

$t(C_{360}).2520$

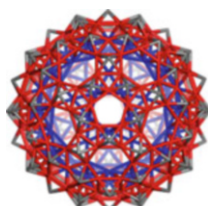
$t(m(C_{92})360).2520$

$C_2 \times A_5$; Classes 21: |21{120}|

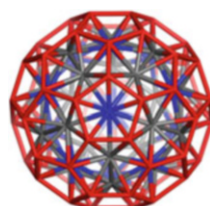
9A2.2.2



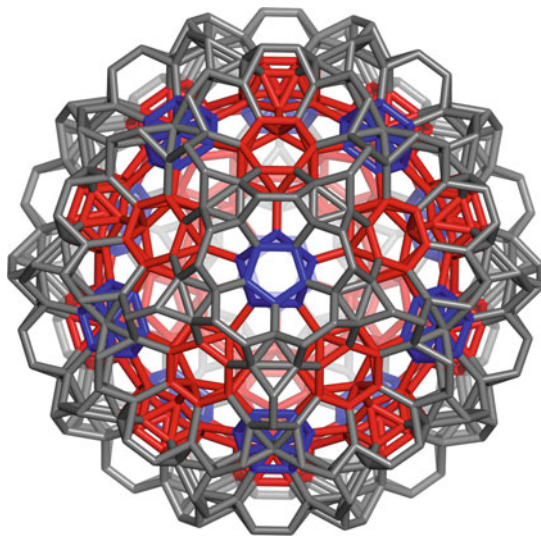
$TO@3TO.78$



$m(C_{92}).360$



$C_{92}=C_{60}@dC_{60}.92$



C₆₀Y(60(TT@3TT/2); f₆).720

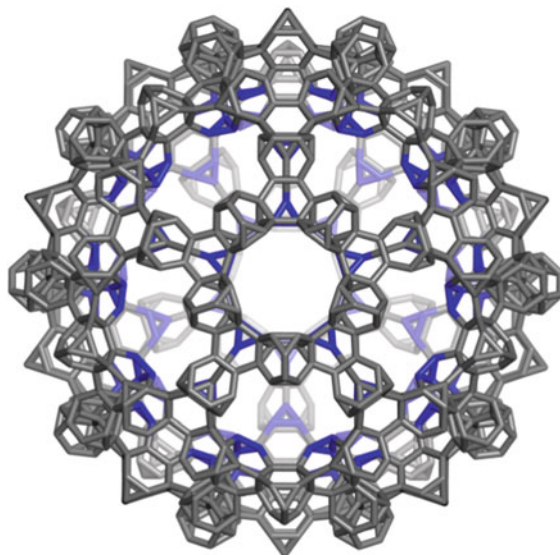
I(C₆₀)@((60(TT@3TT/2);12A₅;20A₆).720

I(C₉₂).720

C₂ × A₅; Classes 9: |3{120};6{60}|

9A2.3

TT@3TT.30	<i>I</i> (C ₆₀).180	C ₉₂ =C ₆₀ @dC ₆₀ .92



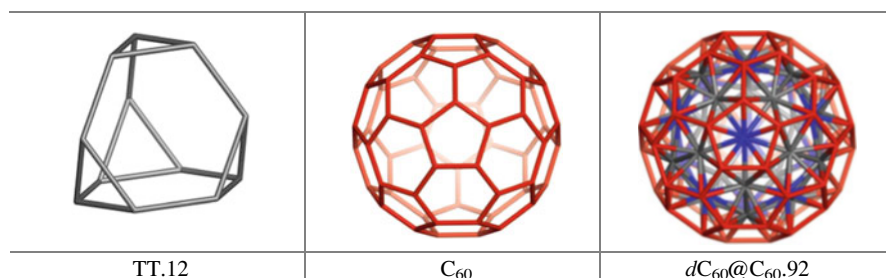
$C_{60}Y(60(TT@3TT/2); f_3).1260$

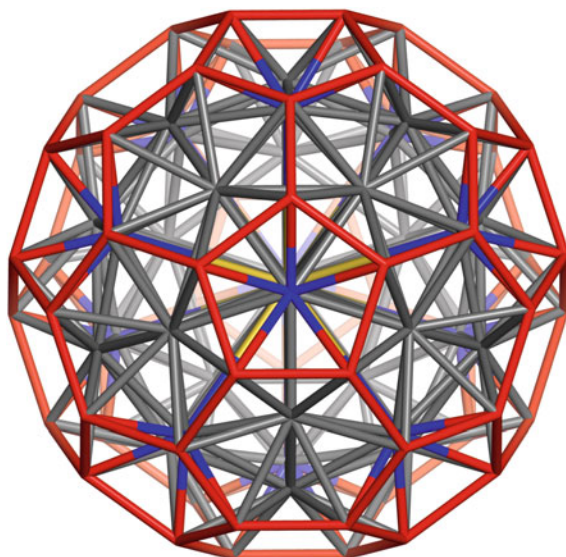
$I(dC_{60}@C_{60.92}).1260$

$I(C_{92}).1260$

$C_2 \times A_5$; Orbits: $13 | 5 \{60\}; 8 \{120\} |$

9A2.4





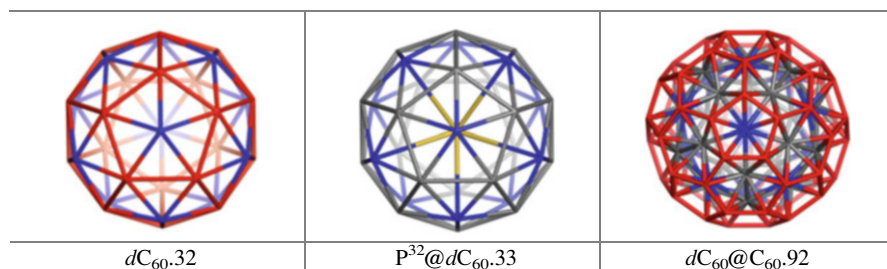
$P^{32}@dC_{60}@C_{60}.93$

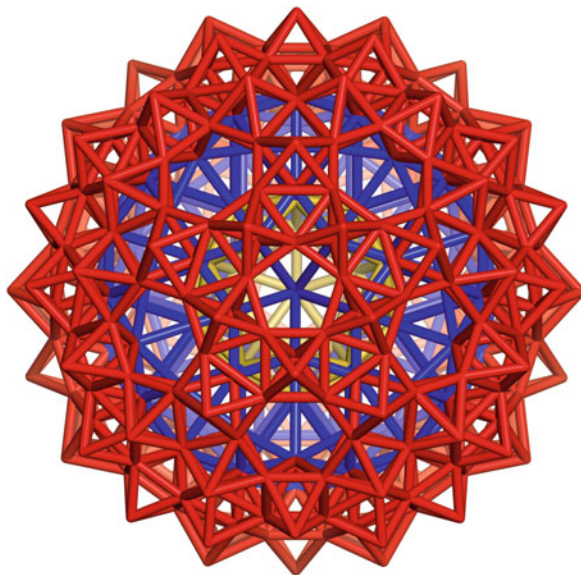
$(P^{32}@dC_{60}.33)@C_{60}.93$

$P^{32}@(dC_{60}@C_{60}.92).93$

$C_2 \times A_5$; Orbits: 4 | {1}; {12}; {20}; {60} |

9A3



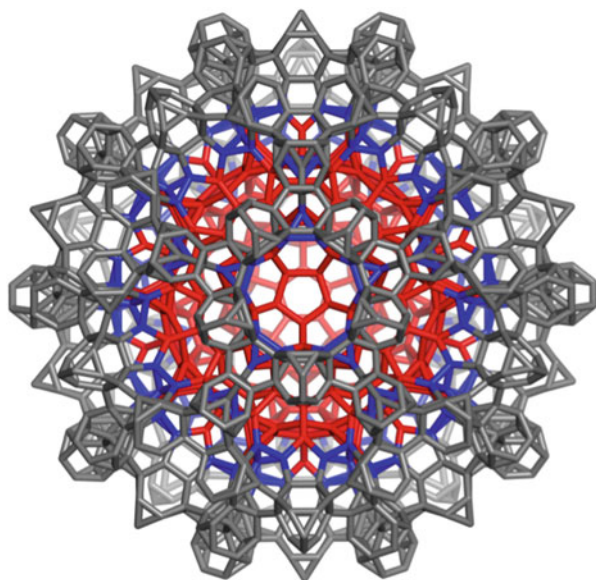


$C_{122}@C_{360}.392$

$m(C_{93}).392$

$C_2 \times A_5$; Orbits: 8 $|\{12\}; \{2\{30\}; 3\{60\}; \{120\}|$
9A3.1

<p>$d(C_{60}).32$</p>	<p>$m(P^{32}@dC_{60}.33).122$</p>	<p>$m(C_{60}@d(C_{60})).360$</p>



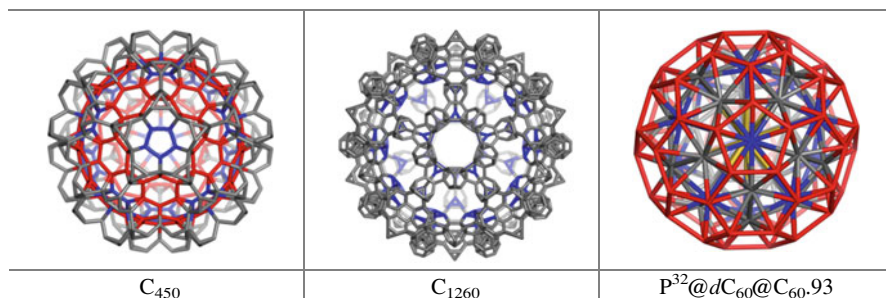
C₄₅₀@C₁₂₆₀·1530

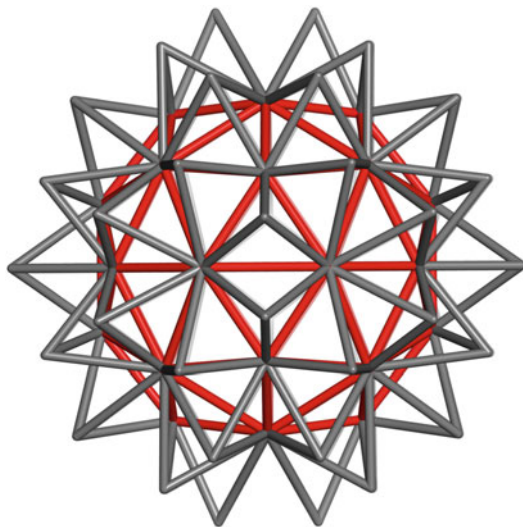
$I(C_{60})@60(2 \times TT)@90TT.1530$

$I(C_{93}).1530$

$C_2 \times A_5$; Orbits: $18 \{30\}; 9 \{60\}; 8 \{120\}$

9A3.2

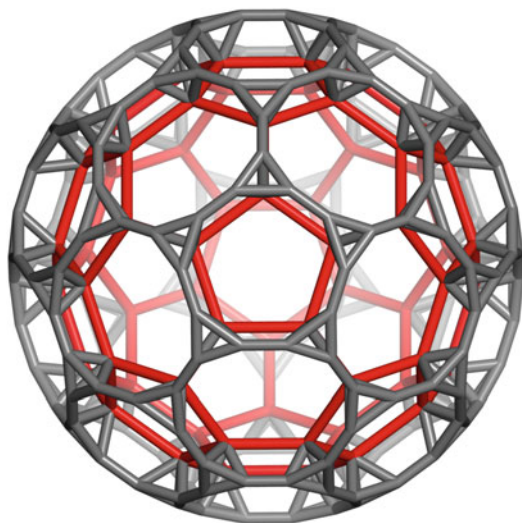




st(dC₆₀).92

$C_2 \times A_5$; Orbits: 3 $\{12\}; [20]; \{60\}$
9A4

<p>C_{60}</p>	<p>$dC_{60.32}$</p>	<p>$st(dC_{60}).92$</p>



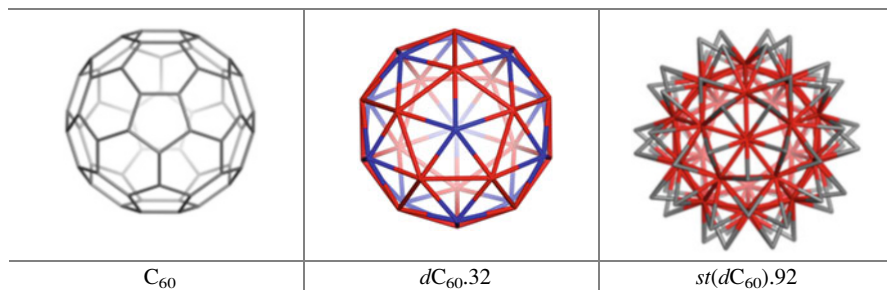
$C_{60}@60T@tC_{60}.240$

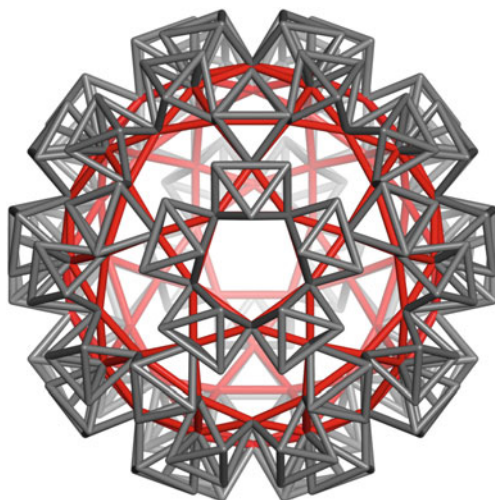
$C_{60}@ (60T; 12HmP_5; 20HmP_6) @ tC_{60}.240$

$d(st(dC_{60})).240$

$C_2 \times A_5$; Orbits: $3 [2\{60\}; \{120\}]$

9A4.1





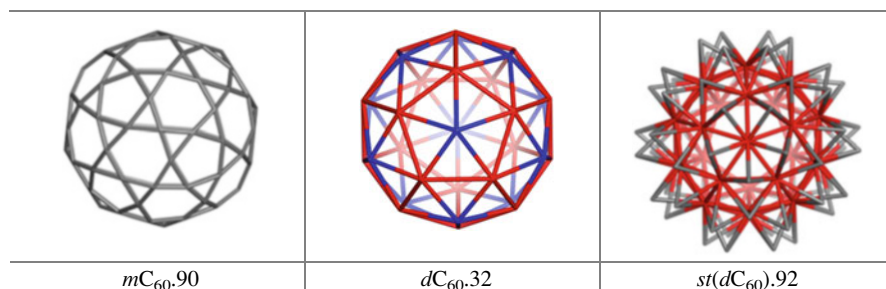
$C_{60} Y(60O;P).270$

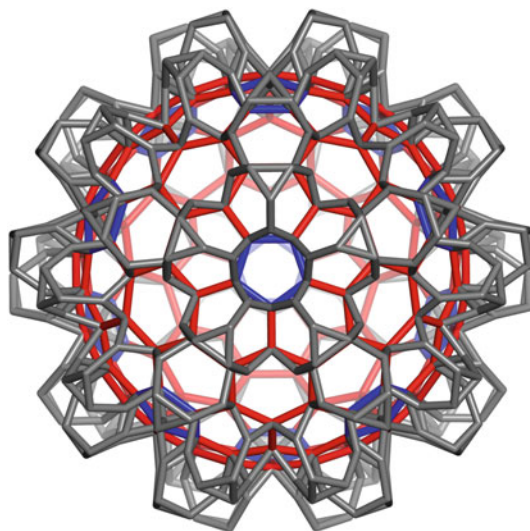
$mC_{60}@ (60O;P).270$

$m(st(dC_{60})).270$

$C_2 \times A_5$; Orbits: 4 $\{30\}$; 2 $\{60\}$; $\{120\}$ |

9A4.2





C₆₀Y(60TT;e).540

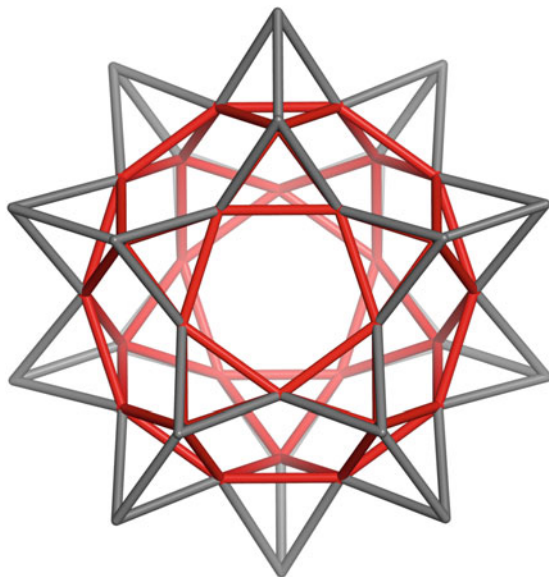
C₁₈₀@(60TT;e).540

t(*st*(*d*C₆₀)).540

C₂×A₅; Orbits: 7 | 5 {60}; 2 {120} |

9A4.3

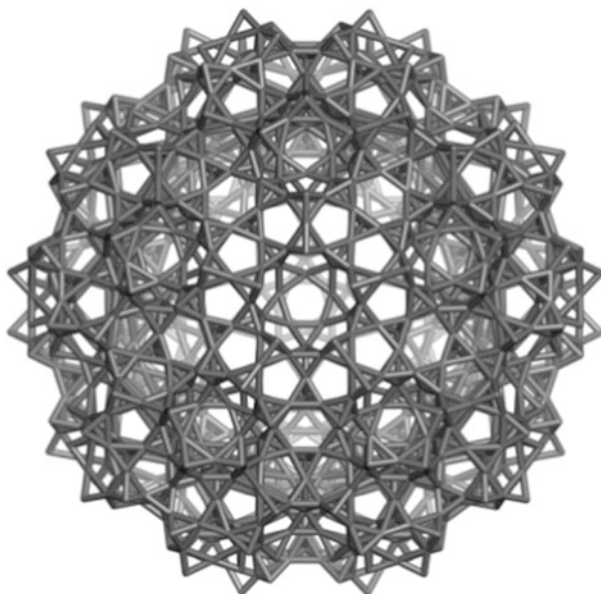
<p>C₁₈₀ = <i>I</i>(C₆₀).180</p>	<p><i>d</i>C₆₀.32</p>	<p><i>st</i>(<i>d</i>C₆₀).92</p>



$st(\text{ID}).50$

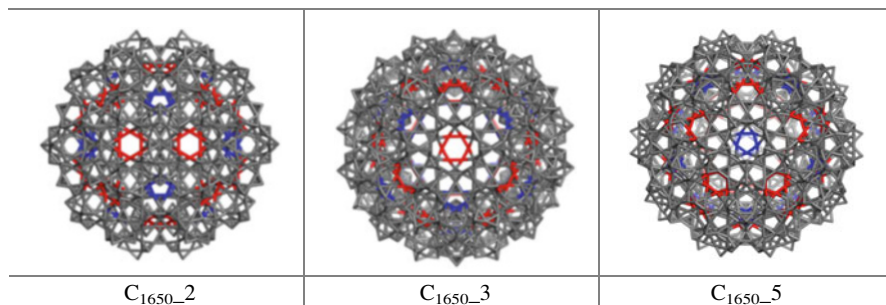
$st(mD).50$
 $C_2 \times A_5$; Orbits: 2 | {20}; {30} |
 9A5

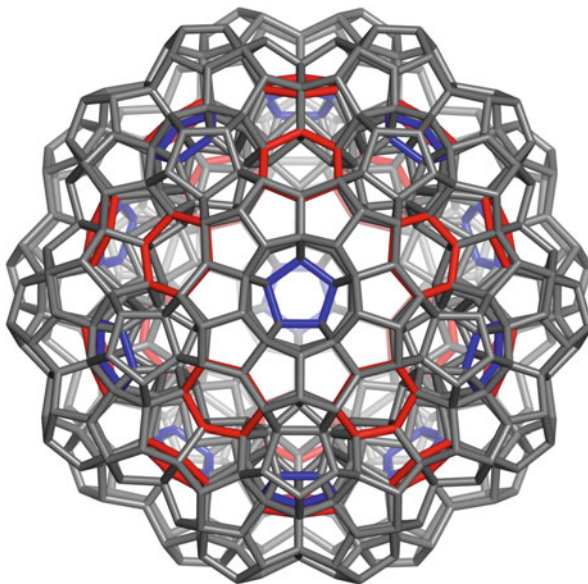
<p>$st(\text{ID}).50$</p>	<p>$6(st(\text{ID}).50).210$</p>	<p>$5(st(\text{ID}).50).175$</p>



$C_{60}Y(60(st(ID); f_5).1650$

$C_2 \times A_5$; Classes 21: $|\{30\}; 13\{60\}; 7\{120\}|$
9A5.1



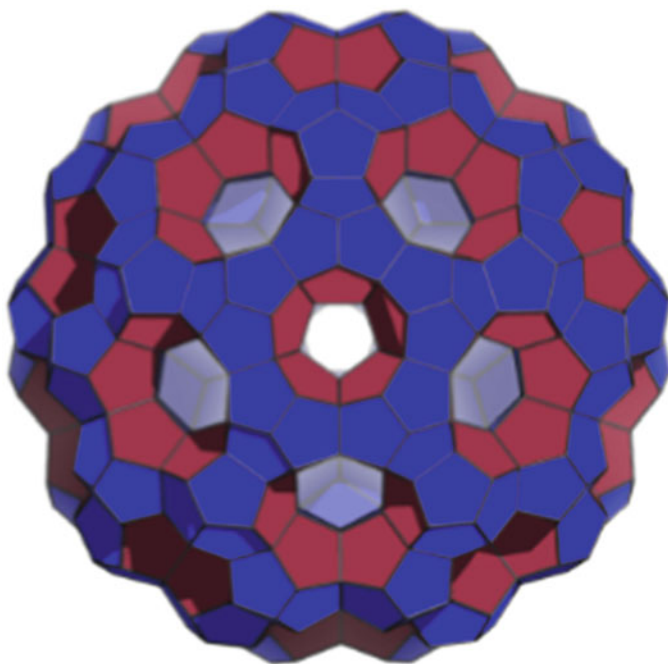


$C_{60}Y(60C_{20}).750$

$t_{set}\{p_4(C_{60})\}@ \{s_2(C_{60})420\}.750$
 $C_{60}Y(60D).750$

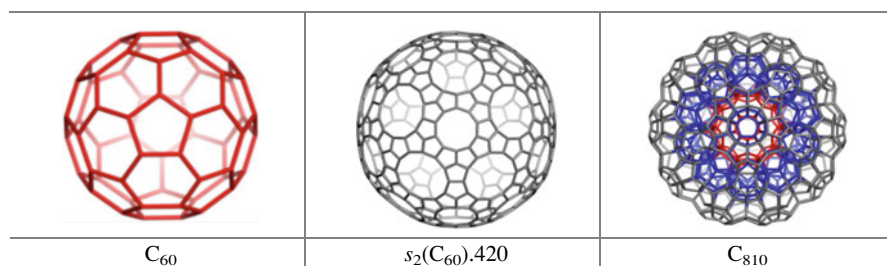
$C_2 \times A_5$; Classes: 12: $|\{30\}; 10\{60\}; \{120\}|$
 9A6

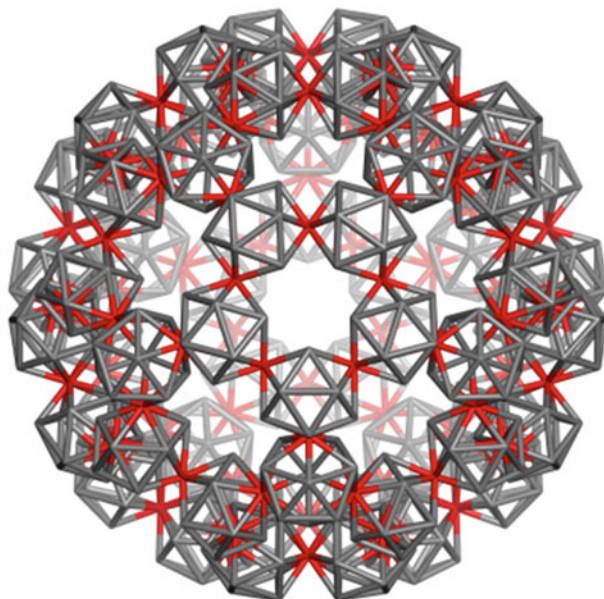
<p>$(12HC_{20}; 20HC_{24}).330$ $t_{set}(p_4(C_{60})).330$ (H=half)</p>	<p>$s_2(C_{60}).420$</p>	<p>$C_{60}P.61$ $P@I.61$ $P^{60}@C_{60}.61$</p>



C₆₀Y(60D).750

9A6a



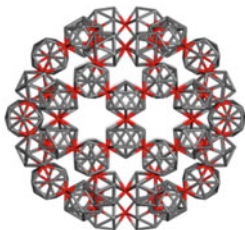


$C_{60}Y(60 I;P).630$

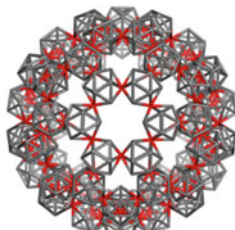
$C_{60}Y(60 dC_{20})_{sp}$
 $d(C_{750}).630_{sp}$

$C_2 \times A_5$; Classes 8: $|\{30\};4\{60\};3\{120\}|$

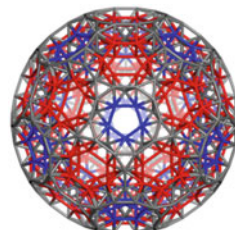
9A6.1



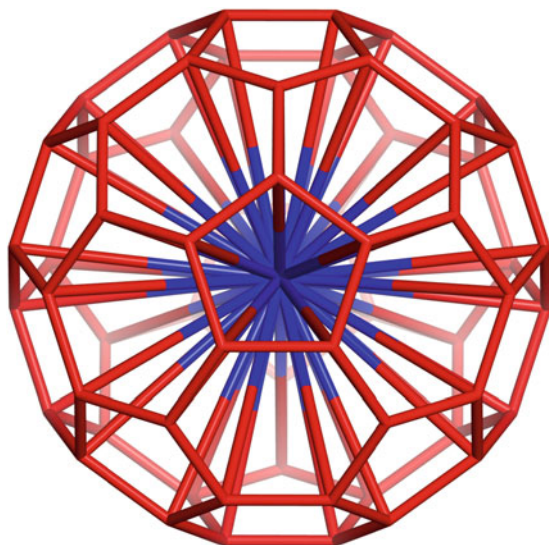
$d(C_{750}).630_{sp_2}$



$d(C_{750}).630_{sp_3}$



$d(C_{750}).630_5$



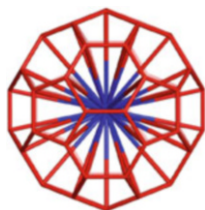
C₆₀P⁶⁰.61

P⁶⁰@C₆₀.61

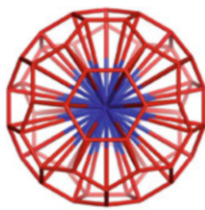
cd(C₇₅₀)

C₂ × A₅; Classes 2 |{1}|; {60}|

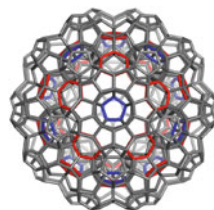
9A6.1a



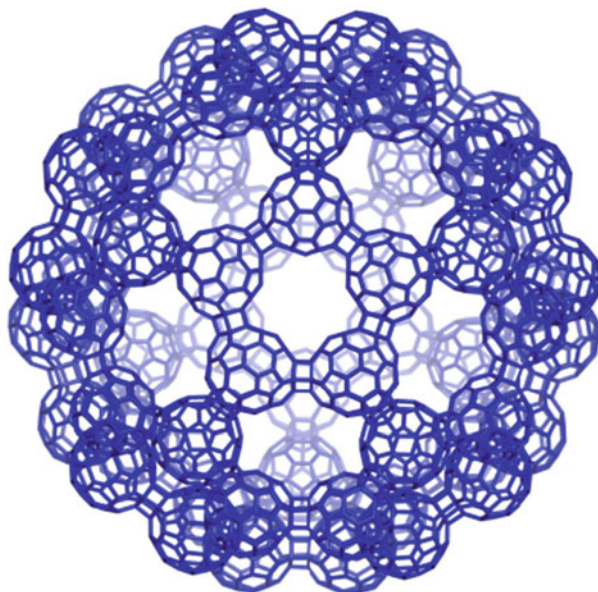
C₆₀P⁶⁰.61_2



C₆₀P⁶⁰.61_3



C₆₀Y(60D).750



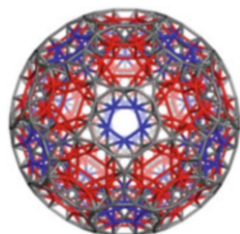
$C_{60}Y(60C_{60};P_5).3600$

$C_{60}Y(60C_{60}; 90P_5).3600$

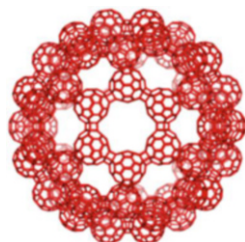
$t(d(C_{750})630).3600$

$C_2 \times A_5$; Classes: 32 |4{60;28{120}}|

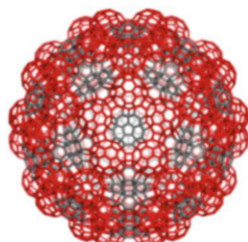
9A6.1.1



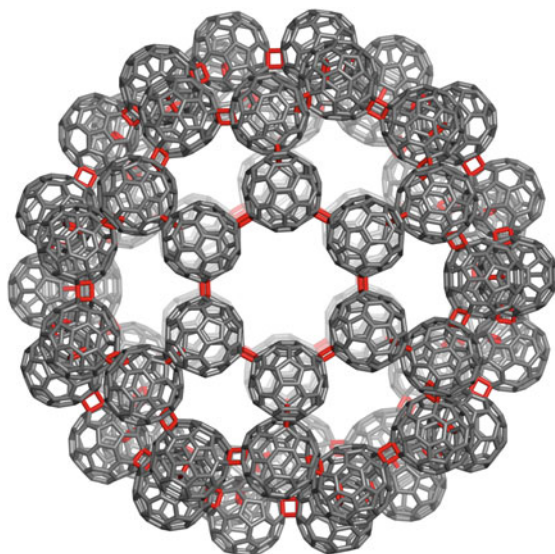
$d(C_{750}).630_5$



C_{3600_3}

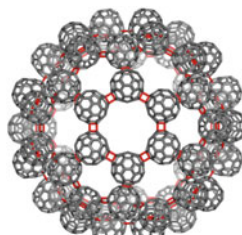
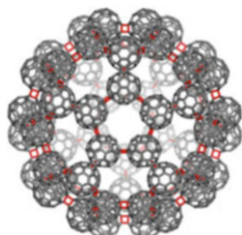
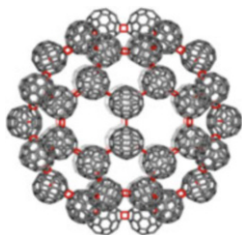


C_{3600}/C_{5040_5}



C₆₀Y(60C₆₀;hh[2+2]).3600

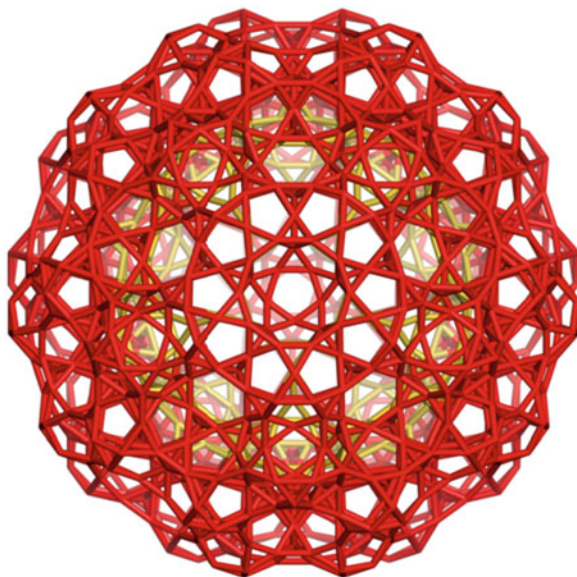
C₆₀Y(60C₆₀; 90sq).3600
 C₂ × A₅; Classes: 32 |4{60};28{120}|
 9A6.1.1a



C₆₀Y(60C₆₀;hh[2+2]).3600_2

C₆₀Y(60C₆₀;hh[2+2]).3600_5

C₆₀Y(60C₆₀;ph[2+2]).3600_3



$C_{60}Y(60 \text{ ID}; f_5).1350$

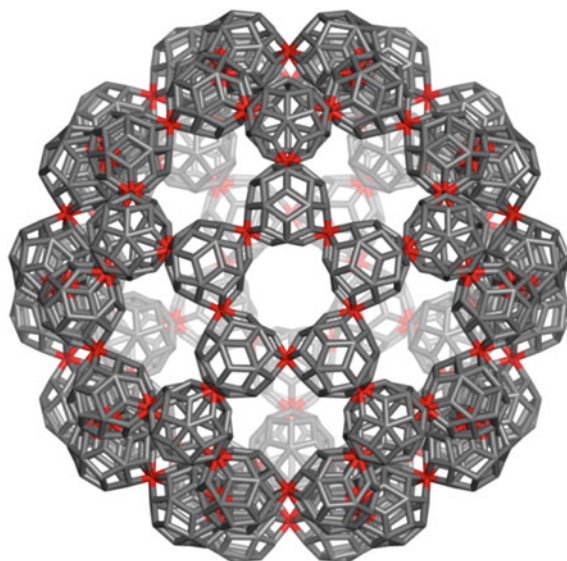
$t(C_{60})@(12(2 \times hm(C_{20})); 20(2 \times hm(C_{24})); 60m(C_{20}); 450T).1350$

$m(C_{750}).1350$

$C_2 \times A_5$; Classes: 17 | {30}; 10 {60}; 6 {120}|

9A6.2

<p>$t(C_{60}).180$</p>	<p>$m(C_{20}).30=ID.30$</p>	<p>C_{24}</p>

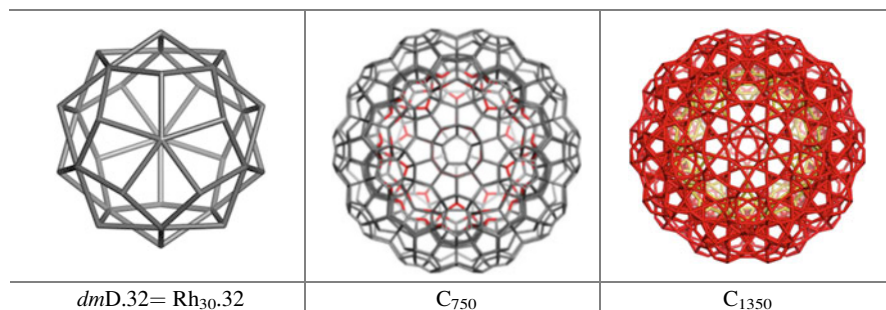


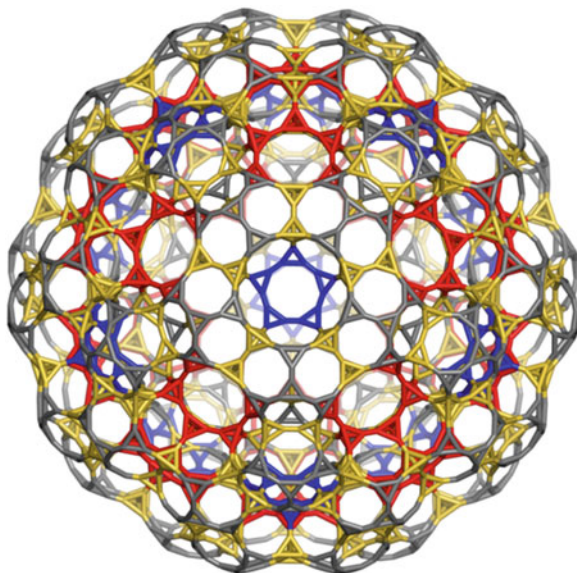
C₆₀Y(60 Rh₃₀;P).1830

$d(m(C_{750})1350).1830$

$C_2 \times A_5$; Classes: 20 |{30};8{60};11{120}|

9A6.2.1



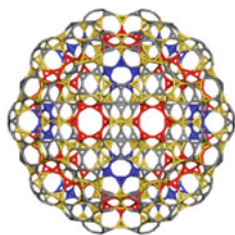


$C_{60}Y(60 \text{ TD}; f_{10}).2700$

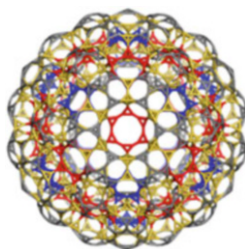
$t(C_{750}).2700$

$C_2 \times A_5$; Classes 32: $|19\{60\}; 13\{120\}|$

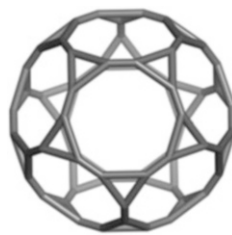
9A6.3



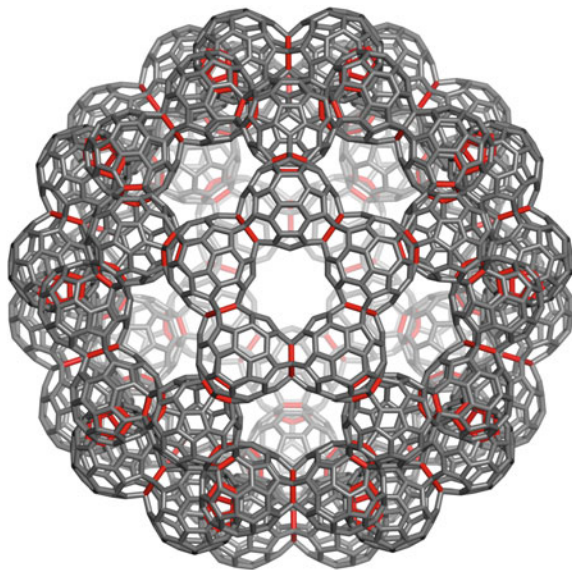
$t(C_{750}).2700_2$



$t(C_{750}).2700_3$



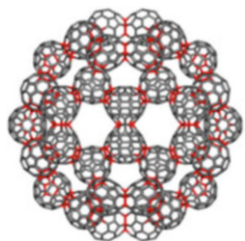
$t(C_{20}).60 = \text{TD}$



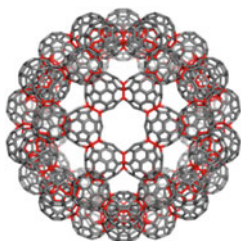
$C_{60}Y(60 C_{60}; f_5).3150$

$I(C_{750}).3150$

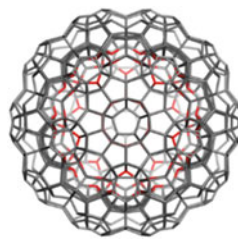
$C_2 \times A_5$; Classes 32: $|\{30\}; 10\{60\}; 21\{120\}|$
9A6.4



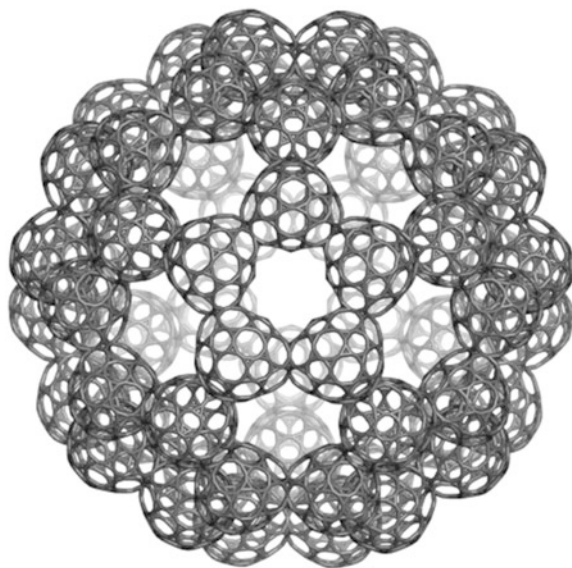
$I(C_{750}).3150_2$



$I(C_{750}).3150_3$



C_{750_5}

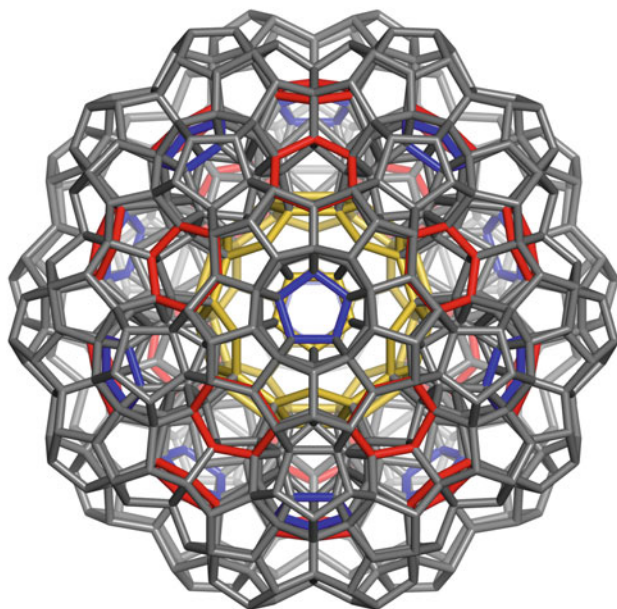


$C_{60}Y(60 \text{ } t(C_{60}); f_{10}).9900$

$t(I(C_{750})3150).9900$
 $C_2 \times A_5$; Classes 92: $|19\{60\}; 73\{120\}|$

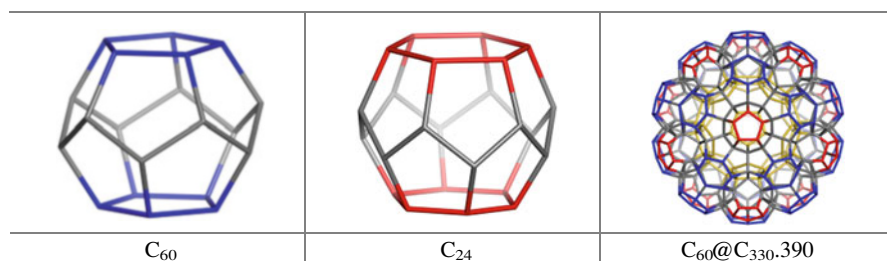
9A6.4.1

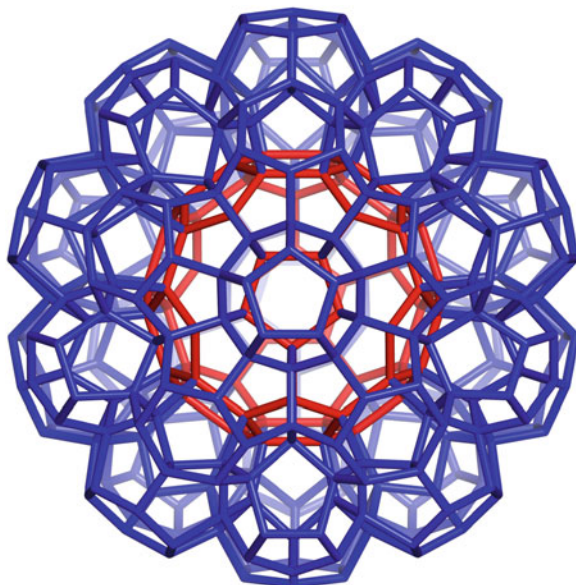
<p>C_{9900_2}</p>	<p>C_{9900_3}</p>	<p>$t(C_{60}).180$</p>



C₆₀@C₇₅₀₋₈₁₀

C₆₀@(12C₂₀;20C₂₄)@(60C₂₀).810
 C₂ × A₅; Classes: 13 |{30};11{60};{120}|
 9A7

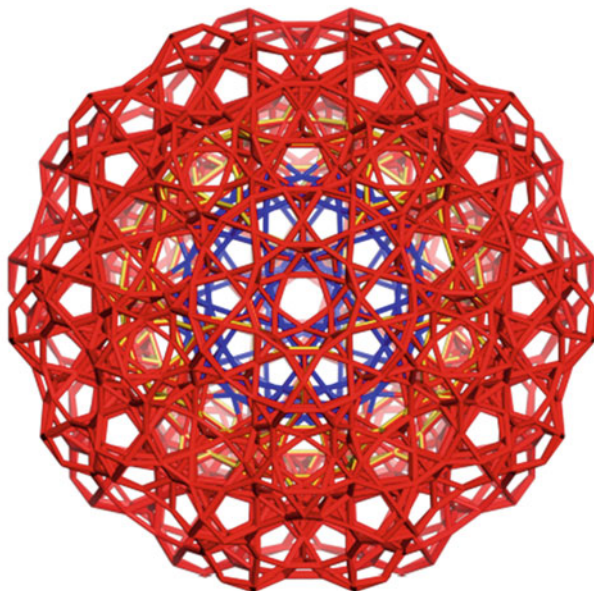




$C_{60}Y(12C_{20};20C_{24};f_5).390$

$C_{60}@((12C_{20};20C_{24}).390$
 $C_2 \times A_5$; Classes: 7 |{30};6{60}|
 9A7a

<p>C_{20}</p>	<p>C_{24}</p>	<p>$(12HC_{20};20HC_{24}).330$ $t_{se}(p_4(C_{60})).330$</p>

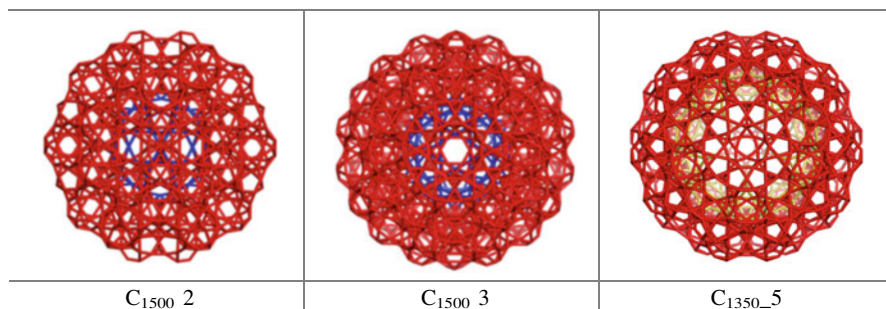


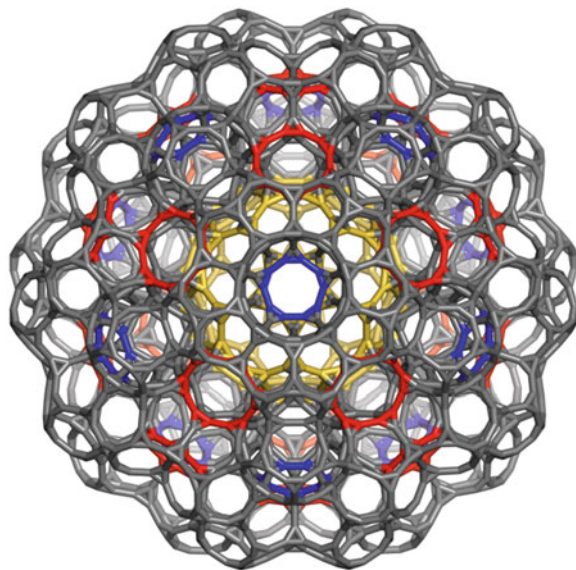
$m(\text{C}_{60})@(12m(\text{C}_{20});20m(\text{C}_{24});60m(\text{C}_{20});570\text{T}).1500$

$m(\text{C}_{810}).1500$

$\text{C}_2 \times \text{A}_5$; Classes: 20 |2{30};12{60};6{120}|

9A7.1

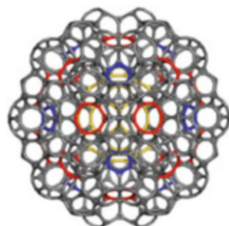




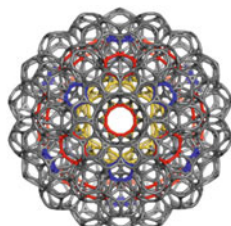
$t(C_{60})@(12t(C_{20});20t(C_{24});60t(C_{20});570T).3000$

$t(C_{810}).3000$

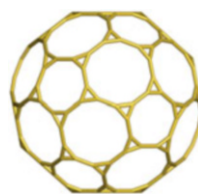
$C_2 \times A_5$; Classes 36: $|22\{60\};14\{120\}|$
9A7.2



$t(C_{810}).3000_2$



$t(C_{810}).3000_3$



$t(C_{60}).180$

References

- Bergman G, Waugh JLT, Pauling L (1952) Crystal structure of the intermetallic compound Mg₃₂(Al, Zn)₄₉ and related phases. *Nature* 169:1057–1058
- Bhattacharya D, Klein DJ, Ortiz Y (2016) The astounding buckyball buckyball. *Chem Phys Lett* 647:185–188
- Diudea MV (2013) Quasicrystals, between spongy and full space filling. In: Diudea MV, Nagy CL (eds) *Diamond and related nanostructures*. Springer, Dordrecht, pp 333–383
- Diudea MV, Rosenfeld VR (2017) The truncation of a cage graph. *J Math Chem* 55:1014–1020
- Euler L (1752–1753) *Elementa doctrinae solidorum-Demonstratio nonnullarum insignium proprietatum, quibus solida hedris planis inclusa sunt praedita*. *Novi Comment Acad Sc Imp Petropol* 4:109–160
- Nagy CL (2016) Symmetry computation by Mathematica (to be published)
- Nagy CL, Diudea MV (2009) Nano studio software. Babes–Bolyai University, Cluj
- Stefu M, Parvan-Moldovan A, Kooperazan-Moftakhar F, Diudea MV (2015) Topological symmetry of C₆₀-related multi-shell clusters. *MATCH Commun Math Comput Chem* 74:273–284

Chapter 10

Chiral Multi-tori

Chirality refers to the dichotomous diversity, as the mirror images of the two human hands, impossible to superpose to each other by rotation-translation in the plane. The mirror images of a chiral molecule are called enantiomers. The term *chirality* comes from the Greek word for hand, χείρ (kheir); this term was introduced by Lord Kelvin in 1894 (1904).

Chirality is one of the basic characteristics of biological structures, starting with aminoacids and glucides, as main constituents of animal body. Chirality is not a condition for biological activity; however, many biologically active molecules are chiral, then optical active. Enzymes, which are chiral, may distinguish between the two enantiomers of a chiral substrate. Chirality is a symmetry property. A chiral molecule has no improper axis of rotation S_n (which includes planes of symmetry and an inversion center) and is always dissymmetric but not asymmetric (no symmetry elements except the identity).

Symmetry (from Greek συμμετρία *symmetria* “agreement in dimensions, due proportion, arrangement”) commonly refers to harmony of proportions in realization of a composition (Hargittai and Hargittai 2010). The simplest symmetry is the mirror symmetry. In Mathematics, symmetry refers to some operations acting on geometric or other regularities of a mathematical object that leave the object invariant. While the classical, geometric symmetry is involved/reflected in several molecular properties, such as dipole moments, IR vibrations, ^{13}C -NMR signals etc., topological symmetry, defined in terms of *connectivity*, is addressed to constitutive aspects of a molecule and is involved in its synthesis and/or its structure elucidation.

10.1 Design of Chiral Multi-tori

An embedding is a representation of a graph on a surface S such that no edge-crossing occurs (Harary 1969). A polyhedral graph, embedded in an orientable surface S obeys the Euler’s formula (Euler 1752–1753):

$$v - e + f = \chi(S) = 2(1 - g)$$

where $\chi(S)$ is the Euler characteristic and g the genus (i.e., the number of consisting simple tori). Positive/negative χ -values indicate positive/negative curvature of a structure embedded in S . A surface is orientable, when it has two sides, or it is non-orientable, when it has only one side, like the Möbius strip.

Curvature (Diudea and Nagy 2007) is the amount by which a geometric object deviates from the planarity; it is usually measured as the Gaussian curvature K , $\int_S K dS = 2\pi\chi$; a combinatorial curvature was also proposed (Klein and Liu 1994; Babić et al. 2001; Higuchi 2001; Klein 2002).

Euler characteristic can be calculated as the alternating sum of figures of dimension/rank k (Schulte 1985, 2014):

$$\chi(S) = f_0 - f_1 + f_2 - f_3 + \dots,$$

where f_0 is a vertex, f_1 is an edge, f_2 is a face, f_3 is a cell . . . f_k being a facet of rank k ; a structure will have the rank k if there are substructures/facets up to the rank $k-1$ and obey relation (4); in case $S = \text{sphere}$, alternates 2 and 0 for odd and even rank, respectively.

Multi-tori are complex structures consisting of more than one torus, embedded in negatively curved surfaces (Diudea and Nagy 2007; Mackay and Terrones 1991; Lenosky et al. 1992; Terrones and Mackay 1997; Lijnen and Ceulemans 2005) they are supposed to result by self-assembling of some repeat units/monomers, formed e.g., by opening of cages/fullerenes and appear in natural zeolites (Meier and Olson 1992) or in spongy carbon (Benedek et al. 2003; Barborini et al. 2002).

Design of multi-tori may be achieved by operations on maps. A map is a combinatorial representation of a (closed) surface, e.g., a polyhedral graph. Several operations on maps are known and used for various purposes. The most used operations are: dual d , medial m , truncation t , leapfrog l , snub s , etc.; applying these operations preserves the symmetry of the parent polyhedron. More about such operations the reader can find in Chap. 2.

A real building process of multi-tori herein studied may occur as a self-assembling of monomers; in this case, the monomer is a snub cage, particularly the snub of Platonic solids. Let's follow such a way, starting from a polyhedron P .

The snub polyhedron $s(P)$ is achieved by dualizing the $p_5(P)$ transform: $s(P) = d(p_5(P))$; since p_5 -operation is *prochiral*, all the consecutive p_5 transforms will be chiral structures. Let now scale $s(P)$ to $k(s(P))$ by an arbitrary k factor and realize a "cage-in-cage" dimer, $s(P)@k(s(P))$, then add a new connection along the diagonal of quadrilaterals appearing by dimerization on the borders of window faces f_w of P , each vertex thus getting the degree 7, that is specified in the name of actual dimer as $s(P)@k(s(P))7$; since this diagonal may be drawn to the right (R) or to the left (S) (the same is true for the operations p_5R and p_5S), so that the number of chiral pair structures will further increase. If the p_5 -operation is explicitly written in the name of dimer $s(P)@k(s(P))7$, the following isomers may result:

- (i) $d(p_5S)@k(d(p_5S))7R$; (ii) $d(p_5R)@k(d(p_5R))7S$; (iii) $d(p_5S)@k(d(p_5S))7S$;
 (iv) $d(p_5R)@k(d(p_5R))7R$; (v) $d(p_5S)@k(d(p_5R))7R$; (vi) $d(p_5S)@k(d(p_5R))7S$

Among these isomers, the last two may be differentiated topologically, contrarily to the first four ones; the operations p_5R/p_5S may commute so that the order is not important. A further dualization of a 7-connected dimer will provide a multi-torus entirely covered by heptagonal faces. Such an all-7 face multi-torus can also be done by identifying the windows of an “open” object made by the sequence: $o(s_1(P))$, P being a Platonic polyhedron, arranged as a “cell-in-cell” dimer (Diudea and Petitjean 2008, 2016).

Snub dodecahedron is shown, together with the corresponding dimer (Fig. 10.1), as chiral pairs. Observe the diagonals (to the left and to the right) in the central pentagonal window.

Design and computations were performed by Nano Studio (Nagy and Diudea 2009) original software developed at TOPO GROUP Cluj. Structures will be presented grouped according to the main polyhedron (Platonics and C_{60}), with additional comments and Atlas figures, numbered 10A n .

Structure elucidation of the snub dimers and multi-tori herein studied was done by: (i) Figure count, (by Euler alternating sum); (ii) Face count (by Ring Signature Index RSI) and (iii) Centrality count (see Chap. 4). The chiral index, as calculated by Petitjean’s (2016) QCM software, is close to unity for most of these structures.

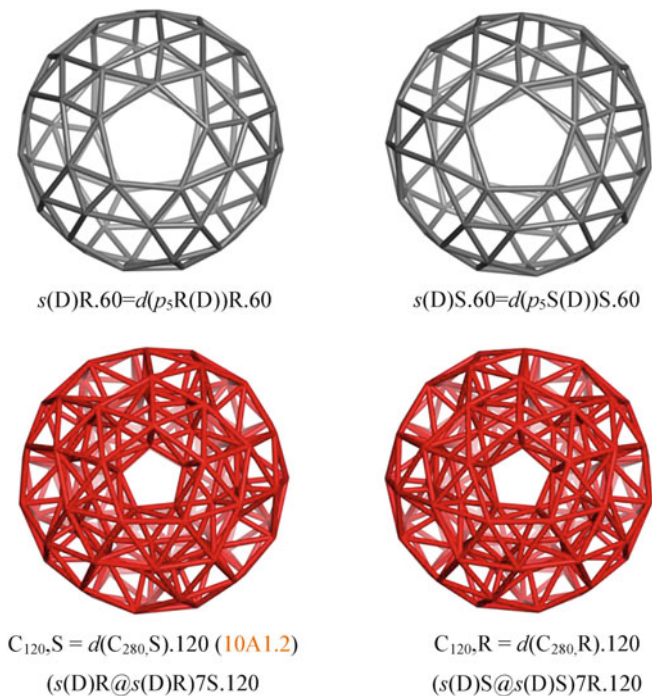


Fig. 10.1 Snub dodecahedron and its dimer (as chiral pairs)

10.2 Dodecahedron Related Structures

Dualization of snub dodecahedron dimers leads to C_{280} (10A1) all-7 faces multi-tori, as shown in Fig. 10.2 (chiral pairs). They belong to the symmetry group A_5 , of order 60. A similar multi-torus may be designed by identifying the window faces of the “open” object $o(s_1(D)).200$ (Fig. 10A1.3b, left), arranged face-to-face, as in a “cage-in-cage” dimer; to relax the strain, several rows of hexagons were added to the incipient cones, so that an object of 1220 vertices (1830 edges, 470 hexagons and 120 heptagons) was obtained; further it was transformed by leapfrog operation to the beautiful object in Fig. 10.3 (right) (Diudea and Nagy 2007; Diudea and Petitjean 2008, 2016).

Dualization may be imagined as a “complementary synthesis” in the “template” of its dual pair, the parent being further “solved” to deliver the desired product.

Among several map operations herein described and used, truncation benefits of a nice theoretical result (Diudea and Rosenfeld 2017) stating that: a necessary and sufficient condition for a simple cubic graph G , without quadrilaterals, to be isomorphic to the truncation $t(H)$ of a simple cubic graph H is possessing by G a cyclic cover C of which all components are triangles (Fig. 10A1.3b, right).

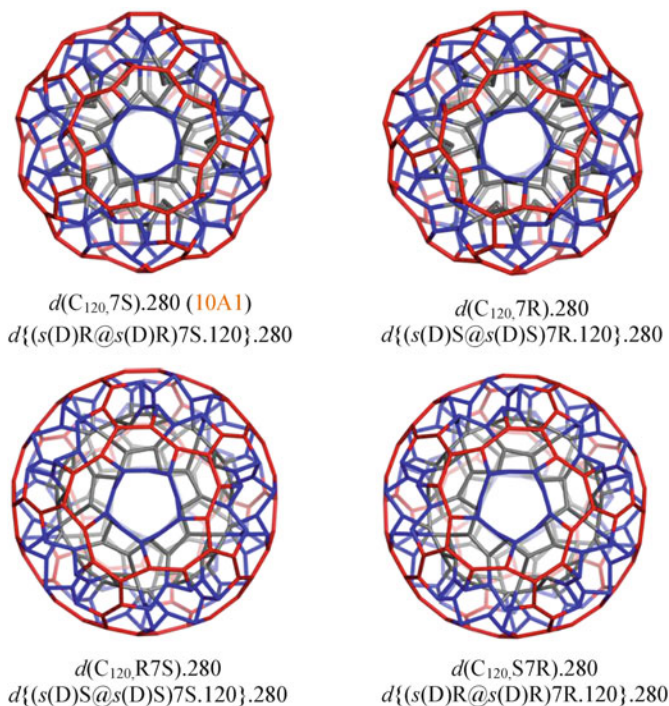


Fig. 10.2 Snub dodecahedron based multi-tori; chiral pairs

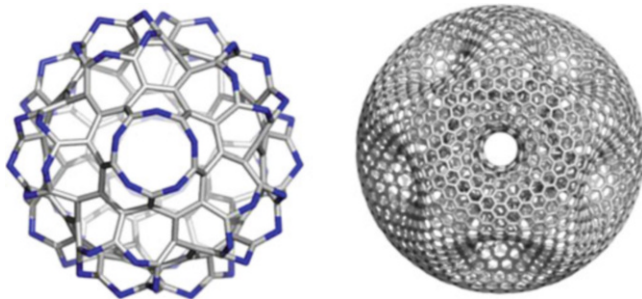


Fig. 10.3 An “open” cage with all-7 faces, derived from the dodecahedron, $o(s_I(D)).200$ (left) used as the core for a multi-torus ($g = 11$), of which leapfrog transform $l(C_{1220}).3660$ is shown in the right part of this figure

Table 10.1 Figure count in snub dodecahedron relatives

Structure	v	e	3(2)	4(2)	5(2)	7(2)	2	3	χ	g	k
$s(D)$	60	150	80	0	12	0	92	0	2	0	3
C_{280} (10A1)	280	420	0	0	0	120	120	0	-20	11	3
C_{280C}	280	420	0	0	0	120	120	2	-22	12	4
$d(C_{280})$ (10A1.2)	120	420	280	90	24	0	394	94	0	0	4
$d(C_{280})_{sp}$	120	420	280	90	0	0	370	80	-10	6	4
$d(C_{280})$ (10A1.2)				A_5	P_3	P_3^*	M	3			
(for 3)				12	20	60	2	94			

P_3^* is a slightly modified P_3

Multi-tori are graphs embedded in surfaces of high genera; Table 10.1 shows a negative value for Euler characteristic: $\chi = -20$; $g = 11$ for C_{280} (a structure of Icosahedral symmetry), meaning the embedding surface has a negative curvature. However, if one considers the multi-torus as being a union of two cells, as in C_{280C} , the result is: $\chi = -22$; $g = 12$, according to the 12 connections of the embedding surface (of each of these halves).

Recall that the snub dimer is the dual of the multi-torus herein studied: $C_{120} = d(C_{280})$ (10A1.2); its 3-facets are detailed at the bottom of Table 10.1. It may be seen as a “spongy” structure, $d(C_{280})_{sp}$, of genus $g = 6$, with the windows seen as hollows.

The genus and rank (or space dimension) of a structure are parameters of its complexity, the balance of their importance being in the looking eye; the genus of these multi-tori equals the number of windows/hollows less 1. Irrespective of the tessellation (read: map operation transform), the embedding surface has the same Euler characteristic, as can be seen in Table 10.2, in case of several relatives of C_{280} (10A1) multi-torus, made by using various map operations. These structures are illustrated in the Atlas of this chapter.

Searching the atom classes by face count provides the “chemical vertex type” if the rings around each atom (counted by RSI—Nagy and Diudea 2017)) are “strong rings” (Blatov et al. 2010); for the majority of snub derivatives a single chemical

Table 10.2 Figure count in C_{280} (10A1) relatives

Structure	v	e	3(2)	4(2)	6(2)	7/14*(2)	2	χ	g	k
C_{280} (10A1)	280	420	0	0	0	120	120	-20	11	3
$t(C_{280})$ (10A1.3)	840	1260	280	0	0	120*	400	-20	11	3
$s(C_{280})$ (10A1.4)	840	2100	1120	0	0	120	1240	-20	11	3
$m(C_{280})$ (10A1.5)	420	840	280	0	0	120	400	-20	11	3
$d(m(C_{280}))(10A1.5.1)$	400	840	0	420	0	0	420	-20	11	3
$l(C_{280})$ (10A1.6)	840	1260	0	0	280	120	400	-20	11	3
$p_4(C_{280})$ (10A1.7)	820	1680	0	840	0	0	840	-20	11	3
$d(p_4(C_{280}))$ (10A1.7.1)	840	1680	280	420	0	120	820	-20	11	3

Face $f=10$ when *

vertex class was found (Table 10.3). However, by enlarging the counted rings to “circuits” of various length, then different vertex classes are revealed. If the “ring signatures” are collected in a layer matrix (Diudea 1994; Diudea and Ursu 2003), the centrality index (calculated cf. Eq. 4.7) may recognize all the topologically distinct vertices, even at the early level of hard rings (Table 10.3).

Remark that the dimer $d(C_{280}).120$ (10A1.2), also those derived from the cube and tetrahedron, have a single class of all central atoms; such self-centered graphs have extensively been studied (Buckley 1979, 1989; Janakiraman and Ramanujan 1992; Negami and Xu 1986; Nazeer et al. 2016).

10.3 Cube Related Structures

Snub cube is shown, together with the corresponding dimer (Fig. 10.4) as chiral pairs. Dualization of dimers leads to C_{112} all-7 faces multi-tori, as shown in Fig. 10.5 (steric isomers). They belong to the symmetry group S_4 , of order 24.

Figure count in snub cube relatives is shown in Table 10.4 while for the transformed C_{112} by map operations data are given in Table 10.5. Excepting symmetry, there is no difference between the structures derived from the cube to those derived from the dodecahedron.

Searching the atom classes, by face count, providing the “chemical vertex type” if the rings counted are “strong rings” and by the centrality index, is shown for the cube derivatives in Tables 10.6 and 10.7.

Here the face count was more detailed, specifying the maximum length ring needed to correctly solve the topological vertex classes. In case of centrality index, even the values changed with R_{\max} changing, the ordering with respect to the center of the graph remained unchanged. The dimer $d(C_{112}).48$ has a single class of all central atoms.

Table 10.3 Atom classes by face count (left) and centrality (right) for C_{280} relatives

Structure	RSI	Class	{ <i>v</i> }	Deg	Ring sign.	C-sign. (class no.)
C_{280} (10A1)	3.000	1	280	3	$7^{\wedge}3$	–
		1	20	3	$7^{\wedge}3$	0.050631
		2	20	3	$7^{\wedge}3$	0.050584
		3	60	3	$7^{\wedge}3$	0.050476
		4	60	3	$7^{\wedge}3$	0.050476
		5	60	3	$7^{\wedge}3$	0.050343
		6	60	3	$7^{\wedge}3$	0.050154
$s(D).60$	2.125	1	60	5	$3^{\wedge}4.5$	0.077345
$d(C_{280}).120$ (10A1.2)	5.917	1	120	7	$3^{\wedge}7.4^{\wedge}5.5^{\wedge}6$	0.053343
$m(C_{280}).420$ (10A1.5)	2.000	1	420	4	$3^{\wedge}2.7^{\wedge}2$	–
		1	60	4	$3^{\wedge}2.7^{\wedge}2$	0.049904
		2	60	4	$3^{\wedge}2.7^{\wedge}2$	0.049858
		3	30	4	$3^{\wedge}2.7^{\wedge}2$	0.049773
		4	30	4	$3^{\wedge}2.7^{\wedge}2$	0.049736
		5	60	4	$3^{\wedge}2.7^{\wedge}2$	0.049632
		6	60	4	$3^{\wedge}2.7^{\wedge}2$	0.049512
		7	60	4	$3^{\wedge}2.7^{\wedge}2$	0.049497
		8	60	4	$3^{\wedge}2.7^{\wedge}2$	0.046636
$d(m(C_{280})).400$ (10A1.5.1)	2.100	1	120	7	$4^{\wedge}7$	–
	–	2	280	3	$4^{\wedge}3$	–
		1	20	3	$4^{\wedge}3$	0.051589
		2	20	3	$4^{\wedge}3$	0.051555
		3	60	7	$4^{\wedge}7$	0.048170
		4	60	7	$4^{\wedge}7$	0.048167
		5	60	3	$4^{\wedge}3$	0.048117
		6	60	3	$4^{\wedge}3$	0.048103
		7	60	3	$4^{\wedge}3$	0.048052
		8	60	3	$4^{\wedge}3$	0.048049
$l(C_{280}).840$ (10A1.6)	1.462	1	840	3	$6^{\wedge}2.7$	$14 \times \{60\}$
$p_4(C_{280}).820$ (10A1.7)	1.366	1	120	7	$4^{\wedge}7$	$16: 2 \times \{20\};$ $2 \times \{30\}; 12 \times \{60\}$
		2	420	4	$4^{\wedge}4$	–
		3	280	3	$4^{\wedge}3$	–
$d(p_4(C_{280})).840$ (10A1.7.1) ((C_{280})).400	2	1	840	4	$4^{\wedge}2$	$14 \times \{60\}$
$t(C_{280}).840$ (10A1.3)	1.824	1	840	3	$3.14^{\wedge}2$	$14 \times \{60\}$

10.4 Tetrahedron Related Structures

Snub tetrahedron is just the icosahedron, and thus non-chiral. The window faces are the same as the triangles promoted by snub operation, thus making difficult the choice. Nevertheless, the window faces proved to be disjoint and problem was solved.

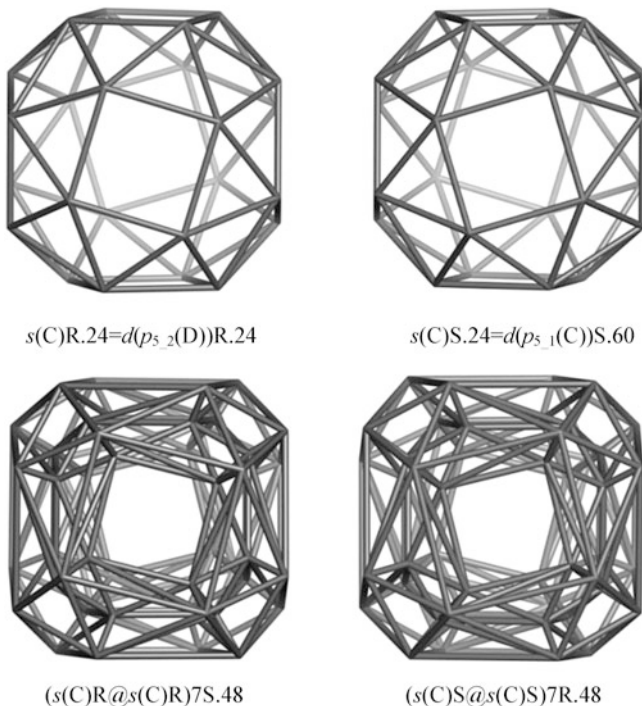


Fig. 10.4 Snub cube and its dimer; chiral pairs

The dimers (R and S) are shown in Fig. 10.6 (top) while their duals are shown in the bottom of this figure. They belong to the symmetry group A_4 , of order 12.

Figure count in snub tetrahedron relatives is shown in Table 10.8 and follows the same rules as in case of cube and dodecahedron.

10.5 C_{60} Related Structures

Departing from Platonic solids but keeping the icosahedral symmetry, let us draw the snub C_{60} ; its dimerization leads to $s(C_{60})@s(C_{60})7.360$ (Fig. 10A2b); then it can be dualized to the multitorus $d(C_{360}, 7).840$ (Fig. 10A2), with all 7-faces and having 32 window faces f_w (12 10-faces and 20 12-faces, respectively) to the central hollow (exactly the number of pentagonal and hexagonal faces of C_{60}).

Figure and genus count for the C_{60} -related structures are given in Tables 10.9 and 10.10. One can see that only the dual of C_{840} (namely the parent snub 7-dimer C_{360} (10A2.1)), in “spongy” state, shows χ and g normal values for C_{60} -related clusters: -30 and 16 ($g = f_w/2 = 16$), respectively. In case of C_{840} (10A2) and its relatives, the normal values are: -60 and 31 , respectively ($g = f_w - 1$), giving account for their “dimer”-state. Indeed, if one considers a structure like $o(s_1(C_{60})).600$ (Fig. 10A2b, right), by identifying the 32 window faces with its copy, the multi-torus C_{840} (10A2)

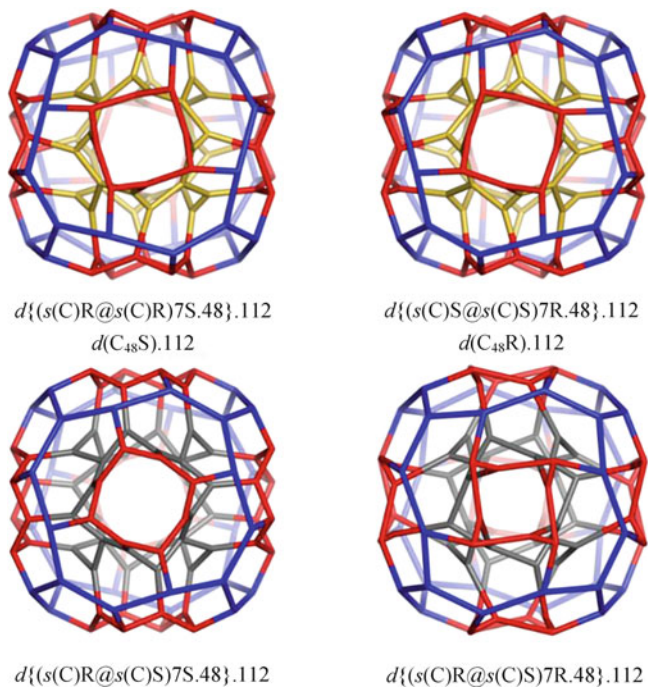


Fig. 10.5 Dual of snub cube dimers

Table 10.4 Figure count in snub cube relatives

Structure	v	e	3(2)	4(2)	7(2)	2	3	χ	g	k
$s(C)$	24	60	32	6	0	38	0	2	0	3
C_{112}	112	168	0	0	48	48	0	-8	5	3
C_{112C}	112	168	0	0	48	48	2	-10	6	4
$d(C_{112})$	48	168	112	48	0	160	40	0	0	4
$d(C_{112})_{sp}$	48	168	112	36	0	148	32	-4	3	4
$d(C_{112})$ (for 3)			A ₄	P ₃	P ₃ *	M	3			
			6	8	24	2	40			

Face $f=10$ when *

Table 10.5 Figure count in C₁₁₂ relatives (Symmetry group S₄; order 24)

Structure	v	e	3(2)	4(2)	6(2)	7(2)	2	χ	g	k
C_{112}	112	168	0	0	0	48	48	-8	5	3
$p_4(C_{112})$	328	672	0	336	0	0	336	-8	5	3
$d(p_4(C_{112}))$	336	672	112	168	0	48	328	-8	5	3
$l(C_{112})$	336	504	0	0	112	48	160	-8	5	3
$s(C_{112})$	336	840	448	0	0	48	496	-8	5	3

Table 10.6 Atom classes by face count and centrality count for C_{112} relatives

Structure	R_{\min}	R_{\max}	Signature (centrality)	Classes {elements}	Deg	RSI
<i>Face count</i>						
$C_{112}(\text{all})$	7	7	$7^{\wedge}3$	1: {112}	3	3.000
$C_{112}(\text{R};\text{RS};\text{SR};\text{S})$	7	14	–	6	3	2.655701
$C_{112}((\text{CP}_5\text{R}@\text{CP}_5\text{S})\text{7R})$	7	10	$7^{\wedge}3.10^{\wedge}2$ $7^{\wedge}3.10^{\wedge}3$ $7^{\wedge}3.8.10^{\wedge}2$	3: {48} {16} {48}	3	0.767395
$C_{112}((\text{CP}_5\text{R}@\text{CP}_5\text{S})\text{7S})$	7	8	$7^{\wedge}3$ $7^{\wedge}3.8$ $7^{\wedge}3.8^{\wedge}2$	3: {16} {48} {48}	3	0.771429
<i>Centrality count</i>						
$\text{LM}(C_{112})$ (R;RS;SR;S)	7	7	(0.090031) (0.089815) (0.089686) (0.089161) (0.088863) (0.088650)	6: {8} {24} {8} {24} {24} {24}	3	–
$C_{112}((\text{CP}_5\text{R}@\text{CP}_5\text{S})\text{7R})$	7	7	(0.090984) (0.090292) (0.090177)	3: {48} {16} {48}	3	–
	7	10	(0.087529) (0.086770) (0.086560)	3: {48} {16} {48}	3	–
$C_{112}((\text{CP}_5\text{R}@\text{CP}_5\text{S})\text{7S})$	7	7	(0.084265) (0.084091) (0.083930)	3: {16} {48} {48}	3	–
	7	8	(0.082919) (0.082463) (0.082076)	3: {16} {48} {48}	3	–

Table 10.7 Symmetry of multi-tori C_{112}

Structure	Symmetry group	Orbit size
$d\{(s(\text{C})\text{S}@\text{s}(\text{C})\text{S})\text{7R}.48\}.112$	S_4	6: 2{8};4{24}
$d\{(s(\text{C})\text{R}@\text{s}(\text{C})\text{R})\text{7S}.48\}.112$	S_4	6: 2{8};4{24}
$d\{(s(\text{C})\text{R}@\text{s}(\text{C})\text{S})\text{7R}.48\}.112$	S_4	6: 2{8};4{24}
$d\{(s(\text{C})\text{R}@\text{s}(\text{C})\text{S})\text{7S}.48\}.112$	S_4	6: 2{8};4{24}
$C_{112}((\text{CP}_5\text{R}@\text{CP}_5\text{S})\text{7R})$	$C_2 \times S_4$	3: 1{16};2{48}
$C_{112}((\text{CP}_5\text{R}@\text{CP}_5\text{S})\text{7S})$	$C_2 \times S_4$	3: 1{16};2{48}

is obtained; if the number of cells (3-faces) is 2 (i.e., dimer—see Table 10.9, entry $C_{840}\text{C}$), the result is $\chi = -62$ and accordingly $g = 32$, in agreement with an idea that the genus counts the number of connections of a given surface (in this case, exactly two surfaces close the connections to each other).

Counting the rings around vertices (Nagy and Diudea 2017) provides the “chemical vertex type” classes (if the rings are the “strong” ones) or the

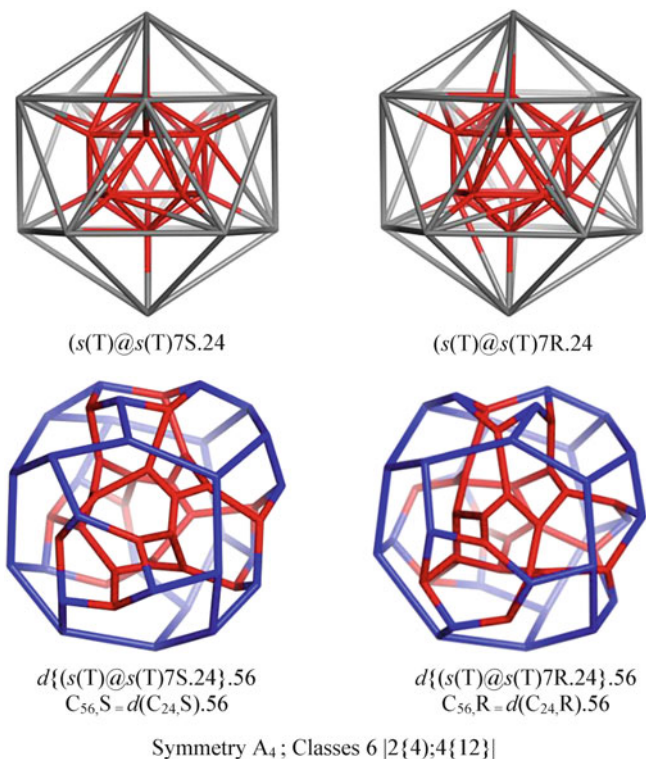


Fig. 10.6 Snub tetrahedron and its chiral derivatives

Table 10.8 Figure count in snub tetrahedron relatives

Structure	v	e	3(2)	4(2)	7(2)	2	3	χ	g	k
$s(T)$	12	30	20	0	0	20	0	2	0	3
C_{56}	56	84	0	0	24	24	0	-4	3	3
C_{56C}	56	84	0	0	24	24	2	-6	4	4
$d(C_{56})$	24	84	64	18	0	82	22	0	0	4
$d(C_{56})_{sp}$	24	84	56	18	0	74	16	-2	2	4
$d(C_{56})$			A_4	P_3	P_3^*	M	3			
(for 3)			4	4	12	2	22			

“topological vertex type” classes (if the rings are circuits long enough), equaling the number of “centrality vertex type” classes (obtained at the early stage of strong rings), as shown in Table 10.11. Structure C_{840} (10A2) is a special hyper- C_{60} structure, as its 14 classes each have exactly 60 vertices/atoms, in agreement with the symmetry group A_5 of order 60. The “chemical” vertices form a single class: $1 \times \{840\}$, that could be important in an eventual synthesis. Recall that all the vertex classes counted by C-index (Nagy and Diudea 2009) have been confirmed by symmetry calculation using the adjacency matrix permutations.

Table 10.9 Figure count in snub C_{60} relatives

Structure	v	e	3(2)	4(2)	5(2)	6(2)	7(2)	2	3	χ	g	k
$s(C_{60})$	180	450	240	0	12	20	0	272	0	2	0	3
C_{840} (10A2)	840	1260	0	0	0	0	360	360	0	-60	31	3
C_{840C}	840	1260	0	0	0	0	360	360	2	-62	32	4
$d(C_{840})$ (10A2.1)	360	1260	840	270	24	40	0	1174	274	0	0	4
$d(C_{840})_{sp}$	360	1260	840	270	0	0	0	1110	240	-30	16	4
$d(C_{840})$ (10A2.1) (for 3)				A_5	A_6	P_3	P_3^*	M	3			
				12	20	60	180	2	274			

Table 10.10 Figure count in C_{840} (10A2) relatives

Structure	v	e	3(2)	4(2)	6(2)	7/14*(2)	2	χ	g	k
C_{840} (10A2)	840	1260	0	0	0	360	360	-60	31	3
$m(C_{840})$ (10A2.2)	1260	2520	840	0	0	360	1200	-60	31	3
$d(m(C_{840}))$ (10A2.2.1)	1200	2520	0	1260	0	0	1260	-60	31	3
$l(C_{840})$ (10A2.3)	2520	3780	0	0	840	360	1200	-60	31	3
$t(C_{840})$ (10A2.4)	2520	3780	840	0	0	360*	1200	-60	31	3

Face $f=10$ when *

Table 10.11 Topological symmetry by RSI and centrality C-index of C_{840} cluster and its relatives

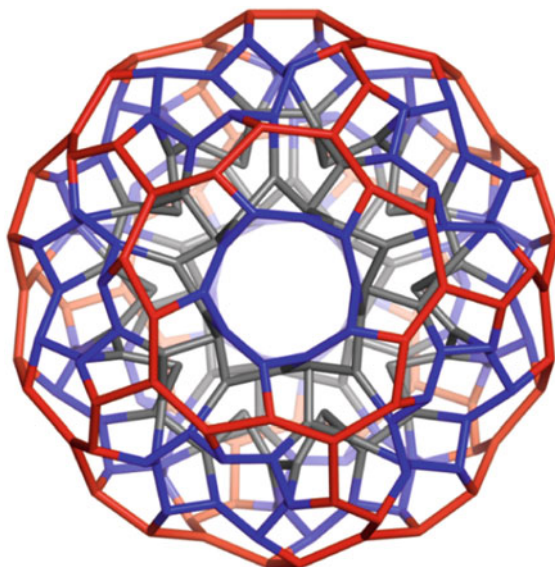
	Structure	R_{min}	R_{max}	Signature ($C_{min};$ C_{max})	Classes {elements}	Deg	RSI
1	C_{840} (10A2)	7	7	$7^{\wedge}3$	$1 \times \{840\}$	3	3
		7	16	—	$14 \times \{60\}$	3	1.410419
	LM(C_{840})	7	7	(0.031336) (0.031245)	$14 \times \{60\}$	3	—
		7	12	(0.028563)	$14 \times \{60\}$	3	—
—	—	—	(0.028473)	—	—	—	
2	$l(C_{840}).2520$ (10A2.3)	6	7	$6^{\wedge}2.7$	$1 \times \{2520\}$	3	1.46154
	LM($l(C_{840}).2520$)	6	7	(0.020287) (0.019819)	$42 \times \{60\}$	3	—
3	$t(C_{840}).2520$ (10A2.4)	3	14	$3.14^{\wedge}2$	$1 \times \{2520\}$	3	1.823529
	LM($t(C_{840}).2520$)	3	14	(0.016973) (0.016659)	$42 \times \{60\}$	3	—

In Diudea and Rosenfeld (2017) it was stated that: a necessary and sufficient condition for a simple cubic graph G , to be isomorphic to the truncation $t(H)$ of a simple cubic graph H is that G has a cyclic cover C of which all components are triangles. Such a triangle disjoint covering is illustrated for the truncated structure, $t(C_{840}).2520$ (10A2.4b, right).

Structures derived from snub C_{60} are illustrated in the Atlas of this section.

Chapter 10 Atlas: Chiral Multi-tori

Dodecahedron Related Structures


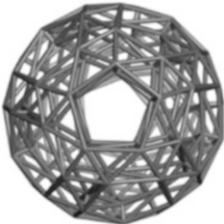
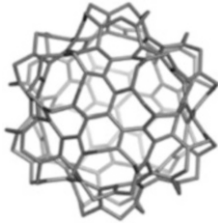


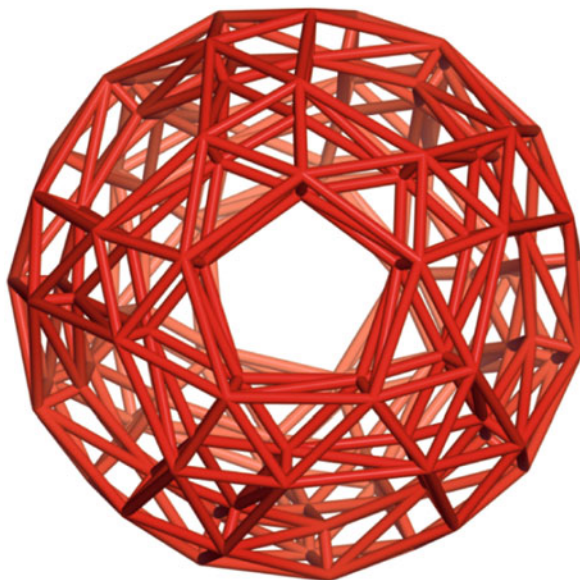
$d(C_{120}, 7S).280$

$d(s(D)@s(D)7S.120).280$

$A_5; |A_5|=60; \text{Classes: } 6 |2\{20\}; 4\{60\}|$

10A1

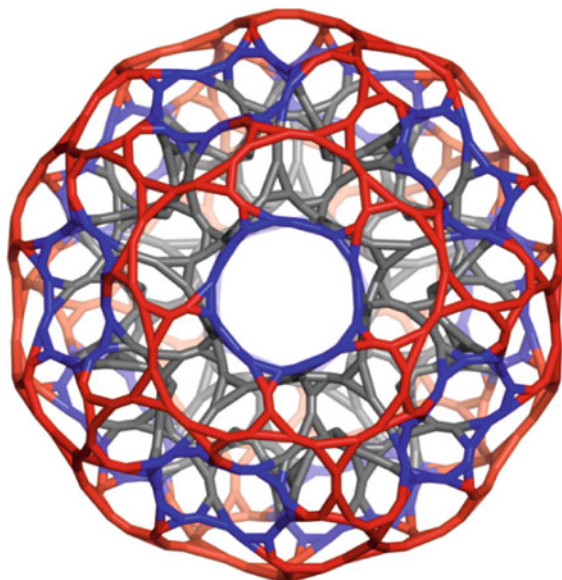
		
$s(D).60$	$s(D)@s(D)7S.120$	$op(ca(D)).200$



$s(\mathbf{D})@s(\mathbf{D})7S.120$

$d(C_{280}, 7S).120$
 A_5 ; Classes: $2 | 2\{60\} |$
 $10A1.2$

<p>$s(\mathbf{D}).60$</p>	<p>$Op(Ca(\mathbf{D})).200$</p>	<p>$C_{280,S}$</p>



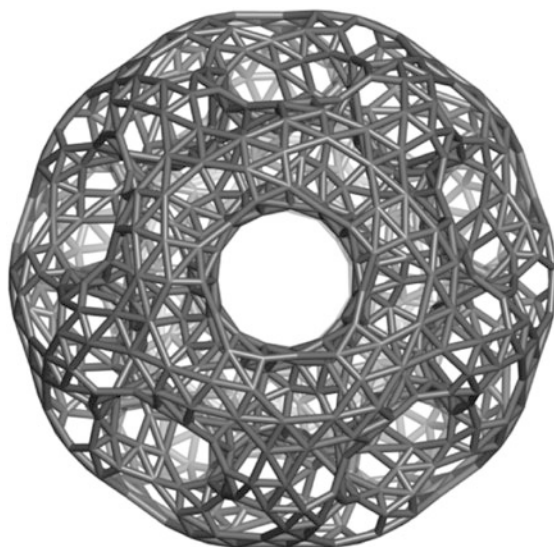
$t(d(C_{120}, 7S)280).840$

$t(C_{280}).840$

A_5 ; Classes: 14 |14{60}|

10A1.3

<p>$op(ca(D)).200$</p>	<p>$C_{280,S}$</p>	<p>$t(C_{280}).840_cyclic\ cover$</p>

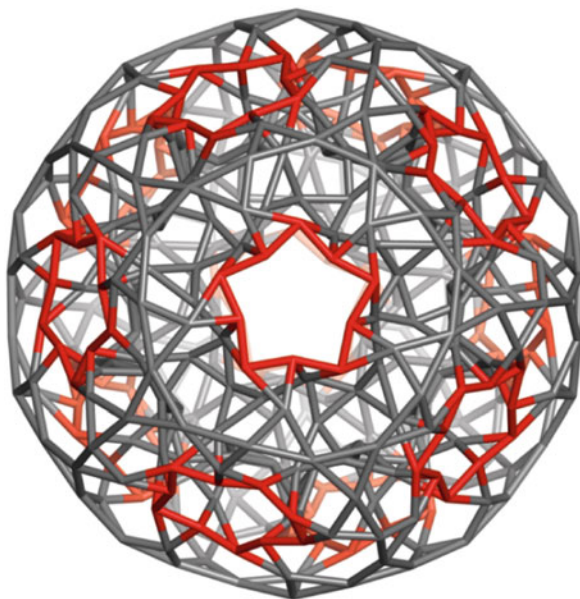


$s(C_{280R}).840$

A_5 ; Classes: 14 |14{60}|

10A1.4

<p>C_{280R}</p>	<p>$P5.1(C_{280R}).1240$</p>	<p>$s(C_{280R}).840$</p>

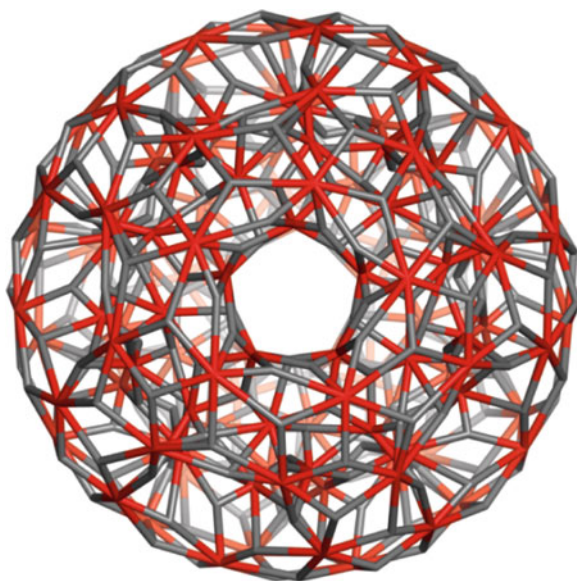


$m(C_{280}).420$

A_5 ; Classes: $8 |2\{30\};6\{60\}|$

10A1.5

<p>$Op(Ca(D)).200$</p>	<p>$d(m(C_{280})).400$</p>	<p>$C_{280,s}$</p>

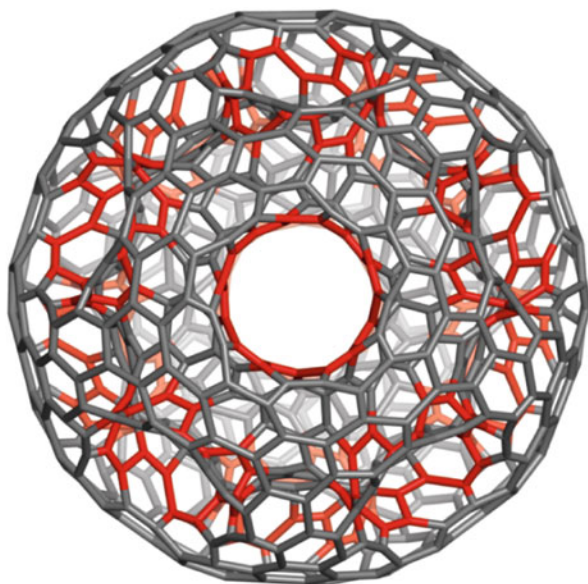


$d(m(C_{280}))-400$

A_5 ; Classes: 8 $|2\{20\}$; 6 $\{60\}$ |

10A1.5.1

<p>$s(D).60_5$</p>	<p>$m(C_{280}).420$</p>	<p>$C_{280,s}$</p>

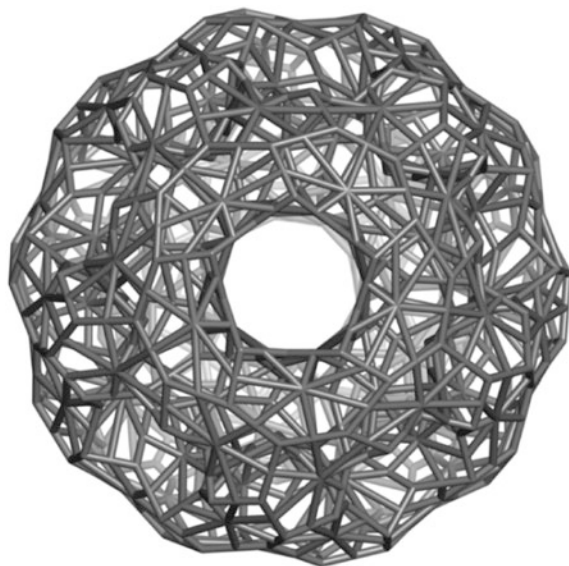


$I(C_{280}).840$

A_5 ; Classes: 14 |14{60}|

10A1.6

<p>$s(D).60_5$</p>	<p>$op(ca(D)).200$</p>	<p>$C_{280,s}$</p>

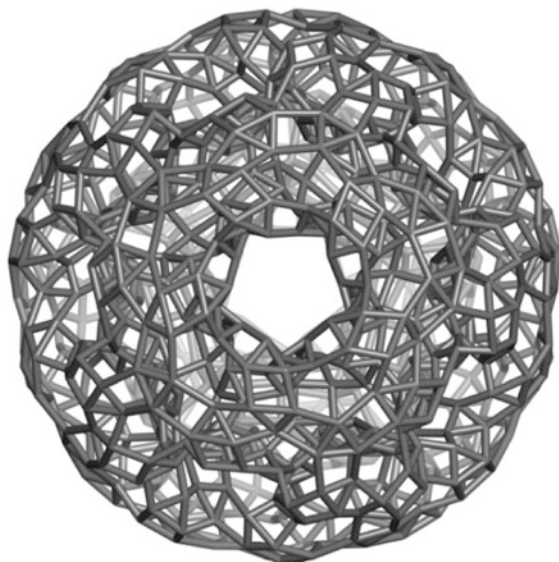


$p_4(C_{280}).820$

A_5 ; Classes: 16 $|2\{20\}; 2\{30\}; 12\{60\}|$

10A1.7

<p>$s(D).60_5$</p>	<p>$Op(Ca(D)).200$</p>	<p>$d(p_4(C_{280})820).840$</p>



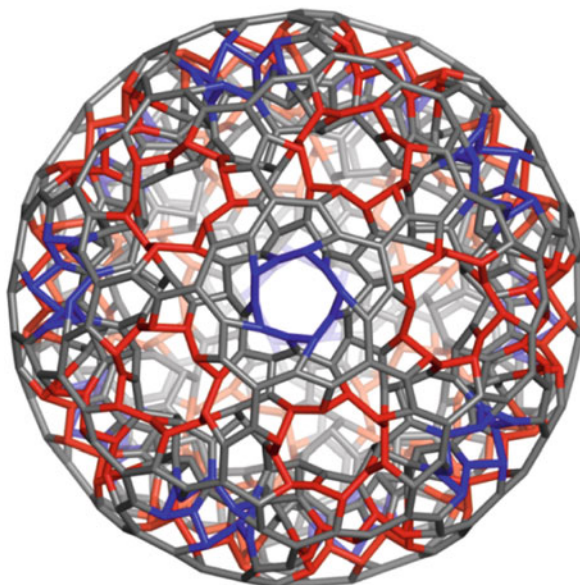
$d(p_4(C_{280})820).840$

A_5 ; Classes: 14 |14{60}|

10A1.7.1

<p>$op(ca(D)).200$</p>	<p>$C_{280,S}$</p>	<p>$p_4(C_{280}).820$</p>

10.2 C_{60} related structures

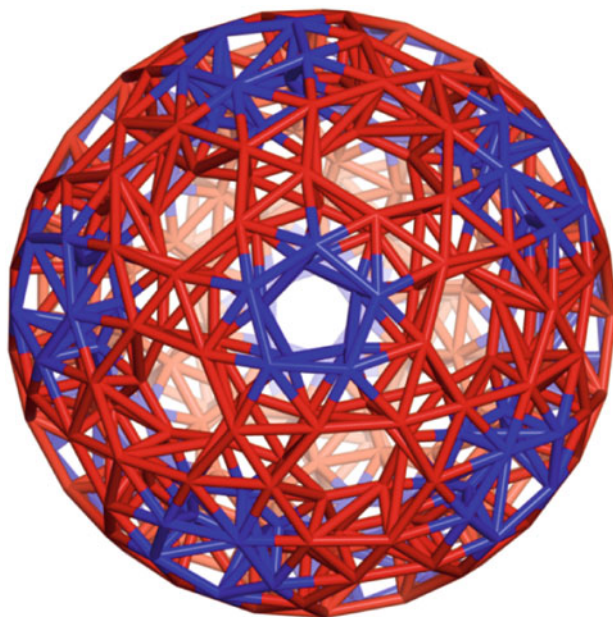


$d(C_{360},7R).840$

$d(s(C_{60})@s(C_{60})7R.360).840$
 $A_5; |A_5| = 60; \text{Classes } 14: |14\{60\}|$

10A2

<p>$s(C_{60}).180$</p>	<p>$s(C_{60})@s(C_{60})7R.360$ $A_5; \text{Classes } 6: 6\{60\}$</p>	<p>$op(ca(C_{60})).600$</p>

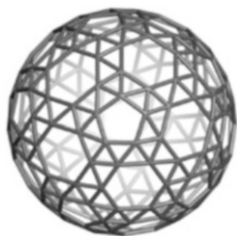


$s(C_{60})@s(C_{60})7R.360$

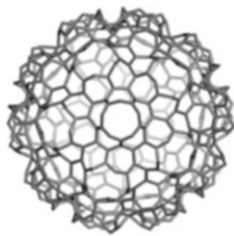
$d(C_{840}, 7R).360$

A_5 ; Classes: 6 |6{60}|

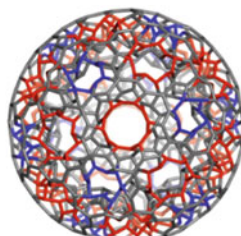
10A2.1



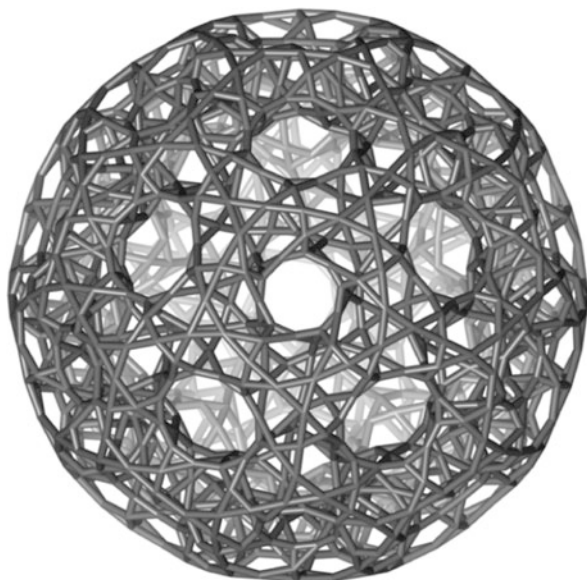
$s(C_{60}).180$



$op(ca(C_{60})).600$



$C_{840}, 7R$

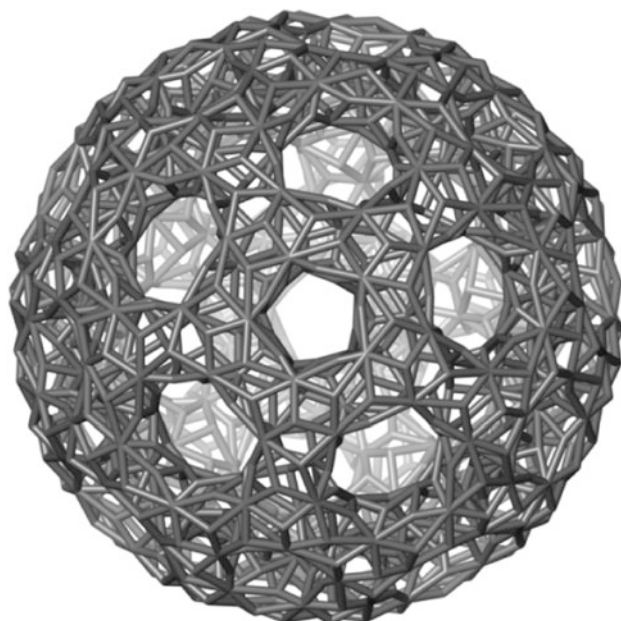


$m(C_{840}).1260$

A_5 ; Classes: $22 | 2 \{30\}; 20 \{60\} |$

10A2.2

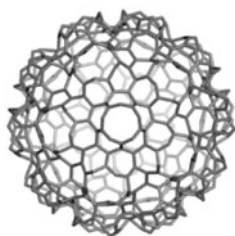
<p>$op(ca(C_{60})).600$</p>	<p>$d(m(C_{840})).1200_3$</p>	<p>$C_{840.7R_3}$</p>



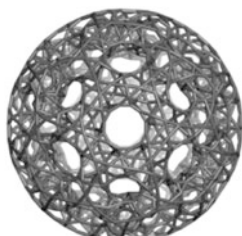
$d(m(C_{840})).1200$

A_5 ; Classes: 20 |20{60}|

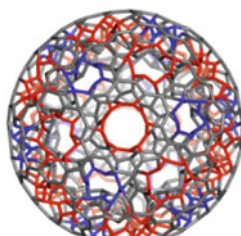
10A2.2.1



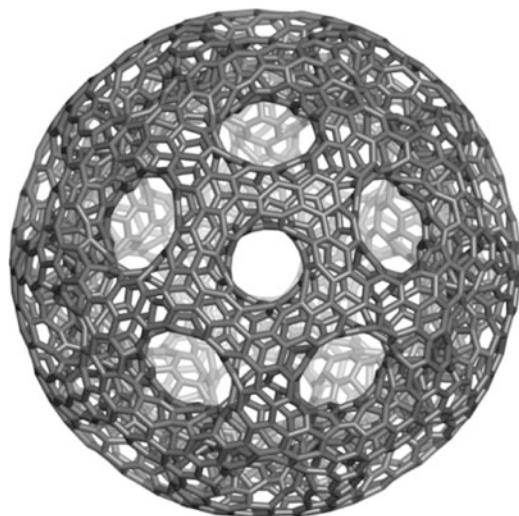
$op(ca(C_{60})).600_5$



$m(C_{840}).1260_3$



$C_{840,7R}_3$

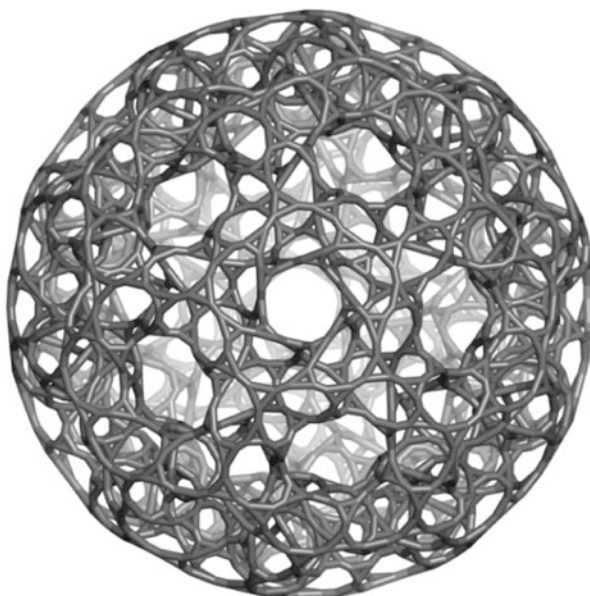


$I(C_{840}).2520$

A_5 ; Classes: $42|42\{60\}$

10A2.3

<p>$s(C_{60}).180$</p>	<p>$op(ca(C_{60})).600$</p>	<p>C_{840,R_5}</p>



$t(C_{840}).2520$

A_5 ; Classes: 42: $|42\{60\}|$

10A2.4

<p>$op(ca(C_{60})).600$</p>	<p>C_{840,R_5}</p>	<p>$t(C_{840}).2520_cyclic\ cover$</p>

References

- Babić D, Klein DJ, Schmalz TG (2001) Curvature matching and strain relief in bucky-tori: usage of sp^3 -hybridization and nonhexagonal rings. *J Mol Graph Model* 19:223–231
- Barborini E, Piseri P, Milani P, Benedek G, Ducati C, Robertson J (2002) Negatively curved spongy carbon. *Appl Phys Lett* 81:3359–3361
- Benedek G, Vahedi-Tafreshi H, Barborini E, Piseri P, Milani P, Ducati C, Robertson J (2003) The structure of negatively curved spongy carbon. *Diam Relat Mater* 12:768–773
- Blatov VA, O’Keeffe M, Proserpio DM (2010) Vertex-, face-, point-, Schläfli-, and Delaney-symbols in nets, polyhedra and tilings: recommended terminology. *Cryst Eng Comm* 12:44–48
- Buckley F (1979) Self-centered graph with given radius. *Congr Numer* 23:211–215
- Buckley F (1989) Self-centered graphs. *Ann NY Acad Sci* 576:71–78
- Diudea MV (1994) Layer matrices in molecular graphs. *J Chem Inf Comput Sci* 34:1064–1071
- Diudea MV, Nagy CL (2007) Periodic nanostructures. Springer, Dordrecht
- Diudea MV, Petitjean M (2008) Symmetry in multi-tori. *Symmetry Cult Sci* 19(4):285–305
- Diudea MV, Petitjean M (2016) Chiral multitori as snub derivatives. *Rev Roum Chim* 61 (4–5):329–337
- Diudea MV, Rosenfeld VR (2017) The truncation of a cage graph. *J Math Chem* 55(4):1014–1020. doi:10.1007/s10910-016-0716-6
- Diudea MV, Ursu O (2003) Layer matrices and distance property descriptors. *Indian J Chem A* 42 (6):1283–1294
- Euler L (1752–1753) *Elementa doctrinae solidorum-Demonstratio nonnullarum insignium proprietatum, quibus solida hedris planis inclusa sunt praedita*. *Novi Comment Acad Sc Imp Petropol* 4:109–160
- Harary F (1969) *Graph theory*. Addison-Wesley, Reading
- Hargittai M, Hargittai I (2010) *Symmetry through the eyes of a chemist*. Springer, Dordrecht
- Higuchi Y (2001) Combinatorial curvature for planar graphs. *J Graph Theory* 38:220–229
- Janakiraman TN, Ramanujan J (1992) On self-centered graphs. *Math Soc* 7:83–92
- Kelvin L (1904) *Baltimore lectures on molecular dynamics and the wave theory of light*, Appendix H, Sect. 22, footnote p. 619. C.J. Clay and Sons, Cambridge University Press Warehouse, London
- Klein DJ (2002) Topo-combinatoric categorization of quasi-local graphitic defects. *Phys Chem Chem Phys* 4:2099–2110
- Klein DJ, Liu X (1994) Elemental carbon isomerism. *Int J Quantum Chem* S28:501–523
- Lenosky T, Gonze X, Teter M, Elser V (1992) Energetics of negatively curved graphitic carbon. *Nature* 355:333–335
- Lijnen E, Ceulemans A (2005) The symmetry of Dyck graph: group structure and molecular realization. *J Chem Inf Model* 45(6):1719–1726
- Mackay AL, Terrones H (1991) Diamond from graphite. *Nature* 352:762–762
- Meier WM, Olson DH (1992) *Atlas of zeolite structure types*, 3rd edn. Butterworth-Heineman, London
- Nagy CL, Diudea MV (2009) *Nano studio software*. Babes-Bolyai University, Cluj
- Nagy CL, Diudea MV (2017) Ring signature index. *MATCH Commun Math Comput Chem* 77 (2):479–492
- Nazeer W, Kang SM, Nazeer S, Munir M, Kousar J, Sehar A, Kwun YC (2016) On center, periphery and average eccentricity for the convex polytopes. *Symmetry* 8:145–168
- Negami S, Xu GH (1986) Locally geodesic cycles in 2-self-centered graphs. *Discret Math* 58:263–268
- Petitjean M (2016) <http://petitjeanmichel.free.fr/itoweb.petitjean.freeware.html>
- Schulte E (1985) Regular incidence-polytopes with Euclidean or toroidal faces and vertex-figures. *J Combin Theory A* 40(2):305–330
- Schulte E (2014) Polyhedra, complexes, nets and symmetry. *Acta Crystallographica A* 70:203–216
- Terrones H, Mackay AL (1997) From C_{60} to negatively curved graphite. *Prog Crystal Growth Charact* 34:25–36

Chapter 11

Spongy Hypercubes

Hypercube Q_n is an n -dimensional analogue of a square ($n = 2$) or a cube ($n = 3$), also called an n -dimensional cube, or simply an n -cube; it is a regular graph of degree n , according to Balinski (1961) theorem.

The hypercube is a special case of a hyper-rectangle (Coxeter 1973, 1974), a generalization of a rectangle for n -dimensions; it can be obtained by the Cartesian product of P_2 graph or can be drawn as a *Hässe* diagram (Baker et al. 1971).

Hypercube is a regular polytope in the space of any number of dimensions (Coxeter 1973). The n -cube $\{4, 3^{n-2}\}$ (by Schläfli symbols (Schläfli 1901) has as its dual the n -orthoplex $\{3^{n-2}, 4\}$. The number of k -cubes contained in an n -cube $Q_n(k)$ comes from the coefficients of $(2k + 1)^n$

$$Q_n(k) = 2^{n-k} \binom{n}{k}; \quad k = 0, \dots, n-1 \quad (11.1)$$

Hypercubes have been considered in the computer architecture (Hillis 1982; Szymanski 1989).

11.1 Simple Toroidal Hypercubes

In the idea of hypercube infinite tessellation (Coxeter 1973), or reminding the abstract polytopes with toroidal faces (Coxeter 1982; Schulte 1985), we tried the embedding of n -cube in the torus. A software program, named Torus, developed by Topo Group Cluj, Romania (Diudea et al. 2003), enables the embedding of n -cube as a double-shell toroidal structure; families of hypertori $T(p,r)$, (with p being the number of points on the small circle while r is the number of small circle copies around the large hollow of the torus) can be generated. The polyhedral hypersurface may be looked as locally curled back on each of the r cuboids Q_n around the large hollow.

Figure 11.1 illustrates the 4-cube and the torus $T((4,8)Q_4).64$, where Q_4 means the 4-cube unit while the last number counts the points/atoms of the whole structure.

Enumeration of the k -faces $T((4,r),Q_n,k)$ in the hypertorus $T((4,r),Q_n)$ is made by the formulas (11.2), derived from the relation for the n -cube (11.1), as exemplified in Table 11.1.

$$\begin{aligned}
 f_r &= (r/2)/n; f_k = (r/2) + k \cdot f_r; k = 0, 1, \dots, n - 1 & (11.2) \\
 T((4,r),Q_n,k) &= Q_n(k) \cdot f_k; \\
 T((4,r),Q_n,(k+1)) &= r
 \end{aligned}$$

The number of rings R around any point in the hypertorus is given by the formula (11.3)

$$R(T((4,r)Q_n)) = 4^{(n-1)(n+2)/2} \tag{11.3}$$

It is known that the Petrie dual of the cube is a torus (see Lijnen and Ceulemans 2005; Schulte 2014); this can be seen in Table 11.1, where the hypertorus $T((4,r)Q_n)$; $r = 8$ has the same number of points as the hypercube Q_{n+2} . The vertex degree

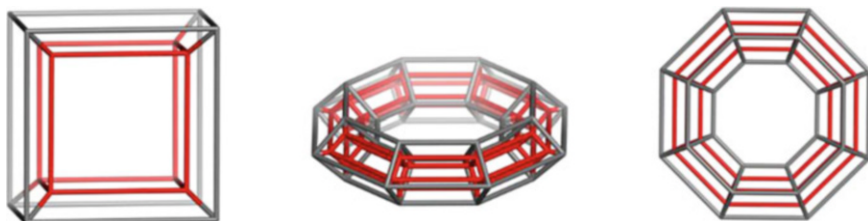


Fig. 11.1 Tesseract $Q_4.16$ hypercube (left) and the toroidal hypercube $T((4,8)Q_4).64$ (middle and right)

Table 11.1 Figure count in the hypertorus $T((4,8),Q_n)$ in comparison to the hypercube Q_n

Struct.\k	0	1	2	3	4	5	6	7	f_r	Deg(v)	χ
$T((4,8),Q_3)$	32	64	40	8	0	0	0	0	4/3	4	0
$T((4,8),Q_4)$	64	160	144	56	8	0	0	0	4/4	5	0
$T((4,8),Q_5)$	128	384	448	256	72	8	0	0	4/6	6	0
$T((4,8),Q_6)$	256	896	1280	960	400	88	8	0	4/6	7	0
$T((4,8),Q_7)$	512	2048	3456	3200	1760	576	104	8	4/7	8	0
Q_3	8	12	6	0	0	0	0	0	0	3	2
Q_4	16	32	24	8	0	0	0	0	0	4	0
Q_5	32	80	80	40	10	0	0	0	0	5	2
Q_6	64	192	240	160	60	12	0	0	0	6	0
Q_7	128	448	672	560	280	84	14	0	0	7	2

in the hypertorus $T((4,r),Q_n)$ equals $n + 1$, n being the rank/dimension of the inside hypercube. The toroidal hyperstructure is vertex transitive but its edges and faces are each split in two equivalence classes.

It is a noticeable difference between the hypercube Q_n and hypertorus $T((4,r),Q_n)$: the alternating figure sum (i.e., the *Euler characteristic* χ —Euler 1753) in Q_n gives either zero or two (for $n =$ even and odd, respectively), cf. relation (3.8), while it is zero, irrespective of n parity, for the hypertorus, because its genus is unity.

11.2 Complex Toroidal Hypercubes

When the two ends of a tube are identified, it results in a closed tube or a torus. The study is focused on hypertori $T(4,r)$ and $T(4,r,s)$ (Fig. 11.2), named according to Diudea’s discretization procedure (Diudea 2002).

In a more complex hypertorus $T((4,r,s),Q_n)$ (Fig. 11.2, right), each unit $T((4,r,1),Q_n)$ is a simple hypertorus $T((4,r),Q_n)$ while there are s -units around the central hollow. The k -rank faces of a hypertorus $T((4,r,s),Q_n)$ are counted from the previous rank faces of the simple hypertorus $T((4,r),Q_n)$, by formulas (11.4)

$$\begin{aligned}
 T((4,r,1),Q_n,k) &= T((4,r),Q_{n-1},k) + T((4,r),Q_{n-1},(k-1)) \\
 T((4,r,s),Q_n,k) &= s \times T((4,r,1),Q_n,k); k = 0, 1, \dots, n-1; n > 3 \quad (11.4)
 \end{aligned}$$

Formulas are confirmed by data listed in Table 11.2; they are valid for any integer $n > 3$. The vertex degree in $T((4,r,s),Q_n)$ is $(n + 2)$; this torus is vertex transitive but its edges and faces are each split in three equivalence classes.

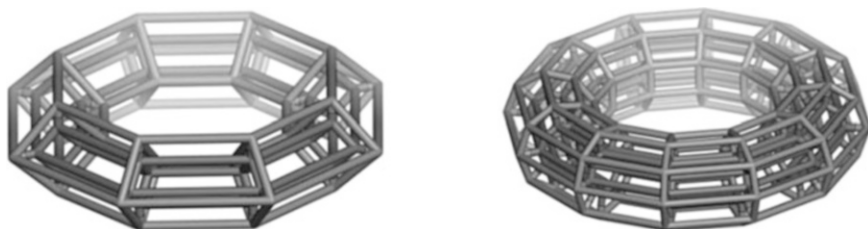


Fig. 11.2 A simple double-wall torus $T((4,8),Q_4).64$, of a square section (left) and $T((4,9,12),Q_3).216$, with an octagonal section and 16 units $T((4,9,1),Q_3).36$ (right)

Table 11.2 Figure count in the hypertorus $T((4,8,16),Q_7).4096$

Structure\k	0	1	2	3	4	5	6	7	χ	k
$T((4,8),Q_6)$	256	896	1280	960	400	88	8	0	0	7
	0	256	896	1280	960	400	88	8	–	–
$T((4,8,1),Q_7)$	256	1152	2176	2240	1360	488	96	8	–	–
$T((4,8,16),Q_7)$	4096	18,432	34,816	35,840	21,760	7808	1536	128	0	8

The figure sum (i.e., the Euler characteristic χ) in the hypertorus $T((4,r,s),Q_n)$ is again only zero (see Table 11.2), irrespective of n parity, as given by the Euler formula (3.1) for an object of the genus $g = 1$.

11.3 Tubular Hypercubes

Hypercube can be embedded in a tube, as shown in Fig. 11.3.

In a simple tubular hypercube $TU((4,r),Q_n)$ (Fig. 11.3, left), the k -rank faces are counted from the hypercube $Q_n(k)$ faces by formulas (11.5) (see Table 11.3).

$$f_r = (r/2 - 1)/n \quad f_k = (r/2) + k \cdot f_r \quad k = 0, 1, \dots, n - 1$$

$$TU((4, r), Q_n, k) = Q_n(k) \cdot f_k \quad TU((4, r), Q_n, (k + 1)) = r \quad (11.5)$$

One can see the alternation of figure count χ : zero and two (for $n =$ even and odd, respectively), cf. relation (3.8). It means that the simple hypertube $TU((4,r),Q_n)$ is like the sphere (i.e., both have the genus $g = 0$).

In a more complex hypertube (Fig. 11.3, right), each unit in the tube $TU((4,r,s),Q_n)$ is a simple hypertorus $T((4,r),Q_n)$ (Fig. 11.2, left) while there are s -units along the tube.

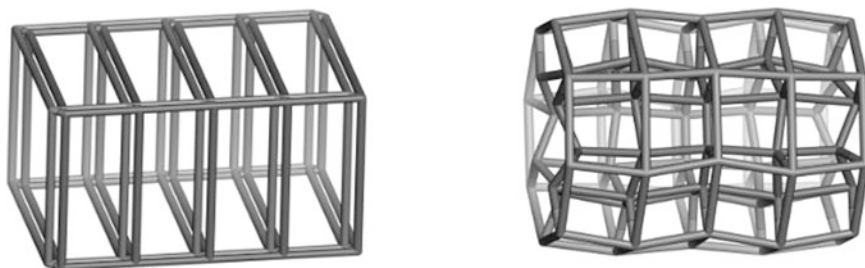


Fig. 11.3 A simple hypertube $TU(4,5),Q_4$.40 (left) and a complex hypertube $TU((4,8,5),Q_3)$.80 (right)

Table 11.3 Figure count in tubular hypercubes $TU((4,r),Q_n)$

Structure\k	0	1	2	3	4	5	6	χ	k
$TU((4,5),Q_5)$.80	80	224	248	136	37	5	–	0	6
Q_5	32	80	80	40	10	0	–	2	5
f_k	2.5	2.8	3.1	3.4	3.7	4	–	–	–
$Q_5 \times f_k \&r$	80	224	248	136	37	5	–	0	6
$TU((4,5),Q_6)$.160	160	528	720	520	210	45	5	2	7
Q_6	64	192	240	160	60	12	–	0	6
f_k	2.5	2.75	3	3.25	3.5	3.75	4	–	–
$Q_6 \times f_k \&r$	160	528	720	520	210	45	5	2	7

Table 11.4 Figure count in the hypertube $TU((4,9,7),Q_5).504$

Structure\k	0	1	2	3	4	5	χ	k
$TU((4,9,7),Q_5).504$	504	1692	2214	1413	441	54	0	6
$T((4,9),Q_4).72$	72	180	162	63	9	–	–	5
–	–	72	180	162	63	9	–	–
$TU((4,9,1),Q_5).72$	72	252	342	225	72	9	–	6
$TU((4,9,1),Q_5) \times 6$	432	1512	2052	1350	432	54	–	–
$+ T((4,9),Q_4).72$	72	180	162	63	9	0	–	–
Sum	504	1692	2214	1413	441	54	0	6

The k -faces of a hypertube $TU((4,r,s),Q_n)$ are counted from the previous rank faces of the simple hypertorus $T((4,r),Q_n)$, by formulas (11.6) (Parvan-Moldovan and Diudea 2015), as exemplified in Table 11.4.

$$\begin{aligned}
 TU((4, r, 1), Q_n, k) &= T((4, r), Q_{n-1}, k) + T((4, r), Q_{n-1}, (k - 1)) \\
 TU((4, r, s), Q_n, k) &= s \times TU((4, r, 1), Q_n, k) + T((4, r), Q_{n-1}, k)
 \end{aligned}
 \tag{11.6}$$

Formulas (11.6) work for any integer $n > 3$.

11.4 Spongy Hypercubes

It is well-known that the Cartesian product of n edges provides the hypercube: $(P_2)^{\square n} = Q_n$. Next, the Cartesian product of two hypercubes is another hypercube: $Q_i \square Q_j = Q_{i+j}$.

Let now take the graph $G(d,v)$ of a d -connected polyhedron on v -vertices and make n -times the Cartesian product with an edge; the operation results in a “spongy hypercube” $G(d, v, Q_{n+1}) = G(d, v) \square^n P_2$. On each edge of the original polyhedral graph, a local hypercube Q_n will evolve; these hypercubes are incident in a hypervertex, according to the original degree, d . It means that, in a spongy hypercube, the original 2-faces will not be counted. Figure 11.4 illustrates such a spongy hypercube, built on the fullerene $C_{60} (I_h)$ (Pirvan-Moldovan and Diudea 2016)

Conjecture 11.1 *The k -faces of a spongy hypercube $G(d, v, Q_n)$, built on a 3-polytope with vertices of degree d , are combinatorially counted from the previous rank faces; their alternating summation accounts for the genus of the embedded surface*

$$G(d, v, Q_n, k) = (v/n)[d \cdot n - (d - 1)(n - k)] \cdot 2^{(n-k-1)} \cdot \binom{n}{k}; n > 1; k = 0, 1, \dots, n \tag{11.7}$$

$$\sum_{k=0}^n (-1)^k f_k = \chi(M) = 2(1 - g); n > 1; k = 0, 1, \dots, n; g = f_2(G)/2 \tag{11.8}$$

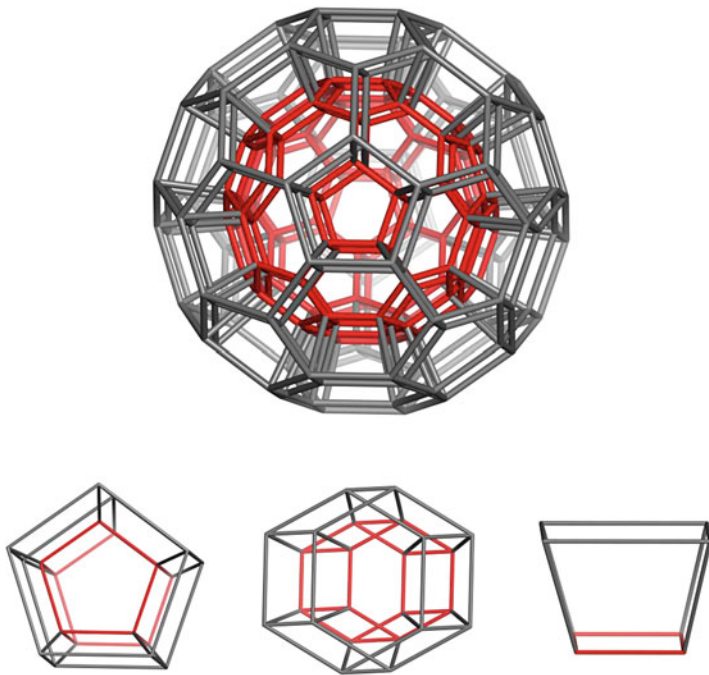


Fig. 11.4 Spongy $C_{60}(Q_4).480$ (top), its hyperfaces (bottom, left and middle) and a hyperedge (bottom, right)

Formula (11.7) represents the “embedding” of the hypercube on any polyhedron of vertex degree d (see the factor in the front of the almost classical hypercube counting), that transforms that cage in a hyper-multi-torus (Pirvan-Moldovan and Diudea 2016). Formula (11.8) expresses the “spongy” character of these structures, by the genus g (Harary 1969) of the hypersurface. Genus means the number of connections of a surface and it equals the half sum of f_2 faces of the embedded polyhedron. Note that (11.8) ignores the (hyper) prisms evolved on each f_2 faces of the original cage. Since f_2 faces are not seen, the rank of spongy structures is counted from the rank of Q_n plus two: $k = n + 2$. In this respect, the case of full-hypercube is compared with the case of spongy-one (Table 11.5).

As can be seen, “spongy” hypercubes follows exact combinatorial rules. Formulas (11.7) and (11.8) are confirmed by the data in Tables 11.5, 11.6, 11.7, 11.8, 11.9, 11.10 and 11.11.

Table 11.5 Figure count for spongy cubic $C_8(Q_n)$ hypercube

$C_8(Q_n) \setminus k$	0	1	2	3	4	5	χ
$(Q_1)3$	8	12	0	0	0	0	-4
$(Q_2)4$	16	32	12	0	0	0	-4
$(Q_3)5$	32	80	56	12	0	0	-4
$(Q_4)6$	64	192	192	80	12	0	-4
$(Q_5)7$	128	448	576	352	104	12	-4
Q_3	8	12	6	0	0	0	2
Q_4	16	32	24	8	0	0	0
Q_5	32	80	80	40	10	0	2
Q_6	64	192	240	160	60	12	0
Q_7	128	448	672	560	280	84	2
$Q_n(C_8(Q_n))$							
3	0	0	6	0	0	0	
4	0	0	12	8	0	0	
5	0	0	24	28	10	0	
6	0	0	48	80	48	12	
7	0	0	96	208	176	72	

Table 11.6 Figure count for spongy dodecahedral $C_{20}(Q_n)$ hypercube

$C_{20}(Q_n) \setminus k$	0	1	2	3	4	5	χ
$(Q_1)3$	20	30	0	0	0	0	-10
$(Q_2)4$	40	80	30	0	0	0	-10
$(Q_3)5$	80	200	140	30	0	0	-10
$(Q_4)6$	160	480	480	200	30	0	-10
$(Q_5)7$	320	1120	1440	880	260	30	-10

Table 11.7 Figure count for spongy tetrahedral $C_4(Q_n)$ hypercube

$C_4(Q_n) \setminus k$	0	1	2	3	4	5	χ
$(Q_1)3$	4	6	0	0	0	0	-2
$(Q_2)4$	8	16	6	0	0	0	-2
$(Q_3)5$	16	40	28	6	0	0	-2
$(Q_4)6$	32	96	96	40	6	0	-2
$(Q_5)7$	64	224	288	176	52	6	-2

Table 11.8 Figure count for spongy icosahedral $C_{12}(Q_n)$ hypercube

$C_{12}(Q_n) \setminus k$	0	1	2	3	4	5	χ
$(Q_1)3$	12	30	0	0	0	0	-18
$(Q_2)4$	24	72	30	0	0	0	-18
$(Q_3)5$	48	168	132	30	0	0	-18
$(Q_4)6$	96	384	432	192	30	0	-18
$(Q_5)7$	192	864	1248	816	252	30	-18

Table 11.9 Figure count for spongy octahedral $C_6(Q_n)$ hypercube

$C_6(Q_n)\setminus k$	0	1	2	3	4	5	χ
$(Q_1)3$	6	12	0	0	0	0	-6
$(Q_2)4$	12	30	12	0	0	0	-6
$(Q_3)5$	24	72	54	12	0	0	-6
$(Q_4)6$	48	168	180	78	12	0	-6
$(Q_5)7$	96	384	528	336	102	12	-6

Table 11.10 Figure count for spongy $C_{60}(Q_n)$ hypercube

$C_{60}(Q_n)\setminus k$	0	1	2	3	4	5	χ
$(Q_1)3$	60	90	0	0	0	0	-30
$(Q_2)4$	120	240	90	0	0	0	-30
$(Q_3)5$	240	600	420	90	0	0	-30
$(Q_4)6$	480	1440	1440	600	90	0	-30
$(Q_5)7$	960	3360	4320	2640	780	90	-30

Table 11.11 Contribution of f_k to f_{k+i} figures in $C_{60}(Q_n)$ hypercube

n	v	Formula i	0	1	2	3
2	120	$(k - 1)(3k - 4)/2$	1	5	12	22
			120	600	1440	2640
3	240	$(k - 1)(k - 2)(3k - 6)/6$	1	6	18	40
			240	1440	4320	9600
4	480	$(k - 1)(k - 2)(k - 3)(3k - 8)/24$	1	7	25	65
			480	3360	12,000	31,200
5	960	$(k - 1)(k - 2)(k - 3)(k - 4)(3k - 10)/120$	1	8	33	98
			960	7680	31,680	94,080

11.5 Truncation of Hypercube

Let now focus attention on the hypercube Q_n ; the truncation replaces any parent vertex in Q_n by a simplex S_{n-1} (Coxeter 1973, 1974) and these all trigonal substructures are disjoint while their union will cover all the vertices in the truncated transform $t(Q_n)$. Squares 4(2) are changed by octagonal 8(2) faces while cubes are changed by truncated cubes (Figs. 11.5 and 11.6).

The number of these simplices equals the number of vertices in Q_n : $|V(Q_n)| = 2^n n$; the number of vertices in each simplex equals n (see Table 11.12). In the above structures, n denotes the dimension or better the rank (McMullen and Schulte 2002), since we refer here to shapes rather than to geometric polytopes. Figure count in the hypercube and its truncated transforms is detailed in Table 11.12. The number of k -facets $t(Q_k)$ is counted by adding to Q_k (that equals the number of substructures with 8(2) faces) the number of facets of the corresponding simplex, as (Pirvan-Moldovan and Diudea 2016).

$$Q_n^k = 2^{n-k} \binom{n}{k}; S_n^k = \binom{n+1}{k+1}; t(Q_n^k) = Q_n^k + S_{n-1}^k \tag{11.9}$$

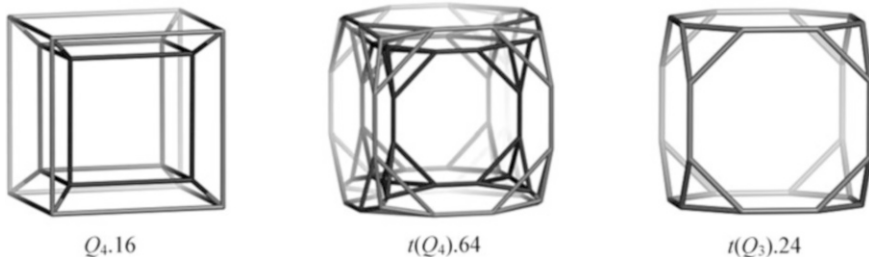


Fig. 11.5 Truncation of the hypercube Q_n

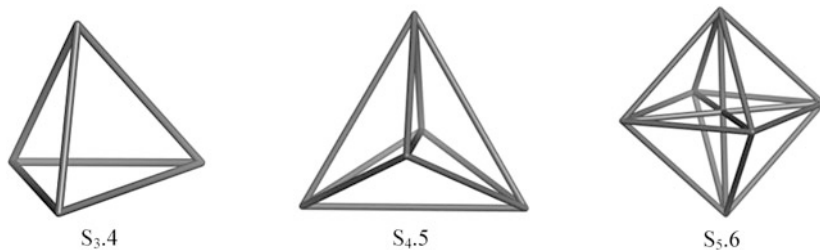


Fig. 11.6 Truncation of hypercube Q_n : simplices S_{n-1} substructures

Table 11.12 Figure count in truncated hypercube Q_n

Q_n										
n	v	e	–	–	4(2)	3	4	5	6	χ
3	8	12	–	–	6	0	0	0	0	2
4	16	32	–	–	24	8	0	0	0	0
5	32	80	–	–	80	40	10	0	0	2
6	64	192	–	–	240	160	60	12	0	0
7	128	448	–	–	672	560	280	84	14	2
$t(Q_n)$	$n \times v(Q_n)$	$n \times e(Q_n)$								
n	v	e	3(2)	8(2)	2	3	4	5	6	χ
3	24	36	8	6	14	–	–	–	–	2
4	64	128	64	24	88	24	–	–	–	0
5	160	400	320	80	400	200	42	–	–	2
6	384	1152	1280	240	1520	1120	444	76	–	0
7	896	3136	4480	672	5152	5040	2968	980	142	2

11.6 Counting Polynomials in Hypercubes

11.6.1 Omega Polynomial

A counting polynomial $P(x) = \sum_a p(a) \cdot x^a$ is a representation of a graph $G(V, E)$, with the exponent a showing the extent of partitions $p(G)$, $\cup p(G) = P(G)$ of a graph property $P(G)$ while the coefficient $p(a)$ is related to the number of partitions of extent a .

Let G be a connected graph, with $V(G)$ and $E(G)$ being the vertex set and edge set, respectively. Two edges $e = (u, v)$ and $f = (x, y)$ of G are called *co-distant* (briefly: *e co f*) if they obey the relation (John et al. 2007; Diudea and Klavžar 2010)

$$d(v, x) = d(v, y) + 1 = d(u, x) + 1 = d(u, y) \quad (11.10)$$

where d is the shortest-path distance function. The relation *co* is reflexive (*e co e*) and symmetric (*e co f*) for any edge e of G but is not necessarily transitive. A graph is called a *co-graph* if the relation *co* is also transitive and thus *co* is an equivalence relation.

If $C(e) := \{f \in E(G); f \text{ co } e\}$ is the set of edges in G , co-distant to $e \in E(G)$, the set $C(e)$ is provided by an orthogonal edge-cutting procedure (Gutman and Klavžar 1995; Klavžar 2008a; Diudea 2010b): take a straight line segment, orthogonal to the edge e , and intersect it and all other edges (of a polygonal plane graph) parallel to e . The set of these intersections is called an *orthogonal cut* of G , with respect to e . If G is a *co-graph* then its orthogonal cuts C_1, C_2, \dots, C_k form a partition in G : $E(G) = C_1 \cup C_2 \cup \dots \cup C_k$, $C_i \cap C_j = \emptyset$, $i \neq j$.

The relation *co* is related to the \sim (Djoković 1973) and Θ (Winkler 1984) relations (Klavžar 2008b).

Two edges e and f of a plane graph G are in relation *opposite*, *e op f*, if they are opposite edges of an inner face of G . Then *e co f* holds by the assumption that faces are isometric. The relation *co* is defined in the whole graph while *op* is defined only in faces/rings. Relation *op* will partition the edges set of G into *opposite edge strips* *ops*, as follows. (i) Any two subsequent edges of an *ops* are in *op* relation; (ii) Any three subsequent edges of such a strip belong to adjacent faces; (iii) In a plane graph, the inner dual of an *ops* is a path (however, in 3D networks, the ring/face interchanging will provide *ops* which are no more paths); (iv) The *ops* is taken as maximum possible, irrespective of the starting edge. The choice about the maximum size of face/ring, and the face/ring mode counting, will decide the length of the strip. Note that *ops* are *qoc* (quasi orthogonal cuts), meaning the transitivity relation is, in general, not obeyed (Diudea and Klavžar 2010).

Omega polynomial $\Omega(x)$ (Diudea 2006; Diudea et al. 2008, Diudea 2010a) is defined on the ground of opposite edge strips *ops* S_1, S_2, \dots, S_k in the graph. Denoting by m the number of *ops* of cardinality/length $s = |S|$, one can write

$$\Omega(x) = \sum_s m \cdot x^s \tag{11.11}$$

The first derivative (in $x = 1$) is used as a graph invariant or a topological index

$$\Omega'(1) = \sum_s m \cdot s = |E(G)| \tag{11.12}$$

An index, called Cluj-Ilmenau $CI(G)$ (John et al. 2007), was defined on $\Omega(x)$

$$CI(G) = \left\{ [\Omega'(1)]^2 - [\Omega'(1) + \Omega''(1)] \right\} \tag{11.13}$$

In tree graphs, the Omega polynomial counts the non-opposite edges, all being included in the term of exponent $s = 1$.

11.6.1.1 Omega Polynomial in Hypercubes

Omega polynomial was thought to describe the covering of polyhedral nano-structures or the tiling of crystal-like lattices, as a complementary description of the crystallographic one.

In hypercubes Q_n Omega polynomial is counted by formulas given in Table 11.13, which are exemplified in Table 11.14.

11.6.1.2 Omega Polynomial in Tubular Hypercubes

In tubular (open-ended or closed/toroidal) hypercubes, Omega polynomial accounts for the structural parameters, r and s ; formulas and examples are given in Tables 11.15, 11.16, 11.17, 11.18, 11.19, 11.20, 11.21 and 11.22.

Table 11.13 Formulas for Omega polynomial in hypercubes Q_n

1	$\Omega(Q_n, x) = n \cdot x^{2^n-1}$
2	$\Omega'(1) = e(Q_n) = E(Q_n) = n \cdot 2^{n-1}$
3	$\Omega''(1) = n \cdot 2^{n-1} \cdot (2^{(n-1)} - 1)$
4	$CI(Q_n) = n(n-1) \cdot 4^{n-1}$

Table 11.14 Omega polynomial in hypercubes Q_n ; examples

Vertices	Edges	$C(n)$	Deg(v)	Omega polynomial	CI
16	32	4	4	$4x^8$	768
32	80	5	5	$5x^{16}$	5120
64	192	6	6	$6x^{32}$	30,720

Table 11.15 Omega polynomial in simple hypertori $T((4,r),Q_n)$

1	$\Omega(T((4,r),Q_n),x) = r \cdot x^{(2^{n-1})} + (n-1) \cdot x^{(r \cdot 2^{n-2})}$
2	$\Omega'(1) = e(T((4,r),Q_n)) = r(n+1) \cdot 2^{n-2}$
3	$v(T((4,r),Q_n)) = r \cdot 2^{n-1}$
4	$\Omega''(1) = (-)r \cdot 2^{n-4}(4n+r \cdot 2^n - 2^{n+2} - r \cdot n \cdot 2^n + 4)$
5	$CI(T((4,r),Q_n)) = r \cdot 4^{n-2}(r \cdot n^2 + r \cdot n + 2r - 4)$

Table 11.16 Omega polynomial in simple hypertori $T((4,r),Q_n)$; examples

Vertices	Edges	n	Deg(v)	Omega polynomial	CI
T(4,8)					
32	64	3	4	$8x^4 + 2x^{16}$	3456
64	160	4	5	$8x^8 + 3x^{32}$	22,016
128	384	5	6	$8x^{16} + 4x^{64}$	129,024
T(4,9)					
288	1008	6	7	$9x^{32} + 5x^{144}$	903,168
576	2304	7	8	$9x^{64} + 6x^{288}$	4,773,888
1152	5184	8	9	$9x^{128} + 7x^{576}$	24,403,968

Table 11.17 Omega polynomial in complex hypertori $T((4,r,s),Q_n)$

1	$\Omega(T((4,r,s),Q_n),x) = s \cdot x^{r \cdot 2^{n-2}} + r \cdot x^{s \cdot 2^{n-2}} + (n-2) \cdot x^{rs \cdot 2^{n-3}}$
2	$\Omega'(1) = e(T((4,r,s),Q_n)) = rs(n+2) \cdot 2^{n-3}$
3	$v(T((4,r,s),Q_n)) = rs \cdot 2^{n-2}$
4	$\Omega''(1) = (-)2^{n-6}rs(8n - 2^{n+2}r - 2^{n+2}s + 2^{n+1}rs - 2^n nrs + 16)$
5	$CI(T((4,r,s),Q_n)) = 2^{2(n-3)}rs(rs n^2 + 3rsn - 4r - 4s + 6rs)$

Table 11.18 Omega polynomial in complex hypertori $T((4,r,s),Q_n)$; examples

Vertices	Edges	n	Deg(v)	Omega polynomial	CI
T(4,5,15)					
150	375	3	5	$15x^{10} + 5x^{30} + 1x^{75}$	129,000
300	900	4	6	$15x^{20} + 5x^{60} + 2x^{150}$	741,000
600	2100	5	7	$15x^{40} + 5x^{120} + 3x^{300}$	4,044,000
T(4,8,8)					
128	320	3	5	$16x^{16} + 1x^{64}$	94,208
256	768	4	6	$16x^{32} + 2x^{128}$	540,672
512	1792	5	7	$16x^{64} + 3x^{256}$	2,949,120

Table 11.19 Omega polynomial in simple hypertubes $TU((4,r),Q_n)$

1	$\Omega(TU((4,r),Q_n),x) = (r-1) \cdot x^{4 \cdot 2^{n-3}} + (n-1) \cdot x^{2r \cdot 2^{n-3}}$
2	$\Omega(1) = e(TU((4,r),Q_n)) = 2^{n-3} \cdot (2r + 2rn - 4)$
3	$v(TU((4,r),Q_n)) = 4r \cdot 2^{n-3}$
4	$\Omega''(1) = 2^{n-4}(4r - 4 \cdot 2^n \cdot r + 4 \cdot 2^n + 2^n \cdot r^2 + 4nr - 2^n \cdot nr^2 - 8)$
5	$CI(TU((4,r),Q_n)) = 4^{n-2}(n^2r^2 + nr^2 - 4nr + 2r^2 - 8r + 8)$

Table 11.20 Omega polynomial in simple hypertubes $TU((4,r),Q_n)$; examples

Structure	v	e	n	Omega polynomial	CI
TU(4,5)	20	36	3	$4x^4 + 2x^{10}$	1032
	40	92	4	$4x^8 + 3x^{20}$	7008
	80	224	5	$4x^{16} + 4x^{40}$	42,752
TU(4,6)	24	44	3	$5x^4 + 2x^{12}$	1568
	48	112	4	$5x^8 + 3x^{24}$	10,496
	96	272	5	$5x^{16} + 4x^{48}$	63,488

Table 11.21 Omega polynomial in complex hypertubes $TU((4,r,s),Q_n)$

1	$\Omega(TU((4,r,s),Q_n),x) = r \cdot x^{2s \cdot 2^{n-3}} + (s-1) \cdot x^{2r \cdot 2^{n-3}} + (n-2) \cdot x^{rs \cdot 2^{n-3}}$
2	$\Omega(1) = e(TU((4,r,s),Q_n)) = 2^{n-3} \cdot (2rs - 2r + nrs)$
3	$v(TU((4,r,s),Q_n)) = 2rs \cdot 2^{n-3}$
4	$\Omega''(1) = 2^{n-6} \cdot r \cdot (16s + 4 \cdot 2^n \cdot r - 4 \cdot 2^n \cdot s^2 + 8 \cdot n \cdot s + 2 \cdot 2^n \cdot r \cdot s^2 - 4 \cdot 2^n \cdot r \cdot s - 2^n \cdot n \cdot r \cdot s^2 - 16)$
5	$CI(TU((4,r,s),Q_n)) = 4^{n-3} \cdot r \cdot (8r + 6r \cdot s^2 - 4s^2 - 12r \cdot s + n^2 \cdot r \cdot s^2 - 4n \cdot r \cdot s + 3n \cdot r \cdot s^2)$

Table 11.22 Omega polynomial in complex hypertubes $TU((4,r,s),Q_n)$; examples

Structure	Vertices	Edges	n	Omega polynomial	r	s	CI
TU(5,5)	50	115	3	$5x^{10} + 4x^{10} + 1x^{25}$	5	5	11,700
	100	280	4	$5x^{20} + 4x^{20} + 2x^{50}$	5	5	69,800
	200	660	5	$5x^{40} + 4x^{40} + 3x^{100}$	5	5	391,200
TU(9,7)	126	297	3	$9x^{14} + 6x^{18} + 1x^{63}$	9	7	80,532
	252	720	4	$9x^{28} + 6x^{36} + 2x^{126}$	9	7	471,816
	504	1692	5	$9x^{56} + 6x^{72} + 3x^{252}$	9	7	2,613,024

11.6.1.3 Omega Polynomial in Spongy Hypercubes

In spongy hypercubes $G(v,e,Q_n)$, Omega polynomial is easily counted by a single general formula (Table 11.23), which is next exemplified in Tables 11.24, 11.25, 11.26, 11.27, 11.28 and 11.29.

In these formulas, v and e refers to the number of vertices and edges, respectively, of the parent polyhedron $G(v,e)$ while n is the actual rank of the local hypercube Q_n (see Sect. 11.4). The opposite, topologically parallel edges are

Table 11.23 Omega polynomial in spongy hypercubes $G(v,e,Q_n)$

	Formulas
1	$\Omega(e, v, n) = ex^{2^{n-1}} + (n - 1)x^{v \cdot 2^{n-2}}$
2	$f'(1) = e2^{n-1} + (n - 1)v2^{n-2} = (2^n/4)(2e - v + nv)$
3	$f''(1) = (2^n/16)(4v - 8e - 2^n \cdot v^2 - 4nv + 4 \cdot 2^n e + 2^n \cdot nv^2)$
4	$CI(e, v, n) = 4^n \left(\frac{n^2 v^2}{16} - \frac{3m^2}{16} + \frac{env}{4} + \frac{v^2}{8} - \frac{ev}{4} - \frac{e}{4} + \frac{e^2}{4} \right)$

Table 11.24 Omega polynomial in spongy cubic hypercube $C_8(Q_n)$; examples

n	v	e	Omega polynomial	CI
1	8	12	–	–
2	16	32	$12x^2 + 1x^8$	912
3	32	80	$12x^4 + 2x^{16}$	5696
4	64	192	$12x^8 + 3x^{32}$	33,024
5	128	448	$12x^{16} + 4x^{64}$	181,248
6	256	1024	$12x^{32} + 5x^{128}$	954,368

Table 11.25 Omega polynomial in spongy dodecahedral $C_{20}(Q_n)$ hypercube; examples

n	v	e	Omega polynomial	CI
1	20	30	–	–
2	40	80	$30x^2 + 1x^{20}$	5880
3	80	200	$30x^4 + 2x^{40}$	36,320
4	160	480	$30x^8 + 3x^{80}$	209,280
5	320	1120	$30x^{16} + 4x^{160}$	1,144,320
6	640	2560	$30x^{32} + 5x^{320}$	6,010,880

Table 11.26 Omega polynomial in spongy tetrahedral $C_4(Q_n)$ hypercube; examples

n	v	e	Omega polynomial	CI
1	4	6	–	–
2	8	16	$6x^2 + 1x^4$	216
3	16	40	$6x^4 + 2x^8$	1376
4	32	96	$6x^8 + 3x^{16}$	8064
5	64	224	$6x^{16} + 4x^{32}$	44,544
6	128	512	$6x^{32} + 5x^{64}$	235,520

Table 11.27 Omega polynomial in spongy icosahedral $C_{12}(Q_n)$ hypercube; examples

n	v	e	Omega polynomial	CI
1	12	30	–	–
2	24	72	$30x^2 + 1x^{12}$	4920
3	48	168	$30x^4 + 2x^{24}$	26,592
4	96	384	$30x^8 + 3x^{48}$	138,624
5	192	864	$30x^{16} + 4x^{96}$	701,952
6	384	1920	$30x^{32} + 5x^{192}$	3,471,360

Table 11.28 Omega polynomial in spongy octahedral $C_6(Q_n)$ hypercube; examples

n	v	e	Omega polynomial	CI
1	6	12		
2	12	30	$12x^2 + 1x^6$	816
3	24	72	$12x^4 + 2x^{12}$	4704
4	48	168	$12x^8 + 3x^{24}$	25,728
5	96	384	$12x^{16} + 4x^{48}$	135,168
6	192	864	$12x^{32} + 5x^{96}$	688,128

Table 11.29 Omega polynomial in spongy $C_{60}(Q_n)$ hypercube; examples

n	v	e	Omega polynomial	CI
1	60	90	–	–
2	120	240	$90x^2 + 1x^{60}$	53,640
3	240	600	$90x^4 + 2x^{120}$	329,760
4	480	1440	$90x^8 + 3x^{240}$	1,895,040
5	960	3360	$90x^{16} + 4x^{480}$	10,344,960
6	1920	7680	$90x^{32} + 5x^{960}$	54,282,240

counted in 2-faces R_4 (i.e. squares). Computations have been done by our original software Nano Studio (Nagy and Diudea 2009)

11.6.2 Cluj Polynomials

In bipartite graphs, the coefficients of CJ polynomial (Diudea 2009) can be calculated by an orthogonal edge-cut procedure (Diudea 2010a, b). In this respect, a more theoretical background is needed.

A graph G is a *partial cube* if it is embeddable in the hypercube Q_n . For any edge $e = (u,v)$ of a connected graph G let n_{uv} denote the set of vertices lying closer to u than to v : $n_{uv} = \{w \in V(G) \mid d(w,u) < d(w,v)\}$. It follows that $n_{uv} = \{w \in V(G) \mid d(w,v) = d(w,u) + 1\}$. The sets n_{uv} and n_{vu} of these vertices are called *semicubes* of G . A graph G is bipartite if and only if, for any edge of G , the opposite semicubes define a partition of G : $n_{uv} + n_{vu} = v = |V(G)|$ (Diudea and Klavžar 2010). These semicubes are just the vertex proximities of (the endpoints of) edge $e = (u,v)$, which CJ_e polynomial counts.

In partial cubes, the semicubes can be estimated by an orthogonal edge-cutting procedure. Function of the mathematic operation, the Cluj polynomials can be written with these semicubes as (Diudea 1997, 2009, 2010a, b)

Cluj-Sum, CJS (obtained by summation)

$$CJS(x) = \sum_e (x^{v_k} + x^{v-v_k}) \tag{11.14}$$

where v_k is the number of vertices lying to the left hand with respect to the orthogonal cut c_k . The first derivative (in $x = 1$) of Cluj polynomial $CJS(x)$ equals

the sum of all entries in UCJ_e matrix, or the column-sum of the shell matrix $ShUCJ_e$ or (in bipartite graphs) the product $|V(G)| \times |E(G)|$ (see Sect. 1.2.10.2).

Cluj-Product, CJP (obtained by pairwise product). It was also named *Szeged* polynomial SZ_v (Khalifeh et al. 2008; Ashrafi et al. 2008; Mansour and Schork 2009)

$$CJP(x) = SZ_v(x) = \sum_e x^{v_k(v-v_k)} \tag{11.15}$$

However, $CJP(x)$ can be derived from CJS only in bipartite graphs and relation with SZ_v (Gutman 1994) is true only there.

11.6.2.1 Cluj Polynomials in Hypercubes

In hypercubes, the formulas for calculating Cluj polynomials and derived topological indices (as the first derivative, in $x = 1$) are given in Table 11.30 while examples are provided in Table 11.31.

11.6.2.2 Cluj Polynomials in Toroidal Hypercubes

In toroidal hypercubes, the formulas (and examples) for calculating Cluj polynomials and derived topological indices are given in Tables 11.32 and 11.33; depending of the structural parameters r and s , several cases of calculation have been considered.

Table 11.30 Cluj polynomials in hypercubes Q_n

Formulas	
$v(C(n)) = V(C(n)) = 2^n$;	$e(C(n)) = E(C(n)) = n \cdot 2^{n-1}$
$CJS(C(n), x) = n(v/2)x^{v/2} + n(v/2)x^{v/2} = n(2^{n-1}) \cdot x^{2^{n-1}} + n(2^{n-1}) \cdot x^{2^{n-1}} = n \cdot 2^n \cdot x^{2^{n-1}}$	
$CJS'(1) = n \cdot 2^{2^n - 1}$	
$CJS''(1) = n \cdot 2^{2^{(n-1)}} \cdot (2^n - 2)$	
$CJP(C(n), x) = n(v/2)x^{(v/2)(v/2)} = n \cdot 2^{n-1} \cdot x^{2^{2(n-1)}}$	
$CJP'(1) = n \cdot 2^{n-1} \cdot 2^{2^{(n-1)}} = SZ_v$	

Table 11.31 Cluj polynomials in hypercubes Q_n ; examples

n	CJS(x)	CJS'(1)	CJP(x)	CJP'(1)
3	$12x^4 + 12x^4$	96	$12x^{(4 \times 4)}$	192
4	$32x^8 + 32x^8$	512	$32x^{(8 \times 8)}$	2048
5	$80x^{16} + 80x^{16}$	2560	$80x^{(16 \times 16)}$	20,480
6	$192x^{32} + 192x^{32}$	12,288	$192x^{(32 \times 32)}$	196,608

Table 11.32 Cluj polynomials in simple toroidal $T((4,r),Q_n)$ hypercubes

$T((4,r),Q_n)$	Formulas				
	$v(T((4,r),Q_n)) = 2r \cdot 2^{n-2}$ $e(T((4,r),Q_n)) = v(n+1)/2 = r(n+1) \cdot 2^{n-2}$				
Case: $r = \text{even}$	$CJS(T((4,r),Q_n),x) = 2e \cdot x^{v/2}$ $CJS(T((4,r),Q_n),1) = 2e \cdot (v/2) = e \cdot v$ $CJP(T((4,r),Q_n),x) = e \cdot x^{(v/2)^2}$ $CJP(T((4,r),Q_n),1) = e \cdot (v/2)^2$				
$r = 8; n:$	v	e	CJS(x)	CJS'(1)	CJP'(1)
4	64	160	$320x^{32}$	10,240	163,840
5	128	384	$768x^{64}$	49,152	1,572,864
6	256	896	$1792x^{128}$	229,376	14,680,064
$r = 10; n:$					
4	80	200	$400x^{40}$	16,000	320,000
5	160	480	$960x^{80}$	76,800	3,072,000
6	320	1120	$2240x^{160}$	358,400	28,672,000
Case: $r = \text{odd}$	$CJS(T((4,r),Q_n),x) = (n-1)v \cdot x^{v/2} + 2v \cdot x^{(v/2)-2(n-2)}$ $CJS(T((4,r),Q_n),1) = (n-1)v \cdot (v/2) + 2v \cdot ((v/2) - 2^{n-2}) = (v/2)(v - 2^n + nv)$				
$r = 9; n:$	v	e	CJS(x)	CJS'(1)	
4	72	180	$216x^{36} + 144x^{32}$	12,384	
5	144	432	$576x^{72} + 288x^{64}$	59,904	
6	288	1008	$1440x^{144} + 576x^{128}$	281,088	
$r = 11; n:$					
4	88	220	$264x^{44} + 176x^{40}$	18,656	
5	176	528	$704x^{88} + 352x^{80}$	90,112	
6	352	1232	$1760x^{176} + 704x^{160}$	422,400	

11.6.2.3 Cluj Polynomials in Spongy Hypercubes

Counting of Cluj polynomials in spongy hypercubes differs from bipartite to non-bipartite graphs, as shown in Table 11.34. To simplify formulas, an additional parameter m was added; it was derived empirically, as a characteristic of pattern polyhedra in Cluj polynomial (see Table 11.35). Examples of Cluj polynomial calculation in spongy hypercubes are given in Tables 11.36, 11.37, 11.38, 11.39, 11.40, 11.41 and 11.42.

Table 11.33 Cluj polynomials in complex toroidal $T((4,r,s),Q_n)$ hypercubes

	Formulas				
$T((4,r,s),Q_n)$	$v(T((4,r,s),Q_n)) = 2rs \cdot 2^{n-3}$ $e(T((4,r,s),Q_n)) = v(n+2)/2 = rs(n+2) \cdot 2^{n-3}$				
Case: (r,s) = even	$CJS(T((4,r,s),Q_n),x) = 2e \cdot x^{v/2}$ $CJS(T((4,r,s),Q_n),1) = 2r^2s^2 \cdot (n+2) \cdot 2^{2(n-3)} = e \cdot v$ $CJP(T((4,r,s),Q_n),x) = e \cdot x^{(v/2)^2}$ $CJP(T((4,r,s),Q_n),1) = e \cdot (v/2)^2 = SZ_v$				
$r = 8; s = 12; n:$	v	e	CJS(x)	CJS'(1)	CJP'(1)
3	192	480	$960x^{96}$	92,160	4,423,680
4	384	1152	$2304x^{192}$	442,368	42,467,328
5	768	2688	$5376x^{384}$	2,064,384	396,361,728
$r = 12; s = 16$					
3	384	960	$1920x^{192}$	368,640	35,389,440
4	768	2304	$4608x^{384}$	1,769,472	339,738,624
5	1536	5376	$10752x^{768}$	8,257,536	3,170,893,824
Case: $r = \text{odd};$ $s = \text{even}$	$CJS(T((4,r,s),Q_n),x) = nv \cdot x^{v/2} + 2v \cdot x^{(v/2)-s \cdot 2^{n-3}}$ $CJS(T((4,r,s),Q_n),1) = nv \cdot (v/2) + 2v \cdot ((v/2) - s \cdot 2^{n-3}) = (v/4)$ $(4v - 2^n s + 2nv)$				
$r = 7; s = 12; n:$	v	e	CJS(x)	CJS'(1)	
3	168	420	$504x^{84} + 336x^{72}$	66,528	
4	336	1008	$1344x^{168} + 672x^{144}$	322,560	
5	672	2352	$3360x^{336} + 1344x^{288}$	1,516,032	
Case: $r = \text{even};$ $s = \text{odd}$	$CJS(T((4,r,s),Q_n),x) = nv \cdot x^{v/2} + 2v \cdot x^{(v/2)-r \cdot 2^{n-3}}$ $CJS(T((4,r,s),Q_n),1) = nv \cdot (v/2) + 2v \cdot ((v/2) - r \cdot 2^{n-3}) = (v/4)$ $(4v - 2^n r + 2nv)$				
$r = 8; s = 11; n:$	v	e	CJS(x)	CJS'(1)	
3	176	440	$528x^{88} + 352x^{80}$	74,624	
4	352	1056	$1408x^{176} + 704x^{160}$	360,448	
5	704	2464	$3520x^{352} + 1408x^{320}$	1,689,600	
Case: (r,s) = odd	$CJS(T((4,r,s),Q_n),x) = (n-2)v \cdot x^{v/2} + 2v \cdot x^{(v/2)-r \cdot 2^{n-3}} + 2v \cdot x^{(v/2)-s \cdot 2^{n-3}}$ $CJS(T((4,r,s),Q_n),1) = ((n-2)/2)v^2 + 2v(v-r \cdot 2^{n-3} - s \cdot 2^{n-3}) = (v/4)$ $(4v - 2^n r - 2^n s + 2nv)$				
$r = 7; s = 13; n:$	v	e	CJS(x)	CJS'(1)	
3	182	455	$182x^{91} + 364x^{84} + 364x^{78}$	75,530	
4	364	1092	$728x^{182} + 728x^{168} + 728x^{156}$	368,368	
5	728	2548	$2184x^{364} + 1456x^{336} + 1456x^{312}$	1,738,464	

Table 11.34 Cluj polynomials in spongy $G(Q_n)$ hypercubes

Case: non-bipartite graphs								
1	$CJS(d, v, n, m)) = 2(n - 1) \cdot v \cdot 2^{n-2} \cdot x^{v \cdot 2^{n-2}} + 2d \cdot v \cdot 2^{n-2} \cdot x^{m \cdot 2^{n-1}}$							
2	$CJS'(1) = (4^n/8) \cdot v \cdot (2dm - v + nv)$; $v, d =$ vertices of degree d of the parent polyhedron; $n =$ actual Q_n rank							
	m	1	2	4	4	8	12	24
	Structure	T	Oct	C	Ico	Do	TO	C_{60}
Case: bipartite graphs								
3	$CJS(v, n, m) = e \cdot x^{m \cdot 2^{n-1}} + e \cdot x^{m \cdot 2^{n-1}} = 2e \cdot x^{m \cdot 2^{n-1}} = 2(2^{n-2} \cdot v \cdot (n + 2) \cdot x^{m \cdot 2^{n-1}})$							
4	$CJS'(1) = e \cdot m \cdot 2^n = 2^{2n-2} \cdot v \cdot (n + 2) \cdot m$; $e = 2^{n-2} \cdot v \cdot (n + 2)$							
5	$CJP(v, n, m) = e \cdot x^{(m \cdot 2^{n-1})(m \cdot 2^{n-1})} = e \cdot x^{(m \cdot 2^{n-1})^2} = 2^{n-2} \cdot v \cdot (n + 2) \cdot x^{(m \cdot 2^{n-1})^2}$							
6	$CJP'(1) = e \cdot (m \cdot 2^{n-1})^2 = 2^{3n-4} \cdot v \cdot (n + 2) \cdot m^2 = SZ(G)$ (Gutman 1994)							

Table 11.35 Cluj polynomials in some parent polyhedral clusters

	v	e	CJS	CJS	CJS'(1)	m	CJP	CJP'(1)
T	4	6	$12x^1$	$6x^1 + 6x^1$	12	1	$6x^{(1*1)}$	6
Oct	6	12	$24x^2$	$12x^2 + 12x^2$	48	2	$12x^{(2*2)}$	48
C	8	12	$24x^4$	$12x^4 + 12x^4$	96	4	$12x^{(4*4)}$	192
Ico	12	30	$60x^4$	$30x^4 + 30x^4$	240	4	$30x^{(4*4)}$	480
Do	20	30	$60x^8$	$30x^8 + 30x^8$	480	8	$30x^{(8*8)}$	1920
TO	24	36	$72x^{12}$	$36x^{12} + 36x^{12}$	864	12	$36x^{(12*12)}$	5184
C_{60}	60	90	$180x^{24}$	$90x^{24} + 90x^{24}$	4320	24	$90x^{(24*24)}$	51,840

Table 11.36 CJS polynomial in spongy tetrahedral $T(Q_n)$ hypercube

n	v	e	CJS	CJS'(1)
1	4	6	$12x^1$	12
2	8	16	$8x^4 + 24x^2$	80
3	16	40	$32x^8 + 48x^4$	448
4	32	96	$96x^{16} + 96x^8$	2304
5	64	224	$256x^{32} + 192x^{16}$	11,264

Table 11.37 CJS polynomial in spongy octahedral $C_6(Q_n)$ hypercube

n	v	e	CJS	CJS'(1)
1	6	12	$24x^2$	48
2	12	30	$12x^6 + 48x^4$	264
3	24	72	$48x^{12} + 96x^8$	1344
4	48	168	$144x^{24} + 192x^{16}$	6528
5	96	384	$384x^{48} + 384x^{32}$	30,720
6	192	864	$960x^{96} + 768x^{64}$	141,312

Table 11.38 Cluj polynomials in bipartite spongy cubic $C_8(Q_n)$ hypercube

n	v	e	CJS	CJS	CJS'(1)	CJP	CJP'(1)
1	8	12	$24x^4$	$12x^4 + 12x^4$	96	$12x^{(4*4)}$	192
2	16	32	$64x^8$	$32x^8 + 32x^8$	512	$32x^{(8*8)}$	2048
3	32	80	$160x^{16}$	$80x^{16} + 80x^{16}$	2560	$80x^{(16*16)}$	20,480
4	64	192	$384x^{32}$	$192x^{32} + 192x^{32}$	12,288	$192x^{(32*32)}$	196,608
5	128	448	$896x^{64}$	$448x^{64} + 448x^{64}$	57,344	$448x^{(64*64)}$	1,835,008
6	256	1024	$2048x^{128}$	$1024x^{128} + 1024x^{128}$	262,144	$1024x^{(128*128)}$	16,777,216

Table 11.39 CJS polynomial in spongy icosahedral $C_{12}(Q_n)$ hypercube

n	v	e	CJS	CJS'(1)
1	12	30	$60x^4$	240
2	24	72	$24x^{12} + 120x^8$	1248
3	48	168	$96x^{24} + 240x^{16}$	6144
4	96	384	$288x^{48} + 480x^{32}$	29,184
5	192	864	$768x^{96} + 960x^{64}$	135,168
6	384	1920	$1920x^{192} + 1920x^{128}$	614,400

Table 11.40 CJS polynomial in spongy dodecahedral D (Q_n) hypercube

n	v	e	CJS	CJS'(1)
1	20	30	$60x^8$	480
2	40	80	$40x^{20} + 120x^{16}$	2720
3	80	200	$160x^{40} + 240x^{32}$	14,080
4	160	480	$480x^{80} + 480x^{64}$	69,120
5	320	1120	$1280x^{160} + 960x^{128}$	327,680
6	640	2560	$3200x^{320} + 1920x^{256}$	1,515,520

Table 11.41 Cluj polynomials in bipartite spongy truncated octahedron TO $C_{24}(Q_n)$ hypercube

n	v	e	CJS	CJS	CJS'(1)	CJP	CJP'(1)
1	24	36	$72x^{12}$	$36x^{12} + 36x^{12}$	864	$36x^{(12*12)}$	5184
2	48	96	$192x^{24}$	$96x^{24} + 96x^{24}$	4608	$96^{(24*24)}$	55,296
3	96	240	$480x^{48}$	$240x^{48} + 240x^{48}$	23,040	$240x^{(48*48)}$	552,960
4	192	576	$1152x^{96}$	$576x^{96} + 575x^{96}$	110,592	$576x^{(96*96)}$	5,308,416
5	384	1344	$2688x^{192}$	$1344x^{192} + 1344x^{192}$	516,096	$1344x^{(192*192)}$	49,545,216
6	768	3072	$6144x^{384}$	$3072x^{384} + 3072x^{384}$	2,359,296	$3072x^{(384*384)}$	452,984,832

Table 11.42 CJS polynomial in spongy C_{60} -hypercube $C_{60}(Q_n)$

n	v	e	CJS	CJS'(1)
1	60	90	$180x^{24}$	4320
2	120	240	$120x^{60} + 360x^{48}$	24,480
3	240	600	$480x^{120} + 720x^{96}$	126,720
4	480	1440	$1440x^{240} + 1440x^{192}$	622,080
5	960	3360	$3840x^{480} + 2880x^{384}$	2,949,120
6	1920	7680	$9600x^{960} + 5760x^{768}$	13,639,680

References

- Ashrafi AR, Jalali M, Ghorbani M, Diudea MV (2008) Computing PI and Omega polynomials of an infinite family of fullerenes. *MATCH Commun Math Comput Chem* 60:905–916
- Baker KA, Fishburn P, Roberts FS (1971) Partial orders of dimension 2. *Networks* 2(1):11–28
- Balinski ML (1961) On the graph structure of convex polyhedra in n -space. *Pac J Math* 11(2): 431–434
- Coxeter HSM (1973) *Regular polytopes*, 3rd edn. Dover, New York
- Coxeter HSM (1974) *Regular complex polytopes*. Cambridge University Press, Cambridge
- Coxeter HSM (1982) Ten toroids and fifty-seven hemi-dodecahedra. *Geom Dedicata* 13:87–99
- Diudea MV (1997) Cluj matrix invariants. *J Chem Inf Comput Sci* 37:300–305
- Diudea MV (2002) Graphenes from 4-Valent tori. *Bull Chem Soc Jpn* 75:487–492
- Diudea MV (2006) Omega polynomial. *Carpath J Math* 22:43–47
- Diudea MV (2009) Cluj polynomials. *J Math Chem* 45:295–308
- Diudea MV (2010a) Nanomolecules and nanostructures – polynomials and indices. In: MCM Ser. 10. University of Kragujevac, Kragujevac
- Diudea MV (2010b) Counting polynomials and related indices by edge cutting procedures. *MATCH Commun Math Comput Chem* 64(3):569–590
- Diudea MV, Klavžar S (2010) Omega polynomial revisited. *Acta Chem Sloven* 57:565–570
- Diudea MV, Parv B, Ursu O (2003) TORUS software. Babes-Bolyai University, Cluj
- Diudea MV, Cigher S, John PE (2008) Omega and related counting polynomials. *MATCH Commun Math Comput Chem* 60:237–250
- Djoković DŽ (1973) Distance preserving subgraphs of hypercubes. *J Combin Theory Ser B* 14: 263–267
- Euler L (1752–1753) *Elementa doctrinae solidorum*. *Novi Comm Acad Sci Imp Petrop* 4:109–160
- Gutman I (1994) A formula for the wiener number of trees and its extension to graphs containing cycles. *Graph Theory Notes NY* 27:9–15
- Gutman I, Klavžar S (1995) An algorithm for the calculation of the szeged index of benzenoid hydrocarbons. *J Chem Inf Comput Sci* 35:1011–1014
- Harary F (1969) *Graph theory*. Addison-Wesley, Reading
- Hillis WD (1982) New computer architectures and their relationship to physics or why computer science is no good. *Int J Theor Phys* 21(3/4):255–262
- John PE, Vizitiu AE, Cigher S, Diudea MV (2007) CI Index in tubular nanostructures. *MATCH Commun Math Comput Chem* 57:479–484
- Khalifeh MH, Yousefi-Azari H, Ashrafi AR (2008) A matrix method for computing szeged and vertex PI indices of join and composition of graphs. *Linear Algebra Appl* 429:2702–2709
- Klavžar S (2008a) Abrid's eye view of the cut method and a survey of its applications in chemical graph theory. *MATCH Commun Math Comput Chem* 60:255–274
- Klavžar S (2008b) Some comments on co graphs and CI index. *MATCH Commun Math Comput Chem* 59:217–222
- Lijnen E, Ceulemans A (2005) The symmetry of the Dyck graph: group structure and molecular realization (Chap. 14). In: Diudea MV (ed) *Nanostructures: novel architecture*. Nova, New York, pp 299–309
- Mansour T, Schork M (2009) The vertex PI index and szeged index of bridge graphs. *Discr Appl Math* 157:1600–1606
- McMullen P, Schulte P (2002) *Abstract Regular Polytopes*, 1st edn. Cambridge University Press, Cambridge
- Nagy CsL, Diudea MV (2009) Nano studio software. “Babes-Bolyai” University, Cluj
- Parvan-Moldovan A, Diudea MV (2015) Hyper-tubes of hyper-cubes. *Iran J Math Chem* 6: 163–168
- Pirvan-Moldovan A, Diudea MV (2016) Euler characteristic of polyhedral graphs. *Croat Chem Acta* (accepted)

- Schläfli L (1901) Theorie der vielfachen Kontinuität Zürcher und Furrer, Zürich (Reprinted in: Ludwig Schläfli, 1814–1895, Gesammelte Mathematische Abhandlungen, Band 1, 167–387, Verlag Birkhäuser, Basel, 1950)
- Schulte E (1985) Regular incidence-polytopes with euclidean or toroidal faces and vertex-figures. *J Combin Theory Ser A* 40(2):305–330
- Schulte E (2014) Polyhedra, complexes, nets and symmetry. *Acta Cryst A* 70:203–216
- Szymanski TH (1989) On the permutation capability of a circuit-switched hypercube. In: Proceedings of the international conference on parallel processing 1, IEEE Computer Society Press, Silver Spring, MD, pp 103–110
- Winkler PM (1984) Isometric embedding in products of complete graphs. *Discret Appl Math* 8: 209–212

Chapter 12

Energetics of Multi-shell Clusters

12.1 Introduction

Nano-era, a period starting since 1985 with the discovery of the C₆₀ fullerene, is characterized by a huge scientific and technologic effort in finding theoretical basis able to predict and explain novel applications of nanostructures. Among the carbon structures, fullerenes (zero-dimensional), nanotubes (one dimensional), graphenes (two dimensional), diamonds and spongy nanostructures (three dimensional) were the most studied. Inorganic compounds were also considered. A novel crystallography, promoting the idea of topological description and classification of crystal structures, has been developed (Blatov et al. 2004, 2007, 2009; Delgado-Friedrichs and O’Keeffe 2005).

Multi-shell clusters discussed in this book may be viewed as molecular realizations of abstract structures, representing ways of the space filling, either in compact or spongy manner, by cells (i.e., 3-polytopes/polyhedra) representing shapes of the geometrical bodies. Homology information is required in this respect; however, many of the discussed structures consist of interlaced substructures (particularly appearing in higher ranked structures), envisaged as rational design or even as real points (i.e., atoms, in Chemistry). If molecular orbitals, computed by DFT or Atoms in Molecules approaches, are not defined to describe some cases existing in these multi-shell clusters, such structures may refer rather to crystal/quasi-crystal state than to molecules, where short-range forces appear to ensure the cohesion of clusters. The task of finding suitable examples from Crystallography is left to the interested scientists. We limited here to compute only carbon-consisting clusters, as shown below.

This chapter brings some computational arguments in the favor of (carbon) nanostructures described within this book.

12.2 C₂₀ Aggregation

C₂₀ (12A1) is the smallest and the most reactive fullerene; scientists devoted huge efforts to prove the existence of all-sp² C₂₀ free cage (Prinzbach et al. 2006) while the hydrogenated dodecahedrane (all-sp³ C₂₀) was synthesized in amounts of grams (Paquette and Vazeux 1981). It may aggregate to form solid phases, e.g., zeolites (Meier and Olson 1992—see below).

Four allotropes of the yet hypothetical diamond D₅ have been designed (Nagy and Diudea 2013) on the basis of C₂₀: a spongy net, a dense hyper-diamond with an “anti”-diamantane structure, the corresponding hyper-lonsdaleite and a quasi-diamond which is a fivefold symmetry quasi-crystal with a “syn”-diamantane structure.

The “anti”-structure of diamond D₅ is the well-known clathrate II, or *mtn* triple periodic 3-nodal net, with the tiling description: {5⁵.6}12{5⁶}5 and 2[5¹²]; [5¹².6⁴]; it belongs to the space group: *Fd-3 m*; this structure exists in the synthetic zeolite ZSM-39 (Adams et al. 1994; Meier and Olson 1992; Böhme et al. 2007) and in germanium allotrope Ge(*cF*136) (Guloy et al. 2006; Schwarz et al. 2008) real materials.

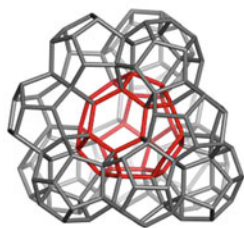
Substructures of D₅ theoretically emerge from the “seed” C₁₇ (Diudea 2010; Diudea and Nagy 2012; Szeffler and Diudea 2012). It can be dimerized (probably by a cycloaddition reaction) to C₃₄ dimer (Benedek called this network *fcc*-C₃₄ (a face-centered cubic lattice—Benedek and Colombo 1996). The dimer can form more complex substructures, such as adamantane-like “Ada”, diamantane-like “Dia”, and fivefold stars (see Fig. 12.1 and the Atlas of Chap. 8) for related structures). Numbers suffixing the name of structures represent the number of (heavy) atoms.

Energetic data (at DFTB level of theory) for the structures in Fig. 12.1 are listed in Table 12.1.

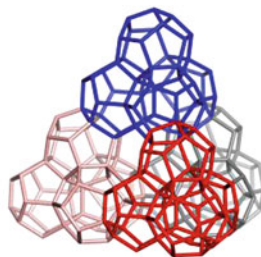
The Ada-units can self-arrange in the net of diamond D₅ (Fig. 12.1). Domains of this diamond network were optimized at the DFTB level of theory (Elstner et al. 1998). Hydrogen atoms were added to the external carbon atoms of the network structures in order to keep the charge neutrality and the sp³ character of C–C bonds at the network surface. Optimized structure data envisaged a well-defined three-clinical lattice, with the following parameters: $a = b = c = 6.79 \text{ \AA}$, and $\alpha = 60^\circ$, $\beta = 120^\circ$, $\gamma = 120^\circ$, even the most symmetrical structure is the *fcc*-one. Density of the D₅ network was calculated to be around 2.8 g/cm^3 .

The C–C bond length varies in a very narrow distance domain of 1.50–1.58 Å, suggesting that all carbon atoms are sp³ hybridized. Considering the one-electron energy levels of HOMO and LUMO, a large energy gap was observed. For two different domains, data were as follows: D₅(C₂₀).860 ($E_{\text{HOMO}} = -5.96 \text{ eV}$, $E_{\text{LUMO}} = +2.10 \text{ eV}$, $\Delta E_{\text{HOMO-LUMO}} = 8.06 \text{ eV}$) and D₅(C₂₈).1022 ($E_{\text{HOMO}} = -6.06 \text{ eV}$, $E_{\text{LUMO}} = +2.45 \text{ eV}$, $\Delta E_{\text{HOMO-LUMO}} = 8.51 \text{ eV}$), which indicates an insulating behavior.

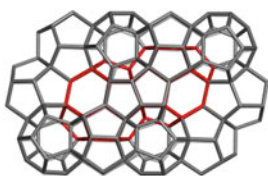
Structural stability of D₅ diamond substructures was evaluated both in static and dynamic temperature conditions by molecular dynamics MD (Kyani and Diudea



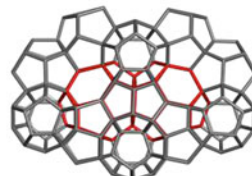
Ada.158
(C₂₈@12C₂₀)ada.158



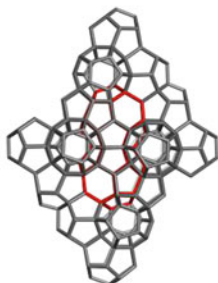
Ada.198
(C₂₈@4(P@4C₂₀))ada.198



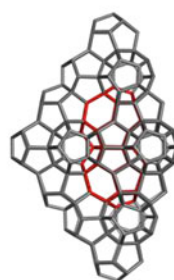
Dia.anti.226



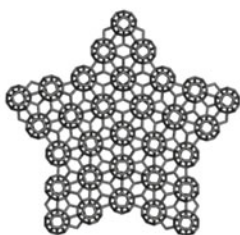
Dia.syn.226



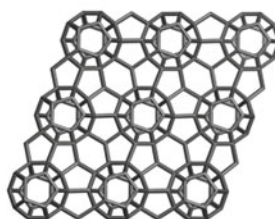
Dia.anti.306



Dia.syn.270



D₅.syn.531s.1185



D₅.anti.333.860

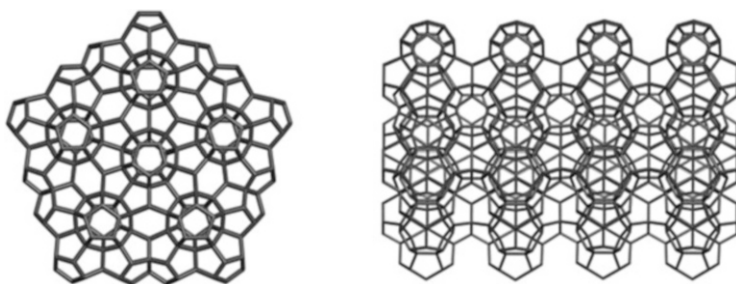
Fig. 12.1 Diamond D₅ and some of its substructures/allotropes

Table 12.1 Energetic data (DFTB) in Diamond D_5 substructures (as hydrogenated species); reference structure was taken the hypothetical $C_{60}H_{60}$

Structure	No C	E_{tot} (au)	E_{tot}/C (au)	GAP (eV)
Ada.158H ₈₄	158	-305.340	-1.957	8.812
Ada.198H ₁₀₀	198	-380.717	1.923	8.725
Dia.anti.226H ₁₀₈	226	-432.311	-1.913	8.584
Dia.syn.226H ₁₀₈	226	-432.264	-1.913	8.514
Dia.anti.306H ₁₄₀	306	-583.049	-1.905	8.482
Dia.syn.270H ₁₂₂	270	-513.845	-1.903	8.448
D_5 .333.860H ₂₇₆	860	-1595.702	-1.855	8.055
D_5 .531s.1185H ₅₁₀	1185	-2244.77	-1.894	8.051
$C_{60}H_{60}$	60	-125.584	-2.093	10.412

Table 12.2 Topology of D_5 . *anti* diamond function of k ($k = 1, 2, \dots$ the number of Ada20-units along the edge of a (k,k,k) -domain)

Formulas
$v(D_5 \text{ . anti}) = -22 - 12k + 34k^3$
$Atoms(sp^3) = -10 - 36k^2 + 34k^3$
$Ring[5] = -18 - 6k - 18k^2 + 36k^3$
$Ring[6] = -1 + 6k - 9k^2 + 4k^3$
$R[5] + R[6] = -19 - 27k^2 + 40k^3$
$\lim_{k \rightarrow \infty} \frac{R[5]}{R[5]+R[6]} = 9/10$

**Fig. 12.2** D_5 .syn.524.1330—top view (*left*) and side view (*right*)

2012; Szefer and Diudea 2012); results shown that D_5 seed C_{17} is the most temperature resistant fragment.

Topology of D_5 .*anti* diamond, in a three-clinical domain (k,k,k) (see Fig. 12.1) is shown in Table 12.2: formulas to calculate the number of atoms, number of rings R and the limits (at infinity) for the ratio R_5 /all Rings are given function of k (i.e., the number of repeating units in the domain).

The quasi-diamond D_5 .*syn* can form a 1-periodic quasicrystal, e.g., D_5 .syn.52 n , of $Amm2$ space group, point symbol: $\{5^2.6\}6\{5^3\} 4\{5^4.6.8\}5 \{5^5.6\}7\{5^6\}3$; 12-nodal net 3,4-c (Fig. 12.2).

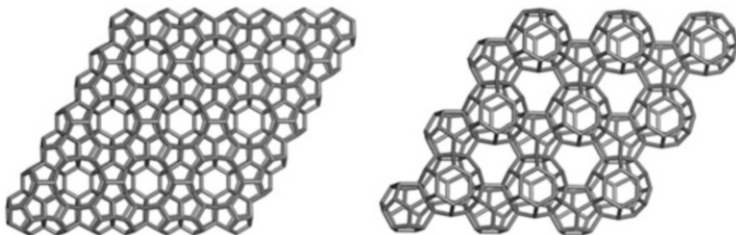


Fig. 12.3 Hypothetical diamond D_5 hyper-graphene layers: a single fullerene layer $C_{20}\text{Hex.333.506}$ (*left*) and a sheet of alternating two fullerenes $(C_{20}C_{28})\text{Hex.331.327}$ (*right*)

12.3 Hyper-graphenes by D_5 Substructures

The small fullerenes C_{20} and C_{28} , filling the space in the frame of D_5 can provide, by “exfoliation”, hyper-graphenes (Diudea 2013).

The corresponding substructures of the hyper-graphenes in Fig. 12.3 are illustrated in Fig. 12.4 (top row). Pentagonal hyper-rings appearing in the core of these stars are illustrated in Fig. 12.4 (bottom row).

Alternating C_{20}/C_{28} hyper-graphene domains with fivefold symmetry (Fig. 12.5) can result by sectioning a D_5 quasi-crystal (Fig. 12.5, right) by an electron beam (Diudea 2013).

Data for some small fullerenes and corresponding fivefold and sixfold hyper-cycles are listed in Table 12.3.

12.4 Hyper-graphenes by C_{60} Units

C_{60} fullerene of I_h symmetry (12A2), also called Buckminster fullerene, in honor of Buckminster Fuller, the architect that used the aesthetic appeal structure of C_{60} cage in architecture, is the most synthesized and most studied graphitic structure. It was discussed in extension in literature so that we limit here only to some aspects appearing in its aggregation (see below).

A hyper-graphene of which nodes are C_{60} units may appear when a thin layer of C_{60} is deposited on a (plane) surface. The polymerization can start with a [2+2] cycloaddition to form dimers (Fig. 12.6) but this could be just the beginning of a more complex process; addition at bonds hh (hexagon-hexagon) is far more favored in comparison to that involving ph (pentagon-hexagon) bonds (see below).

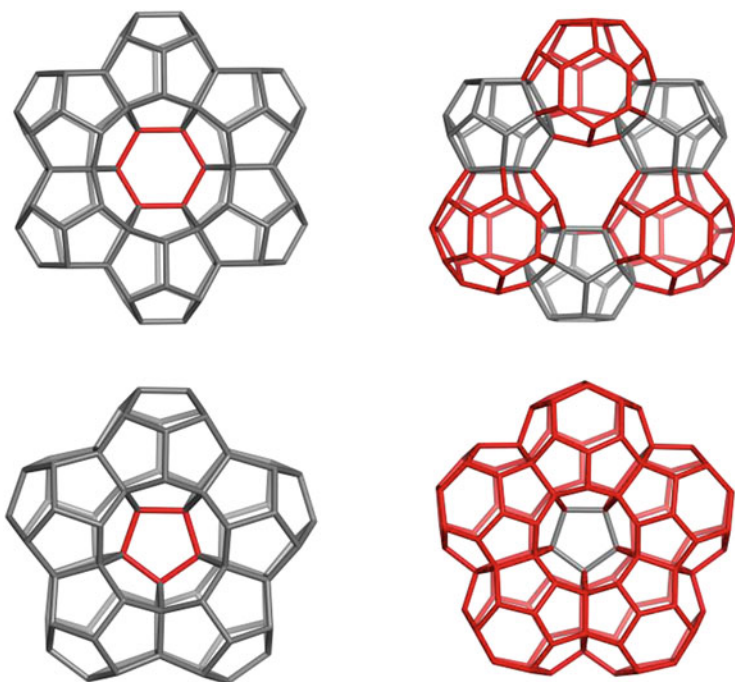


Fig. 12.4 Substructures of C_{20}/C_{28} hyper-graphenes; *Top row*: $(C_{20})_{6,90}$ (*right*); $(C_{20}C_{28})_{3,114}$ (*right*). *Bottom row*: $(C_{20})_{5,75}$ (*left*); $(C_{28})_{5,110}$ (*left*)

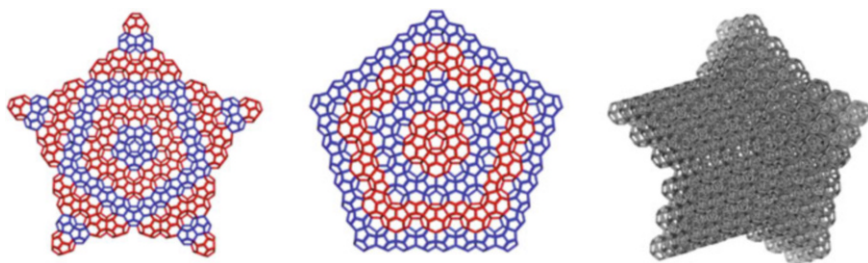
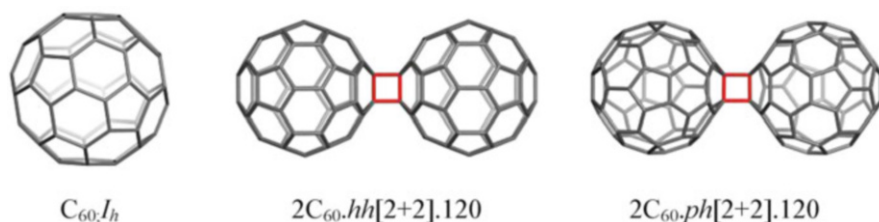


Fig. 12.5 Hyper-graphene domains: C_{20} -centered ($D_5,2028.561s.1345$ (12A1.1) *left*); C_{28} -centered ($D_5,2820.541.1170$ (12A1.2), *middle*) and a D_5 -quasicrystal net ($D_5,2028.533s.5060$ (12A1.3), *right*)

It is also conceivable [Onoe et al. 2012; Diudea and Nagy 2007 (Chap. 5, Stone-Wales isomerization)] that non-closed cages join to each other to form incomplete dimers or trimers, by formal identification of homologous faces (pp or hh), as depicted in Fig. 12.7. Further, these structures can form hyper-pentagons or hyper-hexagons and finally hyper-coronenes (Fig. 12.8) or more extended 2D-structures. Energetic data for such structures are given in Table 12.4, at DFTB level of theory.

Table 12.3 Energetic data (DFTB) for some small fullerenes (C₂₀; C₂₄ and C₂₈) and their hyper-cycles

C ₂₀ -Hyper-graphene	C atoms	E _{tot} (au)	E _{tot} /n (au)	Gap (eV)
C ₆₀	60	-102.185	-1.703	1.930
C ₂₀	20	-33.429	-1.671	0.731
C ₂₄	24	-40.142	-1.673	1.667
C ₂₈	28	-47.101	-1.682	0.351
(C ₂₄) ₅ .90	90	-152.998	-1.700	1.634
(C ₂₀ C ₂₈) ₃ .114	114	-192.488	-1.688	0.166
(C ₂₀) ₅ .75H ₅₀	75	-146.956	-1.959	9.969
(C ₂₄) ₅ .90H ₆₀	90	-175.282	-1.948	9.103
(C ₂₈) ₅ .110H ₈₀	110	-220.185	-2.002	9.270
(C ₂₀) ₆ .90H ₆₀	90	-178.393	-1.982	8.992
(C ₂₀ C ₂₈) ₃ .114H ₈₄	114	-226.346	-1.985	10.278
C ₆₀ H ₆₀	60	-125.584	-2.093	10.412
C ₂₀ H ₂₀	20	-41.659	-2.083	12.295
C ₂₄ H ₂₄	24	-49.752	-2.073	12.247
C ₂₈ H ₂₈	28	-58.301	-2.082	12.384

**Fig. 12.6** C₆₀ dimerization by [2+2] cycloaddition

One can see (Table 12.4) that structures with more hexagonal junction (f6), namely those of entries 2, 6, 8 and 10 are energetically favored.

Computations comparative to DFTB we made on small structures (see Table 12.5) with additional data at Hartree-Fock HF and DFT(B3LYP) level of theory. One can see that, in general, the ordering in the three approaches is preserved, with some exceptions. The main backtracking of DFTB is the underestimation of the gap values in case of *sp*² carbon-only structures. However, DFTB is useful in ordering series of rather large carbon nanostructures.

In following idea of hyper-graphenes, some three-connected nodes with the C₆₀ units separated by pentagonal prisms P₅ (Fig. 12.8) were considered. Constructions

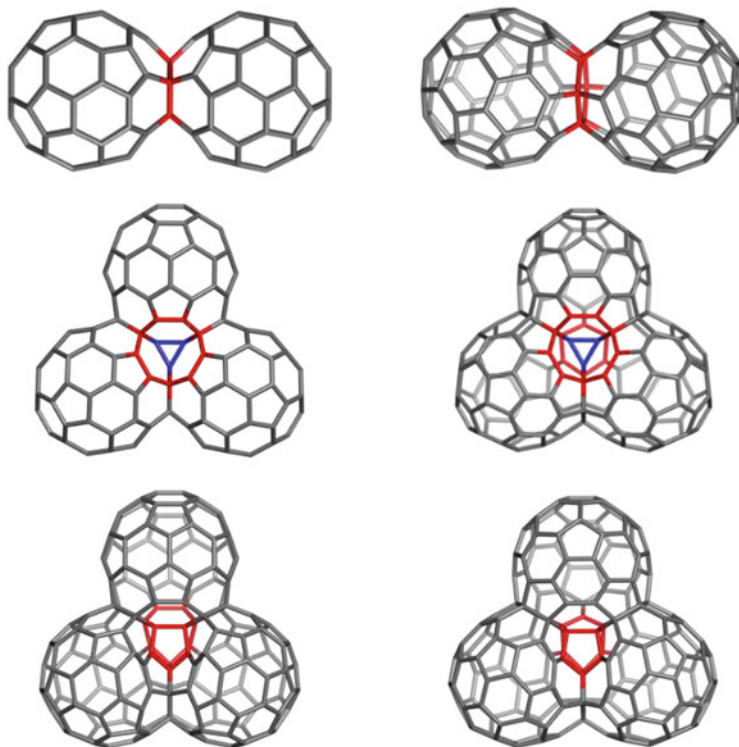


Fig. 12.7 C_{60} oligomers. *Top row:* $C_{60n_2f_5.115}$ (left) and $C_{60n_2f_6.114}$ (right); *Middle row:* $C_{60n_3f_{555}.165}$ (left) and $C_{60n_3f_{666}.162}$ (right); *Bottom row:* $C_{60n_3f_{556}.164}$ (left) and $C_{60n_3f_{566}.163}$ (right)

with these nodes are illustrated in the chapter Atlas, at 12A2.1–12A2.2 (see Fig. 12.9).

If carbon atoms populate such structure, their energetics are rather poor, showing positive binding energy: $E_{\text{bind}} = 298.921$ kcal/mol (see Table 12.6); E_{bind} is calculated as the difference between the total energy of the system and n -times the total energy of C_{60} free-fullerene:

$$E_{\text{bind}} = E_{\text{tot}}(C_{60})_n - n \times E_{\text{tot}}(C_{60})$$

Additional atoms to form TO = C_{24} small cage do not improve the stability of such structures (see the bottom row in Table 12.6).

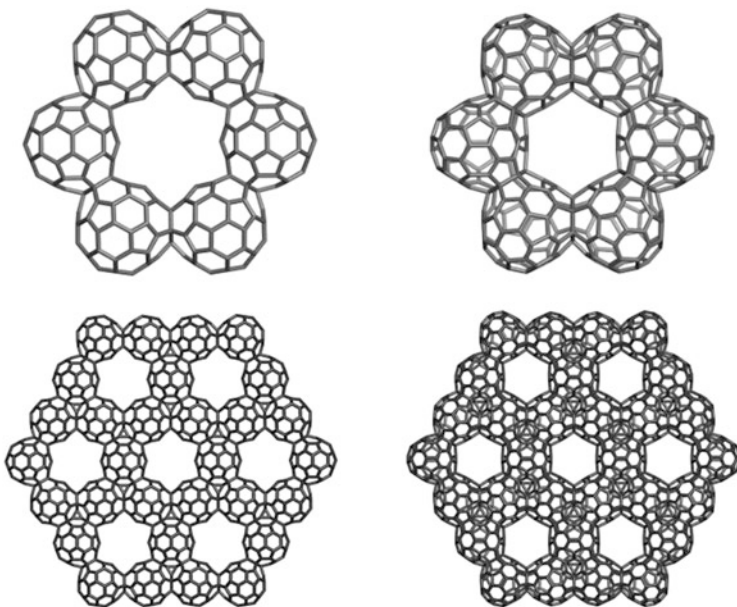


Fig. 12.8 Hyper-graphenes. *Top row:* Hex(C₆₀f₅).330 (*left*); Hex(C₆₀f₆).324 (*right*); *Bottom row:* *l*(Cor(C₂₀)).1560 (*left*); Cor(C₆₀).1512 (*right*)

Table 12.4 Energetic data (DFTB level of theory) for the C₆₀oligomers

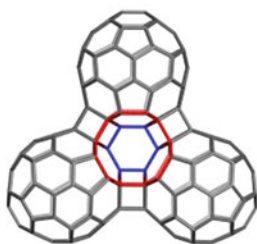
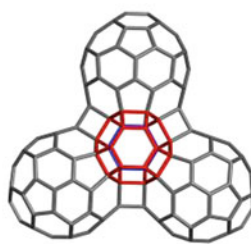
	Structure	<i>n</i>	E _{tot} (au)	E _{tot} / <i>v</i>	Gap (eV)
1	C ₆₀	60	-102.185	-1.703	1.930
2	C ₆₀ n ₂ f ₆	114	-194.183	-1.703	1.444
3	C ₆₀ n ₃ f ₅₅₅	165	-280.787	-1.702	0.608
4	C ₆₀ n ₃ f ₅₅₆	164	-281.658	-1.717	0.333
5	C ₆₀ n ₃ f ₅₆₆	163	-280.238	-1.719	0.391
6	C ₆₀ n ₃ f ₆₆₆	162	-278.935	-1.722	1.481
7	HypHex165f ₅	330	-567.506	-1.710	0.179
8	HypHex162f ₆	324	-557.737	-1.721	1.255
9	<i>l</i> (Cor(C ₂₀))165f ₅	1560	-2652.462	-1.700	0.021
10	Cor(C ₆₀)162f ₆	1512	-2603.270	-1.722	1.095

12.5 C₆₀ Aggregates with Tetrahedral and Icosahedral Symmetry

When three disjoint C₆₀ units join in a hyper-triangle, this may be embedded in the tetrahedron or in the icosahedron (Fig. 12.10), with a hexagon between each of the three C₆₀ units. In case of the tetrahedral cluster, the four C₆₀ units arrange over four

Table 12.5 Comparative data for some small structures involved in hyper-graphenes at Hartree-Fock HF, DFT (B3LYP) and DFTB levels of theory

Structure	n	Theory	E_{tot} (au)	E_{tot}/n (au)	Gap (eV)
$(C_{20})_5f_5$	75	HF	-2838.062	-37.841	4.158
		DFT	-2856.161	-38.082	0.6
		DFTB	-126.324	-1.684	0.113
$(C_{20})_6f_5$	90	HF	-3405.751	-37.842	5.99
		DFT	-3427.462	-38.083	0.9
		DFTB	-151.694	-1.684	0.195
$(C_{28})_5f_6$	110	HF	-4163.361	-37.849	5.533
		DFT	-4189.837	-38.089	1.072
		DFTB	-185.928	-1.69	0.006
$(C_{28})_6f_6$	132	HF	-4996.056	-37.849	5.421
		DFT	-5027.845	-38.090	1.059
		DFTB	-223.166	-1.691	0.035
C_{60}	60	HF	-2271.830	-37.864	7.418
		DFT	-2286.174	-38.103	2.760
		DFTB	-102.185	-1.703	1.930
$C_{60}n_2f_5$	115	HF	-4354.333	-37.864	7.597
		DFT	-4381.797	-38.103	2.907
		DFTB	-195.708	-1.702	2.044
$C_{60}n_2f_6$	114	HF	-4316.491	-37.864	6.270
		DFT	-4343.730	-38.103	1.908
		DFTB	-194.183	-1.703	1.444

 $3(C_{60};P_5).180$ (12A2.1) $2TO@3(C_{60};P_5).192$ (12A2.2)**Fig. 12.9** Trimeric nodes made by C_{60} units (*top view*)**Table 12.6** QM data for C_{60} and some of its aggregates; B3LYP/6-31G(d)

Structure	n	e	PG	E_{gap} (eV)	E_{bind} (kcal/mol)	E_{tot}/v (au)
C_{60}	60	90	I_h	2.763	-	-38.1029
$3(C_{60};P_5)$ (12A2.1)	180	285	D_{3h}	1.204	298.921	-38.1003
$2TO@3(C_{60};P_5)$ (12A2.2)	192	309	D_{3h}	0.213	-	-37.558

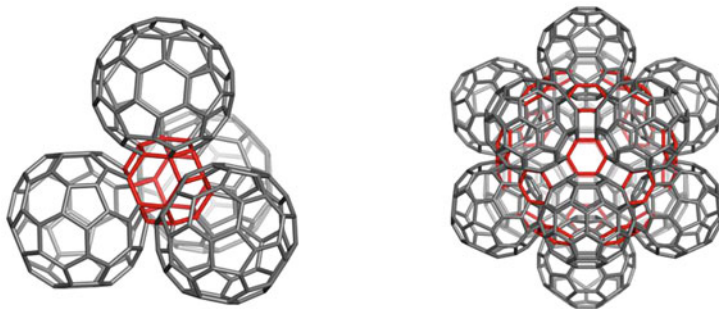


Fig. 12.10 Embedding of C₆₀-triples in the tetrahedron (*left* 12A3) and icosahedron (*right* 12A8)

Table 12.7 QM data for C₆₀ and some of its aggregates; B3LYP/6-31G(d)

Structure	v	e	PG	E_{gap} (eV)	E_{bind} (kcal/mol)	E_{tot}/v (au)
C ₆₀ (12A2)	60	90	I_h	2.763	–	–38.1029
C ₂₄₀ X(TO@4C ₆₀) (12A3)	240	372	T_d	1.723	133.363	–38.102
C ₂₄₀ (TO@(4C ₆₀ ;6P ₅)) (12A4)	240	390	T_d	1.857	420.148	–38.1001
C ₂₆₄ (TO@(4C ₆₀ ;4TO;6P ₅)) (12A4.1)	264	438	T_d	1.790	–	–37.559

Table 12.8 QM data for C₆₀ and some of its aggregates; B3LYP/6-31G(d)

Structure	v	e	PG	E_{gap} (eV)	E_{tot}/v (au)
C ₆₀ (12A2)	60	90	I_h	2.763	–38.1029
(C ₆₀ @(20TT))H60 (5A2.2)	150	270	I_h	6.359	–38.339
C ₆₀ @(20TO;12P ₅) (5A5.6)	300	540	I_h	4.512	–38.089
C ₅₇₀ (6A6.6)	570	960	I_h	1.291	–37.561

of the eight hexagonal faces of truncated octahedron TO. The icosahedral structure is embedded in the C₂₄₀ fullerene, having 12 disjoint corannulene (5@6⁵) flowers (see also Bhattacharya et al. 2014). Energetic data for the tetrahedral structure (12A3) and its congeners with additional TO and P₅ cells (12A4 and 12A4.1) are given in Table 12.7; one can see that the binding energy is still positive.

Details of these structures are given in Chap. 6 (Fig. 6A6.1.3) and in the Atlas 12A (Fig. 12A8). Tetrahedral clusters may join to each other to form “anti”, “syn” or their combinations, as suggested in Figs. 12A3.1–12A3.4.

Other structures including the C₆₀ cage (sharing a face with another C₆₀ or other small cages) were considered for energetic stability (Table 12.8). Their total energy is not far from that of C₆₀ and approaches more when they may be hydrogenated. It is conceivable that additional atoms may form solid phases surrounding the basic

tetrahedral or icosahedral clusters and approaching the hydrogenated state in stability. Embedding of C_{60} units in the tetrahedron, as spongy structures are shown in Figs. 12A11 and 12A12.

An interesting cluster with trigonal symmetry and 11 C_{60} units is envisaged in Figs. 12A5 and 12A5.1.

12.6 C_{60} Network by [2+2] Cycloaddition

Dimerization of C_{60} by a [2+2] cycloaddition is favored by hexagon-hexagon hh (shorter and electron rich) bonds, in comparison to the pentagon-hexagon ph (longer and electron poor) bonds (see also Sect. 4 and Fig. 12.6); data (computed at LDA/3–21 G(d) level of theory) are listed in Table 12.9. The hh dimer shows a negative binding energy, $E_{\text{bind}} = -28.288$ kcal/mol per one C–C adduct; the two ph isomeric dimers (C_{2v} and C_{2h}) do not differ energetically too much and seems to be less stable than the free fullerene C_{60} . The binding is stronger when the cycloadduct is part of a cube (-28.689 kcal/mol, of 12 C–C in $CY(8C_{60};hh).480$ (12A6.4), Table 12.9); in an infinite C_{60} cubic network, the 6-connected C_{60} unit (denoted $CY(7C_{60};hh).420$ in Table 12.9) gave -27.328 kcal/mol per C–C, as expected for a smaller remaining sp^2 C net in the [2+2] adduct.

A detailed topological analysis of C_{60} [2+2] cycloadduct systems revealed three topologically distinct cubic nets: 1. ($C_{60}.hh$); 2. ($C_{60}.ph$) and 3. ($C_{60}.hh-ph(1:2)$); the last one accounts for $30hh+60ph$ of the 90 edges of C_{60} .

$C_{60}.hh$ is the simple cubic lattice, of $Pa\bar{3}$ symmetry, as reported by David et al. (1991); its repeating unit, denoted here $C_{60}.hh(d)$ (12A6.4.1b and Table 12.10), has the topology $6(ph, hp, ph, hp)$ and T_h point group PG symmetry. The unit topology is described by the faces spacing the actual C–C bond to its four neighbor C–C bonds, counted clockwise, in an increasing (smallest faces) order, keeping in mind that $p = 5$ and $h = 6$.

$C_{60}.ph$ may have two arrangements of a same local topology: one is monotonic (the repeating unit consists of a single C_{60} cluster—denoted (1) in Table 12.10) and

Table 12.9 Energetic data for C_{60} [2+2] cycloadducts (LDA/3–21 G(d)); C–C stands for the square joining two C_{60} units in the [2+2] cycloadduct

Structure	n	e	PG	E_{tot}/v (au)	E_{gap} (eV)	E_{bind} (kcal/mol)	#C□C	$E_{\text{bind}}/C□C$ (kcal/mol)
C_{60}	60	90	I_h	-37.559	1.824	–	–	–
$2C_{60}.hh$	120	92	D_{2h}	-37.56	1.541	-28.288	1	-28.288
$2C_{60}.hp$	120	92	C_{2v}	-37.559	0.787	6.211	1	6.211
$2C_{60}.hp$	120	92	C_{2h}	-37.559	0.686	5.815	1	5.815
$CY(8C_{60};hh)$	480	744	T_h	-37.561	1.655	-344.267	12	-28.689
$CY(7C_{60};hh)$	420	648	T_h	-37.56	1.497	-163.969	6	-27.328
$CY(8C_{60};ph)$	480	744	D_{2h}	-37.559	0.472	29.148	12	2.429

Table 12.10 Kekulé count KC and strain energy (kcal/mol) for CY(C₆₀), 333.1620 (12A6.4n) and its fragments (optimized by RPM6; VSTO-6G(5D;7F))

Fragment	#C ₆₀	#C=C	KC	E _{strain}						
				<i>ph</i>	<i>hh-ph</i>	#C(sp ²)	<i>hh</i> (PM6)	<i>hh</i> (MM+)	<i>hh-ph</i> (MM+)	<i>ph</i> (MM+)
<i>a</i>	8	3	1204	238	156	54	7.256	7.648	7.304	7.566
<i>b</i>	12	4	640	28	40	52	6.868	7.409	6.962	7.287
<i>c</i>	6	5	384	10	12	50	6.440	7.141	6.537	6.985
<i>d</i>	1	6	256	4	4	48	5.966	6.847	6.064	6.641
C ₁₆₂₀ (unit)	27	–	6(<i>ph, hp, ph, hp</i>)	3(<i>ph, hp, hh, hh</i>) 3(<i>ph, hh, hh, hp</i>)	2(<i>ph, hh, ph, hh</i>) 4(<i>ph, hp, hp, hh, hp</i>)	1404	6.865 (1)	7.399 (1)	6.927 (2) 7.318 (1)	6.903 (2) 7.298 (1)

the other is alternating (the repeating unit consists of a dimer, the second C_{60} cluster being rotated 180°); its unit $C_{60}.ph(d)$ (12A6.4.2b) is intrinsic chiral, of S_6 PG symmetry and topology ($3(ph, hp, hh, hh)$; $3(ph, hh, hh, hp)$).

$C_{60}.hh-ph$ may also have two arrangements: its unit $C_{60}.hh-ph(d)$ (12A6.4.3b) is not chiral (but the net could be, in the second arrangement); it has the topology ($2(ph, hh, ph, hh)$; $4(php, hp, hh, hp)$) and PG symmetry D_{2h} .

Binding energy is lower in the ph -net (about -22 kcal/mol) than in the $hh-ph$ net (about -32 kcal/mol) and is maximum in the hh -net (about -56 kcal/mol—see Table 12.11, PM6 data). However, these molecular systems are far from equilibrium and the kinetic aspects will prevail in a crystallization process of C_{60} fullerene, favoring the more statistically dominant structures (see Schwerdtfeger et al. 2015); the real net is expected to be a mixture of the five described nets.

A qualitative explanation may be offered by Kekulé count KC (Diudea and Vukičević 2007), in supporting the chance of π -electron conjugation in the $[2+2]$ adduct. A detailed analysis of the remaining sp^2 C net in the $[2+2]$ adducts of cubic C_{60} -333-nets revealed four types of C_{60} fragments (Fig. 12.11), of 3, 4, 5 and 6 connectivity, respectively (see also Table 12.10); it can be seen that the hh -net (and its fragments) has the largest π -system, much more favorable to the π -conjugation than the ph -net and the mixt $hh-ph$ net.

Among the solutions of geometric Kekulé count, there are identical topological isomers, e.g., among 12,500 solutions for C_{60} only 58.06%, represent distinct structures, as detected by the super-index Cluj-Niš (Ilić and Diudea 2010; Diudea et al. 2010). It was suggested that KC alone cannot predict the stability of fullerene structures (Austin et al. 1994; Vukičević and Klein 2005; Zhang et al. 2010; Schwerdtfeger et al. 2015).

Strain energy was calculated by Haddon's (1987, 1990) POAV1 theory; values of strain decrease by increasing the fragment connectivity (as the size of remaining sp^2 C net decreases). Strain tends to a minimum in the d -fragments representing the bulk unit of the infinite C_{60} cubic nets (Table 12.10).

Strain data are also listed in Table 12.11 (PM6 level of theory). In alternating squares ($4C_{60}$ units), the strain of ph -net (entries 2–5) is lower than of $hh-ph$ net (entry 6) and further lower than of hh -net (entry 10). In corresponding cubes ($8C_{60}$ units—entries 7 and 8), the strain ordering is: $hh-ph$ net (entry 8) < ph -net (entry 7) < hh -net (entry 12). In $27C_{60}$ -333 blocks, optimized by MM+ force field, the strain ordering was: ph (2) < $hh-ph$ (2) < ph (1) < $hh-ph$ (1) < hh C_{60} nets (Table 12.10, bottom row).

Clearly, the cubic net is more favorable (both by E_{bind} and E_{strain} values) in comparison to an icosahedral structure (see entries 13 and 14, Table 12.11).

Figure count for some of these structures is given in Table 12.12. Excepting the structure #1 ($3(C_{60};P_5).180$), which is a torus ($g = 1$), the other clusters can be considered as structures (of rank 4) embedded in the sphere ($g = 0$).

The C_{60} $[2+2]$ cycloadducts may be embedded either in the topology of C_{20} (12A9) or C_{60} (12A10) (see Bhattacharya et al. 2016) providing beautiful hyper-clusters. A remark is worthy here for the leapfrog operation “ l ” that transforms clusters with units sharing an edge to each other into $[2+2]$ adducts (see, e.g., Figs. 12A6–12A6.4 or 12A7.2–12A7.2.1).

Table 12.11 Energetics of C₆₀-containing structures (RPM6; VSTO-6G(5D;7F))

	Structure (RPM6; VSTO-6G(5D;7F))	ν	#C ₆₀	PG	E _{tot} (au)	E _{tot} / ν (kcal/mol)	E _{gap} (eV)	#C \square C	E _{bind} (kcal/mol)	E _{bind} /C \square C (kcal/mol)	E _{strain} (kcal/mol)	ν (sp ²)
1	C ₆₀ (12A2)	60	1	I _h	1.294	13.536	6.794	–	–	–	8.256	60
2	4C ₆₀ -ph ₁ _1 (sp(2he)ps (12A3))	240	4	D _{4h}	5.050	13.204	5.836	4	–79.553	–19.888	7.515	224
3	4C ₆₀ -ph ₂ _2 (shhs)	240	4	D _{4h}	5.346	13.978	2.366	4	106.184	26.546	7.583	224
4	4C ₆₀ -ph ₃ _3 (shhe+)	240	4	C _{2v}	5.025	13.140	6.156	4	–95.230	–23.808	7.539	224
5	4C ₆₀ -ph ₄ _4 (sphe)	240	4	C _{2v}	5.055	13.216	6.065	4	–76.859	–19.215	7.542	224
6	4C ₆₀ -hh-ph (shhe) (12A4)	240	4	C _{2v}	4.935	12.90	6.236	4	–151.631	–37.908	7.565	224
7	8C ₆₀ -222_ph	480	8	D _{2h}	9.879	12.915	6.232	12	–297.954	–24.829	7.133	432
8	8C ₆₀ -222_hh-ph	480	8	D _{4h}	9.747	12.743	5.992	12	–380.762	–31.730	7.124	432
9	2C ₆₀ -hh	120	2	D _{2h}	2.499	13.070	6.604	1	–55.8734	–55.873	–	–
10	4C ₆₀ -hh (shpe)	240	4	D _{2h}	4.819	12.599	6.606	4	–224.887	–56.222	7.611	224
11	7C ₆₀ -222_hh	420	7	T _h	8.518	12.727	6.615	6	–339.866	–56.644	7.708	396
12	8C ₆₀ -222_hh (12A6.4)	480	8	T _h	9.271	12.120	6.990	12	–679.565	–56.630	7.251	432
13	27C ₆₀ -333_hh (12A6.4.1)	1620	27	T _h	30.056	11.642	6.957	54	–3067.350	–56.803	6.865	1404
14	DY(20C ₆₀ -hh) (12A9)	1200	20	I _h	23.199	12.132	6.602	30	–1685.130	–56.171	7.234	1080

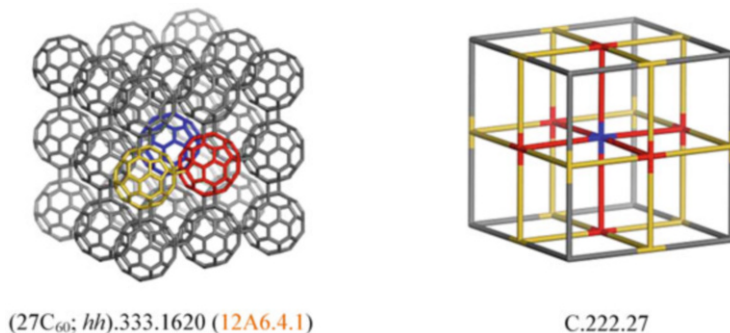


Fig. 12.11 Cubic C₆₀ network, with four distinct units ($a = \text{grey}$, $b = \text{yellow}$, $c = \text{red}$ and $d = \text{blue}$ —*left*), as detailed in the reduced graph (*right*)

Table 12.12 Figure count in some clusters involved in C₆₀aggregation

Structure	v	e	2(3)	2(4)	2(5)	2(6)	2	C ₆₀	P ₅	TO (TT)	M	3	χ	g	k
1 (12A2.1)	180	285	0	15	36	60	111	3	3	0	0	6	0	1	4
2 (12A2.2)	192	309	0	21	36	69	126	3	3	2	1	9	0	0	4
3 (12A3)	240	372	0	6	48	84	138	4	0	0	2	6	0	0	4
4 (12A4)	240	390	0	30	48	84	162	4	6	0	2	12	0	0	4
5 (12A4.1)	264	438	0	42	48	100	190	4	6	4	2	16	0	0	4
6 (5A5.6)	300	540	0	120	24	130	274	1	12	20	1	34	0	0	4
7 (5A2.2)	150	270	50	0	12	80	142	1	0	(20)	1	22	0	0	4
8 (6A6.6)	570	960	50	0	114	260	424	12	0	(20)	2	34	0	0	4

1 = 3(C₆₀;P₅).180; 2 = 2TO@3(C₆₀;P₅).192; 3 = TO@4C₆₀.240X; 4 = TO@(4C₆₀;6P₅).240; 5 = TO@(4C₆₀;4TO;6P₅).264; 6 = C₆₀@(20TO;12P₅).300; 7 = C₆₀@(20TT).150; 8 = 1(D@12D).570

12.7 Computational Methods

Geometry optimizations were performed at the at SCC-DFTB level of theory (Elstner et al. 1998) by using the DFTB+ program (DFTB+; Aradi et al. 2007) with the numerical conjugated gradient method. We used this method because many structures have more than 100 atoms (or more than 1500 atoms).

The DFTB method can be combined with the self-consistent charge technique (SCC-DFTB) to provide more accurate results, comparable with some higher level theoretical methods.

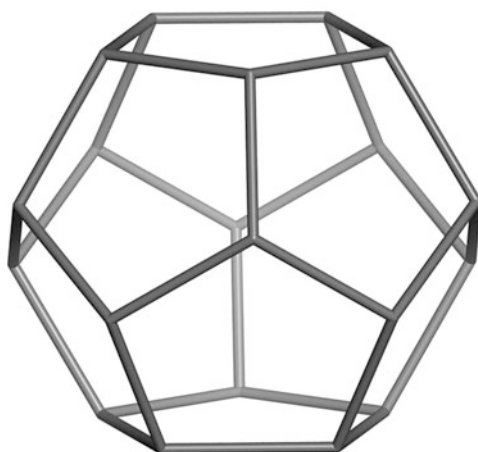
Computations at a higher level of theory: Hartree-Fock and DFT have been performed with the HF/6-31G(d,p), B3LYP/6-31G(d), B3LYP/6-31G(d,p) and LDA/3-21G(d) sets, on Gaussian 09 (Frisch et al. 2009). PM6 computations were done with the VSTO-6G(5D;7F) set.

POAV1 theory of Haddon (1987, 1990) was applied for strain energy calculation. Topological data were calculated by our Nano Studio software (Nagy and Diudea 2009).

Kekulé count was done by our original software (Cigher and Diudea 2006) while the “solutions” were analyzed for isomer discrimination by the super-index Cluj-Niš program (Ilić and Diudea 2010).

The herein discussed structures were seen as molecules; some of them have been considered as carbon structures and molecular energy was computed. However, many others could be models for crystal or quasi-crystal structures. It was not the aim of this book to think about the presented structures as exclusively material structures; these could represent subjects for future mathematical, physical or chemical theoretical and/or practical studies, as well as could inspire architects and plastic artists.

Chapter 12 Atlas: Energetics of Multi-shell Clusters



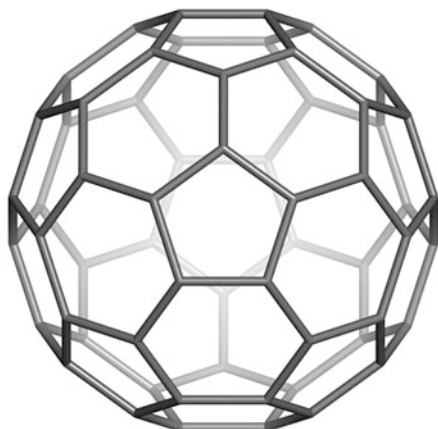
C_{20}

Dodecahedron

Symmetry Group: $C_{2v}A_5$; $|C_{2v}A_5|=120$

12A1

C_{12}	$(C_{20})_{5.75}$	$(C_{20})_{6.90}$



$C_{60} I_h$

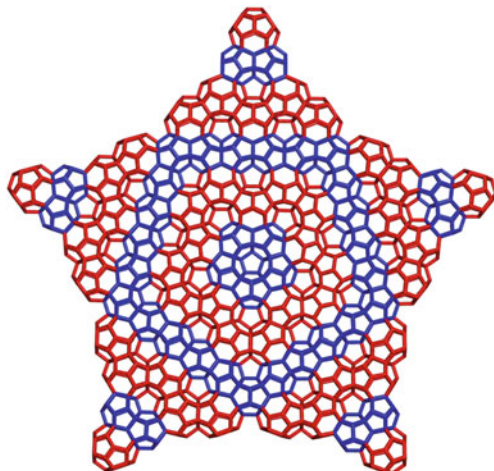
$I/D.60 = I/I.60$

$4((6:3(5.6));6).60$

$C_2.A_5; \text{Classes: } 1 \mid \{60\} \mid$

12A2

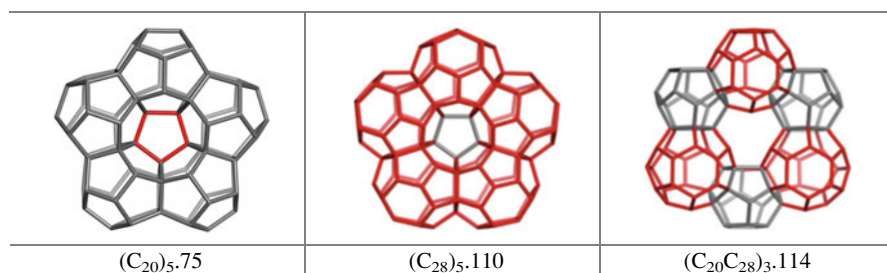
<p>C_{60}; sumanene 6:3(5.6)</p>	<p>C_{60}; empty sumanene</p>	<p>C_{60}; 2(4 sumanene)</p>

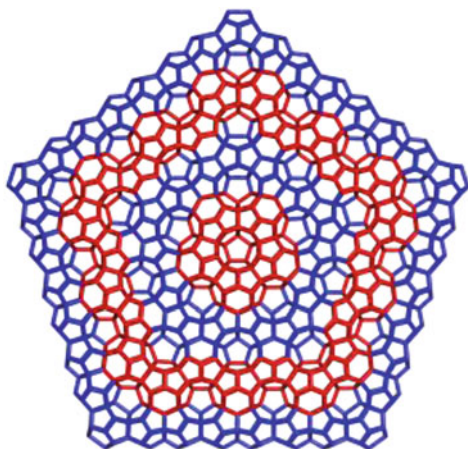


D₅.2028.561s.1345

(C₂₀ centered)

12A1.1



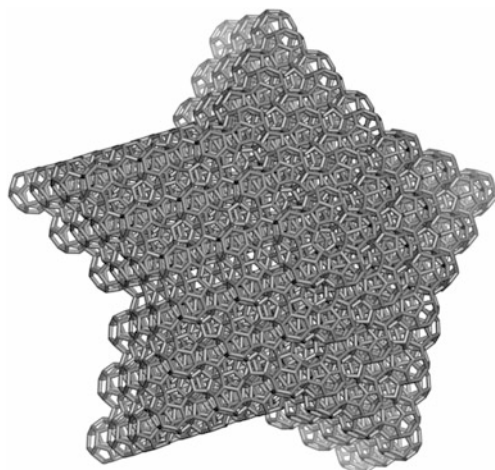


D_{5h}.2820.541.1170

(C₂₈-centered)

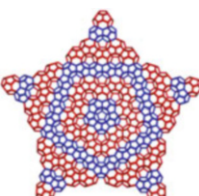
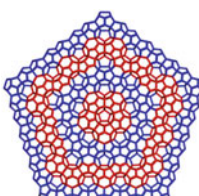
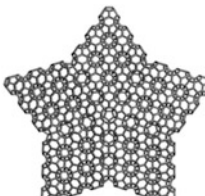
12A1.2

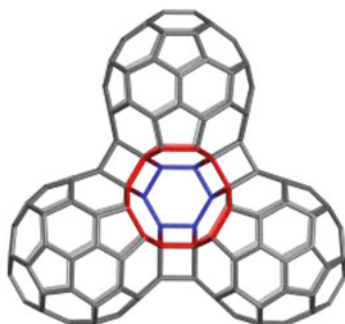
<p>(C₂₈)₅.110</p>	<p>(C₂₀)₅.75</p>	<p>(C₂₀C₂₈)₃.114</p>



D₅.2028.533s.5060

12A1.3

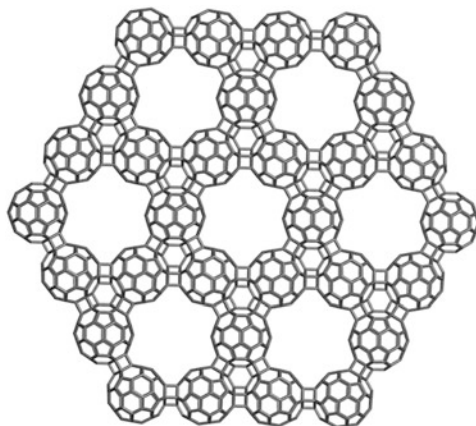
		
D ₅ .2028.561s.1345	D ₅ .2820.541.1170	D ₅ .2028.533s.5060



3(C₆₀;P₅).180

12A2.1

<p>C₆₀</p>	<p>2TO@3(C₆₀;P₅).192</p>	<p>C₁₈₀₀</p>

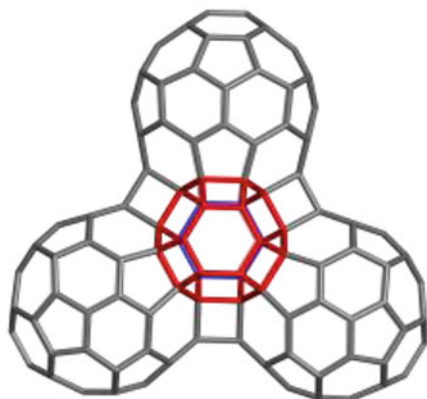


CorY(30C₆₀;P₅).1800

$h(3(C_{60};P_5))@6(h(3(C_{60};P_5))).1800$


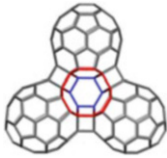
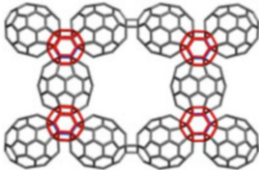
12A2.1.1

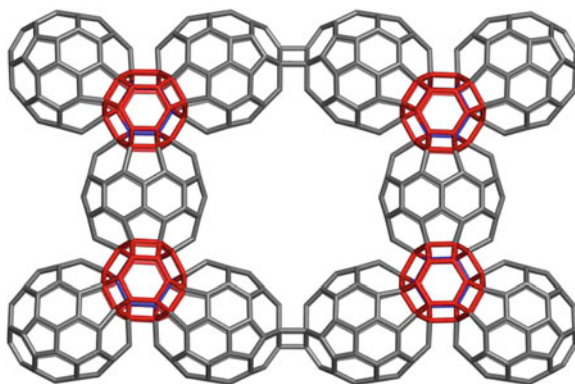
<p>3(C₆₀;P₅).180</p>	<p>6(3(C₆₀;P₅)).720</p>	<p>C₁₈₀₀ (side)</p>



2TO@3(C₆₀;P₅).192

12A2.2

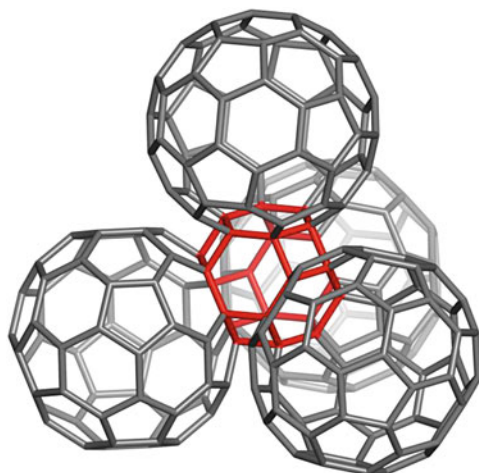
		
C ₆₀	3(C ₆₀ ;P ₅).180	C ₆₄₈



hY(2TO@3(C₆₀;P₅)192).648

12A2.2.1

<p>$3(C_{60};P_5).180$ (top)</p>	<p>$2TO@3(C_{60};P_5).192$ (top)</p>	<p>$hY(C_{192}).2.2.1644$</p>



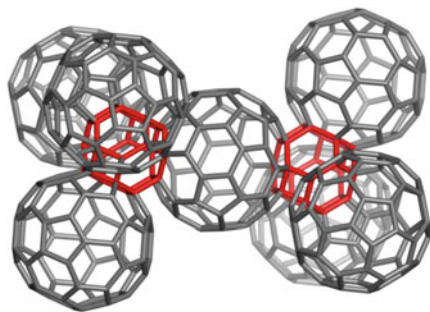
TY(4C₆₀;(TO;f₆)).240

TO@4C₆₀.240

S₄; classes 12:|8{24};4{12}|



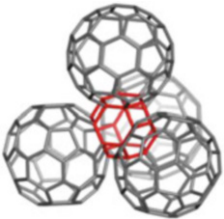
12A3

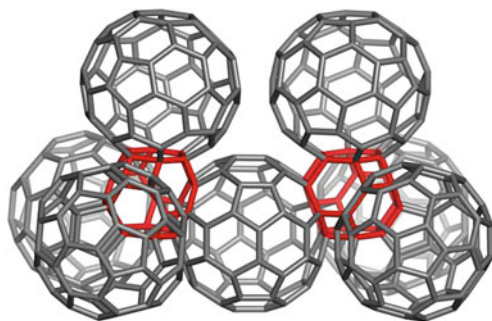
C ₆₀	TO@(4C ₆₀ ;6P ₅).240	TO@(4C ₆₀ ;4TO;6P ₅).264



2×(TY(4C₆₀)240).anti.420

12A3.1

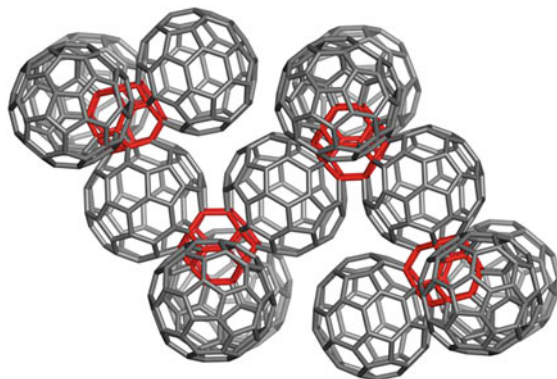
		
TO.24	C ₆₀	TY(4C ₆₀).240



$2 \times (\text{TY}(4\text{C}_{60})\ 240)_{\text{syn.420}}$



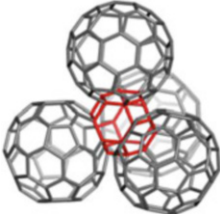
12A3.2

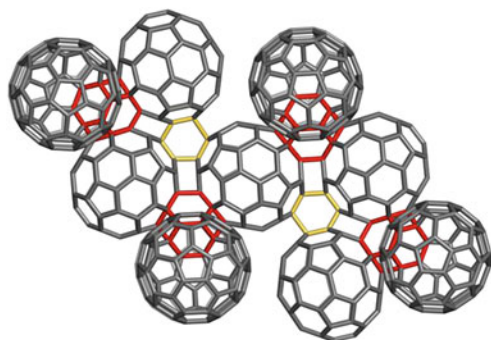
TO.24	C_{60}	$\text{TY}(4\text{C}_{60}).240$



$4 \times (\text{TY}(4\text{C}_{60})240)$.*syn-anti-syn*.780

12A3.3

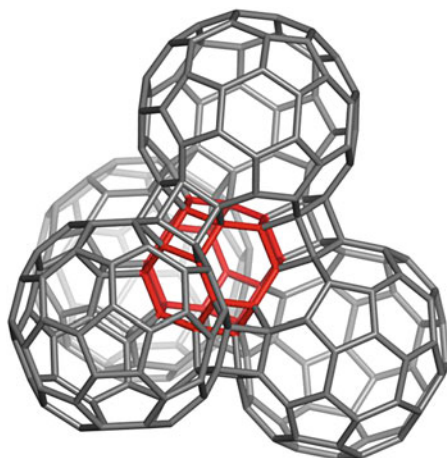
		
TO.24	C_{60}	$\text{TY}(4\text{C}_{60}).240$



$4 \times (\text{TY}(4\text{C}_{60})_{240})_{\text{syn-anti-syn}} \cdot \text{J.780}$

12A3.4

TO.24	C_{60}	C_{348}

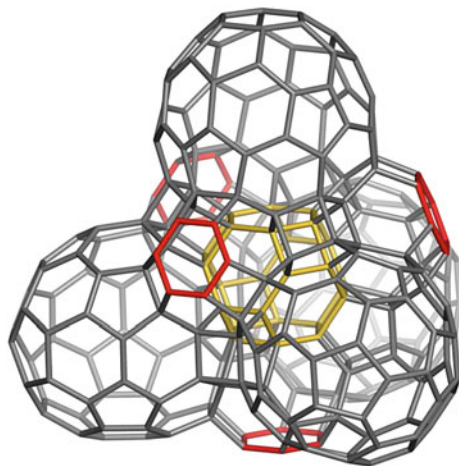


TO@(4C₆₀;6P₅).240

S₄; classes 12: |8{24}, 4{12}|

12A4

TO@(4C ₆₀ ;6P ₅).240_2	TO@(4C ₆₀ ;6P ₅).240_3	TY(4C ₆₀ ;(TO:f ₆)).240

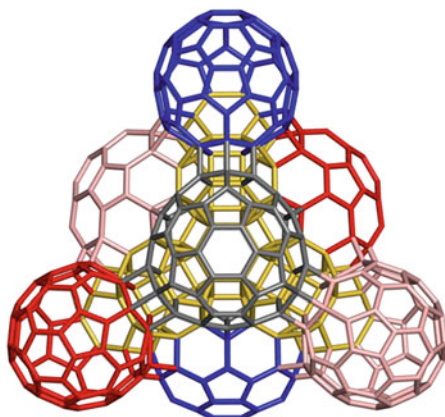


TO@(4C₆₀;4TO;6P₅).264

S₄; classes 13:|4{12}, 9{24}|

12A4.1

<p>TO@(4C₆₀;4TO;6P₅).264_2</p>	<p>TO@(4C₆₀;4TO;6P₅).264_3</p>	<p>TY(4C₆₀;(TO;<i>f</i>₆)).240</p>

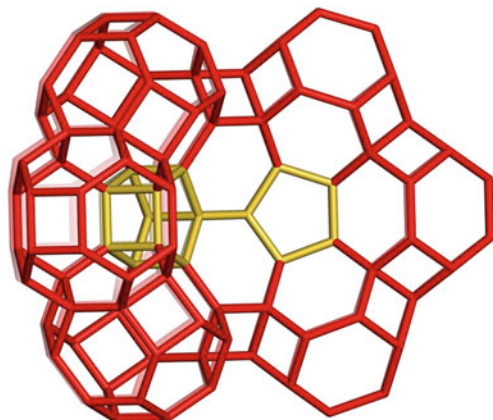


$3((P_5@5TO)@(5C_{60};30P_5)).660$

D_{12} ; classes 61:|49{12},12{6}|

12.A.5

C_{660} (hyperpentagon view)	$(3(P_5@5TO);2TO).186$	$3(P_5@5TO).186_3$

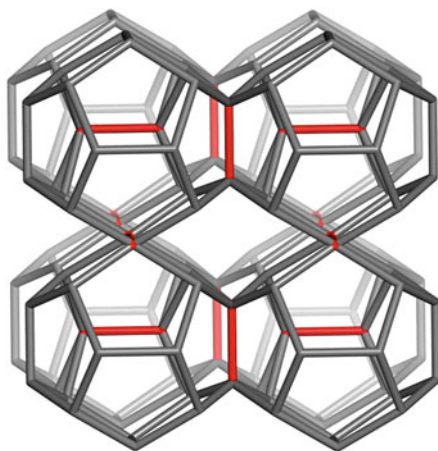


3(P₅@5TO).186

D₁₂; classes 16: |15{12};{6}|

12A5.1

TO.24	C ₁₈₆	C ₆₆₀

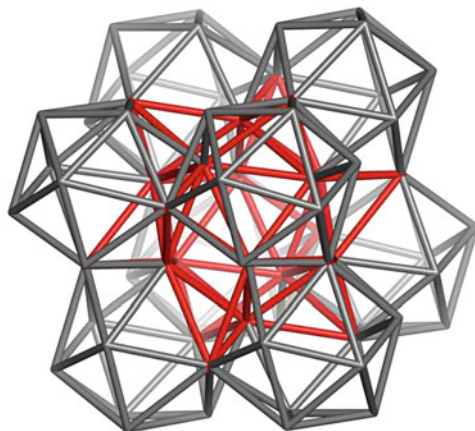


CY(8C₂₀;e).136

D.222.e.136

$C_2 \times A_4$; classes 8: |4{24};2{8};2{12}|
12A6

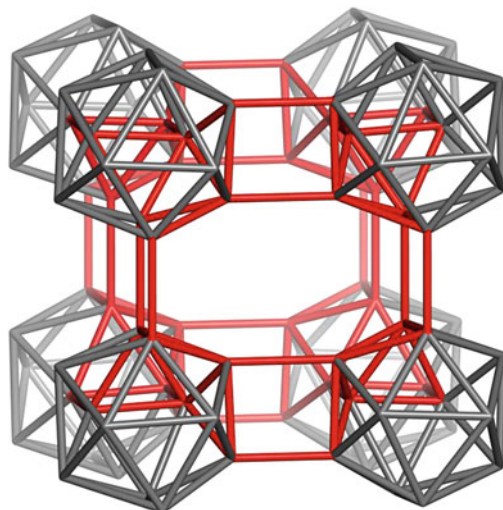
<p>C₂₀-222.136_2</p>	<p>C₂₀-222.136_3</p>	<p>I.222.e.72_2</p>



I.222.e.72

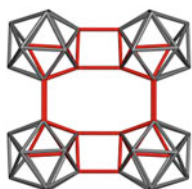
$C_2 \times A_4$; $|C_2 \times A_4| = 24$;
 classes 4: $[2\{24\}, 2\{12\}]$
 12A7

I.222.e.72	I.222.e.72	D.222.e.136

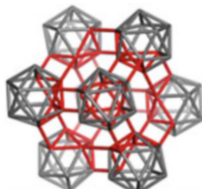


CY(8I;[2+2]).90

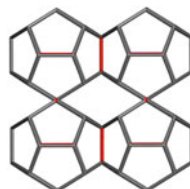
8I.222.90
d(CY(8D;*e*)136).90
12A6.1



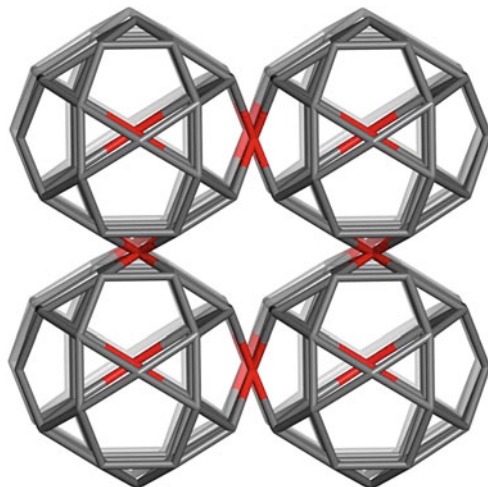
8I.222.90_2



8I.222.90_3



C₂₀.222.136

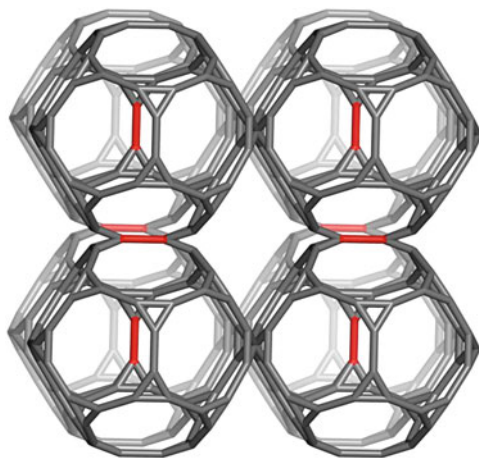


m(D.222.e).228

$C_2 \times A_4$; classes 10: |9{24};{12}|

12A6.2

<p><i>m(D.222.e).228</i></p>	<p><i>m(D.222.e).228</i></p>	<p>D.222.e.136</p>

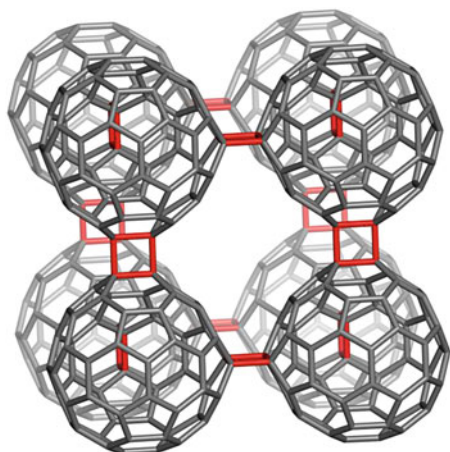


t(D.222.e).456

$C_2 \times A_4$; classes 20: $|18\{24\}; 2\{12\}|$

12A6.3

<i>t(D.222.e).456</i>	<i>t(D.222.e).456</i>	D.222.e.136



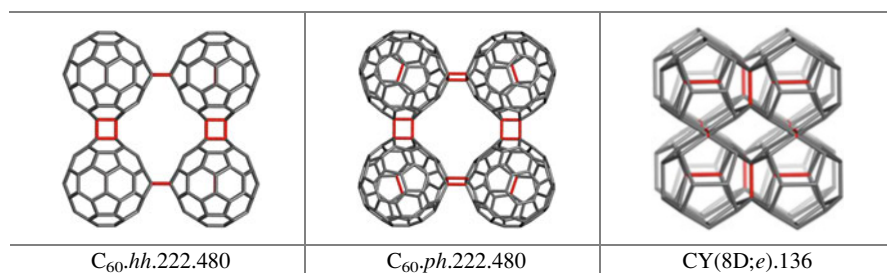
CY(8C₆₀;hh[2+2]).480

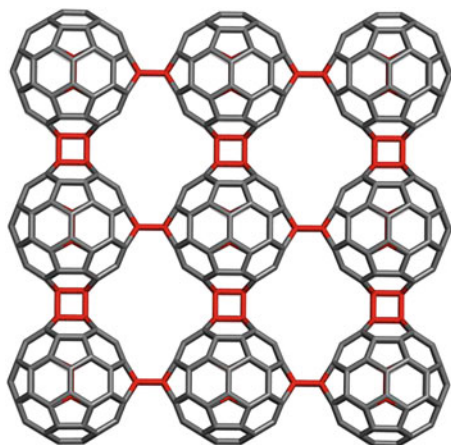
C₆₀.hh.222.480

I(CY(8D:e)136).480

C₂ × A₄; classes 20: [20{24}]

12A6.4

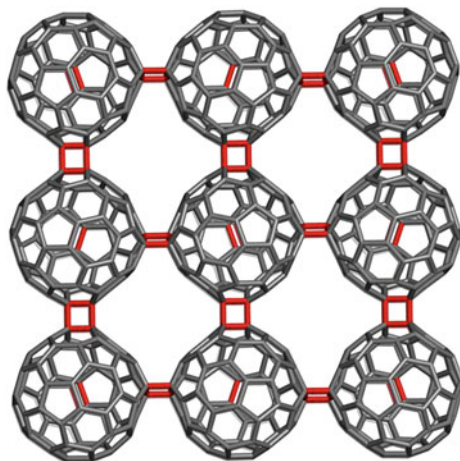




C₆₀. 333.hh.1620

Classes 72: |9{12};63{24}|
12A6.4.1

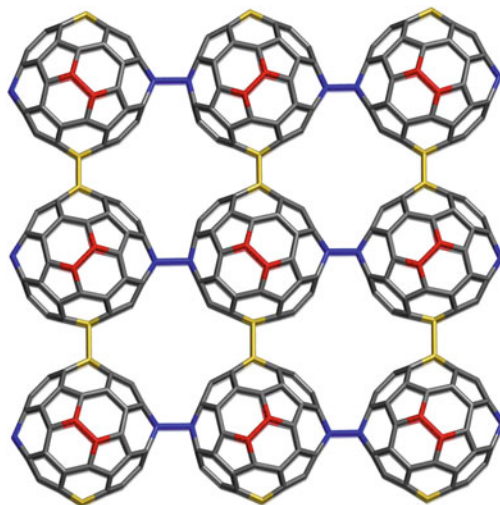
<p>C₆₀.hh.222.480</p>	<p>C₆₀.hh.222.480</p>	<p>C₆₀.hh(d).72; T_h</p>



C_{60} . 333.ph.1620 (2)

Classes 270: $|270\{6\}|$
12A6.4.2

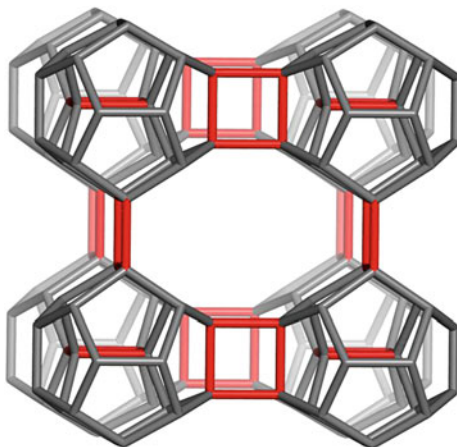
C_{60} .ph.222.480 (2)	C_{60} .ph.222.480 (1)	C_{60} .ph(d).72; S_6



C_{60} .hh-ph.333.1620

Classes 216: $[27\{4\}]$; $189\{8\}$
12A6.4.3

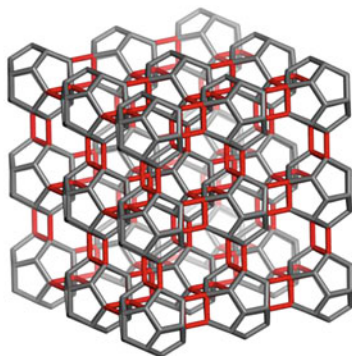
<p>C_{60}.hh-ph.222.480 (2)</p>	<p>C_{60}.hh-ph.222.480 (1)</p>	<p>C_{60}.hh-ph(d).72; D_{2h}</p>



CY(8C₂₀; $[2+2]$).160

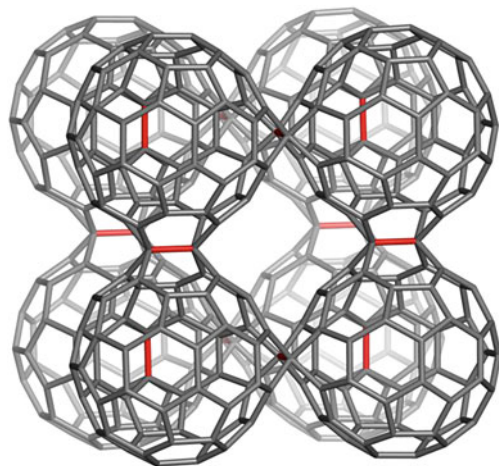
d(I.222.e.72).160
 $C_2 \times A_4$; classes 8: $|6\{2\}; 2\{8\}|$
 12A7.1

<p><i>d</i>(I.222.e.72).160</p>	<p><i>d</i>(I.222.e.72).160</p>	<p>I.222.e.72</p>

**D.333.[2+2].540**
 $C_2 \times A_4$; classes 29: |17{24};3{8};9{12}|

12A7.1.1

D.333.[2+2].540	D.333.[2+2].540	D.333.[2+2].540 (corner)

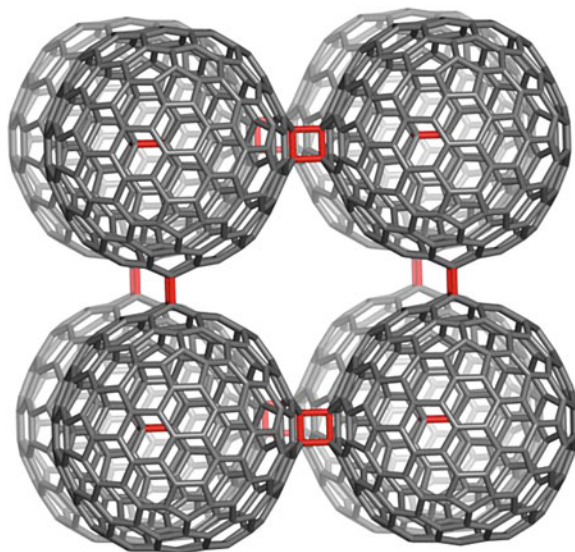


t(I.222.e.72).456

$C_2 \times A_4$; classes 20: |18{24};2{12}|

12A7.2

<p><i>t(I.222.e.72).456</i></p>	<p><i>t(I.222.e.72).456</i> (corner)</p>	<p><i>I.222.e.72</i></p>

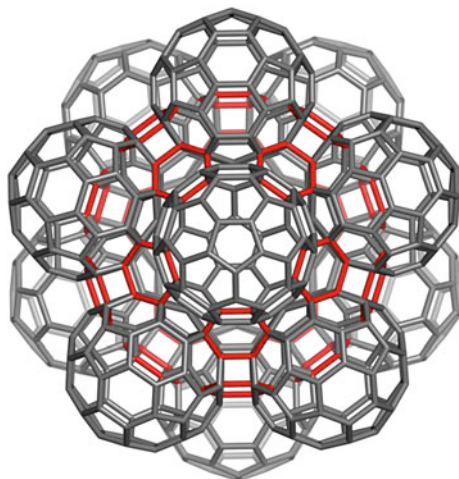


CY(8C₁₈₀;hh[2+2]).1440

l(t(I.222.e.72)456).1440

12A7.2.1

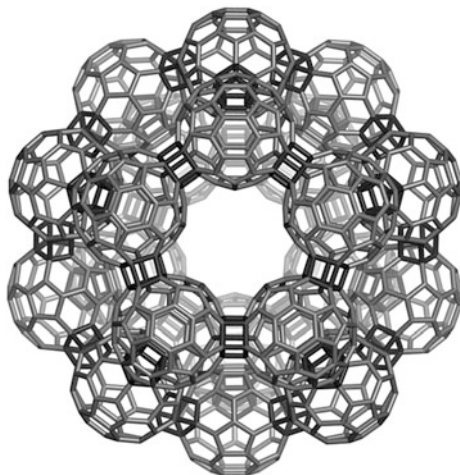
<p><i>l(t(I.222.e.72)456).1440</i></p>	<p><i>l(t(I.222.e.72)456).1440</i></p>	<p><i>t(I.222.e.72).456</i></p>



IY(12C₆₀;(e_{jn})).720X

C₂₄₀@12C₆₀.720X sp
t(d(C₁₃₀)).720X sp
 C₂ × A₅; classes 8:|4{60};4{120}|
 12A8

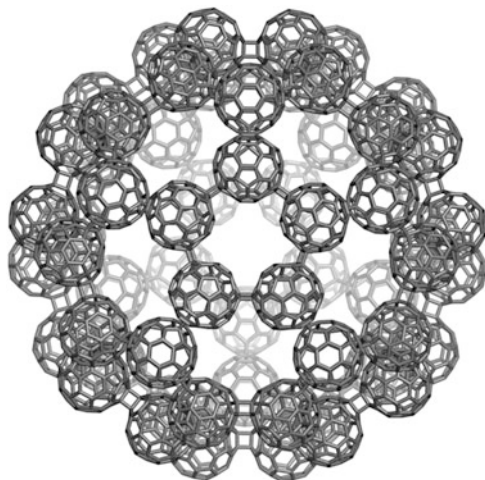
<p><i>t(d(C₁₃₀)).720X_2</i></p>	<p><i>t(d(C₁₃₀)).720X_3</i></p>	<p>C₂₄₀ disjoint corannulenes</p>



DY(20C₆₀;P₅).1200

$t(d(C_{250})).1200$
 $C_2 \times A_5$; classes 12: $8\{120\};4\{60\}$
 12A9

$t(d(C_{250})).1200$	$C_{20}Y(20C_{60};ph[2+2]).1200$	$C_{20}Y(20C_{60};hh[2+2]).1200$

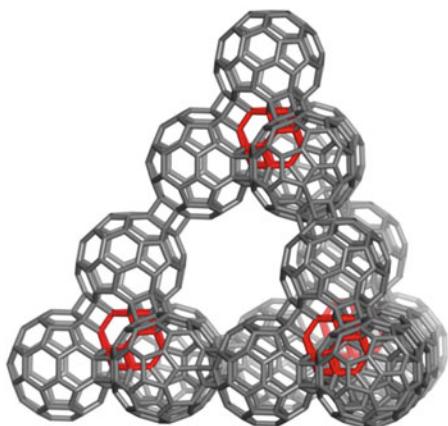


$C_{60}Y(60C_{60};hh[2+2]).3600$

$C_2 \times A_5$; classes 32:28{120},4{60}|

12A10

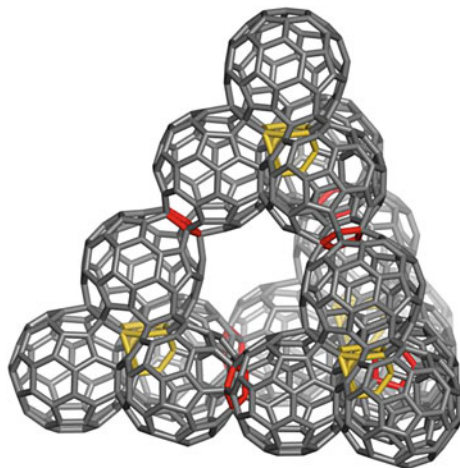
<p>$C_{60}Y(60C_{60};hh[2+2]).3600$</p>	<p>$C_{60}Y(60C_{60};ph[2+2]).3600$</p>	<p>$C_{60}Y(60C_{60};P_5).3600$</p>



TY(4C₂₄₀;P₅).960

(16C₆₀;4TO;30P₅).960
 S₄; classes 44: [36{24};8{12}]
 12A11

<p>TO@(4C₆₀;6P₅).240_3</p>	<p>(TO@4TO)@ (4C₆₀;6P₅).264_3</p>	<p>C₈₁₀</p>



TY(4C₂₁₀;5).810

I(Ada20.198)834X.810
 S₄ classes 41: |27{24};13{12};{6}|
 12A12

Ada20.198	(TT@4TT)@(4C ₆₀).210	C ₆₃₀

References

- Adams GB, O’Keeffe M, Demkov AA, Sankey OF, Huang Y-M (1994) Wide-band-gap Si in open fourfold-coordinated clathrate structures. *Phys Rev B* 49(12):8048–8053
- Aradi B, Hourahine B, Frauenheim T (2007) DFTB+, a sparse matrix-based implementation of the DFTB method. *J Phys Chem A* 111:5678–5684
- Austin SJ, Fowler PW, Hansen P, Manolopoulos DE, Zheng M (1994) Fullerene isomers of C₆₀ Kekulé counts versus stability. *Chem Phys Lett* 228:478–484
- Benedek G, Colombo L (1996) Hollow diamonds from fullerenes. *Mater Sci Forum* 232:247–274
- Bhattacharya D, Klein DJ, Oliva JM, Griffin LL, Alcoba DR, Massaccesi GE (2014) Icosahedral symmetry super-carborane and beyond. *Chem Phys Lett* 616–617:16–19
- Bhattacharya D, Klein DJ, Ortiz Y (2016) The astounding buckyball buckyball. *Chem Phys Lett* 647:185–188

- Blatov VA, Carlucci L, Ciani G, Proserpio DM (2004) Interpenetrating metal-organic and inorganic 3D networks: a computer-aided systematic investigation. Part I. Analysis of the Cambridge structural database. *CrystEngComm* 6:377–395
- Blatov VA, Delgado-Friedrichs O, O’Keeffe M, Proserpio DM (2007) Three-periodic nets and tilings: natural tilings for nets. *Acta Crystallogr Sect A Found Crystallogr* 63(5):418–425
- Blatov VA, O’Keeffe M, Proserpio DM (2009) Vertex-, face-, point-, Schläfli-, and Delaney-symbols in nets, polyhedra and tilings: recommended terminology. *CrystEngComm* 12 (1):44–48
- Böhme B, Guloy A, Tang Z, Schnelle W, Burkhardt U, Baitinger M, Yu G (2007) Oxidation of M_4Si_4 ($M = Na, K$) to clathrates by HCl or H_2O . *J Am Chem Soc* 129:5348–5349
- Cigher S, Diudea MV (2006) Kekulé structure counter. “Babes-Bolyai” University, Cluj
- David WIF, Ibberson RM, Matthewman JC, Prassides K, Dennis TJS, Hare JP, Kroto HW, Taylor R, Walton DRM (1991) Crystal structure and bonding of ordered C_{60} . *Nature* 353:147–149
- Delgado-Friedrichs O, O’Keeffe M (2005) Crystal nets as graphs: terminology and definitions. *J Solid State Chem* 178(8):2480–2485
- Diudea MV (2010) Diamond D_5 , a novel allotrope of carbon. *Stud Univ Babes-Bolyai Chem* 55 (4):11–17
- Diudea MV (2013) Hyper-graphenes. *Int J Chem Model* 5:211–220
- Diudea MV, Nagy CL (2007) Periodic nanostructures. Springer, Dordrecht
- Diudea MV, Nagy CL (2012) All pentagonal ring structures related to the C_{20} fullerene: diamond D_5 . *Diam Relat Mater* 23:105–108
- Diudea MV, Vukičević D (2007) Kekulé structure count in corazulenic fullerenes. *J Nanosci Nanotechnol* 7:1321–1328
- Diudea MV, Ilić A, Varmuza K, Dehmer M (2010) Network analysis using a novel highly discriminating topological index. *Complexity* 16(6):32–39
- Elstner M, Porezag D, Jungnickel G, Elsner J, Haugk M, Frauenheim T, Suhai S, Seifert G (1998) Self-consistent-charge density-functional tight-binding method for simulations of complex materials properties. *Phys Rev B* 58:7260–7268
- Frisch MJ, Trucks GW, Schlegel HB, Scuseria GE, Robb MA, Cheeseman JR, Scalmani G, Barone V, Mennucci B, Petersson GA, Nakatsuji H, Caricato M, Li X, Hratchian HP, Izmaylov AF, Bloino J, Zheng G, Sonnenberg JL, Hada M, Ehara M, Toyota K, Fukuda R, Hasegawa J, Ishida M, Nakajima T, Honda Y, Kitao O, Nakai H, Vreven T, Montgomery JA, Peralta JE, Ogliaro F, Bearpark M, Heyd JJ, Brothers E, Kudin KN, Staroverov VN, Kobayashi R, Normand J, Raghavachari K, Rendell A, Burant JC, Iyengar SS, Tomasi J, Cossi M, Rega N, Millam NJ, Klene M, Knox JE, Cross JB, Bakken V, Adamo C, Jaramillo J, Gomperts R, Stratmann RE, Yazyev O, Austin AJ, Cammi R, Pomelli C, Ochterski JW, Martin RL, Morokuma K, Zakrzewski VG, Voth GA, Salvador P, Dannenberg JJ, Dapprich S, Daniels AD, Farkas Ö, Foresman JB, Ortiz JV, Cioslowski J, Fox DJ (2009) Gaussian 09 Rev. A.1. Gaussian Inc., Wallingford
- Guloy A, Ramlau R, Tang Z, Schnelle W, Baitinger M, Yu G (2006) A quest-free germanium chlatrate. *Nature* 443:320–323
- Haddon RC (1987) Rehybridization and π -orbital overlap in nonplanar conjugated organic molecules: π -Orbital axis vector (POAV) analysis and three-dimensional hückel molecular orbital (3D-HMO) theory. *J Am Chem Soc* 109:1676–1685
- Haddon RC (1990) Measure of nonplanarity in conjugated organic molecules: which structurally characterized molecule displays the highest degree of pyramidalization? *J Am Chem Soc* 112:3385–3389
- Ilić A, Diudea MV (2010) Super-index Cluj-Niș software program. “Babes-Bolyai” University, Cluj
- Kyani A, Diudea MV (2012) Molecular dynamics simulation study on the diamond D_5 sub-structures. *Central Eur J Chem* 10(4):1028–1033

- Meier WM, Olson DH (1992) Atlas of zeolite structure types, 3rd edn. Butterworth-Heineman, London
- Nagy CL, Diudea MV (2009) Nano studio. Babes–Bolyai University, Cluj
- Nagy CL, Diudea MV (2013) Diamond D_5 . In: Nagy CL, Diudea MV (eds) Diamond and related nanostructures. Springer, Dordrecht, pp 91–105
- Onoe J, Ito T, Kimura SI, Shima H, Toda Y, Yoshioka H (2012) One-dimensional uneven peanut-shaped C_{60} polymer: a quantum electronic system in Riemannian space. *Fullerenes Nanotubes Carbon Nanostruct* 20:1–16
- Paquette LA, Vazeux M (1981) Threefold transannular epoxide cyclization. Synthesis of a heterocyclic C_{17} -hexaquinane. *Tetrahedron Lett* 22:291–294
- Prinzbach H, Wahl F, Weiler A, Landenberger P, Wörth J, Scott LT, Gelmont M, Olevano D, Sommer F, von Issendoef B (2006) C_{20} carbon clusters: Fullerene-boat-sheet generation, mass selection, photoelectron characterization. *Chem Eur J* 12:6268–6280
- Schwarz U, Wosylus A, Böhme B, Baitinger M, Hanfland M, Grin Y (2008) A 3D network of four-bonded germanium: a link between open and dense. *Angew Chem Int Ed* 47:6790–6793
- Schwerdtfeger P, Wirz LN, Avery J (2015) The topology of fullerenes. *WIREs Comput Mol Sci* 5:96–145
- Szefer B, Diudea MV (2012) On molecular dynamics of the diamond D_5 seed. *Struct Chem* 23(3):717–722
- Vukičević D, Klein DJ (2005) Characterization of distribution of pi-electrons amongst benzenoid rings for Randić's "algebraic" Kekulé structures. *J Math Chem* 37:163–170
- Zhang H, Ye D, Liu Y (2010) A combination of Clar number and Kekulé count as an indicator of relative stability of fullerene isomers of C_{60} . *J Math Chem* 48:733–740

Index

A

- Adamantane, 248, 386
- Aggregation, 251, 287, 386–389, 400
- Atlas, 78–80, 130, 132, 133, 187, 189, 190,
193, 194, 247, 248, 251, 282, 287,
337, 339, 346, 386, 392, 395
- Automorphism, 3, 18, 46, 47, 57

B

- Balinski, M.L., 40, 66, 363
- Benedek, G., 336, 386
- Blatov, V.A., 59, 130, 135, 339, 385
- Bonding polygon, 27

C

- Cartesian product, 42, 66, 367
- Cell-in-cell, 49, 50, 77, 247, 337
- Ceulemans, A., 336, 364
- Chiral, 29, 335–346
- Cluster
 - Bergman's cluster, 126
 - P-centered cluster, 47–50, 126, 187, 247
 - rhombic cluster, 80, 135
 - spongy cluster, 135, 287
- Co-distant, 372
- Co-graph, 372
- Complexity, 74, 339
- Co-net, 61, 192, 194
- Connectivity, 5, 18, 45, 55, 69, 282, 335, 398
- Conway, J.H., 23, 25

Count

- figure count, 47, 49–52, 64, 66, 73, 77–81,
83, 85, 126–129, 132–135, 187–192,
247, 249–252, 282–284, 286–289,
337, 339, 340, 342, 343, 346,
364–367, 369, 370, 398
- Kekulé count, 397, 398, 401
- Coxeter, H.S.M., 24, 37, 40–43, 67, 80, 130,
190, 248, 363, 370

Crystal

- crystallography, 57, 61, 69, 385
- quasicrystal, 388, 390
- Curvature, 38, 46, 56, 69, 336, 339

Cycle

- cyclic cover, 67, 291, 338, 346
- cycloaddition, 287, 386, 389, 391, 396–398

D

- Diamantane, 248, 386
- Diamond
 - diamond D_5 , 248, 386–389
- Dimer, 336, 337, 339, 340, 342, 343, 386, 389,
396, 398
- Discretization, 365
- Diudea, M.V., 1, 3, 4, 6, 8, 9, 11, 14, 15, 17,
26, 28–30, 47, 49, 55, 56, 58–61,
67, 69, 74, 77, 78, 80, 130, 187,
192, 193, 248, 251, 284, 291, 337,
339, 344, 346, 363, 365, 367, 368,
370, 372, 377, 386, 389, 390,
398, 400

E

Eberhart, V., 27
 Edges, 1–4, 8–10, 16–18, 23–26, 28–30, 37, 38,
 40–46, 51, 56, 57, 63, 66, 67, 70,
 77–80, 251, 335, 336, 338, 365, 367,
 372, 373, 375, 377, 388, 396, 398
 Embedding, 30, 55, 56, 66, 69, 73, 74, 132,
 135, 190, 335, 339, 363, 366, 368,
 395, 396, 398
 Endo, 125, 187–189, 251, 284
 Endohedral, 47, 61, 125, 286
 Energy
 binding energy, 392, 395, 396, 398
 HOMO-LUMO, 386
 strain energy, 397, 398, 400
 Euler, L., 2, 38, 43, 56, 80, 135, 335, 365
 Euler characteristic, 38, 43, 46, 55–57, 69–71,
 73, 74, 77, 336, 339, 365, 366
 Eulerian, 3
 Exo, 187, 188

F

Figure count, 47, 49–52, 64, 66, 73, 77, 79–81,
 83, 84, 126–128, 130–135, 187–192,
 247, 249–253, 282, 284–290, 337,
 339, 340, 342, 343, 345, 346,
 365–367, 369–371, 398, 400
 Flags, 37, 44, 46
 Fluorite, 194
 Fowler, P.W., 27
 Frank-Kasper phase, 130
 Fullerene, 45, 126, 248, 251, 281, 286, 287,
 367, 385, 386, 389, 391, 392, 395,
 396, 398

G

Gaussian curvature, 56, 336
 Genus, 38, 56, 69, 78, 132, 133, 135, 189, 190,
 251, 282, 336, 339, 342, 344,
 365–368
 Goldberg, M., 29, 30, 193
 Graovac, A., 6, 59
 Graph
 bipartite graph, 1, 2, 378, 381, 382
 chemical graph, 1–19
 graph invariant, 373
 n-partite graph, 1, 51, 52, 135, 136
 reaction graph, 4
 regular graph, 4, 28, 363
 self-centered graph, 247, 340
 Grünbaum, B., 23, 39, 40, 42, 43, 135, 193

H

Haddon, R.C., 398, 400
Hamiltonian, 3
 Hasse diagram, 44, 46
 Hexagonal, 193, 284, 342, 391, 395
 Hyper
 hypercube, 42, 60, 66, 67, 363–370,
 372–380, 382
 hyper-graphene, 389–391, 394
 hyper-ring, 389
 hyper-structure, 77, 127, 133, 135, 187,
 248, 251, 281, 287, 290
 hypertorus, 364, 365, 367
 hypertube, 366, 367, 375

I

Isomer
 “anti”, “syn” isomer, 395
 Isomorphism, 3–5, 57

K

Klein, D.J., 8, 11, 56, 287, 336, 398

J

Johnson, C.R., 9
 Johnson, N.W., 23, 25, 39, 80

M

Mackay, A.L., 336
 Map, 18, 23, 24, 27–29, 56, 61, 63, 69–74,
 78, 80, 133, 187, 188, 190, 193,
 194, 247, 251, 281, 282, 336,
 338–340
 Map operation, 24, 74, 131, 282, 364
 capra/whirl, 29
 dual
 cell dual, 131, 282
 Petrie dual, 24, 74, 364
 leapfrog, 27, 28
 medial, 25, 51, 63, 64, 80, 81, 135,
 190, 251
 polygonal mapping, 26, 27
 quadrupling, 28
 septupling, 29, 30
 snub, 27
 stellation, 28
 truncation, 26
 Maps, 23, 28, 30, 38, 39, 43, 46, 47, 51, 70, 77,
 125, 284, 286, 336

Matrix

- adjacency matrix, 5, 6, 16, 18, 19, 130, 284, 287, 345
- Cluj matrix, 9–11, 16, 17
- combinatorial matrix, 8, 9
- Detour matrix, 5, 7, 8
- distance matrix, 6, 7, 10, 14
- layer matrix, 14, 15, 58, 59, 131, 193, 287, 340
- reciprocal matrix, 14
- shell matrix, 14–17, 58, 59
- walk matrix, 12–14
- Wiener matrix, 7–9, 11, 14, 16, 17

Molecular dynamics, 386

Monomers, 281, 336

Multi-shell clusters, 30, 37, 187, 247, 251, 385, 401

Multi-torus, 135, 337–339, 342, 368

N

Nagy, C.L., 26, 29, 30, 56, 59, 63, 74, 78, 80, 130, 131, 192, 248, 251, 284, 287, 336, 337, 339, 344, 377, 386, 390, 401

Network

three-clinical network, 386, 388

Net

- hh*-net, 398
- hh-ph* net, 398
- ph*-net, 398

O

Oligomer, 392, 393

Opposite edge strip, 372

Orthogonal edge-cut, 372, 377

P

Parent tessellation, 28

Parvan-Moldovan, A., 47, 49, 77, 80, 187, 367

Partial cube, 377

Penrose, R., 135

Pentagonal, 26, 28–30, 77, 80, 125, 132, 190, 251, 284, 287, 337, 342, 389–391

Permutations, 3, 18, 47, 57, 345

Petitjean, M., 18, 337

pi-conjugation, 398

Pisanski, T., 26, 59, 78

Plato, 37, 125, 187

Point-centered cluster, 247, 286

Polygons, 24, 25, 28, 29, 37, 39–41, 43, 46, 73

Polyhedron

- regular polyhedron, 37
- uniform polyhedron, 39, 40, 45

Polymer, 389

Polynomial

- Cluj polynomial, 11, 16, 377–382
- Omega polynomial, 372–377

Polytope

- abstract polytope, 43–47, 363
- convex hull, 41–43
- cross polytope, 42
- n*-cube, 42, 363, 364
- n*-dimensional structure, 40–43
- n*-polytope, 25, 45, 46, 69
- n*-simplex, 41
- regular polytope, 24, 25, 39–42, 45, 47

Poset, 43, 44, 46

Primitive cubic lattice, 194

Propellane, 135, 136

Q

Quasicrystal, 388, 390

Quasi-diamond, 386, 388

R

Randić, M., 5, 8, 16, 23, 26, 78

Rank, 43, 44, 46, 49, 50, 55, 57, 63, 64, 69, 77–80, 83–85, 125, 126, 130, 132, 135, 136, 187, 189, 190, 192, 248, 250, 251, 281, 287, 336, 339, 365–368, 375, 398

Ring

- ring signature, 56, 59–69, 130, 136, 190, 192, 194, 337
- strong ring, 60, 130, 284, 345

Rosenfeld, V.R., 67, 291, 338, 346

S

Samson cluster, 130

Samson, S., 130

Schläfli, L., 66, 73, 77, 125, 363

Schulte, E., 37, 43, 57, 80, 130, 248, 336, 363, 364, 370

Self-arranging, 284

Semicubes, 377

Similarity, 192

- Sodalite, 194
- Software
- CVNET, 74
 - Nano Studio, 74, 80, 131, 248, 251, 337, 377, 400
 - Topos, 30, 131, 192, 337
- Solid, 23, 37, 77, 187, 193
- Archimedean solid, 39, 40
 - Catalan solid, 39, 40, 60
 - Platonic solid, 23, 24, 37–40, 43, 47, 50, 51, 247, 336, 342
 - cube, 23, 37, 187, 193
 - dodecahedron, 37, 77, 187
 - icosahedron, 23, 37
 - octahedron, 23, 37, 187
 - tetrahedron, 23, 37, 187
- Space
- filler, 193
 - filling, 193, 385
- Spongy hypercube, 66, 68, 367–370, 375, 379, 382
- Steinitz, E., 40, 135
- Strain, 132, 338, 397, 398, 400
- Structures, 1, 5, 18, 25, 29, 30, 37, 38, 40, 45–50, 55–57, 59–61, 63, 64, 69, 73, 77–80, 82, 125–133, 135, 136, 187, 189, 190, 192, 193, 248, 251, 281, 282, 286, 287, 290, 291, 335–346, 363, 364, 368, 370, 373, 385, 386, 388–392, 394–396, 398–401
- Symmetry
- icosahedral symmetry, 37, 77, 79, 125–127, 136, 339, 342, 393–396
 - octahedral symmetry, 37, 187–193
 - point group symmetry, 77, 396
 - symmetry group, 18, 37, 41, 46, 127, 187, 247, 338, 340, 343–345
 - tetrahedral symmetry, 37, 393–396
- T**
- Terrones, H., 336
- Tessellation, 28, 30, 41, 135, 282, 339, 363
- Theory**
- DFT, 385, 394
 - DFTB, 386, 388, 390, 391, 393, 394, 400
 - LDA, 396, 400
 - PM6, 398
 - POAV1 theory, 398, 400
 - SCF Hartree-Fock, 391, 400
- Tiling, 29, 56, 63, 73, 135, 194, 373, 386
- Topo Group Cluj, 30, 251, 363
- Topology, 59–61
 - topological distance, 3, 4
 - topological index
 - centrality index, 17, 58, 59, 193, 340, 346
 - chromatic number, 51
 - Cluj-Ilmenau index, 373
 - Cluj-Niš index, 398, 401
 - ring signature index, 59–61
 - topological symmetry, 18, 19, 55, 57, 58, 130, 131, 284, 335
- Toroidal hypercube, 363–366, 378
- Torus, 24, 69, 71, 72, 336, 337, 339, 342, 363–365, 398
- U**
- Uninodal, 61, 69, 194
- Ursu, O., 15, 17, 59, 130, 193, 340
- V**
- Vertex
- equivalence class, 59, 63, 136, 248, 287, 365
 - figure, 25, 39–43, 45, 46
 - orbit, 60, 247
 - vertex degree, 2, 3, 28, 60, 67, 364, 367, 368
- Z**
- Zeolite, 248, 336, 386